Characteristics of Reinforced Concrete Bond at High Strain Rates

by

Eric Jacques

Thesis submitted to the
Faculty of Graduate and Postdoctoral Studies
in partial fulfillment of the requirements for the degree of
Doctorate of Philosophy
in Civil Engineering

uOttawa

Department of Civil Engineering
Faculty of Engineering
University of Ottawa
June, 2016

Executive Summary

The effect of blast and impact on constitutive material behaviour, structural response, and dynamic analysis is currently of great interest to the civil engineering community. Despite the on-going intensity of research in the field of protective structural design, one topic that has been largely ignored in the literature is the effect of high strain rates on reinforced concrete bond. Few researchers have investigated this highly specialized area of study owing to the technical challenges associated with simulating short-duration dynamic loads. Those that have studied the topic have primarily used small-scale pull-out type specimens, which unfortunately generate an unrealistic internal stress-state. While previous tests have clearly demonstrated that bond characteristics are sensitive to strain rate, the use of a poorly-suited test specimen makes it impossible to correlate results obtained using pull-out tests with bond conditions encountered in actual engineering practice.

A comprehensive research program was undertaken to establish the effects of high strain rates on the bond between reinforcing steel and the surrounding concrete. To maximize applicability of the results to the engineering community, the study was focused exclusively on flexural members, where the reinforcing bar and surrounding concrete are in tension, with reinforcement bearing surfaces acting in compression. A combined experimental and analytical investigation was performed to achieve the objectives of the program.

The experimental program was divided into two phases. The first phase consisted of the construction and testing of fourteen flexural beam-end bond specimens having 20M deformed reinforcement. The second phase examined the high strain rate response of a total of twenty-five lap-spliced reinforced concrete beams divided into twelve companion pairs. The physical and material properties of the companion pairs were selected based on a range of design parameters known to significantly influence bond strength, including the size of spliced reinforcement, cover depth, concrete strength and the presence of transverse reinforcement. In order to establish a baseline for comparison, approximately half of the total number of specimens were subjected to

static testing ($\dot{\varepsilon} = 10^{-6} s^{-1}$) while the remainder were subjected to dynamic loading using a shock tube ($\dot{\varepsilon} = 0.1 - 1\ s^{-1}$). The first series of tests demonstrated that the elastic bond strength of beam-ends improved by a factor of 1.45. Furthermore, the general shape of the bond stress-slip curve in the elastic range was not significantly affected by dynamic loading. Results of the lap splice beam tests showed that the flexural behaviour of reinforced concrete was significantly stronger and stiffer when subjected to dynamic loading. Furthermore, high strain rate bond strength was always greater than corresponding low strain rate values, yielding an average dynamic increase factor (DIF) applied to ultimate bond strength of 1.28.

A database of low and high strain rate flexural bond test results was assembled to evaluate the effect of various physical and material properties on the strain rate sensitivity of bond. The database was comprised of a total of 41 bond tests, with the results of this study complemented by other relevant data obtained from the literature. Analysis of the database led to the development of empirical expressions describing the observed strain rate sensitivity of reinforced concrete bond for spliced and developed bars with and without transverse reinforcement. The strain rate sensitivity of bond strength for bars not confined by transverse reinforcement was found to be proportional to bar size, and inversely proportional to an idealized failure plane defined by the development length and the distance between the smallest concrete cover and the centre of the developed bar. The predictive accuracy of the proposed DIF expressions were evaluated against the database and the results showed that dynamic bond strength can be predicted with reasonably good accuracy and can be used for analysis and design of protective structures.

An analytical method was developed to predict the flexural behaviour of reinforced concrete members containing tension lap splices. The methodology incorporated the effect of reinforcement slip, in addition to giving consideration to the effect of high strain rates on bond characteristics and on the material properties of concrete and steel. The proposed model has the advantage of capturing bond-slip phenomenon through the use of pseudo-material stress-strain relationships, rather than giving consideration to the continuum of reinforcement and slippage over the entire structural element. Material properties and associated dynamic increase factors (DIF) were defined using accepted formulations. A suitable bond-slip law was presented, and modified to account for the influence of strain rates on bond characteristics. Beam failure criteria were expressed in terms of a flexural failure of the member or a bond splitting failure of the splice. A comparison of the analytical predictions with experimental data demonstrated that the proposed analysis technique can reasonably predict the flexural response of beams with tension lap splices. The results also show that the model is equally applicable for use at low and high strain rate loading, such as those generated during blast and impact.

Acknowledgements

It's been 5 years since I first began this academic adventure. When I first started, I wasn't entirely sure what I was signing up for, and I certainly didn't have a good idea of what one does with a Ph.D. once they've earned it. However, I knew that I could not pass on an opportunity to pursue new ideas and contribute to the profession. And so the journey began. Now that this particular adventure is coming to a close, I would like to acknowledge the support and assistance of a number of individuals.

Foremost, I want to thank Dr. Murat Saatcioglu for his continued guidance, encouragement and support during the course of this research project. I appreciate the trust that you placed in me to work independently, while always making yourself available to provide mentorship and expertise.

To my wife, Jennifer, I am deeply indebted to you for your unwavering love, support and patience. Without you at my side, none of this would have been possible. Thank you for putting up with endless late nights of rallying, and my seemingly innate ability to continuously find myself overcommitted to any number of academic and professional endeavours.

Thank you to my family – Haydn, Heather, Amanda, Walter, Donna, Andy, and Mr. Bird – for your support and encouragement during the course of my studies. I also greatly appreciate your patience every time I changed the subject whenever you asked how my thesis was going and when I'd finish.

I'm also grateful for the many friendships that I've made at the University of Ottawa. Thank you to Alan Lloyd, Dan Lacroix and Joey Barreiro for your assistance with the shock tube and for the opportunity to collaborate with you on joint projects. To Christian Viau, Steve Castonguay and Fred Dagenais, I am thankful for your help completing my experimental tests.

And so, another journey begins… *E.J. - June 27, 2016*

Table of Contents

Executive Summary ii

Acknowledgements iv

Table of Contents v

Symbols and Notations ix

I Introduction and State of the Art 1

1 Introduction 2

2 State-of-the-Art 5

State of the Art 5

2.1 Mechanism of Bond 5

2.2 Factors Affecting Bond 6

2.2.1 Concrete cover and bar spacing 7

2.2.2 Concrete properties 7

2.2.3 Reinforcement properties 8

2.2.4 Presence of transverse reinforcement 8

2.2.5 Development length 9

2.2.6 Bar casting position 9

2.3 High Strain Rates 9

2.4 Literature Review of Bond at High Strain rates 10

2.4.1 Shah and Hansen (1963) 10

2.4.2 Rezansoff et al. (1975) 11

2.4.3 Vos and Reinhardt (1982), Reinhardt (1982), and Vos (1983) 11

2.4.4 Chung and Shah (1987) 12

2.4.5 Yan (1992) 12
2.4.6 Malvar and Crawford (1998b) 13
2.4.7 Weathersby (2003) 13
2.4.8 UFC 03-340-02 (DoD, 2008) 13
2.4.9 Solomos and Berra (2010) 13
2.4.10 Canadian Standards Association CSA S850 (2012) 14
2.4.11 Toikka (2012), Toikka et al. (2015) 14
2.4.12 Yao, Wu and Huang (2013) 16
2.4.13 Michal et al. (2015) 16
2.5 Protective Design Requirements 17
2.6 Research Needs 18
2.7 Objectives 18
2.8 Scope 19
2.9 Organization of Thesis 20

II Experimental and Analytical Studies 29

3 High Strain Rate Response of Reinforced Concrete Beam-ends 30
3.1 Introduction 31
3.2 Beam-end Tests 32
3.2.1 Low Strain Rate Test Fixture 34
3.2.2 High Strain Rate Test Fixture 34
3.3 Test Procedure 35
3.4 Test Results 35
3.4.1 Failure Mode & Ultimate Bond Strength 35
3.4.2 Steel Strain Distribution Curves 37
3.4.3 Slip Distribution Curves 38
3.4.4 Elastic Bond Stress-Slip Behaviour 38
3.5 Discussion 40
3.6 Summary and Conclusions 42

4 High Strain Rate Response of Reinforced Concrete Lap Splice Beams 52
4.1 Introduction 53
4.2 Experimental Methodology 54
4.2.1 Test Specimens and Parameters 54
4.2.2 Material Properties 55
4.2.3 Test Setup 56
4.3 Instrumentation 57

4.4 Test Procedure & Blast Loading Program 58
4.5 Experimental Results 59
4.5.1 Loading Rate 59
4.5.2 Strain Rate 59
4.5.3 General Behaviour 60
4.5.4 Description of Beam Behaviour 63
4.5.5 Bond Energy 64
4.5.6 Splice Toughness 65
4.5.7 Reinforcement Strains 66
4.5.8 Influence of Strain rate on Bond Strength 66
4.6 Summary and Conclusions 68

5 Bond Strength of Reinforced Concrete at High Strain Rates 85
5.1 Introduction 86
5.2 High Strain rate Bond Database 87
5.2.1 Database Overview 87
5.2.2 Database Structure 88
5.2.3 Sectional Analysis to Obtain Splice Steel Stress 89
5.2.4 Review of Test Data 90
5.3 Analysis of Test Results 93
5.3.1 Bars without Transverse Reinforcement 93
5.3.2 Bars with Transverse Reinforcement 96
5.3.3 Evaluation of Descriptive Expressions 98
5.4 Application to Protective Design 100
5.4.1 Canadian Blast Standard, CSA S850 100
5.4.2 Recommendations for Protective Design 102
5.5 Summary and Conclusions 103

6 Structural Response of Lap Spliced RC Beams at Low and High Strain Rates 113
6.1 Introduction 114
6.2 Analytical Model 116
6.2.1 General Approach 116
6.2.2 Reinforcement Stress-Strain Incorporating Bond-Slip 117
6.2.3 Bond-Slip Response at High Strain rates 119
6.2.4 Material Behaviour at Low and High Strain rates 122
6.2.5 Solution Procedure for Structure Behaviour 125
6.3 Model Validation 126

6.3.1 Test Specimens and Parameters 126
6.3.2 Analysis of Test Beams 127
6.4 Summary and Conclusions 130

III Conclusions and Future Work **145**

7 Conclusions **146**

8 Future Work **152**

9 References **153**

IV Appendices **159**

A Beam-end Bond Test Data **160**

B Reinforced Concrete Lap Splice Beam Test Data **200**

C Dynamic Support Reactions **324**

D List of Tables **328**

E List of Figures **329**

Symbols and Notations

Acronym	Definition
BE	Beam-end
COV	Coefficient of variation
CP	Companion pair
DIF	Dynamic increase factor
DPL	Dynamic point loader
HSR	High strain rate
HSS	Hollow Structural Section
LSR	Low strain rate
LTD	Load transfer device
LVDT	Linear variable displacement transducer
SHPB	Split-Hopkinson Pressure Bar

Symbol	Definition
A	Area of the LTD
A_b	Bar area
$A_{F.R.}$	Area of an equivalent fully rigid structure
A_{tr}	Area of each stirrup or tie crossing a potential splitting place adjacent to the reinforcement being developed
b	Width
B	Blast load
BE	Bond energy
c_b	Bottom cover
c_{max}	Maximum of (c_b, c_s)
c_s	Minimum of $(c_{so}, c_{si} + 6.35)$
c_{si}	½ the clear bar spacing
c_{so}	Side cover
d	Reinforcement depth
d_b	Bar diameter
d_{cs}	The smaller of (a) the distance from the closest concrete surface to the centre of the bar being developed; or (b) two-thirds the centre-to-centre spacing of the bars being developed
D	Dead load

DIF_c	Dynamic increase factor applied to bond strength for splices with transverse reinforcement
DIF_{f_c}	Dynamic increase factor applied to concrete compressive strength
DIF_{f_u}	Dynamic increase factor applied to steel ultimate strength
DIF_{f_y}	Dynamic increase factor applied to steel yield strength
DIF_{l_d}	Dynamic increase factor used for design of dynamic development lengths
DIF_{T_c}	Dynamic increase factor applied to the concrete contribution to normalized total bond force
DIF_{T_s}	Dynamic increase factor applied to the contribution of transverse reinforcement to normalized total bond force
DIF_u	Dynamic increase factor applied to bond stress
DIF_{uc}	Dynamic increase factor applied to bond strength for splices without transverse reinforcement
E_c	Modulus of elasticity of concrete
E_s	Modulus of elasticity of steel
f_c'	Compressive strength of concrete
f_{dc}'	Dynamic compressive strength of concrete
f_{cr}	Cracking strength of concrete
f_{dcr}	Dynamic cracking strength of concrete
f_{dy}	Dynamic yield strength of concrete
f_s	Steel stress
$f_{s,exp}$	Experimental steel stress
$f_{s,pred}$	Predicted steel stress
f_s^{cal}	Calculated splice stress
f_{sh}	Steel strain hardening stress
f_s^t	Experimental splice stress
f_u	Ultimate strength of reinforcement
f_y	Yield strength of reinforcement
f_{yt}	Yield strength of transverse reinforcement
$F(t)$	Time-varying force
h	Height
h_r	Reinforcement rib height
h_x	Maximum horizontal centre-to-centre spacing between longitudinal bars on all faces of the column that are laterally supported by seismic hoops or crosstie legs
I_r	Reflected impulse
jd	Internal lever arm
k	Calibration constant
k_1	Bar location factor
k_2	Coating factor
k_3	Concrete density factor
k_4	Bar size factor
K_{tr}	Transverse reinforcement index
l_b	Bonded length
l_d	Development length
l_s	Spliced length
l_{dd}	Development length required to resist dynamic loads
L	Length, live load
L_s'	Effective splice length
m	Parameter to account for bond on tensile concrete strength
$\bar{m}$	Distributed mass

m_c	Concentrated mass
$M(t)$	Time-varying moment
M_f	Moment at failure
$M \cdot \phi$	Moment-curvature relationship
n	Number of bars being developed or spliced, or calibration constant
N	Number of transverse stirrups or ties within l_d
P_r	Pressure
$P_r(t)$	Time-varying pressure
$R(\delta)$	Resistance-displacement Function
$R(t)$	Time-varying resistance
R_{exp}	Experimental peak resistance
R_f	Peak resistance
R_{pred}	Predicted peak resistance
R_r	Relative rib ratio
s	Bar slip or spacing of transverse reinforcement
s_1	Slip at which u_o is attained
s_2, s_3, s_4	Slip parameters
s_L	Reinforcement lug spacing
s_{max}	Maximum bar slip
s_r	Reinforcement rib spacing
s_x	Longitudinal spacing of transverse reinforcement
S	Snow load
$S_{f_c'}$	Dynamic in-situ concrete strength
S_{f_y}	Dynamic in-situ steel yield strength
t_f	Time to peak resistance
t_m	Time to maximum material strain
t_r	Effect of relative rib area on T_s $(9.6R_r + .028)$
t_d	Effect of bar size on T_s $(0.03d_b + 0.22)$
T_b	Bond force
$T_b^{A23.3}$	Bond force predicted using CSA A23.3
T_b^{cal}	Bond force obtained from calculations
T_b^t	Bond force obtained from test measurements
T_c	Concrete contribution to total bond force
T_{db}	Dynamic bond force
T_{dc}	Dynamic concrete contribution to total bond force
T_{ds}	Dynamic contribution of transverse reinforcement to total bond force
$T.I.$	Toughness index
T_s	Contribution of transverse reinforcement to total bond force
u	Bond stress
u_f	Fictional bond stress
u_m	Maximum bond stress
u_o	Bond strength corresponding to yield of reinforcement
$V(t)$	Time-varying support reactions
x	Distance
$x(t)$	Time-varying centroid of inertia force
α_s	Coefficient in Eq.(5.1)
α	Calibration factor
β	Exponent in Eq. (6.5)
Δ	Mid-span beam deflection obtained by numerical integration of $M \cdot \phi$
δ_{exp}	Experimental displacement at peak resistance
δ_f	Displacement at peak resistance

δ_{pred}	Predicted displacement at peak resistance
δ_u	Ultimate deflection
$\dot{\varepsilon}$	Strain rate
ε	Strain
ε_{avg}	Average strain
ε_c	Concrete strain
ε_m	Maximum material strain
ε_o	Strain corresponding with f_c'
ε_s	Steel strain
ε_s'	Effective reinforcement strain within a splice
ε_{sh}	Strain at the onset of reinforcement strain hardening
ε_{slip}	Slippage strain
ε_u	Rupture strain of reinforcement
ε_y	Yield strain of reinforcement
ϕ	Curvature
$\phi(x)$	Curvature distribution
γ_s	Coefficient in Eq. (5.1)

Part I

Introduction and State of the Art

Chapter 1

Introduction

Concrete's economic potential and viability can be traced to a number of beneficial characteristics which make it one of the most common building materials in use throughout the world. For example, concrete is less likely to decay or corrode as compared with other building materials. As a result, concrete structures have a long service life and relatively low maintenance requirements. Concrete can be cast into practically any desired shape and provides inherent fire resistance without the need for supplemental fire protection. As a poor thermal conductor having considerable density, concrete structures have a high thermal mass which can aid in offsetting daily temperature fluctuations. However, concrete has relatively low tensile strength and poor ductility. This necessitates the addition of reinforcing steel to fully realize the potential of the material in modern infrastructure.

Reinforced concrete members are designed on the basis of composite action between two dissimilar materials. A force transfer is required to permit equilibrium of compressive stresses, resisted by concrete, with tensile stresses, resisted by reinforcing steel. This mechanism of force transfer is achieved through bond stresses, which ensure composite behaviour of concrete and reinforcement.

The phenomenon of bond, a fundamental characteristic of reinforced concrete behaviour, is a topic whose origins may be traced to the early 20^{th} century. Extensive research in this area has led to a fundamental understanding of the bond phenomena and has generated substantial knowledge on the factors affecting bond. It is widely accepted that bond is caused by the cumulative effect of surface friction, chemical adhesion and mechanical interlock of rebar lugs with surrounding concrete. Unlike the crushing strength of concrete or the yield strength of steel, bond is not a generic material property. Rather, it is a complex behaviour that is sensitive to a host of material and

structural parameters, such as the material properties of steel and concrete, the surface condition and geometric configuration of the reinforcement, and the construction of the structural element. Due to the depth and breadth of the knowledgebase, numerous publications have been written on the topic of bond. However, the vast majority of these have focused on bond under slowly applied static load conditions. Very few studies have examined the effect of high strain rates, such as those generated during blast and impact events, on reinforced concrete bond characteristics.

Owing to the technical challenges of simulating short-duration dynamic loads on structural members, few researchers have investigated the highly specialized topic of reinforced concrete bond behaviour at high strain rates. Those that have studied the topic have primarily used small-scale pull-out type specimens subjected to dynamic loads. Split-Hopkinson Pressure Bars (SHPB) and high-speed actuators are commonly reported as dynamic load sources. The results of these tests have demonstrated that bond strength experiences an apparent increase when subjected to short-duration, dynamic loads. The previous studies also suggest that the degree of dynamic bond strength improvement is a function of: the rate of loading; the construction details and geometry of the developed or spliced bar, and; the properties of the constituent materials.

The pull-out bond test has a number of issues which limit researchers' ability to correlate their test results with bond in real members. Although pull-out tests are relatively simple to perform, they generate a stress field in which the reinforcement is placed in tension and the surrounding concrete is in compression. In actual structures, the stress field surrounding developed reinforcement is such that reinforcement and concrete are both in tension. As the tensile behaviour of concrete is significantly different from its compression response, it is impossible to correlate results obtained using pull-out tests with bond conditions encountered in actual engineering practice. In consequence, there is a lack of a quantitative understanding of the influence that high strain rates have on bond as a function of the geometric and material parameters that are commonly encountered in practice.

Despite the lack of firm data on the dynamic behaviour of reinforced concrete bond, protective design documents do make reference to the importance of maintaining bond during blast and impact events. For instance, both CSA S850 and UFC 03-340-02 impose stringent detailing requirements to reduce the likelihood of bond-related failures under blast and impact loading. Although the literature suggests otherwise, these documents recommend that any strain rate-related bond strength enhancement be ignored. Therefore, in blast-resistant design, spliced and anchored reinforcement are proportioned to resist dynamic loads using static bond strength design expressions. The rationale for using the static bond strength to design for dynamic loads is to ensure that the development or splice length provided will always be greater than what is required.

Given the sheer lack of knowledge with which high strain rates may or not affect reinforced concrete bond, ignoring its influence is consistent with the overriding life-safety objective of protective design. In doing so, a number of issues and contractions arise. Firstly, ignoring dynamic bond strength makes it impossible to establish to what degree an existing splice or developed region is sufficient or deficient. Secondly, this approach doesn't provide any meaningful guidance to researchers or analysts conducting a sophisticated design or analysis of a blast-loaded structure. Finally, if the justification for ignoring dynamic bond is to obtain an enhanced level of conservatism against undesirable failure modes, why then are dynamic material strength increases not ignored when proportioning blast-resistant structural elements? Based on the above, it would appear that the effect of high strain rates on bond strength, and the implications for protective design, are far from certain.

From the perspectives of advancing the state of the art in the field of blast research and ensuring the resiliency of critical infrastructure, it is evident that some clarity is required regarding how high strain rates affect reinforced concrete bond. The Chemical, Biological, Radiological, Nuclear and Explosives (CBRNE) Research and Technology Initiative (CRTI) recently funded a project (CRTI 06-0150TD) to investigate the vulnerability of building components to bomb damage and develop risk assessment tools to improve Canada's response preparedness and capabilities against blast threats. As part of this study, the University of Ottawa led a research initiative to establish the effect of high strain rates on the bond between reinforcing steel and concrete in developed and spliced reinforcement. The motivation of this thesis came with the aim of providing a quantitative measure of the influence that high strain rates have on reinforced concrete bond in large-scale structures. Another equally important outcome of this work is to propose a unified, consistent means of incorporating dynamic bond strength into the protective design process.

Chapter 2

State of the Art

Bond between reinforcing steel and concrete is a topic of study whose origins may be traced to the early 20th century. Exhaustive research in this area has led to a significant understanding of bond phenomenon, extensive knowledge of the factors affecting bond, and the development of expressions which can accurately predict bond strength of reinforced concrete members. The following discussion is a general overview of bond phenomenon. It is intended to serve as a basis for the research activities presented in this thesis. For a detailed treatise on the topic of reinforced concrete bond, the reader is directed to the comprehensive report published by ACI Committee 408 (ACI, 2003).

Table 2.1 lists a set of standard terminology which was adopted to describe reinforced concrete bond throughout this dissertation. The terminology is consistent with those recommended by ACI Committee 408 (ACI, 2003).

2.1 Mechanism of Bond

Reinforced concrete members are designed on the basis of composite action between two dissimilar building materials. A force transfer is required to permit equilibrium of compressive stresses resisted by concrete and tensile stresses resisted by reinforcing steel. This mechanism of force transfer is achieved through bond stresses, which ensure composite action between the two materials.

The components which contribute to the mechanism of bond transfer, illustrated in Figure 2.1, are: chemical adhesion between the concrete and the reinforcing bar; frictional forces at the bonded interface, and; mechanical bearing of deformations (lugs) on the surface of the bar. Chemical

adhesion is lost once slippage of the bar occurs, at which point bond is primarily caused by mechanical bearing. This phenomenon generates longitudinal and radial stresses in the surrounding concrete. If the radial stress demand exceeds the capacity of the surrounding concrete, a splitting failure will occur. However, pull-out failures are also possible if the longitudinal stresses are sufficient to crush concrete in the vicinity of the lugs prior to splitting. A number of factors, including concrete strength, cover depth, and presence of transverse reinforcement, influence the mechanism of bond transfer.

Bond exists when a finite length of reinforcement, such as the one illustrated in Figure 2.2, experiences a change in stress. A bond stress (u) is required to maintain equilibrium if steel stress f_{s2} is different than f_{s1}. The average bond stress acting on a bar experiencing a change in steel stress $\Delta f_s = f_{s2} - f_{s1}$ is given by:

$$u = \frac{\Delta f_s d_b}{4 l_d} \tag{2.1}$$

where d_b is the bar diameter and l_d is the bonded length. If the bonded length becomes infinitesimally small with length ∂x, the above equation becomes

$$u = \frac{d_b}{4} \frac{\partial f_s}{\partial x} \tag{2.2}$$

where u represents the bond stress acting on length ∂x.

Examining Eq. (2.2) indicates that the true distribution of bond is proportional to the rate of change of steel stress along the development length. The variation of steel, concrete, and bond stresses in a cracked reinforced concrete beam subjected to four-point bending are illustrated in Figure 2.3 (a). At the location of the cracks in Figure 2.3 (a), all tensile force in the member is carried by reinforcing steel. Between the cracks, a portion of the tensile force is carried by concrete due to tension stiffening, shown in Figure 2.3 (d). As a result, steel stresses between cracks are less than those at a crack. Based on the rate of change of the steel stress distribution, the bond stress along the length of the prism can be computed. This distribution, illustrated in Figure 2.3 (e), is referred to as the "true bond stress distribution." Accurately predicting the distribution of cracks in a reinforced concrete member is an extremely challenging endeavor. As a result, computing the true distribution of bond stresses is not practical for most applications. Therefore, it is common to assume bond forces are uniformly distributed over the length of reinforcement being developed or spliced.

2.2 Factors Affecting Bond

Unlike the crushing strength of concrete or the yield strength of steel, bond is not a generic material property. Rather, it is a complex phenomenon that is sensitive to a host of material and structural parameters, such as the material properties of steel and concrete, the surface condition

and geometric configuration of the reinforcement, and the construction of the structural element. The following provides a summary of the main factors which exert influence on bond phenomenology.

2.2.1 Concrete cover and bar spacing

Concrete cover and bar spacing exert significant influence on bond characteristics. Increased cover and bar spacing results in greater bond strength, while also increasing the likelihood of pull-out type failures (Orangun, Jirsa, and Breen, 1977). However, for typical structural members, splitting failures are most common. Splitting failures can be classified by the nature of splitting crack propagation, either occurring between bars, between the bars and the nearest free-surface, or some combination thereof (ACI, 2003). In many cases, splitting failures are related to the relative values of the side and bottom covers, as well as the separation between bars (Darwin et al., 1992). Face splitting failures, shown in Figure 2.4 (a), generally occur when the bottom cover, c_b, is smaller than the side cover, c_{so}, and ½ the clear bar spacing, c_{si}. Similarly, side splitting failures, Figure 2.4 (b), tend to occur when c_b is larger than c_{so} or c_{si}. In the case of anchored bars, splitting failures are likely to occur at locations of stress concentrations at transverse flexural cracks or at a free surface. For the case of spliced bars, splitting failures tend to occur at the end of the splice and propagate along the rest of the splice. "V-notch failures," characterised by face splitting with inclined cracking, can also occur when $c_{si} \gg c_b$.

2.2.2 Concrete properties

Bond is affected by both the tensile and compressive strength of concrete. The effect of concrete properties on bond has typically been expressed as being proportional to $\sqrt{f_c'}$. However, researchers have reported a better representation can be obtained for a greater range of concrete strengths when bond is expressed as being proportional to $f_c'^{1/4}$ (Darwin et al., 1996). Higher strength concrete results in increased bond due to enhancements to both concrete tensile and compressive strengths (Azizinamini et al., 1995). Similarly, higher strength aggregates, such as basalt, tend to produce higher bond strengths than weaker aggregates, such as limestone, in splices with and without transverse reinforcement (Zuo and Darwin, 1998). This is attributed to higher fracture energies of higher strength aggregates resisting the onset of internal splitting cracks. In regards to concrete density, design codes typically penalize bond strength whenever lightweight cementitious materials are used. ACI Committee 408 (ACI, 2003) noted that the literature does not indicate a clear consensus on its effect, with the bond strength of lightweight concrete ranging from between 65% to 100% of the strength obtained from normalweight concrete.

2.2.3 Reinforcement properties

The physical characteristics of the reinforcing bar also influence development and splice length. For bars not confined by transverse reinforcement, increases in bar size require larger bonded lengths to achieve the same steel stress as smaller bars. For the case of anchored or spliced bars confined by transverse reinforcement, larger bars generate greater radial strains in the surrounding concrete. In turn, these radial strains activate the transverse reinforcement which generate passive confining pressures leading to increased bond strength (Darwin et al., 1996). Deformation pattern also influences bond characteristics by affecting the mechanical bond between concrete and reinforcement lugs. Larger bond strengths are obtained for bars with greater rib bearing areas (Darwin and Graham, 1993). The surface condition of the reinforcement can also affect bond strength, with clean, rust-free bars being preferable. As reported by ACI Committee 408, epoxy-coated rebar generally has lower bond strength due to a reduction in the coefficient of friction (ACI, 2003).

2.2.4 Presence of transverse reinforcement

The presence of transverse reinforcement improves bond strength by limiting the development of splitting cracks in the spliced region (Zuo and Darwin, 1998). Passive confining pressures, generated by the transverse reinforcement due to wedging action of the bars, resist lateral expansion of concrete due to splitting. Greater bond strengths are obtained in proportion to the amount of transverse reinforcing crossing a potential splitting crack plane. However, there is an upper limit on the amount of transverse reinforcement beyond which no increase in bond is noted (ACI, 2003).

The likelihood of a pull-out bond failure increases as the amount of confinement provided by transverse reinforcement increases. Darwin et al. (1996) proposed a combined variable $t_r t_d N A_{tr}/n$ to describe the contribution of transverse reinforcement to bond strength. Parameters t_r and t_d, characteristics inherent to a particular type of rebar, account for the wedging action of the lugs against the surrounding substrate. Larger rebar sizes (resulting in greater values of t_r) and more aggressive deformation patterns (resulting in greater values of t_d) generate greater values of bond force provided by transverse reinforcement (T_s). The parameter $N A_{tr}/n$ represents the effective quantity of transverse reinforcement mobilized to resist splitting failure along a critical plane. Research has shown that increasing one or any combination of reinforcement size, relative rib ratio, or quantity of transverse reinforcement will lead to greater increases in T_s due to increased wedging action (Darwin et al., 1996). For bars confined by transverse reinforcement, $f_c'^{3/4}$ was found to best represent the effect of concrete properties on bond strength due to transverse reinforcement (Zuo and Darwin, 1998). Furthermore, transverse reinforcement confining developed or spliced regions will generally not yield and the grade of steel used does not influence T_s. (ACI, 2003)

2.2.5 Development length

Intuitively, bond strength is increased by providing larger development and splice lengths. This occurs as a greater area of concrete must be split for a crack to initiate. However, the increase in bond strength is not proportional to the bonded length since the rate of increase in energy required to form a splitting crack is less than the increase in bonded length (Brown et al., 1993).

2.2.6 Bar casting position

Bar casting position also influences bond strength. Research has shown that bottom cast bars have a higher bond strength than top cast bars. This reduction in bond efficiency occurs due to the settlement of aggregates, as well as the bleeding of concrete, which increases the local water-cement ratio in the vicinity of top cast bars (ACI, 2003). Combined, these effects decrease the adhesion of concrete and steel in top cast reinforcement.

2.3 High Strain Rates

Structures subjected to short-duration dynamic loads, such as blast or impact, experience an apparent increase in material strength. This dynamic behaviour is generally only present for the duration of the loading event, and can significantly affect the strength and stiffness of structural elements over that time period. While static design is commonly associated with strain rates ($\dot{\varepsilon}$) on the order of 10^{-5} – 10^{-6} s^{-1}, strain rates of 0.1 s^{-1} and 0.3 s^{-1} are associated with blast-resistant design in the far- and mid-field design ranges, respectively (Department of Defense, 2008). The temporal and spatial distribution of strain rate is highly non-uniform, with regions of maximum stress (*e.g.* critical sections) typically experiencing the greatest material increases due to rate-effects.

A scaling factor, known as a dynamic increase factor (DIF), is applied to a static material property to account for strain rate sensitivity. The DIF is defined as the ratio of the dynamic material property to the static material property. The DIF of a material is primarily a function of strain rate, increasing as strain rate increases, although material quality and sample geometry also contributes. Strain rate is typically defined as

$$\dot{\varepsilon} = \frac{\varepsilon_m}{t_m} \tag{2.3}$$

where: ε_m is the maximum strain in a material and t_m is the time-to-maximum strain ε_m.

The tensile and compressive strength of concrete are both affected by high strain rates. For a given strain rate, tensile strength generally exhibits greater strain rate sensitivity than compressive strength (Malvar and Crawford, 1998b). Figure 2.5 shows the influence of high strain rates on concrete properties. For moderately high strain rates, the relative dynamic strengths of concrete remain low. However, a sharp transition occurs where the relative dynamic strengths increase

rapidly at higher strain rates. The discontinuous change observed in *DIF* is indicative of a change in physical response of the material to dynamic loading (Biscoff and Perry, 1991). At strain rates below 1 s^{-1}, porosity and free water within concrete pores exert considerable influence on dynamic strength (Toutlemonde et al., 1995). However, at strain rates above 1 s^{-1}, a time lag in radial acceleration associated with Poisson's effect, known as lateral inertial confinement, results in a sharp increase in *DIF* (Biscoff and Perry, 1995).

As is the case for concrete, reinforcing steel experiences an increase in material properties due to dynamic loading. Typical increase factors for reinforcing steel are illustrated in Figure 2.6. Unlike concrete, the *DIF* for steel is understood with a much higher degree of statistical confidence. This is attributed to the high degree of standardization and precision employed during the steel manufacturing process, and due to the isotropic nature of steel (Fu et al., 1991). Malvar (1998a) performed a review of existing research on dynamic material behaviour of reinforcing steel and found that the *DIF* of both yield and ultimate stress are inversely proportional to yield stress; higher grade reinforcing steel experiences a smaller *DIF* than lower grade steel. Furthermore, the ultimate strength of steel experiences a much smaller increase than the yield strength. Modulus of elasticity is independent of strain rate.

2.4 Literature Review of Bond at High Strain rates

Owing to the technical challenges of simulating short-duration dynamic loads on structural members, few researchers have investigated the highly specialized topic of reinforced concrete bond behaviour at high strain rates. The following is a summary of the limited research findings on reinforced concrete bond subjected to high strain rates.

2.4.1 Shah and Hansen (1963)

The authors studied the effect of concrete strength and deformed bar diameter on the bond properties of reinforcing steel at high loading rates. A pull-out type test was employed. Three concrete strengths were considered: 13.8 MPa, 24.1 MPa and 41.4 MPa. Three bar diameters were studied: #8 (25M), #10 (30M) and #14 (45M). Bonded length for each specimen was three times the bar diameter to ensure a bond failure as opposed to bar rupture failure. A dynamic loading machine was used to apply a triangular loading pulse of up to 1337 kN with a rise of between 15 ms and 30 ms. Assuming that bars just achieved yield at bond failure, this translates to an approximate strain rate of 10^{-2} to 10^{-1} s^{-1}. Loading pulses were selected such that bond failure would occur during the "rising" portion of the pulse.

The results showed that for both static and dynamic load cases, ultimate bond stress increases with concrete compressive strength: the static ultimate bond strength reported was in the range of 0.5-0.6f_c' while the dynamic ultimate bond strength was in the range of 0.6-0.9f_c' (*DIF*=1.36). The

ratio of bond stress to concrete strength remained constant for static testing. When subjected to dynamic loading, the bond stress ratio was found to decrease with increasing concrete strength. Ultimate bond stress was reported to be inversely proportional to bar diameter. Furthermore, tests seemed to indicate that increasing bar diameter and concrete strength increased the likelihood of splitting failure of the specimens, as opposed to pull-out failure.

2.4.2 Rezansoff et al. (1975)

Rezansoff et al. (1975) performed drop-weight impact tests on doubly reinforced concrete beams constructed with tension lap splices, with and without transverse reinforcement. Impact tests generated strain rates of approximately 0.3 s^{-1} in the tensile reinforcement. The simply supported beams were 380 mm tall, and 430 mm wide and subjected to four point bending. Primary flexural reinforcement consisted of 2-#8 (25M) bars lapped in the constant moment region. Lap lengths varied between 450 mm and 1060 mm. Beam length varied between 3700 mm to 5300 mm, depending on the spliced length. Various beams were subjected to either single, incrementally increasing, or cyclically applied impact loads. The mass of the drop weight, illustrated in Figure 2.7, was 1180 kg with drop heights ranging from 200 mm to 1200 mm.

Higher mode effects were evident from oscillation in the load cell data, as well as in the steel strain gauge data. Dynamic moment capacity of the beams was larger than the static moment capacity: increases of 1.33 for a 200 mm drop height, 1.35 for a 400 mm drop, 1.41 for a 600 mm drop, and 1.69 for a 1200 mm drop were observed. Dynamic increase factors for the yield strength of steel were reported to be in the range of 1.16 to 1.29, while the tensile strength of concrete experienced an estimated increase between 35% and 65%. The performance of beams with splices confined by stirrups was superior to beams without transverse reinforcement. Beams with transverse reinforcement in the spliced region sustained deflections at least twice as large as those for beams without transverse reinforcement.

The authors did not report on the static and dynamic bond strength directly. However, an analysis of the test data (discussed in detail in Chapter 0) indicates that bond strength of lap splices not confined by transverse reinforcement experienced a DIF in the range of 1.25 – 1.43 depending on splice construction, material properties and loading sequence.

2.4.3 Vos and Reinhardt (1982), Reinhardt (1982), and Vos (1983)

Vos and Reinhardt used a SHPB to perform impact testing of smooth reinforcing bars, prestressing strands and deformed reinforcement. Bar diameter was maintained at a constant 10 mm for all tests. The circular concrete pull-out specimens, shown in Figure 2.8, had a diameter of 100 mm, and a bonded length of 30 mm. The maximum loading rate was approximately 100-160 MPa/ms. This roughly translates into a strain rate of 0.65 s^{-1}. The investigators reported that the bond

characteristics of plain reinforcement and prestressing strands were independent of loading rate. It was suggested that the bond mechanisms of adhesion and friction are not affected by loading rate. However, the bond resistance of deformed reinforcement is significantly affected by loading rate: higher loading rates resulted in greater peak bond resistance and lower slip displacements, indicative of increased bond stiffness. Furthermore, the increase in bond under dynamic loading was greater for lower quality concrete. The researchers also suggest that the use of static bond-slip relationships with appropriate material increase factors can adequately describe the dynamic bond-slip characteristics.

2.4.4 Chung and Shah (1987)

Small-scale beam-column joints and anchorage bond specimens were subjected to large-displacement cyclic load reversals. Strain gauges were installed into grooves in the reinforcement to monitor strain development in the anchored regions. The authors noted a number of behaviours linked directly to high strain rate effects. Tests on both beam-column joints and anchorage bond specimens indicated that ultimate load capacity was improved with greater damage and more localized cracking occurring for higher loading rates. Analysis of the strain distribution within the anchored regions also showed that strain was more localized when subjected to dynamic loads. The concentration of strain observed by the authors was attributed to improved reinforced concrete bond resistance.

2.4.5 Yan (1992)

Pull-out and push-in tests were performed to study the effect of bond between reinforcing steel and concrete at high loading rates. Smooth bars with a diameter of 12.7 mm and 10M deformed steel bars were tested. Plain, polypropylene fibre reinforced, and steel fibre reinforced concretes were considered. The bars were embedded into the centre of 152.4 mm × 152.4 mm × 63.5 mm concrete prisms. Details of the specimens are shown in Figure 2.9. Embedment length was 63.5 mm for all tests. A 345 kg drop hammer impact machine, with a maximum drop height of 2.4 m, was used to apply high loading rates. Failure occurred on the order of 20 ms after the impact of the drop mass.

The results indicated that the bond strength for smooth reinforcing bars is independent of loading rate, concrete quality, and use of additional fibrous reinforcement within the concrete mix. For deformed bars, the dynamic bond characteristics are enhanced by loading rate, concrete quality and fibre content. A linear bond-slip relationship was observed for smooth bars, whereas deformed bars exhibited nonlinear bond-slip relationship.

2.4.6 Malvar and Crawford (1998b)

A literature review was performed to characterise the dynamic increase factors of concrete in tension and compression at high strain rates. As a part of this study, the authors discussed the effect of strain rate on bond between concrete and reinforcing steel. It was suggested that existing bond-slip relationships developed from static test data could be applied to dynamic loads, provided dynamic increase factors were applied to concrete and steel material properties.

2.4.7 Weathersby (2003)

The primary objective of this study was to investigate the dynamic interaction between bond of reinforcement and concrete at various loading rates. A 900 kN hydraulic test fixture was used as the primary experimental apparatus. This setup is shown in Figure 2.10 (a). Three load types were considered: quasi-static loading with a time to peak load of several hundred seconds, dynamic loading with a rise time of approximately 132 ms and impact loads with a rise of around 4 ms.

Thirty-three circular pull-out specimens were tested. Specimens had circular diameter of either 254 mm or 356 mm with a constant embedment depth of 254 mm. #8 (25M) and #10 (35M) deformed steel reinforcement, along with #8 smooth steel reinforcement were considered. A typical specimen prior to testing is shown in Figure 2.10 (b).

Weathersby reported a general decrease in development length as loading rates and confinement (*i.e.* diameter of the concrete cylinder) increased. Impact failure loads for all specimens were 70% to 100% larger than their corresponding quasi-static values, provided the failure mode remained the same. An approximately 300% increase in the bond stress associated with static friction and chemical adhesion was reported as loading rate increased from quasi-static to impact loading. Furthermore, bar deformations contributed approximately 75% of total pull-out resistance for all loading rates.

2.4.8 UFC 03-340-02 (DoD, 2008)

This protective design document assumed that any increase in bond under dynamic loading may be attributed to strain rate effects of reinforcing steel only. No justification for ignoring the increase in concrete strength at high strain rates is given, beyond ensuring that conservative development lengths are provided in design.

2.4.9 Solomos and Berra (2010)

Solomos and Berra studied the effect of loading rate on cast-in-place and post-installed ribbed 20 mm diameter DYWIDAG reinforcement. The effect of confinement, anchorage length and concrete strength were considered for cast-in-plate and post-installed reinforcement. A schematic

of the specimens is shown in Figure 2.11. All specimens had a diameter of 100 mm, with a 50 mm bond breaker at either end of the cylinder. Anchorage length was either 100 mm or 200 mm. Concrete strength was 35 MPa or 68 MPa. More than 50 specimens were tested. A SHPB was used to apply a rectangular pulse loading with a duration of 40 ms. Typical pull-out response occurred within approximately 2 ms for unconfined specimens and 16 ms for confined specimens. The authors estimated that the strain rate observed during testing was on the order of 10 s^{-1}.

The results for unconfined specimens indicated that peak dynamic pull-out forces were up to 90% greater than corresponding static values. The primary failure mode for unconfined specimens was tensile splitting of concrete. The increase in dynamic pull-out force relative to static force was attributed primarily to the increase in the tensile strength of concrete at high strain rates. For confined specimens, where the primary failure mode is due to rebar pull-out, the dynamic pull-out forces were 22% larger for 100 mm anchorage length and 11% for 200 mm anchorage. The confinement of concrete by steel jackets resisted the radial expansion of concrete, and increased the compressive strength of concrete in the region of the mechanical lugs. The moderate increase in dynamic pull-out forces relative to static pull-out for confined specimens was attributed to the reduced strain rate sensitivity of concrete in compression, relative to tension. In general, confinement of concrete increased the peak loads required to fail specimens by a factor of 2.5 compared to unconfined specimens.

The authors noted that higher grade concrete exhibited increased bond characteristics. However, higher grade concrete also exhibited reduced strain rate sensitivity. Therefore, the relative increase between the dynamic and static pull-out forces for high grade concrete is less than for low grade concrete. The authors also noted that post-installed reinforced concrete exhibited equal, or better, pull-out resistance than cast-in-place specimens. This result is attributed to the mechanical properties of the particular bonding agent used during construction.

2.4.10 Canadian Standards Association CSA S850 (2012)

As with UFC 03-340-02 document, CSA S850 implicitly suggests that dynamic bond strength be ignored and the static bond strength be used for design and analysis. However, a caveat is provided whereby appropriate values for *DIF* may be used if more accurate information is available.

2.4.11 Toikka (2012), Toikka et al. (2015)

The authors published two pieces of literature detailing an investigation into the effect of high strain rates on the development length of steel reinforcement in reinforced concrete beams. The two publications are Toikka (2012), henceforth referred to as the “thesis”, and Toikka et al. (2015), the “paper”.

Rectangular beams were constructed, each 170 mm wide by 220 mm tall and 2440 mm long. The beams were detailed with one longitudinal reinforcement bar with a bottom cover of approximately 80 mm and side covers of approximately 70 mm. The development length for each specimen, located at either end near the supports (low moment/high shear zone), was the minimum required by CSA A23.3 (Canadian Standards Association, 2004). Longitudinal reinforcement consisted of 15M (f_y =465 MPa), 20M (f_y =437 MPa), and 25M (f_y =449 MPa) bars with development lengths of 423 mm (15M), 523 mm (20M) and 830 mm (25M). The static strength of concrete was 37.0 MPa. The beams were simply supported and subjected to four-point bending for both static and dynamic testing. Dynamic loads were generated using a shock tube and load transferring device. The bonded region was confined by 6.3 mm diameter non-deformed steel wire stirrups at 100 mm. Strain gauges were installed along the developed length to measure the distribution of reinforcement strains. A 25 mm vinyl tube was used as a bond breaker, sheathed around the longitudinal reinforcement. A schematic of the specimens is illustrated in Figure 2.12.

The authors noted that the development length of reinforcement for dynamic tests was always less than or equal to the development length required for static tests for a given level of reinforcement strain. This observation was based on strain profiles constructed from strain readings taken in the developed region. Reinforcement slip at the unloaded ends of the developed bars was not observed, and beams exhibited a concrete crushing flexural failure, rather than a bond failure. The authors conducted an analysis of the distribution of strain in the bonded region to establish *DIF*'s applied to average bond strength. In the thesis, it was reported that values of bond *DIF* were proportional to bond strength, with a *DIF* applied to bond of 1.13 for 15M bars, 1.71 for 20M bars, and 1.97 for 25M bars. However, significantly different values were presented in the paper. Based on the same experimental data, a *DIF* of 1.11 for 15M bars, 2.24 for 20M bars and 3.98 MPa for 25M bars was reported. No explanation was provided as to why the results for the same data were different. These values, particularly for 20M and 25M bars, are considerably larger than what is commonly reported in the literature.

With an intent to cite and build upon the results of Toikka (2012) and Toikka et al. (2015), a thorough reanalysis of the raw experimental data and the underlying assumptions was conducted as part of the present study. In doing so, a serious issue was identified which call into question the results.

In both the thesis and the paper, values of *DIF* were obtained based on an unweighted mean of local bond strengths calculated at four stations along the development length. However, the local bond data was not equally spaced since one of the stations had a length a fraction of that of the other three stations. Coincidently, the greatest values of local bond were obtained for the station with the narrowest width. Therefore, the use of an unweighted mean artificially inflates the reinforcement

bond DIF. It would have been more appropriate to use a weighted arithmetic mean to compute average bond strength. If a weighted arithmetic mean is used, much more reasonable values of bond strength are obtained, yielding bond strength DIF's of 1.06 for 15M bars, 1.08 for 20M bars, and 1.06 for 25M bars.

The main conclusion highlighted in both the paper and the thesis was that the development length requirements for concrete beams designed to resist static loading according to CSA A23.3 (Canadian Standards Association, 2004) were sufficient for the design of beams to resist high strain rate loading. While the body of evidence available in the literature seems to uphold this observation, the analysis of the experimental data presented in Toikka (2012) and Toikka et al. (2015) is flawed and cannot be relied upon to substantiate that claim.

2.4.12 Yao, Wu and Huang (2013)

The authors conducted pull-out tests using a SHPB to investigate the dynamic bond-slip relationship between reinforcing steel and concrete. Deformed reinforcement with 12 mm diameter was studied. Development lengths of 110 mm and 220 mm were considered. The cylindrical specimens had a diameter of 200 mm and length equal to the developed length of reinforcement. The static strength of concrete was 48.9 MPa while the static yield strength of reinforcement was not specified. Impact velocities between 9 m/s and 29 m/s were generated by the SHPB. No information was reported on the strain rate obtained during testing.

The peak bond strength and the shape of the bond-slip curve were both affected by high strain rate loading. The dynamic bond strength was always greater than the static bond strength, with a $DIF \approx 3.5$ reported for bond strength of tests with 110 mm embedment. No comparison of dynamic and static bond conditions for specimens with embedment of 220 mm was presented since no companion static test was performed. Yao, Wu and Huang also reported that the bond stress-slip relationship of deformed reinforcement exhibits increased stiffness under rapid loading. Furthermore, the slip at peak stress (s_1) was reported to decrease as loading rate increased for specimens with long embedment, while an increase in s_1 was noted as loading rate increased for specimens with short embedment.

2.4.13 Michal et al. (2015)

This conference paper describes the introductory part of an ongoing research project to characterize the bond behaviour of reinforced concrete. A brief literature review wass presented in which the authors concluded that comparing results from various literature sources was challenged by the lack of consistent test methods and boundary conditions. The authors conducted preliminary experimental investigations using a SHPB to subject cylindrical rebar push-in and pull-out specimens to dynamic loads. The diameter of the test specimens was 100 mm with 20 mm diameter

deformed reinforcement. Two embedment lengths of 100 mm and 200 mm were studied. No experimental results are provided, although a sample bond-slip curve, shown in Figure 2.13, was presented. The approximate range of strain rates was not presented. Although the work contains no results, the authors do state that their investigations show that bond strength is rate-dependent. Future work, described in the conference paper, will include the development of a new dynamic bond testing apparatus, similar in concept to a SHPB, that can accommodate both cylindrical pull-out and RILEM beam test specimens.

2.5 Protective Design Requirements

From a Canadian perspective, the two most commonly referenced protective design documents are the Canadian Standard Association's CAN/CSA S850 "Design and Assessment of Buildings Subjected to Blast Loads" and the Department of Defense's UFC 03-340-02 "Structures to Resist the Effects of Accidental Explosions". To offset the lack of data and certainty on dynamic bond characteristics, these documents impose stringent detailing requirements on anchorage and development of reinforcement. The following list is a compilation of requirements and recommendations present in CAN/CSA S850 and UFC 03-340-02:

- Structural members containing spliced reinforcement cannot be relied upon to develop tension membrane action;
- Splices should be located in regions of relatively low stress, away from critical sections and plastic hinge regions;
- The potential for load reversal should be accounted for in the design of lap splices;
- It is implied that any potential for high strain rate bond strength enhancement, caused by improvements to concrete strength or other means, be ignored;
- The construction of splices must meet or exceed "Class A" (development length provided at least $\geq 1.0 l_d$) of CAN/CSA A23.3;
- Splices in beams must be enclosed by hoops with max. spacing of $d/4$ or 100 mm;
- Splices in columns must be enclosed by special transverse reinforcement. Depending on the geometric configuration of the column, this may consist of single or overlapping spirals, circular hoops or rectilinear hoops with or without seismic cross-ties;
- The max. spacing of special transverse reinforcement in columns should not exceed:
    - One-quarter of the minimum cross-sectional dimension;
    - Six times the diameter of the smallest longitudinal bar;
    - $s_x = 100 + \left(\frac{350 - h_x}{3}\right) \leq 150\ mm$ where $h_x \leq 350\ mm$;
- Not more than 50% of the bars at a cross-section may be spliced at a given location;
- All lap splices separated along the axis of an element by at least two the lap length.

2.6 Research Needs

The literature review summarized in the preceding sections clearly indicates a lack of sufficient experimental data on the bond characteristics between reinforcing steel and concrete at high strain rates. As demonstrated by previous researchers, bond experiences some level of strain rate enhancement. However, many of the tests reported in the literature were performed on small scale specimens subjected to unrealistic internal stress states. A lack of consistent testing methodology, specimen construction and boundary conditions limits the applicability of the literature data to engineering practice.

Given the limitations in the current body of knowledge, it is unclear how high strain rates affect the bond properties of full-scale structural members. Furthermore, it is not clear how dynamic bond properties are influenced by the factors which are known to affect static bond (*e.g.* cover, bar diameter, presence of transverse reinforcement, concrete properties).

Part of the difficulty with performing dynamic testing on large-scale specimens is the prohibitive cost and restrictive security concerns associated with live explosive testing. Lack of facilities suitable for performing simulated dynamic testing of specimens having an appropriate scale further compounds the problem.

Current design provisions for development and splice length at high strain rates compensate for a lack of experimental data by increasing detailing requirements to reduce the likelihood of bond failure (Department of Defence, 2008). While existing protective design requirements for development and anchorage of reinforcement are conservative, they are largely empirical in nature and few experimental tests – let alone actual explosions impacting protective structures – are available to validate this approach. In addition, there are no known expressions or analytical tools for assessing whether bonded lengths are sufficient or deficient when subjected to blast loading.

The knowledge gap indicated above demonstrates the urgent need for research focusing on the effect of high strain rates on development and splice lengths of reinforcement.

2.7 Objectives

The overall aim of this study is to establish the effects of high strain rates on bond between reinforcing steel and the surrounding concrete in reinforced concrete structural members. The focus of the study is restricted to flexural members, where the reinforcing bar and surrounding concrete are in tension, with reinforcement bearing surfaces acting in compression.

The objectives include generation of experimental data on the effect of high strain rates on bond characteristics, evaluation of the experimental and analytical results to characterize high strain rate

bond, and development of descriptive expression(s) and analytical modelling techniques to properly predict the observed phenomenon.

2.8 Scope

The scope includes a combined experimental and analytical research methodology consisting of the following tasks:

- Compilation of the existing literature on the effect of high strain rates on reinforced concrete bond to gain an overall understanding of the factors affecting the rate-sensitivity of bond.
- Design, construction, instrumentation and testing of beam-end test specimens with different reinforcement embedment lengths under static and dynamic loads, following the requirements of ASTM A944 (2010) to establish the basic characteristics of reinforcement bond in concrete under high strain rates.
- Evaluation of test data and the assessment of reinforcement bond stresses in the beam-end tests conducted under task 2, as well as the determination of a *DIF* to be applied to bond under high strain rates.
- Design, construction, instrumentation and testing of large-scale beams under static and dynamic loads to establish reinforcement bond, and development and splice length requirements under high strain rates. The tests will focus on beams with lap splices designed and proportioned according to CSA A23.3 (Canadian Standards Association, 2004) with and without transverse reinforcement.

  The outcomes of this task will be judged based on the ability to generate static and dynamic experimental data – primarily, average bond strength at failure – considering a variety of relevant physical parameters affecting bond, including: (i) cover; (ii) bonded length; (iii) concrete strength; (iv) bar diameter, and; (v) the presence of transverse reinforcement.
- Evaluation of test data obtained from the beam tests conducted under task 4 for assessment of high strain rates on reinforcement bond, and development and splice lengths.
- Development of design expressions for reinforcement bond under high strain rates, *DIFs* as well as reinforcement development and splice lengths that can be codified for use in structural design based on the tests conducted under tasks 3, and 4, and using any relevant data from the literature identified under task 1.
- Generating resistance curves incorporating bond-slip phenomenon modified to incorporate the *DIFs* generated under task 6. Comparing the aforementioned resistance functions against experimental data, collected in task 4, to validate the applicability of the analysis methodology, while assessing its accuracy.
- Presentation of results and design recommendations.

2.9 Organization of Thesis

This dissertation is primarily written in an article based format. The structure and organizations of the thesis is as follows:

- The **Introduction** (Chapter 1) presents a brief overview of the topic of reinforced concrete bond at high strain rates, and provides the reader with the context of the thesis.
- The **State of the Art** (Chapter 2) provides an exploratory discussion on reinforced concrete bond, summarizes a literature survey of high strain rate bond tests, and identifies the scope and major objectives of the research project. Task 1 is addressed in this chapter.
- **Chapter 3** presents the methodology, results, and discussion of the high strain rate beam-end bond tests, addressing tasks 2 and 3.
- **Chapter 4** presents the results of tasks 4 and 5, consisting of dynamic experimental testing and assessment of large-scale reinforced concrete beams with tension lap splices subjected to high strain rate loads.
- **Chapter 5** presents a database of relevant high strain rate bond tests collected under task 1, 2, and 4. The database is used to develop simple empirical expressions suitable for predicting the bond strength of reinforced concrete flexural members subjected to high strain rates. Chapter 5 also includes a series of recommendations for the proportioning of development and splice length for use in protective design.
- **Chapter 6**, addressing task 7, investigates the low and high strain rate load-deformation response of the beam tests. The empirical expressions developed under task 6 are applied to existing bond stress-slip models to present an analytical approach to predict the load-deformation response of the beams incorporating strain rate sensitivity. The analytically-derived resistance functions are then compared against experimental data, collected in task 4, to validate the applicability and accuracy of the analysis methodology.
- The **Conclusions** (Chapter 7) summarize the findings detailed in the previous chapters. This section provides closure to the thesis and is not intended for publication.
- The **Future Work** (Chapter 8) makes recommendations for future research. This chapter is not intended for publication.
- **Appendix A** lists the experimental results for the beam-end tests collected under task 2.
- **Appendix B** lists the experimental results for the lap splice beam tests under task 4.
- **Appendix C** provides the derivation of an equation relating the dynamic support reactions to the internal resistance of a beam subjected to high stain rate loading.

Table 2.1: List of common reinforced concrete bond terminology (ACI, 2003)

Phrase	**Meaning**
Bond force	Force that tends to move a reinforcing bar parallel to its length with respect to the surrounding concrete
Bond strength	The maximum bond force that may be sustained by a bar
Development strength Splice strength	Bond strength of bars that are not spliced Bond strength of bars that are spliced
Developed length Development length	Bonded length of a bar that is not spliced with another bar
Spliced length Splice length	Bonded length of bars that are lap-spliced

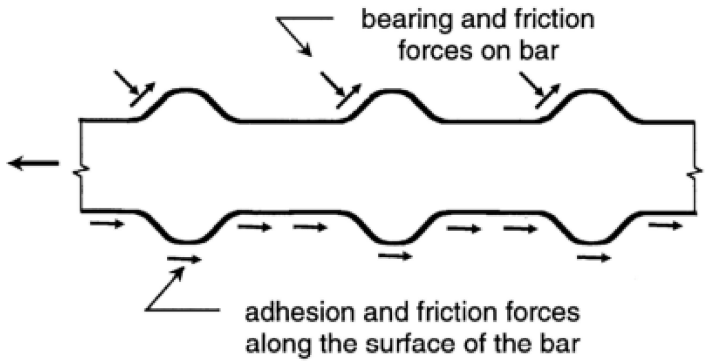

Figure 2.1: Bond force transfer mechanisms (ACI, 2003).

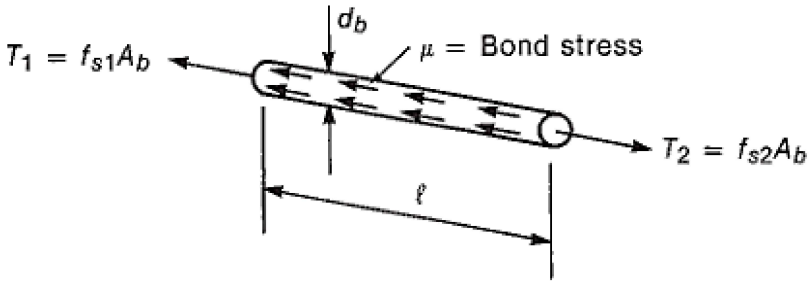

Figure 2.2: Free-body diagram of a bonded bar subjected a change in stress. (Wight and MacGregor, 2009)

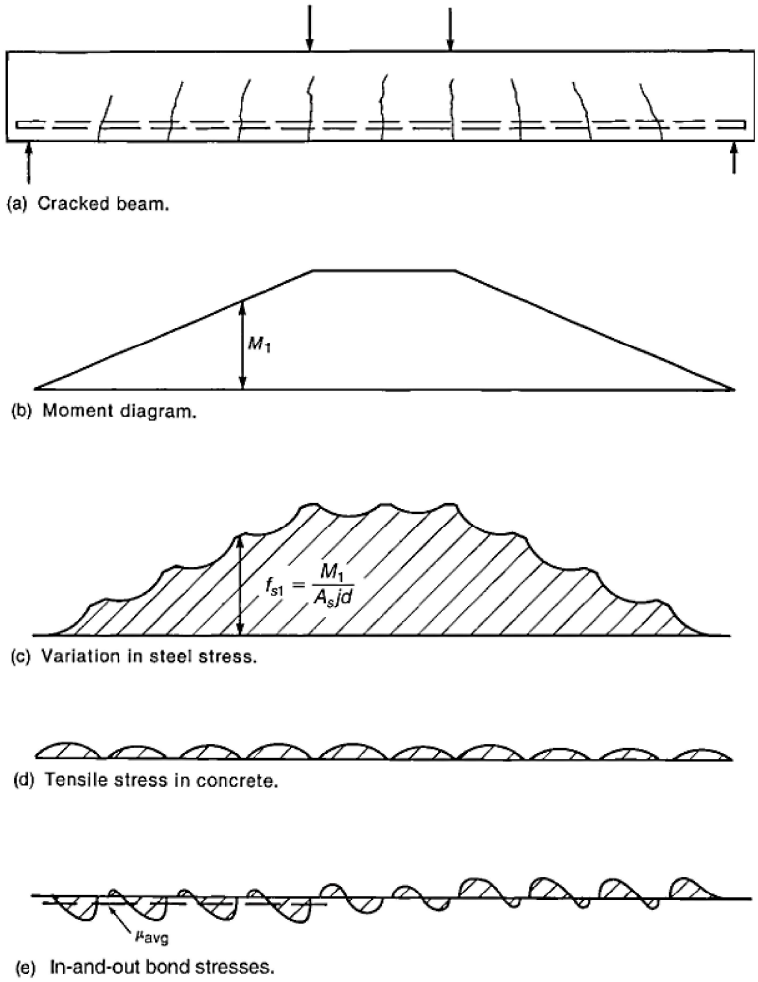

Figure 2.3: Variation in stress in a reinforced concrete beam: (a) reinforced concrete beam; (b) moment diagram; (c) tensile steel stress; (c) variation in tensile stress in reinforcement, and; (d) distribution of bond stress along the reinforcement (Wight and MacGregor, 2009).

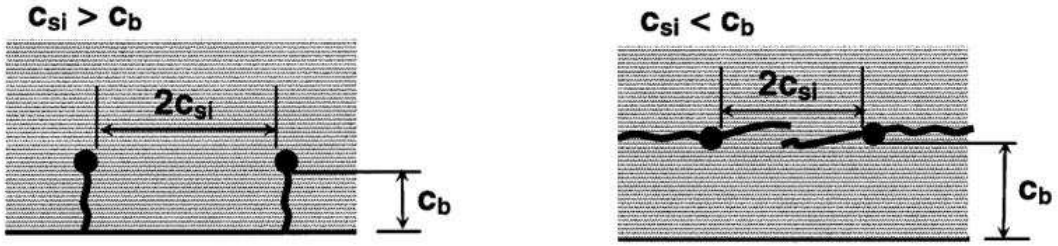

(a) Face splitting
$c_{si} > c_b$

(b) Side splitting
$c_{si} < c_b$

Figure 2.4: Typical bond splitting cracks (ACI, 2003).

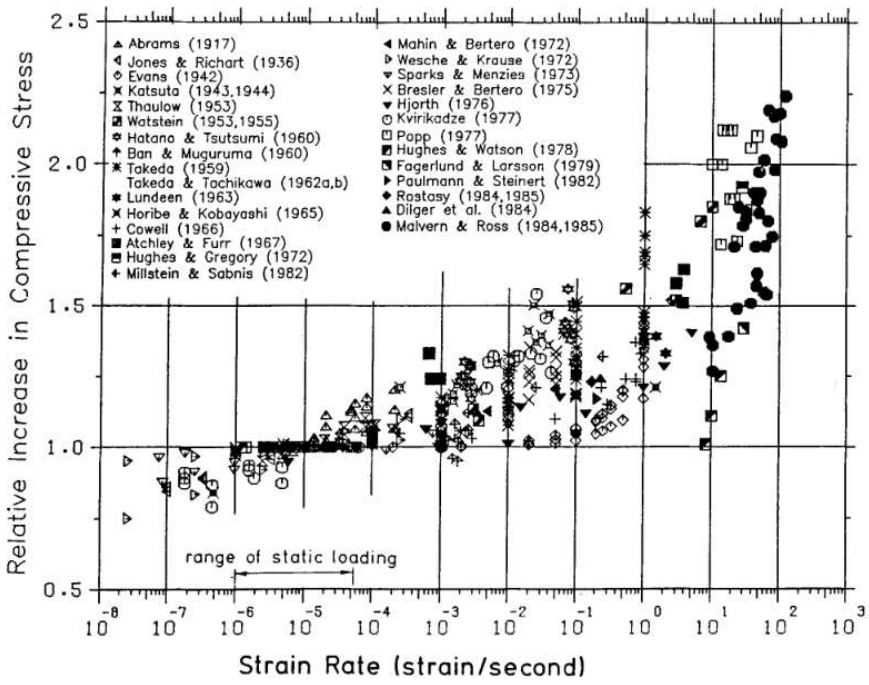

(a)

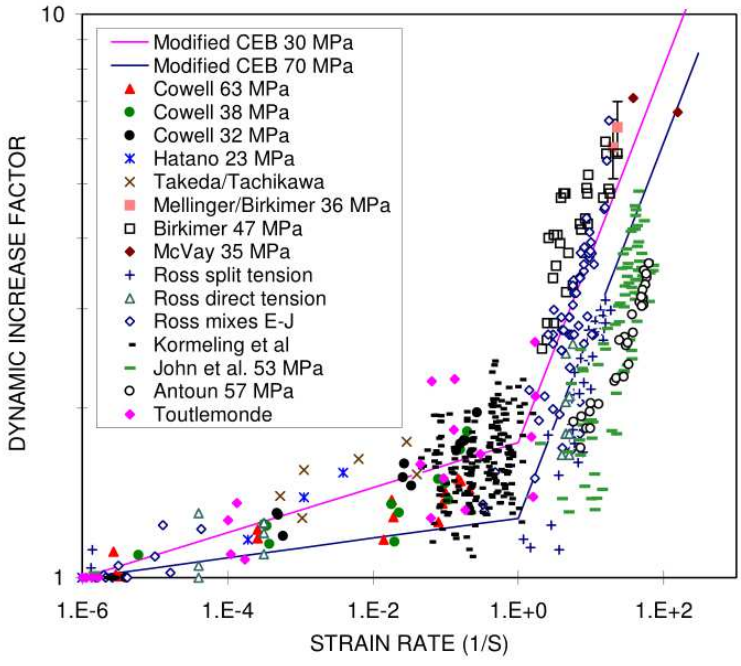

(b)

Figure 2.5: Influence of high strain rates on concrete properties: (a) compressive strength (Biscoff and Perry, 1991), and; (b) tensile strength of concrete (Malvar and Crawford, 1998b).

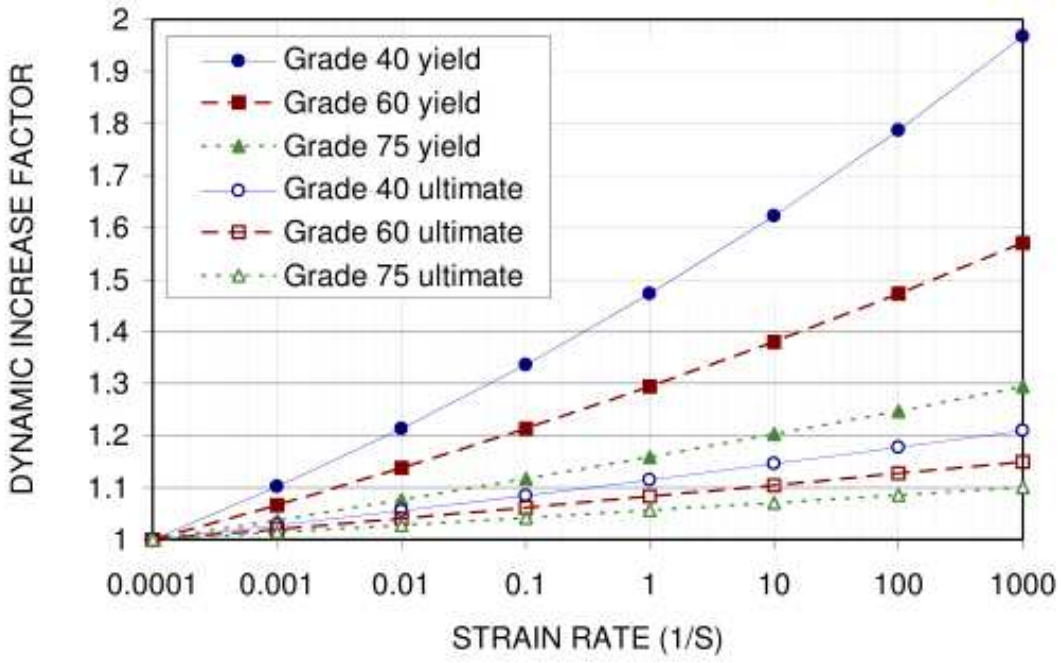

Figure 2.6: Influence of high strain rates on the yield and ultimate strengths of various steels (Malvar, 1998a).

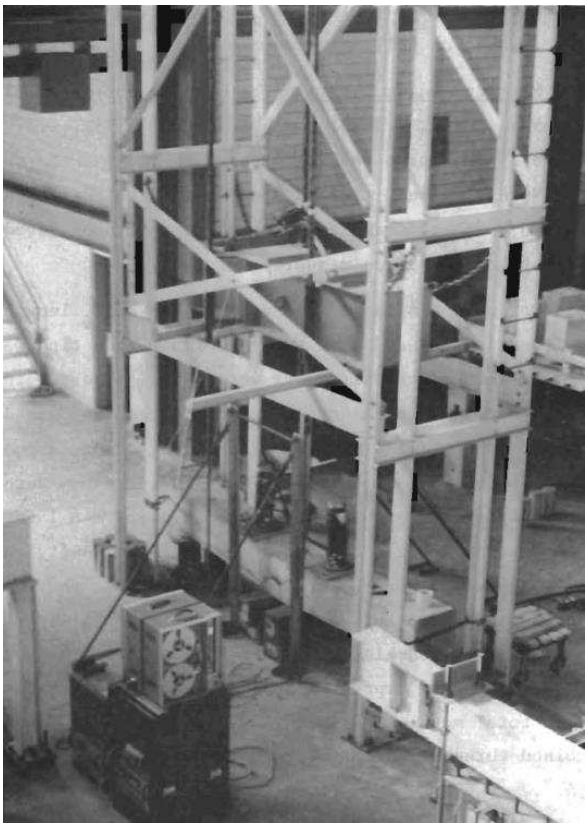

Figure 2.7: Drop weight impactor used by Rezansoff et al. (1975).

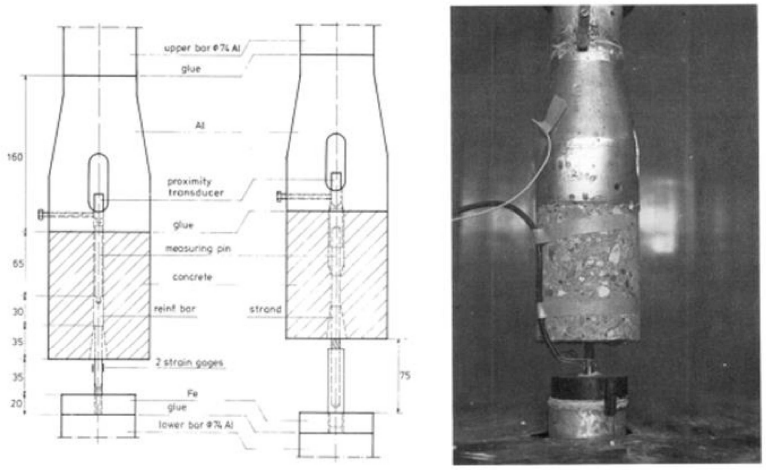

Figure 2.8: Pull-out specimen studied by Vos and Reinhardt (1982).

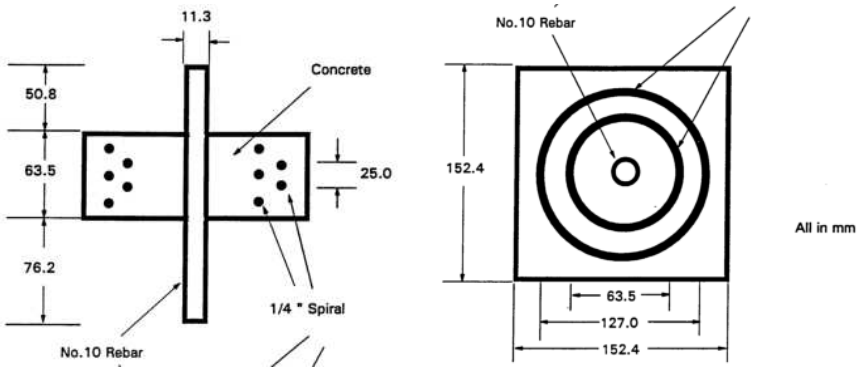

Figure 2.9: Push-in/pull-out specimen used by Yan (1992).

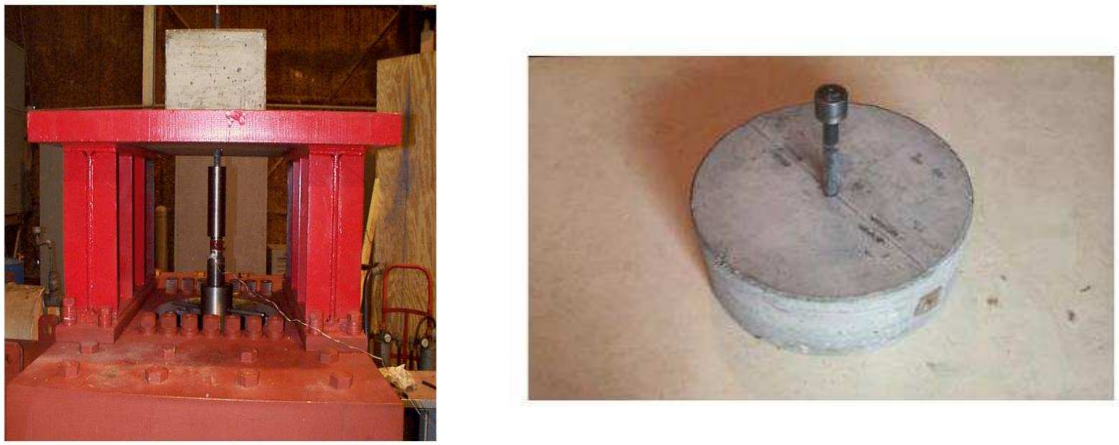

(a) Hydraulic testing apparatus (b) Typical cylindrical specimen

Figure 2.10: Test apparatus and typical pull-out specimens used by Weathersby (2003).

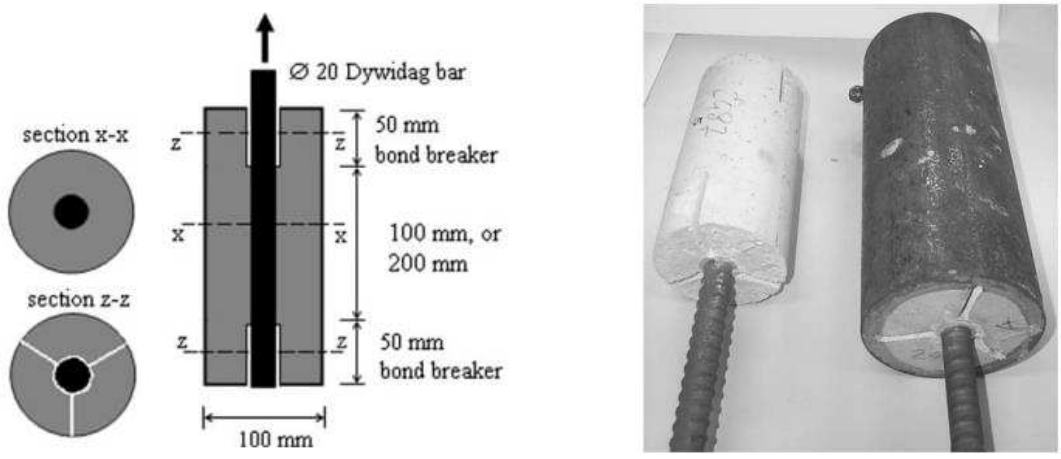

(a) Geometry and dimensions of specimens (b) Unconfined (left) and confined specimens (right)

Figure 2.11: Typical pull-out specimens studied by Solomos and Berra (2010).

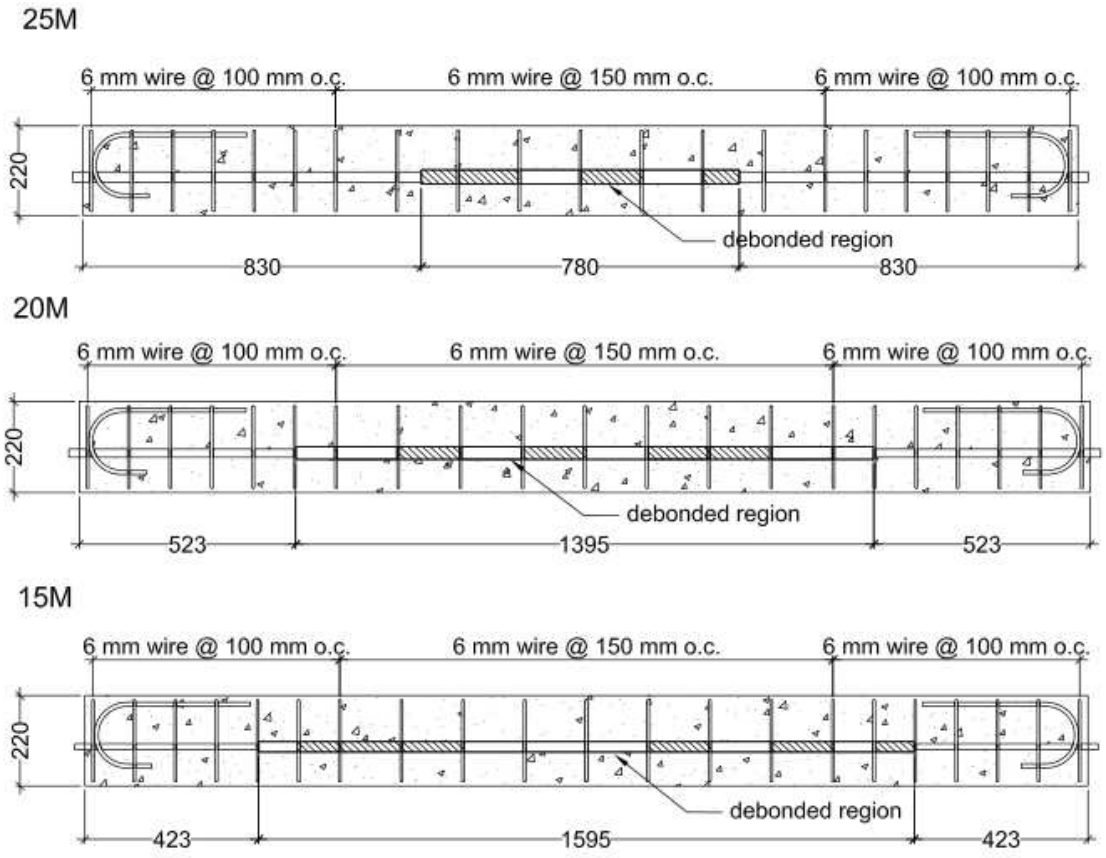

Figure 2.12: Beam specimens tested by Toikka (2012) and Toikka et al. (2015) (adaopted from Toikka et al. , 2015).

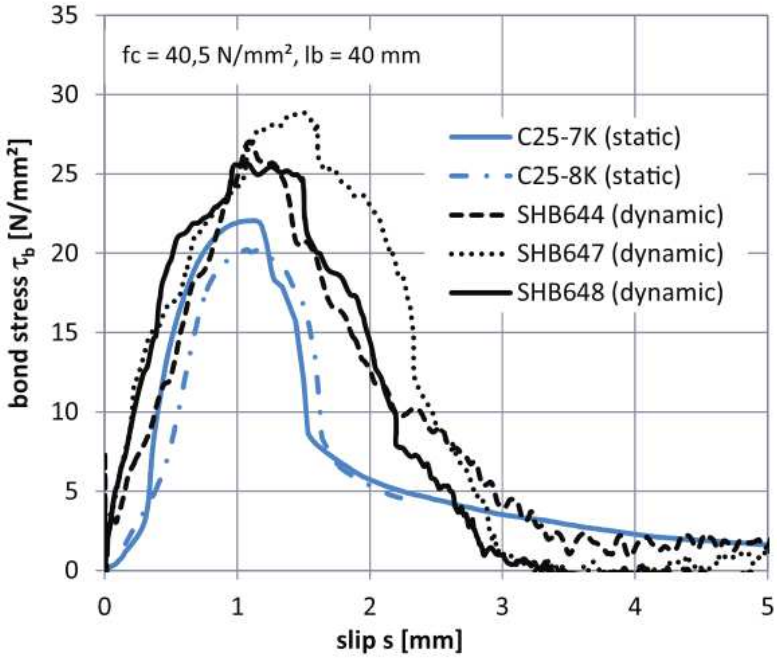

Figure 2.13: Sample bond-slip data presented by Michal et al. (2015).

Part II

Experimental & Analytical Studies

Chapter 3

High Strain Rate Response of Reinforced Concrete Beam-ends

Abstract The suitability of using flexural beam-end tests to characterise the effect of high strain rates on reinforced concrete bond has been investigated. A total of 14 flexural beam-end bond specimens, constructed with 20M deformed reinforcement embedded in 50 MPa concrete, was tested. Beam-ends were subjected to a range of low and high strain rates of approximately 5.0×10^{-6} s^{-1} and 1.2 s^{-1}. Two lengths of bonded reinforcement were considered, with a short embedment of 200 mm and long embedment of 400 mm. The bond stress-slip response of the specimens was constructed using elastic strain measurements obtained from the bonded region. High strain rates were found to significantly enhance the bond strength of the beam-ends, whereas they did not significantly influence the general shape of the bond stress-slip curves. Bond strength obtained under rapid loading conditions exhibited approximately the same strain rate sensitivity as has been observed by others in the literature for similar high strain rate tests. Flexural beam-end tests were found to be well suited for high strain rate testing, and are recommended for future studies provided a safe and convenient dynamic loading fixture can be employed.

Keywords Bond strength; bond stress-slip; high strain rates; reinforced concrete; blast;

3.1 Introduction

Reinforced concrete members are designed on the basis of composite action between compressive stresses resisted by concrete, and tensile and compressive stresses resisted by reinforcing steel. Bond, primarily caused by mechanical bearing of deformations (lugs) on the surface of the reinforcement against the surrounding substrate and influenced by surface fiction and chemical adhesion, is responsible for this phenomenon. The resistance of the substrate to bond failure is typically governed by concrete strength, cover depth, reinforcement type and distribution, as well as presence of transverse reinforcement. Extensive research under static conditions has led to the development of design equations (*e.g.* CSA, 2014) and predictive expressions (*e.g.* ACI, 2003) which accurately describe the bond characteristics within development lengths and spliced regions under slowly applied gravity and lateral load conditions.

The effect of blast and impact on constitutive material behaviour, structural response, and dynamic analysis is currently of great interest to the civil engineering community. Despite this enthusiasm, an almost virgin field of study exists in characterising high strain rate reinforced concrete bond behaviour. A survey of the limited number of studies in the literature devoted to this topic in the literature has identified several common findings. For example, most studies reported that bond strength exhibits strain rate sensitivity, with greater values of bond obtained at increasing loading rates (Shah and Hansen, 1963; Vos and Reinhardt, 1982; Weathersby, 2003). Inferior quality concrete experiences greater relative increases in dynamic bond than for superior quality concretes (Shah and Hansen, 1963; Solomos and Berra, 2010). Confinement can significantly increase dynamic pullout resistance (Weathersby, 2003) and also improve the toughness and durability of tension lap splices in beam tests (Rezansoff et al., 1975). Finally, the bond stress-slip relationship of deformed reinforcement is reported to exhibit increased stiffness under rapid loading (Yao, Wu, and Huang, 2013).

Reconciling the quantitative results of these studies is complicated by the lack of uniformity in experimental methodologies. Pull-out tests, which place concrete surrounding a developed bar in compression, are most commonly reported (Shah and Hansen, 1963; Vos and Reinhardt, 1982; Yan, 1992; Weathersby, 2003; Solomos and Berra, 2010; Yao, Wu, and Huang, 2013). Although this type of test is relatively simple to perform, it does not accurately simulate the internal stress state found in real structures (ACI, 2003). Less common are flexural beam tests, in which the bar and surrounding concrete are in tension with reinforcement bearing surfaces acting in compression (Rezansoff et al., 1975; Toikka, 2012). Although flexural bond tests are preferred, a lack of research facilities capable of performing large-scale dynamic flexural tests limits their wide scale adoption. As a result, the depth and breadth of existing studies is insufficient to serve as a basis for the development of dynamic

increase factors ($DIFs$) applied to reinforced concrete bond suitable for design and analysis of protective structures.

The aim of this chapter is to present the results of experimental research investigating the suitability of flexural beam-end tests to characterise reinforcement bond in concrete under high strain rates. The beam-ends, consisting of a deformed bar embedded in an unconfined concrete block, were subjected to static and high strain rate excitations. The boundary conditions applied to the block generated a flexural internal stress state. The effect of loading rate on bond strength is presented, and the strain rate sensitivity of the bond stress-slip relationship is evaluated. The implications of the study, as well as recommendations for future tests, are also discussed.

3.2 Beam-end Tests

Flexural beam-end tests provide a standard experimental method for comparing the static bond strength of steel reinforcement embedded in concrete (ASTM A944, 2010). This type of bond test was selected due to its simplicity of construction and ease of testing, as well as for generating an internal stress state similar to that observed in full scale flexural members (ACI, 2003). The objectives of the beam-end bond tests were to:

1. Investigate the effect of high strain rates on reinforced concrete bond strength;
2. Evaluate the rate-sensitivity of bond stress-slip response of deformed reinforcement;
3. Determine the effect of embedment length on dynamic bond properties; and,
4. Assess the suitability of beam-end bond tests for future dynamic bond characterisation studies.

Fourteen reinforced concrete flexural beam-end specimens were constructed. Each sample was bottom cast with 20M steel reinforcement embedded in 50 MPa concrete. A standard naming convention was adopted for each beam, beginning with the prefix "BE" followed by a number. Strain rate and bonded length varied during the study, while all other parameters were held constant. Strain rate was defined by taking the ratio of a given strain value by the time after the start of loading required to achieve said strain. The development length required to yield the reinforcement under static conditions, 430 mm, served as the basis for specimen design (Canadian Standards Association, 2004). Half of the specimens (referred to as BE1 through BE7) were constructed with a bonded length, l_b, equal to approximately 50% of the design development length (200 mm), with the remainder having l_b equal to approximately the design value of 400 mm (BE8 through BE14). Clear cover between the reinforcement and the bottom face, c_b, was 38 mm. The experiment followed the requirements of ASTM A944 (2010) as closely as possible.

Construction and reinforcement details of the beam-ends are illustrated in Figure 3.1. All specimens were 600 mm long and 225 mm wide, with depth proportioned according to bonded

length; specimens with $l_b = 200$ mm were 400 mm deep, while specimens with $l_b = 400$ mm were 600 mm deep. A 50 mm bond breaker on the loaded end of the test bars was used to prevent the formation of a pull-out cone. Lengths of PVC tubing were inserted over the unbonded portions of reinforcement and sealed with plugs to serve as bond breakers.

Additional detailing was provided to eliminate undesirable flexure or shear failure without affecting bond characteristics of the test bar. Two 15M bars, located at the same depth as the 20M test bar, were provided as secondary reinforcement. Shear reinforcement consisted of four 10M closed stirrups placed on either side of the primary reinforcement, parallel to the side faces, rather than being oriented in the cross-sectional plane. The shear reinforcement was situated above the plane of the primary reinforcement. A typical beam-end with reinforcement installed prior to casting is shown in Figure 3.2 (a).

The nominal area (A_b) of the 20M reinforcements was 300 mm^2 with a diameter (d_b) of 19.5 mm. The static stress-strain properties of the reinforcement, illustrated in Figure 3.3, were determined based on an average of 4 standard coupon tests. The static yield strength, f_y, was 486 MPa and the ultimate strength, f_u, was 683 MPa. All beam-ends were cast from the same batch of ready mix concrete with a specified 28-day strength of 35 MPa, with a maximum coarse aggregate size of 20 mm and a slump of 150 mm. The peak cylinder compressive strength of concrete, f_c', at the time of testing was 50 MPa based on an average of 8 standard 100 mm × 200 mm cylinder tests.

The 20M bars were instrumented with strain gauges to measure the formation and propagation of steel stresses due to bond. Tokyo Sokki Kenkyujo Co., Ltd. FLA-6-350-11 350Ω electrical resistance strain gauges, each 3.0 mm wide by 6.5 mm long, were placed in a 6.4 mm wide by 3 mm deep slot that was milled into the test bar. The cross-section of a typical test bar after milling is illustrated in Figure 3.2 (b). The slot extended over the entire bonded length and was milled along a rib so as not to interfere with the load bearing lugs. Strain gauges were placed inside the reinforcement to mitigate local disruptions in bond that occur when strain gauges are installed on the exterior surface (Beconcini et al., 2008). The net cross-sectional area was reduced to 272 mm^2 due to milling. Beam-ends with $l_b = 200$ mm contained 7 gauges, with the first placed 10 mm from the loaded end of the test bar with subsequent gauges spaced at 30 mm. Beam-ends with $l_b = 400$ mm contained 9 gauges, with spacing of 47.5 mm beginning 10 mm from the loaded end. Positioning and nomenclature for the strain gauges is illustrated in Figure 3.4. A layer of electrical tape was used to insulate the gauges and act as a bond break. The entire slot was filled flush to the exterior surface with a protective layer of epoxy, as illustrated in Figure 3.2 (c). The bar was oriented such that the slot and strain gauges were on the plane of the neutral axis.

3.2.1 Low Strain Rate Test Fixture

A photograph of the static test fixture is illustrated in Figure 3.5 (a). Linear variable displacement transducers (LVDTs) were used to measure the slippage of the free-end of the test bars. Load was applied using a general purpose through-hole hydraulic jack, and was measured using a strain gauge load cell. A mechanical shear bolt rebar coupler was used to fix the jack and load cell against the reaction frame.

3.2.2 High Strain Rate Test Fixture

The University of Ottawa shock tube was designed to subject large-scale planar structural components to uniformly distributed shock pressures (Lloyd et al., 2011). A dynamic point loader (DPL) was constructed to extend the capabilities of the shock tube to include dynamic beam-end tests. A photograph of the DPL is illustrated in Figure 3.5 (b). Figure 3.6 shows an idealized schematic of the test fixture. One end of a rigid steel beam was loaded by shock wave pressures generated by the shock tube. The other end of the steel beam was fixed to the beam-end test bar. A force-couple between the test bar and shock wave pressure generated a dynamic force in the reinforcement suitable for high strain rate point load testing.

The DPL was located in the Blast Research Laboratory of the University of Ottawa, which is situated immediately below the Structures Laboratory with a strong floor (callout 1 in Figure 3.6). The DPL was supported by a reaction frame (callout 2) suspended from the underside of the 914 mm thick strong floor using post-tensioned DYWIDAG bars (callout 3). Beam-end specimens (callout 4) were tested in a bar down configuration and positioned such that the edge of the strong floor provided restraint against the horizontal reaction (callout 5). Restraint against vertical reactions (callout 5) was provided by the reaction frame. The vertically oriented load beam (callout 6) consisted of a 1400 mm long W310×52 steel section. The top end of the beam had a ball and socket connection through which the test bar was attached using a shear-off type mechanical rebar coupler (callout 7). The load beam was connected to the reaction frame by a 75 mm diameter circular steel pivot located 250 mm below the test bar (callout 8). An 812 mm square pressure collector panel (callout 9), centred 1000 mm below the pivot, was fixed to the beam. Shock wave pressures, generated in the 1830 mm long, 600 mm diameter circular shock tube driver section (callout 10), were applied to the load beam at the pressure collector panel. These pressures formed a force-couple with the test bar about the shear pin. Due to the small horizontal displacement required to generate bond failure, rotation of the load beam was negligible up to the point of bond failure. The system was capable of generating an effectively horizontal point load with peak force greater than 200 kN and rise time of 15 milliseconds.

LVDTs were used to measure slippage at the free end of the test bar. Numerical integration of the strain profile within the bonded region was used to calculate slip at the loaded end of the test bar. Shock wave pressures in the driven section were measured using a piezoelectric pressure sensor. A high-speed camera directed at the underside of the test specimens recorded the response of the beam-ends to dynamic load at 1000 frames per second. Experimental data was collected using a data acquisition system recording at 100 kilo-samples per second. The connection point between the test bar and the rigid load beam could not accommodate a load cell for direct measurement of applied load. Dynamic loads were therefore computed based on strain measurements in the bonded region.

3.3 Test Procedure

Beam-ends subjected to static tests were loaded to failure with loading rate of 30 kN/min to satisfy the ASTM A944 (2010) requirement that failure not occur within 180 seconds of load being applied. A hydraulic hand pump was used, with loading rate controlled manually using a real-time data acquisition feed from the load cell.

Beam-ends subjected to high strain rate loading were typically subjected to 2 shock wave tests. The pressure time-histories applied to the load beam had an approximately rectangular profile. A ping test, with an applied pressure of 80 kPa and impulse of 900 kPa-ms, was first performed to verify that the instrumentation and specimen were properly configured. Ping tests generated elastic stresses in the 20M reinforcement in the range of 150 MPa. The second, destructive test was selected to just achieve bond failure. The applied pressure and impulse for l_b = 200 mm beam-ends were 335 kPa, and 3710 kPa-ms, respectively. For l_b = 400 mm beam-ends, the destructive test typically consisted of a shock wave with applied pressure of 390 kPa and impulse of 4450 kPa-ms. Strain gauges were not rebalanced after each subsequent test to account for the effect of repeated loading on bond characteristics.

3.4 Test Results

3.4.1 Failure Mode & Ultimate Bond Strength

Static testing of l_b = 200 mm

Beam-ends BE1, BE2, and BE3, with l_b = 200 mm, were subjected to static testing. As illustrated by the typical crack profile shown in Figure 3.7 (a), these specimens failed by tensile face splitting of the cover concrete with no cover loss. The primary splitting crack on the bottom face ran parallel with the test bar, and intersected perpendicular cracks at the end of the bonded region. Secondary splitting of the specimens was also observed on the front and side faces. Failure occurred at an average static load of 107.9 kN at a time of 250 seconds. This generated an elastic stress in the

reinforcement of 395 MPa, consistent with strain measurements in the bonded region. The ultimate static bond strength at failure for $l_b = 200$ mm was 8.81 MPa at a strain rate of 7.8×10^{-6} s^{-1}.

High strain rate testing of $l_b = 200$ mm

Beam-ends BE4, BE5, BE6, and BE7, with $l_b = 200$ mm, were subjected to high strain rate testing. These specimens failed by tensile face splitting of the concrete, with exactly the same crack pattern as that observed for static tests, and illustrated in Figure 3.7 (a). Crack widths narrower than those of static tests were noted. High speed video footage showed that splitting cracks on the bottom face took approximately 5 ms to completely form, after which bond was lost and the bar experienced significant slippage. On average, loss of bond occurred 24.9 ms after load was first applied to the pressure collector panel.

Analysis of strain data in the bonded region of the four specimens indicated that failure occurred at the onset of dynamic yielding of reinforcement. Using a DIF of 1.20 applied to the static yield strenbgth computed for a strain rate in the range of 0.1 s^{-1} (Malvar and Crawford, 1998a), the stress in reinforcement at bond failure was estimated to be 585 MPa. The corresponding load at failure was approximately 159 kN. The ultimate dynamic bond strength for $l_b = 200$ mm was 13.0 MPa at a strain rate of 0.1 s^{-1}. This yields a DIF applied to ultimate bond strength of 1.47 for specimens with $l_b = 200$ mm embedment that experienced a face splitting failure.

Static testing of $l_b = 400$ mm

Beam-ends BE8 and BE10, with $l_b = 400$ mm failed by a tensile face splitting of the cover concrete when subjected to static loads. Note that specimen BE9 was not tested due to poor concrete consolidation. The splitting failure mode exhibited by BE8 and BE10, illustrated in Figure 3.7 (b), was nominally similar to that of the specimens with shorter bonded lengths. Bond failure occurred 344.6 seconds after load was first applied at an average load of 151.4 kN. Steel response was in the strain hardening range with a stress of 558.6 MPa. The ultimate static bond strength at failure for $l_b = 400$ mm was 6.2 MPa at a strain rate of 4.3×10^{-5} s^{-1}.

High strain rate testing of $l_b = 400$ mm

Beam-end BE14 was the first specimen with $l_b = 400$ mm to undergo high strain rate testing. It was subjected to a test performed at maximum capacity of the shock tube, generating an applied pressure of 425 kPa and an impulse of 4500 kPa-ms. Unlike other beam-ends with $l_b = 200$ mm, BE14 failed due to rupture of reinforcement. The crack pattern of the specimen after testing, illustrated in Figure 3.7 (c), consisted of a narrow crack running parallel to the test bar on the bottom face and another crack spanning the width of the bottom face at the end of the bonded region. The reinforcement, shown in Figure 3.7 (d), ruptured 15 mm into the bonded region at the loaded end of the test bar. Time-to-rupture was 15 ms giving a strain rate of 1.20 s^{-1}. The dynamic rupture stress

was estimated to be 738 MPa using a *DIF* applied to ultimate strength of 1.08 (Malvar and Crawford, 1998a). Analysis of the strain gauge data in the bonded region indicated that the entire bonded length of 400 mm was stressed at the time of rupture. The ultimate dynamic bond strength at failure for l_b = 400 mm was estimated to be 8.2 MPa at a strain rate of 1.20 s^{-1}. This yields a *DIF* applied to ultimate bond strength of 1.33 for specimens with longer embedment.

Concerns were raised regarding the safety of operating the DPL at maximum shock tube capacity. The loaded end of the ruptured test bar was propelled 15 meters across the laboratory and the test fixture experienced severe vibrations after the rupture had occurred. As a result, the remaining beam-ends with l_b = 400 mm, BE11, BE12, and BE13, were subjected to the same pressure-impulse which resulted in debonding failure of the l_b = 200 mm specimens. Although this pressure-impulse combination was not sufficient to generate bond failure in the l_b = 200 mm specimens, the bars were stressed past their dynamic yield point and high strain rate bond characteristics in the elastic range were recorded.

3.4.2 Steel Strain Distribution Curves

Typical steel strain distribution curves for l_b = 200 mm beam-ends subjected to static and high strain rate loads are illustrated in Figure 3.8 (a) and (b), respectively. Similar static and high strain rate distribution curves for l_b = 400 mm specimens are presented in Figure 3.8 (c) and (d), respectively. These figures show the effect of bond on steel response as a function of position along the bonded length. As the effectiveness of the strain gauges was significantly reduced upon yielding of reinforcement, incremental strain profiles were generated for response of steel in the elastic range. The maximum strain considered for development of the strain profiles was 2430 $\mu\varepsilon$ (486 MPa) for static tests, and 2925 $\mu\varepsilon$ (585 MPa) for dynamic tests. The term 'elastic bond' was introduced to describe bond characteristics when steel stress was within the elastic range. Strain values at the loaded end of the bonded region, extrapolated from strain gauge measurements, were used to determine values of load for each strain profile. Strain profiles were constructed in increments of 250 $\mu\varepsilon$ at the loaded end of the test bar, resulting in approximately 10 profiles constructed for each test. The number of profiles shown in Figure 3.8 has been reduced for clarity.

The static strain profiles for beam-ends with l_b = 200 mm, illustrated in Figure 3.8 (a), had an approximately linear distribution until the entire bonded length had been strained, at a load P = 50 kN. Once the entire embedment length had been activated, the shape of the static strain profiles became increasingly convex with large regions of reinforcement undergoing small changes in strain. As bond stress is proportional to changes in steel stress, this indicates a gradual decrease in localized bond near the loaded end of the test bar consistent with yielding of reinforcement. For the case of l_b = 200 mm subjected to dynamic loads, the strain profiles exhibited a linear shape for all levels of applied load up to failure. Comparing static and high strain rate profiles for the same load

increments, the high strain rate profiles had noticeably greater strain gradient than that of static tests. For beam-ends with the relatively short embedment length of 200 mm, the greatest enhancement in bond distribution due to strain rate effects occurred after the full embedment length had been stressed.

The static and high strain rate strain profiles for beam-ends with $l_b = 400$ mm are illustrated in Figure 3.8 (c) and Figure 3.8 (d). The profiles exhibited predominantly linear shape up to yielding of reinforcement. The strain gradient for high strain rate tests was greater than that of the static tests for loads up to the static reinforcement yield strength. Once applied load increased beyond that of static yield, high strain rates significantly improved the distribution of strain along the bonded length. For example, Figure 3.8 (c) shows the partial strain profile constructed for a static load at splitting failure of 151 kN. At this load level, the entire bonded length was stressed and a significant portion of the bar had yielded. At a similar level of load, 159 kN, the high strain rate strain profile shown in Figure 3.8 (d) exhibited markedly improved behaviour, with much shorter length of reinforcement being stressed and the strain profile maintaining an approximately linear shape. Collectively, these results indicate that the distribution of bond stresses along the length of developed reinforcement are sensitive to strain rate enhancement.

3.4.3 Slip Distribution Curves

Local slippage of reinforcement is caused by a strain differential between reinforcement and concrete. Typical loaded-end slip distribution curves for $l_b = 200$ mm beam-ends tested at static and high strain rate tests are presented in Figure 3.9 (a) and (b), respectively. Static and high strain rate slip curves for $l_b = 400$ mm beam-ends are shown in Figure 3.9 (c) and (d), respectively. Slip was computed by numerical integration of the steel strain distribution. The strain in concrete was neglected and slip at the far end of the bar was assumed to be zero. Slip profiles were generated for increments of load within the elastic range of steel response.

The slip distribution curves were parabolic at all rates of strain. However, high strain rates had several beneficial effects on the distribution of slip. Larger slip gradients resulting in steeper parabolic distributions were observed under dynamic loads. Secondly, lower magnitudes of slip were obtained for similar levels of load at high strain rates than for static loads. For the same level of applied load, beam-ends subjected to high strain rates experienced reductions in slip of 10-20% when compared with similar static results. This trend was consistent for beam-ends with both short and long bonded length.

3.4.4 Elastic Bond Stress-Slip Behaviour

The bond stress-slip behaviour of the beam-ends was constructed using incremental values of the average bond stress, u, acting over the surface of the reinforcing bar and corresponding loaded

end slip, s. These incremental quantities were computed using slip profiles generated from the slip distribution curves. Bond stress was computed for each increment according to Eq. (3.1).

$$u = \frac{\varepsilon_s E_s A_b}{\pi d_b l_d} \tag{3.1}$$

where ε_s is the strain at the loaded end of the test bar, E_s is the modulus of elasticity of steel (assumed to be 200 GPa), A_b is the area of the bar, d_b is the bar diameter, and l_d is the developed length. Developed length was taken as the intercept of a linear regression curve fit to the strain data with the horizontal axis. Loaded-end slips were obtained from the slip distribution profiles. Detailed calculations of the loaded-end slips are showed in Appendix A.

A comparison of static and high strain rate bond-slip response for l_b = 200 mm beam-ends is shown in Figure 3.10 (a), while a similar comparison for l_b = 400 mm beam-ends is shown in Figure 3.10 (b). The bond stress-slip data presented in Figure 3.10 was limited to the elastic range of reinforcement response. This figure was aggregated from test data having the same bonded length.

The results show that high strain rate bond stresses were greater than corresponding static values for a given slip interval. Furthermore, the general shape of the bond stress-slip curves was similar for tests performed on beam-ends with the same bonded length. The initial ascending branch of the bond-slip curves for l_b = 200 mm and l_b = 400 mm beam-ends was characterised by a gradual parabolic function. The consistency in the shape of the bond stress-slip curves suggests that the fundamental mechanism of reinforced concrete bond is unaffected by strain rates on the order of 0.1 to 1.0 s^{-1}.

Some scatter is present in the bond stress-slip data shown in Figure 3.10. This scatter was caused by minor variations in developed length calculated from curve fitting the strain profiles obtained during beam-end tests. To overcome the scatter, a two-step analytical bond stress-slip expression (Ciampi et al., 1981; Eligenhausen et al., 1983) was fitted to the data using a least squares regression analysis. This expression was developed for deformed bars embedded in concrete subjected to monotonic and reverse cyclic loads. The initial ascending branch, described by Eq. (3.2), is followed by a plateau of constant bond for increasing values of slip, given in Eq. (3.3). Lack of strain data beyond the elastic range of reinforcement response limited the extent of the regression analysis to these regions.

$$u = u_o \left(\frac{s}{s_1}\right)^{\alpha} \text{ for } s < s_1 \tag{3.2}$$

$$u = u_o \text{ for } s > s_1 \tag{3.3}$$

where u_o is the bond strength corresponding to yield in the reinforcement, s_1 is the slip at which u_o is attained, and the exponent α is a calibration factor. The least squares regression was performed to

determine the values of s_1, u_o, and α which generated the best-fit with experimental data by maximizing the coefficient of determination, R^2.

Regression parameters for static and high strain rate bond tests for $l_b = 200$ mm are presented in Table 3.1 (a). A comparison of experimental bond stress-slip data and best-fit curves for $l_b = 200$ mm is illustrated in Figure 3.10 (a). Based on the regression analysis, the low strain rate elastic bond strength for beam-ends with $l_b = 200$ mm was 9.2 MPa at a slip of 0.27 mm. Under dynamic loading, elastic bond strength was 13.6 MPa at a slip of 0.30 mm for strain rates in the range of 0.1 s^{-1}. A calibration factor $\alpha = 0.65$ was found to best represent the data for $l_b = 200$ mm beam-end tests. The results indicated that values of elastic bond strength were sensitive to rate-enhancement while slip and calibration factor were not. The R^2 value for static and high strain rate curve fits was 0.96 and 0.92, respectively. A DIF applied to elastic bond strength for $l_b = 200$ mm beam-ends tests was 1.48 at strain rates of 0.1 s^{-1}.

Regression parameters for static and high strain rate bond tests for $l_b = 400$ mm are presented in Table 3.1 (b). A comparison of experimental bond stress-slip data and best-fit curves for $l_b = 400$ mm is illustrated in Figure 3.10 (b). The low strain rate elastic bond strength for beam-ends with $l_b = 400$ mm obtained from regression analysis was 8.2 MPa at a slip of 0.25 mm. The dynamic elastic bond strength was 11.9 MPa at a slip of 0.25 mm for strain rates of 0.1 s^{-1}. A calibration factor $\alpha = 0.40$ was found for beam-end tests with longer embedment indicating stiffer response than that of shorter embedment. As was the case for beam-ends with shorter embedment, values of bond strength were sensitive to rate-enhancement, while slip and calibration factor were not. The R^2 value for static and dynamic curve fitting was 0.89 and 0.83, respectively. The DIF applied to elastic bond for beam-ends with $l_b = 400$ mm was 1.45 for strain rates of 0.1 s^{-1}. This was consistent with the DIF for elastic bond of beam-ends with $l_b = 200$ mm embedment.

3.5 Discussion

Regardless of bonded length, beam-ends subjected to strain rates in the range of 0.1 s^{-1} experienced increases in elastic bond equal to approximately 1.45 times their static value. At splitting failure, beam-ends with $l_b = 200$ mm experienced increases in ultimate bond of 1.47 at strain rates in the range of 0.1 s^{-1}. Beam-ends with $l_b = 400$ mm, which experienced splitting failures at low strain rates and reinforcement rupture at high strain rates, were found to have increases in ultimate bond of 1.33 at strain rates in the range of 1.2 s^{-1}. The primary difference in ultimate bond DIFs between $l_b = 200$ mm and $l_b = 400$ mm beam-ends is thought to be related to the failure mode. For the case of beam-ends with shorter embedment, the ultimate capacity of the anchorage was attained as the member experienced a splitting failure. However, the same cannot be said for beam-ends with longer embedment as they experienced reinforcement rupture when subjected to high strain rates. This meant that dynamic bond strength was limited by the dynamic rupture strength of the

reinforcement. Future studies could utilize high strength reinforcement to ensure ultimate bond conditions are attained for all embedment/splice lengths by favoring bond failures, rather than reinforcement rupture.

In general, the *DIF*s obtained during this study compare reasonably well with the literature. For example, the values compare favorably with the results of Rezansoff et al. (1975) whose data indicated that bond strength of unconfined tension lap splices increased by a factor of 1.33 at strain rates of 0.3 s^{-1}. The beam-end results also fall within the range of increases reported in the literature for dynamic pullout tests. Hjorth, as cited by Vos and Reinhardt (1982), found that static bond strength increased by a factor of 1.30 at strain rates of approximately 0.1 s^{-1}. Vos and Reinhardt (1982) reported an increase in bond strength at failure of 1.44 for strain rates of 5.4 s^{-1}. Solomos and Berra (2010) published increases of 1.90 at a strain rate of 10 s^{-1}. However, caution should be exercised when comparing bond strengths reported in the literature as significant differences in experimental methodology most certainly influenced the comparison. Despite this caution, the consistency noted in the range of *DIFs* suggests that a universal high strain rate phenomenon does affect bond.

Strain rate did not influence the failure mechanism of beam-ends when bond failure occurred in the concrete substrate. For example, beam-ends with short bonded lengths experienced a cover splitting failure regardless of strain rate. Weathersby (2003) noted that specimens which suffered pullout or splitting bond failures under static conditions were likely to experience the same failure mode under high strain rate loading, provided that failure did not occur as a result of rupture of reinforcement. Shah and Hansen (1963) also reported consistent pull-out failures accompanied by splitting cracks in the surrounding cover concrete independent of strain rate. The aforementioned authors also noted that the likelihood and severity of splitting cracks was reduced under dynamic loads. This reduction was also observed for the case of the beam-end bond tests of this study.

Although bond strength was sensitive to strain rate, the bond stress-slip characteristics of the beam-ends were not significantly affected by rapid loading. The bond stress-slip characteristics were, however, influenced by embedment length. As evidenced by the best-fit bond curves illustrated in Figure 3.10, beam-ends with longer embedment exhibited greater stiffness than those with shorter embedment independent of strain rate. Furthermore, the magnitude of static and dynamic bond for beam-ends with $l_b = 200$ mm was 13% greater than those with $l_b = 400$ mm. The overall sensitivity of bond characteristics to embedment length at strain rates of 0.1 to 1.0 s^{-1} is consistent with the results of pullout tests performed by Yao, Wu, and Huang (2013) who reported that shorter bonded lengths experience greater relative increases in bond under dynamic load conditions.

Less clear is the effect of strain rate on the slip at peak stress, s_1. Results of the beam-ends tests show no discernable effect of strain rate or embedment length on s_1. On the other hand, Yao, Wu,

and Huang reported a decrease in s_1 as loading rate increased for specimens with long embedment, while an increase in s_1 was noted as loading rate increased for specimens with short embedment. Although larger values of slip are expected for shorter lengths of bonded reinforcement stressed to the cut-off point (Alsiwat and Saatcioglu, 1992), the effect of rapid loading on s_1 remains uncertain.

A number of observations were made in regards to the use of beam-end specimens for comprehensive investigations into the rate-sensitivity of reinforced concrete bond. Beam-end bond tests, an accepted means of comparing the relative bond strength of reinforcing steel in concrete under static conditions, were successfully adapted to dynamic testing. As expected, specimens were found to be relatively simple to construct and experimental tests were straightforward. The bonded regions were well-suited to instrumentation using internally mounted strain gauges and detailed bond stress-slip curves in the elastic range were generated based on strain gauge data. Furthermore, the propagation of splitting cracks and development of bond failure was recorded using a high speed camera. Analysis of the test data also demonstrated that reinforced concrete bond is improved under rapid loading conditions. As a result, it is reasonable to conclude that beam-end tests are a suitable method to establish and compare the bond strength of reinforcing steel embedded in concrete at high strain rates.

A shock tube was used in conjunction with a DPL to perform the dynamic tests. The apparatus produced repeatable dynamic loads capable of rupturing 20M reinforcement and generated strain rates consistent with those used in protective design (Dept. of Defense, 2008). The test fixture was generally well suited to rapid testing of beam-ends. However, a major deficiency in the design of the shock tube test fixture, noted during the commissioning phase, was lack of suitable dynamic load measurement. In spite of this, strain gauge measurements proved to be an acceptable means of quantifying bond increases, although direct measurement of applied load remains the preferred method. It should also be noted that an electro-hydraulic actuator capable of generating dynamic point loads could also be used in place of a shock tube.

3.6 Summary and Conclusions

The effect of high strain rate on reinforced concrete bond was studied using flexural beam-end specimens. Beam-ends were constructed using 20M deformed reinforcement embedded in 50 MPa concrete. The clear cover to the bottom of the reinforcement was 38 mm. Strain gauges were installed in a slot milled into the reinforcement to reduce local disruptions in bond. The effect of bonded length on bond characteristics was also studied. Half of the specimens were constructed with a bonded length of 200 mm, while the remainder had a bonded length of 400 mm. Static tests were performed at strain rates on the order of 10^{-6} to 10^{-5} s^{-1}. A shock tube apparatus was used to generate high strain rates in the range of 0.1 to 1.0 s^{-1}. These tests were undertaken with the goal of assessing the suitability of using beam-end tests for dynamic bond testing.

The following conclusions were drawn based on the results presented in this study:

- Bond strength of deformed reinforcement in concrete was improved when subjected to dynamic loads.
- Based on analysis of strain readings obtained from the embedment length, elastic bond strength experienced a *DIF* of 1.45 at strain rates on the order of 0.1 s^{-1} under all conditions of bonded length.
- Ultimate bond strength experienced *DIFs* which varied between 1.47 for specimens with 200 mm bonded length and 1.33 for specimens with 400 mm bonded length, both at a strain rate on the order of 0.1 to 1.0 s^{-1}.
- Bond strengths obtained under rapid loading conditions exhibited approximately the same strain rate sensitivity as had been reported by others in the literature for similar high strain rate tests.
- Beam-ends subjected to high strain rate loads experienced loaded end slips that were similar in magnitude to those measured under low strain rate static conditions.
- The general shape of the bond stress-slip characteristics of the beam-ends, and the slip displacement at which peak bond stress was attained, were not significantly affected by high strain rates considered in this study.
- Beam-end test specimens were well-suited to high strain rate bond testing provided a safe and convenient dynamic loading fixture can be employed.

Table 3.1: Elastic bond-slip parameters obtained through beam-end tests: (a) l_b = 200 mm beam-ends, and; (b) l_b = 400 mm beam-ends.

Property	Strain rate (s^{-1})	u_o (MPa)	s_1 (mm)	α	R^2
(a) Average of l_b = 200 mm beam-ends					
Static	7.8×10^{-6}	9.2	0.27	0.65	0.96
High strain rate	1.1×10^{-1}	13.6	0.30		0.92
DIF		1.48	1.11		
(b) Average of l_b = 400 mm beam-ends					
Static	4.3×10^{-5}	8.2	0.25	0.40	0.87
High strain rate	1.2×10^{0}	11.9	0.25		0.81
DIF		1.45	1.00		

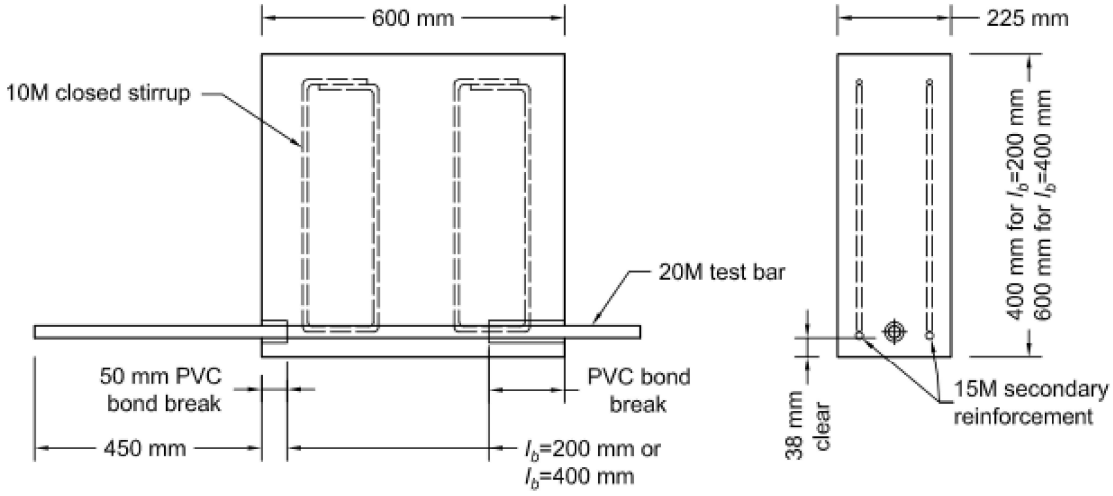

Figure 3.1: Construction and reinforcement details of beam-end specimens.

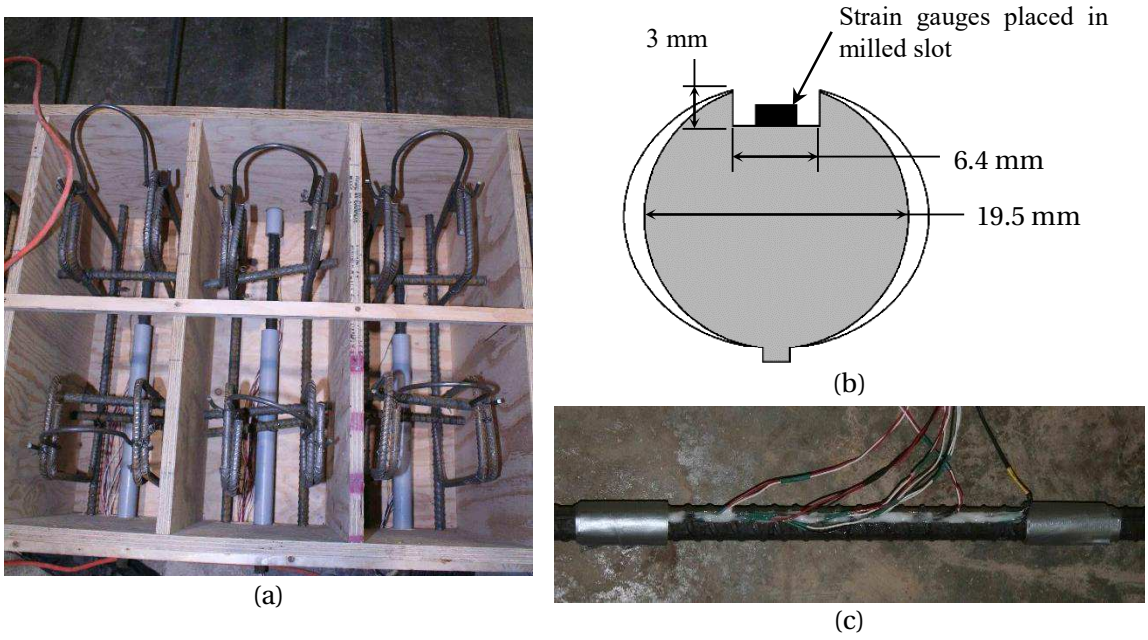

Figure 3.2: Details of the bonded test bar: (a) photograph of formwork construction and PVC bond breakers; (b) schematic of milled slot and strain gauge placement, and; (c) photograph of completed test bar.

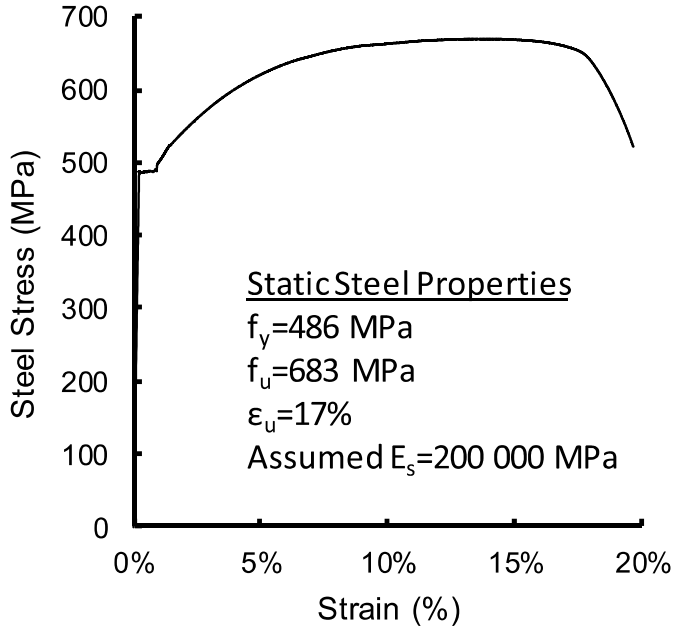

Figure 3.3: Measured static stress-strain relationship of 20M reinforcement.

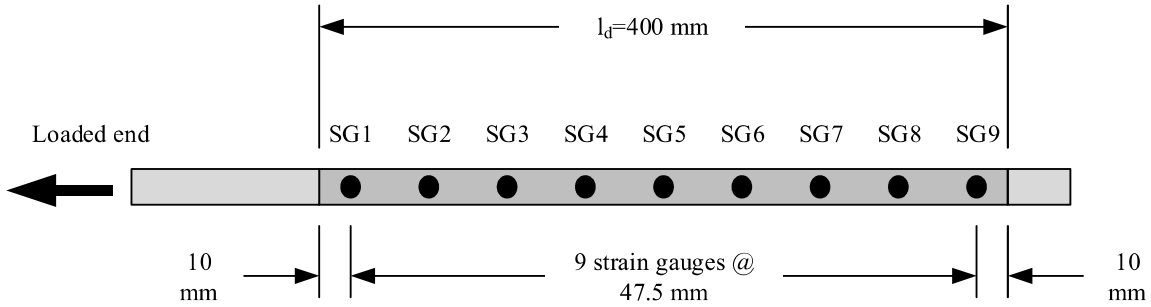

(a) Specimens with 400 mm bonded length

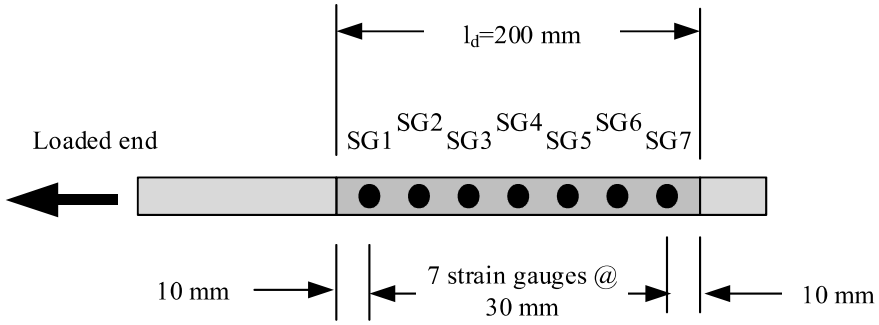

(b) Specimen with 200 mm bonded length

Figure 3.4: Spacing and nomenclature of strain gauges for beam-end tests.

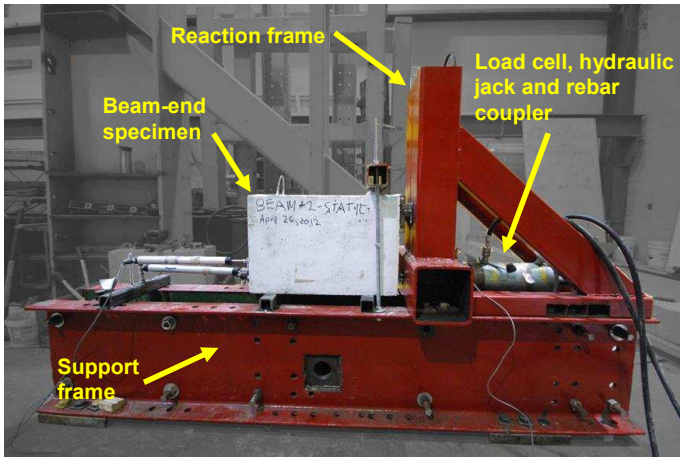

(a)

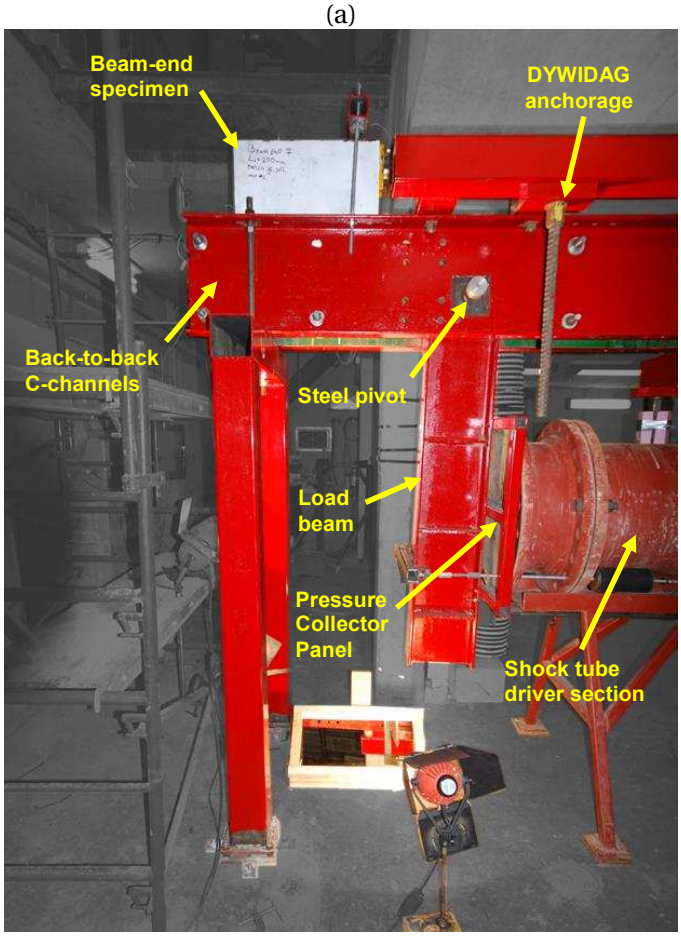

(b)

Figure 3.5: Test fixture for (a) static tests, and (b) dynamic tests.

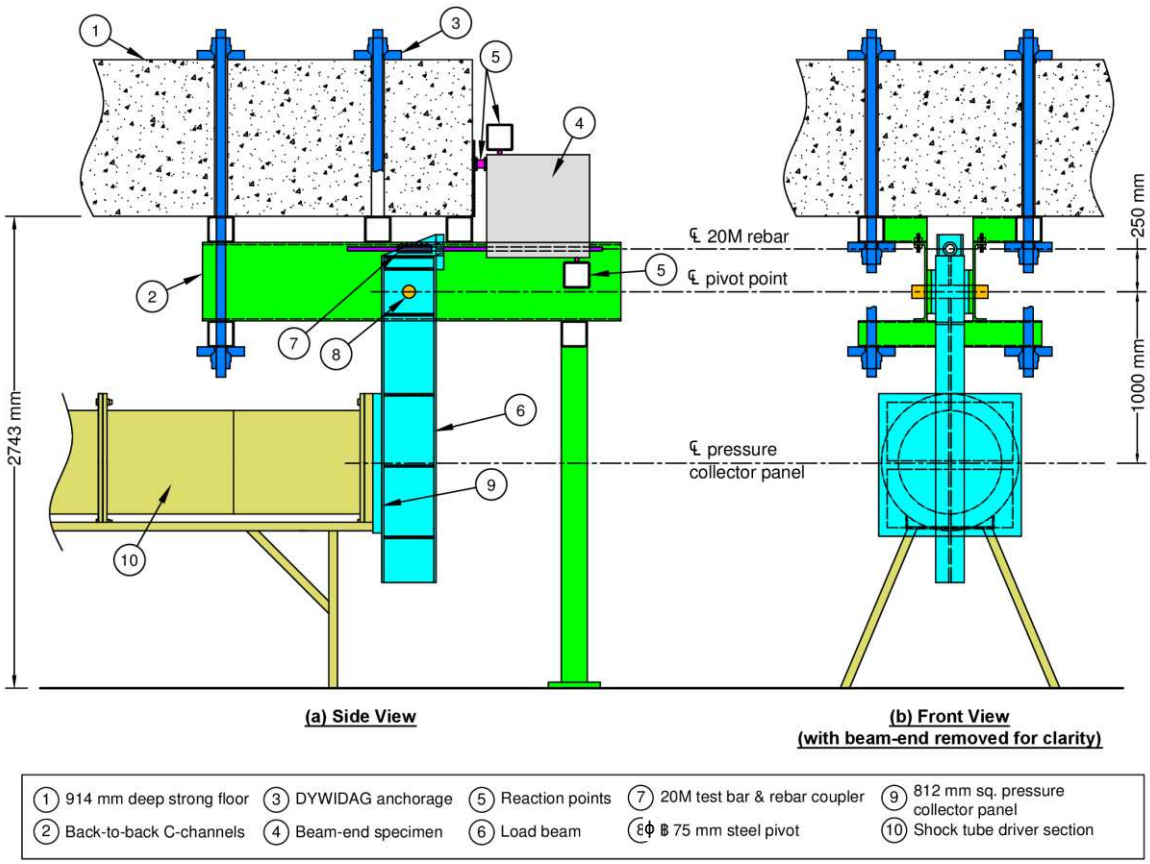

Figure 3.6: Idealized schematic of the high strain rate test fixture.

(a) (b) (c) (d)

Figure 3.7: Typical specimen failure modes: (a) face splitting failure for static and high strain rate $l_b = 200$ mm; (b) face splitting failure for static $l_b = 400$ mm; (c) face splitting failure for dynamic $l_b = 400$ mm, and; (d) rupture of test bar for high strain rate $l_b = 400$ mm.

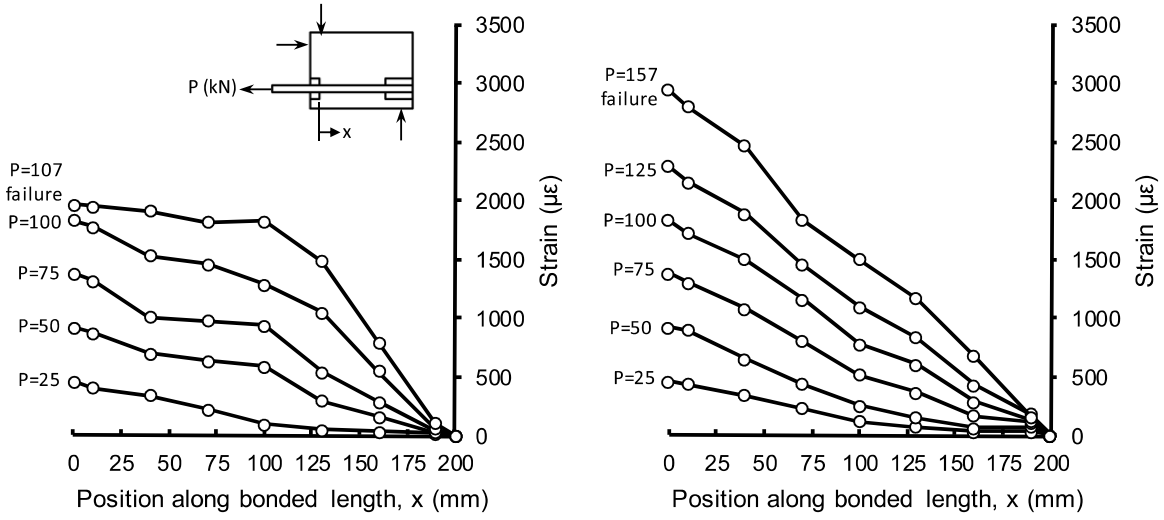

(a) Static $l_b = 200$ mm

(b) High strain rate $l_b = 200$ mm

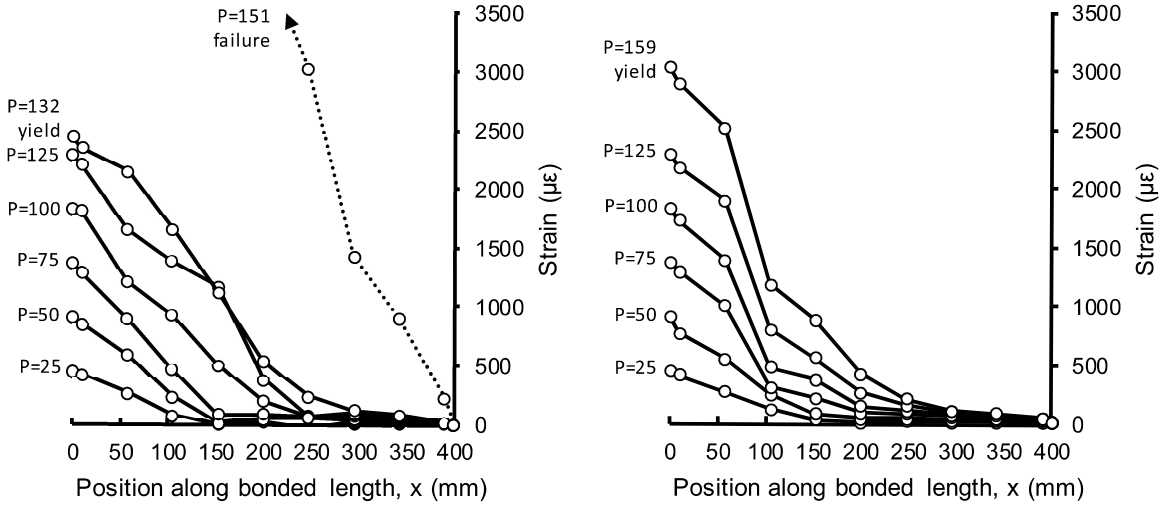

(c) Static $l_b = 400$ mm

(d) High strain rate $l_b = 400$ mm

Figure 3.8: Typical distribution of steel strains in the bonded region.

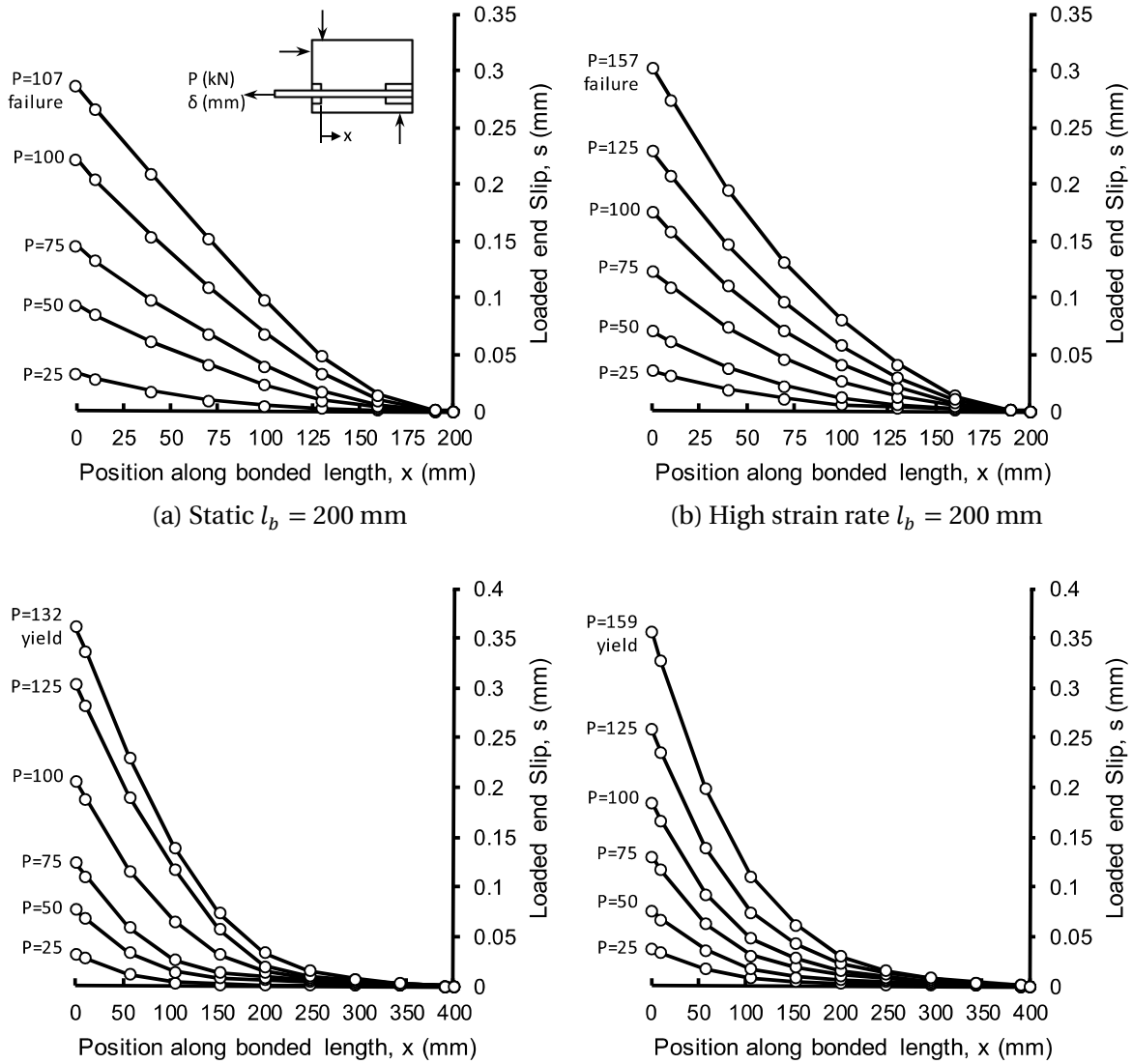

(a) Static $l_b = 200$ mm

(b) High strain rate $l_b = 200$ mm

(c) Static $l_b = 400$ mm

(d) High strain rate $l_b = 400$ mm

Figure 3.9: Typical distribution of bar slip in the bonded region.

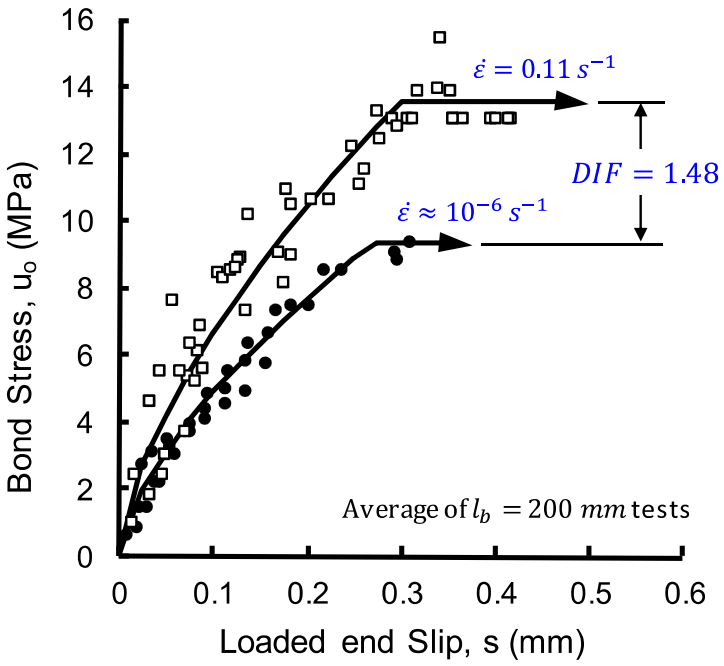

(a)

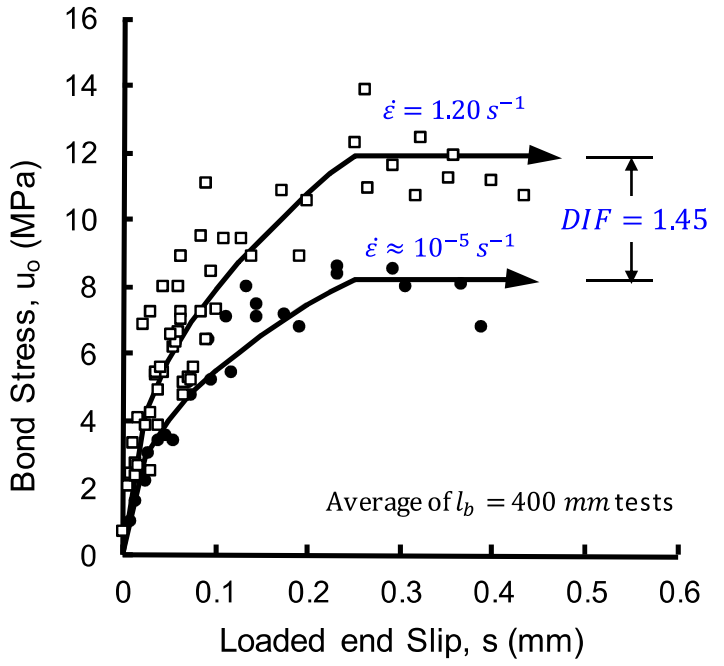

(b)

Figure 3.10: Static and high strain rate elastic bond-slip relationships for beam-ends: (a) l_b = 200 mm specimens, and; (b) l_b = 400 mm specimens.

Chapter 4

High Strain Rate Response of Reinforced Concrete Lap Splice Beams

Abstract The experimental behaviour of lap-spliced reinforced concrete beams subjected to high strain rates was studied. Eleven companion pairs of beams, each consisting of two nominally identical specimens, were designed, built and tested. The physical and material properties of the companion pairs were selected based on a range of design parameters known to significantly influence bond strength (*i.e.* size of spliced reinforcement, cover depth, concrete strength, presence of transverse reinforcement). In order to establish a baseline for comparison, one beam from each companion pair was subjected to static loads generating an average strain rate of 10^{-5} s^{-1}, while the other was subjected to high strain rates in the range of 1.0 s^{-1} generated using a shock tube.

Results of the experiments demonstrated that although the underlying flexural response and nature of bond splitting failure was not affected by dynamic loads, the strength and stiffness of reinforced concrete beams was significantly improved when subjected to blast loading. An increase in the average peak dynamic beam resistance of 30% relative to the reference static conditions was attributed to high strain rate effects. Part of this increase was attributed to improvements in the load carrying capacity of the lap splices. Without exception, high strain rate bond strength was always greater than corresponding low strain rate values, yielding an average dynamic increase factor (*DIF*) applied to bond of 1.28. Regardless of strain rate, it was found that the bond strength of splices with and without transverse reinforcement increased in proportion to the ratios of the minimum cover depth and the splice length to bar diameter, respectively.

Keywords reinforced concrete bond; high strain rates; lap splice; dynamic increase factor.

4.1 Introduction

Recent world events have demonstrated the vulnerability of structures to the extreme effects of accidental or man-made explosions for which they have not been designed. As a result, the performance of buildings subjected to blast loading is an active area of ongoing research. For example, numerous studies have shown that the mechanical properties of concrete and steel are sensitive to strain rate enhancement (Bischoff and Perry, 1991; Malvar and Crawford, 1998a; Malvar and Crawford, 1998b). For a typical reinforced concrete member subjected to blast loading, concrete and steel exhibit strength increases ranging between 10% to 30% of their reference static value (Department of Defense, 2008). As a result of these so-called "strain rate effects", improvements in material strengths directly impact the strength of reinforced concrete members (Fu et al., 1991). For example, loading rate has been shown to increase the load carrying capacity of reinforced concrete beams, in addition to providing improved energy dissipation and ductility (Xiao et al., 2012). The mitigation of the blast risk associated with terrorist attacks and accidental explosions threatening critical infrastructure is dependent on the ability of the civil engineering community to fully understand the underlying physical behaviours. One area in particular need of further study is the effect of high strain rate loading on the bond characteristics between reinforcing steel and concrete.

Owing to the technical challenges of simulating short-duration dynamic loads on structural members, few researchers have investigated the highly specialized topic of reinforced concrete bond behaviour at high strain rates. Those that have studied the topic have primarily used small-scale pull-out type specimens subjected to dynamic loads generated using Split-Hopkinson Pressure Bars (SHPB) and high-speed actuators (Shah and Hansen, 1963; Vos and Reinhardt, 1982; Yan, 1992; Weathersby, 2003; Solomos and Berra, 2010; Yao, Wu and Huang, 2013; Michal et al., 2015). The results of these tests have demonstrated that bond strength experiences an apparent increase when subjected to short-duration, dynamic loads. Furthermore, it has been reported that the degree of dynamic bond strength improvement is a function of: the rate of loading; the construction details and geometry of the developed or spliced bar; as well as the properties of the constituent materials. However, unlike the crushing strength of concrete or the yield strength of steel, bond is not a generic material property. Rather, it is a complex phenomenon that is sensitive to a host of material and structural parameters, such as the properties of steel and concrete, the surface condition and geometric configuration of the reinforcement, and the construction of the structural element itself (ACI, 2003). Since the construction, geometry and internal stress state of pull-out specimens is entirely different from in-situ bond conditions in actual reinforced concrete construction, test results obtained from these tests cannot be used to substantiate design and analysis of actual infrastructure subjected to extreme loads.

The objective of this chapter is to present the design, construction, instrumentation and testing of large-scale reinforced concrete beams with tension lap splices subjected to static and dynamic loads. The University of Ottawa Shock Tube Testing Facility was used to generate high strain rate bond failure of the test samples. Specimens were instrumented such that shock wave pressures, reaction forces, displacement response, and steel strains were recorded during testing. The test results are presented, and the strength and ductility capacity of the lap splices subjected to low and high strain rates is assessed. Finally, a discussion is presented on the influence of the strain rate sensitivity of bond strength as a function of the construction parameters of the spliced beams.

4.2 Experimental Methodology

Eleven companion pairs of beams, each consisting of two nominally identical specimens, were designed, built and tested for this experimental study. Table 4.1 lists the test matrix and properties for each of the companion pairs. The physical and material properties of the companion pairs were selected based on a range of design parameters known to significantly influence bond strength. The test variables consisted of the size of longitudinal reinforcement (10M, 15M, and 20M); the cover depth (25 mm, and 50 mm); the concrete strength (30 MPa and 50 MPa), and; the presence of transverse reinforcement (confined or unconfined splices). In order to establish a baseline for comparison, one beam from each companion pair was subjected to low strain rate static tests. The other companion beam specimen of each pair was subjected to high strain rate loading generated using a shock tube.

A standard naming convention was adopted. Each companion pair was referred to with the prefix "CP" (Companion Pair) followed by a number denoting specimen type. Companion pairs were designated CP1 through CP11. The suffix "-LSR" or "-HSR" was used to indicate whether a particular specimen was subjected to low or high strain rates, respectively. Strain rate was defined based on the time required to achieve the maximum tensile strain in the spliced reinforcement. For the purposes of this investigation, a "low" strain rate test was one with strain rates in the range of 10^{-5} to 10^{-6} s^{-1}. A "high" strain rate was one where the strain rate exceeded 10^{-1} s^{-1}. Details of the lap splice beams, test fixtures and instrumentation are presented in the following section.

4.2.1 Test Specimens and Parameters

Table 4.1 shows the as-built geometric and material properties of the test specimens. The dimensions and reinforcement details of a typical beam specimen are illustrated in Figure 4.1. All of the bottom cast beams were doubly reinforced with two contact tensile lap splices at mid-span and continuous compression reinforcement. The overall length of the beams was 2440 mm with a clear span between supports of 2232 mm. The beams were subjected to four-point bending generating a constant moment region with a length of 744 mm. Shear reinforcement was provided throughout

the shear spans with stirrups constructed from diameter 6.3 mm smooth steel wires spaced at 75 mm [Figure 4.1 (c)].

A generic cross section of the spliced region is illustrated in Figure 4.1 (d). As suggested by Briggs et al. (2007), the nominal side cover (c_{so}) was set equal to the bottom cover (c_b) to ensure that neither a face nor a side splitting cover failure mode would be favoured. The clear spacing between splices (c_{si}) was equal to twice the side cover. As a result, the cross-sectional width of all beams was equal to $4d_b + 4c_{so}$ rounded up to the nearest multiple of 5 mm. Beam height was proportioned such that concrete would not crush until after the stress level in the reinforcement reached at least $1.25f_y$ based on an assumed design yield stress $f_y = 400$ MPa.

Splice length (l_s) of the lap splices was proportioned such that a cover splitting bond failure would occur under low strain rates at a stress level in the reinforcement of 400 MPa. Values of l_s for each companion pair were computed using the descriptive expressions for bond strength proposed by ACI Committee 408 (ACI, 2003). The splices for companion pairs CP1 through CP8 were constructed without transverse reinforcement and hence, were unconfined. However, the splices for CP9 through CP11 were confined by double leg closed transverse reinforcement constructed from diameter 6.3 mm smooth steel wires. The spacing of the ties was not greater than $d/4$, as required by CSA S850 for tension lap splices in reinforced concrete beams subjected to blast loads (Canadian Standards Association, 2012).

4.2.2 Material Properties

All beams were constructed using normal strength concrete with a maximum crushed limestone aggregate size of 10 mm. Concrete was supplied by a ready-mix company and cast in four separate batches. Two of the batches were specified to have a 28-day compressive strength (f_c') of 30 MPa, while the remainder were specified as 50 MPa. This range represents typical concrete strengths encountered in practice and provided a baseline for evaluating the influence of strain rate on bond characteristics at different concrete strengths. The compressive strength of concrete at the time of testing was determined by crushing an average of six standard 100 mm × 200 mm cylinders. Companion pairs CP1, CP2, CP3, CP4, and CP7 each had a compressive strength of 32.5 MPa at the time of testing, while CP9 and CP10 had f_c' of 36.9 MPa. Similarly, companion pairs CP5, CP6, and CP8 had a compressive strength of 48.7 MPa, while f_c' for CP11 was 45.2 MPa.

Grade 400 reinforcing bars were used for both the continuous and spliced longitudinal reinforcement. Stress-strain relationships for the three sizes of rebar, shown in Figure 4.2, were determined based on an average of three coupon tests. The 10M (CP1, and CP2), 15M (CP3, CP4, CP5, CP6, CP9, CP10, and CP11), and 20M reinforcement (CP7, and CP8) had a static yield strength

f_y of 431.2 MPa, 448.4 MPa, and 491.0 MPa, respectively. The diameter 6.3 mm smooth steel wire used for the transverse reinforcement had a static yield strength (f_{yt}) of 580 MPa.

4.2.3 Test Setup

Low Strain Rate Tests

Figure 4.3 shows the low strain rate test fixture used for the static tests performed at the University of Ottawa Structures Laboratory on a strong floor. A hydraulic jack with manual hand pump was used to apply two point loads to the test specimens through a spreader beam. Special care was taken to ensure that the support conditions and span lengths in the static tests were the same as those of the high strain rate tests.

High Strain Rate Tests

High strain rate tests were conducted at the University of Ottawa Shock Tube Testing Facility. Previous research had demonstrated that the pneumatically-driven shock tube can generate positive phase blast waveforms which are nominally identical to those produced by the detonation of high explosives (Lloyd et al., 2011) and that shock tube testing can consistently generate repeatable blast pressure time-histories (Jacques, 2011). The facility can accommodate high strain rate testing of a broad variety of structural components, including planar (*e.g.* slabs, wall, windows) and non-planar elements (*e.g.* columns, beams, beam-ends).

The shock tube test fixture, illustrated in Figure 4.4, was designed to closely replicate the support conditions and load conditions used for static tests. The ends of the vertically oriented lap splice beam (callout 1 in Figure 4.4) were connected to the shock tube test frame (callout 2) by two reaction assemblies. For the lap splice beams of this study, a load transfer device (LTD) was constructed to collect the pressure generated by the shock tube and transfer the loading to the beams as two point loads. The load transfer system, first used to test dimensional lumber subjected to high strain rates (Jacques et al., 2014), consisted of two individual rigid steel panels (callout 3). Each steel panel was 2032 mm tall × 1000 mm wide and, when placed side-by-side, completely covered the 2032 mm by 2032 mm opening at the front of the shock tube test frame. Sliding hinges (callout 4) increased the efficiency of the transfer system by permitting the entire load transfer device to translate laterally without causing a reaction at the hinge locations. The maximum lateral displacement of the load transfer system was 200 mm. A set of steel wires was used to prevent excessive lateral deflections and rebound of the load transfer system into the shock tube.

Two reaction assemblies provided lateral support to the lap splice beams and consisted of a front support and a rear support. The front support was a 1200 mm long, 152 mm × 152 mm × 6.4 mm square hollow structural section (HSS) stiffened on both flexural faces with 6.4 mm thick steel plates extending the full length of the HSS (callout 5). A load cell with integral pin-joint (callout 6) was

mounted to the front support. The rear support (callout 7) was a 500 mm long, 51 mm × 51 mm × 6.4 mm square HSS. A 440 mm long, 19 mm diameter steel rod was welded to the front and rear HSS supports. Four 19 mm diameter Grade 5 threaded steel rods (callout 8) were used to bolt each of the top and bottom reaction assemblies to the shock tube test frame. The front supports tended to drop under their own weight when bolted to the shock tube. To prevent this undesirable condition, the elevation of the front supports was maintained by wedging them between the concrete floors above and below the test fixture by means of two shoring jacks and wedging blocks (callout 9). Stiffened W150x30 steel beams were used to fix the two steel panels together at the load application points (callout 10).

The entire load transfer system had a mass of 283.6 kg and an effective tributary area of 3.55 m^2. A photograph of the load transfer system is shown in Figure 4.5. Previous tests on similarly proportioned beams have demonstrated that this configuration of end supports can generate boundary conditions which closely simulate ideal simple reactions (Jacques, 2011; Toikka, 2012).

As the experimental results will subsequently demonstrate, the load transfer system proved to be an effective means of generating high strain rates in a four-point bending configuration. However, the system did have several drawbacks. First, the load transfer system added significant mass to the dynamic system. This mass was accurately measured and accounted for during the analysis. Second, the load applied to the test specimens was not measured directly. Rather, it was calculated based on the applied pressure time-history and the area of the LTD. Finally, the LTD was not directly connected to specimens preventing transfer of negative pressure forces. However, this did not prove to have any significant impact on response as the beams generally failed before the end of the first positive phase of the blast pressure waveform and during the initial inbound displacement phase.

4.3 Instrumentation

All beams were instrumented in a similar fashion with strain gauges, load cells and displacement transducers. Strain in the bottom spliced longitudinal reinforcement was measured using a total of eight Tokyo Sokki Kenkyujo Co., Ltd. FLA-6-350-11 350Ω electrical resistance strain gauges. Hardware limitations precluded installation of a greater number of strain gauges. The placement and naming convention of strain gauges is shown in Figure 4.1 (b). Each bar was instrumented with a strain gauge placed at mid-splice and another placed outside of the spliced length, but within the constant moment region. This configuration allowed the development of strains within the spliced and non-spliced regions of reinforcement to be monitored. The gauges were oriented along the neutral axis of the reinforcement, and care was taken to ensure the installation of the strain gauges and placement of lead wires did not significantly disturb the integrity of the splices.

Strain gauge based load cells were used to measure reaction forces. The same load cells were used for both low- and high-strain rate tests. Shock wave reflected pressure-time histories were recorded using two piezeoelectric pressure sensors located 50 mm away from the end of the test frame inside the shock tube. The general response and crack propagation of the specimens was recorded using a high definition digital video camera during low strain rate tests, and a high-speed digital video camera recording at 500 frames per second during high strain rate tests. During shock tube testing, experimental data was recorded using a high-speed data acquisition unit recording at 100,000 samples per second (10 μs between samples).

Specimen displacements were monitored using linear variable displacement transducers (LVDTs) with a stroke of 312 mm. For static and dynamic tests, LVDTs were mounted at mid-span and at each of the load application points. These sensors recorded the displacement of the beams relative to a fixing attached to the laboratory floor. Unlike the supports used in static tests, the dynamically tested beams were fixed directly to the shock tube. Since the shock tube recoils and vibrates during blast testing, not accounting for the support motion can lead to significant error in displacement measurements (Lloyd, 2015). Therefore, the movement of the shock tube was also recorded using an LVDT. Consequently, the "true" or net deflection of the beams was computed by subtracting the movement of the shock tube from the beam deflections measured relative to the floor.

4.4 Test Procedure & Blast Loading Program

To facilitate direct comparison of experimental results, beam tests followed a standard destructive test procedure. Prior to testing, the beams were photographed and the surface condition of the beams was noted. Specimens were then prepared, instrumented and installed into the appropriate test fixture. Care was taken to ensure consistent span lengths and test configuration between the low and high strain rate tests. Tests were then conducted with the objective of achieving a bond failure of the splice. Bottom and side covers were measured at several locations along the splices, and average values were obtained. Once the respective test was conducted, photographs of the beams were taken, the post-test condition of the specimens was noted, and measurements to confirm the depths of the bottom- and side-cover in the spliced region were taken.

For low strain rate tests, the target loading rate was set to 20 kN/min (0.3 kN/s). This loading rate was selected to satisfy the ASTM requirement for similar flexural beam-end tests that bond failure not occur within 180 seconds of load first being applied (ASTM, 2010).

For high strain rate tests, beams were subjected to a single destructive pressure-impulse combination selected to generate a bond failure. Beams with different sizes of reinforcement were subjected to different pressure parameters reflecting differences in ultimate capacity. Sample

reflected pressure and reflected impulse time-histories are shown in Figure 4.6. Beams constructed with 10M reinforcement were subjected to a shock wave with reflected pressure (P_r) of 53.7 kPa and reflected impulse (I_r) of 415 kPa-ms. Beams with 15M reinforcement experienced a shock wave with $P_r = 85.0$ kPa and $I_r = 662$ kPa-ms, while beams with 20M reinforcement were subjected to a shock wave with $P_r = 93.5$ kPa and $I_r = 709$ kPa-ms.

4.5 Experimental Results

The following is a brief description of the observations and experimental data obtained during the low- and high-strain rate bond tests. Table 4.2 presents the experimental results and other parameters which summarize the behaviour of the specimens. Key parameters of study included the peak resistance of the beam (R_f) and the corresponding time (t_f), the strain rate ($\dot{\varepsilon}$), and mid-span displacement at failure (δ_f). Failure was defined as the time required to generate a loss of load carrying capacity in the splice, as recorded by either reaction load cell data or strain gauge data. Steel stress at failure (f_s) was established by converting strain gauge readings into stress using an appropriate stress-strain relation obtained from static coupon tests, shown in Figure 4.2. For a broad presentation of all the experimental data, the reader is directed to Appendix B of this dissertation.

4.5.1 Loading Rate

For the lap splice beams subjected to high strain rate loads, failure was on a significantly shorter time scale than the statically tested companion pairs. Typically, values of t_f for high strain rate tests was between 7.6 and 28.0 ms, compared with failure times between 2 and 10 minutes for low strain rate tests. The equivalent loading rate for shock tube tests was much greater than those obtained under static conditions, with an average loading rate (R_f/t_f) for high strain rate tests of 872 MN/min, compared with an average loading rate of 23 kN/min for static tests.

4.5.2 Strain Rate

Strain rate ($\dot{\varepsilon}$) was computed based on the ratio of the strain developed in non-spliced portions of reinforcement at failure to the time required to achieve failure, t_f. This definition, known as an "average" strain rate, considers the strain variation over the entire loading history of reinforced concrete, from initial uncracked response through to incipient failure. However, the challenge lies in determining the strain at failure. Strain readings are typically not relied upon since strain gauges become progressively less reliable as steel strain exceeds the elastic limit. Therefore, a nonlinear sectional analysis, incorporating the effect of high strain rates for dynamic tests, was performed to compute the failure strain in the reinforcement corresponding to the failure moment ($M_f = 6R_f/L$). This approach was used for both low- and high-strain rate beam tests. Details of this analysis are presented in Chapter 5, while Table 4.2 shows the average strain rate obtained for the low- and high-strain rate beam tests

Figure 4.7 shows a sample tension steel strain-time history from beam CP3-HSR. This strain history was recorded by a gauge located on the tension steel in the constant moment region outside of the spliced zone. The recorded strain profile shows the development of approximately 4050 με beginning at a time of 4.4 ms until 10.5 ms. In this region, the rate of change of steel strain gives an instantaneous strain rate of 0.66 s^{-1}. After 10.5 ms, the strain readings experience an increase of 20,000 με over 1 ms which was attributed to instrumentation failure. Hence strain readings in this region cannot be relied upon to determine the failure strain of the lap splice. Comparatively, the sectional analysis predicted a failure strain for CP3-HSR of 5850 με at a failure moment of 57.7 kNm. Based on a time-to-failure of 9.0 ms, the average strain rate over the entire loading history was 0.65 s^{-1}. In general, good agreement was found between the two methods of defining strain rate for all low- and high-strain rate tests. This confirmed that the average strain rate at failure, defined based on the ratio of the computed failure strain to the time required to achieve failure, reasonably captured the rate of change of steel strain recorded in the strain-time histories.

The average strain rate at failure attained during shock tube tests were consistent with those commonly accepted for protective design. The average strain rate obtained during static tests was 8.6×10^{-6} s^{-1}, compared with an average strain rate of 0.60 s^{-1} ranging between 0.28 s^{-1} and 1.13 s^{-1} for high strain rate tests. Previous researchers have reported similar strain rates when flexural beam specimens were used to study high strain rate bond properties (Rezansoff et al., 1975), while others have reported an order of magnitude greater strain rates when pull-out type specimens were used (Solomos and Berra, 2010). Furthermore, the range of strain rates achieved during this study was consistent with behaviour commonly accepted for structures subjected to the low range of impact loadings and for design of blast-resistant structures (Bischoff and Perry, 1991; Department of Defense, 2008).

4.5.3 General Behaviour

The resistance of a structural member is an internal restoring force which acts to return the member to its unloaded neutral position (Biggs, 1964). Unlike applied load or reaction forces, internal restoring forces cannot be measured directly. Assuming an ideal case of no damping, equilibrium necessitates that member resistance, inertia forces, applied load, and reaction forces must be resolved. Since accelerations are generally small for static loading, internal member resistance is implicitly known if either the applied loading or external reactions are measured. However, inertia forces cannot be ignored for the case of high strain rate loads that generate large accelerations.

The internal resistance of the high strain rate companion beams was computed by considering equilibrium between the support reactions, the applied force, and the inertia forces. Consider the free-body diagram of one-half beam shown in Figure 4.9. The two support reactions $V(t)$, recorded

by load cells, were in most cases approximately equal. The time-varying applied pressure force $F(t)$ was taken as the applied pressure-history $P_r(t)$ multiplied by the area of the load transfer device $A = 3.55\ m^2$. In calculating the inertia forces, consideration was given to the distributed mass of the beam ($\bar{m}$) and the concentrated mass of the LTD (m_c). Following the work of Biggs (1964), it was assumed that the distribution of inertia forces followed the elastic flexural mode shape of a simply supported beam subjected to equally spaced four-point loading. As will be discussed subsequently, this assumption was justified on the basis that spliced reinforcement generally remained elastic during high strain rate response. An expression for the dynamic support reaction was computed by taking sum of moments about the centroid of inertia forces, computed assuming the inertia distribution followed the same mode shape as the beam (Biggs, 1964). In the elastic range, the resulting expression for $V(t)$ is given by:

$$V(t) = R(t)\frac{L}{6x_t} + F(t)\frac{(x_t - L/3)}{2x_t} \tag{4.1}$$

$$x_t = \frac{0.101L^2\bar{m} + 0.290Lm_c}{0.318L\bar{m} + 0.870m_c} \tag{4.2}$$

where x_t is the distance from the support to the centroid of the inertia force. A thorough derivation of Eq. (4.1) and (4.2) can be found in Appendix C. Note that as m_c approaches zero, substituting Eq. (4.2) into Eq. (4.1) yields the correct solution for the dynamic support reactions of a system distributed mass along the length $V(t) = 0.525R(t) - 0.025F(t)$ as given by Biggs (1964).

The time-varying internal resistance for each beam subjected to high strain rates was obtained by inserting experimental data for $V(t)$ and $F(t) = P_r(t)A$ into Eq. (4.1) and rearranging to extract $R(t)$. In doing so it was found that the resulting peak resistance of the high strain rate beams was roughly equal to 97% of the corresponding peak support reaction, with the difference between peak support reaction and resistance being attributed to inertial restoring forces.

A typical plot of $R(t)$, computed from reaction load cell readings for CP6-HSR, versus mid-span displacement is shown in Figure 4.10. Generally, all high strain rate beam tests showed an unusual oscillation in resistance immediately after the initial flexural cracking stage. This oscillation was present in measured $V(t)$ and was therefore not introduced in the calculation to determine $R(t)$. If the observed oscillation in resistance was an actual phenomenon, it should have been evident in the strain gauge data since reinforcement stress in the elastic range is proportional to resistance. This hypothesis was tested by comparing the resistance calculated using Eq. (4.1) against resistance computed using strain gauges following $R = 6A_sE_s\varepsilon jd/L$. The internal lever arm jd was assumed to be equal to $0.9d$. Figure 4.10 also shows a comparison between dynamic resistance computed from strain gauges and load cells for CP6-HSR. For high strain rate tests, strain gauge resistance showed greater strength and stiffness over the range of displacements where the unusual dip was noted in the reaction resistance measurements. Near peak response, the strain gauge measurements and load

cell resistance curve were in good agreement. Since the strain gauge data did not capture the strength decrease observed in reaction load cell readings, it was concluded that the test fixture somehow interfered with the load readings. One plausible explanation was that dynamic interaction between the beam and the support reaction fixture was responsible for the localized drop in load recorded by the load cells. However, further study beyond the scope of this chapter would be required to confirm this explanation. To compensate for the strength drop evident in the resistance function at low displacement levels, a composite resistance function was generated by tracing the backbone curve created by the load cell and strain gauge resistance functions. A composite resistance curve constructed for CP6-HSR is shown in Figure 4.10.

Resistance-central deflection curves for the low and high strain rate beams are shown in Figure 4.11 (for CP1, CP2 with unconfined 10M lap splices), Figure 4.12 (for CP3, CP4, CP5, CP6 with unconfined 15M lap splices), Figure 4.13 (for CP7, CP8 with unconfined 20M lap splices) and Figure 4.14 (for CP9, CP10, CP11 with confined 15M lap splices). Note than nominal specimen and material properties are listed alongside the resistance curves shown in Figure 4.11-Figure 4.14, and that the reader is directed to Table 4.1 for a precise listing of actual construction parameters.

In all cases, the high strain rate flexural resistance of the lap splice specimens was greater than the corresponding reference static value. Furthermore, the peak resistance of beams subjected to high strain rates was on average 30% greater than was obtained under static conditions. In addition, beams subjected to high strain rates exhibited initially very rigid behaviour, as compared to those under low strain rate loading. This was attributed to improvements in the cracking strength of concrete when subjected to dynamic loads.

The test data in Table 4.2 and the resistance curves shown in Figure 4.11-Figure 4.14 demonstrated that beam response was primarily controlled by reinforcement size, and to some extent the presence of transverse reinforcement. Comparison of results from all eleven companion pairs showed that for both low and high strain rates, beams constructed with the same size of reinforcement failed at similar levels of applied load. For example, beams with 10M, 15M, and 20M reinforcement experienced static bond failure at loads in the range of 40, 115, and 180 kN, respectively. A similar trend was observed for high strain rate tests, albeit with failure occurring at greater load levels of approximately 50, 145, and 250 kN for 10M, 15M, and 20M reinforcement. Comparison of R_f for increasing d_b demonstrates that the larger bar diameters experienced greater relative increases in peak resistance under high strain rates. For splices without transverse reinforcement, the average relative increase in peak resistance for 10M reinforcement was 19%, increasing to 27% for 15M and 33% for 20M reinforcement. Splices confined by transverse reinforcement, despite failing at lower peak resistances than unconfined splices, experienced the greatest average relative increase in resistance of 37%. It was noted that while concrete strength and

cover depth did exert some influence in the load-carrying capacity of the beams, the steel controlled nature of the specimens limited their influence on flexural capacity.

4.5.4 Description of Beam Behaviour

The flexural behaviour of the lap splice beams could be discretized according to four distinct stages of response, beginning with flexural uncracked response, following by cracked response, attainment of peak resistance of the splice, and post-peak flexural response. Figure 4.8 shows the typical stages of flexural response observed during low- and high-strain rate beam tests.

Prior to cracking, the flexural response of beams subjected to high strain rates showed increased stiffness but negligible strength increase relative to statically tested companion pairs. This phenomenon was primarily attributed to improvements in the mechanical properties of concrete due to high strain rate effects (Bertero et al., 1973).

The appearance of flexural cracks at the load points signalled the beginning of the cracked flexural response stage. This behaviour was associated with a decrease in member stiffness as the tensile capacity of concrete in flexure became less effective with increasing curvature. Splitting cracks delineating the spliced region occurred during this stage, typically at relatively low resistance levels. The quantity and width of the splitting cracks increased in proportion to resistance. The post-cracking flexural stiffness of beams subjected to high strain rates showed a similar level of stiffness, but greater strength than companion beams tested under reference conditions. During post-cracked response, the behaviour of the beams was controlled by the elastic response of the reinforcement. Accordingly, the stiffness of the beams during this stage was unaffected by strain rate since the modulus of elasticity of steel is not sensitive to rate enhancement. However, the modest improvement in strength observed in most high strain rate specimens was attributed to dynamic strength of concrete resulting in increased internal moment couple for the same level of curvature as in the reference static tests.

The third stage of response consisted of a bond failure which naturally occurred at peak member resistance. Figure 4.15 (CP1, CP2 splices with 10M reinforcement), Figure 4.16 (CP3, CP4, CP5, CP6, CP9, CP10, CP11 splices with 15M reinforcement), and Figure 4.17 (CP7, CP8 splices with 20M reinforcement) show photographs of the post-test condition of the high strain rate beams, grouped according to bar size. During low strain rate tests, an appropriately equal mix of side splitting (where the principal splitting crack forms across the plane of the reinforcement through the side cover) and face splitting failures (where the principal splitting crack forms perpendicular to the plane of reinforcement through the bottom cover) were observed, usually associated with minimal loss of cover concrete. Most high strain rate beams experienced a side splitting failure with significant cover loss. In many cases, dangerous projectiles were formed when cover was explosively ejected during

bond failure. For example, CP7-HSR experienced a side splitting cover failure and a 14 kg piece of cover was ejected at an average velocity in excess of 4 m/s. However, not all high strain rate specimens exhibited catastrophic bond failure. The experimental strain and reaction data indicated a loss of load carrying capacity for CP2-HSR, CP3-HSR and CP8-HSR. Visual inspection of these samples showed the clear development of splitting cracks without significant cover loss.

Close examination of the spliced regions after splitting failure showed crushing of concrete along the leading edges of the rebar lugs in the concrete keys. Crushing, noted in both low and high strain rate tests, was most pronounced for splices with transverse reinforcement. This was attributed to the confinement provided by the closely spaced ties. The ties served to limit splitting cracks and increased the amount of damage in the concrete keys at the point of contact with the bar lugs. Based on a qualitative comparison, there did appear to be a greater amount of crushing present in the keys for the case of HSR test series, but the cursory nature of the examination limited more specific conclusions. Furthermore, the transverse reinforcement also served to ensure contact between spliced bars even after concrete cover failure, with residual slip of the spliced reinforcement approximately equal to the tie spacing $l_s/(N-1)$.

The final stage of response consisted of a decrease in load carrying capacity after splice failure. For beams without transverse reinforcement, failure was generally characterised by a sudden drop in strength immediately after peak resistance. The response of pair CP2 shown in Figure 4.11 (b), for example, highlights this type of failure. The implication is that splices without transverse reinforcement have negligible toughness, or the ability to sustain inelastic deformation without splice disintegration. The post-peak portion of the resistance curves for beams with transverse reinforcement, shown in Figure 4.14, show a sudden drop in resistance to approximately $0.5R_f$, followed by gradual strength decay with increasing displacement.

4.5.5 Bond Energy

The area under the resistance curve up to the point of splice failure was used to define the bond energy, $BE = \int_0^{\delta_f} R(\delta)d\delta$. The bond energy parameter, BE, was used as a relative measure of the energy dissipation capacity of the splice. Portions of the resistance curve after splice failure were not considered in calculating BE as splices with and without transverse reinforcement showed significantly different post-peak strength capacity.

Values of BE computed for all beam pairs are listed in Table 4.2. The average bond energy of splices subjected to high strain rates was 160% greater than the corresponding low strain rate data. However, significant scatter in the data (COV=70%) indicates that the energy dissipation capacity of the beams was dependent on various parameters. For example, beams experiencing the largest increases in ductility, particularly CP1-HSR and CP2-HSR with 10M reinforcement, showed the

greatest increase in BE ranging between 370% and 243%. The next largest relative increase in BE occurred for splices constructed with 20M reinforcement (270% greater), followed by splices with 15M rebar confined by transverse reinforcement (116% greater), and finally splices with 15M reinforcement without confinement (65% greater). It is worth noting that CP6-HSR showed no increase in BE as bond failure occurred at a displacement less than the corresponding static value, thus offsetting the increase in peak resistance.

The results show that the high strain rate beams had improved energy dissipation capacity. This is consistent with the work of Xiao et al. (2012) who reported that the energy-dissipation capacity of reinforced concrete is improved as a result of increases to the cracked, ultimate and post-peak strengths of dynamically loaded members. The improvements observed in this study were attributed to increases in material strength of steel and concrete, in addition to improvements in the load carrying capacity of the lap splices.

4.5.6 Splice Toughness

As was previously discussed, splices with transverse reinforcement showed significantly better post-peak strength capacity than splices without transverse reinforcement, which exhibited effectively no post-peak strength. Aoude et al. (2014) proposed a toughness index ($T.I.$) as a measure of the toughness and post-peak ductility of steel fibre-reinforced concrete columns. A similar approach was adopted here to examine the effect of high strain rates on lap splice toughness. For this study, the $T.I.$ was defined as the ratio of the area under the resistance curve up to displacement δ_u to the area of an equivalent fully rigid structure, $A_{F.R.} = R_f \times \delta_u$, as illustrated in Figure 4.18. The formulation for $T.I.$ is given as follows:

$$T.I. = \frac{\int_0^{\delta_u} R(\delta) d\delta}{R_f \times \delta_u} \tag{4.3}$$

where, for convenience, δ_u was assumed to be 25 mm for all comparisons.

A comparison of the $T.I.$ for all splices with transverse reinforcement is provided in Table 4.2. The results show that the toughness values obtained for beam CP9-LSR ($T.I. = 0.50$), CP10-LSR ($T.I. = 0.53$), and CP11-LSR ($T.I. = 0.52$) were similar. Toughness of splices confined by transverse reinforcement subjected to high strain rates was improved for CP9-HSR ($T.I. = 0.58$), CP10-HSR ($T.I. = 0.63$), and CP11-HSR ($T.I. = 0.74$). These increases, however, were not uniform: CP9 and CP10 experienced increases in $T.I.$ of 18%, while the splice toughness for CP11 increased by 41%, due to strain rate effects The variation observed in splice toughness was believed to be attributed to differences in concrete strength and differences in the number of stirrups in the spliced region between the various samples.

4.5.7 Reinforcement Strains

To investigate whether reinforcement remained elastic prior to splice failure, strain gauge readings taken in the constant moment region outside of the spliced zone were converted into stresses using an appropriate stress-strain relation. For the case of static tests, stress-strain curves obtained from tensile coupon tests were used directly in the comparison. For high strain rate tests, the coupon test data was modified to account for rate enhancement by applying separate *DIF*s to the yield and ultimate strengths of reinforcement. For values between yield and ultimate, a linear variation in *DIF* was applied. The expressions proposed by Malvar and Crawford (1998a) were used to establish values of DIF_{f_y} and DIF_{f_u} for each bar size using the actual strain rate observed during beam tests. Based on the range of strain rates and the reinforcement grades used in beam construction, the predicted values of DIF_{f_y} and DIF_{f_u} varied between 1.27 – 1.31 and 1.08–1.09, respectively.

Stress developed in the reinforcement at failure for all tests is presented in Table 4.2. The average static failure stress was 444 MPa with a COV of 7%, with values ranging from a minimum of 391 MPa (beam CP9-LSR) and a maximum of 491 MPa (beams CP7-LSR and CP8-LSR). Comparing the static reinforcement stress level at failure against the yield strength indicates that only CP2-LSR, CP3-LSR and CP4-LSR yielded prior to failure. Although the average stress level in reinforcement was 11% greater than the target failure stress of 400 MPa, the strain data indicated that most statically tested beams did not yield prior to splice failure.

Greater steel stresses were developed in all high strain rate beam tests relative to their statically tested companion specimen. The average high strain rate failure stress in the reinforcement was 567 MPa, with a COV of 4% with values between a minimum of 514 MPa (beam CP11-HSR) and maximum of 600 MPa (beam CP7-HSR). Furthermore, only two specimens, CP1-HSR and CP2-HSR, experienced steel stresses greater than the dynamic yield strength of the reinforcement. Deliberately configuring test specimens for predominantly elastic steel response ensured steel strains were within the acceptable measurement range of the strain gauges.

4.5.8 Influence of Strain rate on Bond Strength

The effect of the test parameters on the splitting bond strength of the lap splices, u, was investigated to establish the influence of strain rate on reinforced concrete bond. Constant bond was assumed in the spliced region. Bond strength was computed according to Eq. (4.4), provided below:

$$u = \frac{A_b f_s}{\pi d_b l_d} = \frac{f_s d_b}{\pi l_d} \tag{4.4}$$

where f_s is the steel stress at failure obtained by converting strain readings into stress, A_b is the bar area and d_b is the bar diameter. A *DIF* to be applied to bond, computed as the ratio between the

dynamic bond strength to corresponding static value, was established for each companion pair to study the effect of high strain rates on reinforced concrete bond. Values of u for each specimen, as well as a DIF applied to bond strength for each companion pair, are presented in Table 4.2.

Figure 4.19 shows the effect of strain rate on the bond strength of splices not confined by transverse reinforcement as a function of c_{min}/d_b, where c_{min} is the smaller of the minimum concrete cover ½ of the clear spacing between bars. The parameter c_{min}/d_b provides a non-dimensional measure of the influence of cover depth on bond strength.

It was found that the bond strength of splices without transverse reinforcement increased in proportion to the ratio of c_{min}/d_b for all rates of strain. For constant reinforcement sizes, greater depths of cover generated greater bond strengths in the splices. Furthermore, high strain rate bond was always greater than the corresponding low strain rate bond. The average DIF applied to bond strength for splices without transverse reinforcement (DIF_{uc}) was 1.28 with a COV of 5% and values ranging between 1.21 (CP4) and 1.39 (CP2). A power function was fitted to the low and high strain rate bond strength data. The quotient of the resulting best-fit curves was used to define a DIF_{uc} as a function of c_{min}/d_b. It was found that the bond strength of splices without transverse reinforcement could be expressed as $DIF_{uc} = 1.28\left(\frac{c_{min}}{d_b}\right)^{0.02}$. This indicates that as the ratio of cover depth to bar diameter increases, bond strength becomes more sensitive to strain rate. This observation is attributed to the improved splitting resistance of splices with large cover depths when subjected to short duration dynamic loads.

Figure 4.20 shows the effect of strain rate on the bond strength of splices confined by transverse reinforcement. Although only a small number of data points are available, bond strength for splices without transverse reinforcement increased in proportion to c_{min}/d_b. Furthermore, values of high strain rate bond were always greater than low strain rate bond. Comparing the bond strength of splices with and without transverse reinforcement indicates that the rate of bond strength increase as a function of c_{min}/d_b was greater for splices with transverse reinforcement. The average DIF applied to bond strength for splices with transverse reinforcement (DIF_c) was 1.29 with a COV of 10% and values ranging between 1.16 (CP11) and 1.42 (CP9). A power function was again fitted to each of the low and high strain rate bond strength data. The best-fit curves were used to define DIF_c as function of c_{min}/d_b. The resulting expression for the DIF of confined bond strength was $DIF_c = 1.70\left(\frac{c_{min}}{d_b}\right)^{-0.29}$. This indicates that as the ratio of cover depth to bar diameter increases, bond strength for splices with transverse reinforcement becomes slightly less sensitive to strain rate.

Figure 4.21 shows the effect of strain rate on the bond strength of splices with and without transverse reinforcement as a function of the ratio of splice length to bar diameter (l_s/d_b). Regardless of strain rate, bond strength was found to decrease as the ratio of l_s/d_b increased. Holding bar size

constant, longer lengths of developed reinforcement experienced splitting failure at lower bond strengths. Although splices with transverse reinforcement had greater bond strength, there was no discernible difference in the variation of bond strength as a function of l_s/d_b for spliced regions with or without transverse reinforcement. A power function was fitted to both the low and high strain rate bond strength data to obtain an expression for DIF_u as a function of l_s/d_b. The resulting expression $DIF_u = 1.27(l_s/d_b)^{0.003}$ indicated that improvements in bond due to rate effects were insensitive to the ratio of l_s/d_b.

Several conclusions can be made regarding the bond data obtained during the course of this study. First, it was clear that the bond strength of tension lap splices was improved when subjected to high strain rate loads. In addition, the strain rate sensitivity of bond was influenced by a number of parameters, including c_{min}, d_b, l_s and the presence of transverse reinforcement. However, the results pertaining to bond strengths and associated DIF's are not necessarily suitable for design or analysis of reinforced concrete protective structures subjected to dynamic loads for the following reasons: (i) bond strengths should be normalized to account for the effect of strain rate enhancement on the tensile and compressive properties of concrete; (ii) contemporary studies show a preference for reporting total bond force, rather than bond stress, as it facilitates decomposition of the contribution of transverse reinforcement and concrete properties on total bond strength (ACI, 2003); (iii) the quantity, arrangement and size of stirrups should be considered in analysis of bond strength for splices confined by transverse reinforcement, and; (iv) bar stresses developed in spliced reinforcement have historically been computed using sectional analysis, rather than indirect measurement using strain gauges (ACI, 2003). A more thorough assessment of the bond strength of reinforced concrete subjected to high strain rates is presented in the subsequent chapter (Chapter 0).

4.6 Summary and Conclusions

Twenty-two reinforced concrete beams were constructed with tension lap splices and tested under four-point bending. The beams contained varying configurations of reinforcement size, cover depth, concrete strength and splice confinement. The specimens were divided into eleven companion pairs of nominally identical beams, with one beam from each pair subjected to low strain rate static loading and the other subjected to high strain rate, shock tube-induced dynamic loads. Static tests were performed at strain rates on the order of 10^{-6} to 10^{-5} s^{-1}, while high strain rates in the range of 0.28 to 1.13 s^{-1} were generated using a shock tube. The objective of the tests was to examine the effect of strain rate on the load-carrying capacity of reinforced concrete beams containing lap splices. The following conclusions were reached based on the tests presented in this chapter:

1. The strength and stiffness of reinforced concrete beams was significantly improved when subjected to dynamic loading. The peak resistance of the beams studied was found

to increase by an average of 30%, while the average bond energy (area under the resistance curve) increased by 163%, both relative to the reference static conditions;

2. Comparison of the general behaviour of specimens showed that the underlying flexural response and nature of the bond splitting failure was not affected by dynamic loads, despite clear increases in member strength and stiffness attributed to strain rate enhancement;
3. The use of transverse reinforcement to confine spliced regions led to significant improvements in post-peak strength and splice toughness relative to splices without transverse reinforcement. These improvements were further amplified by high strain rate effects;
4. Without exception, high strain rate bond strength was always greater than corresponding low strain rate values, yielding an average DIF applied to bond strength of 1.28, and;
5. Regardless of strain rate, the bond strength of splices with and without transverse reinforcement was found to increase in proportion to the ratio of c_{min}/d_b, and decrease in proportion to l_s/d_b.

Table 4.1: Construction details and material properties for lap splice companion pairs.

Companion Pair	Materials		Cross-Section					Splice Details						
	f'_c MPa	f_y MPa	b mm	h mm	Bar Size	d_b mm	A_b mm^2	c_b mm	c_{so} mm	c_{si} mm	l_s mm	n	N	A_{tr} mm^2
CP1-LSR	32.5	431.2	150	200	10M	11.3	100	26	27	37	275	-	-	-
CP1-HSR								27	25	39	276			
CP2-LSR	32.5	431.2	240	200	10M	11.3	100	51	49	60	168	-	-	-
CP2-HSR								52	49	60	160			
CP3-LSR	32.5	448.4	165	300	15M	16.0	200	26	24	43	493	-	-	-
CP3-HSR								26	26	41	494			
CP4-LSR	32.5	448.4	265	300	15M	16.0	200	52	52	65	272	-	-	-
CP4-HSR								51	50	67	282			
CP5-LSR	48.7	448.4	165	300	15M	16.0	200	28	27	40	409	-	-	-
CP5-HSR								27	25	42	395			
CP6-LSR	48.7	448.4	265	300	15M	16.0	200	53	52	65	235	-	-	-
CP6-HSR								51	47	70	230			
CP7-LSR	32.5	491.0	280	300	20M	19.5	300	53	54	67	415	-	-	-
CP7-HSR								52	55	66	397			
CP8-LSR	48.7	491.1	280	300	20M	19.5	300	53	54	67	360	-	-	-
CP8-HSR								51	53	68	361			
CP9-LSR	36.9	448.4	165	300	15M	16.0	200	25	28	39	325	2	6	62.3
CP9-HSR								24	27	40	327			
CP10-LSR	36.9	448.4	265	300	15M	16.0	200	48	52	65	187	2	4	62.3
CP10-HSR								49	50	67	185			
CP11-LSR	45.2	448.4	265	300	15M	16.0	200	49	48	69	164	2	4	62.3
CP11-HSR								53	48	69	175			

Table 4.2: Low and high strain rate experimental results for lap splice companion pairs.

Companion Pair	Time-to-failure	Deflection at failure	Resistance at failure	Average strain rate	Measured splice stress	Bond Energy Parameter	Toughness Index	Bond Stress	Dynamic Increase Factor
	t_f (s or ms)	δ_f mm	R_f kN	$\dot{\varepsilon}$ s^{-1}	f_s^t MPa	BE Joules	$T.I.$	u MPa	DIF
CP1-LSR	146.3 s	14.8	38.4	1.5×10^{-5}	431	410	-	4.4	
CP1-HSR	15.6 ms	50.7	47.7	0.31	571	1925	-	5.8	1.32
CP2-LSR	123.5 s	25.8	45.6	1.8×10^{-5}	441	827	-	7.4	
CP2-HSR	28.4 ms	66.8	52.0	0.28	583	2836	-	10.3	1.39
CP3-LSR	320.0 s	16.0	122.9	7.0×10^{-6}	450	1333	-	3.7	
CP3-HSR	9.0 ms	19.0	155.0	0.65	566	2181	-	4.6	1.26
CP4-LSR	412.5 s	9.6	114.6	5.5×10^{-6}	450	646	-	6.6	
CP4-HSR	10.6 ms	15.6	164.0	1.13	566	1261	-	8.0	1.21
CP5-LSR	544.0 s	10.0	130.6	4.1×10^{-6}	448	768	-	4.4	
CP5-HSR	8.0 ms	14.1	153.2	0.60	565	1528	-	5.7	1.31
CP6-LSR	350.6 s	14.1	121.6	6.3×10^{-6}	443	1093	-	7.5	
CP6-HSR	9.5 ms	12.2	149.8	0.78	566	1096	-	9.8	1.31
CP7-LSR	322.8 s	8.7	182.4	7.6×10^{-6}	491	872	-	5.8	
CP7-HSR	12.7 ms	20.3	245.0	0.80	600	3381	-	7.4	1.28
CP8-LSR	570.0 s	10.1	185.5	4.3×10^{-6}	491	999	-	6.6	
CP8-HSR	14.0 ms	20.0	244.0	0.75	595	3514	-	8.0	1.21
CP9-LSR	147.6 s	9.5	109.2	1.3×10^{-5}	391	569	0.50	4.8	
CP9-HSR	7.6 ms	11.1	154.4	0.70	557	1130	0.58	6.8	1.42
CP10-LSR	289.5 s	7.6	100.1	7.4×10^{-6}	428	408	0.53	9.2	
CP10-HSR	8.8 ms	10.1	135.5	0.32	556	857	0.63	12.0	1.31
CP11-LSR	347.7 s	7.4	99.4	6.0×10^{-6}	417	447	0.52	10.2	
CP11-HSR	9.0 ms	11.0	134.5	0.33	514	1067	0.74	11.7	1.16

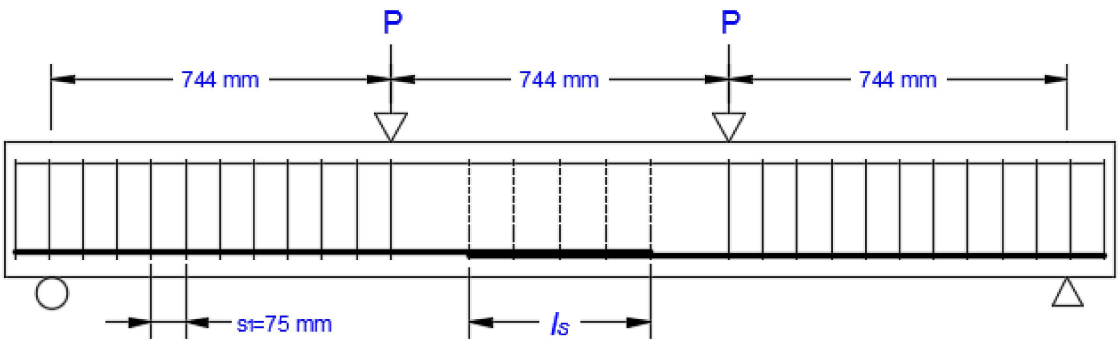

(a) Elevation view

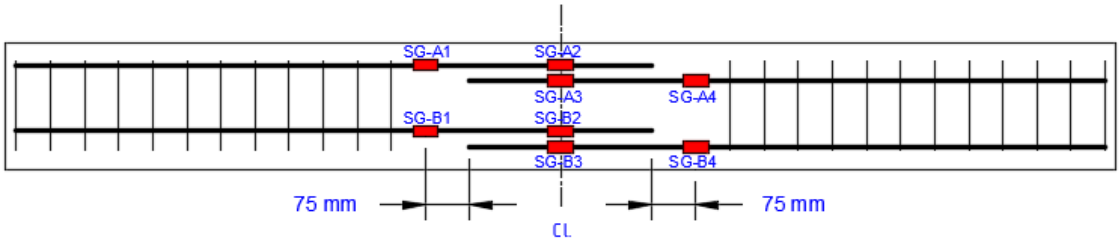

(b) Strain gauge positioning

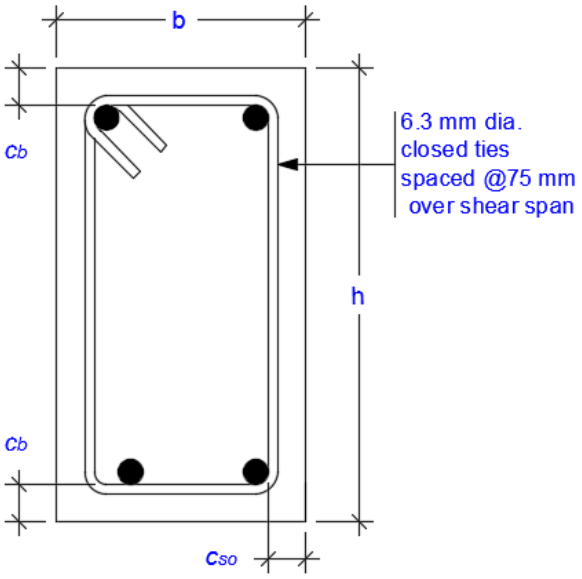

(c) Cross-section through shear span

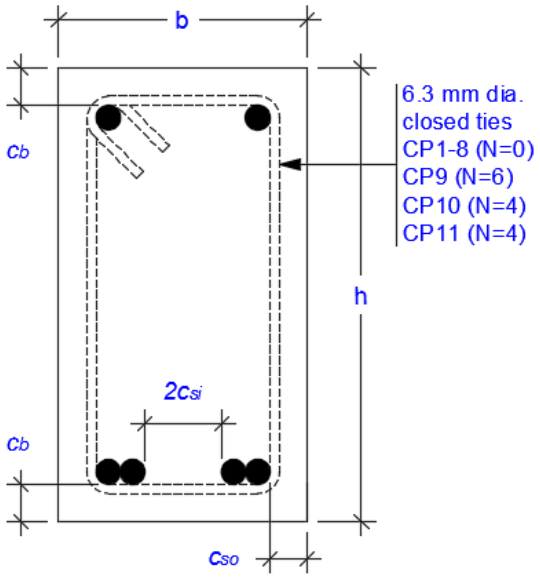

(d) Cross-section through spliced region

Figure 4.1: Construction and reinforcement details of lap splice beams.

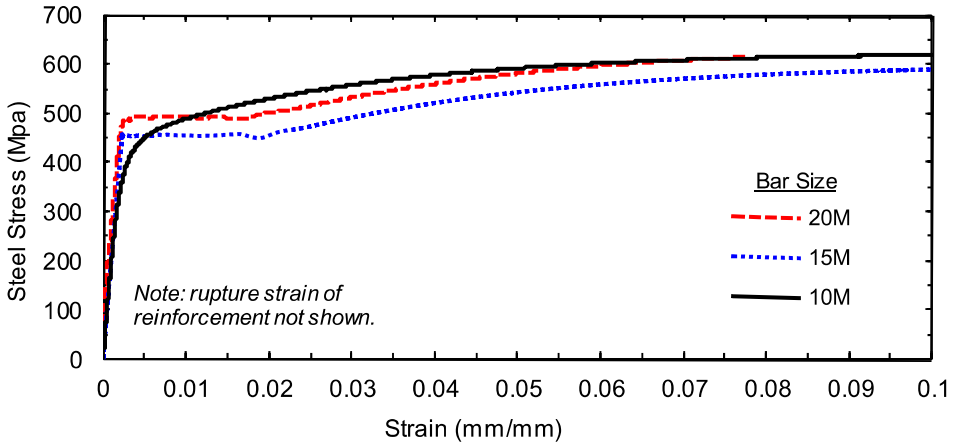

Figure 4.2: Static stress-strain relationships of reinforcement.

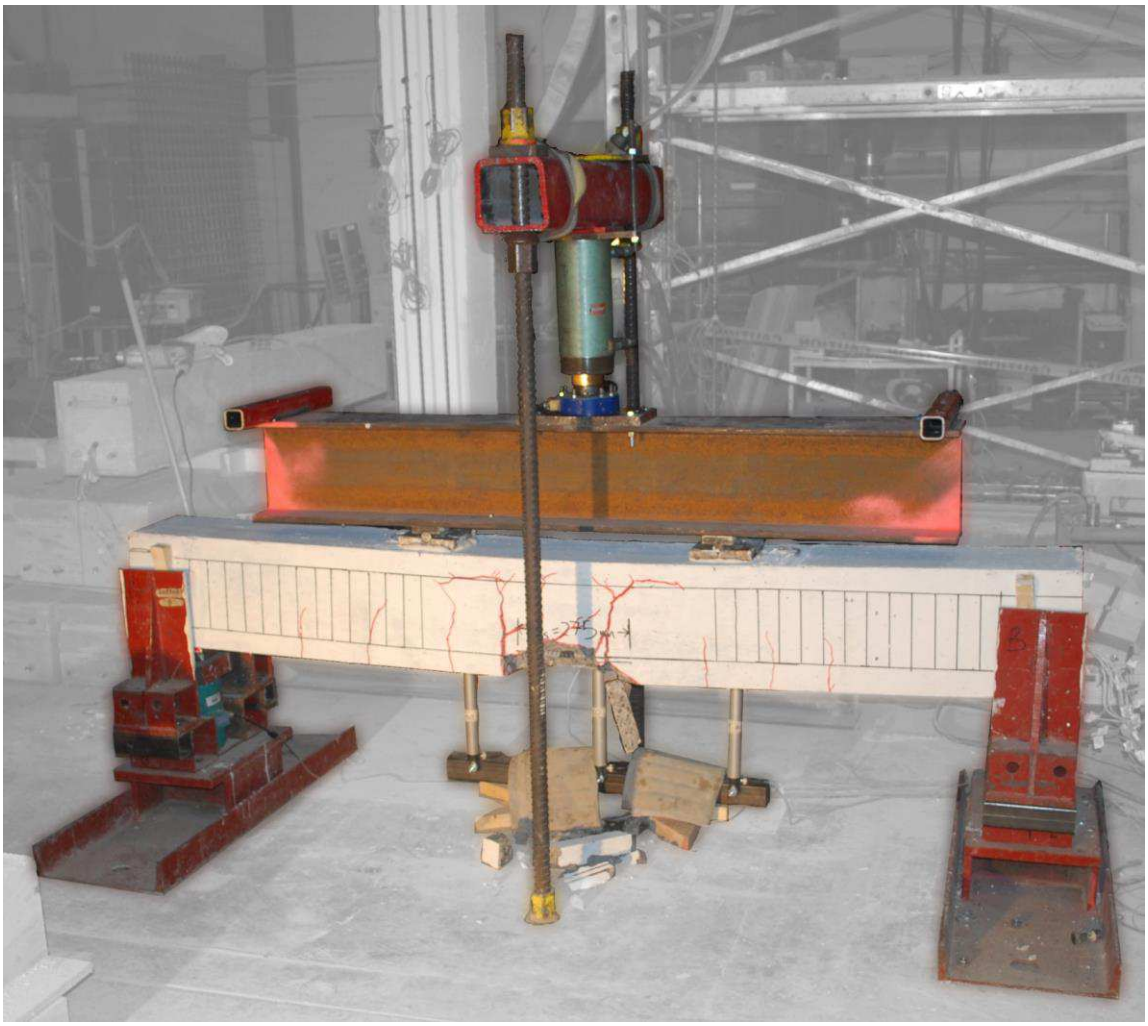

Figure 4.3: Photograph of low strain rate test fixture.

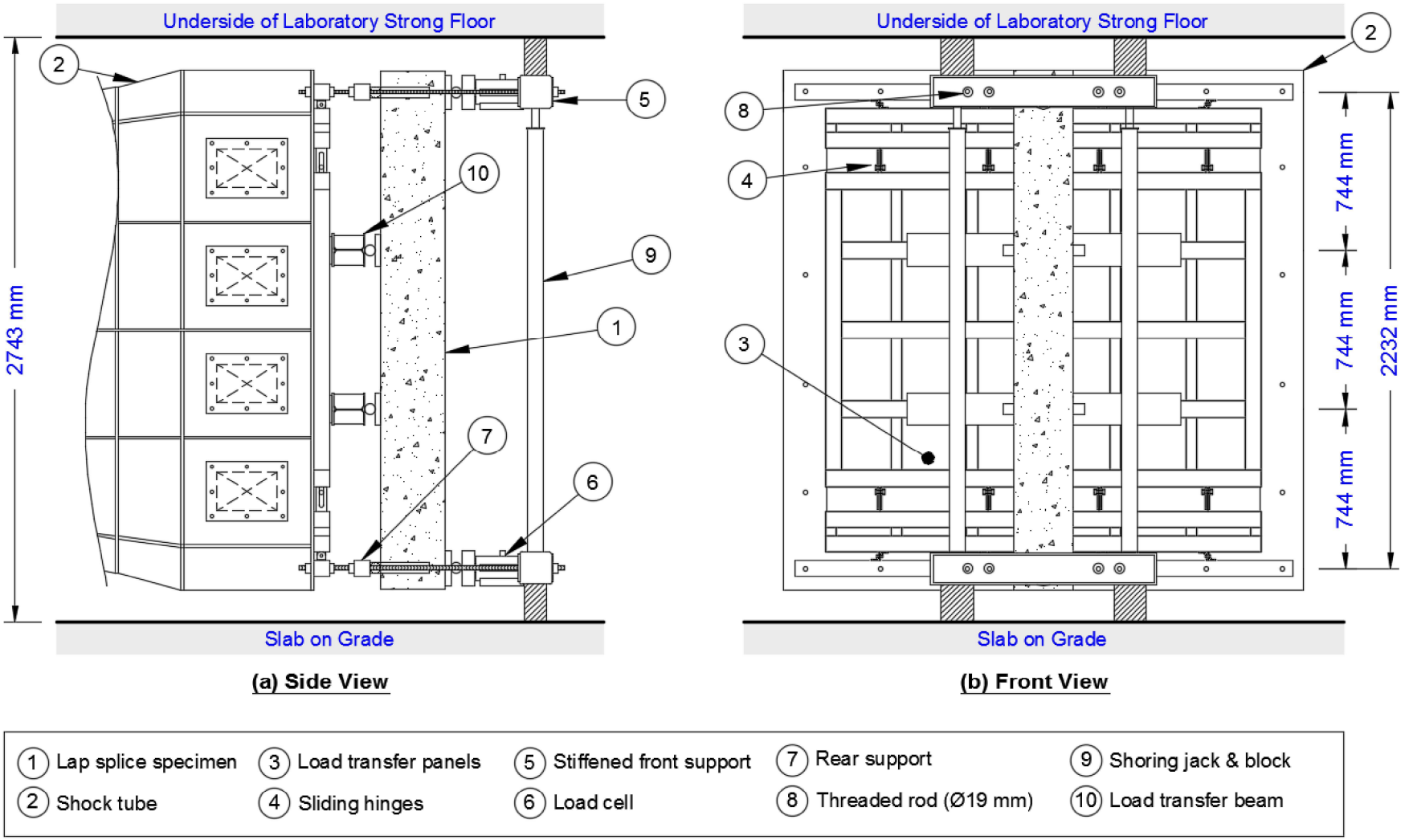

Figure 4.4: Illustration of the high strain rate test fixture.

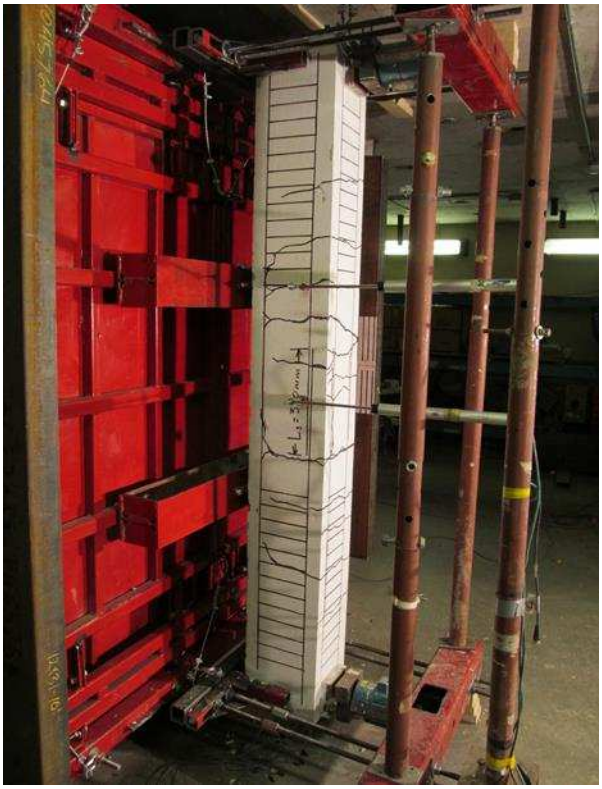

(a) Side view

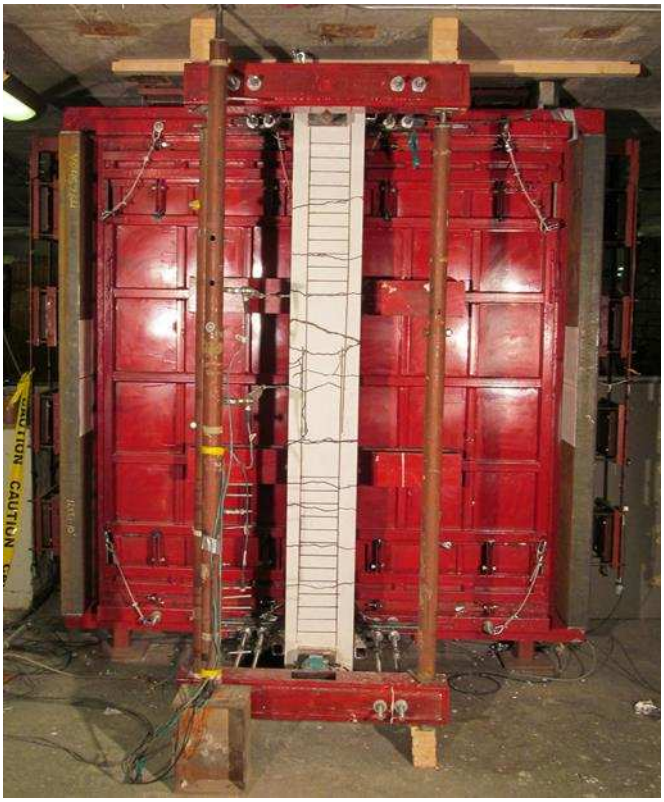

(b) Front view

Figure 4.5: Photographs of high strain rate test fixture.

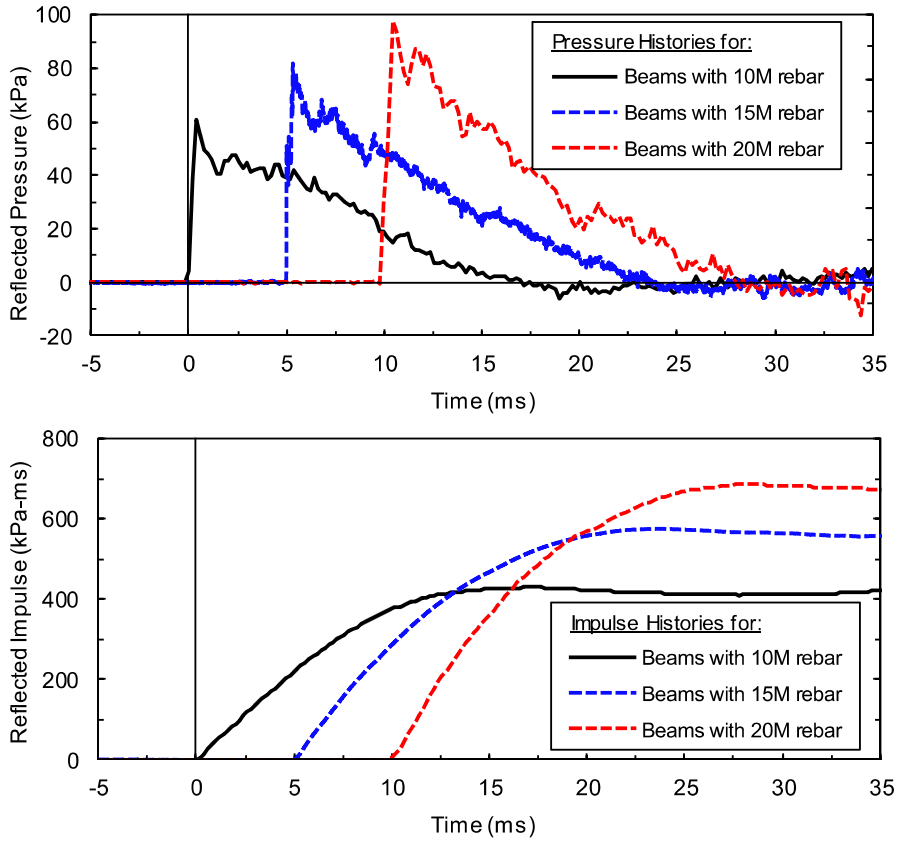

Note: Time scale of plots offset for clarity.

Figure 4.6: Sample reflected pressure and impulse time-histories.

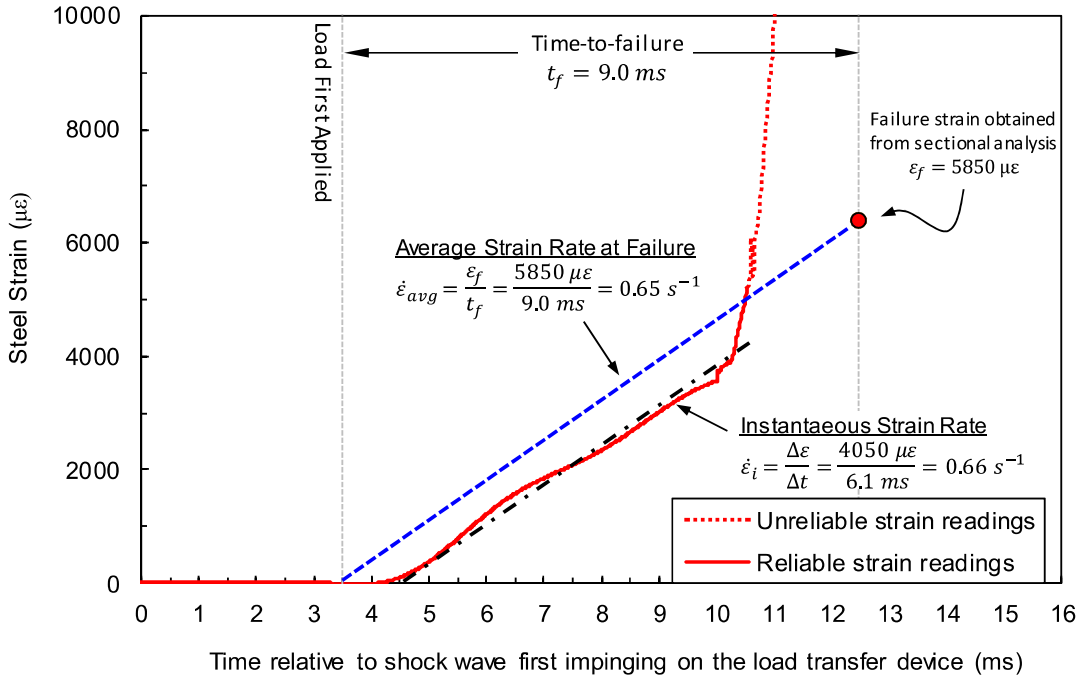

Figure 4.7: Definition of strain rate.

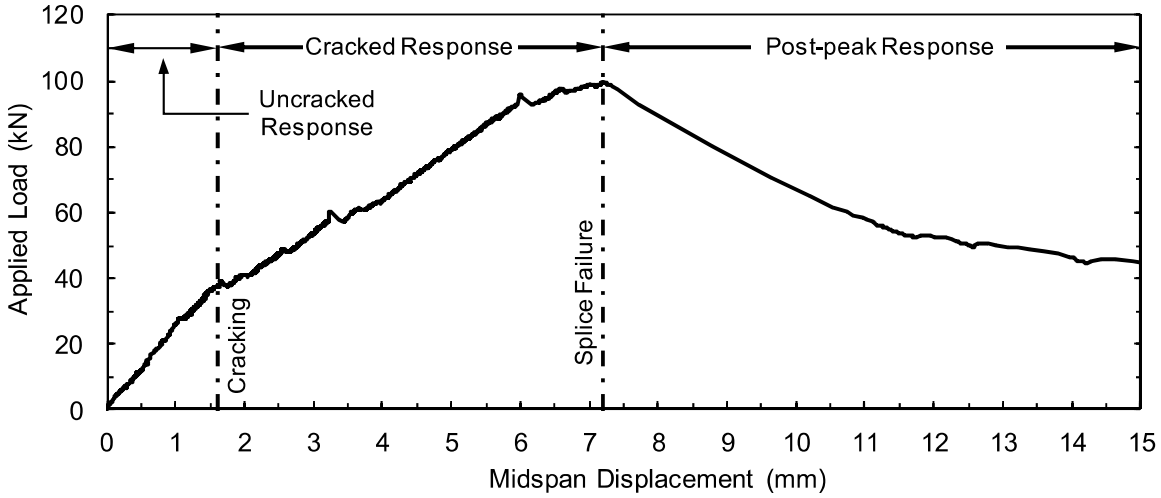

Figure 4.8: Typical stages of response observed during low- and high-rate beam tests.

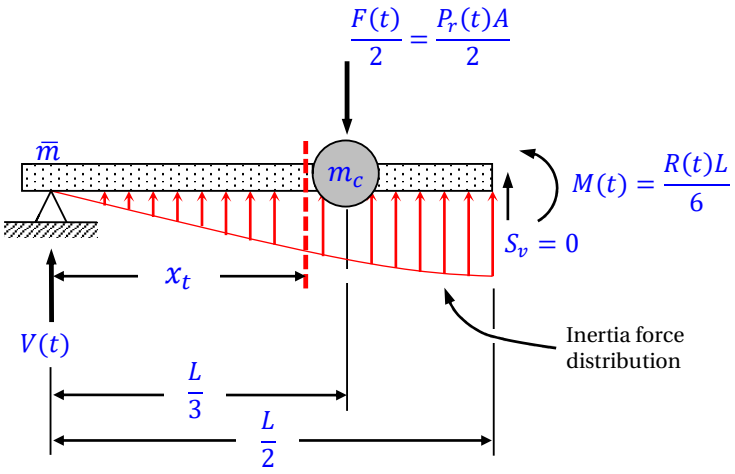

Figure 4.9: Free-body-diagram of idealized beam and load transfer device used for derivation of dynamic support reactions.

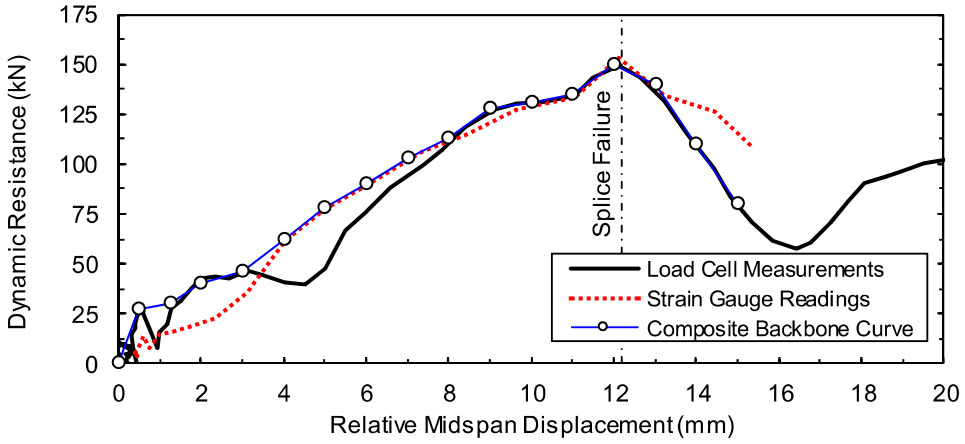

Figure 4.10: Comparison of resistance functions obtained for CP6-HSR.

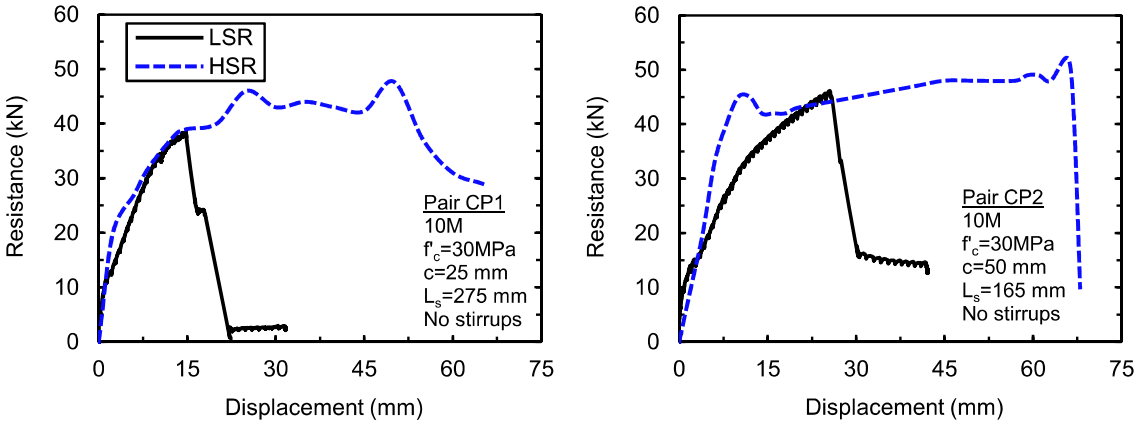

(a) Companion Pair CP1 (b) Companion Pair CP2

Figure 4.11: Comparison of low and high strain rate member response for lap splices constructed with 10M rebar and not confined by transverse reinforcement.

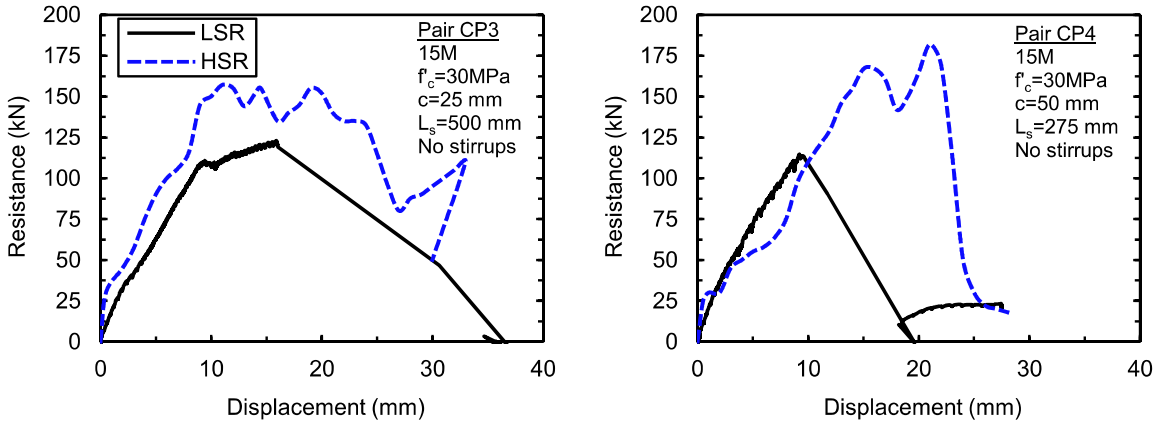

(a) Companion Pair CP3 (b) Companion Pair CP4

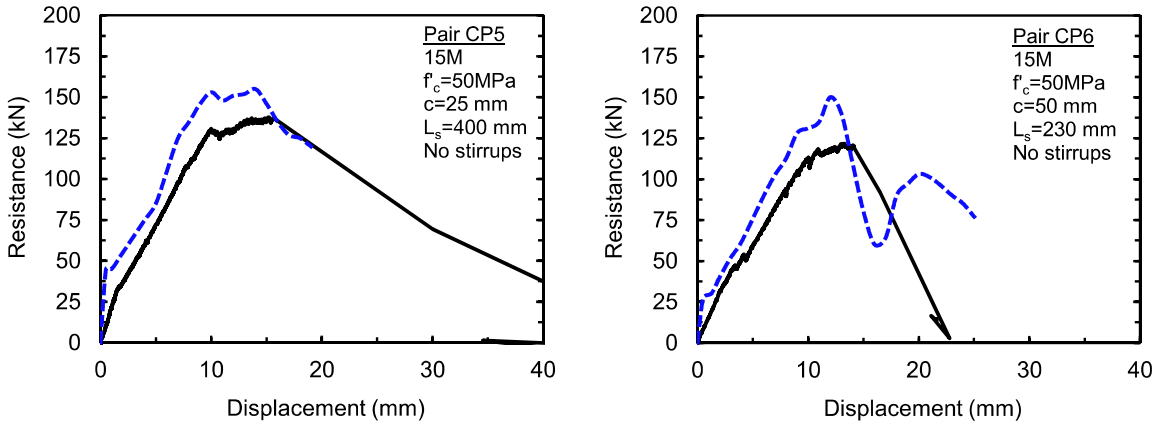

(c) Companion Pair CP5 (d) Companion Pair CP6

Figure 4.12: Comparison of low and high strain rate member response for lap splices constructed with 15M rebar and not confined by transverse reinforcement.

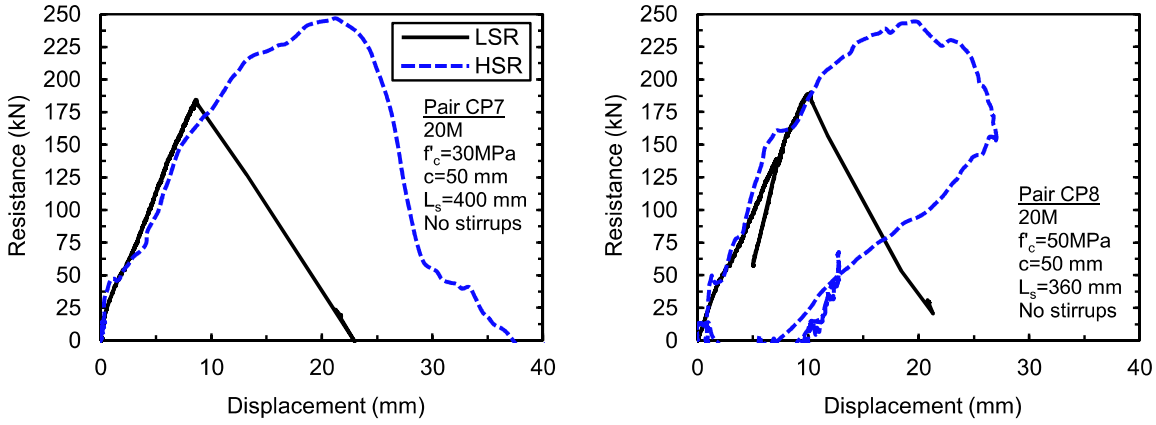

(a) Companion Pair CP7 (b) Companion Pair CP8

Figure 4.13: Comparison of low and high strain rate member response for lap splices constructed with 20M rebar and not confined by transverse reinforcement.

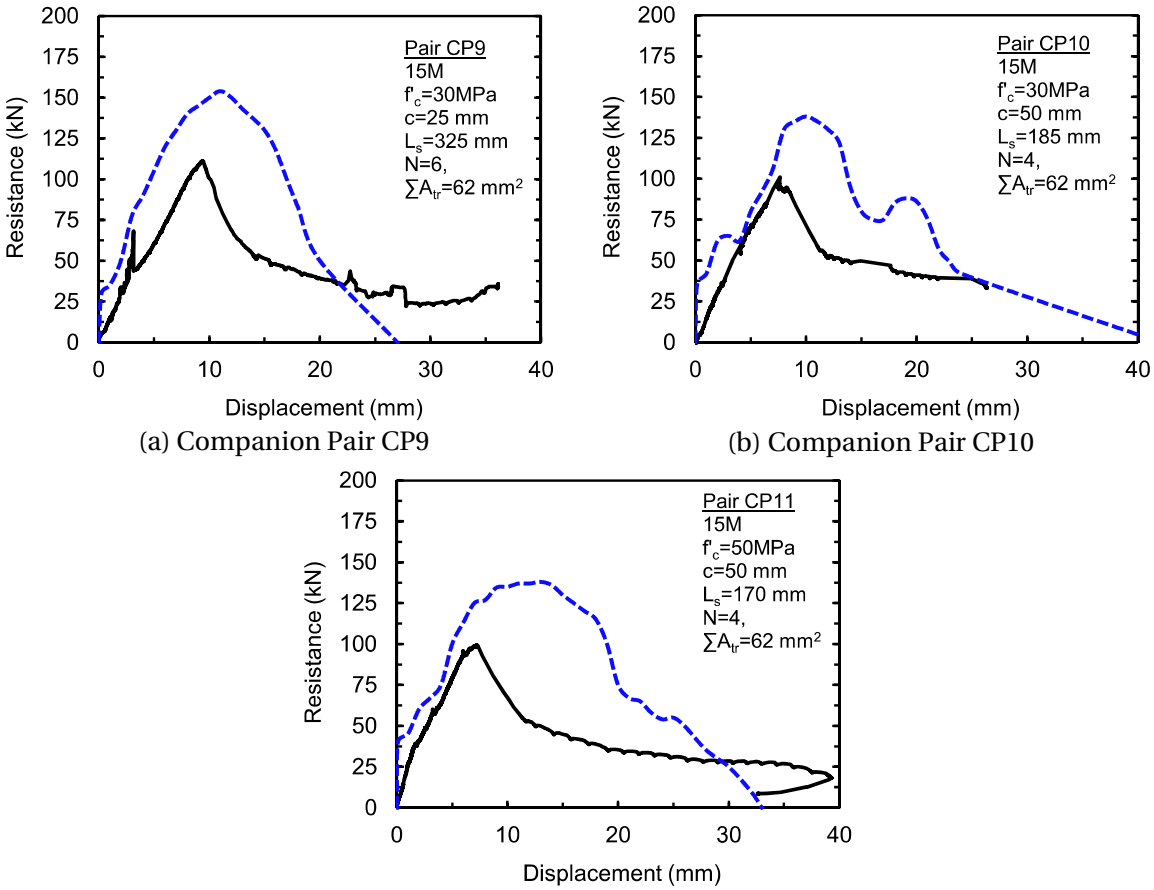

(a) Companion Pair CP9

(b) Companion Pair CP10

(c) Companion Pair CP11

Figure 4.14: Comparison of low and high strain rate member response for lap splices constructed with 15M rebar and confined by transverse reinforcement.

Figure 4.15: Comparison of splice damage for beams with 10M reinforcement.

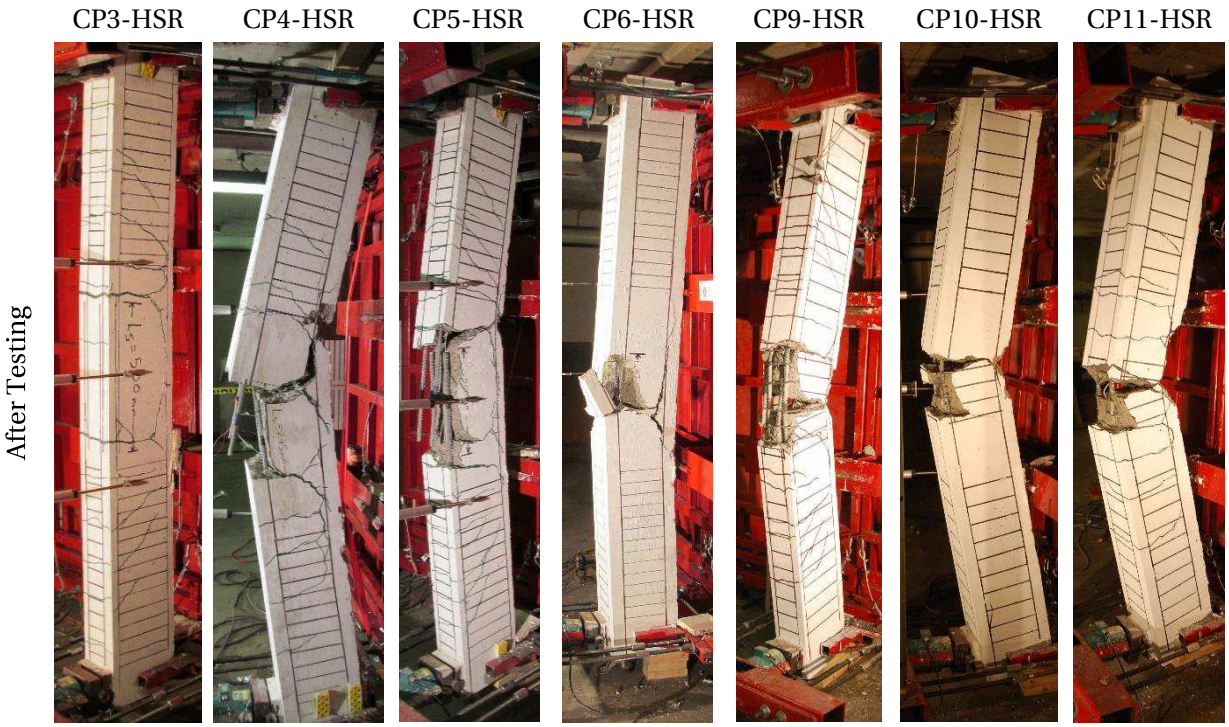

Figure 4.16: Comparison of splice damage for beams with 15M reinforcement.

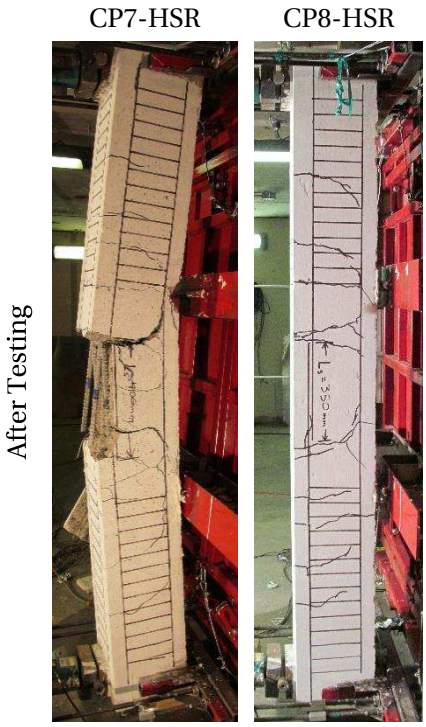

Figure 4.17: Comparison of splice damage for beams with 20M reinforcement.

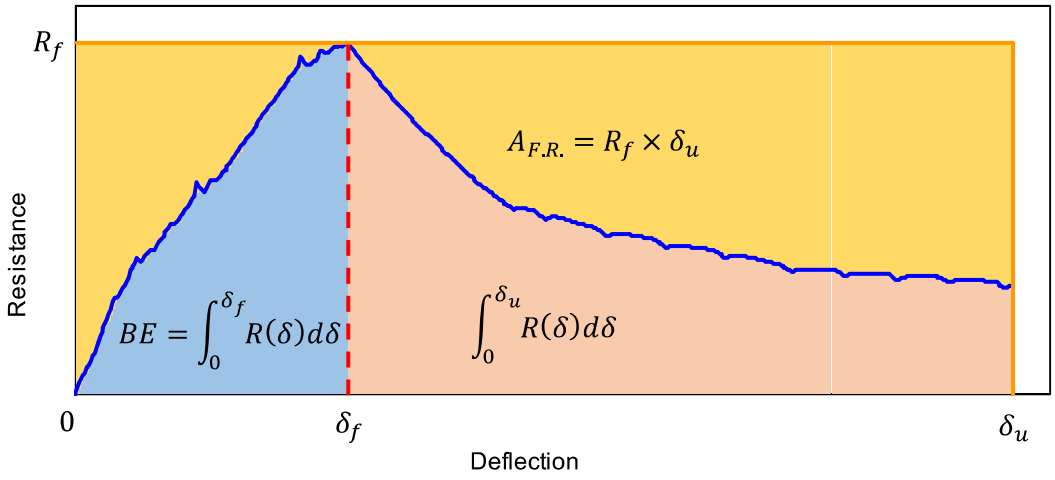

Figure 4.18: Definition of bond energy and toughness parameters (adapted from Aoude et al., 2014).

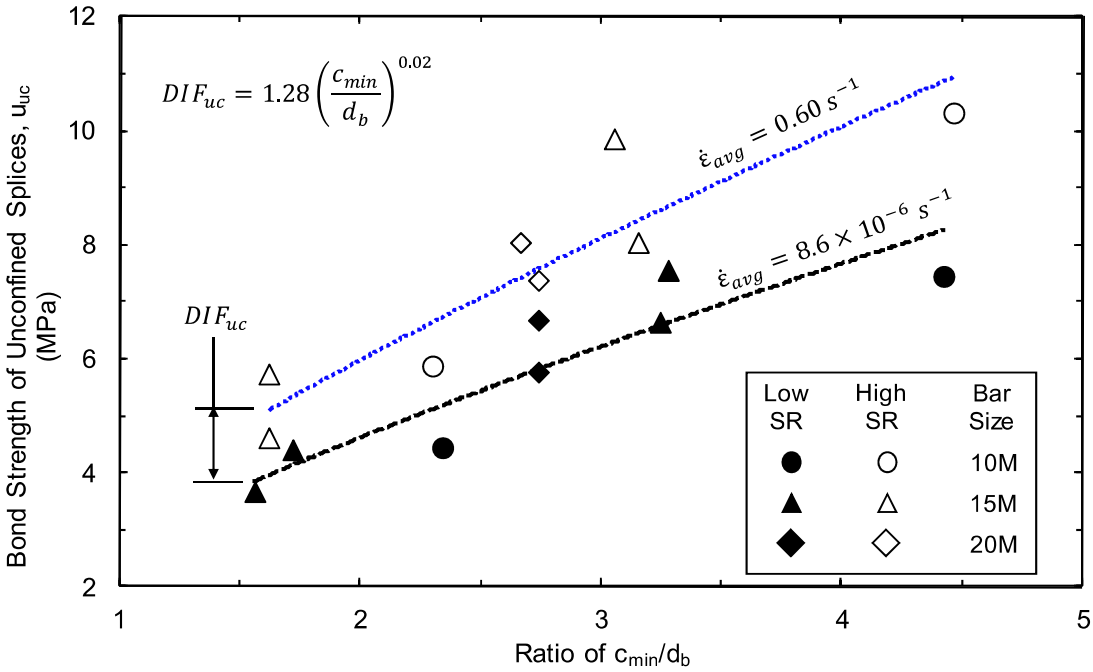

Figure 4.19: Effect of high strain rate on bond strength of splices not confined by transverse reinforcement with respect to c_{min}/d_b.

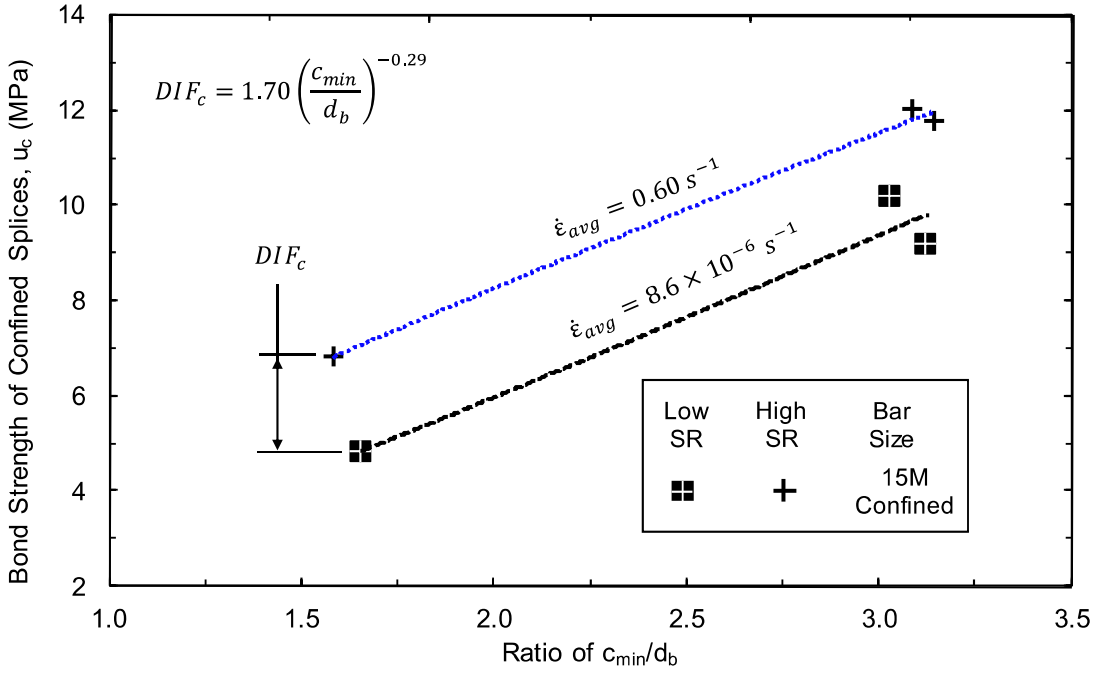

Figure 4.20: Effect of high strain rate on bond strength of splices confined by transverse reinforcement with respect to c_{min}/d_b.

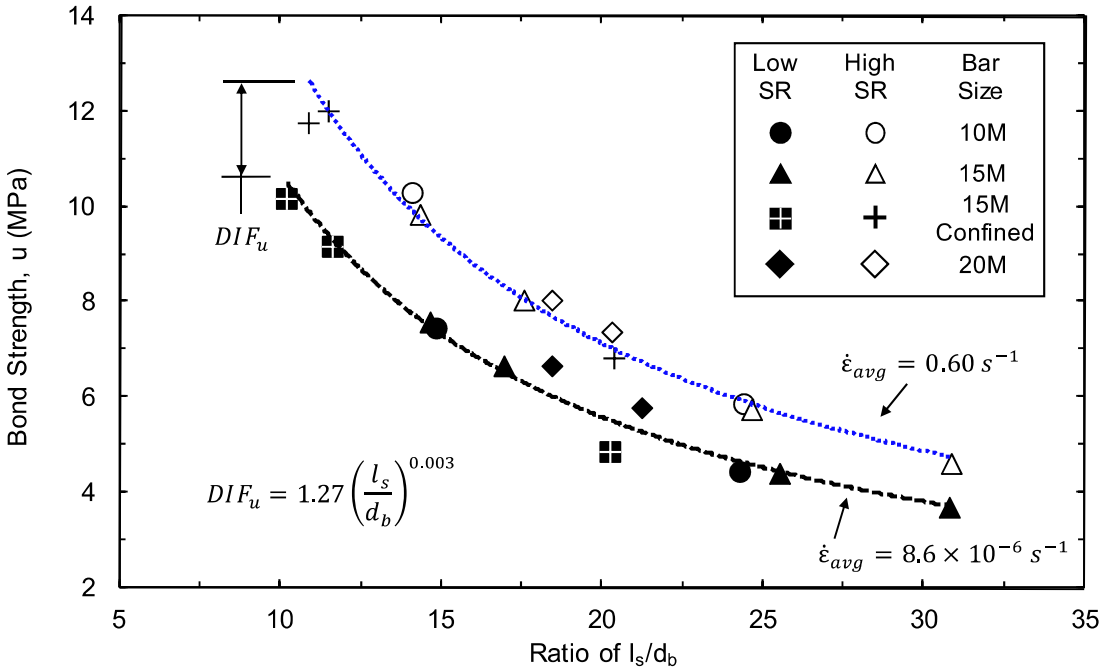

Figure 4.21: Effect of high strain rate on bond strength of splices with and without transverse reinforcement with respect to l_s/d_b.

Chapter 5

Bond Strength of Reinforced Concrete at High Strain Rates

Abstract This chapter presents a database investigation undertaken to review and correlate the results of relevant high strain rate flexural bond tests from the literature with those of this dissertation. The objective was to formulate an expression to predict dynamic bond strength as a function of the major factors known to affect bond. Although several authors have experimentally observed that bond experiences an apparent increase in strength when anchored or developed reinforcement is subjected to high strain rates, none of the aforementioned authors have correlated their own data with the results of other studies.

A database of 41 flexural bond tests, consisting of reinforced concrete lap splice beams and cantilever beam-ends, was assembled. Approximately half of the data points were obtained at low strain rates ($\dot{\varepsilon} = 10^{-6}$ s^{-1}), while the remainder were collected at high rates of strain commonly associated with protective design ($\dot{\varepsilon} = 0.1–1.0$ s^{-1}). Analysis of the database led to the development of empirical expressions describing the observed strain rate sensitivity of reinforced concrete bond. When used in conjunction with the descriptive expression for static bond strength proposed by ACI 408R, excellent predictions of high strain rate bond strength were obtained. The strain rate sensitivity of bond strength for bars not confined by transverse reinforcement was found to be proportional to bar size, and inversely proportional to an idealized concrete splitting failure plane defined by the development length and the distance between the smallest concrete cover and the centre of the developed bar. The predictive accuracy of the proposed *DIF* expressions was evaluated against the database. The results indicated that dynamic bond can be predicted with reasonable accuracy for the purposes of analysis and design of protective structures.

Keywords bond strength; high strain rate; dynamic increase factor; *DIF*; reinforced concrete.

5.1 Introduction

Reinforced concrete members are designed on the basis of composite action between two dissimilar building materials. A force transfer is required to permit equilibrium of compressive stresses resisted by concrete and tensile stresses resisted by reinforcing steel. This force transfer, known as bond, is a structural property influenced by the constituent materials, member geometry, and the presence of transverse reinforcement. A large volume of research has been published regarding the bond strength of deformed reinforcement, including a number of comprehensive studies (Orangun et al., 1977; Zuo and Darwin, 1998; 2000) that form the basis of the development length expressions in modern building codes (*e.g.* ACI 318, CSA A23.3). Studies have shown that the total bond force generated in developed or spliced reinforcement (T_b) can be decomposed into the relative contributions of concrete properties by normalizing bond with respect to compressive strength f_c' raised to a given power, the bond force developed in a bar without transverse reinforcement (T_c) and the additional bond force provided by the presence of transverse reinforcement (T_s) (ACI, 2003). Notwithstanding the ongoing intensity of bond research, the effect of high strain rates on reinforced concrete bond is a specialized topic that has been largely neglected by the research community.

Only a limited number of studies are reported for reinforced concrete bond at high strain rates. The majority of these were small-scale studies using pull-out type specimens (Shah and Hansen, 1963; Vos and Reinhardt, 1982; Yan, 1992; Weathersby, 2003; Solomos and Berra, 2010; Michal et al., 2015). A common finding of each was that bond strength was improved under dynamic loads generated by blast and impact events. Furthermore, the rate-sensitivity of bond is reported to be inversely proportional to concrete quality (Shah and Hansen, 1963; Solomos and Berra, 2010). In addition, confinement, provided by steel reinforcement or increased cover depth, results in greater bond resistance but reduced strain rate sensitivity (Weathersby, 2003; Solomos and Berra, 2010). While these findings confirm that bond strength is sensitive to strain rate enhancement, the relevance of the test results to engineering practice is severely limited as pull-out specimens are not recommended for bond testing due to an unrealistic internal stress state (ACI, 2003).

A handful of authors have investigated the effect of strain rates on reinforced concrete bond using flexural beam tests (Rezansoff et al., 1975; Toikka, 2012). From a qualitative perspective, the consensus view is that strain rate sensitivity of reinforced concrete bond characteristics of flexural members is generally similar to that obtained using pull-out tests. However, existing studies considered only a narrow range of material strengths, cover spacing, and reinforcement sizes meaning that there are too few data to generalize about the influence of high strain rates on bond strength for the type of structures commonly found in practice. As a result, no expression has been developed that can estimate the strain rate sensitivity of bond strength for design or assessment of

protective reinforced concrete structures. Currently, reinforced concrete structures are being designed to resist blast and impact loads with no more than a rudimentary understanding of how bond strength is influenced by high strain rate load conditions.

This chapter describes a numerical study whose objective was to investigate and quantify the increase in bond strength which occurs when reinforced concrete members are subjected to high strain rate loads. A database was developed and populated with test data from lap splice and cantilever beam-end bond tests. The database was populated with a total of 41 test data from three sources, of which 23 were obtained at an average high strain rate of 0.60 s^{-1} with the remainder being static reference tests. Using the high strain rate bond database, empirical expressions were developed to obtain a dynamic increase factor (DIF) applied to reinforced concrete bond as a function of the contributions of concrete properties, structural characteristics, and presence of transverse reinforcement. The predictive accuracy of the proposed DIF expressions were evaluated against the database. The results indicated that dynamic bond can be predicted with reasonable accuracy for the purposes of analysis and design of protective structures. To the best knowledge of the author, the collection of test results and associated analysis presented in this chapter provide the first direct comparison of low and high strain rate bond strength observed in large-scale flexural members.

5.2 High Strain rate Bond Database

5.2.1 Database Overview

A database of high strain rate bond tests was constructed. The purpose of the database was to study the effect of dynamic loads on the bond strength of developed and spliced reinforcement. Experimental data described in this thesis was supplemented with additional data from the literature. A "low" strain rate test was one with strain rates ($\dot{\varepsilon}$) of 10^{-5} to 10^{-6} s^{-1}, while a "high" strain rate was one where $\dot{\varepsilon}$ exceeded 0.1 s^{-1}.

To be included in the database, tests had to satisfy three criteria to ensure a fair comparison between data sets:

(i) Tests must have been performed on specimens which experienced an internal flexural stress state (*e.g.* beams and beam-ends);
(ii) Only tests which resulted in failure of the specimen were included; and
(iii) High strain rate data must correspond to strain rates in the range of $0.1 \leq \dot{\varepsilon} \leq 10\ s^{-1}$.

The first criterion severely restricted the pool of studies considered for inclusion in the database since most of the relevant literature focused on pull-out behaviour. The second criterion limited the database to bond conditions corresponding to ultimate strength. The third criterion served two

purposes, one of which was to ensure that the data represented strain rates commonly accepted for protective design (Department of Defense, 2008). Furthermore, by ensuring the data was collected over a narrow band of strain rates, any differences due to the rate sensitivity of material properties were minimized due to the logarithmic nature of the variation in DIF. As a result, it was assumed that any DIF applied to bond strength was constant over the range of strain rates considered in the database. The cantilever beam-end (Chapter 3) and lap splice beam tests (Chapter 4) presented in this thesis were included in the database. An exhaustive literature search was conducted to identify relevant studies which met the necessary criteria. However, only the research by Rezansoff et al. (1975) satisfied the conditions.

5.2.2 Database Structure

The database was comprised of a total of 41 entries, with 32 tests reported for bars not confined by transverse reinforcement (presented in Table 5.1) and an additional 9 tests for bars confined by transverse reinforcement (presented in Table 5.2). Of the total number of tests, 23 were subjected to dynamic loads representing an average strain rate of 0.60 s^{-1}, while the remaining 18 static tests correspond to an average strain rate of 10^{-5} s^{-1}.

To facilitate direct comparison of static and dynamic data, the database was structured with companion tests grouped together in adjacent rows. The specimen nomenclature used in the source literature was adopted with the addition of a tag to indicate loading rate (*i.e.* "HSR" for high strain rate and "LSR" for static tests). The cross-sectional dimensions and construction details of the developed reinforcement were provided for each specimen, including beam width (b) and height (h), bottom cover (c_b), side cover (c_{so}), ½ the clear splice spacing (c_{si}), the length of the spliced or developed reinforcement (l_d), the number of spliced bars (n), the number of transverse stirrups or ties within l_d (N), and the total area of the stirrups or ties crossing a potential splitting plane adjacent to reinforcement being developed ($\sum A_{tr}$).

Values for compressive strength (f_c') and reinforcement yield stress (f_y) were tabulated in the database. For the LSR series of tests, these values were the static data reported in the source literature. For the case of HSR series of tests, the material properties provided have been scaled to account for the apparent increase in strength due to rate effects. A dynamic increase factor (DIF_{f_c}) was applied to f_c' according to the CEB Model Code equation (CEB-FIP, 1993), given below:

(5.1)
$$DIF_{f_c} = \begin{cases} \left(\dfrac{\dot{\varepsilon}}{30 \times 10^{-6}}\right)^{1.026\alpha_s} & \text{for } \dot{\varepsilon} \leq 30\ s^{-1} \\ \gamma_s \left(\dfrac{\dot{\varepsilon}}{30 \times 10^{-6}}\right)^{\frac{1}{3}} & \text{for } \dot{\varepsilon} > 30\ s^{-1} \end{cases}$$

where

$$\log \gamma_s = 6.156\alpha_s - 2$$

$$\alpha_s = 1/(5 + \frac{9f_c}{10})$$

Similarly, the reinforcement yield stress for the HSR series was appropriately scaled following the expressions proposed by Malvar and Crawford (1998a) for a dynamic increase factor applied to the yield (DIF_{f_y}) and ultimate (DIF_{f_u}) strengths, respectively.

$$DIF_{f_y} = \left(\frac{\dot{\varepsilon}}{10^{-4}}\right)^{0.074-0.040f_y/414} \tag{5.2}$$

$$DIF_{f_u} = \left(\frac{\dot{\varepsilon}}{10^{-4}}\right)^{0.019-0.009f_y/414} \tag{5.3}$$

where Eq. (5.2) and (5.3) are valid for $10^{-4}\ s^{-1} \leq \dot{\varepsilon} \leq 225\ s^{-1}$ and for $f_y \leq$710 MPa.

Test results were provided for each database entry, including the moment at failure (M_f), strain rate ($\dot{\varepsilon}$), and the measured stress in the reinforcement (f_s^t). If reinforcement stress at failure was not explicitly provided in the source literature, it was obtained by converting strain measurements into stresses using the appropriate low or high strain rate stress-strain relationship. In addition to experimental data, several calculated quantities were also listed in the bond database. These include the calculated stress in the reinforcement at failure (f_s^{cal}) and total bond force (T_b). The force T_b developed in the spliced reinforcement was computed based on the calculated stress f_s^{cal} at bond failure and the nominal area of continuous reinforcement in the splice (A_b).

5.2.3 Sectional Analysis to Obtain Splice Steel Stress

Of the calculated quantities, the most critical was f_s^{cal} which was used to compute T_b. The work of Zuo and Darwin (1998) demonstrated that the moment-curvature method provides the most realistic prediction of bar stresses, when compared with transformed section (linear elastic analysis) and strength methods (stress block). Therefore, the majority of stresses at failure shown in Table 5.1 and Table 5.2 were computed using the moment-curvature method. However, the strength method was used in cases where sectional analysis could not satisfactorily predict the target failure moment.

Non-linear material stress-strain relationships were used in the moment-curvature analysis. The stress-strain behaviour of concrete at low and high strain rates was modeled using the base curve for concrete in compression proposed by Thorenfeldt et al., (1987), illustrated in Figure 5.1 (a). The calibration constants developed by Porasz (1989) were used to establish model parameters. As recommended by ACI 408R (2003), the tensile strength of concrete was ignored in the sectional analysis.

Whenever possible, steel stress-strain relationships obtained from low strain rate tensile coupon tests were used in the sectional analysis. When coupon test data was not available, the idealized reinforcing steel model described by Jacques et al. (2012) was used. This stress-strain relationship, shown in Figure 5.1 (b), consisted of two linear segments to describe the elastic and post-yield behaviour of steel, and a parabolic function to describe the effect of strain hardening. For the purposes of the analysis, the strain hardening stress (f_{sh}) was set equal to the yield stress (f_y) at a strain $\varepsilon_{sh} = 0.01$, and the ultimate stress (f_u) was $1.25f_y$ at a rupture strain (ε_u) of 0.015. By eliminating the post-yield plateau, the idealized stress-strain relationship can be modified to suit the behaviour of 10M reinforcement which does not typically exhibit a strain plateau after yield. For the case of high strain rate moment-curvature computations, the experimental and idealized stress-strain relationships were modified to include dynamic increase factors applied to yield strength [Eq. (5.2)] and ultimate strength [Eq. (5.3)]. A linear variation in DIF was applied to stress values between yield and ultimate.

The accuracy of the analysis was assessed by comparing computed f_s^{cal} against measured f_s^t developed in the steel. Bar stresses were computed using the moment-curvature or strength methods for 35 beams of the total 41 tests in the database. The moment-curvature method was used for 32 of these predictions, while the strength method was used on 3 occasions. Tests that relied on the strength method were flagged in the database. The average ratio of f_s^t/f_s^{cal} for all tests was 0.97 with a coefficient of variation (COV) of 4%. The ratio of f_s^t/f_s^{cal} varied between a maximum of 1.06 and a minimum of 0.88. No statistical difference was found between ratios of f_s^t/f_s^{cal} for low and high strain rate tests, as well as those for splices with and without transverse reinforcement. The results indicated that bar stresses calculated using the moment-curvature and strength methods correlated well with those obtained from strain readings.

5.2.4 Review of Test Data

The following provides a brief overview of the construction details and test results of the bond data included in the database. A justification for inclusion of the tests in the database is also provided.

Lap splice beam tests described in Chapter 4

The results of all 22 large-scale reinforced concrete lap splice beams described in Chapter 4 were included in the bond database. An additional 3 lap splice beams of the CP0 series, intended as commissioning tests not covered in Chapter 4, were also included in the database. Details of the CP0 series are provided in Appendix B.

The companion pairs of beams were established to study the effect of varying cover depth, concrete strength, bar diameter, and presence of transverse reinforcement on high strain rate bond

strength. The range of parameters considered in the tests included: cover depths of 25 mm, 38 mm, and 50 mm; concrete strength of 30 MPa or 50 MPa.; three longitudinal rebar sizes (10M, 15M, 20M), and; splices with or without transverse reinforcement. The specimens were divided into twelve companion pairs, denoted by the prefix "CP" followed by a unique numeric identifier. The suffixes "-LSR" and "-HSR" were used to denote whether a specimen was subjected to low or high strain rate testing, respectively.

Figure 5.2 shows the geometry and reinforcement of a typical splice beam. Pertinent details of each of the specimens are tabulated Table 5.1 (a),(b) and Table 5.2 (a). Companion pairs CP1-CP11 were constructed as shown in Figure 5.2 (a), and were doubly reinforced with two bottom cast contact tension lap splices per specimen. Figure 5.2 (b) illustrated the construction of beams in companion pair CP0, each singly reinforced with one bottom cast contact tension lap splice. The nominal bottom, c_b, and side covers, c_{so}, to the spliced reinforcement for CP1-CP11 were equal to ensure neither a bottom or side splitting failures would be favored. The spliced length of all beams was proportioned to experience a bond splitting failure of the cover concrete prior to flexural failure. The splices for companion pairs CP0 through CP8 were unconfined, while the splices for companion pairs CP9 through CP11 were confined by double leg closed ϕ6.3 mm smooth steel wires with spacing (s_2) not greater than $d/4$. Dynamic test specimens were subjected to a single destructive shock tube test.

Static tests were performed at strain rates on the order of 10^{-6} to 10^{-5} s^{-1}, while high strain rates in the range of 0.28 to 1.13 s^{-1} were generated using a shock tube.

It was found that the strength and stiffness of reinforced concrete beams was significantly improved when subjected to dynamic loading. The peak resistance of the beams increased by an average of 30%, while the average bond energy (area under the resistance curve) increased by 160%, relative to the reference static conditions. A comparison of the general behaviour of the specimens showed that the underlying flexural response and nature of the bond splitting failure was not affected by dynamic loads, despite a clear increase in member strength and stiffness attributed to strain rate enhancement. The use of transverse reinforcement to confine spliced regions led to significant improvements in post-peak strength and splice toughness compared to splices without transverse reinforcement at all rates of loading. Regardless of strain rate, the bond strength of splices with and without transverse reinforcement was found to increase in proportion to the ratio of c_{min}/d_b, and decrease in proportion to l_s/d_b. Without exception, the high strain rate bond strength was greater than the corresponding low strain rate values, yielding an average DIF to be applied to bond strength of 1.28.

Rezansoff et al. (1975) – Lap splice beam tests

Rezansoff et al. (1975) performed drop-weight impact tests on 20 doubly reinforced concrete beams constructed with tension lap splices, with and without transverse reinforcement. Impact tests generated strain rates of approximately 0.2-0.3 s^{-1} in the tensile reinforcement. The simply supported beams were 380 mm tall by 430 mm wide and subjected to four-point bending. Primary flexural reinforcement consisted of 2 - #8 (25M) bars lapped in the constant moment region. The main parameter of study was splice length (457, 762, and 1067 mm) and the presence of transverse reinforcement. The bottom and side covers were 38 and 83 mm, respectively, and concrete strength was approximately 20 MPa. Four series of impact tests were conducted producing failure in either one cycle (IO series), in three to five cycles of incrementally increasing magnitude (IM series), and in unidirectional cyclic (C series) or reversed cyclic (CR series) impact loading. The static companion tests (RS series) were originally conducted by Ferguson and Breen (1966).

The authors reported that splice capacity was dependent on the rate of loading affecting strain rate related enhancements in the apparent strength of concrete and steel. For example, dynamic increase factors for the yield strength of steel were reported to be in the range of 1.16 to 1.29, while the tensile strength of concrete experienced an estimated increase between 35% and 65%. It was also observed that the dynamic moment capacity of the beams was always larger than the static moment capacity, with increases in moment capacity as high as 1.74 reported. The performance of beams with splice stirrups was superior to beams without transverse reinforcement. Beams with transverse reinforcement in the spliced region sustained deflections at least twice as large as those for beams without transverse reinforcement. The authors concluded that, based on their findings, splice lengths proportioned using static design requirements should be sufficient to resist dynamic loads. However, the authors did not explicitly report on the static and dynamic bond characteristics (*e.g.* bond strength) and limited their assessment to flexural member response.

Table 5.1 (c) and Table 5.2 (b) show the Rezansoff dataset for unconfined splices and splices with transverse reinforcement, respectively. A total of 4 static and 8 dynamic tests were included, covering all of the RS, IO and IM series of tests. All of the tests in the IM series were included despite the fact that the progressively increasing load regime would have induced some damage into the sample. However, the failure moments recorded for similar specimens in both the IO and IM series were similar. As a result, any potential effect of accumulated damage affecting the results of the IM tests was ignored. It is also important to note that specimens IO-30-T and IM-30-T (both with 762 mm splice length with transverse reinforcement), and IO-42 and IM-42 (with 1067 mm splice length without transverse reinforcement) experienced flexural failures rather than bond failures. Although the ultimate strength of the splice was not attained, these data points were included in the database as they provide a lower bound estimate of the dynamic strength of reinforced concrete bond.

The C and CR series were excluded from the database as many of these tests consisted of over a dozen impact loads, the cumulative effects of which would undoubtedly have influenced the results.

Cantilever beam-end tests described in Chapter 3

A pilot study was conducted using cantilever beam-end specimens constructed according to ASTM A944 (2010) and subjected to high strain rate bond tests. A total of 14 beam-ends were constructed, with 7 having a bonded length l_b = 200 mm, and the remainder having l_b = 400 mm. None of the developed bars were confined by transverse reinforcement and f_c' for the specimens was 50 MPa. Strain rates in the range of 0.1 to 1.2 s^{-1} were obtained. Under low strain rates, all beam-ends failed by cover splitting regardless of the development length. At high strain rates, l_b = 200 mm beam-ends failed by splitting, while l_b = 400 mm beam-ends experienced rupture of the reinforcing bar. Ultimate and elastic bond strengths, as well as bond stiffness, increased under rapid loading.

Table 5.1 (d) lists the beam-end bond tests included in the database. The average results of all low and high strain rate beam-ends with l_b = 200 mm, referred to by the name "BE-200 AVG" were included. All specimens with l_b = 200 mm experienced a bond splitting failure, yielding an average DIF to be applied to ultimate bond force of 1.47, at a strain rate of 0.50 s^{-1}. The data for BE-14, with l_b = 400 mm, experienced rupture of reinforcement corresponding to an ultimate bond force DIF of 1.33 at a strain rate of 1.20 s^{-1}.

5.3 Analysis of Test Results

The results of the lap splice tests, supplemented by data from other sources, were analyzed to establish correlations between high strain rates and bond strength.

Table 5.1 lists the test data for bars without transverse reinforcement. The average strain rate for the 14 static tests was 1.1×10^{-5} s^{-1}, and 0.59 s^{-1} for the 18 high strain rate tests. Several observations were noted regarding the stresses developed in the spliced reinforcement. Steel stresses f_s^{cal} exceeded the static yield strength in 8 of 14 low strain rate tests, and exceeded the theoretical dynamic yield strength in 5 of 18 high strain rate tests. Greater steel stresses were developed in all companion pairs as a result of high strain rate loading. The average f_s^{cal} for all low strain rate tests was 453 MPa, which exceeds the typical design yield of 400 MPa by 13%. The average f_s^{cal} for high strain rate tests was 566 MPa.

5.3.1 Bars without Transverse Reinforcement

Considerable research has shown that the influence of concrete quality on static bond is best represented by the compressive strength f_c' raised to a given power (ACI, 2003). Therefore, following the work of Darwin et al. (1996), the term $f_c'^{1/4}$ was adopted to account for the influence of concrete properties on bond. This assumption was assumed valid for low and high strain rates provided

appropriately selected material $DIF's$ were employed. In making this assumption, the author acknowledges that it is unclear "whether compressive strength or tensile strength is the more relevant property (…) because both show a similar dependence on loading rate" (Vos and Reinhardt, 1982). Nonetheless, the relative strain rate sensitivity exhibited by tensile and compressive strengths should be minimal due to the logarithmic nature of dynamic material properties coupled with the narrow range of loading rates considered in this study.

Since the tests contained no transverse reinforcement, the total bond force is equal to the bond force developed without transverse reinforcement, $T_b = T_c$. Accordingly, the effect of structural characteristics on bond strength was evaluated by normalizing T_c with respect to $f_c'^{1/4}$. Absolute values of bond strength ($T_c = f_s^{cal} A_b$), as well as normalized bond strength ($T_c/f_c'^{1/4}$), for bars without transverse reinforcement were computed. The term $T_c/f_c'^{1/4}$ represents the effect of structural characteristics and geometry on bond strength. For low strain rate tests, normalization was performed with the static compressive strength of concrete, f_c'. For the case of high strain rate tests, the dynamic compressive strength of concrete $DIF_{f_c} \times f_c'$ was used, where DIF_{f_c} was obtained using Eq. (5.1).

Figure 5.5 shows the influence of strain rate on the variation of $T_c/f_c'^{1/4}$ with respect to $l_s(c_{min} + 0.5d_b)$. Test results were grouped according to bar size and loading rate. The term $l_s(c_{min} + 0.5d_b)$ provides a measure of the influence of the structural characteristics and geometry on bond strength. It represents the area of an idealized failure plane spanning from the most critical cover dimension to the centre of a developed bar extending over the entire developed length. The results shown in Figure 5.5 include the 19 lap splice tests not confined by transverse reinforcement of this study, the 9 unconfined splice beam tests by Rezansoff et al. (1975) and an additional 4 cantilever beam-end tests by presented in Chapter 3.

The results suggest that an increase in the area of the idealized splitting failure plane, or increasing bar diameter, will increase the stress developed in the reinforcement. In other words, increases in $T_c/f_c'^{1/4}$ occur due to increases in one or some combination of l_s, c_{min}, and d_b. This trend was observed to occur regardless of strain rate. However, high strain rate values of bond strength were always greater than corresponding low strain rate strengths.

Absolute values of $T_c/f_c'^{1/4}$, shown in Figure 5.5, suggest that the bond strength resulting from structural characteristics were dependent on strain rate. A dynamic increase factor DIF_{T_c} was introduced to quantify this increase. This term reflects the apparent increase in normalized bond force for bars not confined by transverse reinforcement subjected to rapid strain rates. The scale factor DIF_{T_c} was taken as the ratio of the dynamic normalized strength $T_c/f_c'^{1/4}$ to the corresponding static value. Values of DIF_{T_c} are listed in Table 5.1 and plotted in Figure 5.6.

Several trends are discernible from the data. First, larger bars experienced greater values of DIF_{T_c} under rapid strain rates than smaller bars. This contradicts Shah and Hansen (1963) whose results indicated that the strain rate sensitivity of bond is inversely proportional to reinforcement diameter. The aforementioned authors conducted pull-out tests on short bonded lengths, which could explain this discrepancy. Secondly, failure planes with greater values of $l_d(c_{min} + 0.5d_b)$ yielded lower values of DIF_{T_c}. This suggests that the strain rate sensitivity of bond is reduced as the area of the bond splitting failure plane increases for all sizes of reinforcement. This finding was consistent with Weathersby (2003) who found that while absolute bond resistance was improved with increasing cover depth, the relative increase in bond resistance at high strain rates was reduced. This finding was also consistent with Solomos and Berra (2010) who reported that increasing bonded length was less effective at increasing bond resistance under dynamic conditions. Lastly, the results shown in Figure 5.6 suggest that there exists an upper limit on the value of $l_d(c_{min} + 0.5d_b)$ for which no increase in DIF_{T_c} is observed. This of course assumes that negative values of DIF_{T_c} are not possible.

A two-variable regression analysis was performed to generate an expression describing the strain rate sensitivity of bars not confined by transverse reinforcement using the results listed in Table 5.1. Given the influence of the failure plane area and bar size on bond strength noted in Figure 5.6, the regression parameters selected were $l_d(c_{min} + 0.5d_b)$ and A_b. The results of the regression analysis gave the following expression for DIF_{T_c}:

$$DIF_{T_c} = -1.20 \times 10^{-5} l_d(c_{min} + 0.5d_b) + 1.04 \times 10^{-3} A_b + 1.18 \geq 1.00 \text{ for } 0.1 \leq \dot{\varepsilon} \leq 1.2 \text{ s}^{-1} \quad (5.4)$$

This expression is valid for deformed reinforcement developed or spliced in flexural members subjected to strain rate loading in the range of $0.1 \leq \dot{\varepsilon} \leq 1.2$ s^{-1} and having concrete with a static compressive strength between $18 \leq f_c' \leq 50$ MPa. The values of DIF_{T_c} shall not be taken less than 1.0, and Eq. (5.4) is valid only for describing the rate-sensitivity of bond strength normalized with respected to $f_c'^{1/4}$.

The regression model presented in Eq. (5.4) was used to generate contour lines of DIF_{T_c} over a range of $l_d(c_{min} + 0.5d_b)$ values for common bar sizes. These contour lines are illustrated alongside the experimental data in Figure 5.6. All of the contour lines have negative slope and reasonably match the trends evident in the experimental data. Within the range of measured values used in the regression analysis, Eq. (5.4) can reasonably predict the rate-sensitivity of $T_c/f_c'^{1/4}$ with a coefficient of determination $R^2 = 0.87$ and standard error of regression $S = 0.04$ based on 18 observations.

The physical interpretation of Eq. (5.4) is understood as follows. First, increasing the size of the reinforcement, reflected in the A_b term, increases the strain rate sensitivity of normalized bond force. This is attributed to lateral inertial confinement provided by the cover concrete when the bar is

subjected to dynamic loading. Inertia forces in the concrete are activated by radial acceleration of the cover due to wedging action of the rebar lugs against the surrounding concrete. The greater strain rate sensitivity exhibited by increasing reinforcement size can be explained by the activation of a greater degree of wedging, and hence greater confinement provided by the inertial resistance of the cover. The strain rate sensitivity of normalized bond force for bars not confined by transverse reinforcement was also found to be inversely proportional to the idealized bond splitting failure plane $l_d(c_{min} + 0.5d_b)$. Although increasing the area of the idealized failure plane, either by providing increased development length, cover, or bar size, did yield greater total bond force, it resulted in a decrease in strain rate sensitivity. This is attributed to the fact that bond stresses are not uniformly distributed over the developed length, and that bond failures are localized and incremental. Finally, the normalized bond force obtained for bars not confined by transverse reinforcement when subjected to dynamic loading was always greater than the corresponding static bond force. Therefore, the strain rate sensitivity of bond was always greater than or equal to unity. This indicates that there is an upper limit on the idealized crack splitting failure plane beyond which normalized bond force exhibited no strain rate sensitivity.

5.3.2 Bars with Transverse Reinforcement

The presence of transverse reinforcement improves bond strength by limiting the development of splitting cracks in the spliced region (Zuo and Darwin, 1998). Passive confining pressures, generated by the transverse reinforcement due to wedging action of the bars, resist lateral expansion of concrete due to splitting. Darwin et al. (1996) proposed a combined variable $t_r t_d N A_{tr}/n$ to describe the contribution of transverse reinforcement on total bond strength. Parameters t_r and t_d, characteristics inherent to a particular type of rebar, account for the wedging action of the lugs against the surrounding substrate. Larger rebar sizes (resulting in greater values of t_r) and more aggressive deformation patterns (resulting in greater values of t_d) generate greater values of T_s. The parameter NA_{tr}/n represents the effective quantity of transverse reinforcement mobilized to resist splitting failure along a critical plane. Research has shown that increasing one or any combination of reinforcement size, relative rib ratio, or quantity of transverse reinforcement will lead to greater increases in T_s due to increased wedging action (Darwin et al., 1996). For bars confined by transverse reinforcement, $f_c'^{3/4}$ was found to best represent the effect of concrete strength on bond strength due to transverse reinforcement (Zuo and Darwin, 1998).

The increase in total bond force due to the presence of transverse reinforcement cannot be measured directly. Therefore, it was computed as the difference $T_s = T_b - T_c$, where $T_b = f_s^{cal} A_b$ was obtained through experiments and the contribution T_c was computed following the descriptive expression developed by ACI Committee 408R (2003), shown below:

(5.5) $$T_c = [1.43 l_d (c_{\min} + 0.5 d_b) + 57.4 A_b] \left(\frac{0.1 c_{max}}{c_{min}} + 0.9 \right) {f_c'}^{1/4}$$

where: A_b is the bar area (mm^2); f_s is the steel stress at failure (MPa); f_c' is the compressive strength of concrete (MPa); l_d is the development or splice length (mm); c_{min} is the minimum of c_b or c_s (mm); c_b is the bottom cover to the bar being developed or spliced (mm); c_s is the minimum of c_{so} and c_{si} + 6.35 (mm); c_{so} is the side cover to the bar being develop or spliced (mm); c_{si} is ½ of the clear bar spacing (mm); c_{max} is the maximum of c_b and c_s (mm); d_b is the bar diameter (mm).

ACI Committee 408R also developed an expression to predict the additional bond force developed due to the contribution of transverse reinforcement (T_s):

(5.6) $$T_s = \left(8.9 t_r t_d \frac{N A_{tr}}{n} + 558 \right) {f_c'}^{3/4}$$

where R_r is the relative rib ratio, approximately equal to 0.8 to 0.9 h_r/s_r (ACI, 2003); h_r is the reinforcement rib height (mm); s_r is the reinforcement rib spacing (mm); t_r is the effect of relative rib area on T_s ($9.6R_r + 0.28$); t_d is the effect of bar size on T_s ($0.03d_b + 0.22$); N is the number of transverse stirrups or ties within l_d; A_{tr} is the area of each stirrup or tie crossing a potential splitting place adjacent to reinforcement being developed (mm^2), and; n is the number of bars being developed or spliced.

Test data for bars with transverse reinforcement are listed in Table 5.2, including total bond force T_b, the additional bond force due to transverse reinforcement $T_s = T_b - T_c$, where T_c was computed using Eq. (5.5). Dynamic increase factors DIF_{f_c} [Eq. (5.1)] and DIF_{T_c} [Eq. (5.4)] were incorporated into the expression for T_c to account for the strain rate sensitivity of concrete properties and splice geometry on bond strength of bars not confined by transverse reinforcement.

Shown in Table 5.2 are values of T_s normalized with respect to ${f_c'}^{3/4}$ (or $\left[DIF_{f_c} \times f_c'\right]^{3/4}$ for high strain rate tests) to remove the influence of concrete properties on bond provided by transverse reinforcement. As expected, the high strain rate data for the "CP" series of tests, described in Chapter 4, showed an increase in $T_s/{f_c'}^{3/4}$ compared with corresponding static results. However, the high strain rate data for the Rezansoff series of tests showed a *decrease* in normalized bond force $T_s/{f_c'}^{3/4}$ when compared against static results. This divergence is attributed to the fact that IM-30-T and IO-30-T, subjected to dynamic loading, experienced a flexural beam failure rather than a splice failure which occurred for the static baseline test, RS-30-T. Therefore, the apparent decrease in splice strength was attributed to the fact that splices were not stressed to their ultimate condition. As a result, the proceeding discussion on the effect of high strain rates on bars with transverse reinforcement excludes the Rezansoff data set.

Figure 5.7 shows the influence of strain rate on the variation of $T_s/f_c'^{3/4}$ for splices confined with transverse reinforcement with respect to $t_r t_d NA_{tr}/n$. The parameter $t_r t_d NA_{tr}/n$ reflects the degree of confinement provided by transverse reinforcement as well as the contribution of the wedging action of rebar deformations. As expected, high strain rate values of $T_s/f_c'^{3/4}$ were consistently greater than corresponding low strain rate values. Unexpectedly however, both low and high strain rate $T_s/f_c'^{3/4}$ showed no consistent variation with respect to degree of confinement. It was anticipated that the additional strength provided by transverse reinforcement would be proportional to increases in the degree of confinement. For example, under low strain rate conditions, the ACI 408R expression in Eq. (5.6) predicts an increase in the normalized bond force of 26% over the range of $t_r t_d NA_{tr}/n$ reflected in Table 5.2 for the CP-series of lap splice beam tests. The results in Figure 5.7 show no discernible trend, with the deviation between observed and expected behaviour likely due to variations consistent with such a small sample size.

A dynamic increase factor (DIF_{T_s}) was introduced to account for the apparent increase in the contribution to normalized bond force provided by transverse reinforcement. Values of DIF_{T_s} are listed in Table 5.2, with relative increases ranging from 1.24 for CP9, 1.15 for CP10, and 1.01 for CP11 obtained at an average strain rate of 0.45 s^{-1}.

Given the small number of data and the lack of a clear trend governing the rate sensitivity of $T_s/f_c'^{3/4}$, a constant value of $DIF_{T_s} = 1.14$ is proposed. This dynamic increase factor is valid for 15M deformed reinforcement having a relative rib ratio $R_r \approx 0.056$ confined by transverse reinforcement in flexural members subjected to strain rate loading in the range of $\dot{\varepsilon} = 0.45$ s^{-1} and having concrete with a static compressive strength between $36.9 \leq f_c' \leq 45.2$ MPa. The value of DIF_{T_s} is only valid for values of T_s normalized with respect to $f_c'^{3/4}$.

The singular value of DIF_{T_s} was developed based on a small number of tests for a narrow range of NA_{tr}/n, and a single bar size with a constant value of R_r. Although the results indicate that T_s does experience some level of strain rate enhancement, the limited size of the dataset precludes any further in-depth discussion on effect of t_r, t_d and NA_{tr}/n on the high strain rate response of $T_s/f_c'^{3/4}$. Further research is required to confirm and expand upon these findings.

5.3.3 Evaluation of Descriptive Expressions

Analysis of the test data indicated that the strain rate sensitivity of total bond can be decomposed into the relative effects of material properties (based on the assumed relationship for DIF_{f_c}), contribution to bond force of a bar without transverse reinforcement (DIF_{T_c}), and the contribution due to the presence of transverse reinforcement (DIF_{T_s}). The significance of this observation was assessed through a prediction of the bond strength of the tests listed in Table 5.1 and Table 5.2 for

splices without and with transverse reinforcement, respectively. The descriptive expression for bond force developed by ACI 408R given in Eqs. (5.5) and (5.6) formed the basis of the predictions. Although several other descriptive expressions are available in the literature (Orangun et al., 1977; Zuo and Darwin, 2000), the ACI 408R expression was selected as it yields superior predictions of bond strength over a wide range of structural configurations and concrete strengths (ACI, 2003).

The values of bond strength calculated using ACI 408R (T_b^{408R}) were compared against the corresponding strength obtained from tests (T_b^t). The ACI 408R expression was used to calculate low strain rate bond strength without modification. For the case of high strain rate bond strength, T_{db}^{408R}, the ACI expressions were modified to incorporate DIF_{T_c} and DIF_{T_s} proposed in this chapter. Incorporating the effect of strain rate sensitivity yields:

$$T_{db}^{408R} = T_{dc} + T_{ds} \tag{5.7}$$

$$T_{dc} = DIF_{T_c} \times [1.43 l_d (c_{\min} + 0.5 d_b) + 57.4 A_b] \left(\frac{0.1 c_{max}}{c_{min}} + 0.9 \right) {f'_{dc}}^{1/4} \tag{5.8}$$

$$T_{ds} = DIF_{T_s} \times \left(8.9 t_r t_d \frac{N A_{tr}}{n} + 558 \right) {f'_{dc}}^{3/4} \tag{5.9}$$

where DIF_{T_c} was computed using Eq. (5.4), DIF_{T_s} was taken as 1.14, and the dynamic strength of concrete f'_{dc} was calculated by applying a dynamic increase factor DIF_{f_c} to f'_c following Eq. (5.1)

A comparison between the experimental and calculated bond strengths are plotted in Figure 5.9. Comparisons are grouped according to strain rate and bar size. Not surprisingly, the results show that the ACI 408R expression can reasonably predict the low stain rate bond strength of deformed reinforcement, with and without transverse reinforcement, with a high degree of accuracy. For the 18 low strain rate tests, the average ratio of experimental strength to calculated strength (T_b^t/T_b^{408R}) was 1.04 with a coefficient of variation of 9% at an average strain rate of $\dot{\varepsilon} = 1.3 \times 10^{-5}$ s^{-1} with maximum and minimum ratios of 1.18 and 0.85, respectively. This confirms that the ACI 408R expression can reasonably predict the low strain rate bond strength for the reinforced concrete members contained in the database.

Similarly, the modified ACI 408R bond expression incorporating DIF_{f_c}, DIF_{T_c} and DIF_{T_s} yield accurate predictions of high strain rate bond strength. For the 23 high strain rate tests included in the database, the average ratio of T_b^t/T_b^{408R} was 1.02 with a coefficient of variation of 10% at an average strain rate of $\dot{\varepsilon} = 0.56$ s^{-1} with maximum and minimum T_b^t/T_b^{408R} ratios of 1.23 and 0.87, respectively.

Based on the above, it is not unreasonable to conclude that the analysis approach used to develop dynamic increase factors applied to bond phenomenon can generate acceptable predictions of high strain rate bond strength for the flexural members of this study. Similarly,

acceptable predictions of high strain rate bond strength for reinforcement with transverse reinforcement were made, although the data set is of limited size. The results indicate that the ACI 408R bond expression can serve as a basis for predicting high strain rate bond strength when modified to incorporate strain rate increase factors.

5.4 Application to Protective Design

5.4.1 Canadian Blast Standard, CSA S850

In protective design of reinforced concrete structures, loss of bond is, to say the least, a catastrophic failure mode. The current CSA S850 code provisions (Canadian Standards Association, 2012) for blast-resistant reinforced concrete design impose strict detailing requirements to reduce the likelihood of bond failure. These requirements include: (i) increasing the quantity and type of transverse reinforcement confining a developed bar; (ii) limiting the number of bars which can be spliced at any location along the length of a structural member, and; (iii) restricting members with lap splices to a flexural response mode. Currently, the development and splice length of reinforcement subjected to dynamic loads are proportioned by ignoring any apparent increase in bond strength due to strain rate phenomenon (Canadian Standards Association, 2012). This deliberate conservatism reflects the lack of a comprehensive understanding of the behaviour of bond between reinforcing steel and concrete in large-scale structural elements subjected to dynamic loads (Department of Defense, 2008). However, the results of this study and others clearly demonstrate that bond is improved under high strain rates. This should be reflected in protective design without sacrificing life safety objectives.

The basic development and splice length expression used in Canada traces its origin to the work of Orangun et al. (1977). Based on their work and the work of others, the design expression for development length l_d according to CSA A23.3 (Canadian Standards Association, 2014) is given as

$$l_d = \frac{1.15 k_1 k_2 k_3 k_4}{(d_{cs} + K_{tr})} \frac{f_s}{\sqrt{f_c'}} A_b \tag{5.10}$$

$$K_{tr} = \frac{A_{tr} f_{yt}}{10.5 s n} \tag{5.11}$$

where: k_1 is a bar location factor, equal to 1.0 for bottom-cast splices; k_2 is a coating factor, equal to 1.0 for uncoated reinforcement; k_3 is a concrete density factor, equal to 1.0 for normal-density concrete; k_4 is a bar size factor, equal to 0.8 for 20M and smaller bars; A_b is the area of reinforcing bar being spliced; d_{cs} is the lesser of the smallest concrete cover depth to the centre of the bar or two-thirds the centre-to-centre spacing of the bars; A_{tr} is the total cross-sectional area of reinforcement that is within spacing s and crosses the potential plane of bond splitting through the reinforcement being developed; f_{yt} is the yield strength of transverse reinforcement; s is the maximum centre-to-

centre spacing of transverse reinforcement within the spliced region; n is the number of bars being developed or lap-spliced along a plane of splitting.

The expressions for DIF_{T_c} and DIF_{T_s} were developed using regression parameters normalized with respect to $f_c'^{1/4}$ and are not compatible with the CSA A23.3 development length equation. Therefore, a re-examination of the test data was necessary to develop an expression for DIF applied to bond compatible with CSA A23.3 and CSA S850.

Two assumptions were made in the re-examination which were not present in the original analysis. First, in the Canadian standard, the effect of concrete properties on bond are assumed to be proportional to $\sqrt{f_c'}$. While research has shown that $f_c'^{1/4}$ gives a better representation of the effect of concrete properties on bond, particularly for high strength concrete, $\sqrt{f_c'}$ is adequate provided $f_c' \leq 64$ MPa (ACI, 2003). Second, the strain rate sensitivity of the additional bond force provided by transverse reinforcement is ignored. An analysis of the 342 bond tests for bars with transverse reinforcement listed in the ACI Committee 408 Database 10-2001 (ACI, 2003) indicates that, on average, the presence of transverse steel accounts for approximately 25% of the total bond force. Therefore, ignoring any potential strain rate increase affecting this relatively small portion of the total bond is conservative. From a practical standpoint, another justification for ignoring the rate sensitivity of transverse steel is that the limited sample size makes it difficult to generalize its associated high strain rate behaviour.

The results of the re-examination were expressed in terms of the parameter DIF_{l_d}. This parameter represents the apparent increase in the bond force for bars not confined by transverse reinforcement subjected to rapid strain rates with the effect of concrete properties proportional to $\sqrt{f_c'}$. Values of bond strength T_c in Table 5.1 were normalized with respect to $\sqrt{f_c'}$. Values of DIF_{l_d} were computed as the ratio between high and low strain rate $T_c/\sqrt{f_c'}$. A two-variable regression analysis was performed to generate an expression for DIF_{l_d}. The regression parameters were $l_d d_{cs}$ and A_b. The variable d_{cs} is equivalent to $c_{min} + 0.5d_b$ and has been used to remain consistent with CSA A23.3. The results of the regression analysis gave the following expression for DIF_{l_d}:

$$DIF_{l_d} = -1.1 \times 10^{-5} l_d \mathrm{d_{cs}} + 8.5 \times 10^{-4} A_b + 1.1 \geq 1.0 \text{ for } 0.1 \leq \dot{\varepsilon} \leq 1.2 \text{ s}^{-1} \tag{5.12}$$

This expression is valid for deformed reinforcement developed or spliced in flexural members subjected to strain rate loading in the approximate range of $0.1 \leq \dot{\varepsilon} \leq 1.2$ s^{-1} and having concrete with a static compressive strength between $18 \leq f_c' \leq 50$ MPa. The values of DIF_{l_d} shall not be less than 1.0, and Eq. (5.12) is only valid for describing the rate-sensitivity of bond strength normalized with respected to $\sqrt{f_c'}$.

Setting all k-factors equal to unity, inserting DIF_{f_c} and DIF_{l_d} to account for rate effects, and rewriting the CSA A23.3 development length expression to extract the dynamic bond force $T_b^{A23.3}$ yields the following:

$$T_b^{A23.3} = DIF_{l_d} \times \frac{l_d(d_{cs} + K_{tr})}{1.15}\sqrt{DIF_{f_c} \times f_c'} \tag{5.13}$$

A comparison of bond force predicted using the CSA A23.3 design expression in Eq. (5.13) with the test data are shown in Figure 5.10. All test data, including splices with and without transverse reinforcement, were included in the comparisons. The limitation imposed on $(d_{cs} + K_{tr}) \leq 2.5d_b$ was relaxed for the comparisons as pull-out failures did not occur during the tests. For low strain rate tests, the average ratio of $T_b^t/T_b^{A23.3}$ was 1.16 with a COV of 22% based on 17 samples, with a maximum ratio of 1.83 and minimum of 0.77. For high strain rate tests, the average ratio of $T_b^t/T_b^{A23.3}$ was 1.20 with a COV of 24% based on 21 samples, with a maximum ratio of 1.98 and minimum of 0.81. Compared with ACI 408R, the CSA A23.3 expression modified for high strain rate bond strength under-predicts bond and exhibits significantly greater scatter. However, these results are not unreasonable when applied to design of protective structures as they produce conservative results.

5.4.2 Recommendations for Protective Design

For the purposes of protective design following the requirements of CSA S850 (Canadian Standards Association, 2012), it is recommended that the basic dynamic development length l_{dd} for a deformed bar subjected to high strain rate stresses be computed using the following expression

$$l_{dd} = \frac{1.15k_1k_2k_3k_4}{DIF_{l_d}(d_{cs} + K_{tr})}\frac{S_{f_y}}{\sqrt{S_{f_c'}}}A_b \geq 300 \text{ mm} \tag{5.14}$$

where: S_{f_y} and S_{f_c}' are dynamic design strengths of steel and concrete, respectively. Solution to Eq. (5.14) requires an iterative approach as DIF_{l_d} is itself a function of l_{dd}. No dynamic increase factor should be applied to the strength of transverse reinforcement f_{yt} in the term K_{tr} as yielding of transverse reinforcement is unlikely to occur. Furthermore, detailing requirements specified in CSA S850 should be satisfied.

The value of l_{dd} obtained from Eq. (5.14) is valid only for the load combination for ultimate limit states design of blast-loaded structures, $1.0D + 0.5L + 0.25S + 1.0B$. Development lengths required for all other load combinations (*e.g.* static, wind, earthquake) should be verified separately and the most critical value selected for design.

Figure 5.11 shows a comparison of low- and high-strain rate experimental development lengths compared against those calculated using DIF_{l_d} incorporated into the CSA A23.3 design expression presented in Eq. (5.12). The results demonstrated that the proposed dynamic development length

expression can conservatively predict the development length of the test specimens included in the database. This suggests that for the purposes of design or assessment of protective structures, the dynamic development length expression in Eq. (5.14) could be used with an acceptable level of accuracy. Alternatively, the ACI 408R descriptive expression for bond force, incorporating detailed values of DIF_{T_c} and DIF_{T_s}, could be used to obtain a greater level of precision in predictions of high strain rate bond strength.

5.5 Summary and Conclusions

A database of high strain rate bond tests containing 41 reinforced concrete flexural tests was constructed. Approximately half of the data points were obtained at low strain rates ($\dot{\varepsilon}$ =10^{-6} s^{-1}), while the remainder were collected at high rates of strain commonly associated with protective design ($\dot{\varepsilon}$ =0.1–1.0 s^{-1}). Analysis of the database led to the development of empirical expressions describing the observed strain rate sensitivity of reinforced concrete bond. The study can be summarized as follows:

1. The bond strength of bars with and without transverse reinforcement was always increased under high strain rates.
2. Bond tests included in the database showed an average increase in bond force T_b of 1.31 at an average strain rate of 0.58 s^{-1}.
3. The strain rate sensitivity of bond force due to concrete properties (DIF_{f_c}) was assumed to be proportional to improvements in the dynamic compressive strength of concrete f'_{dc} to the exponent $1/4$.
4. The strain rate sensitivity of bond force normalized with respect to concrete properties was divided into two components, each affected by rapid loading: improvements to the bond force developed without transverse reinforcement, and to improvements in the additional bond force provided by transverse reinforcement.
5. The strain rate sensitivity of normalized bond force for bars not confined by transverse reinforcement (DIF_{T_c}) was proportional to bar area A_b, and inversely proportional to an idealized failure plane defined by the development length and the distance between the smallest concrete cover and the centre of the developed bar $l_s(c_{min} + 0.5d_b)$.
6. There is an upper limit on the area of the idealized crack splitting failure plane beyond which normalized bond force exhibited no strain rate sensitivity.
7. Limited test data indicates that the contribution to normalized bond force provided by transverse reinforcement (DIF_{T_s}) is sensitive to strain rate enhancement and suggests that greater relative increases in bond occur as $t_r t_d N A_{tr}/n$ increases.
8. Empirical expressions were developed for the observed strain rate sensitivity of each the components affecting bond force. When used in conjunction with the descriptive

expression for bond strength under static loads recommended by ACI 408R, good predictions of high strain rate bond strength were obtained.

9. The current CSA A23.3-14 bond and development length design expressions were modified to account for strain rate effects. These expressions were found to be more conservative than the modified ACI 408R equation, but provided conservative estimates of bond strength for design purposes.

Table 5.1: Database of specimen properties and test results for lap splices without transverse reinforcement.

Specimen Designation	f'_c* MPa	f_y* MPa	b mm	h mm	d_b mm	A_b mm^2	c_b mm	c_{so} mm	c_{si} mm	l_d mm	n	M_f kNm	$\dot{\varepsilon}$ s^{-1}	f_s^t MPa	f_s^{cal} MPa	$T_c = f_s^{cal} A_b$ kN	$T_c/f_c'^{1/4}$	DIF_{T_c} ††
(a) Commissioning lap splice beams (Appendix B)																		
CP0-LSR	45.2	470.0	150	300	16.0	200	38	59	-	500	1	36.3	3.1×10^{-5}	470	517	103.4	39.9	
CP0-HSR1	57.2	613.3					38	59	-	500		-	1.10	-	624	124.8	45.4	1.14
CP0-HSR2	57.2	613.3					38	59	-	500		-	1.10	-	631	126.2	45.9	1.15
(b)Lap splice beams (Chapter 4)																		
CP1-LSR	32.5	431.2	150	200	11.3	100	26	27	37	275	2	14.3	1.5×10^{-5}	431	457	45.7	19.1	
CP1-HSR	42.9	559.2					27	25	39	276		17.8	0.31	571	575	57.5	22.5	1.17
CP2-LSR	32.5	431.2	240	200	11.3	100	51	49	60	168	2	17.0	1.8×10^{-5}	441	468	46.8	19.6	
CP2-HSR	42.7	557.4					52	49	60	160		19.3	0.28	583	602	60.2	23.5	1.20
CP3-LSR	32.5	448.4	165	300	16.0	200	26	24	43	493	2	45.7	7.0×10^{-6}	450	462	92.4	38.7	
CP3-HSR	43.8	587.0					26	26	41	494		57.7	0.65	566	585	117.0	45.5	1.18
CP4-LSR	32.5	448.4	265	300	16.0	200	52	52	65	272	2	42.6	5.5×10^{-6}	450	458	91.6	38.4	
CP4-HSR	44.6	597.0					51	50	67	282		61.0	1.13	566	570	114.0	44.1	1.15
CP5-LSR	48.7	448.4	165	300	16.0	200	28	27	40	409	2	48.6	4.1×10^{-6}	448	485	97.0	36.7	
CP5-HSR	60.0	585.6					27	25	42	395		57.0	0.60	565	584	116.8	42.0	1.14
CP6-LSR	48.7	448.4	265	300	16.0	200	53	52	65	235	2	45.2	6.3×10^{-6}	443	467	93.3	35.3	
CP6-HSR	60.3	590.3					51	47	70	230		55.7	0.78	566	588	117.6	42.2	1.19
CP7-LSR	32.5	491.0	280	300	19.5	300	53	54	67	415	2	67.9	7.6×10^{-6}	491	491	147.3	61.7	
CP7-HSR ¶	44.1	623.4					52	55	66	397		91.1	0.80	600	623	186.9	72.5	1.18
CP8-LSR	48.7	491.0	280	300	19.5	300	53	54	67	360	2	69.0	4.3×10^{-6}	491	491	147.3	55.8	
CP8-HSR ¶	60.2	622.3					51	53	68	361		90.8	0.75	595	604	181.2	65.0	1.17
(c) Rezansoff et al. (1975) lap splice beams																		
RS-18 *(LSR)*	23.0	413.4	432	381	25.4	509	38	83	83	457	2	98.1	10^{-5}	325	327	165.5	75.6	
IM-18 (HSR)	31.6	547.6					38	83	83	457		152.5	0.20	479	503	256.1	108.0	1.43
IO-18 (HSR)	32.4	547.6					38	83	83	457		146.9	0.36	488	485	246.7	103.4	1.37
RS-30 *(LSR)*	20.9	516.8	432	381	25.4	509	39	83	83	762	2	109.6	10^{-5}	365	365	185.9	86.9	
IM-30 (HSR)	31.6	547.6					38	83	83	762		159.3	0.22	>508	526	267.5	112.9	1.30
IO-30 (HSR)	31.9	547.6					38	83	83	762		153.7	0.28	537	507	258.3	108.7	1.25
RS-42 (LSR)	18.3	516.8	432	381	25.4	509	38	83	83	1067	2	138.3	10^{-5}	454	456	231.2	111.7	
IM-42 (HSR) §	32.3	547.6					38	83	83	1067		162.7	0.23	>478	537	273.5	114.7	1.03
IO-42 (HSR) §	32.4	547.6					38	83	83	1067		159.3	0.25	524	526	267.9	112.3	1.01
(d) Catilever beam-ends (Chapter 3)																		
BE-200 AVG LSR	50.0	460.0	225	400	19.5	272	38	103	-	200	1	-	7.8×10^{-6}	395	-	107.4	40.4	
BE-200 AVG HSR	61.0	588.8					38	103	-	200		-	0.50	585	-	159.1	56.9	1.41
BE14-400 LSR	50.0	460.0	225	600	19.5	272	38	103	-	400	1	-	4.3×10^{-5}	559	-	151.9	57.1	
BE14-400 HSR	62.1	607.2					38	103	-	400		-	1.20	738	-	200.7	71.5	1.25

* Material properties for high strain rate tests multiplied by appropriate *DIF*

†† DIF_{T_c} = ratio of high strain rate $T_{dc}/f_{dc}'^{1/4}$ to comparable low strain rate value $T_c/f_c'^{1/4}$

§ Flexural failure, rather than splice failure

¶ Strength method used to obtain f_s^{cal}

Table 5.2: Database of specimen properties and test results for lap splices with transverse reinforcement.

Specimen Designation	f'_c* MPa	f_y* MPa	b mm	h mm	d_b mm	A_b mm²	c_b mm	c_{so} mm	c_{si} mm	l_d mm	n	N	$\sum A_{tr}$ mm²	M_f kNm	$\dot{\varepsilon}$ s⁻¹	f_s^t MPa	f_s^{cal} MPa	$T_b = f_s^{cal} A_b$ kN	$T_s = T_b - T_c^\dagger$ kN	$T_s/f'^{3/4}_c$	DIF_{T_s} ††
(a) Lap splice beams (Chapter 4)																					
CP9-LSR	36.9	448.4	165	300	16.0	200	25	28	39	325	2	6	62.4	40.6	1.3×10^{-5}	391	426	85.2	18.3	1.22	
CP9-HSR	48.3	588.3					24	27	40	327				57.4	0.70	557	585	117.0	27.9	1.52	1.24
CP10-LSR	36.9	448.4	265	300	16.0	200	48	52	65	187	2	4	62.4	37.2	7.4×10^{-6}	428	423	84.6	18.9	1.26	
CP10-HSR	47.3	574.1					49	50	67	185				50.4	0.32	556	571	114.2	26.1	1.45	1.15
CP11-LSR	45.2	448.4	265	300	16.0	200	49	48	69	164	2	4	62.4	37.0	6.0×10^{-6}	417	417	83.3	19.4	1.11	
CP11-HSR	55.7	574.9					53	48	69	175				50.0	0.33	514	561	112.2	22.9	1.12	1.01
(b) Rezansoff et al. (1975) lap splice beams																					
RS-30-T (LSR)	18.0	516.0	432	381	25.4	509	39	83	83	762	1	6	32.2	119.8	10^{-5}	404	400	203.6	9.1	1.04	
IM-30-T (HSR) §¶	34.8	547.6					38	83	83	762	1	6	32.2	187.6	0.23	528	575	292.6	7.1	0.50	0.48
IO-30-T (HSR) §	35.2	547.6					38	83	83	762	1	6	32.2	174.0	0.31	506	574	291.9	5.6	0.39	0.37

* Material properties for high strain rate tests multiplied by appropriate *DIF*

† T_c computed following Eq. (5.5) and incorporating appropriate *DIF* for concrete strength Eq. (5.1) and bond Eq. (5.5)

†† DIF_{T_s} = ratio of high strain rate $T_{ds}/f'^{3/4}_{dc}$ to comparable low strain rate value $T_s/f'^{3/4}_c$

§ Flexural failure, rather than splice failure

¶ Strength method used to obtain f_s^{cal}

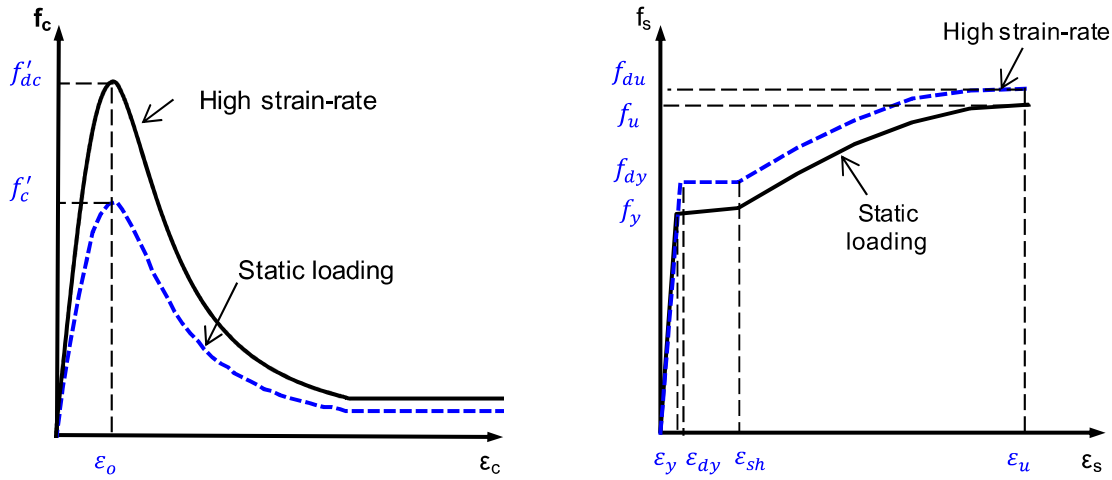

(a) Concrete (b) Reinforcing steel

Figure 5.1: Idealized stress-strain relationships.

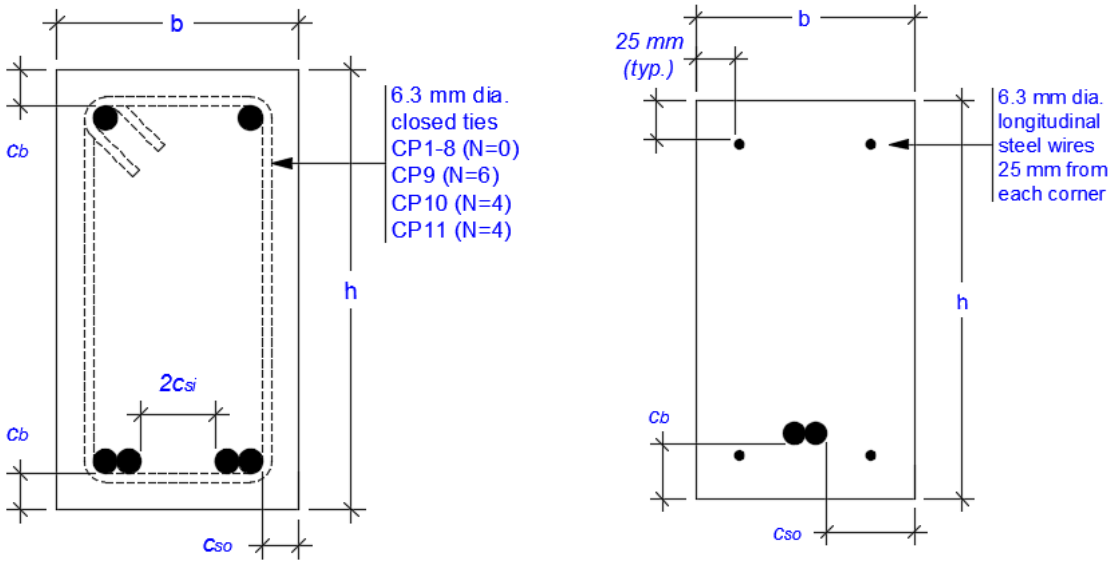

(a) Cross-section through spliced region for CP1-CP11

(b) Cross-section through spliced region for CP0

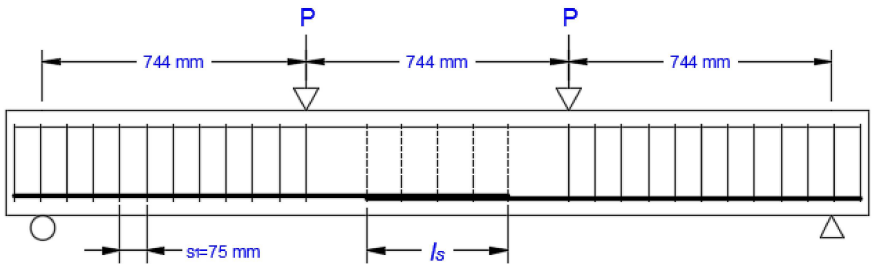

(c) Elevation view

Figure 5.2: Specimen details of the lap splice beams [Chapter 4].

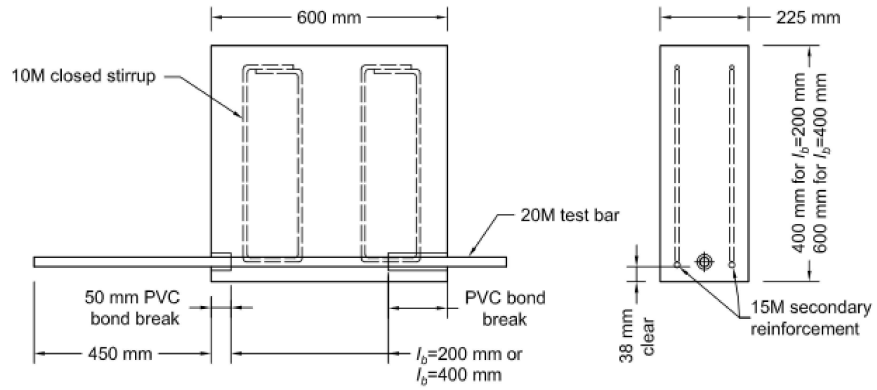

Figure 5.3: Specimens details of the cantilever beam-ends [Chapter 3].

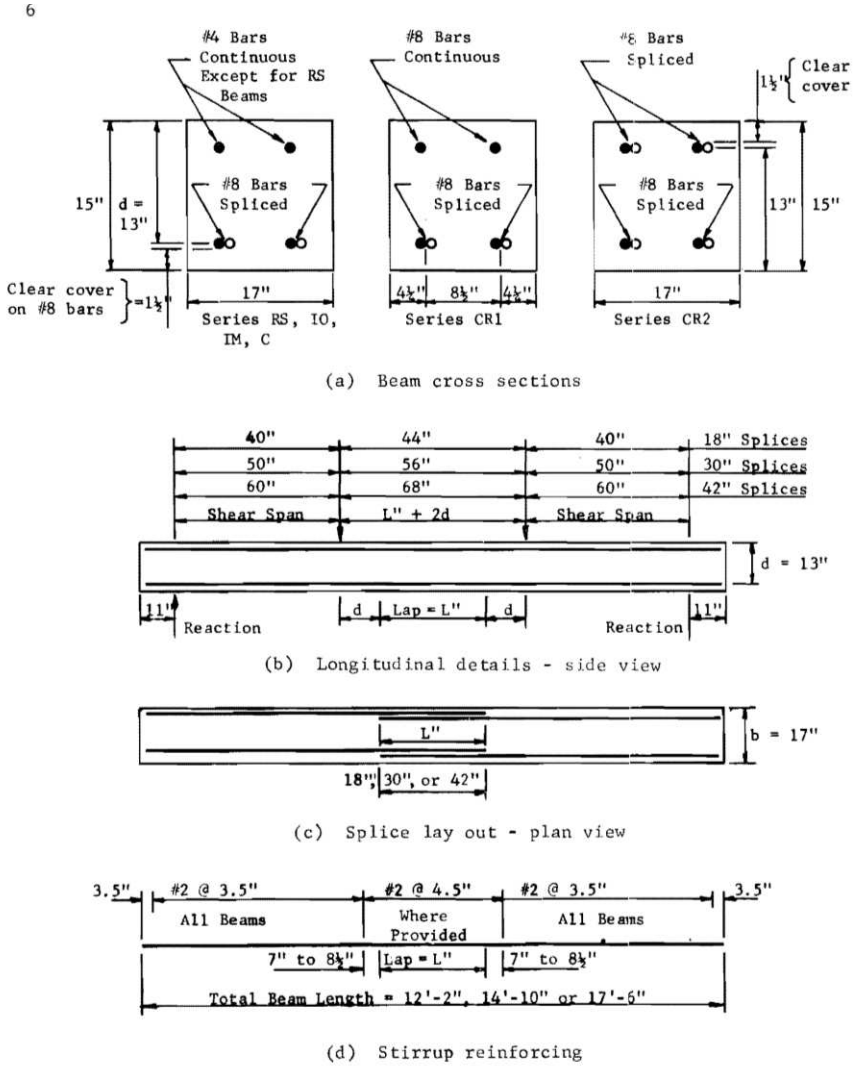

Figure 5.4: Specimen details of the lap splice beams tested by Rezansoff et al. (1975).

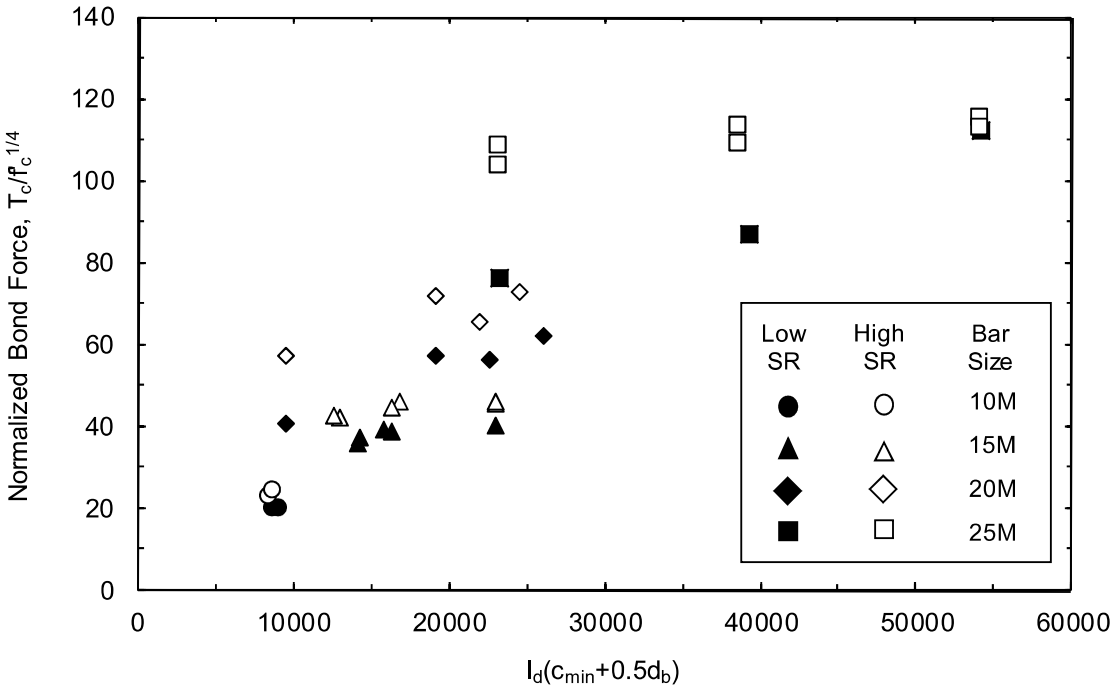

Figure 5.5: Influence of strain rate on the variation of $T_c/f_c'^{1/4}$ with respect to $l_d(c_{min} + 0.5d_b)$.

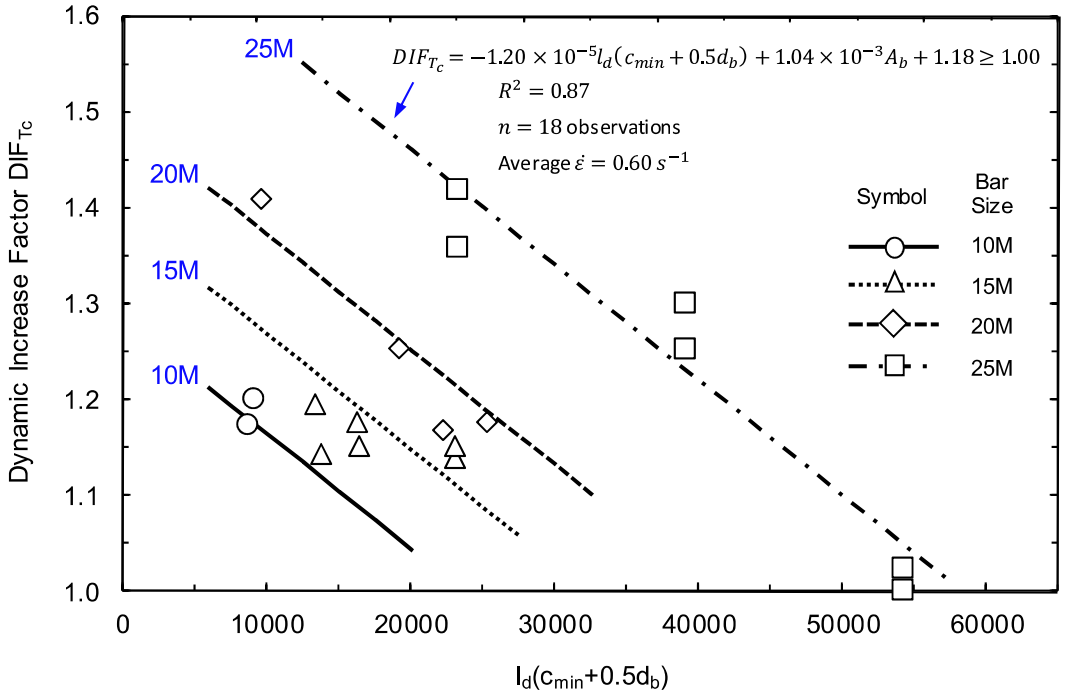

Figure 5.6: Variation of DIF_{T_c} with respect to $l_d(c_{min} + 0.5d_b)$ and rebar size.

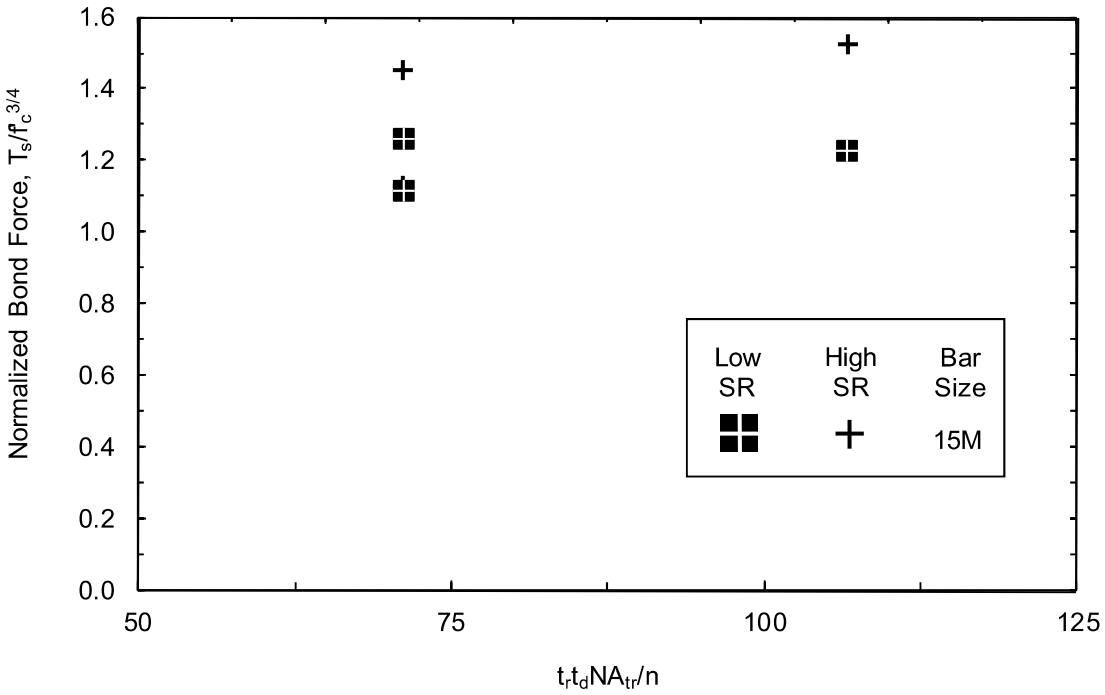

Figure 5.7: Influence of strain rate on the variation of $T_s/f_c'^{3/4}$ for splices confined with transverse reinforcement with respect to NA_{tr}/n.

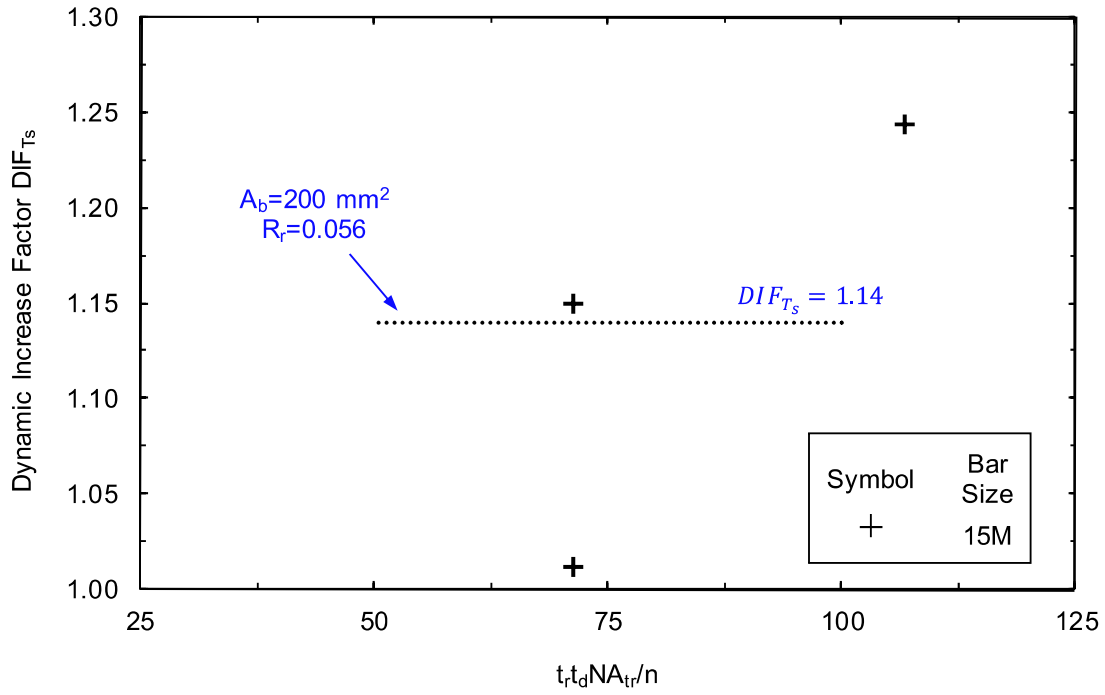

Figure 5.8: Variation of DIF_{T_s} with respect to $t_r t_d NA_{tr}/n$.

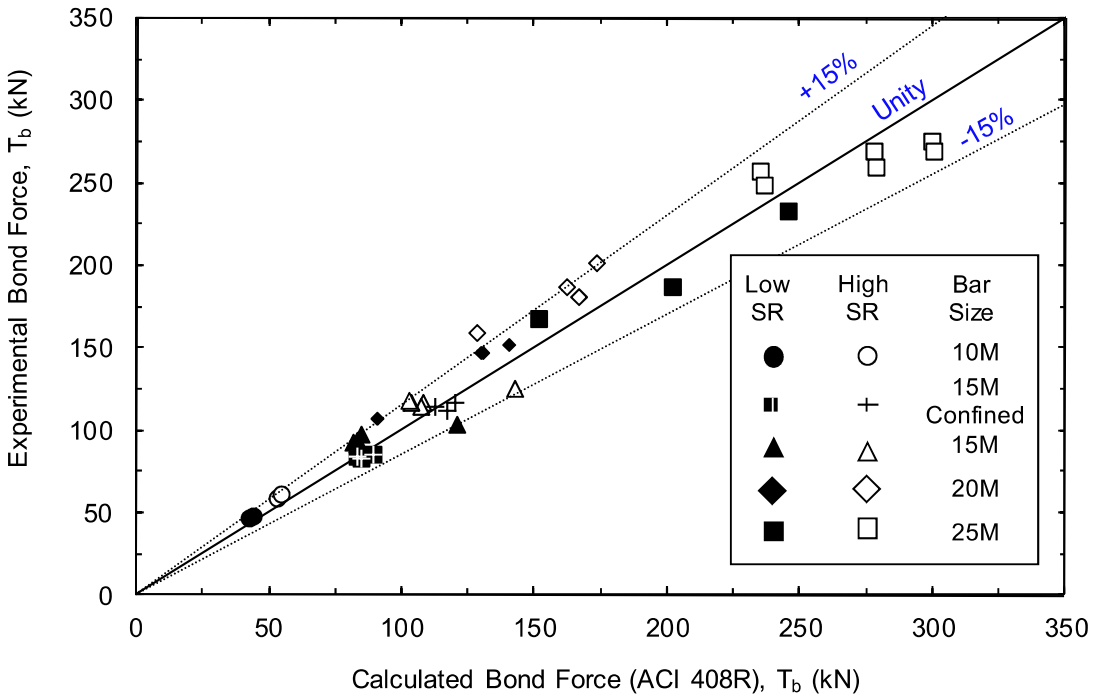

Figure 5.9: Low and high strain rate experimental bond strengths compared against those calculated using DIF_{T_c} and DIF_{T_s} incorporated into the ACI 408R descriptive expression.

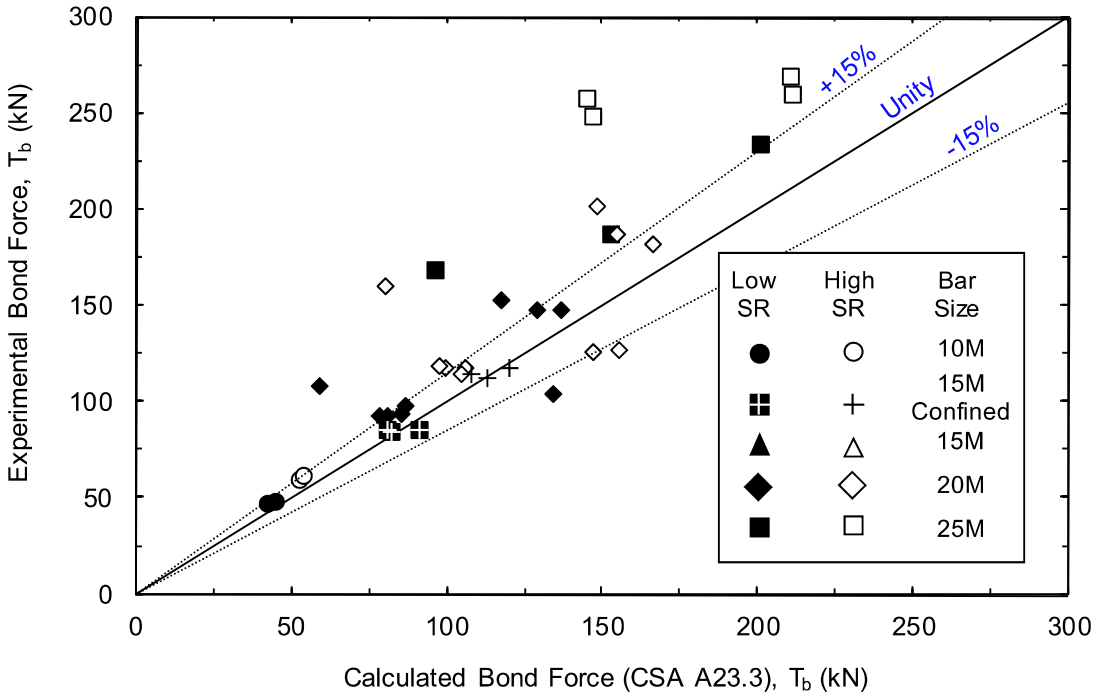

Figure 5.10: Low and high strain rate experimental bond strengths compared against those calculated using DIF_{l_d} incorporated into the CSA A23.3 design expression.

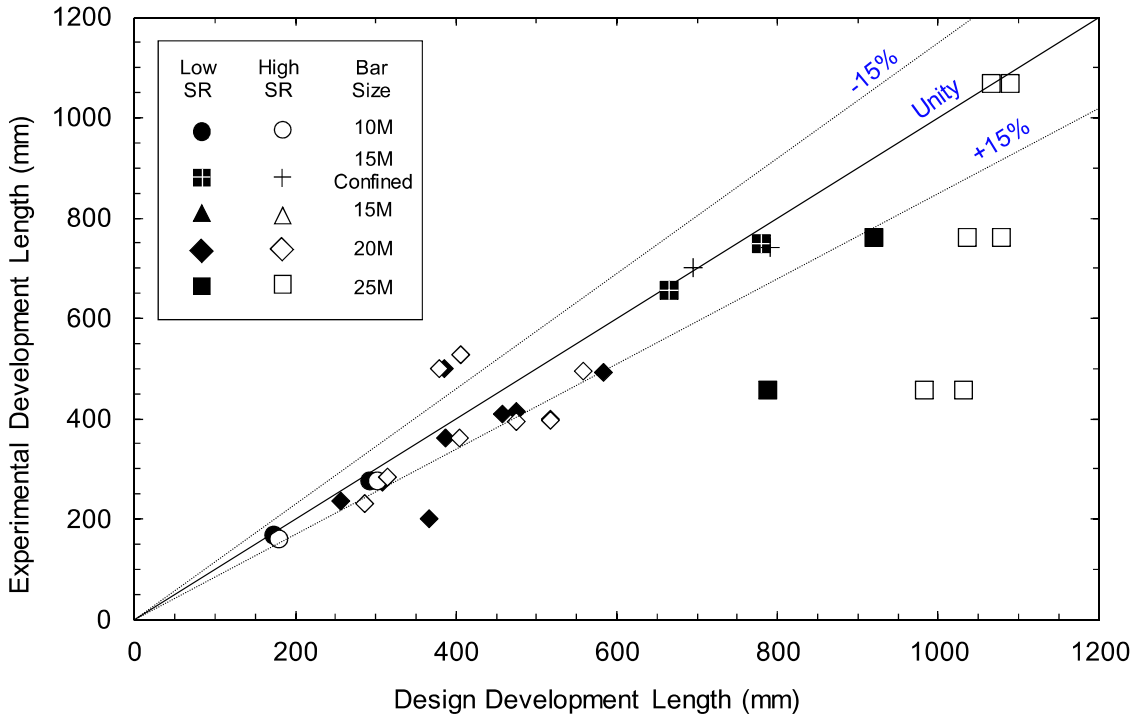

Figure 5.11: Comparison of low and high strain rate experimental development lengths compared against those calculated using DIF_{l_d} incorporated into the CSA A23.3 design expression presented in Eq. (5.12).

Chapter 6

Structural Response of Lap-Spliced RC Beams at Low and High Strain Rates

Abstract This chapter presents an analytical model developed to predict the flexural behaviour of reinforced concrete members containing tension lap splices. The proposed model incorporates the effect of reinforcement slip of the lap splice and the effect of high strain rates on bond characteristics and material properties of concrete and steel. The main advantages of the proposed model are that bond-slip phenomena are captured through the use of pseudo-material stress-strain relationships, rather than giving consideration to the continuum of reinforcement and slippage over the entire structural element. Material properties and associated dynamic increase factors (DIF) are defined using accepted formulations. A suitable bond-slip law is presented, and modified to account for the influence of strain rates on bond characteristics. Beam failure criteria are expressed in terms of a flexural failure of the member or a bond splitting failure of the splice. A comparison of the analytical predictions with experimental data demonstrated that the proposed analysis technique can reasonably predict the flexural response of beams with tension lap splices. The results also show that the model is equally applicable for use at low- and high- strain rate loading, such as those generated during blast and impact loading.

Keywords blast; high strain rates; bond; reinforced concrete; structural response; explosion simulation.

6.1 Introduction

Bond, the mechanism of force transfer between reinforcing steel and concrete, is a fundamental characteristic of reinforced concrete behaviour. This phenomenon is caused by the cumulative effect of surface friction, chemical adhesion and mechanical interlock of rebar lugs with surrounding concrete. It is affected by the material properties of steel and concrete, the surface condition of the reinforcement, and the construction and configuration of the structural element (ACI, 2003). For the purposes of design, a condition of perfect bond is assumed to exist between reinforcing steel and concrete. Generally, this premise is valid only for low load levels, prior to significant cracking of concrete (Gan, 2000). The assumption of perfect bond is no longer valid in regions of high stress transfer near cracks, where a difference in strain between steel and concrete occurs as a result of the relative displacement between the two materials. This relative displacement, known as bond-slip, can significantly alter the flexural response of reinforced concrete through a number of mechanisms, including:

1. Tension stiffening, where concrete between crack planes can carry a portion of the total tension force resisted by the section, is a bond phenomenon which causes an apparent increase in member stiffness after cracking of concrete (Bentz, 2000).
2. Anchorage slip can occur when inelastic strains penetrate into adjoining structural members causing extension and/or slippage of reinforcement within concrete joints, producing significant rigid body end rotations that increase the lateral deformation of the element (Alsiwat and Saatcioglu, 1992).
3. Force transfer between adjacent reinforcing bars in a tension lap splice can generate extension and/or slippage of the bars within the splice. Otherwise referred to as lap splice slip, the relative movement of rebar within the splice has the effect of softening the section and increasing the flexibility of the spliced member (Pimanmas and Thai, 2011).

Considerable research over the past century has led to a thorough and exhaustive understanding of the factors affecting bond strength in reinforced concrete structures for the case of slowly applied static loading (ACI, 2003). However, little effort has been directed towards establishing the influence of short duration, dynamic loads on bond characteristics. Strain rate ($\dot{\varepsilon}$), defined as the rate of change of strain with respect to time, varies from 10^{-5} s^{-1} for static loading and up to 10^{3} s^{-1} for hard impact and blast events (Bischoff and Perry, 1991).

Much of the limited research that has been published on dynamic bond confirms that bond strength is improved under high strain rate dynamic loading (Rezansoff et al., 1975; Vos and Reinhardt, 1982; Yan, 1992). The degree of bond strength improvement is related to the construction details of the developed or spliced reinforcement. For example, dynamic bond strength is inversely proportional to concrete quality (Shah and Hansen, 1963; Solomos and Berra, 2010). In addition,

confinement, provided by steel reinforcement or increased cover depth, results in greater bond resistance but reduced strain rate sensitivity (Weathersby, 2003; Solomos and Berra, 2010). However, since the majority of these studies were conducted using pull-out type bond specimens, extrapolating the results to establish the anticipated level of dynamic bond strength in realistically proportioned reinforced concrete structures is not possible.

The Chemical, Biological, Radiological, Nuclear and Explosives (CBRNE) Research and Technology Initiative (CRTI) recently funded a project (CRTI 06-0150TD) to investigate the vulnerability of building components to bomb damage and develop risk assessment tools to improve Canada's response preparedness and capabilities against blast threats. As part of this study, the University of Ottawa led a research initiative to establish the effect of high strain rates on the bond between reinforcing steel and concrete in large-scale structures containing developed and spliced reinforcement (described in Chapter 3 and Chapter 4, respectively) The results showed that, on average, the total bond force developed in anchored/spliced reinforcement increased by a factor of 1.28 at strain rates on the order of 0.1-1.0 s^{-1}. The strain rate sensitivity of bond was found to be proportional to the dynamic strength of concrete, the size of reinforcement, and the presence of transverse reinforcement, in addition to being inversely proportional to an idealized crack splitting failure plane defined by the development length and the distance between the smallest concrete cover and the centre of the developed bar. However, the results demonstrated that the assumption of perfect bond between steel and concrete is not entirely applicable. It was observed that the flexural strength and stiffness of lap-spliced reinforced concrete beams is markedly less than that predicted using conventional flexural theory. This observation, consistently noted for all beams regardless of strain rate, suggests that accounting for the bond-slip response of flexural reinforcement and the surrounding concrete can be critical when structures are subjected to extreme loads generated during blast and impact events.

Considerable effort has been directed towards developing analytical methods to describe the mechanics of bond-slip as it affects reinforced concrete flexural behaviour. The most common approach reported in the literature for modeling the load-deformation behaviour of partially-bonded reinforcement has been the use of flexibility-based fibre elements (Monti et al., 1997; Ayoub and Filippou, 1999; Monti and Spacone, 2000; Orakcal and Chowdhury, 2012). The flexibility-based method mathematically approximates the smooth steel stress distribution within anchored regions, rather than attempting to approximate the highly nonlinear strain distribution. This approach serves to simplify solution of the differential equations of equilibrium and compatibility of anchored/developed reinforcement. The major differences between various flexibility-based techniques has been the manner in which the stress transfer length has been defined, the degree of the polynomial used to distribute bond stresses along said transfer length, and the weighting and order of the interpolation functions used for relative slip and reinforcement steel forces. Other,

simpler methods of approaching the bond-slip problem also exist. Xiao and Ma (1997) incorporated bond-links into a moment-curvature analysis, while Alsiwat and Saatcioglu (1992) computed rigid body end rotation of flexural members through integration of the strain distribution along anchored reinforcement.

Regardless of the solution scheme adopted, each of the aforementioned studies obtained reasonable predictions of the global load-deformation response of reinforced concrete members. The common, unifying characteristic of each of the analyses was the use of appropriate constitutive bond-slip relationships selected based on the type of reinforcement and expected bond failure mode. However, the scope of these studies was limited to static loading. To the best knowledge of the authors, no study has examined the effect of high strain rates on the flexural response of reinforced concrete members experiencing slippage of reinforcement lap splices. Addressing this gap in the knowledge is especially important for advancing the state of the art of protective design to ensure the continued safety and resilience of concrete infrastructure.

Presented in this chapter is an analytical model that can predict the behaviour of reinforced concrete flexural members at high strain rates and the effect of reinforcement slippage of tension lap splices. Details of the analytical model are discussed, including an appropriate bond-slip law, material properties for steel and concrete, and dynamic increase factors (DIF). The effectiveness of the methodology was validated against comprehensive resistance curve data recorded during experimental testing of reinforced concrete beams subjected to four-point static and dynamic shock tube loading. The objective of the analytical study was to demonstrate that the response of tension lap splices subjected to dynamic loads can be predicted satisfactorily using the proposed analysis technique.

6.2 Analytical Model

6.2.1 General Approach

The model for partial-bond discussed in this chapter builds upon the work of Monti and Spacone (2000). Moment-curvature relationships were used to trace the load-deflection response of a reinforced concrete beam in the entire range from uncracked response up to collapse. The moment-curvature analysis explicitly considered the effect of slippage of lap-spliced longitudinal bars through the use of an effective reinforcement stress-strain curve incorporating bond-slip phenomenon. For the case of rapidly applied loads generating high strain rates, material properties and bond parameters were modified using appropriately selected dynamic increase factors (DIF).

6.2.2 Reinforcement Stress-Strain Incorporating Bond-Slip

Two assumptions form the basis of reinforced concrete flexural analysis. The first is Bernoulli's principle, which states that plane sections before bending remain plane after bending. The second is perfect bond which requires compatibility between the strains in reinforcing steel (ε_s) and concrete (ε_c) such that $\varepsilon_c = \varepsilon_s$. Combined, the mathematical implication of these assumptions is that the strain at any location within a section (ε) is a function of the average strain (ε_{avg}), curvature (ϕ), and the distance from the neutral axis to the location under consideration (y) through the relation

$$\varepsilon_c = \varepsilon_s = \varepsilon = \varepsilon_{avg} + \phi y \tag{6.1}$$

If the assumption of perfect bond is relaxed, and steel is permitted to slip relative to the surrounding concrete, strain compatibility requires that

$$\varepsilon_c = \varepsilon_s + \varepsilon_{slip} \tag{6.2}$$

where ε_{slip} is the slippage strain due to imperfect reinforced concrete bond.

Whereas values of ε_c and ε_s can be obtained from constitutive stress-strain relationships, bond-slip expressions may be used to obtain appropriate values for ε_{slip}. Consider the spliced region with length L_s subject to constant axial tension force $f_s A_b$ illustrated in Figure 6.1. From the perspective of the observer, the starter bar and surrounding concrete are assumed fixed, while the spliced bar experiences a slip displacement (s) relative to the starter bar. Slippage of reinforcement leads to a reduction in the effective splice length available for bond transfer, expressed as $L_s' = L_s - s$. The slippage strain may now be defined as $\varepsilon_{slip} = s/L_s$. The effective strain in reinforcement within the splice (ε_s'), incorporating the effects of bond-slip, can be conveniently written as

$$\varepsilon_s' = \varepsilon_s + \frac{s}{L_s} = \varepsilon_s + \varepsilon_{slip} \tag{6.3}$$

Assuming that a state of constant bond stress (u) exists in the splice, the steel stress developed over L_s' can be written as

$$f_s = \frac{u L_s' \pi d_b}{A_b} = \frac{4 u L_s'}{d_b} \tag{6.4}$$

provided that the values of ε_s and f_s satisfy compatibility with the stress-strain law for the bare reinforcing steel.

A bond-slip law describes the transfer of interfacial stresses between the reinforcing bar and concrete as a function of the displacement, or slip, of the bar relative to the surrounding substrate. The components which contribute to the mechanism of bond transfer, illustrated in Figure 6.2, are:

chemical adhesion between the concrete and the reinforcing bar; frictional forces at the bonded interface, and; mechanical bearing of deformations (lugs) on the surface of the bar. Plain reinforcing bars, reliant on chemical adhesion and friction, generally have the lowest capacity for bond. For the case of deformed bars, chemical adhesion is lost once any appreciable slippage of the bar occurs, at which point bond is primarily caused by mechanical bearing. This phenomenon generates longitudinal and radial stresses in the surrounding concrete. If the radial stress demand exceeds the capacity of the surrounding concrete, a splitting failure will occur. However, pull-out failures are also possible if the longitudinal stresses are sufficient to crush concrete in the vicinity of the lugs prior to splitting. A number of factors, including concrete strength, cover depth, and presence of transverse reinforcement, influence the mechanism of bond transfer (ACI, 2003). Therefore, a well-defined bond-slip law is essential for tracing the evolution of steel stress within the splice as a function of rebar slippage.

It is evident that the effective steel stress developed within the splice is a function of the degree of reinforcement slippage and of the bond-slip characteristics of the steel-concrete interface. Stress-strain relationships for spliced reinforcement, incorporating the effect of bond deterioration, can be obtained by solving Eqs. (6.3) and (6.4) for progressively increasing values of bar slip obtained from bond-slip expressions, whilst ensuring compatibility with the steel stress-strain relationship.

The analytical procedure to develop stress-strain response of rebar that includes bond-slip effects is described by the flowchart in Figure 6.3. A displacement field is assumed along the length of the spliced region. From there, the effective load carrying capacity of the splice is computed by ensuring compatibility between the bond-slip and material stress-strain relationship is maintained. The analytical procedure can be summarized as follows:

1. Select a small, incremental slip s;
2. Obtain the corresponding bond stress u from the bond-slip relationship;
3. Calculate ε_{slip} and L_s';
4. Solve for f_s from Eq. (6.4);
5. Obtain steel strain ε_s from the steel stress-strain relationship corresponding to f_s;
6. Calculate ε_s' from Eq. (6.3);
7. Store ε_s' and f_s for the current slip s;
8. Check termination criterion ($\varepsilon_s > \varepsilon_u$ or $s > s_{max}$);
9. Return to step 1.

Information regarding the failure mechanism of the splice can also be obtained. For example, a splice failure due to bond loss is likely to occur if rebar slip s exceeds the maximum bar slip s_{max} defined in the bond-slip law prior to steel stress ε_s exceeding the material rupture strain ε_u. Splice failure due to steel rupturing is predicted if $\varepsilon_s > \varepsilon_u$ is achieved prior to $s > s_{max}$.

To demonstrate the effect of bond-slip on spliced reinforcement, a comparison of stress-strain responses for different bond levels is shown in Figure 6.4. For the case of superior bond conditions, the response of partially bonded reinforcement closely follows that of the bare rebar, with only a small decrease in initial stiffness due to slippage. As bond conditions deteriorate, as is evident for the case of an intermediate level of bond, the initially stiff bond-slip response follows the bare rebar response only for relatively low load levels. As stress in the splice is increased, slippage has the effect of reducing the effective strength and stiffness of reinforcement, while also limiting the maximum attainable strain. A splice failure, either by splitting or pull-out, is indicated when the ultimate strain defined in the effective stress-strain response is exceeded prior to achieving the ultimate rupture strain of the reinforcement. If the structural element provides a weak level of bond, (*e.g.* insufficient cover depth or inadequate developed length) the stress-strain response of the spliced region is expected to closely follow the general shape of the bond-slip curve. In such cases, it is unlikely that the splice will develop the yield strength and will exhibit considerably lower stiffness than what is expected for continuous reinforcement.

It is important to note that the effective stress-strain relationship developed for spliced reinforcement cannot be considered a true material property. Rather, it is a pseudo-material property, whose characteristics are dependent on the size and grade of reinforcement, and of the construction of the splice itself. They serve as a convenient mathematical representation of an otherwise complicated physical phenomenon. The primary advantage of this formulation is that the fundamental characteristics of bond-slip can be described using modified material properties, rather than implementing overly detailed and time-consuming finite-element methods. The relatively straightforward development of the effective bond-slip stress-strain relationships is ideal for use in practice through either hand calculations or spreadsheet implementation of reinforced concrete flexural analyses.

6.2.3 Bond-Slip Response at High Strain rates

Bond-Slip Law

Vos (1983) suggested the use of static bond-slip relationships modified with appropriate material increase factors to describe dynamic bond-slip behaviour. On that basis, the monotonic envelope curve proposed by Eligehausen, Popov and Bertéro (1983), describing the variation in bond strength and bond stiffness as a function of reinforcement slip, was adopted for this study. The envelope bond-slip curve, shown in Figure 6.5, consisted of four stages. During the initial ascending stage, the variation in bond stress up to slip s_1 is given by:

$$u = u_m \left(\frac{s}{s_1}\right)^{\beta} \tag{6.5}$$

where u_m is the maximum bond stress corresponding to bond failure and the exponent β is used to calibrate the expression to experimental data. The second stage consists of a region of constant bond u_m until slip s_2. The third stage, a descending branch of linearly decreasing bond up to slip s_3, is followed by a region of constant frictional bond u_f until incipient failure at s_4.

Bond Strength

The maximum bond stress u_m attained in the bond-slip envelope curve was computed assuming a constant distribution of bond over the development length such that $u_m = T_b/(\pi d_b l_d)$. The total bond force (T_b) developed in the splice was computed using the descriptive expression proposed by ACI Committee 408 (ACI, 2003). In this expression, T_b is the sum of the bond force developed without transverse reinforcement (T_c) and the additional bond force developed due to the contribution of transverse reinforcement (T_s). The expression for T_b, shown in Eqs. (6.6) - (6.8), was reported to provide the best overall correlation with experimental data for a range of material properties and structural configurations of spliced and developed bars (ACI, 2003).

$$T_b = T_c + T_s \tag{6.6}$$

where the concrete contribution to bond force equal to the bond force that would be developed without transverse reinforcement is:

$$T_c = [1.43 l_d (c_{\min} + 0.5 d_b) + 57.4 A_b] \left(\frac{0.1 c_{max}}{c_{min}} + 0.9 \right) f_c'^{1/4} \tag{6.7}$$

and the additional strength provided by the transverse reinforcement is:

$$T_s = \left(8.9 t_r t_d \frac{N A_{tr}}{n} + 558 \right) f_c'^{3/4} \tag{6.8}$$

where: A_b is the bar area (mm^2); f_s is the steel stress at failure (MPa); f_c' is the compressive strength of concrete (MPa); l_d is the development of splice length (mm); c_{min} is the minimum of c_b or c_s (mm); c_b is the bottom cover to the bar being developed or spliced (mm); c_s is the minimum of c_{so} and c_{si} + 6.35 (mm); c_{so} is the side cover to the bar being developed or spliced (mm); c_{si} is ½ of the clear bar spacing (mm); c_{max} is the maximum of c_b and c_s (mm); d_b is the bar diameter (mm); R_r is the relative rib ratio, approximately equal to 0.8 to 0.9 h_r/s_r (ACI, 2003); h_r is the reinforcement rib height (mm); s_r is the reinforcement rib spacing (mm); t_r is the effect of relative rib area on T_s ($9.6R_r + 0.28$); t_d is the effect of bar size on T_s ($0.03d_b + 0.22$); N is the number of transverse stirrups or ties within l_d; A_{tr} is the area of each stirrup or ties crossing a potential splitting plane adjacent to reinforcement being developed (mm^2), and; n is the number of bars being developed or spliced.

Strain rate Sensitivity of Bond Strength

A number of researchers have confirmed that bond is sensitive to strength enhancement when subjected to blast and impact loading (Shah and Hansen, 1963; Vos and Reinhardt, 1982; Yan, 1992; Weathersby, 2003; Solomos and Berra, 2010). Chapter 5 of this thesis demonstrated that the strain rate sensitivity of bond strength can be divided into three components each affected by rapid loading consisting of the dynamic concrete properties (f'_{dc}), the dynamic bond force developed without transverse reinforcement (T_{dc}), and the additional dynamic bond force developed when splices are confined by transverse reinforcement (T_{ds}). Using the ACI descriptive expression as a foundation (ACI, 2003), it was found that the dynamic total bond force (T_{db}) in developed or spliced reinforcement subjected to high strain rates can be expressed as

$$T_{db} = T_{dc} + T_{ds} \tag{6.9}$$

$$T_{dc} = DIF_{T_c} \times [1.43 l_d (c_{\min} + 0.5 d_b) + 57.4 A_b] \left(\frac{0.1 c_{max}}{c_{min}} + 0.9 \right) {f'_{dc}}^{1/4} \tag{6.10}$$

$$T_{ds} = DIF_{T_s} \times \left(8.9 t_r t_d \frac{N A_{tr}}{n} + 558 \right) {f'_{dc}}^{3/4} \tag{6.11}$$

where f'_{dc} is the dynamic compressive strength of concrete, and DIF_{T_c} and DIF_{T_s} are dynamic increase factors which account for the apparent increase in concrete compressive strength, bond force developed without transverse reinforcement and additional bond force provided by transverse reinforcement, respectively.

For strain rates $0.1 \leq \dot{\varepsilon} \leq 1.2$ s^{-1}, values of DIF_{T_c} and DIF_{T_s} can be computed as follows:

$$DIF_{T_c} = -1.20 \times 10^{-5} l_d (c_{min} + 0.5 d_b) + 1.04 \times 10^{-3} A_b + 1.18 \geq 1.00 \tag{6.12}$$

$$DIF_{T_s} = 1.14 \tag{6.13}$$

For splices with transverse reinforcement, it was proposed that a constant value of DIF_{T_s}=1.14 be used. However, this DIF was based on a limited dataset for a narrow range of confinement ratios and relative rib geometries, and the author cautioned that further study was required to confirm the value for DIF_{T_s}.

Bond Parameters at Low and High Strain rates

Ciampi et al. (1981) proposed that values of bond parameters u_m, u_f, $s_{1\to4}$ and β be selected to provide a suitable match with experimental bond-slip data. Eligehausen et al. (1983) found that $\beta = 0.4$ provided good correlation between the shape of the initial ascending branch with experimental data for unconfined concrete under static loading. For elastic bond at high strain rates, the results described in Chapter 3showed that the parameter β was insensitive to loading rate for $\dot{\varepsilon} \approx 1\ s^{-1}$ and that $\beta = 0.4$ reasonably captured the shape of the ascending branch for unconfined concrete with

bonded lengths of 400 mm. Therefore, $\beta = 0.4$ was selected for the analysis of both low and high strain rates.

Bar slips $s_{1\to4}$ are commonly expressed in terms of the clear distance, s_L, between rebar lugs. Values of slip proposed by Harajli et al. (2002), specifically $s_1 = 0.15s_L$, $s_2 = 0.35s_L$, $s_3 = s_L$, were adopted in this study. It was assumed that these were valid for both low and high strain rate bond response based on the findings described in Chapter 3, where is was shown that s_1 was not particularly sensitive to strain rates on the order of 1 s^{-1}. By extension, it was assumed that s_2, s_3 and s_4 were similarly not sensitive to strain rates and the static values were valid for dynamic loading. Finally, the frictional bond stress u_f was assumed to be equal to $u_m/4$ for both static and dynamic loading.

No distinction was made in the bond-slip parameters selected for unconfined and confined lap splices beams.

6.2.4 Material Behaviour at Low and High Strain rates

The following describes the stress-strain relationships for concrete and reinforcing steel used in the analysis. As necessary, the relationships were modified with dynamic increase factors to account for the effect of high strain rates on the constitutive behaviour of the materials.

Concrete

The Thorenfeldt et al. (1987) uniaxial stress-strain curve for concrete in compression, shown in Figure 6.6 (a), was used in the analysis. The expression for the ascending and descending branches is given as follows:

$$f_c = \frac{f_c' \cdot n \cdot \left(\frac{\varepsilon_c}{\varepsilon_o}\right)}{n - 1 + \left(\frac{\varepsilon_c}{\varepsilon_o}\right)^{nk}} \tag{6.14}$$

in which calibration constants n, ε_o, k were computed following the approach presented in Collins and Mitchell (2001), selected on the basis that only the cylinder strength f_c' was required to obtain the appropriate constants.

$$n = 0.8 + \frac{f_c'}{17} \tag{6.15}$$

$$\varepsilon_o = \frac{f_c'}{E_c} \times \frac{n}{n-1} \tag{6.16}$$

$$E_c = 3320\sqrt{f_c'} + 6900 \tag{6.17}$$

(6.18) $$k = \begin{cases} 1 \text{ for} \dfrac{\varepsilon_c}{\varepsilon_o} \leq 1.0 \\ 0.67 + \dfrac{f_c'}{62} \text{ for} \dfrac{\varepsilon_c}{\varepsilon_o} > 1.0 \end{cases}$$

Concrete exhibits an increase in strength and stiffness when subjected to high strain rate loading (Department of Defense, 2008). To account for this phenomenon, the peak static compressive strength of concrete, f_c' in Eqs. (6.14) - (6.18) was substituted by the dynamic compressive strength f_{dc}', for which:

(6.19) $$f_{dc}' = DIF_{f_c} \times f_c'$$

where DIF_{f_c} is the dynamic increase factor to account for high strain rate effects on concrete compressive strength. The CEB Model Code expression (CEB-FIP, 1993) was used to predict values of DIF_{f_c} for concrete in compression according to:

(6.20) $$DIF_{f_c} = \left(\frac{\dot{\varepsilon}}{30\times10^{-6}}\right)^{1.026\alpha} \text{ for } \dot{\varepsilon} \leq 30\ s^{-1}$$

(6.21) $$\alpha = \frac{1}{5 + \frac{9f_c'}{10}}$$

The tensile stress-strain curve for concrete was modelled following the work of Bentz (2000). The initial ascending portion up to first cracking was represented by a linear curve with slope given by the initial tangent stiffness of concrete given in Eq. (6.17). The peak tensile cracking strength of concrete (f_{cr}) was taken as

(6.22) $$f_{cr} = 0.45(f_c')^{0.4}$$

The second portion of the tensile curve, accounting for tension stiffening of concrete which can occur after first cracking, was expressed following:

(6.23) $$f_t = \frac{f_{cr}}{1 + \sqrt{3.6m \cdot \varepsilon_t}}$$

where the parameter $m = A_c/\sum d_b\pi$ accounts for the influence of bond characteristics on the area of concrete in tension (A_c) by the perimeter of all the reinforcing bars in the area ($\sum d_b\pi$).

The dynamic tensile strength of concrete (f_{dcr}) was computed by applying a dynamic increase factor, $DIF_{f_{cr}}$ to account for the effect of high strain rates on the tensile properties of concrete as follows:

(6.24) $$f_{dcr} = DIF_{f_{cr}} \times f_{cr}$$

where $DIF_{f_{cr}}$ was defined according to the formulation proposed by Malvar and Crawford (1998b). They defined the dynamic increase factor for concrete strength in tension as:

$$DIF_{f_{cr}} = \begin{cases} \left(\frac{\dot{\varepsilon}}{10^{-6}}\right)^{\delta} & \text{for } \dot{\varepsilon} \leq 1\ s^{-1} \\ \beta\left(\frac{\dot{\varepsilon}}{10^{-6}}\right)^{\frac{1}{3}} & \text{for } \dot{\varepsilon} > 1\ s^{-1} \end{cases} \tag{6.25}$$

$$\delta = \frac{1}{1 + \frac{8f_c'}{10}} \tag{6.26}$$

$$\log\beta = 6\delta - 2 \tag{6.27}$$

Steel Reinforcement

The stress-strain relationships for each of the reinforcement sizes, provided in Figure 6.6 (b), were obtained from tension coupon tests. Instability failure of compression reinforcement, common when reinforced concrete is subjected to large inelastic displacements (Yalcin and Saatcioglu, 2000), was ignored in the analysis. Therefore, coupon data was assumed to be applicable for both tension and compression reinforcement response.

Reinforcing steel experiences an increase in material properties due to dynamic loading. However, unlike concrete, the effect of loading rate on stress-strain response for steel is understood with a greater level of confidence, partially due to material isotropy and the high degree of standardization and precision associated with steel manufacturing (Fu et al., 1991). The strain rate sensitivity of reinforcing steel is inversely proportional to strength, with yield strength exhibiting greater sensitivity than ultimate strength (Department of Defense, 2008).

The work of Malvar (1998a) was used to obtain values of DIF for both f_y and f_u to construct dynamic stress-strain relationships used in the analysis. The static stress-strain coupon data was modified by applying a linear variation in DIF to stress values between yield and ultimate. Strain rate and static yield strength were used as inputs to obtain values of DIF according to:

$$DIF = \left(\frac{\dot{\varepsilon}_s}{10^{-4}}\right)^{\alpha} \tag{6.28}$$

valid for $10^{-4} \leq \dot{\varepsilon}_s \leq 225\ s^{-1}$ and $290 \leq f_y \leq 710\ MPa$.

The DIF applied to the static yield strength to obtain the dynamic yield strength $f_{dy} = DIF_{f_y} \times f_y$ may be determined by substituing $\alpha = \alpha_{f_y}$ in Eq. (6.28) according to:

$$\alpha_{f_y} = 0.074 - \frac{0.040 f_y}{414} \tag{6.29}$$

A similar procedure was followed to obtain the dynamic ultimate strength $f_{du} = DIF_{f_u} \times f_u$ where $\alpha = \alpha_{f_u}$ is substituted in Eq. (6.28) as follows:

$$\alpha_{f_u} = 0.019 - \frac{0.009 f_y}{414} \tag{6.30}$$

6.2.5 Solution Procedure for Structure Behaviour

A standard solution procedure was employed to predict the structural behaviour of lap-spliced reinforced concrete beams. The first step in the solution procedure was to establish the static material properties for concrete and steel (*i.e.* Figure 6.6). As necessary, appropriately selected dynamic increase factors (DIF) were applied to material properties and bond-slip parameters to account for the effect of high strain rates on member response. Strain rate $\dot{\varepsilon}$ obtained from experimental tests was used to establish DIFs. The effective stress-strain relationship for spliced reinforcement incorporating bond-slip was constructed following the procedure outlined in Figure 6.3 and described in Section 6.2.2.

Two moment-curvature ($M \cdot \phi$) relationships were established for each beam: one for regions of fully-bonded reinforcement and the other for regions of spliced reinforcement. Both $M \cdot \phi$ relationships were constructed with the same geometric configuration and concrete constitutive material properties. The $M \cdot \phi$ relationship for fully-bonded reinforcement was developed with the bare steel stress-strain curve, while the $M \cdot \phi$ for spliced reinforcement was developed using the effective stress-strain bond-slip element. The $M \cdot \phi$ analysis was terminated when reinforcing steel strain exceeded the material rupture strain or the effective bond splitting failure strain of reinforcement as defined by either the bare bar or effective bond-slip stress-strain curves.

Bending moment was assumed to be the dominant action, while the effect of shear and axial forces were neglected. The reinforced concrete beam was discretized into a number of segments along its length. Using a small, incremental load, the bending moment at the midpoint of each segment was computed. The curvature for segments having fully bonded reinforcement was mapped onto the beam from the $M \cdot \phi$ relationship developed for fully-bonded reinforcement, while the curvature for segments located in the spliced region was established from the partially-bonded $M \cdot \phi$ diagram. Mid-span deflection was then computed by numerical integration of the curvature distribution $\phi(x)$ along the length of the beam such that $\Delta = \int_0^{L/2} \phi(x) \cdot x \cdot dx$. The total load, mid-span deflection and steel stress in the lap splice were stored for later use. A new incremental applied load was then selected and the procedure was repeated. The stopping criterion defined in the analysis was when the beam mid-span moment exceeded the moment capacity of the lap splice. Piecewise linear functions were then constructed describing the load-deflection response and the

variation in stress in the lap splice as a function of applied load. The predicted behaviour of the beams was then compared against experimentally obtained data.

6.3 Model Validation

6.3.1 Test Specimens and Parameters

The accuracy of the model was assessed by comparing the predicted results against low and high strain rate experimental data described in Chapter 4. A total of 22 large-scale reinforced concrete beams were constructed and tested under four-point bending. One beam from each companion pair was subjected to low strain rate static loading, while the other was subjected to high strain rates. Dynamic loading was generated using a shock tube and load application device. Strain rates on the order of 1 s^{-1} were achieved using the shock tube loading system, while strain rates of 10^5 s^{-1} were obtained using conventional static testing equipment.

The beams were divided into eleven companion pairs established to study the influence of concrete strength, cover depth, reinforcement size and presence of transverse reinforcement on dynamic bond strength. Beam cross-section and geometry is illustrated in Figure 6.7, while construction details and material properties are summarized in Table 6.1. The test variables consisted of the size of longitudinal reinforcement (10M, 15M, and 20M); the cover depth (25 mm, and 50 mm); the concrete strength (30 MPa and 50 MPa), and; the presence of transverse reinforcement (confined or unconfined splices). Proportioning of the cross-sectional dimensions and splice length for each companion pair was conducted to ensure that the spliced regions would experience bond failure once the stress in the reinforcement achieved 400 MPa.

The overall length of all beams was 2440 mm, with each having a clear span between supports of 2232 mm. The four-point bending configuration of the low and high strain rate tests was similar, with both generating a constant moment region over a length of 744 mm. Displacement transducers recorded the mid-span deflection, while load cells placed in the supports were used to obtain reaction forces. For the case of high strain rate tests, dynamic analysis was performed to compute the internal member resistance based on equilibrium of reaction load cell readings, applied pressure distribution and inertia of the beam system. In addition, strain gauges were installed on the reinforcement within the splices to monitor the magnitude and distribution of stress within the spliced region.

Previously in this thesis, it was reported that the strength and stiffness of reinforced concrete beams was significantly improved when subjected to dynamic loading. The peak resistance of the beams increased by an average of 30%, while the average bond energy (area under the resistance curve) increased by 163%, relative to the reference static conditions. A comparison of the general behaviour of the specimens showed that the underlying flexural response and nature of the bond

splitting failure was not affected by dynamic loads, despite clear increase in member strength and stiffness attributed to strain rate enhancement. The use of transverse reinforcement to confine spliced regions led to significant improvements in post-peak strength and splice toughness as compared to splices without transverse reinforcement. These improvements were further amplified by high strain rate effects. Regardless of strain rate, the bond strength of splices with and without transverse reinforcement was found to increase in proportion to the ratio of c_{min}/d_b, and decrease in proportion to l_s/d_b. Without exception, high strain rate bond strength was always greater than corresponding low strain rate values, yielding an average DIF applied to bond strength of 1.28.

6.3.2 Analysis of Test Beams

The analytical methodology described in Section 6.2 was used to predict the flexural response of the twenty-two lap splice beam tests incorporating the effect of bond-slip. A comparison of experimental and analytical beam resistance curves at low and high strain rates is shown in Figure 6.8 and Figure 6.9 for splices with and without transverse reinforcement, respectively. To assess the significance of bond-slip on flexural response, the analysis was also performed considering perfect bond between reinforcing steel and concrete. The perfect bond flexural predictions are also presented for comparison in Figure 6.8 and Figure 6.9.

The predicted resistance curves in Figure 6.8 and Figure 6.9 for lap splices having perfect bond showed poor correlation with experimental data. The fully-bonded predictions consistently overestimated the flexural stiffness of the beams, despite yielding reasonable predictions of peak resistance. The load corresponding to cracking of concrete appeared to be the threshold after which reinforcement slippage began to exert a measureable influence on flexural response. This trend, consistently observed for both low- and high-strain rate tests, indicated that bond was lost partially even at the initial stages of loading. Although all anchored and spliced reinforcement experiences some level of slip under service conditions, the degree to which the test specimens exhibited flexural softening was initially surprising. However, a number of factors are believed to have contributed to this phenomenon. First, the spliced lengths provided were relatively short, and in many cases much less than that required by CSA A23.3. Secondly, many of the splices were stressed well beyond their design stress level of 400 MPa, particularly those subjected to dynamic loads. Third, most of the splices were unconfined, and hence relatively brittle and susceptible to slip-related deficiency. These types of lap splices are generally not permitted in many flexural members (with the exception of slabs, for example). Finally, all tension reinforcement was spliced at the critical section, whereas in practice spliced bars are typically staggered such that at least some of the reinforcement is continuous over the critical section. Combined, these contributing factors served to exacerbate the slip behaviour observed during the static and dynamic tests. In essence, purposely detailing the

specimens to promote a bond-related failure likely contributed to the observed slip softening behaviour.

Results of the analysis for the case of partial-bond are reported in Table 6.2. The experimental and predicted quantities compared include: the peak resistance (R_{exp} and R_{pred}, respectively) and peak resistance ratios (R_{exp}/R_{pred}); the displacement at peak resistance (δ_{exp} and δ_{pred}) and displacement ratios ($\delta_{exp}/\delta_{pred}$), and; the splice stress at peak resistance ($f_{s,exp}$ and $f_{s,pred}$) and splice stress ratios ($f_{s,exp}/f_{s,pred}$). Summary statistics (mean, coefficient of variation [COV], minimum, maximum) for each of the prediction ratios are listed in Table 6.3.

With regard to the experimental resistance curves shown, the peak strength of beams tested at high strain rates was in all cases significantly greater than the strength of beams subjected to slowly applied static loading. This characteristic, common for structures subjected to short duration, dynamic loads (Department of Defense, 2008; Lloyd, 2015; Jacques and Saatcioglu, 2016), can be attributed to an apparent increase in material strength due to rate effects. Figure 6.8 and Figure 6.9 show that the fully- and partially-bonded flexural analyses yield reasonably good predictions of the peak strength of the lap splice beams for the cases of low and high strain rates. Furthermore, partial-bond flexural predictions, incorporating appropriate material *DIF*s, were able to capture the initially very rigid behaviour of the high strain rate beams. The results suggest that the expressions for *DIF* applied to concrete properties and steel reinforcement (discussed in Section 6.2.4), in addition to the Jacques expression for dynamic bond strength [*i.e.* Eq. (6.12)], can be relied upon to provide reasonable predictions of the ultimate strength of flexural members subjected to high strain rate loading.

A focused comparison of experimental stress developed in the splice against splice stress predicted using fully- and partially-bonded analysis techniques is shown in Figure 6.10, Figure 6.11, and Figure 6.12 for companion pairs CP4, CP6 and CP8, respectively. Experimental splice stress was obtained by converting strain readings taken in the constant moment region – but outside the spliced zone – into stress using appropriate stress-strain relations (discussed in Section 6.2.4). In general, the comparisons indicate that fully-bonded flexural analysis does not adequately capture the evolution of stress in the splice as a function of internal resistance. The reason for this is that spliced reinforcement must develop a greater level of stress than fully-bonded continuous reinforcement to achieve the same internal restoring moment. Achieving this greater stress level, however, requires that the section experience greater curvatures, which in turn has the effect of softening flexural response. The partially-bonded analysis methodology described in the chapter can reasonably capture the effect of splice slippage on the flexural behaviour of the test samples, and appears to be equally applicable at both low and high strain rates.

Good agreement between predicted and experimental data was obtained when the phenomenology of bond-slip in lap-spliced reinforcement was expressed through the use of an effective reinforcement stress-strain relationship. A comparison between the experimental and predicted peak resistances is plotted in Figure 6.13, with comparisons grouped according to strain rate. A mean peak resistance ratio (R_{exp}/R_{pred}) of 1.04 (COV=9%) was obtained for the partial-bond analysis of all 22 tests. No significant statistical difference was observed in the accuracy of the predictions of peak resistance conducted at low or high strain rates. Similarly, the stress in the splice at failure was predicted with a good level of accuracy: the mean splice stress at peak resistance ratio $f_{s,exp}/f_{s,pred}$ for all twenty-two tests was 1.08 with a corresponding COV of 5%.

Unlike predictions of peak resistance and splice stress, the predictions of the displacement corresponding to splice failure were predicted with a lower level of accuracy. The mean ratio of $\delta_{exp}/\delta_{pred}$ for all tests was 1.04 (COV=62%). However, the peak displacement for low strain rate tests were consistently overestimated (Average $\{\delta_{exp}/\delta_{pred}\}_{LSR} = 0.81$), while the high strain rate tests were over-predicted by approximately the same margin (Average $\{\delta_{exp}/\delta_{pred}\}_{HSR} = 1.28$). Despite some inaccuracy in predicting the displacement at splice failure, the comparisons presented in Figure 6.8 and Figure 6.9 show that the partial-bond resistance curves can accurately trace the evolution of flexural strength and stiffness over the entire displacement range up to failure. This justifies the analysis procedure when used to predict the response of beams with tension lap splices subjected to static and dynamic loading with strain rates in the range of 10^{-5} s^{-1} and 1 s^{-1}.

Another important observation was the influence of transverse reinforcement on flexural response. A comparison of the fully bonded flexural predictions against experimental data demonstrated that the effect of bond-slip was more pronounced for splices not confined by transverse reinforcement, as was the case for results illustrated in Figure 6.8. However, the effect of reinforcement slip was reduced for the case of splices with transverse reinforcement (*i.e.* Figure 6.9). The improvement in member stiffness observed for beams having splices confined by transverse reinforcement was due to a passive clamping pressure provided by the transverse reinforcement which resists splitting of the cover concrete (ACI, 2003).

The results presented in this chapter demonstrate that effective steel stress-strain relationships, incorporating partially-bonded reinforcement response, provide an acceptable means of capturing the fundamental characteristics of bond-slip along the splice length. The major advantages of the methodology are that it can provide reasonably accurate predictions and can be conveniently incorporated into existing moment-curvature or finite element software. However, further validation is required to assess the suitability and limitations of the methodology when applied to a broader range of reinforced concrete flexure members containing tension lap splices.

In some cases, however, the analytical model did have some difficultly. For example, the predictions for CP7-LSR [Figure 6.8 (m)] and CP8-LSR [Figure 6.8 (o)] underestimated flexural stiffness. One explanation was that the use of the Haraliji, Hamad and Karam (2002) formulation for slip parameters based on reinforcement lug spacing gave unrealistically large slips for the case of larger bars. The methodology also had difficulty predicting the significant splice ductility exhibited by CP1-HSR [Figure 6.8 (b)] and CP2-HSR [Figure 6.8 (d)]. Despite these minor variances, the shape of the partially-bonded predictions showed much better correlation with experimental data that did the fully-bond predictions. Furthermore, the analysis does provide the opportunity for some future refinements. For example, the use of a local bond-slip model developed specifically to trace evolution of bond stress for developed/spliced bars susceptible to splitting failures, such as the one described by Harajli (2004) could be investigated.

6.4 Summary and Conclusions

An analytical model was presented which could predict the flexural behaviour of reinforced concrete members constructed with tension lap splices. The model incorporated the effect of slippage of the lap-spliced reinforcement, in addition to accounting for the effect of high strain rates on material and bond properties. The effectiveness of the methodology was validated against comprehensive resistance curve data recorded during experimental testing of reinforced concrete beams subjected to four-point static and dynamic shock tube loading. Good agreement between experimental and predicted displacement responses was obtained when considering a condition of partial-bond within the spliced region. Additional analyses were also conducted to demonstrate that conventional, fully-bonded reinforced concrete flexural analysis over-predicted the strength and stiffness characteristics of the lap-spliced beams at both low and high strain rates. The results clearly demonstrated that the response of reinforced concrete beams with tension lap splices subjected to static and dynamic loads can be predicted satisfactorily using the proposed partial-bond analysis technique. However, further study is required to assess the suitability and limitations of the methodology when applied to a broader range of reinforced concrete members containing tension lap splices.

Table 6.1: Construction and reinforcing details of lap splice beams.

Specimen Designation	f_c'* MPa	f_y* MPa	b mm	h mm	d_b mm	A_b mm^2	c_b mm	c_{so} mm	c_{si} mm	l_d mm	n	N	A_{tr} mm^2
CP1-LSR	32.5	431.2	150	200	11.3	100	26	27	37	275	2	-	-
CP1-HSR	42.9	559.2					27	25	39	276			
CP2-LSR	32.5	431.2	240	200	11.3	100	51	49	60	168	2	-	-
CP2-HSR	42.7	557.4					52	49	60	160			
CP3-LSR	32.5	448.4	165	300	16.0	200	26	24	43	493	2	-	-
CP3-HSR	43.8	587.0					26	26	41	494			
CP4-LSR	32.5	448.4	265	300	16.0	200	52	52	65	272	2	-	-
CP4-HSR	44.6	597.0					51	50	67	282			
CP5-LSR	48.7	448.4	165	300	16.0	200	28	27	40	409	2	-	-
CP5-HSR	60.0	585.6					27	25	42	395			
CP6-LSR	48.7	448.4	265	300	16.0	200	53	52	65	235	2	-	-
CP6-HSR	60.3	590.3					51	47	70	230			
CP7-LSR	32.5	491.0	280	300	19.5	300	53	54	67	415	2	-	-
CP7-HSR	44.1	623.4					52	55	66	397			
CP8-LSR	48.7	491.0	280	300	19.5	300	53	54	67	360	2	-	-
CP8-HSR	60.2	622.3					51	53	68	361			
CP9-LSR	36.9	448.4	165	300	16.0	200	25	28	39	325	2	6	62.4
CP9-HSR	48.3	588.3					24	27	40	327			
CP10-LSR	36.9	448.4	265	300	16.0	200	48	52	65	187	2	4	62.4
CP10-HSR	47.3	574.1					49	50	67	185			
CP11-LSR	45.2	448.4	265	300	16.0	200	49	48	69	164	2	4	62.4
CP11-HSR	55.7	574.9					53	48	69	175			

* Material properties for high strain rate tests multiplied by appropriate *DIF*

Table 6.2: Comparison of experimental and predicted low and high strain rate results for the case of partial bond.

Beam	Strain rate $\dot{\varepsilon}$	Peak Resistance			Displacement at peak resistance			Splice stress at peak resistance		
		R_{exp} (kN)	R_{pred} (kN)	$\frac{R_{pred}}{R_{exp}}$	δ_{exp} (mm)	δ_{pred} (mm)	$\frac{\delta_{pred}}{\delta_{exp}}$	$f_{s,exp}$ (MPa)	$f_{s,pred}$ (MPa)	$\frac{f_{s,pred}}{f_{s,exp}}$
CP1-LSR	1.5×10^{-5}	38.4	37.0	0.96	14.8	17.9	1.21	457	430	0.94
CP1-HSR	0.31	47.7	46.9	0.98	50.7	19.5	0.38	575	534	0.93
CP2-LSR	1.8×10^{-5}	45.6	41.4	0.91	25.8	23	0.89	468	446	0.95
CP2-HSR	0.28	52.0	50.7	0.98	66.8	20.5	0.31	602	544	0.90
CP3-LSR	7.0×10^{-6}	122.9	108.4	0.88	16.0	13.3	0.83	462	404	0.87
CP3-HSR	0.65	155.0	144.5	0.93	19.0	18.8	0.99	585	539	0.92
CP4-LSR	5.5×10^{-6}	114.6	109.4	0.95	9.6	13.4	1.40	458	409	0.89
CP4-HSR	1.13	164.0	141.4	0.86	15.6	15.4	0.99	570	531	0.93
CP5-LSR	4.1×10^{-6}	130.6	122.5	0.94	10.0	13.4	1.34	485	417	0.86
CP5-HSR	0.60	153.2	138.5	0.90	14.1	14.8	1.05	584	511	0.88
CP6-LSR	6.3×10^{-6}	121.6	118.4	0.97	14.1	14.3	1.01	467	410	0.88
CP6-HSR	0.78	149.8	142.4	0.95	12.2	15.5	1.27	588	512	0.87
CP7-LSR	7.6×10^{-6}	182.4	159.9	0.88	8.7	14.6	1.68	491	433	0.88
CP7-HSR	0.80	245.0	202.8	0.83	20.3	15.7	0.78	623	548	0.88
CP8-LSR	4.3×10^{-6}	185.5	171.8	0.93	10.1	15.5	1.53	491	434	0.88
CP8-HSR	0.75	244.0	218.8	0.90	20.0	20.8	1.04	604	561	0.93
CP9-LSR	1.3×10^{-5}	109.2	117.9	1.08	9.5	12.7	1.34	426	441	1.04
CP9-HSR	0.70	154.4	156.7	1.01	11.1	17.6	1.59	585	584	1.00
CP10-LSR	7.4×10^{-6}	100.1	112.0	1.12	7.6	11.5	1.51	423	411	0.97
CP10-HSR	0.32	135.5	147.4	1.09	10.1	12.8	1.27	571	553	0.97
CP11-LSR	6.0×10^{-6}	99.4	117.1	1.18	7.4	11.3	1.53	417	416	1.00
CP11-HSR	0.33	134.5	153.1	1.14	11.0	13.9	1.26	561	561	1.00

Table 6.3: Summary statistics for low and high strain rate resistance curve predictions for the case of partial bond.

	Peak Resistance, R_{exp}/R_{pred}			Displacement at peak resistance, $\delta_{exp}/\delta_{pred}$			Splice stress at peak resistance, $f_{s,exp}/f_{s,pred}$		
	LSR Tests	HSR Tests	All Tests	LSR Tests	HSR Tests	All Tests	LSR Tests	HSR Tests	All Tests
Average	1.03	1.05	1.04	0.81	1.28	1.04	1.09	1.08	1.08
COV.	9%	9%	9%	25%	66%	62%	6%	5%	5%
Min.	0.85	0.88	0.85	0.60	0.63	0.60	0.97	1.00	0.97
Max.	1.14	1.21	1.21	1.20	3.26	3.26	1.16	1.15	1.16
Count	11	11	22	11	11	22	11	11	22

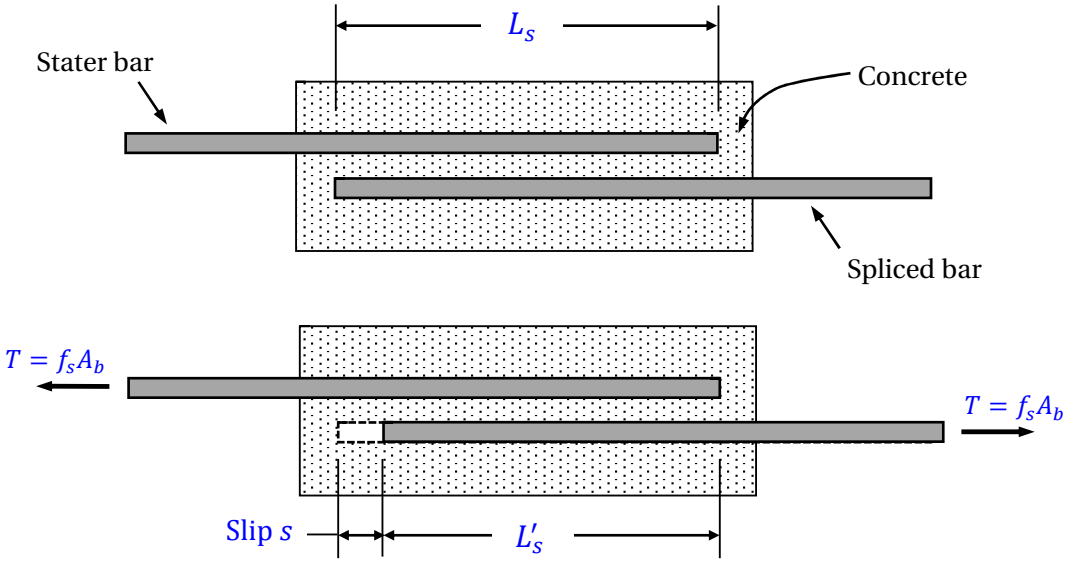

Figure 6.1: Idealized reinforcement lap splice region.

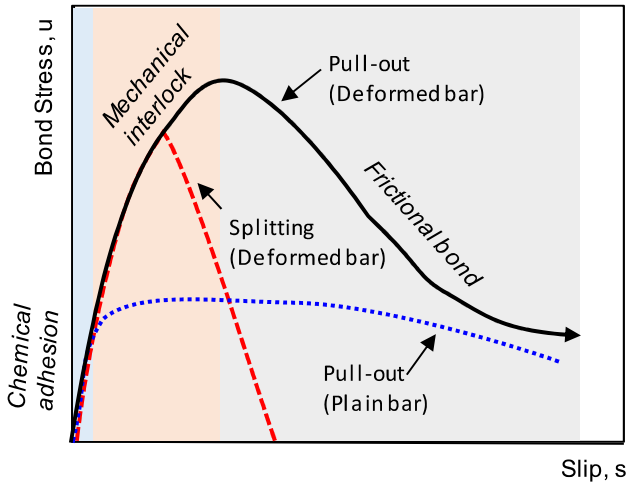

Figure 6.2: Idealized bond-slip diagram (adapted from Michal et al, 2015).

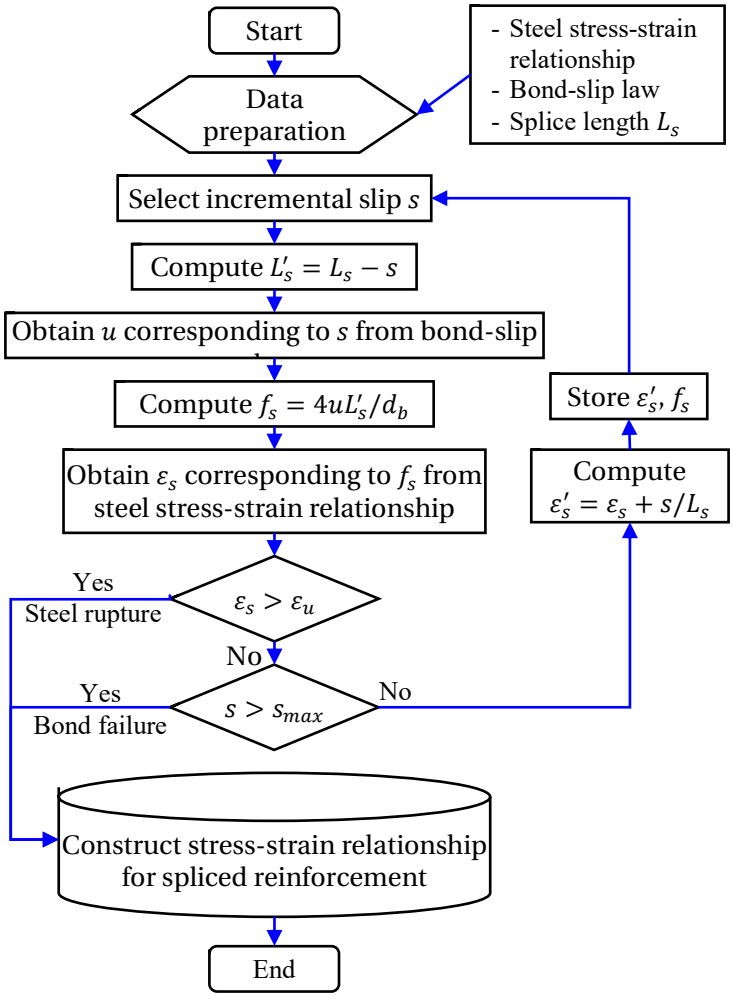

Figure 6.3: Flowchart for the development of pseudo stress-strain relationships.

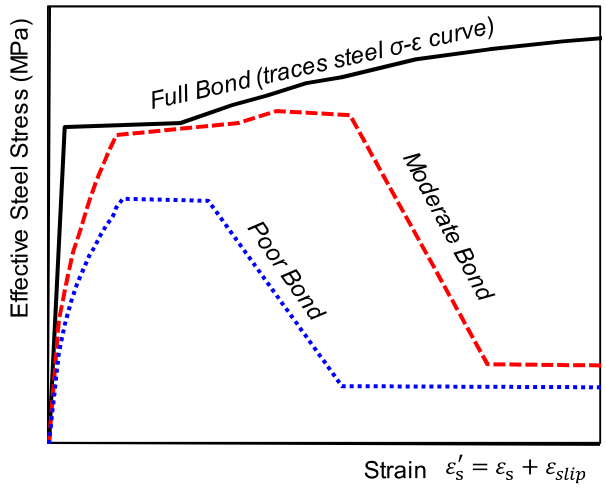

Figure 6.4: Typical pseudo stress-strain relationship developed for different bond levels.

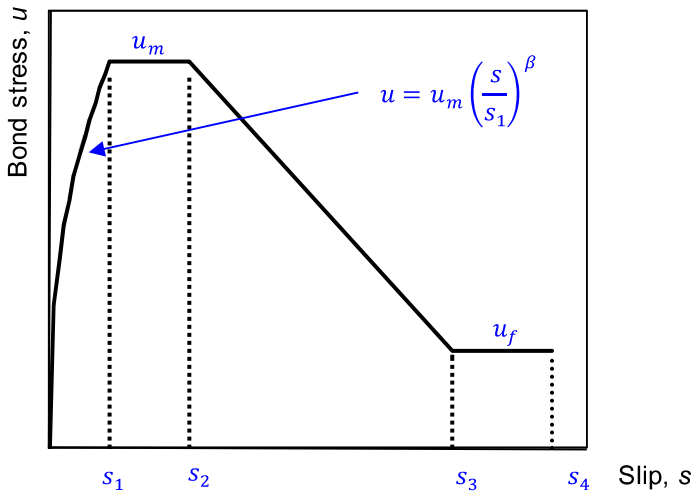

Figure 6.5: Bond-slip relationship proposed by Eligehausen, Popov and Bertéro (1983).

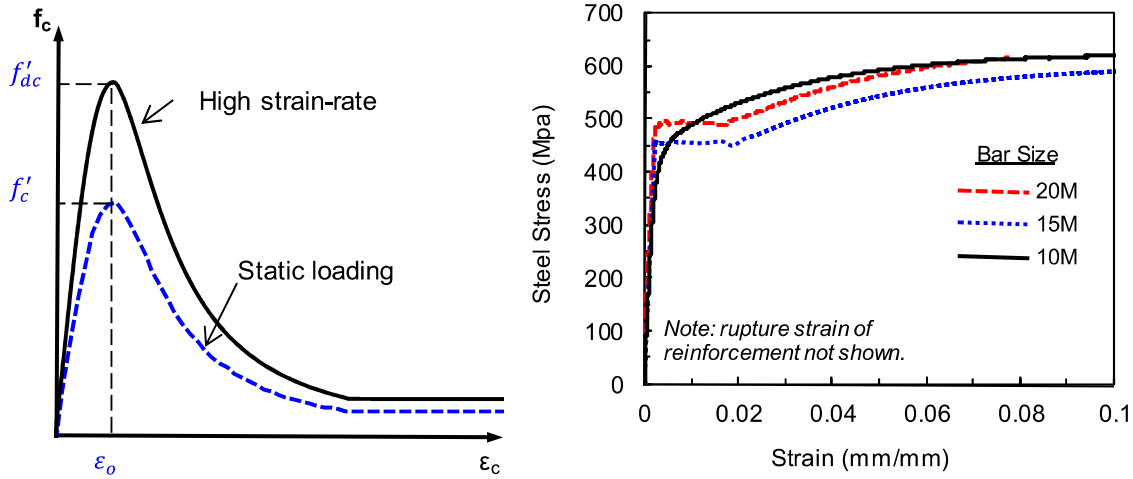

(a) Concrete in compression (b) Static steel tension coupon data

Figure 6.6: Stress-strain relationships used in the analytical model.

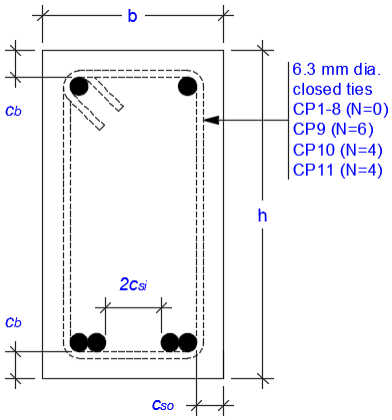

(a) Cross-section through spliced region

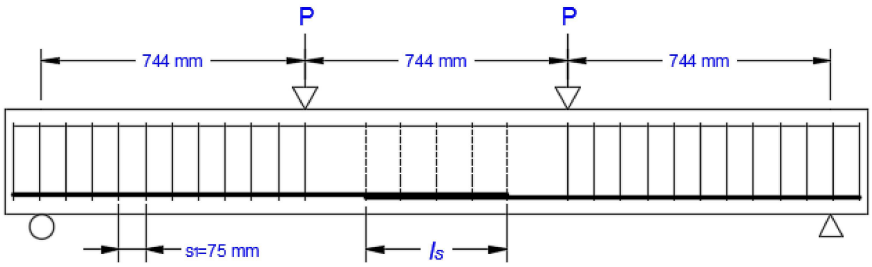

(b) Elevation view

Figure 6.7: Specimen details of the lap splice beams tested Chapter 4.

Figure 6.8: Comparison of low and high strain rate experimental resistance curves against those predicted considering full- and partial-bond conditions for splices not confined by transverse reinforcement.

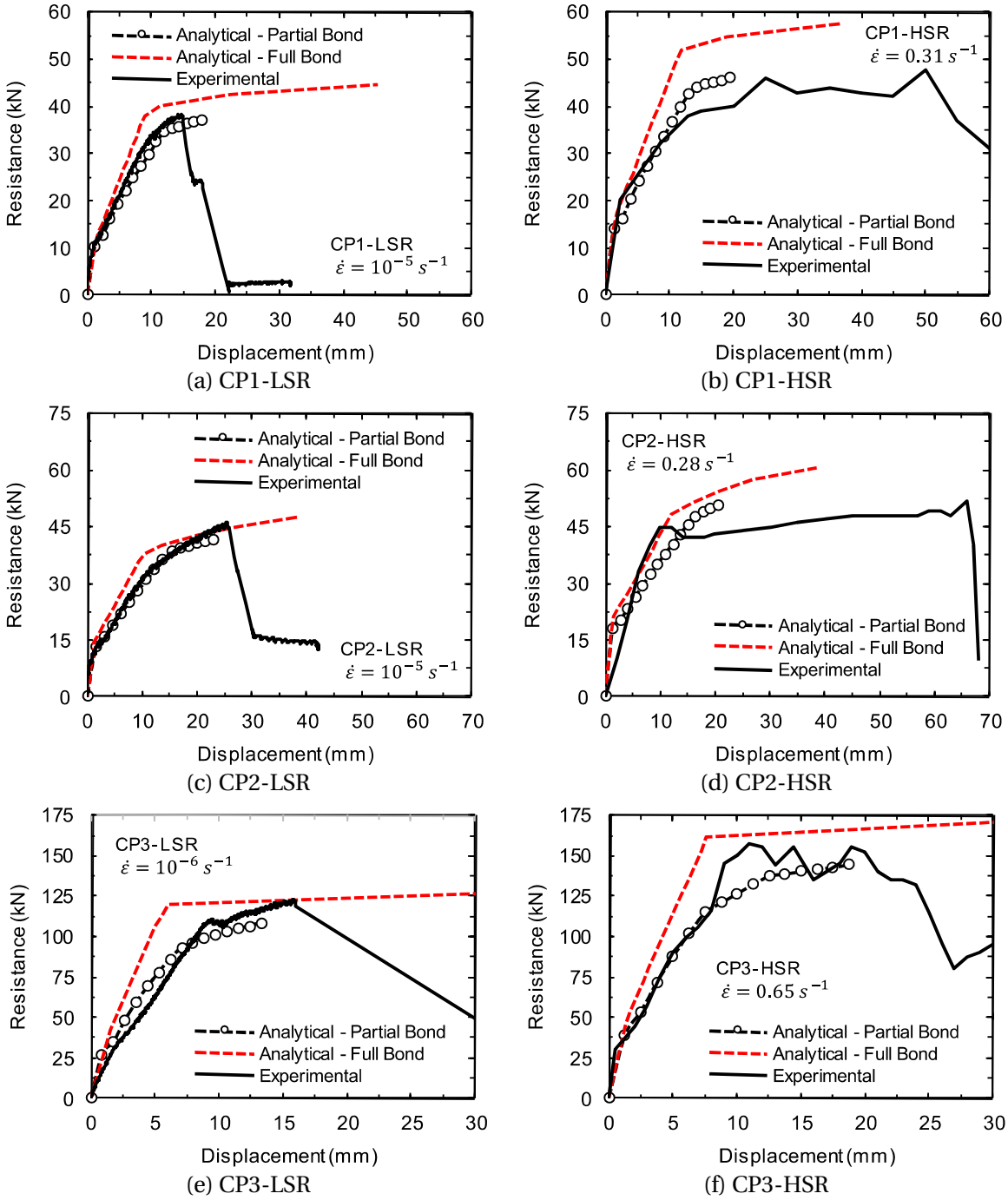

Figure 6.8: Comparison of low and high strain rate experimental resistance curves against those predicted considering full- and partial-bond conditions for splices not confined by transverse reinforcement.

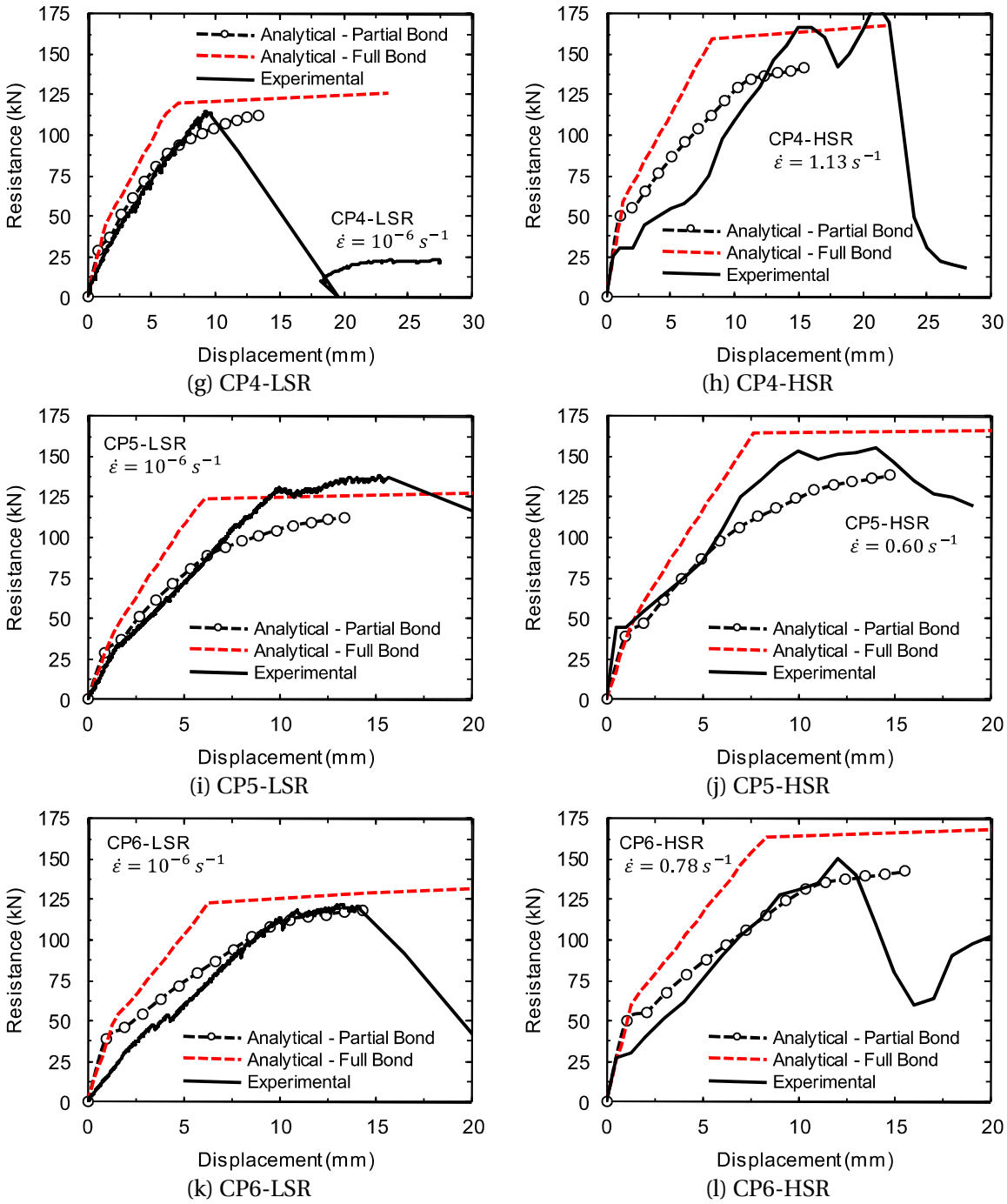

(g) CP4-LSR (h) CP4-HSR

(i) CP5-LSR (j) CP5-HSR

(k) CP6-LSR (l) CP6-HSR

Figure 6.8: Comparison of low and high strain rate experimental resistance curves against those predicted considering full- and partial-bond conditions for splices not confined by transverse reinforcement.

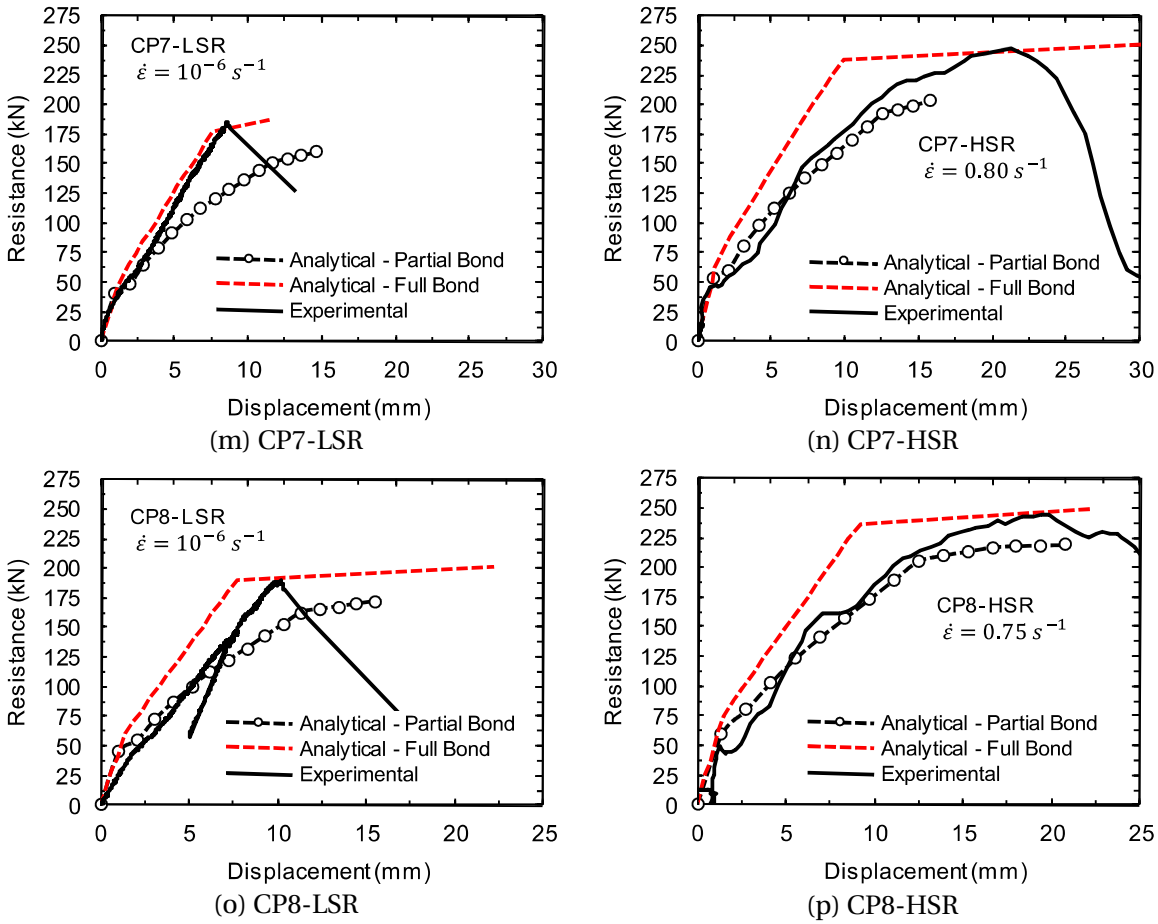

(m) CP7-LSR (n) CP7-HSR

(o) CP8-LSR (p) CP8-HSR

Figure 6.9: Comparison of low and high strain rate experimental resistance curves against those predicted considering full- and partial-bond conditions for splices confined by transverse reinforcement.

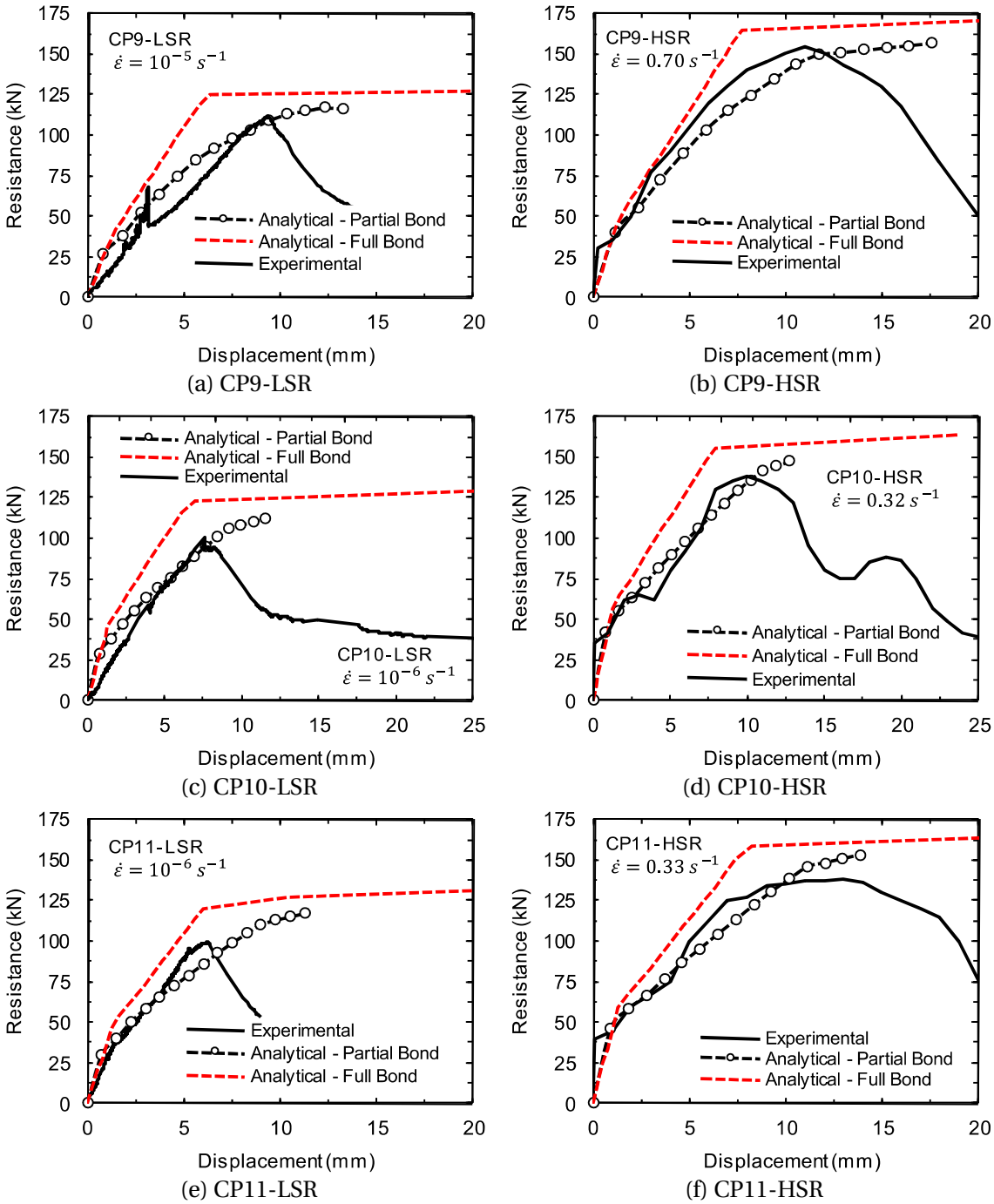

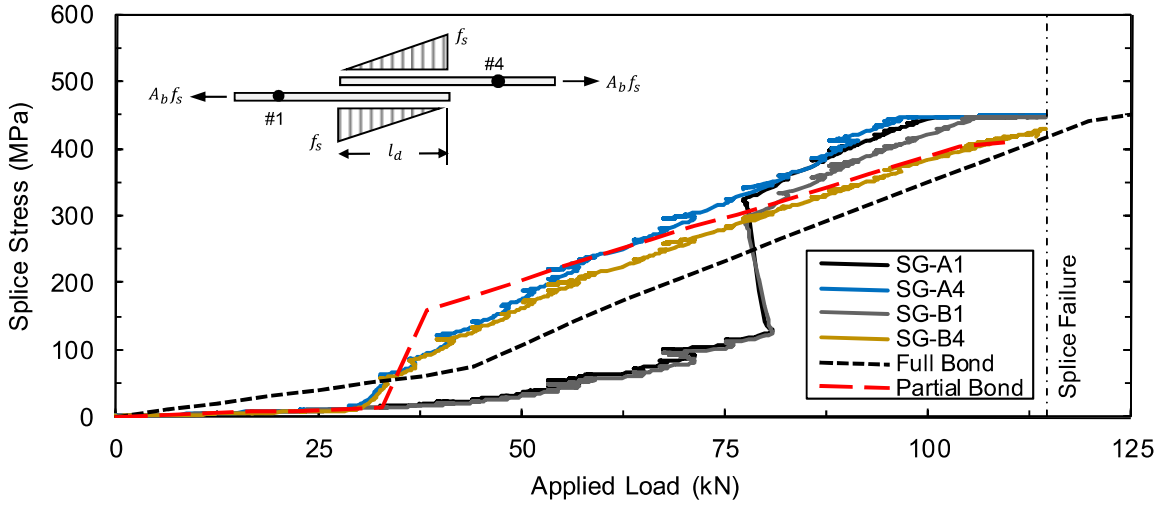

(a) CP4-LSR

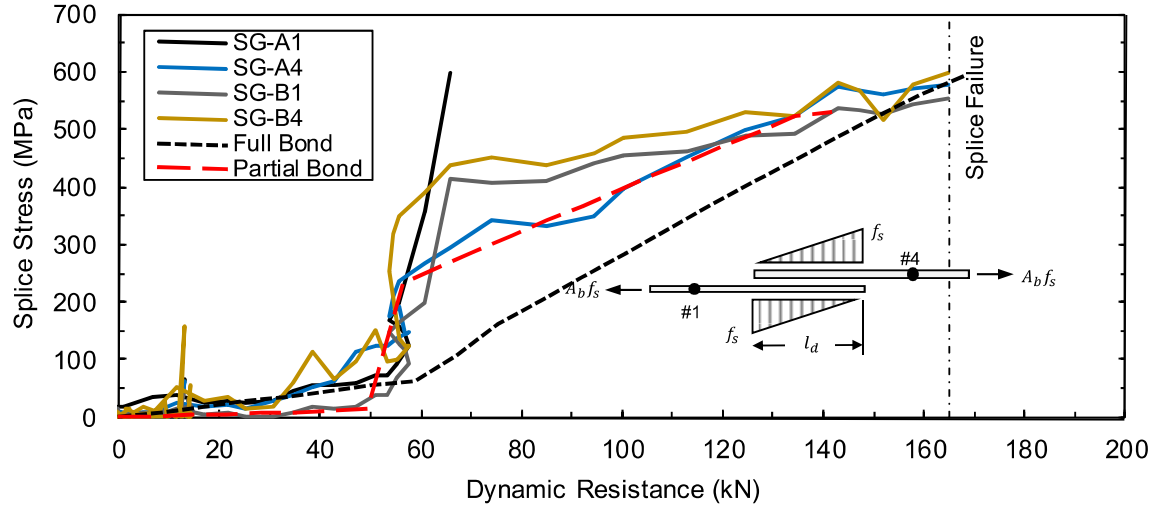

(b) CP4-HSR

Figure 6.10: Comparison of experimental and predicted splice stress for companion pair CP4.

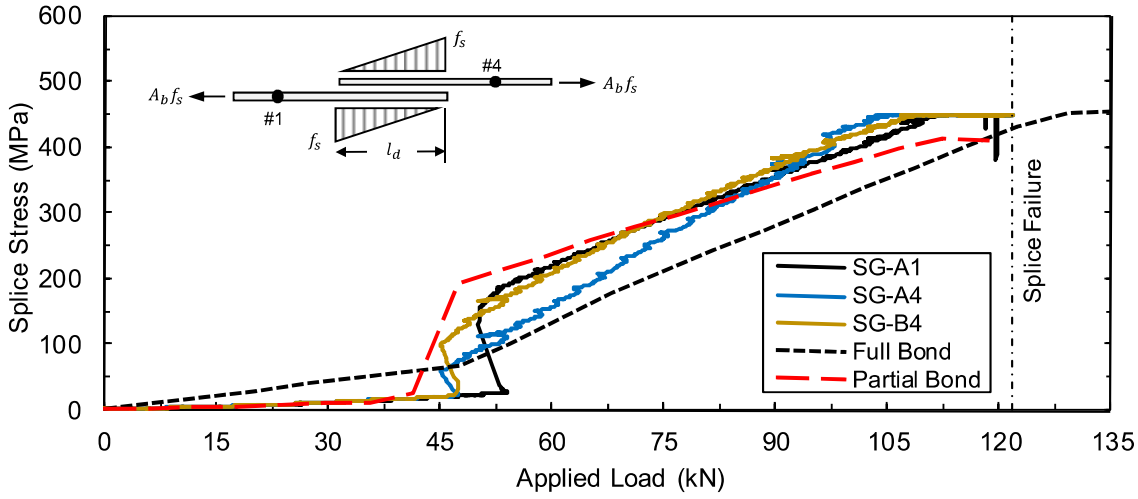

(a) CP6-LSR

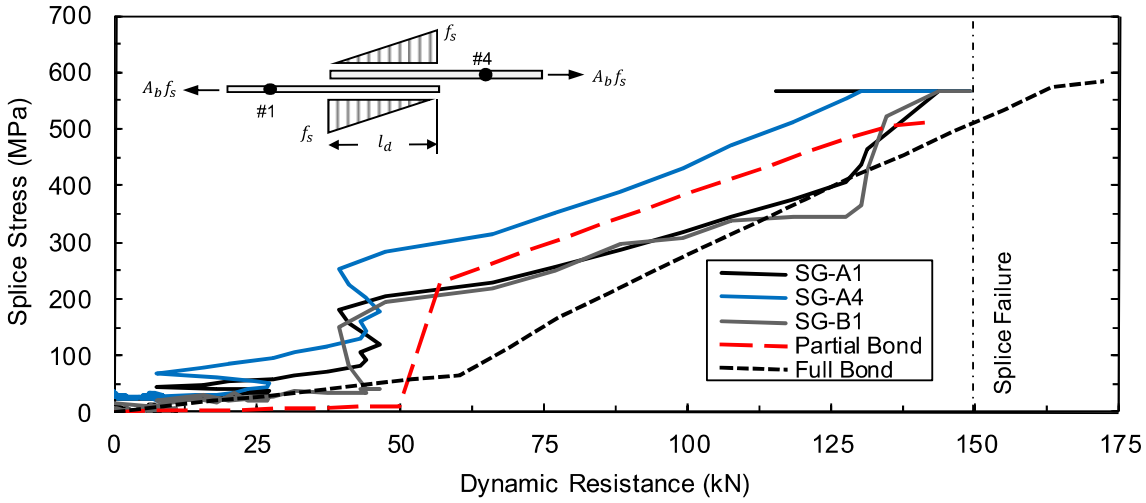

(b) CP6-HSR

Figure 6.11: Comparison of experimental and predicted splice stress for companion pair CP6.

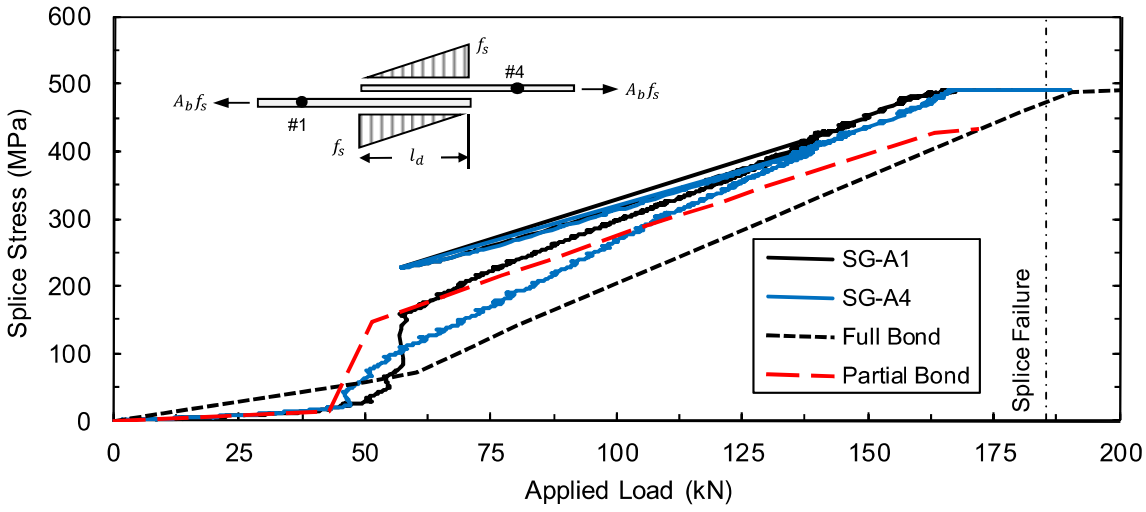

(a) CP8-LSR

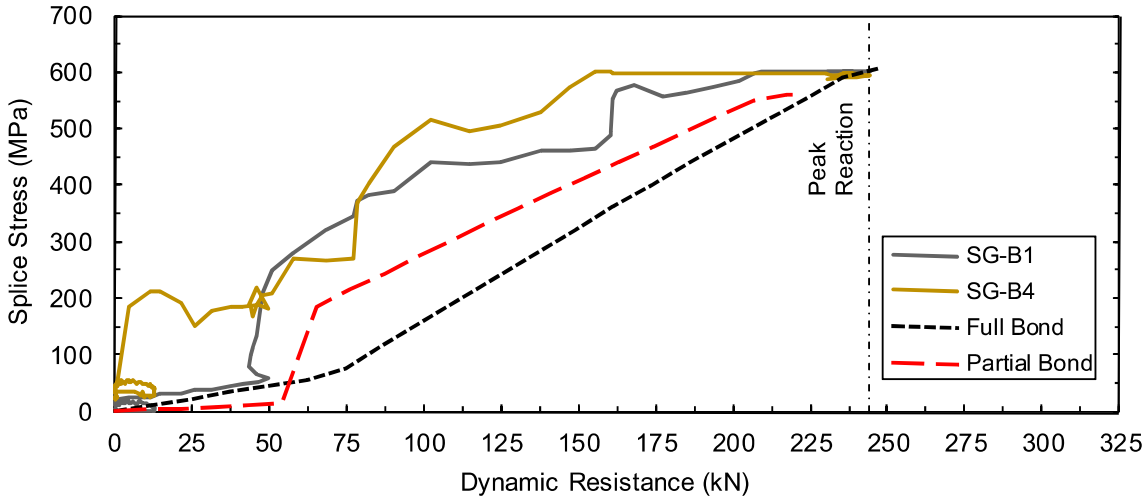

(b) CP8-HSR

Figure 6.12: Comparison of experimental and predicted splice stress for companion pair CP8.

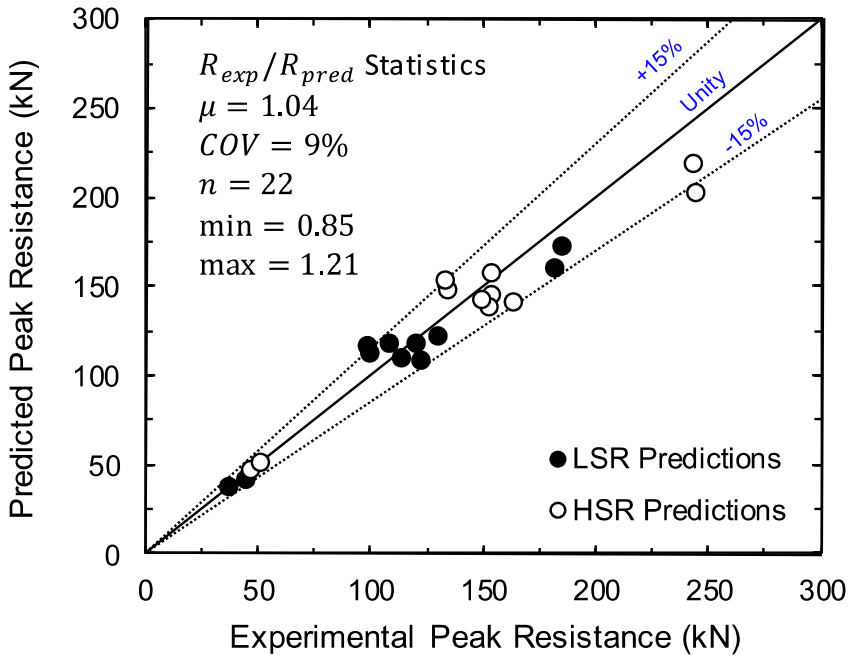

Figure 6.13: Experimental peak resistance compared against peak resistance predicted using the partially-bonded analysis methodology.

Part III

Conclusions & Future Work

Chapter 7

Conclusions

This thesis presented a comprehensive experimental and analytical research program undertaken to establish the effect of high strain rates on the characteristics of reinforced concrete bond. The research was motivated by the lack of design information on dynamic bond strength in protective design documents, such as CSA S850 in Canada and UFC 03-340-02 in the United States. The objectives of the study were to generate experimental data on the effect of high strain rates on reinforced concrete bond, evaluate the experimental results to characterize high strain rate bond characteristics, and develop descriptive expression(s) and analytical modelling techniques to properly predict the observed behaviours. The following is an overview of the work and summary of the main conclusions.

7.1 Summary of the Experimental Program

The experimental program consisted of subjecting companion pairs of reinforced concrete flexural specimens to low- and high-strain rates. This loading scheme allowed for direct comparison of results which facilitated assessment of the dynamic bond characteristics. A total of 39 reinforced concrete flexural members were tested, of which 22 were cantilever beam-ends having 20M deformed reinforcement with bonded length of 200 or 400 mm. The remaining 25 specimens were reinforced concrete beams containing tension lap splices divided into 12 companion pairs. The primary test variables governing construction of the companion pairs were the size of spliced reinforcement, concrete cover depth, concrete strength and the presence of transverse reinforcement. The test variables were varied based on factors known to significantly influence bond strength. Low strain rate static tests were conducted at the University of Ottawa Structures Laboratory, while high strain rate tests were conducted at the University of Ottawa Shock Tube Testing Facility. Two load transfer devices were designed and constructed to convert the planar

shock wave generated by the shock tube into dynamically-applied point loads required for the cantilever beam-end and lap splice beam tests. Static tests generated average reinforcement strain rates of approximately 10^{-6} s^{-1}, while dynamic tests achieved strain rates on the order of 0.1 – 1.0 s^{-1}. This range of high strain rates is consistent with those encountered in protective design against mid- and far-field explosive detonation.

7.2 Effect of Dynamic Loading on Cantilever Beam-ends

A comparison of the low- and high-strain rate test results obtained for the cantilever beam-end specimens showed that the bond strength of deformed reinforcement embedded in concrete was improved when subjected to dynamic loads. Based on strain gauge readings obtained over the bonded length, the elastic bond strength of cantilever beam-ends experienced a *DIF* applied to bond strength of 1.45 at strain rates on the order of 0.1 s^{-1} under all conditions of bonded length. For steel response limited to the elastic region, it was found that the general shape of the bond stress-slip curve, and the slip displacement at which peak bond stress was attained, were not significantly affected by dynamic loads.

Considering bond characteristics at ultimate conditions, the improvement in bond strength due to high strain rate effects was not sufficient to alter the bond splitting failure mode observed for beam-ends with 200 mm bonded length when subjected to static or dynamic loading. However, for beam-ends with 400 mm bonded length, high strain rate effects were sufficient to transition from a splitting type failure under static loads to a rupture of reinforcement when subjected to dynamic loading. The ultimate bond strength of beam-ends experienced *DIFs* which varied between 1.47 for samples with 200 mm bonded length and 1.33 for those beam-ends with 400 mm bonded length, both at a strain rate on the order of 0.1 to 1.0 s^{-1}.

7.3 Effect of Dynamic Loading on Lap Splice Beams

The dynamic strength and stiffness of lap spliced reinforced concrete beams was improved when beams were subjected to strain rates between 0.28 to 1.13 s^{-1}. The peak resistance of the dynamically-tested beams was on average 30% greater than the reference static resistance. In addition, the area under the resistance curve up to bond failure, defined as the bond energy, increased by 163% when subjected to dynamic loads, relative to reference static conditions. Despite improvements to the strength and stiffness of the lap splice beams, the general behaviour of specimens showed that the underlying flexural response and nature of the bond splitting failure was not affected by dynamic loads. Furthermore, the use of transverse reinforcement to confine spliced regions led to improvements in post-peak strength and splice toughness relative to splices without transverse reinforcement. When the results of the beam tests are examined with respect to bond strength, the

high strain rate bond strength of the tension lap splices was, without exception, always greater than corresponding low strain rate values, yielding an average *DIF* applied to bond strength of 1.28.

7.4 Reinforced Concrete Bond Characteristics at High Strain Rates

A database of 41 low and high strain rate flexural bond tests was constructed. The majority of the database was composed of cantilever beam-end and lap splice beam test results obtained during the course of this study, and was further supplemented by relevant literature data. In order to establish a baseline for comparison, approximately half of the total number of specimens were subjected to static testing ($\dot{\varepsilon} = 10^{-6} s^{-1}$) while the remainder were subjected to dynamic loading using a shock tube or drop weight impactor ($\dot{\varepsilon} = 0.1 - 1\ s^{-1}$). The results showed that the total bond strength of deformed reinforcement, with and without transverse reinforcement, was improved when subjected to high strain rate loading. The total bond force of all tests included in the database experienced an average *DIF* of 1.31 at an average high strain rate of 0.58 s^{-1}.

The influence of the geometry and material properties on the dynamic bond strength of developed and spliced reinforcement was analyzed using the aforementioned database. As is customary in the analysis of bond under static loads, it was assumed that the influence of concrete properties on bond could be accounted for by normalizing total bond force with respect to the static or dynamic compressive strength of concrete raised to the exponent 1/4. The strain rate sensitivity of normalized bond force was then divided into two components, consisting of the bond force developed without transverse reinforcement, and the additional bond force provided by transverse reinforcement.

The strain rate sensitivity of normalized bond force for bars not confined by transverse reinforcement was found to be proportional to the reinforcement cross-sectional area A_b. This is attributed to lateral inertial confinement provided by the cover concrete when the bar is subjected to dynamic loading. Inertia forces in the concrete are activated by radial acceleration of the cover due to wedging action of the rebar lugs against the surrounding concrete. The greater strain rate sensitivity exhibited by increasing reinforcement size can be explained by the activation of a greater degree of wedging, and hence greater confinement provided by the inertial resistance of the cover.

The strain rate sensitivity of normalized bond force for bars not confined by transverse reinforcement was also found to be inversely proportional to the idealized bond splitting failure plane $l_d(c_{min} + 0.5d_b)$. Although increasing the area of the idealized failure plane, either by providing increased development length, cover, or bar size, did yield greater total bond force, it resulted in a decrease in strain rate sensitivity. This stems from the fact that bond stresses are not uniformly distributed over the developed length, and that bond failures are localized and incremental. Finally, the normalized bond force obtained for bars not confined by transverse reinforcement when

subjected to dynamic loading was always greater than the corresponding static bond force. Therefore, the strain rate sensitivity of bond was always greater than or equal to unity. This indicates that there is an upper limit on the idealized crack splitting failure plane beyond which normalized bond force exhibited no strain rate sensitivity.

Although only limited test data was available on the strain rate sensitivity of the additional bond force provided by transverse reinforcement, the results indicated that the contribution of normalized bond force provided by transverse reinforcement was sensitive to strain rate enhancement. Greater strain rate sensitivity was generally observed in proportion to the quantity of transverse reinforcement confining the developed or spline reinforcement, and also in proportion to the size and deformation pattern of the deformed reinforcement. However, additional tests are recommended to elaborate on the effect of transverse reinforcement on dynamic bond strength.

Empirical expressions were developed for the observed strain rate sensitivity of each the components affecting bond force. When used in conjunction with the descriptive expression for static bond strength developed by ACI Committee 408R, excellent predictions of high strain rate bond strength were obtained. The descriptive expressions developed in this thesis for high strain rate bond strength correspond to the typical range of strain rates encountered in protective design against mid- and far-field explosive detonation, $\dot{\varepsilon} \approx 0.1 - 1\ s^{-1}$.

7.5 Limitations of the Experimental Study

The experimental investigation had two main limitations. First, only a narrow band of high strain rates (0.1 – 1.0 s^{-1}) were studied. It was not possible to generate higher strain rates during the beam-end and lap splice beam tests as a result of practical limitations in the pressure-impulse combinations generated by the shock tube. Offsetting this limitation is the fact that the strain rates which were achieved are consistent with those associated with mid- and far-field response of reinforced concrete structures. Therefore, the results presented in this thesis were obtained at strain rates which encompass the band of strain rates most often encountered in protective design.

The second limitation in the work was that lap splices confined by transverse reinforcement comprised only a small number of the total number of test specimens. Since in protective design practice development lengths and spliced regions are never detailed without transverse reinforcement, focusing on bars without transverse reinforcement could be viewed as limiting the applicability of the work. However, since the bond force generated in bars without transverse reinforcement accounts for approximately 75% of the total bond force developed in bars confined by transverse reinforcement, it was logical to focus on the largest component contributing to bond strength. Expanding the research to further examine the effect of transverse reinforcement on high strain rate bond sensitivity is acknowledged as an area requiring further study.

7.6 Structural Modeling of Bond-Slip Phenomenon

Load-deformation resistance curves for lap splice beams subjected to low- and high-strain rates exhibited reduced strength and stiffness relative to what was predicted using conventional flexural theory. The observed reduction in capacity was attributed to slippage of reinforcement in the lap splices. The bond-slip response of spliced reinforcement was modelled using pseudo-material stress-strain relationships, which accounted for the apparent reduction in reinforcing steel strength and stiffness that occurs due to bond degradation.

The pseudo-material stress-strain relationships were constructed by first assuming a displacement field distributed along the spliced bar. The effective load carrying capacity of the splice was then computed ensuring compatibility between the bond-slip law and material stress-strain relationship. Material properties and dynamic increase factors were defined using accepted formulations. The influence of strain rate on bond-slip response was accounted for by applying the descriptive expressions developed for DIF_{T_c} and DIF_{T_s} to bond strength and modifying the shape of the bond-slip curve based on experimental observations obtained during the cantilever beam-end tests. Beam failure criteria were expressed in terms of a flexural failure of the member or a bond splitting failure of the splice.

A comparison of the predicted resistance curves with those obtained experimentally demonstrated that the proposed analysis technique can reasonably predict the flexural response of beams with tension lap splices having only partially-bonded reinforcement. The results also showed that the analytical model was equally applicable for use at low- and high-strain rate loading, such as those generated during blast response in the mid- to far-field. However, further validation is required to assess the suitability and limitations of the methodology when applied to a broader range of reinforced concrete flexure members beyond those considered in this research.

7.7 Implications for Protective Design

Currently, any strain rate-related strength enhancement is ignored when proportioning the length of reinforcement required to resist dynamic forces. This approach, adopted in CSA S850 and UFC 03-340-02, reflects the general lack of understanding on the rate sensitivity of reinforced concrete bond and the factors which influence bond sensitivity. While the use of static bond strength to proportion the reinforcement length required to resist dynamic loads is undoubtedly conservative, it is an inconvenient philosophy for a number of reasons. First, ignoring dynamic bond strength makes it impossible to establish to what degree an existing splice or developed region is sufficient or deficient. Second, this approach does not provide adequate understanding of the problem for a detailed design. Finally, the conservative philosophy does not contribute to the

advancement of the state of the art of protective design. Clearly, experimental and analytical work conducted as part of this thesis is badly needed by the protective design community.

To support codification of the experimental results presented in this thesis, an empirical expression was generated to obtain the minimum dynamic development length (l_{dd}) required to resist high strain rate loads. The design expression, the first of its kind to be developed, incorporated the influence of high strain rates on reinforced concrete bond strength. To maintain consistency with the Canadian standard for concrete design, CSA A23.3, the strain rate sensitivity of bond force due to concrete properties was assumed to be proportional to the square root of the dynamic compressive strength of concrete f'_{dc}. The expression for l_{dd} was found to under-predict the total bond force developed in anchored and spliced reinforcement. In other words, the dynamic development lengths predicted using the design expression were consistently greater than those provided experimentally. This indicated a level of conservatism suitable to the purposes of design and assessment of protective concrete structures subjected to blast loads. The design expression for dynamic development length l_{dd} is valid only for the load combination for ultimate limit states design of blast-loaded structures, $1.0D + 0.5L + 0.25S + 1.0B$ and protective design for mid- and far-field detonations. Development lengths required for all other load combinations (*e.g.* static, wind, earthquake) should be verified separately and the most critical length selected for design. It is recommended that the lap splice and development length detailing requirements specified in CSA S850 be satisfied at all times for additional conservatism in design.

Chapter 8

Future Work

Based on the research detailed in this thesis, the following are highlighted for further study:

- Continue to investigate the influence of strain rate on bond strength for a greater range of physical parameters (cover depth, beam size, reinforcement size, splice spacing, number of splices, etc.);
- Expand the investigation to include a greater range of high strain rates;
- Conduct additional tests to elaborate on the effect of transverse reinforcement on bond strength and dynamic load-deformation characteristics;
- Establish the influence of concrete properties on the strain rate sensitivity of bond by testing beams with identical construction varying only concrete strength;
- Investigate the effect of blast-induced high strain rates on bond strength when normal strength concrete is replaced with high-performance, self-consolidating and fibre reinforced concretes;
- Assess the predictive capability of the pseudo-material stress-strain relations developed for spliced reinforcement when different bond-slip relationships are used;
- Assess the general suitability of the analytical bond-slip model for tension lap splices against experimental load-deflection data collected by other researchers;
- Conduct detailed finite element analysis of the static and dynamic lap splice beams to further advance the state of the art of analytical modelling of structures subject to extreme load events.

Chapter 9

References

ACI. (2003). ACI Committee 408: Bond and Development of Straight Reinforcing Bars in Tension. American Concrete Institute, Farmington Hills, Michigan.

ACI. (2014). ACI Committee 318: Building Code Requirements for Structural Concrete. American Concrete Institute, Farmington Hills, Michigan.

Alsiwat. J. M., and Saatcioglu, M. (1992). Reinforcement Anchorage Slip under Monotonic Loading. Journal of Structural Engineering. American Society of Civil Engineering, ASCE, 118(9): 2421-2438.

Aoude, H., Hosinieh, M., Cook, W., and Mitchell, D. (2014). "Behaviour of Rectangular Columns Constructed with SCC and Steel Fibers," ASCE Journal of Structural Engineering, American Society of Civil Engineers, 141(8).

ASTM A944-10. (2010). Standard Test Method for Comparing Bond Strength of Steel Reinforcing Bars to Concrete Using Beam-End Specimens. Annual Book of ASTM Standards, American Society for Testing and Materials, West Conshohocken, Pennsylvania, USA, 4 pages.

Ayoub, A. and Filippou, F.C. (1999). Mixed Formulation of Bond-Slip Problems under Cyclic Loads. ASCE Journal of Structural Engineering, 125(6): 661-671.

Azizinamini, A., Chisala, M., and Ghosh, S.K. (1995). Tension Development Length of Reinforcing Bars Embedded in High-Strength Concrete. Engineering Structures, 17(7): 512-522.

Beconcini, M.L., Croce, P., and Formichi, P. (2008). Influence of bond-slip on the behaviour of reinforced concrete beam to column joints. In Walraven, J.C., and Stoelhorst, D. (Eds.) Tailor Made Structures: Tailor Made Concrete Structures, pp. 533-539.

Bentz, E.C. (2000). Sectional Analysis of Reinforced Concrete Members. Ph.D. Thesis, Department of Civil Engineering, University of Toronto, Toronto, Ontario, 310 pages.

Bertero, V.V., Rea, D., Mahin, S., and Atalay, M.B. (1973). "Rate of Loading Effects on Uncracked and Repaired Reinforced Concrete Members." Proceedings of the 5th World Conference on Earthquake Engineering, Istanbul, Turkey, pp. 271-278.

Biggs, J. M. (1964). Introduction to Structural Dynamics. McGraw-Hill, New York, NY.

Bischoff, P. H., and Perry, S. H. (1991). "Compressive behaviour of concrete at high strain rates," Materials Research Society Symposia Proceedings, 64, pp. 151-165.

Bischoff, P. H., and Perry, S. H. 1995. Impact behaviour of plain concrete loaded in uniaxial compression. Journal of Engineering Mechanics, 121(6): 685-693.

Briggs, M., Miller, S., Darwin, D., and Browning, J. (2007). Bond Behavior of Grade 100 ASTM A1035 Reinforcing Steel in Beam-Splice Specimens. SL Report 07-01, University of Kansas Center for Research, Lawrence, Kansas, 92 pages.

Brown, C.J., Darwin, D., and McCabe, S.L. (1993). Finite Element Fracture Analysis of Steel-Concrete Bond. SM Report No. 36, University of Kansas Center for Research, Lawrence, Kans., Nov., 100 pages.

CEB-FIP (1993). Model Code 90 for Concrete Structures, Federation International de la preconstraint, CEB Bulletin No. 213/214, Paris.

Chung, L., and Shah, S. (1987). Strain rate effects on bond stresses during earthquake loading. Proceedings of the Pacific Conference on Earthquake Engineering, Wairakei, New Zealand, 5-8 August 1987, Vol. 1.

Ciampi, V., Eligehausen, R., Bertero, V.V., and Popov, E.P. (1981). Analytical model for deformed bar bond under generalized excitations, IABSE Colloquium on Advanced Mechanics in Reinforced Concrete, Delft, The Netherlands.

Collins, M.P., and Mitchell, D. (2001) Prestressed Concrete Structures. Response Publicatios.

Canadian Standards Association (2004). Design of concrete structures. CSA Standard A23.3-04. Canadian Standards Association, Mississauga, Ontario.

Canadian Standards Association (2014). Design of concrete structures. CSA Standard A23.3-14. Canadian Standards Association, Mississauga, Ontario.

Canadian Standards Association. (2012). Design and assessment of buildings subjected to blast Loads. CSA Standard S850-12, Mississauga, ON, Canada.

Darwin, D., and Graham, E. K. (1993). Effect of Deformation Height and Spacing on Bond Strength of Reinforcing Bars, SL Report 93-1, University of Kansas Center for Research, Lawrence, Kans., Jan., 68 pages.

Darwin, D., McCabe, S.L., Idun, E.K., and Schoenekase, S.P. (1992). Development Length Criteria: Bars Not Confined by Transverse Reinforcement. ACI Structural Journal, 89(6): 709-720.

Darwin, D., Tholen, M.L., Idun, E.K., and Zuo, J. (1996). Splice Strength of High Relative Rib Area Reinforcing Bars. ACI Structural Journal, 93(1): 95-107.

Department of Defense. (2008). Structures to Resist the Effects of Accidental Explosions. United Facilities Code (UFC) 03-340-02. United States of America Department of Defense, Washington, D.C.

Eligehausen, R., Popov, E.P., and Bertero, V. (1983). Local Bond Stress-slip Relationships of Deformed Bars Under Generalized Excitations. Rep. No. UCB/EERC 83/23, Earthquake Engineering Research Center, University of California, Berkeley.

Ferguson, P.M., and Breen, J.E. (1965) Lapped Splices for High Strength Reinforcing Bars. Journal of the American Concrete Institute, 62(9): 1063-1076.

Fu, H. C., Erki, M. A., and Seckin, M. (1991). Review of Effects of Loading Rate on Reinforced Concrete. ASCE Journal of Structural Engineering, 117(12): 3660-3679.

Gan, Y. (2000). Bond Stress and Slip Modeling in Nonlinear Finite Element Analysis of Reinforced Concrete Structures. M.A.Sc. Thesis. Graduate Department of Civil Engineering, University of Toronto, Toronto, Ontario, 269 pages.

Harajli, M.H. (2004). Comparison of Bond Strength of Steel Bars in Normal and High-Strength Concrete. ASCE Journal of Materials in Civil Engineering, 16(10): 365-374.

Harajli, M.H., Hamad, B., and Karam, K. (2002). Bond-slip Response of Reinforcing Bars Embedded in Plain and Fiber Concrete. ASCE Journal of Materials in Civil Engineering, 14(6): 503-511.

Jacques, E. (2011). Blast Retrofit of Reinforced Concrete Walls and Slabs. M.A.Sc. Thesis, Department of Civil Engineering, University of Ottawa, Ottawa, Ontario, 286 pages.

Jacques, E., and Saatcioglu, M., (2016) “Blind Simulation of Blast Loaded Slabs Using RCBlast Software,”. ACI-SP 306: Analytical and Finite Element Concrete Material Models - Comparison of Blast Response Analysis of One Way Slabs with Experimental Data, American Concrete Institute, Farmington Hills, Michigan.

Jacques, E., Lloyd, A., Braimah, A., Saatcioglu, M., Doudak, G., and Abdelalim, O. (2014) “Influence of High Strain Rates on the Dynamic Flexural Material Properties of Spruce-Pine-Fir Wood Studs,” Canadian Journal of Civil Engineering, 41(1): 56-64.

Jacques, E., Lloyd, A., and Saatcioglu, M. (2012). “Predicting reinforced concrete response to blast loads.” Canadian Journal of Civil Engineering, 40(5): 427–444.

Lloyd, A., Jacques, E., Saatcioglu, M., Palermo, D., Nistor, I., and Tikka, T. (2011). Capabilities and Effectiveness of using a Shock Tube to Simulate Blast Loading on Structures and Structural Components. ACI-SP 281: Behavior of Concrete Structures Subjected to Blast and Impact, American Concrete Institute, Farmington Hills, Michigan.

Lloyd, A.E.W. (2015). Blast Retrofit of Reinforced Concrete Columns. Ph.D. Thesis. Department of Civil Engineering, University of Ottawa, Ottawa, Ontario, 466 pages.

Malvar, L.J., and Crawford, J.E. (1998a). Dynamic Increase Factors for Steel Reinforcing Bars. Proceedings of the Twenty-Eighth DDESB Seminar, DoD Explosives Safety Board, Orlando, Florida.

Malvar, L. J., and Crawford, J. E. (1998b). “Dynamic Increase Factors for Concrete.” Proceedings of the Twenty-Eighth DDESB Seminar, DoD Explosives Safety Board, Orlando, FL.

Michal, M., Keuser, M., Solomos, G., Peroni, M., Larcher, M., and Esteban, B. (2015). Experimental Investigation of Bond Strength under High Loading Rates. Proceedings of the 11th International DYMAT Conference p. 01044 vol. 94.

Monti, G., Filippou, F.C., and Spacone, E. (1997). Finite Element for Anchored Bars Under Cyclic Load Reversals, Journal of Structural Engineering., 123(5): 614-623.

Monti, G., and Spacone, E. (2000). Reinforced Concrete fiber beam Element with Bond-slip. Journal of Structural Engineering, 126(6): 654-661.

Orakcal, K., and Chowdhury, S.R. (2012). Bond Slip Modeling of Reinforced Concrete Columns with Deficient Lap Splices. Proceedings of the 15th World Conference on Earthquake Engineering 2012 (15WCEE), Lisbon, Portugal, September 24-28, 2013.

Orangun, C.O., Jirsa, J.O., and Breen, J.E. (1977). A Reevaluation of Test Data on Development Length and Splices. ACI Journal, 74(3): 114-122.

Pimanmas, A., and Thai, D.X. (2011). Response of Lap Splice of Reinforcing Bars Confined by FRP Wrapping: Application to Nonlinear Analysis of RC Column. Structural Engineering and Mechanics, 37(1): 111-129.

Porasz, A. (1989). An Investigation of the Stress-Strain Characteristics of High Strength Concrete in Shear. M.A.Sc. Thesis, University of Toronto, Toronto, Ontario.

Reinhardt, H.W. (1982). Concrete under Impact Loading, Tensile Strength and Bond, HERON, 27(3), 48 pages.

Rezansoff, T., Bufkin, M.P., Jirsa, J.O., and Breen, J.E. (1975). The Performance of Lapped Splices Under Rapid Loading. Research Report 154-2, Center for Highway Research, The University of Texas at Austin, Austin Texas. 104 pages.

Shah, I.K., and Hansen, R.J. (1963). Behavior of Bond Under Dynamic Loading. Department of Civil Engineering, Massachusetts Institute of Technology, Cambridge Massachusetts.

Solomos, G., and Berra, M. (2010). Rebar Pullout Testing Under Dynamic Hopkinson Bar Induced Impulsive Loading. Materials and Structures, 43(1-2), pp. 247-260.

Thorenfeldt, E., Tomaszewicz, A., and Jensen, J.J. (1987). Mechanical Properties of High Strength Concrete and Application in Design. Proceedings of the Symposium Utilization of High Strength Concrete, Tapir, Trondheim, pp. 149-159.

Toikka, L., Braimah, A., Razaqpur, G., and Foo, S. (2015). Strain Rate Effect on Development Length of Steel Reinforcement. Journal of Structural Engineering, 141(11).

Toikka, L. (2012). Strain Rate Effect on Development Length of Steel Reinforcement Using Shock Tube Testing. M.A.Sc. Thesis, Department of Civil Engineering, Carleton University, Ottawa, Ontario. 251 pages.

Toutlemonde, F., Rossi, P., Boulay, C., Gourraud, C., and Guedon, D. 1995. Dynamic Behaviour of Concrete: Tests of Slabs with a shock Tube. Materials and Structures, 28(179): 293-298.

Vos, E. (1983). Influence of Loading Rate and Radial Pressure on Bond in Reinforced Concrete: A Numerical and Experimental Approach, Ph.D. Thesis, Delft University of Technology, The Netherlands, 250 pages.

Vos, E., and Reinhardt, H.W. (1982) Influence of Loading Rate on Bond Behaviour of Reinforcing Steel and Prestressing Strands. Materials and Structures, 15(85): 3-10.

Weathersby, J.H. (2003). Investigation of Bond Slip Between Concrete and Steel Reinforcement Under Dynamic Loading Conditions. Ph.D. Thesis, Department of Civil and Environmental Engineering, Louisiana State University and Agricultural and Mechanical College, Baton Rouge, Louisiana, 280 pages.

Wight, J. K., and MacGregor, J. G. (2009). Reinforced Concrete: Mechanics and Design (5th edition). Pearson Prentice Hall, Upper Saddle River, NJ.

Xiao, Y. and Ma, R. (1997). Seismic Retrofit of RC Circular Columns using Prefabricated Composite Jacketing, ASCE Journal of Structural Engineering, 123(10): 1357-1364.

Xiao S., Cao, W., and Pan, H. (2012) Experiment of Reinforce Concrete Beams at Different Loading Rates, Proceedings of the 15th World Conference on Earthquake Engineering 2012 (15WCEE), Lisbon, Portugal, September 24-28.

Yalcin, C., and Saatcioglu, M. (2000). Inelastic Analysis of Reinforced Concrete Columns. Computers & Structures, 77(5): 539–555.

Yan, C. (1992). Bond Between Reinforcing Bars and Concrete Under Impact Loading. Ph.D. Thesis, Department of Civil Engineering, University of British Colombia, Vancouver, B.C., 412 pages.

Yao, W., Wu, H., and Huang, F. (2013). Experimental Investigation about Dynamic Bond-slip between Reinforcing Steel Bar and Concrete. Applied Mechanics and Materials, Vols. 249-250: 1073-1081.

Zuo, J., and Darwin, D. (1998). Bond Strength of High Relative Rib Area Reinforcing Bars. SM Report No. 46, University of Kansas Center for Research, Lawrence, Kansas, 350 pages.

Zuo, J., and Darwin, D. (2000). Splice Strength of Conventional and High Relative Rib Area Bars in Normal and High-Strength Concrete. ACI Structural Journal, 97(4): 630-641.

Part IV

Appendices

Appendix A

Beam-end Bond Test Data

Appendix A contains the experimental results collected during the course of the experimental study on the performance of fourteen reinforced concrete cantilever beam-ends subjected to low and high strain rates. Chapter 3 contains a concise presentation of the results, as well as an analysis and discussion. Typical data presented in the appendix includes a brief written synopsis of each test, the material and cross-sectional properties, and a summary of the relevant experimental results. Strain values in the developed region are tabulated for each beam-end. Strain at the end of the bonded region ($x = 0$ mm) was computed by extrapolation. In cases were individual strain readings became corrupted during testing, substitute values were obtained by interpolation. The nomenclature and spacing of strain-gauges is provided in the figure below.

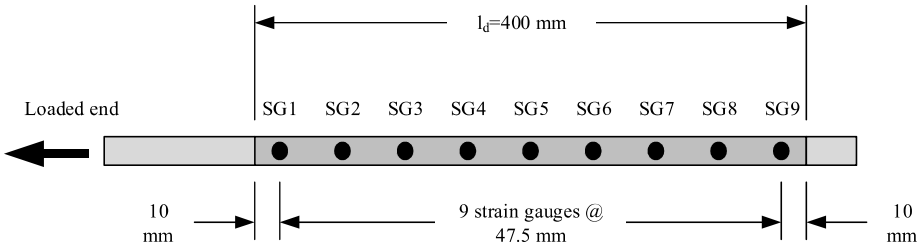

(a) Specimens with 400 mm bonded length

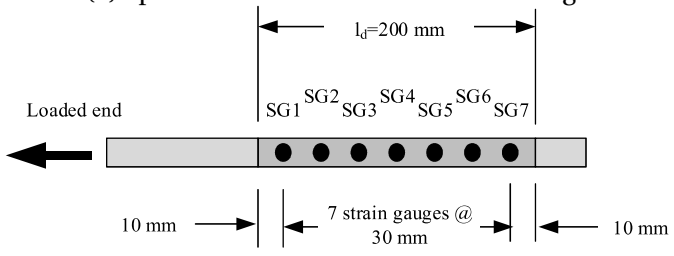

(b) Specimens with 200 mm bonded length

Figure A.1: Spacing and nomenclature of strain gauges for beam-end tests.

A.1: Beam-end BE1

BE1 with l_b = 200 mm was subjected to low strain rate testing on April 26, 2012. The specimen failed by tensile splitting of the cover concrete at an applied load of 114.2 kN generating a stress in the reinforcement of 419.9 MPa. Time-to-failure was 236.0 seconds and strain rate was 3.2×10^{-5} s^{-1}.

Table A.1.1: Experimental data for beam-end BE1.

General Test Data						Strain data in the bonded region ($\times10^{-6}$)								
Time **s**	$\dot{\varepsilon}$ **s^{-1}**	P_{exp} **kN**	f_s **MPa**	l_d **mm**	δ_{LE} **mm**	**LE**	**SG1**	**SG2**	**SG3**	**SG4**	**SG5**	**SG6**	**SG7**	**FE**
0	0	0	0	0	0	0	0	0	0	0	0	0	0	0
17.2	9.1×10^{-6}	10.7	31.3	176	0.019	157	150	127	115	98	111	39	6	0
41.6	6.6×10^{-6}	20.0	55.2	179	0.030	276	260	223	189	152	143	56	7	0
56.2	7.6×10^{-6}	30.0	85.1	179	0.043	425	401	340	281	219	186	73	10	0
91.4	6.5×10^{-6}	40.4	117.9	177	0.059	590	555	469	385	297	250	90	12	0
114.2	6.4×10^{-6}	50.0	145.7	176	0.075	728	677	594	485	381	343	119	14	0
122.2	7.0×10^{-6}	60.2	170.7	177	0.091	853	782	716	583	467	443	158	17	0
139.8	6.9×10^{-6}	70.1	192.2	189	0.113	961	919	848	739	643	544	196	22	0
171.0	6.4×10^{-6}	80.2	218.4	200	0.135	1092	1029	1012	877	784	681	260	29	0
184.2	7.0×10^{-6}	90.0	257.1	200	0.158	1286	1194	1214	1032	923	796	261	37	0
197.6	8.4×10^{-6}	100.1	332.7	200	0.202	1664	1535	1577	1326	1181	1009	311	55	0
218.2	9.3×10^{-6}	110.1	404.9	200	0.293	2024	2113	2201	2141	1709	1369	481	184	0
236.0	*3.2×10^{-5}*	*114.2*	*419.9*	*200*	*0.310*	*7645*	*3360*	*3405*	*3449*	*2135*	*934*	*498*	*498*	*0*

Note: Italicized data indicates questionable strain gauge readings.

(a) Prior to testing (b) After testing

Figure A.1.1: Photographs of BE1 before and after testing.

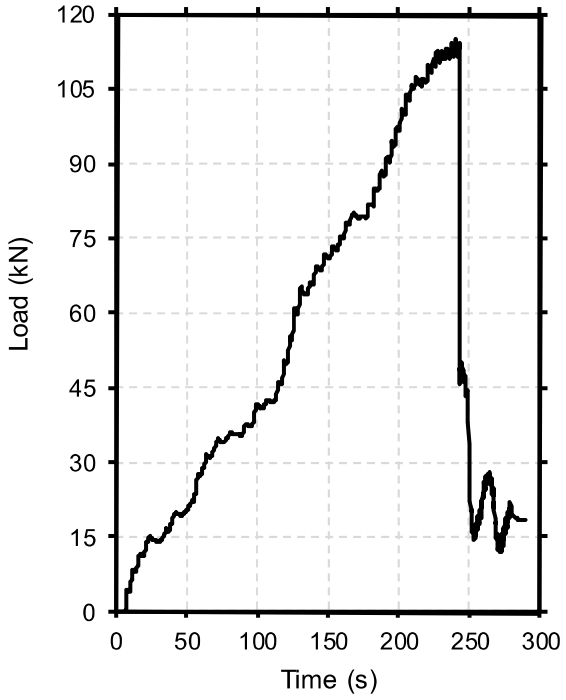

Figure A.1.2: Load-time history.

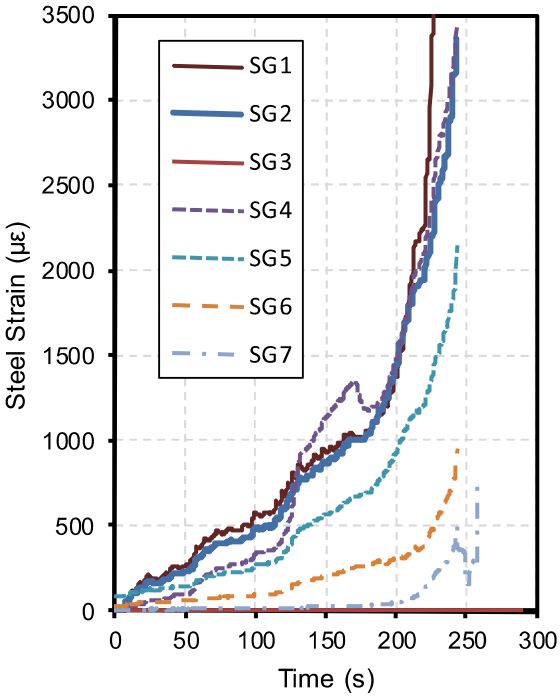

Figure A.1.3: Strain-time history.

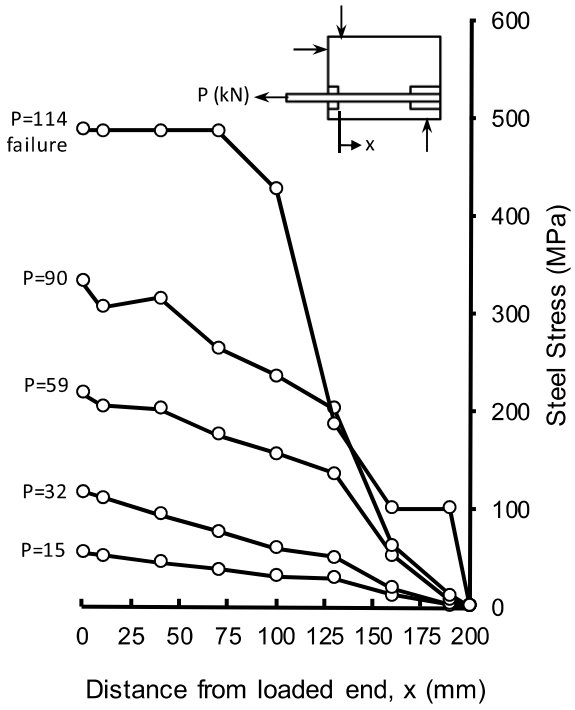

Figure A.1.4: Distribution of steel stresses in the bonded region.

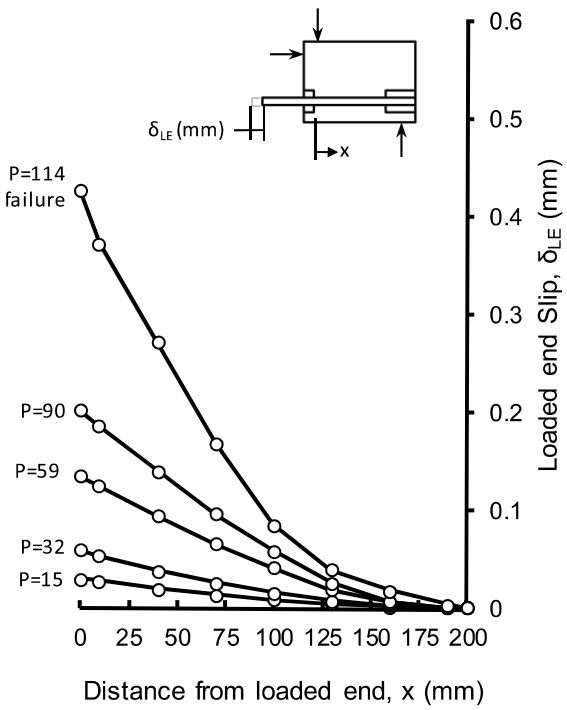

Figure A.1.5: Distribution of slip in the bonded region.

A.2: Beam-end BE2

BE2 with l_b = 200 mm was subjected to low strain rate testing on April 26, 2012. The specimen failed by tensile splitting of the cover concrete at an applied load of 107.9 kN generating a stress in the reinforcement of 395.8 MPa. Time-to-failure was 232.6 seconds and strain rate was 8.5×10^{-6} s^{-1}.

Table A.2.1: Experimental data for beam-end BE2.

General Test Data						Strain data in the bonded region ($\times10^{-6}$)								
Time s	$\dot{\varepsilon}$ s^{-1}	P_{exp} kN	f_s MPa	l_d mm	δ_{LE} mm	LE	SG1	SG2	SG3	SG4	SG5	SG6	SG7	FE
0	0	0	0	0	0	0	0	0	0	0	0	0	0	0
10.6	3.7×10^{-5}	10.4	78.5	130	0.026	393	345	297	159	60	27	20	13	0
18.4	2.7×10^{-5}	20.2	99.4	144	0.037	497	431	364	258	119	62	38	14	0
70.2	8.9×10^{-6}	30.2	125.3	164	0.053	626	543	460	371	263	114	65	16	0
90	8.5×10^{-6}	40.2	153.5	187	0.072	767	726	577	491	411	192	105	18	0
120.6	7.5×10^{-6}	50.4	179.9	200	0.091	899	857	688	618	574	280	150	21	0
129.8	8.5×10^{-6}	60.1	221.6	200	0.113	1108	1054	809	760	717	373	198	24	0
148.2	8.7×10^{-6}	70.3	258.9	200	0.136	1294	1234	947	910	864	486	256	26	0
162	9.1×10^{-6}	80.4	295.9	200	0.159	1480	1413	1083	1060	1015	601	316	31	0
183.6	9.1×10^{-6}	90.3	335.4	200	0.184	1677	1604	1256	1217	1123	755	396	38	0
221.6	8.6×10^{-6}	101.4	381.8	200	0.239	1909	1854	1656	1565	1357	1170	616	62	0
232.6	8.5×10^{-6}	107.9	395.8	200	0.296	1979	1971	1972	1876	1926	1551	831	110	0

Note: Italicized data indicates questionable strain gauge readings.

(a) After testing

(b) After testing

Figure A.2.1: Photographs of BE2 before and after testing.

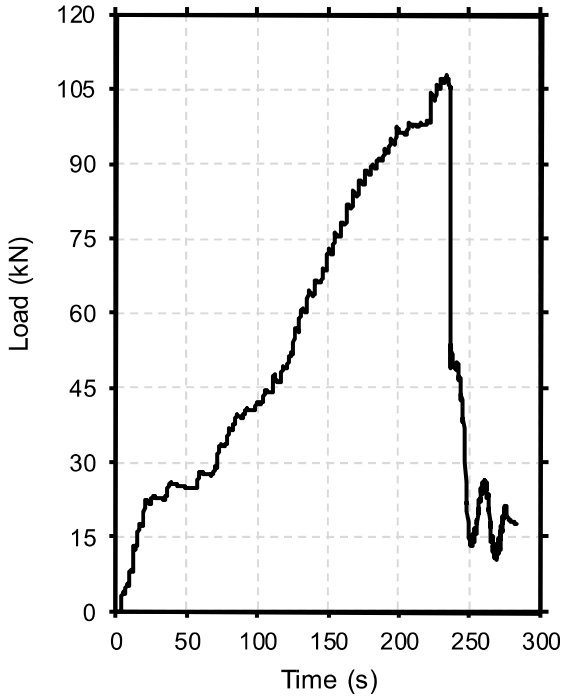

Figure A.2.2: Load-time history.

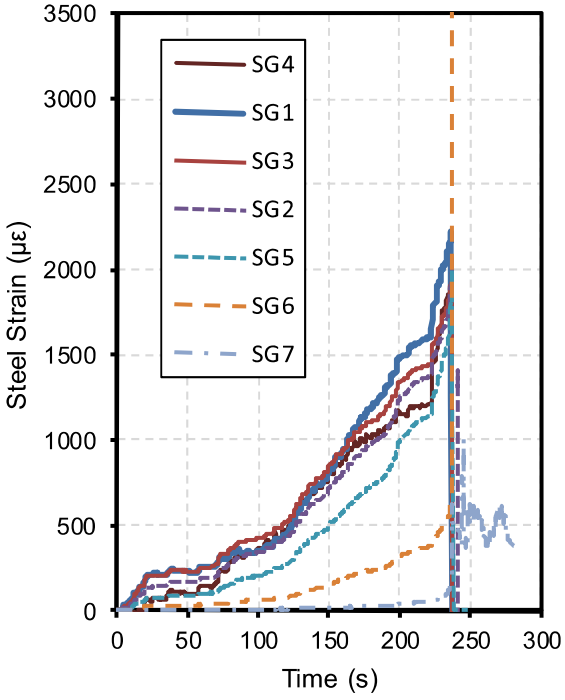

Figure A.2.3: Strain-time history.

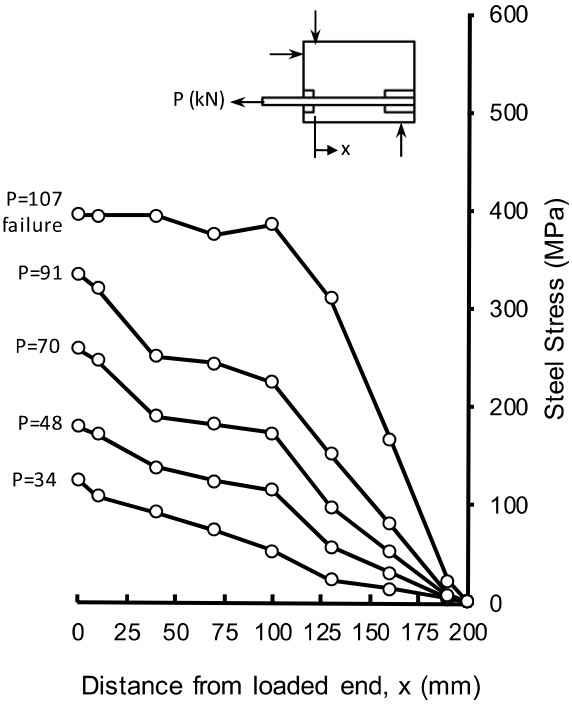

Figure A.2.4: Distribution of steel stresses in the bonded region.

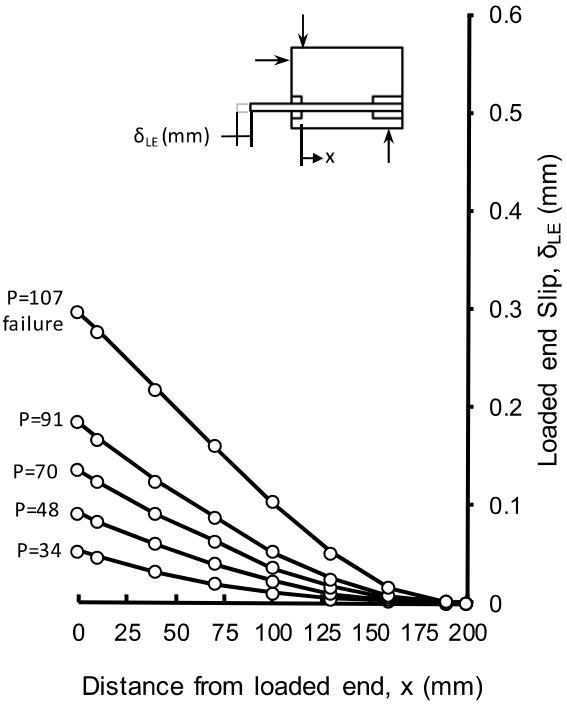

Figure A.2.5: Distribution of slip in the bonded region.

A.3: Beam-end BE3

BE3 with l_b = 200 mm was subjected to low strain rate testing on April 25, 2012. The specimen failed by tensile splitting of the cover concrete at an applied load of 100.4 kN generating a stress in the reinforcement of 380.0 MPa. Time-to-failure was 178.6 seconds and strain rate was 1.1×10^{-5} s^{-1}.

Table A.3.1: Experimental data for beam-end BE3.

General Test Data						Strain data in the bonded region ($\times10^{-6}$)								
Time s	$\dot{\varepsilon}$ s^{-1}	P_{exp} kN	f_s MPa	l_d mm	δ_{LE} mm	LE	SG1	SG2	SG3	SG4	SG5	SG6	SG7	FE
0	0	0	0	0	0	0	0	0	0	0	0	0	0	0
26.4	3.9×10^{-6}	10.1	20.7	172	0.009	104	86	93	68	34	23	11	3	0
37.2	6.8×10^{-6}	20.3	50.9	166	0.022	255	229	200	167	86	54	23	5	0
54.2	7.9×10^{-6}	30.0	85.8	178	0.038	429	390	331	291	164	100	36	8	0
91.4	6.9×10^{-6}	40.5	126.2	175	0.056	631	575	496	417	250	155	54	11	0
110	7.5×10^{-6}	50.0	164.0	189	0.076	820	742	652	562	366	238	76	13	0
119.4	8.7×10^{-6}	60.9	206.6	191	0.096	1033	932	816	700	464	311	98	18	0
134.8	9.1×10^{-6}	70.3	245.9	200	0.118	1230	1102	979	856	591	417	133	22	0
143.4	9.9×10^{-6}	79.8	284.2	200	0.139	1421	1271	1137	1003	707	514	172	28	0
170.6	9.6×10^{-6}	90.4	327.1	200	0.167	1636	1451	1325	1199	866	656	241	35	0
178.6	1.1×10^{-5}	100.4	380.0	200	0.219	1900	1648	1594	1541	1250	989	453	72	0

Note: Italicized data indicates questionable strain gauge readings.

(a) Before testing

(b) After testing

Figure A.3.1: Photographs of BE3 before and after testing.

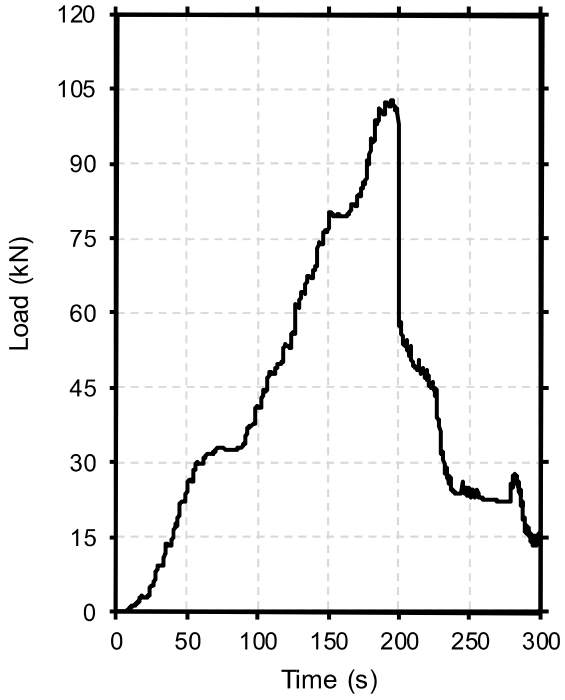

Figure A.3.2: Load-time history.

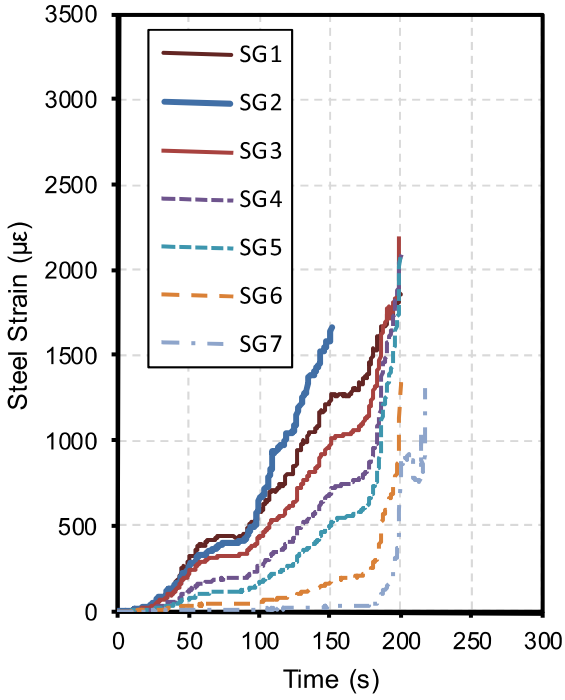

Figure A.3.3: Strain-time history.

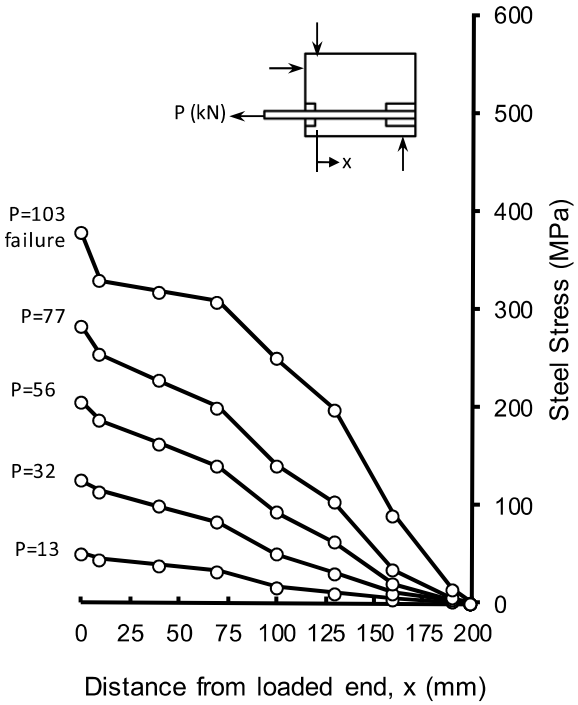

Figure A.3.4: Distribution of steel stresses in the bonded region.

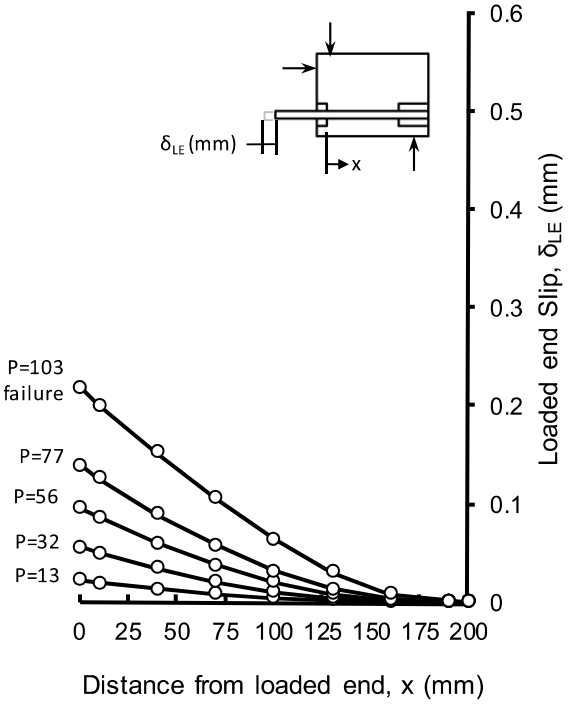

Figure A.3.5: Distribution of slip in the bonded region.

A.4: Beam-end BE4

BE4 with l_b = 200 mm was subjected to high strain rate testing on March 22, 2012. The DPL was used to subject this specimen to a shock wave with a reflected pressure of 292 kPa and reflected impulse of 3385 kPa-ms. The specimen failed by tensile splitting of the cover concrete and the reinforcement was stressed into the strain hardening range. The peak load considered in the analysis was 159.4 kN generating a stress in the reinforcement of 585.0 MPa. Time-to-failure was 30.7 milliseconds and strain rate was 0.14 s^{-1}.

Table A.4.1: Experimental data for beam-end BE4.

General Test Data						Strain data in the bonded region (×10^{-6})								
Time ms	$\dot{\varepsilon}$ s^{-1}	P_{exp} kN	f_s MPa	l_d mm	δ_{LE} mm	LE	SG1	SG2	SG3	SG4	SG5	SG6	SG7	FE
0	0	0	0	0	0	0	0	0	0	0	0	0	0	0
1.2	0.30	18.9	69.4	177	0.032	347	295	288	268	106	69	57	38	0
2.2	0.25	29.6	109.0	162	0.049	545	579	369	388	178	103	69	78	0
2.7	0.34	49.1	180.5	151	0.073	902	843	657	513	265	142	83	100	0
4.4	0.23	55.9	205.3	164	0.090	1027	964	733	665	380	203	101	148	0
6.2	0.30	100.7	370.2	183	0.171	1851	1640	1375	1248	840	499	196	222	0
7.9	0.36	155.9	573.1	193	0.276	2865	2717	2238	1879	1368	923	398	137	0
9.7	0.41	159.3	585.5	168	0.342	3921	3688	3179	2048	1510	1031	451	90	0
16.7	0.21	159.0	584.5	187	0.340	3572	3381	2808	2247	1620	1137	498	251	0
20.2	0.18	158.9	584.3	188	0.354	3552	3375	2841	2413	1698	1228	551	318	0
23.7	0.17	159.3	585.6	200	0.397	4064	3857	3238	2778	1889	1313	599	243	0
27.2	0.15	159.3	585.6	200	0.403	4068	3863	3249	2635	2064	1411	667	234	0
30.7	0.14	159.4	585.9	200	0.418	4222	4009	3371	2733	2145	1449	695	230	0
Dynamic loading continued until splitting failure														

Note: Italicized data indicates questionable strain gauge readings.

(a) After testing (b) After testing

Figure A.4.1: Photographs of BE4 before and after testing.

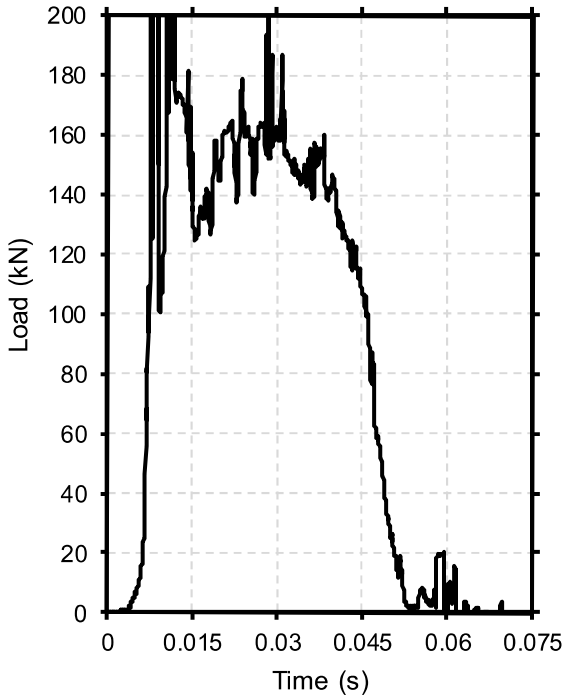

Figure A.4.2: Load-time history.

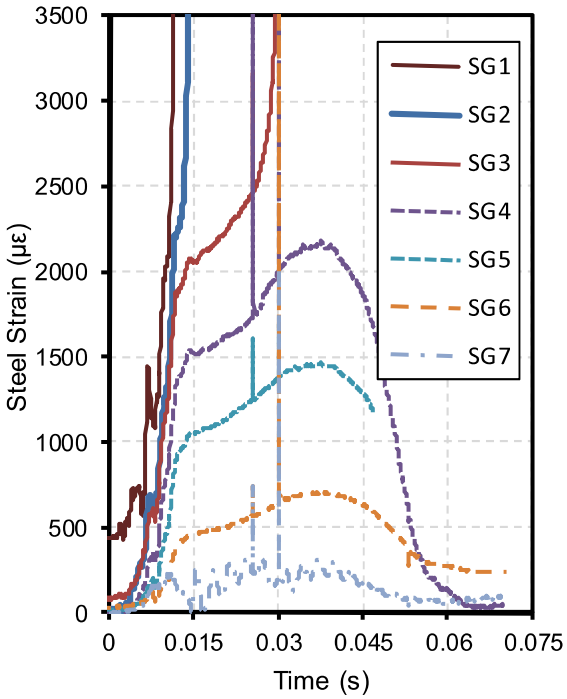

Figure A.4.3: Strain-time history.

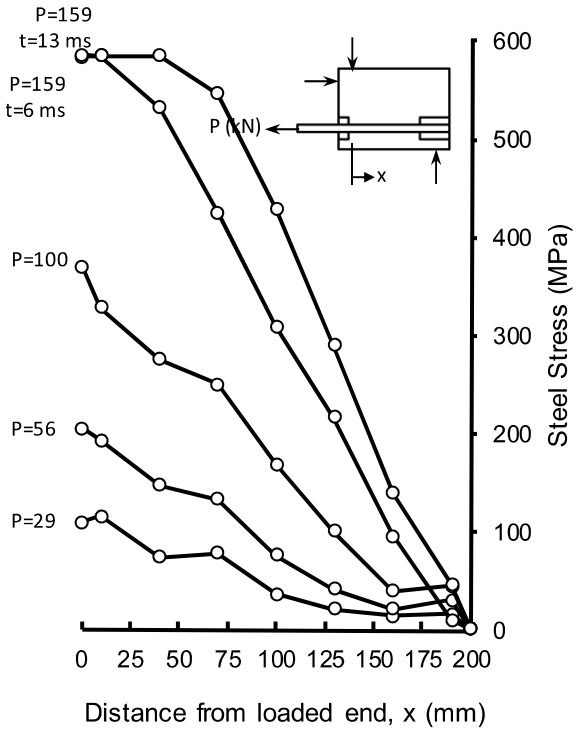

Figure A.4.4: Distribution of steel stresses in the bonded region.

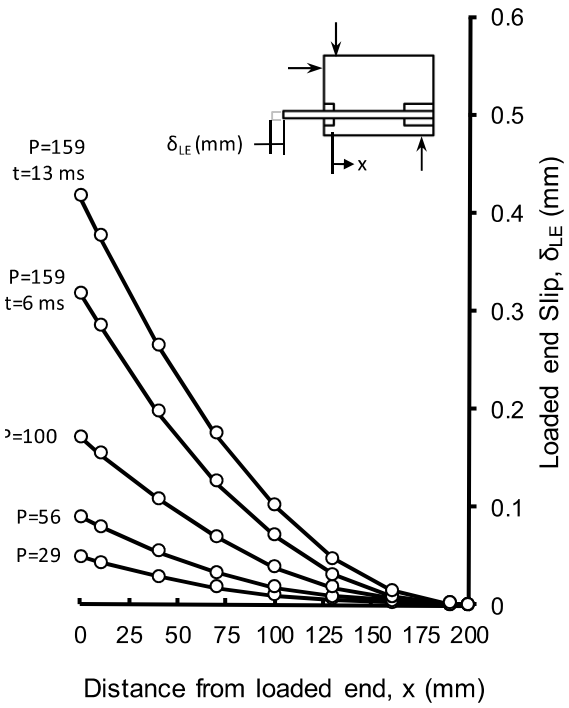

Figure A.4.5: Distribution of slip in the bonded region.

A.5: Beam-end BE5

BE5 with l_b = 200 mm was subjected to high strain rate testing on March 25, 2012. The DPL was used to subject this specimen to a shock wave with a reflected pressure of 325 kPa and reflected impulse of 3726 kPa-ms. The specimen failed by tensile splitting of the cover concrete. The precise load at failure is unknown, although analysis of the strain gauge data indicated the peak load was at least 159.3 kN, generating a stress in the reinforcement of 586.0 MPa. Time-to-peak load was 10.0 milliseconds and strain rate was 0.41 s^{-1}.

Table A.5.1: Experimental data for beam-end BE5.

General Test Data						Strain data in the bonded region (×10^{-6})								
Time ms	$\dot{\varepsilon}$ s^{-1}	P_{exp} kN	f_s MPa	l_d mm	δ_{LE} mm	LE	SG1	SG2	SG3	SG4	SG5	SG6	SG7	FE
0	0	0	0	0	0	0	0	0	0	0	0	0	0	0
2.5	0.21	28.2	103.7	177	0.039	519	483	418	204	161	75	0	25	0
3.8	0.26	53.4	196.5	162	0.078	982	918	838	368	342	206	0	111	0
5.0	0.27	73.9	271.6	151	0.115	1358	1275	1173	562	532	358	37	132	0
6.3	0.32	110.4	405.9	164	0.195	2029	1922	1825	941	956	747	312	168	0
7.5	0.33	133.7	491.4	183	0.250	2457	2335	2228	1210	1233	996	499	293	0
8.8	0.36	159.1	585.1	193	0.309	3137	2976	2914	1379	1528	1256	563	209	0
10.0	0.41	159.3	585.6	168	0.358	4051	3817	3745	1465	1709	1322	304	239	0
Dynamic loading continued until splitting failure														

Note: Italicized data indicates questionable strain gauge readings.

(a) Front view

(b) Side and bottom face video

Figure A.5.1: Photographs of BE5 after testing.

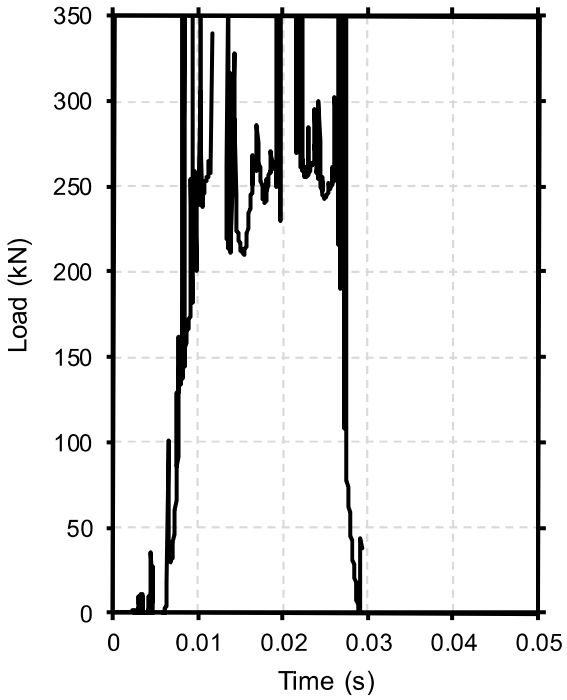

Figure A.5.2: Load-time history.

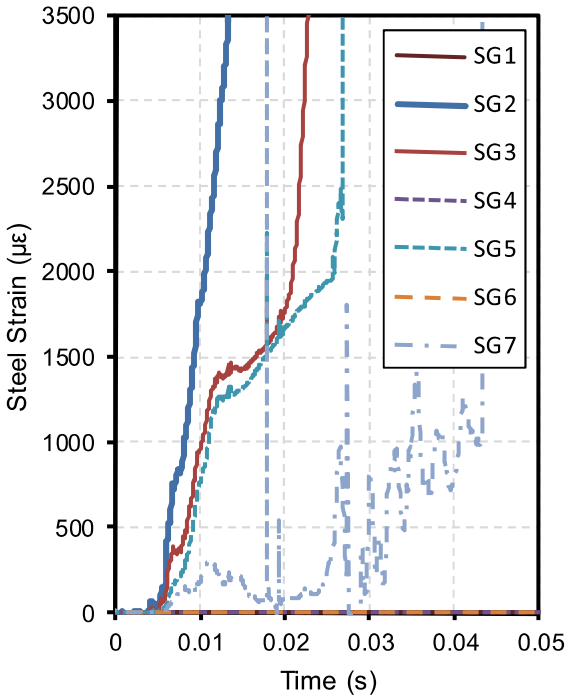

Figure A.5.3: Strain-time history.

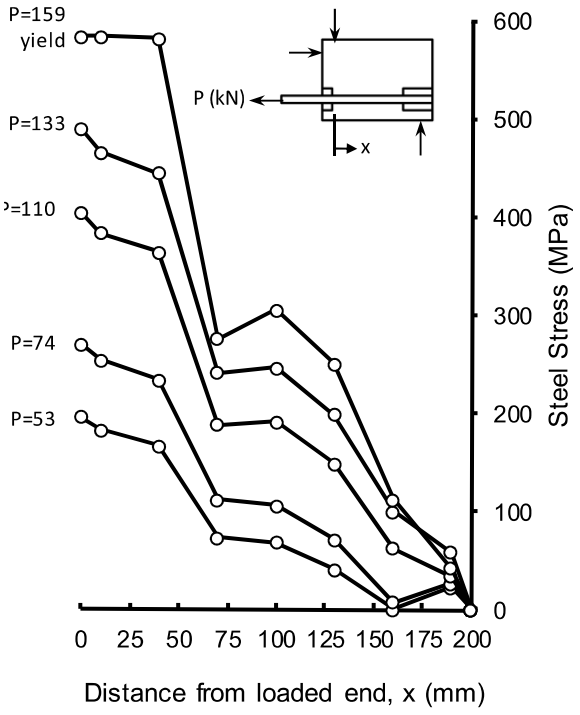

Figure A.5.4: Distribution of steel stresses in the bonded region.

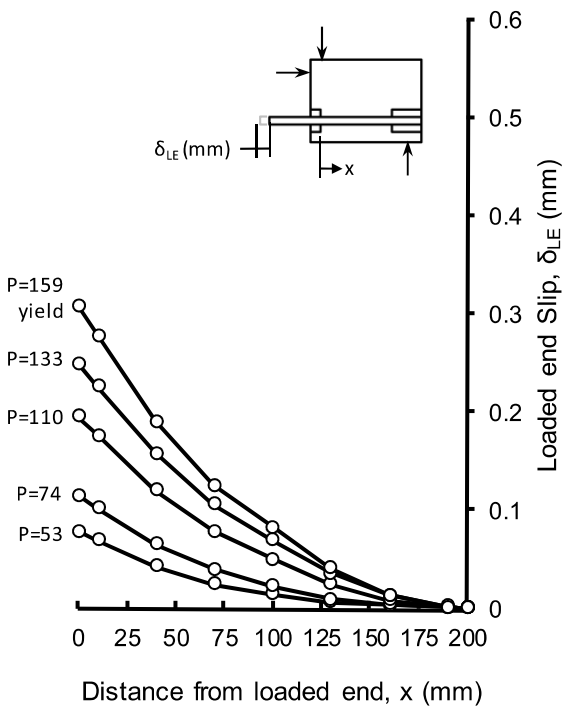

Figure A.5.5: Distribution of slip in the bonded region.

A.6: Beam-end BE6

BE6 with l_b = 200 mm was subjected to high strain rate testing on March 21, 2012. The DPL was used to subject this specimen to a shock wave with a reflected pressure of 284 kPa and reflected impulse of 3362 kPa-ms. No clear failure mode was identified, although a single flexural crack was noted. No outward sign of bond failure was visible after testing. The precise load at failure is unknown, although analysis of the strain gauge data indicated the peak load was at least 159.4 kN, generating a stress in the reinforcement of 585.9 MPa. Time-to-peak load was 13.9 milliseconds and strain rate was 0.30 s^{-1}.

Table A.6.1: Experimental data for beam-end BE6.

General Test Data						Strain data in the bonded region (×10^{-6})								
Time ms	$\dot{\varepsilon}$ s^{-1}	P_{exp} kN	f_s MPa	l_d mm	δ_{LE} mm	LE	SG1	SG2	SG3	SG4	SG5	SG6	SG7	FE
0	0	0	0	0	0	0	0	0	0	0	0	0	0	0
1.9	0.09	9.3	34.2	163	0.015	171	138	158	107	50	31	16	8	0
3.4	0.26	47.2	173.7	142	0.065	868	856	600	398	223	128	54	52	0
4.9	0.21	56.5	207.6	152	0.084	1038	987	771	538	319	188	78	102	0
6.4	0.30	103.6	381	190	0.184	1905	1781	1559	1213	815	641	305	131	0
7.9	0.33	140.3	516	200	0.262	2580	2428	2134	1632	1302	973	516	214	0
9.4	0.32	159.1	585.1	200	0.307	2980	2837	2497	1854	1518	1183	683	149	0
10.9	0.31	159	584.5	200	0.356	3417	3255	2885	2131	1756	1381	830	212	0
12.4	0.29	159.1	585	200	0.368	3632	3454	3151	2123	1751	1379	849	143	0
13.9	0.30	159.4	585.9	200	0.415	4175	4149	3973	2195	1805	1414	864	184	0
15.4	0.21	159.1	584.8	200	0.357	3294	3147	2706	2232	1842	1452	892	196	0
Dynamic loading continued until splitting failure														

Note: Italicized data indicates questionable strain gauge readings.

(a) After testing (b) After testing

Figure A.6.1: Photographs of BE6 after testing.

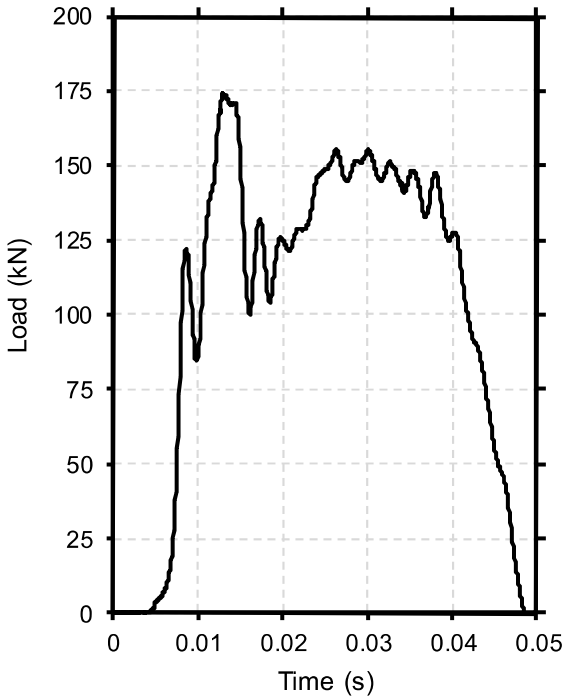

Figure A.6.2: Load-time history.

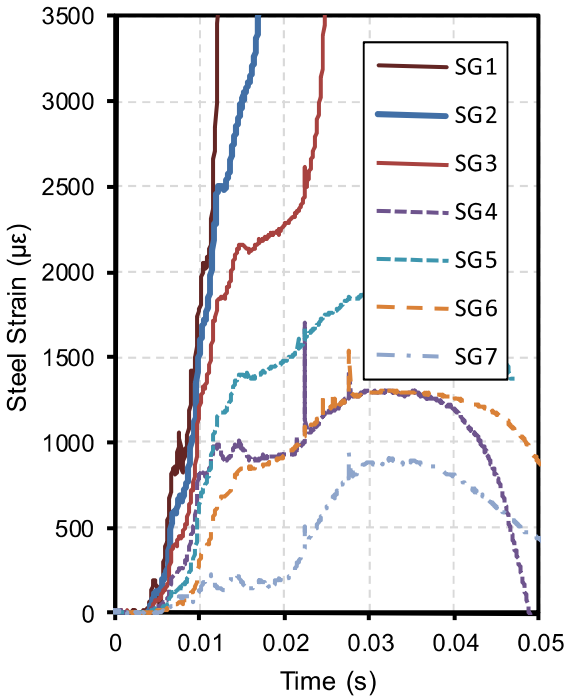

Figure A.6.3: Strain-time history.

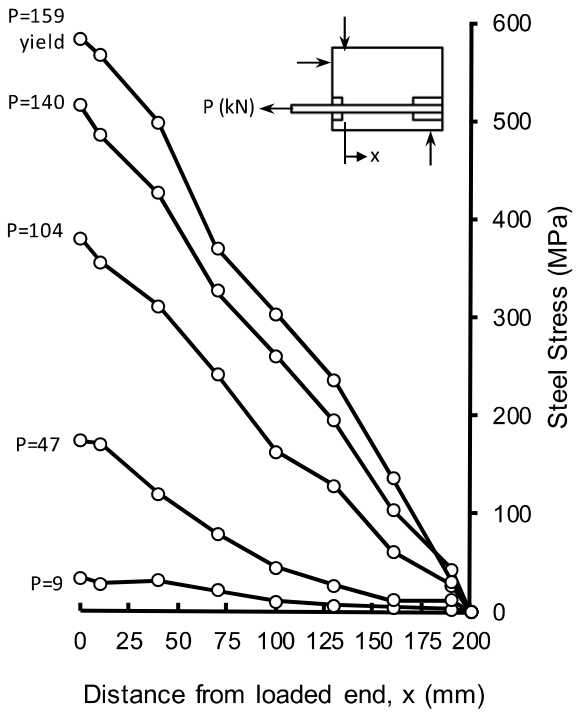

Figure A.6.4: Distribution of steel stresses in the bonded region.

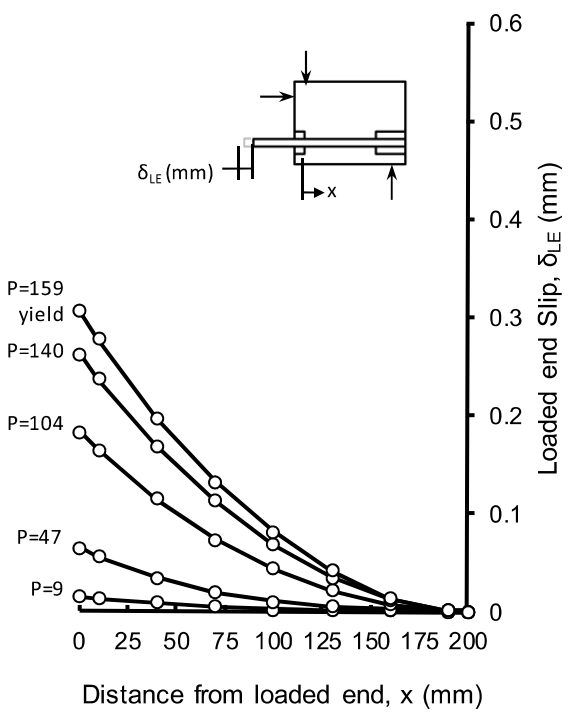

Figure A.6.5: Distribution of slip in the bonded region.

A.7.1: Beam-end BE7 – Test 1

BE7 with l_b = 200 mm was subjected to a total of three high strain rate tests. This test, the first of three, was conducted on March 19, 2012. The DPL was used to subject this specimen to a shock wave with a reflected pressure of 160 kPa and reflected impulse of 1898 kPa-ms. The specimen did not fail during this test. Analysis of the strain gauge data indicated the peak load was 91.1 kN, generating a stress in the reinforcement of 334.8 MPa. Time-to-peak load was 10.5 milliseconds and strain rate was 0.16 s^{-1}.

Table A.7.1.1: Experimental data for beam-end BE7 Test 1.

General Test Data						Strain data in the bonded region (×10^{-6})								
Time ms	$\dot{\varepsilon}$ s^{-1}	P_{exp} kN	f_s MPa	l_d mm	δ_{LE} mm	LE	SG1	SG2	SG3	SG4	SG5	SG6	SG7	FE
0	0	0	0	0	0	0	0	0	0	0	0	0	0	0
0.5	0.56	15.2	56.0	104	0.016	280	266	166	66	29	26	8	18	0
1.5	0.36	29.6	109.0	107	0.033	545	520	328	137	75	51	33	34	0
2.5	0.27	37.3	137.1	112	0.044	685	655	425	194	118	72	63	56	0
3.5	0.27	51.1	187.9	110	0.057	939	893	578	263	142	97	40	55	0
4.5	0.25	61.7	227.0	160	0.077	1135	1156	771	386	221	147	52	63	0
5.5	0.22	67.0	246.2	160	0.086	1231	1245	847	448	263	176	62	58	0
6.5	0.24	84.6	311.1	165	0.107	1556	1476	1024	573	357	243	82	72	0
7.5	0.21	85.5	314.5	170	0.111	1573	1491	1051	612	388	268	79	45	0
8.5	0.20	90.6	333.1	175	0.119	1666	1576	1129	683	433	299	92	18	0
9.5	0.18	94.9	348.8	175	0.130	1744	1649	1208	768	500	349	112	6	0
10.5	0.16	91.1	334.8	170	0.128	1674	1584	1170	757	501	350	113	79	0

Note: Italicized data indicates questionable strain gauge readings.

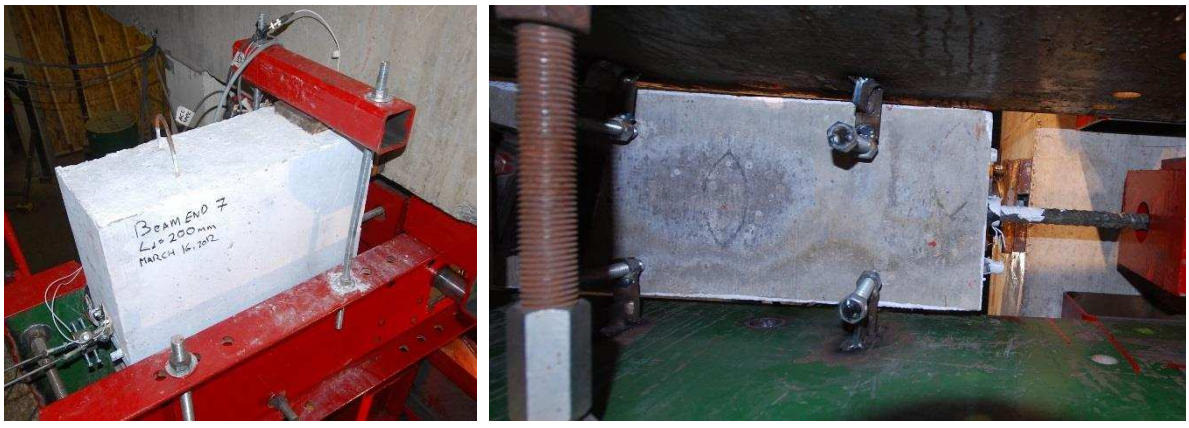

(a) Before testing (b) Underside of specimen after testing

Figure A.7.1.1: Photographs of BE7 before and after Test 1.

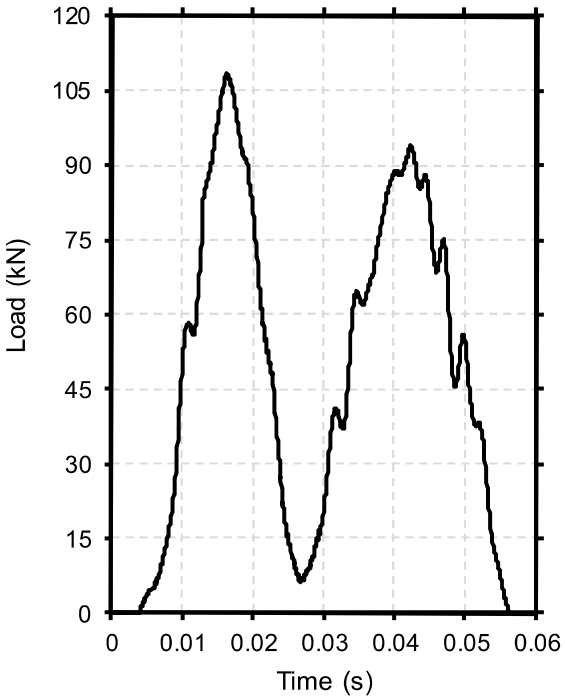

Figure A.7.1.2: Load-time history.

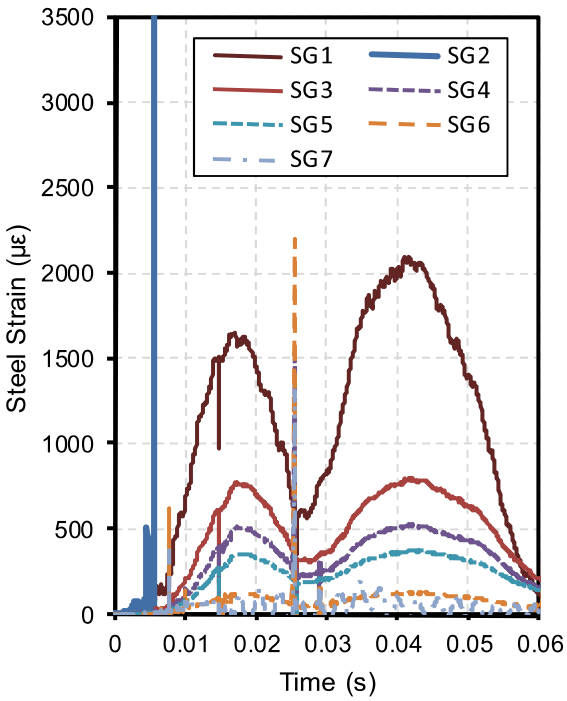

Figure A.7.1.3: Strain-time history.

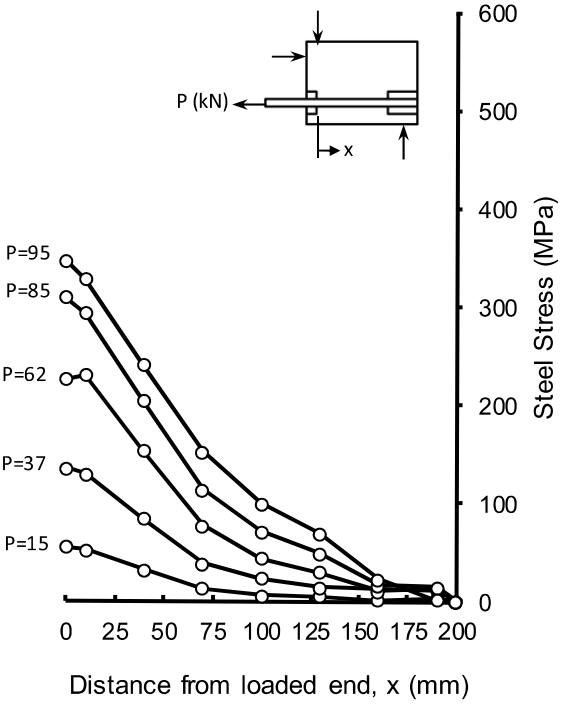

Figure A.7.1.4: Distribution of steel stresses in the bonded region.

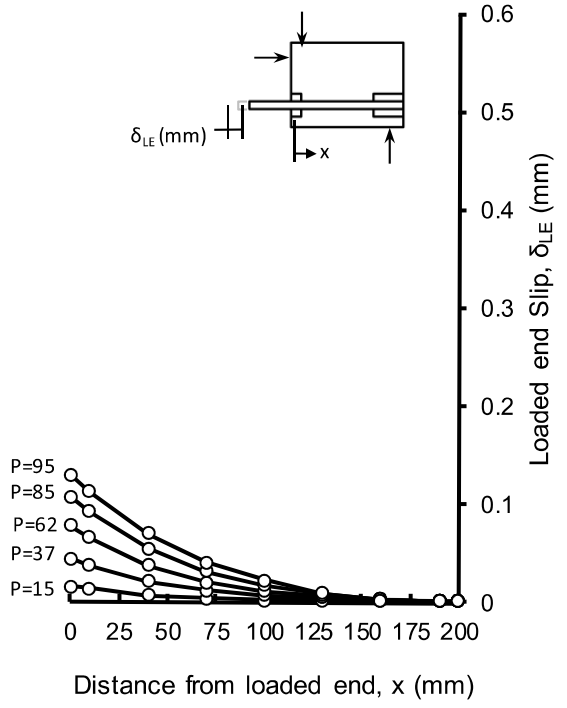

Figure A.7.1.5: Distribution of slip in the bonded region.

A.7.2: Beam-end BE7 – Test 2

BE7 with l_b = 200 mm was subjected to a total of three high strain rate tests. This test, the second of three, was conducted on March 19, 2012. The DPL was used to subject this specimen to a shock wave with a reflected pressure of 221 kPa and reflected impulse of 2540 kPa-ms. The specimen did not fail during this test. Analysis of the strain gauge data indicated the peak load was at least 158.9 kN, generating a stress in the reinforcement of 584.3 MPa. Time-to-peak load was 13.5 milliseconds and strain rate was 0.26 s^{-1}.

Table A.7.2.1: Experimental data for beam-end BE7 Test 2.

General Test Data						Strain data in the bonded region (×10^{-6})								
Time ms	$\dot{\varepsilon}$ s^{-1}	P_{exp} kN	f_s MPa	l_d mm	δ_{LE} mm	LE	SG1	SG2	SG3	SG4	SG5	SG6	SG7	FE
0	0	0	0	0	0	0	0	0	0	0	0	0	0	0
1.5	0.29	23.4	86.0	160	0.046	430	395	361	327	207	163	74	114	0
3.0	0.31	50.6	186.2	160	0.083	931	1051	760	468	284	214	86	140	0
4.5	0.34	83.6	307.4	159	0.124	1537	1577	1147	717	438	311	106	170	0
6.0	0.30	97.0	356.8	156	0.138	1784	1805	1337	870	434	351	84	59	0
7.5	0.28	112.2	412.6	168	0.178	2063	2036	1574	1112	707	504	179	212	0
9.0	0.23	111.9	411.5	175	0.184	2057	1983	1595	1207	779	558	219	187	0
10.5	0.21	121.2	445.6	187	0.206	2228	2184	1782	1380	893	667	242	114	0
12.0	0.23	149.1	548.0	200	0.248	2740	2841	2182	1523	1013	774	290	213	0
13.5	0.26	158.9	584.3	200	0.291	3559	3967	2732	1544	1037	818	312	37	0
Dynamic loading continued but splitting did not occur														

Note: Italicized data indicates questionable strain gauge readings.

Figure A.7.2.1: Photograph of the underside of BE7 after Test 2.

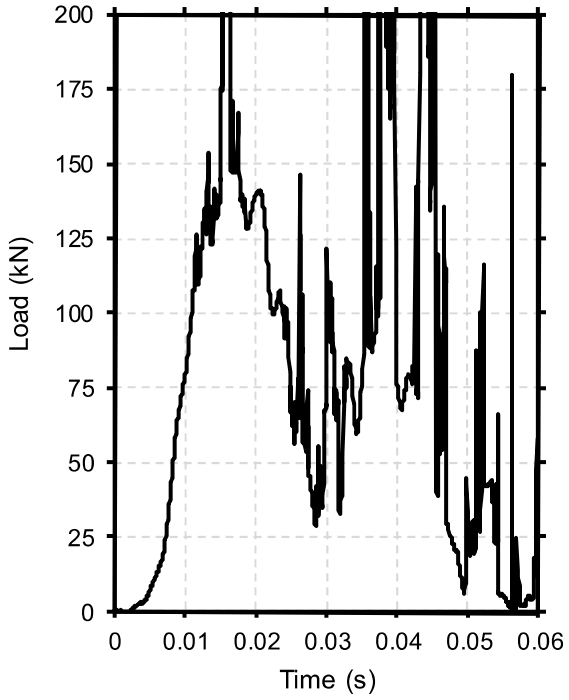

Figure A.7.2.2: Load-time history.

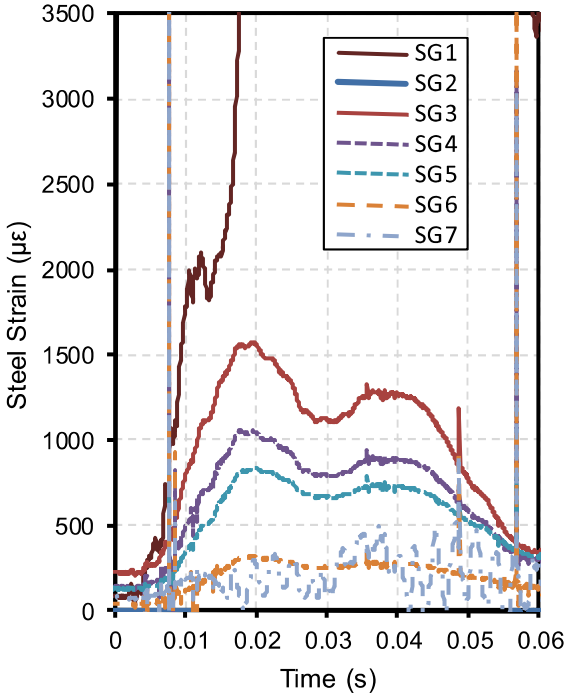

Figure A.7.2.3: Strain-time history.

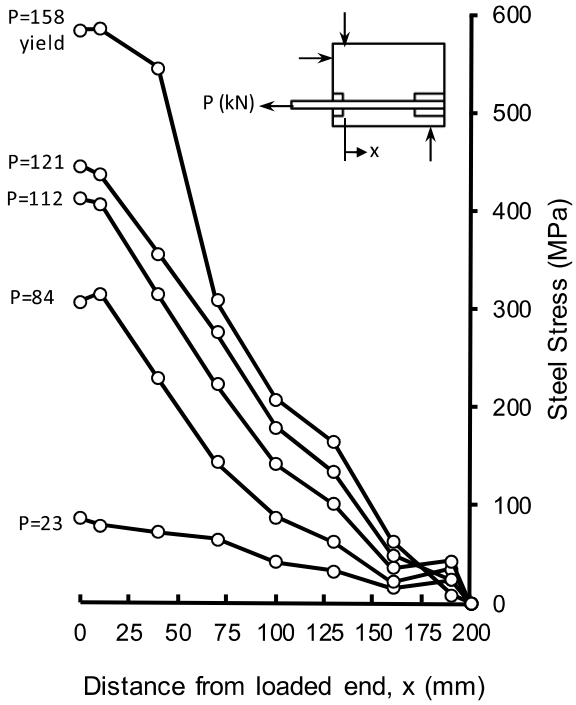

Figure A.7.2.4: Distribution of steel stresses in the bonded region.

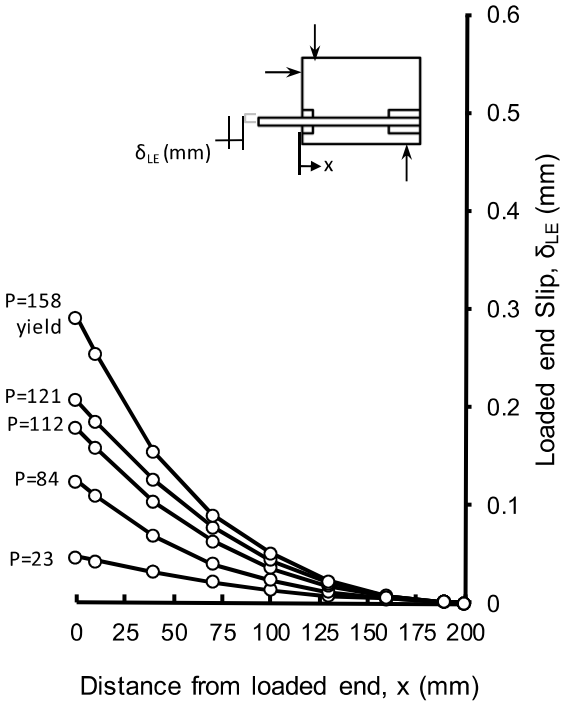

Figure A.7.2.5: Distribution of slip in the bonded region.

A.7.3: Beam-end BE7 – Test 3

BE7 with l_b = 200 mm was subjected to a total of three high strain rate tests. This test, the third of three, was conducted on March 19, 2012. The DPL was used to subject this specimen to a shock with a reflected pressure of 302 kPa and reflected impulse of 3410 kPa-ms. The specimen failed by tensile splitting of the cover concrete. The load at failure was unknown, although analysis of the strain gauge data indicated the peak load of at least 159.7 kN, generating a stress in the reinforcement of 587.1 MPa. Time-to-peak load was 20 milliseconds and strain rate was 0.33 s^{-1}.

Table A.7.3.1: Experimental data for beam-end BE7 Test 3.

General Test Data						Strain data in the bonded region (×10^{-6})								
Time ms	$\dot{\varepsilon}$ s^{-1}	P_{exp} kN	f_s MPa	l_d mm	δ_{LE} mm	LE	SG1	SG2	SG3	SG4	SG5	SG6	SG7	FE
0	0	0	0	0	0	0	0	0	0	0	0	0	0	0
0.5	1.32	35.9	132.1	160	0.071	661	601	542	486	290	323	178	36	0
2.0	0.76	82.4	302.9	186	0.136	1515	988	1189	952	624	585	150	179	0
3.5	0.50	94.9	348.8	192	0.177	1744	1588	1445	1188	773	708	258	269	0
5.0	0.46	124.2	456.6	192	0.224	2283	2164	1807	1506	926	903	323	289	0
6.5	0.39	137.5	505.6	204	0.256	2528	2404	2030	1749	1090	1088	401	228	0
8.0	0.34	149.8	550.8	197	0.277	2754	2617	2206	1841	1201	1197	473	164	0
9.5	0.30	156.6	575.7	200	0.298	2878	2739	2320	1956	1286	1290	539	338	0
11.0	0.29	159.1	585.1	200	0.314	3176	3015	2534	2074	1364	1396	542	39	0
12.5	0.26	159.1	584.8	200	0.345	3279	3123	2654	2217	1518	1520	650	483	0
14.0	0.26	159.1	585.1	200	0.374	3635	3458	2926	2414	1648	1636	728	323	0
15.5	0.26	159.3	585.6	200	0.418	4003	3810	3234	2803	1756	1730	817	577	0
17.0	0.28	159.6	586.7	200	0.484	4814	4575	3858	3486	1900	1858	883	456	0
18.5	0.31	159.6	586.9	200	0.569	5757	5468	4599	4375	2042	2003	999	514	0
20.0	0.33	159.7	587.1	200	0.670	6594	6270	5297	4867	2520	2569	1318	732	0
Dynamic loading continued until splitting failure														

Note: Italicized data indicates questionable strain gauge readings.

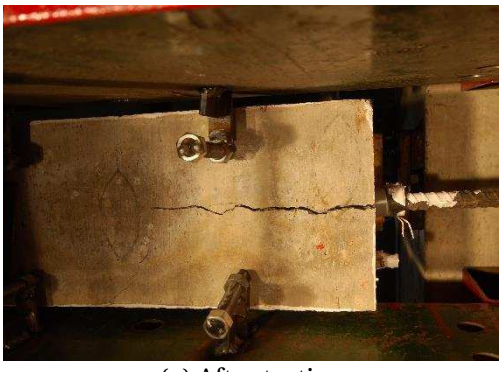

(a) After testing

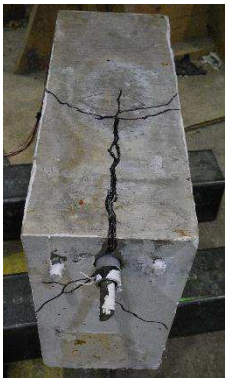

(b) After testing

Figure A.7.3.1: Photographs of BE7 after Test 3.

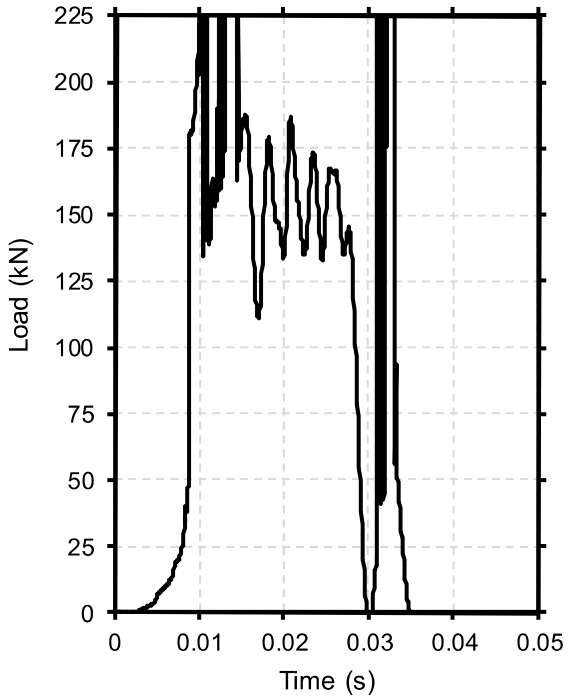

Figure A.7.3.2: Load-time history.

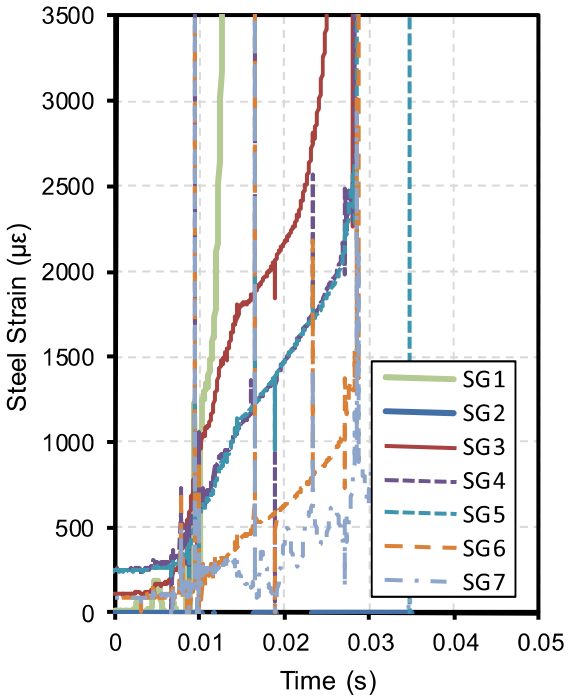

Figure A.7.3.3: Strain-time history.

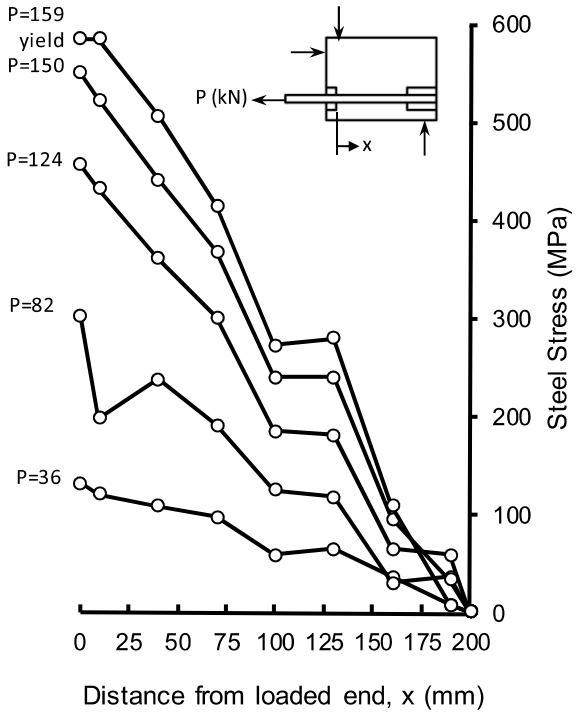

Figure A.7.3.4: Distribution of steel stresses in the bonded region.

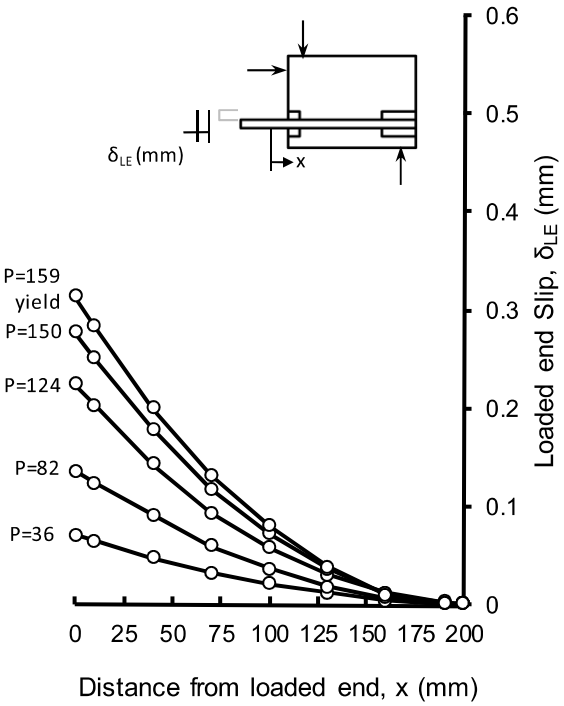

Figure A.7.3.5: Distribution of slip in the bonded region.

A.8: Beam-end BE8

BE8 with l_b = 400 mm was subjected to low strain rate testing on April 26, 2012. The specimen failed by tensile splitting of the cover concrete at an applied load of 143.9 kN generating a stress in the reinforcement of 529.0 MPa. Time-to-failure was 334.8 seconds and strain rate was approximately 10^{-6} s^{-1}.

Table A.8.1: Experimental data for beam-end BE8.

General Test Data						Strain data in the bonded region ($\times 10^{-6}$)										
Time	$\dot{\varepsilon}$	P_{exp}	f_s	l_d	δ_{LE}	LE	SG1	SG2	SG3	SG4	SG5	SG6	SG7	SG8	SG9	FE
s	s^{-1}	kN	MPa	mm	mm											
0	0	0	0	0	0	0	0	0	0	0	0	0	0	0	0	0
6.2	2.7×10^{-5}	10.6	33.1	161	0.010	165	128	70	38	6	8	8	6	-13	1	0
13.8	2.6×10^{-5}	20.5	70.7	147	0.025	353	329	161	88	16	17	14	12	-11	1	0
58.6	9.3×10^{-6}	30.2	108.9	146	0.040	545	507	275	140	5	27	21	17	-15	0	0
78.0	8.6×10^{-6}	40.3	134.8	178	0.055	674	712	400	204	8	37	28	24	-53	2	0
104.6	9.1×10^{-6}	50.9	190.0	179	0.074	950	897	569	300	13	49	38	32	-79	3	0
120.6	9.0×10^{-6}	60.0	216.0	186	0.096	1080	1022	691	471	32	60	45	39	-49	5	0
134.6	9.3×10^{-6}	70.9	250.8	207	0.118	1254	1193	866	560	64	74	55	48	-44	8	0
142.2	1.1×10^{-5}	80.1	306.3	192	0.147	1531	1452	1080	695	110	93	66	55	-48	9	0
155.2	1.1×10^{-5}	91.2	343.2	226	0.191	1716	1640	1396	919	201	133	84	66	48	11	0
167.6	1.2×10^{-5}	100.0	395.0	210	0.233	1975	1947	1658	1023	370	194	106	78	80	13	0
204.0	1.1×10^{-5}	110.4	434.4	228	0.294	2172	2223	2006	1256	616	330	151	98	154	15	0
238.2	8.2×10^{-6}	121.0	391.4	294	0.390	1957	2591	2157	1723	1200	728	341	167	104	19	0
265.6	8.8×10^{-6}	130.7	480.5	-	-	2330	-	-	-	2688	2020	1150	911	390	48	0
319.0	8.8×10^{-6}	140.4	516.1	-	-		1764	-	-	7270	2461	1586	1370	656	126	0
334.8	8.8×10^{-6}	143.9	529.0	-	-	-	4214	-	-	12368	2955	2018	1731	951	294	0

Note: Italicized data indicates questionable strain gauge readings.

(a) Before testing

(b) After testing

Figure A.8.1: Photographs of BE8 before and after testing.

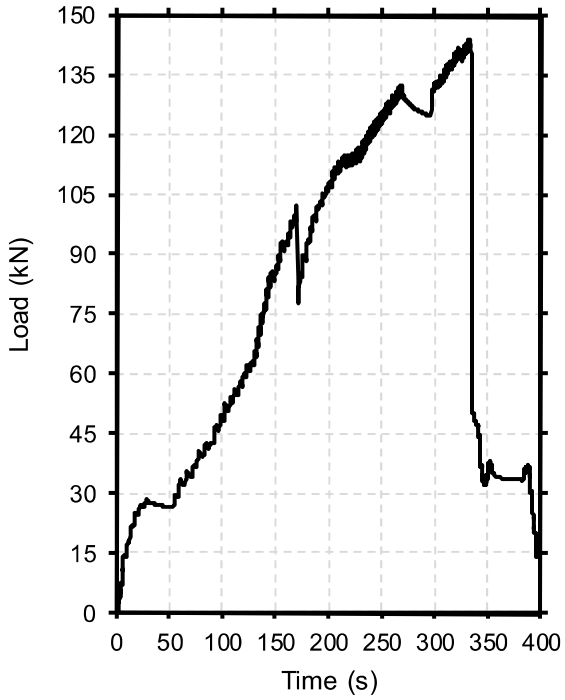

Figure A.8.2: Load-time history.

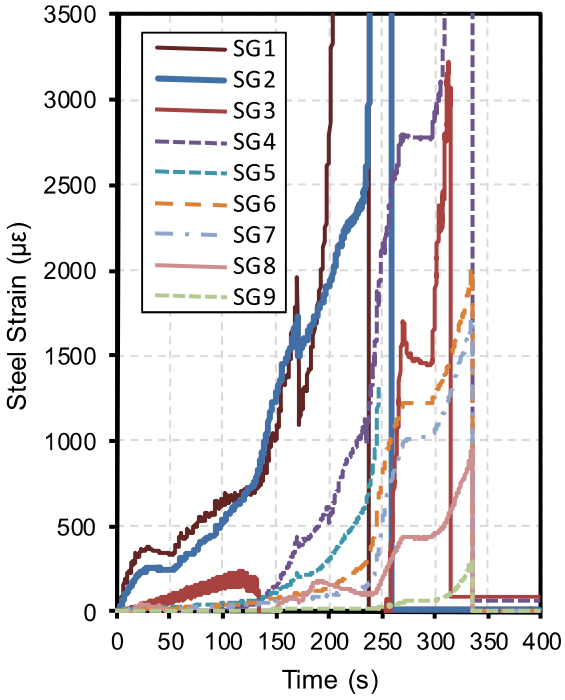

Figure A.8.3: Strain-time history.

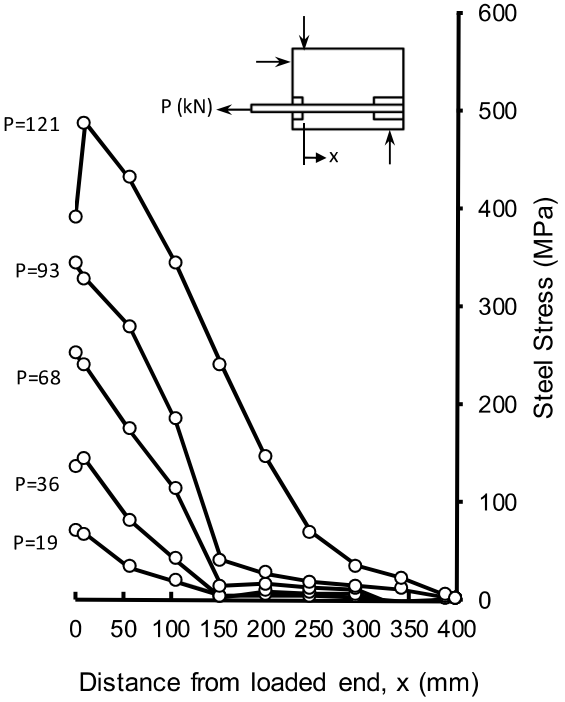

Figure A.8.4: Distribution of steel stresses in the bonded region.

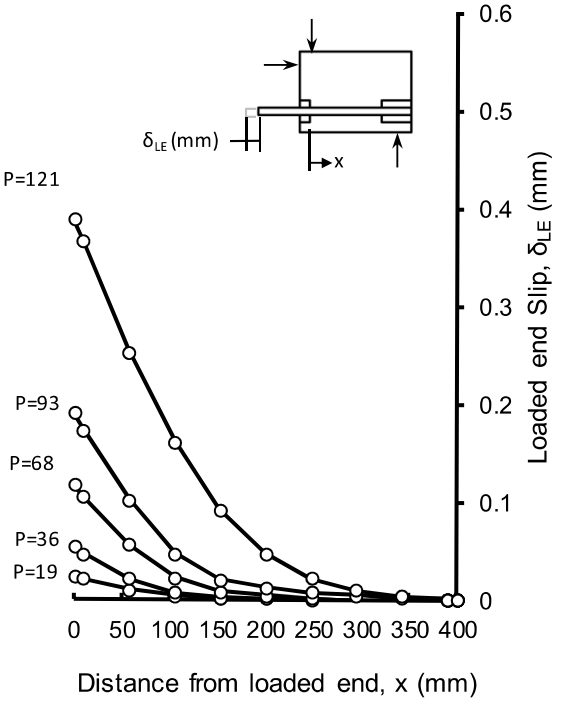

Figure A.8.5: Distribution of slip in the bonded region.

A.9: Beam-end BE9

BE9 with l_b = 400 mm was intended to be subjected to low strain rate testing. However, concrete was poorly consolidated in this specimen and was unsuitable for experimentation.

A.10: Beam-end BE10

BE10 with l_b = 400 mm was subjected to low strain rate testing on April 26, 2012. The specimen failed by tensile splitting of the cover concrete at an applied load of 153.5 kN generating a stress in the reinforcement of 565.0 MPa. Time-to-failure was 345.4 seconds and strain rate was approximately 10^{-5} s^{-1}.

Table A.10.1: Experimental data for beam-end BE10.

General Test Data						Strain data in the bonded region ($\times 10^{-6}$)										
Time	$\dot{\varepsilon}$	P_{exp}	f_s	l_d	δ_{LE}	LE	SG1	SG2	SG3	SG4	SG5	SG6	SG7	SG8	SG9	FE
s	s^{-1}	kN	MPa	mm	mm											
0	0	0	0	0	0	0	0	0	0	0	0	0	0	0	0	0
2.8	1.3×10^{-5}	2.0	7.4	10	0.000	37	39	18	20	6	3	-86	5	4	0	0
4.8	4.5×10^{-5}	11.6	42.8	126	0.015	214	197	117	36	16	9	-13	8	7	2	0
6.2	6.7×10^{-5}	22.8	83.7	125	0.028	418	385	226	68	5	16	-34	13	11	2	0
9.6	6.1×10^{-5}	32.1	118.1	148	0.047	590	551	386	125	8	27	10	19	15	3	0
55.2	1.6×10^{-5}	47.1	173.3	151	0.072	867	809	560	212	13	42	55	26	22	5	0
128.4	8.6×10^{-6}	60.0	220.4	154	0.094	1102	1031	711	315	32	57	62	32	27	5	0
132.4	9.5×10^{-6}	68.8	252.8	159	0.112	1264	1184	821	398	64	71	82	40	32	7	0
139.4	1.1×10^{-5}	80.2	294.7	164	0.134	1474	1384	962	522	110	91	58	47	39	6	0
176.0	8.5×10^{-6}	81.1	298.0	179	0.147	1490	1407	990	662	201	120	8	57	45	8	0
186.2	8.6×10^{-6}	87.5	321.6	201	0.175	1608	1528	1130	807	370	155	14	67	52	9	0
195.4	1.0×10^{-5}	110.5	406.2	211	0.232	2031	2057	1289	1028	616	235	123	78	60	12	0
216.2	1.1×10^{-5}	125.6	461.9	258	0.308	2309	2220	1673	1405	1200	383	56	98	69	10	0
258.2	9.5×10^{-5}	132.6	487.4	270	0.367	2464	2372	2205	1692	1118	543	250	122	81	15	0
283.0	4.2×10^{-5}	139.4	512.6	350	0.689	12000	7215	2430	2298	1723	1148	870	273	122	23	0
Dynamic loading continued until splitting failure																

Note: Italicized data indicates questionable strain gauge readings.

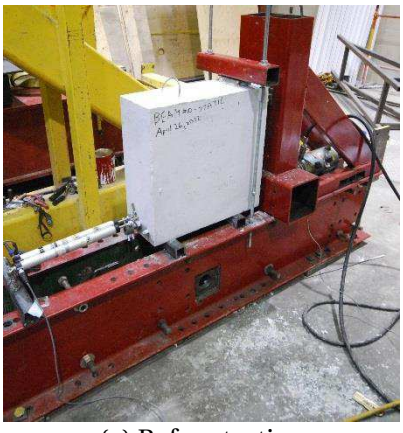

(a) Before testing

(b) After testing

Figure A.10.1: Photographs of BE10 before and after testing.

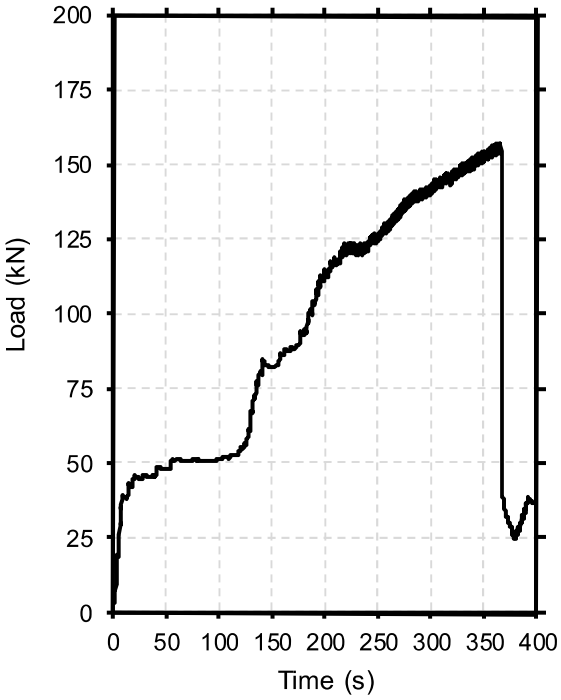

Figure A.10.2: Load-time history.

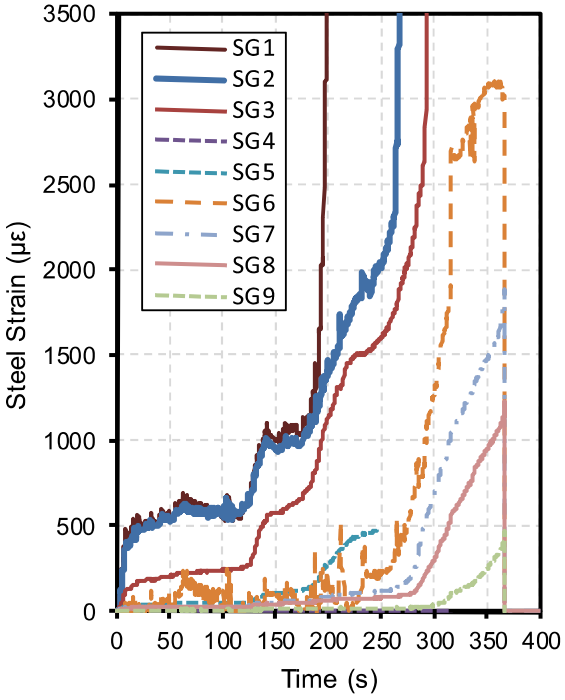

Figure A.10.3: Strain-time history.

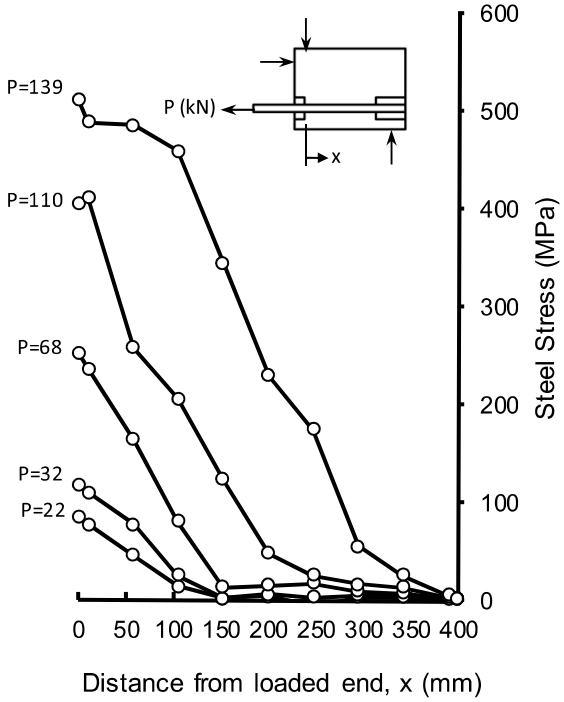

Figure A.10.4: Distribution of steel stresses in the bonded region.

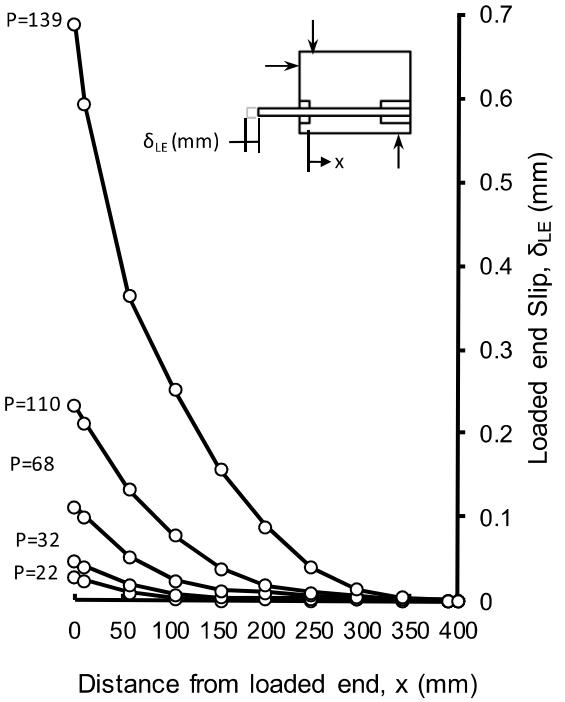

Figure A.10.5: Distribution of slip in the bonded region.

A.11.1: Beam-end BE11 – Test 1

BE11 with l_b = 400 mm was subjected to a total of two high strain rate tests. This test, the first of two, was conducted on March 30, 2012. The DPL was used to subject this specimen to a shock wave with a reflected pressure of 82 kPa and reflected impulse of 853 kPa-ms. The specimen did not fail during this test. Analysis of the strain gauge data indicated the peak load was 54.7 kN, generating a stress in the reinforcement of 201.1 MPa. Time-to-peak load was 17.2 milliseconds and strain rate was 0.06 s^{-1}.

Table A.11.1.1: Experimental data for beam-end BE11 Test 1.

General Test Data						Strain data in the bonded region ($\times 10^{-6}$)										
Time ms	$\dot{\varepsilon}$ s^{-1}	P_{exp} kN	f_s MPa	l_d mm	δ_{LE} mm	LE	SG1	SG2	SG3	SG4	SG5	SG6	SG7	SG8	SG9	FE
0	0	0	0	0	0	0	0	0	0	0	0	0	0	0	0	0
0.7	0.08	2.9	10.6	72	0.002	53	46	11	8	0	0	0	0	0	0	0
2.2	0.09	10.6	38.8	73	0.009	194	168	42	22	0	0	0	0	0	0	0
3.7	0.10	19.5	71.8	80	0.018	359	315	103	42	0	0	0	0	0	0	0
5.2	0.09	26.5	97.4	113	0.025	487	432	166	57	0	0	0	0	0	0	0
6.7	0.08	30.4	111.8	119	0.032	559	503	233	80	0	0	0	0	0	0	0
8.2	0.08	35.9	132.1	120	0.039	661	598	298	96	0	0	0	0	0	0	0
9.7	0.08	40.4	148.4	122	0.045	742	675	358	112	0	0	0	0	0	0	0
11.2	0.08	46.7	171.7	124	0.055	858	799	440	141	0	0	0	0	0	0	0
12.7	0.07	49.1	180.4	125	0.058	902	837	476	153	0	0	0	0	0	0	0
14.2	0.06	48.7	179.1	126	0.058	895	828	480	155	0	0	0	0	0	0	0
15.7	0.06	50.8	186.6	125	0.060	933	868	486	162	0	0	0	0	0	0	0
17.2	0.06	54.7	201.2	125	0.065	1006	941	510	173	0	0	0	0	0	0	0

Note: Italicized data indicates questionable strain gauge readings.

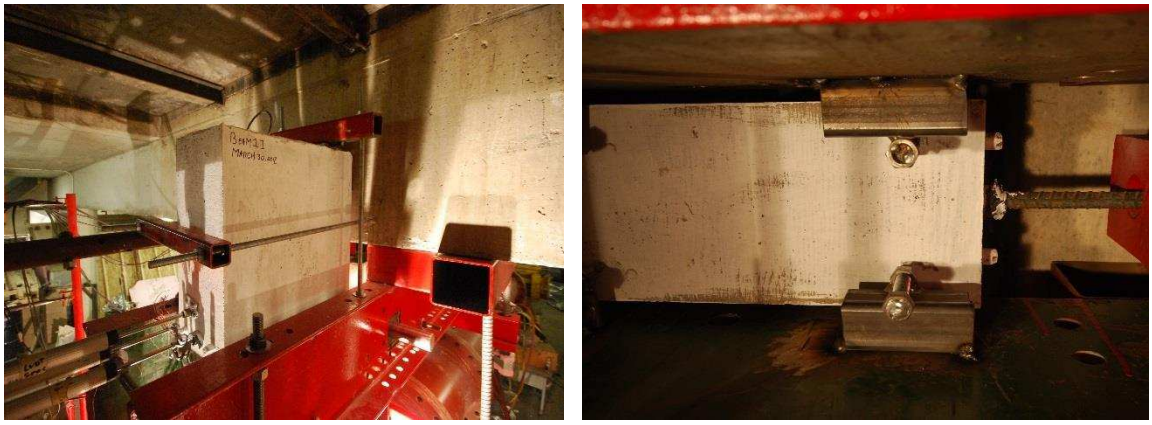

(a) Before testing (b) After testing

Figure A.11.1.1: Photographs of BE11 before and after Test 1.

Load-time history data not available.

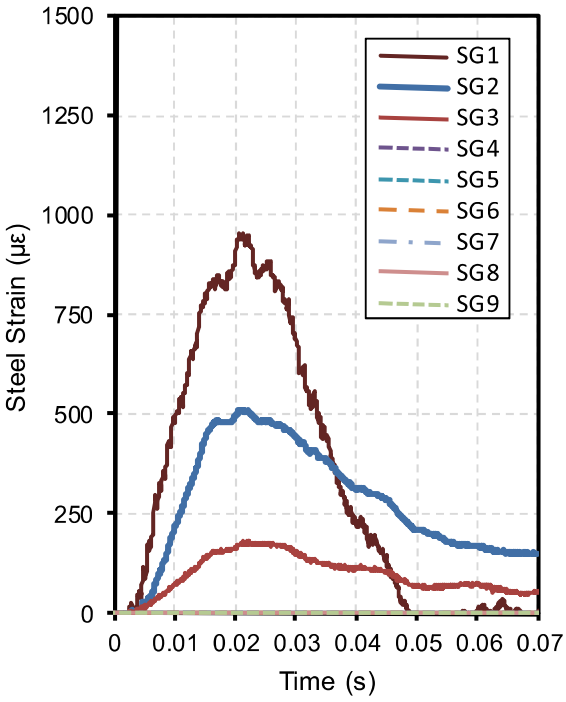

Figure A.11.1.2: Load-time history.

Figure A.11.1.3: Strain-time history.

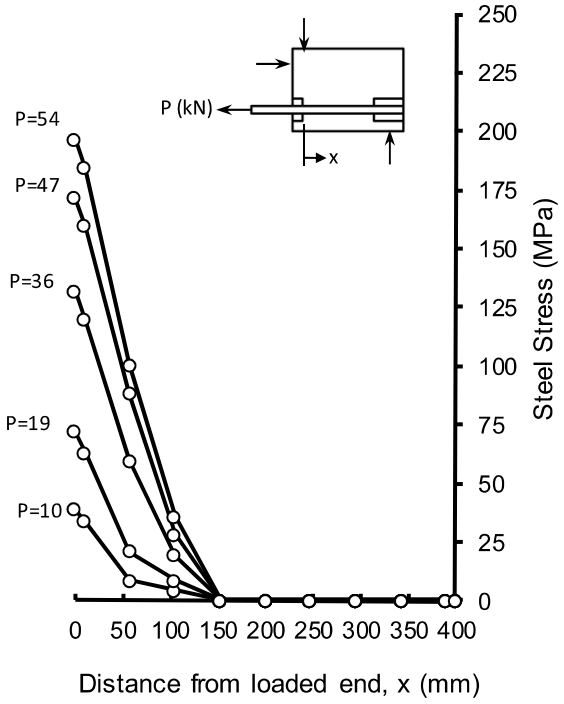

Figure A.11.1.4: Distribution of steel stresses in the bonded region.

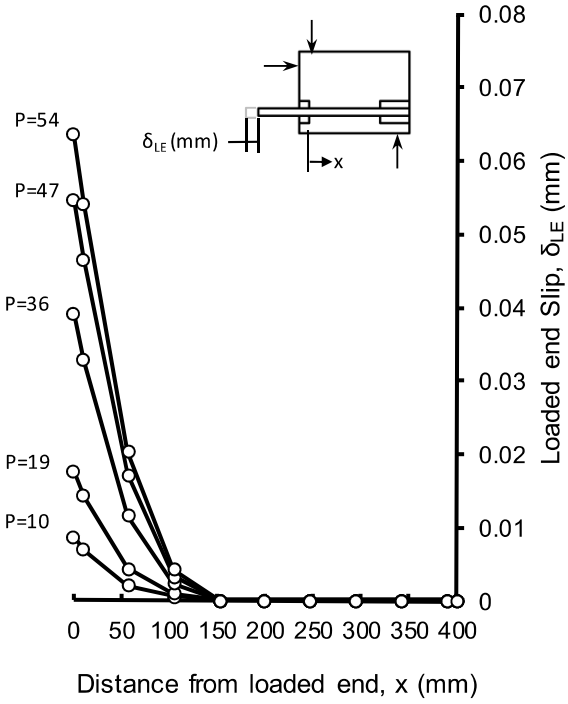

Figure A.11.1.5: Distribution of slip in the bonded region.

A.11.2: Beam-end BE11 – Test 2

BE11 with l_b = 400 mm was subjected to a total of two high strain rate tests. This test, the second of two, was conducted on March 30, 2012. The DPL was used to subject this specimen to a shock wave with a reflected pressure of 323 kPa and reflected impulse of 3808 kPa-ms. The specimen did not fail during this test but the reinforcement was stressed into the strain hardening range. Analysis of the strain gauge data indicated the peak load was at least 159.1 kN, generating a stress in the reinforcement of at least 585.1 MPa. Time-to-peak load was 9.0 milliseconds and strain rate was 0.35 s^{-1}.

Table A.11.2.1: Experimental data for beam-end BE11 Test 2.

General Test Data						Strain data in the bonded region ($\times 10^{-6}$)										
Time ms	$\dot{\varepsilon}$ s^{-1}	P_{exp} kN	f_s MPa	l_d mm	δ_{LE} mm	LE	SG1	SG2	SG3	SG4	SG5	SG6	SG7	SG8	SG9	FE
0	0	0	0	0	0	0	0	0	0	0	0	0	0	0	0	0
1.5	0.45	36.5	134.4	112	0.038	672	598	244	68	14	21	12	8	0	-7	0
4.0	0.37	79.8	293.5	118	0.092	1467	1311	568	213	58	45	32	28	0	62	0
6.5	0.25	87.7	322.5	161	0.141	1613	1503	979	457	149	89	72	62	0	138	0
9.0	0.35	159.1	585.1	188	0.262	3145	2906	1767	1008	229	192	127	100	0	15	0
Dynamic loading continued beyond this load but bond failure did not occur.																

Note: Italicized data indicates questionable strain gauge readings.

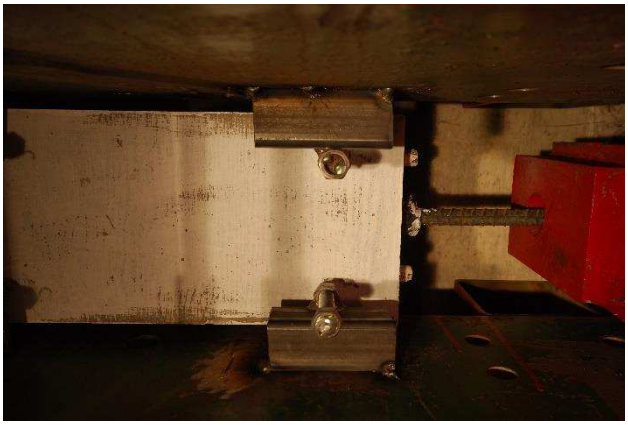

Figure A.11.2.1: Photographs of BE11 after Test 2.

Load-time history data not available.

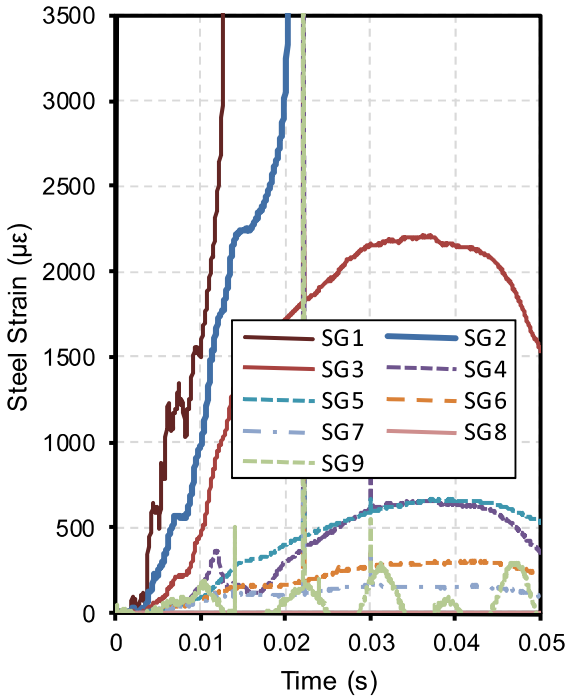

Figure A.11.2.2: Load-time history.

Figure A.11.2.3: Strain-time history.

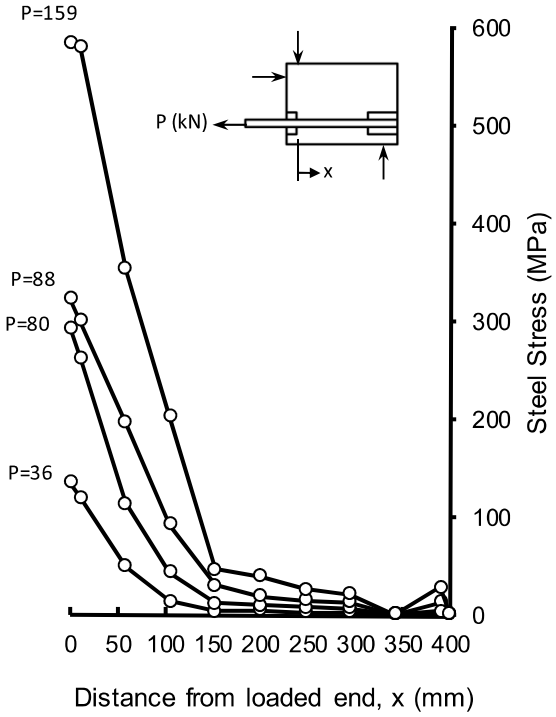

Figure A.11.2.4: Distribution of steel stresses in the bonded region.

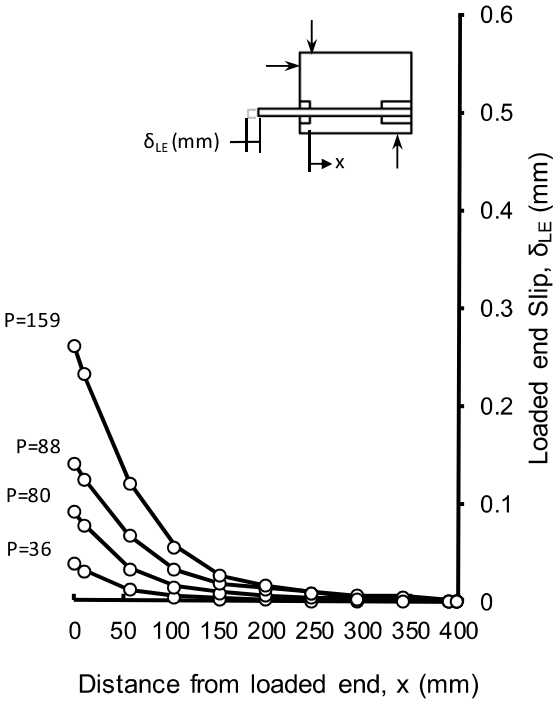

Figure A.11.2.5: Distribution of slip in the bonded region.

A.12.1: Beam-end BE12 – Test 1

BE12 with l_b = 400 mm was subjected to a total of two high strain rate tests. This test, the first of two, was conducted on March 29, 2012. The DPL was used to subject this specimen to a shock wave with a reflected pressure of 90 kPa and reflected impulse of 987 kPa-ms. The specimen did not fail during this test and reinforcement response was in the elastic range. Analysis of the strain gauge data indicated the peak load was 48.9 kN, generating a stress in the reinforcement of 179.7 MPa. Time-to-peak load was 21.4 milliseconds and strain rate was 0.04 s^{-1}.

Table A.12.1.1: Experimental data for beam-end BE12 Test 1.

General Test Data						Strain data in the bonded region ($\times 10^{-6}$)										
Time ms	$\dot{\varepsilon}$ s^{-1}	P_{exp} kN	f_s MPa	l_d mm	δ_{LE} mm	LE	SG1	SG2	SG3	SG4	SG5	SG6	SG7	SG8	SG9	FE
0	0	0	0	0	0	0	0	0	0	0	0	0	0	0	0	0
1.4	0.11	8.2	30.2	67	0.006	151	128	22	9	3	3	1	1	1	7	0
3.9	0.07	14.7	54.1	104	0.014	270	234	62	18	11	8	3	3	2	26	0
6.4	0.05	17.5	64.2	106	0.016	321	264	80	23	12	8	5	3	1	29	0
8.9	0.03	14.6	53.9	92	0.017	269	240	101	32	17	14	10	7	4	-9	0
11.4	0.05	28.9	106.3	125	0.039	532	488	287	82	38	27	19	13	9	-23	0
13.9	0.06	42.8	157.3	138	0.066	786	707	502	166	65	44	32	26	22	49	0
16.4	0.05	41.7	153.5	146	0.066	767	682	531	182	71	47	33	27	23	-16	0
18.9	0.04	45.7	168.2	143	0.072	841	752	565	195	77	52	37	31	33	-43	0
21.4	0.04	48.9	179.7	144	0.078	898	807	599	215	81	53	38	32	33	5	0
23.9	0.04	45.9	168.8	146	0.074	844	755	575	207	77	47	34	29	34	17	0

Note: Italicized data indicates questionable strain gauge readings.

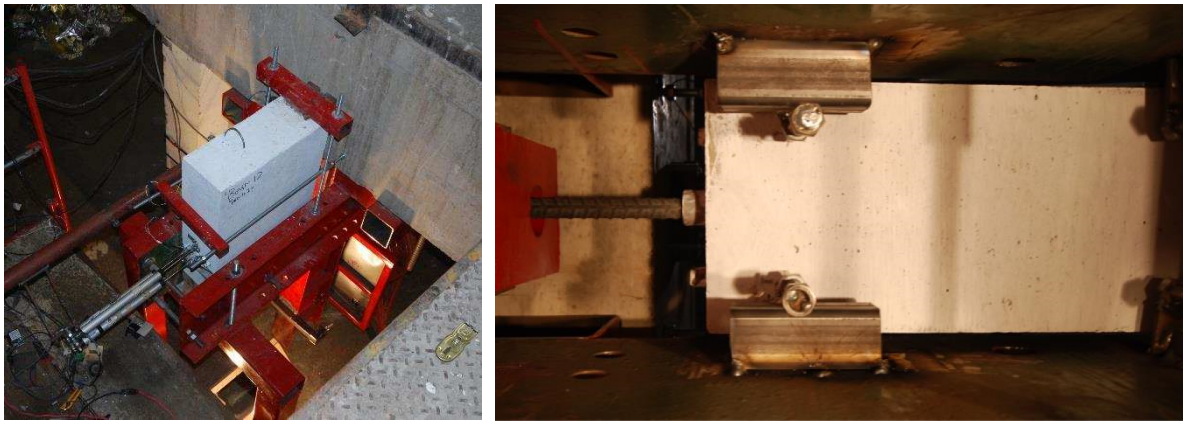

(a) Before testing (b) After testing

Figure A.12.1.1: Photographs of BE12 before and after Test 1.

Load-time history data not available.

Figure A.12.1.2: Load-time history.

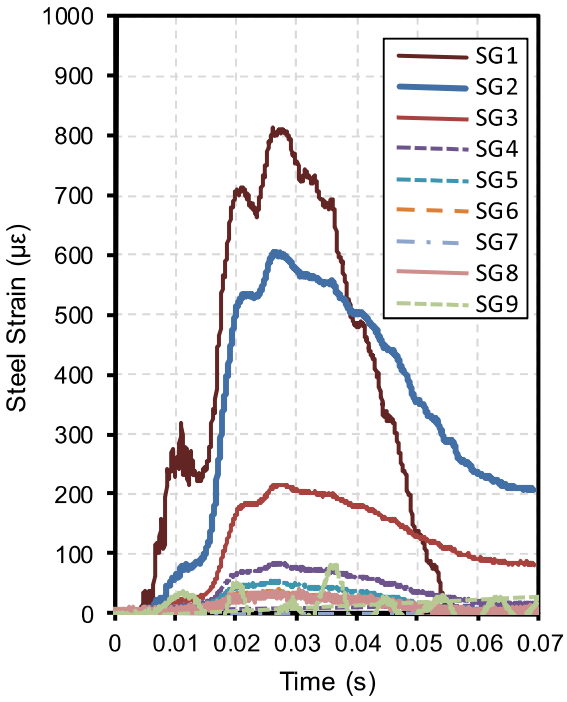

Figure A.12.1.3: Strain-time history.

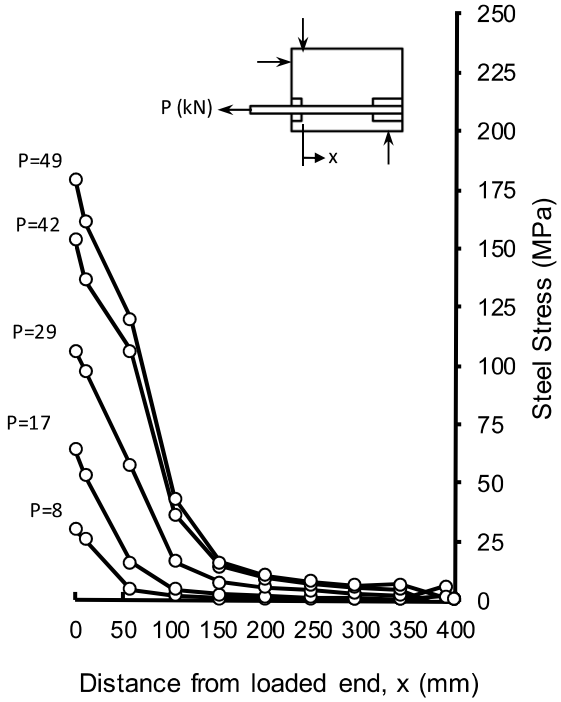

Figure A.12.1.4: Distribution of steel stresses in the bonded region.

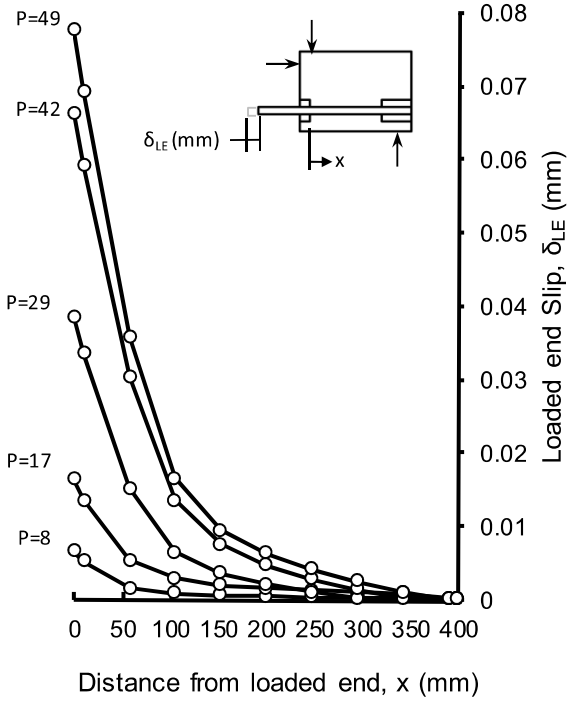

Figure A.12.1.5: Distribution of slip in the bonded region.

A.12.2: Beam-end BE12 – Test 2

BE12 with l_b = 400 mm was subjected to a total of two high strain rate tests. This test, the second of two, was conducted on March 29, 2012. The DPL was used to subject this specimen to a shock wave with a reflected pressure of 334 kPa and reflected impulse of 3672 kPa-ms. The specimen did not fail during this test and reinforcement response was in the strain hardening range. Analysis of the strain gauge data indicated the peak load was at least 159.1 kN, generating a stress in the reinforcement of at least 584.8 MPa. Time-to-peak load was 18 milliseconds and strain rate was 0.18 s^{-1}.

Table A.12.2.1: Experimental data for beam-end BE12 Test 2.

General Test Data						Strain data in the bonded region ($\times 10^{-6}$)										
Time ms	$\dot{\varepsilon}$ s^{-1}	P_{exp} kN	f_s MPa	l_d mm	δ_{LE} mm	LE	SG1	SG2	SG3	SG4	SG5	SG6	SG7	SG8	SG9	FE
0	0	0	0	0	0	0	0	0	0	0	0	0	0	0	0	0
3.0	0.32	51.5	189.2	106	0.045	946	826	256	71	25	22	3	6	-50	41	0
6.0	0.18	58.8	216.2	134	0.086	1081	1002	625	231	89	58	36	33	6	34	0
9.0	0.20	99.4	365.6	184	0.193	1828	1667	1369	709	322	143	91	82	110	51	0
12.0	0.22	145.4	534.4	222	0.318	2672	2552	2083	1258	827	319	143	113	120	17	0
15.0	0.19	158.4	582.4	231	0.355	2912	2786	2264	1463	1014	420	161	108	66	-35	0
18.0	0.18	159.1	584.8	233	0.400	3283	3142	2563	1657	1166	497	177	107	14	-25	0
Dynamic loading continued beyond this load but bond failure did not occur.																

Note: Italicized data indicates questionable strain gauge readings.

Figure A.12.2.1: Photographs of BE12 after Test 2.

Load-time history data not available.

Figure A.12.2.2: Load-time history.

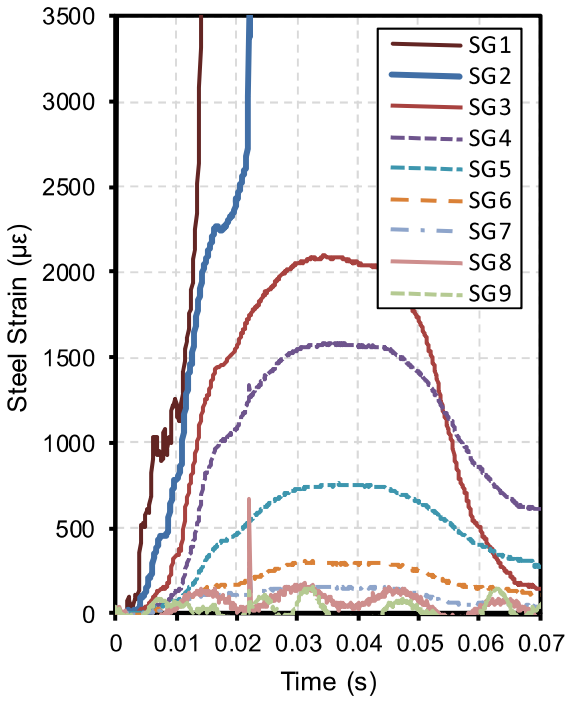

Figure A.12.2.3: Strain-time history.

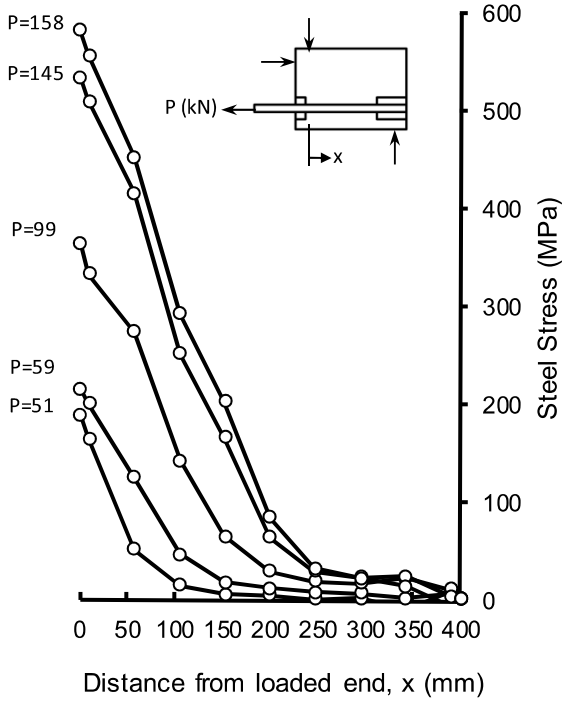

Figure A.12.2.4: Distribution of steel stresses in the bonded region.

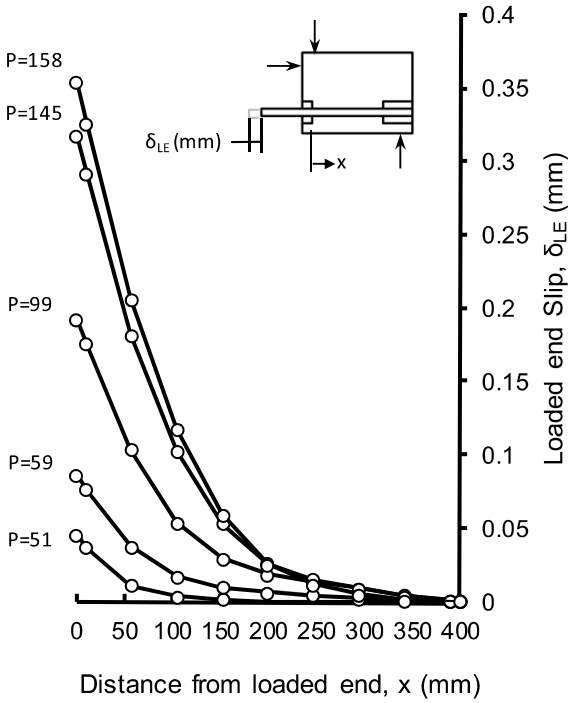

Figure A.12.2.5: Distribution of slip in the bonded region.

A.13: Beam-end BE13

BE13 with $l_b = 200$ mm was subjected to high strain rate testing on March 28, 2012. The DPL was used to subject this specimen to a shock wave with a reflected pressure of 331 kPa and reflected impulse of 3782 kPa-ms. The specimen did not fail but the reinforcement was stressed into the strain hardening range. Analysis of the strain gauge data indicated the peak load was at least 171.1 kN, generating a stress in the reinforcement of 629.0 MPa. Time-to-peak load was 34.6 milliseconds and strain rate was 0.41 s^{-1}.

Table A.13.1: Experimental data for beam-end BE13.

General Test Data						Strain data in the bonded region ($\times 10^{-6}$)										
Time ms	$\dot{\varepsilon}$ s^{-1}	P_{exp} kN	f_s MPa	l_d mm	δ_{LE} mm	LE	SG1	SG2	SG3	SG4	SG5	SG6	SG7	SG8	SG9	FE
0	0	0	0	0	0	0	0	0	0	0	0	0	0	0	0	0
4.6	0.08	21.1	77.5	141	0.031	388	360	229	98	28	9	19	8	9	5	0
7.1	0.16	60.2	221.3	154	0.091	1107	918	666	302	105	53	51	35	29	15	0
9.6	0.12	61.6	226.5	138	0.103	1132	1062	804	235	133	73	68	46	31	15	0
12.1	0.15	96.4	354.5	145	0.174	1772	1671	1322	435	355	130	103	71	42	21	0
14.6	0.16	127.3	468.2	191	0.265	2341	2230	1947	839	575	273	158	99	73	36	0
17.1	0.15	138.5	509.2	196	0.294	2546	2427	2111	945	689	313	181	96	98	49	0
19.6	0.14	151.6	557.4	200	0.324	2787	2659	2309	1069	788	370	190	107	72	36	0
22.1	0.14	159.1	585.1	219	0.358	3051	2911	2530	1188	887	425	208	109	80	40	0
24.6	0.19	159.6	586.7	245	0.435	4643	4324	2809	1294	985	483	239	118	93	46	0
29.6	0.31	160.5	590.0	299	0.696	9115	8381	4895	1409	1154	596	302	139	101	50	0
34.6	0.41	171.1	629.1	301	0.969	14085	12884	7177	1470	1227	639	329	140	102	51	0
Dynamic loading continued beyond this load but bond failure did not occur.																

Note: Italicized data indicates questionable strain gauge readings.

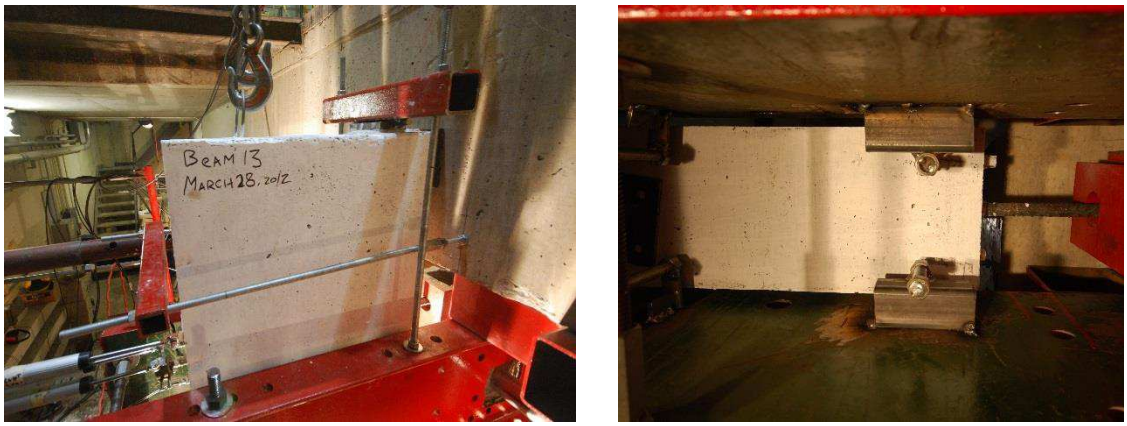

(a) Before testing (b) After testing

Figure A.13.1: Photographs of BE13 before and after testing.

Load-time history data not available.

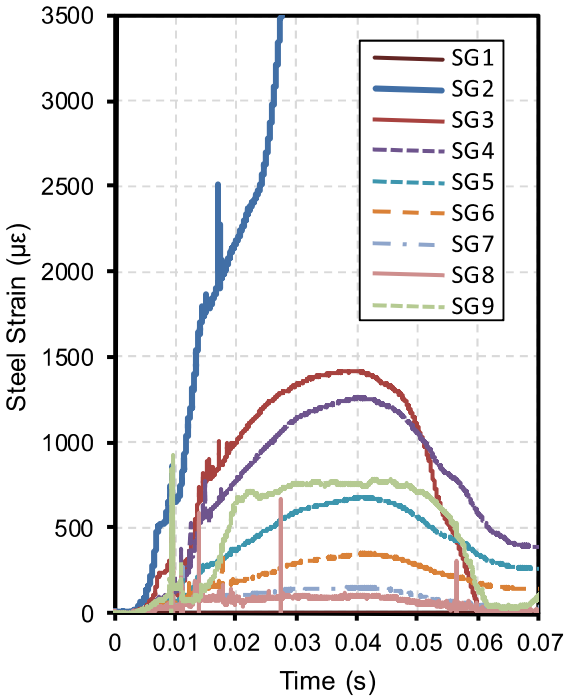

Figure A.13.2: Load-time history.

Figure A.13.3: Strain-time history.

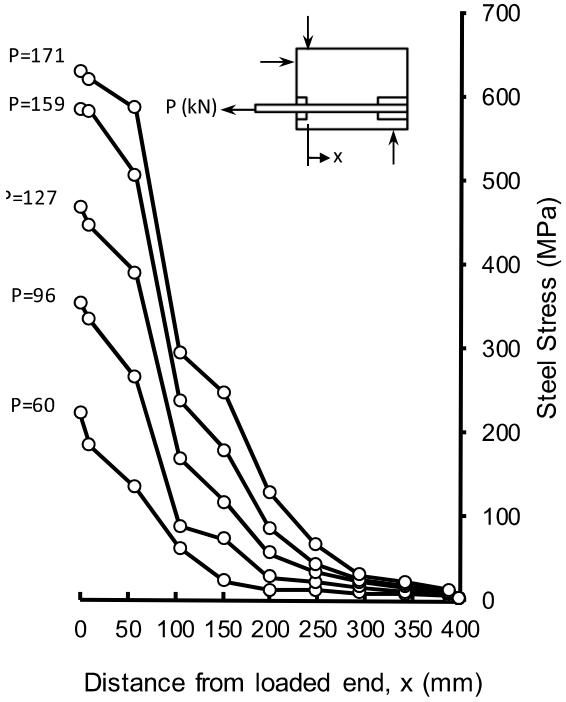

Figure A.13.4: Distribution of steel stresses in the bonded region.

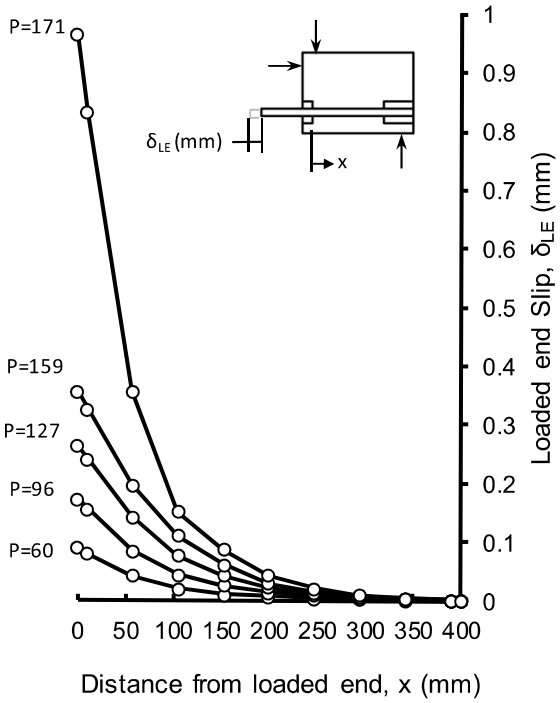

Figure A.13.5: Distribution of slip in the bonded region.

A.14.1: Beam-end BE14 – Test 1

BE14 with l_b = 400 mm was subjected to a total of three high strain rate tests. This test, the first of three, was conducted on March 25, 2012. The DPL was used to subject this specimen to a shock wave with a reflected pressure of 76 kPa and reflected impulse of 786 kPa-ms. The specimen did not fail during this test and reinforcement response was in the elastic range. Analysis of the strain gauge data indicated the peak load was 61.8 kN, generating a stress in the reinforcement of 226.5 MPa. Time-to-peak load was 21.5 milliseconds and strain rate was 0.05 s^{-1}.

Table A.14.1.1: Experimental data for beam-end BE14 Test 1.

General Test Data						Strain data in the bonded region (×10^{-6})										
Time ms	$\dot{\varepsilon}$ s^{-1}	P_{exp} kN	f_s MPa	l_d mm	δ_{LE} mm	LE	SG1	SG2	SG3	SG4	SG5	SG6	SG7	SG8	SG9	FE
0	0	0	0	0	0	0	0	0	0	0	0	0	0	0	0	0
1.5	0.17	13.7	50.3	69	0.012	252	215	41	16	10	4	7	5	-1	13	0
4.0	0.13	28.9	106.4	69	0.024	532	455	90	29	18	11	11	9	4	14	0
6.5	0.09	33.5	123.3	76	0.032	617	536	152	47	26	15	16	12	7	12	0
9.0	0.07	35.8	131.5	108	0.036	657	576	188	60	31	20	18	14	5	22	0
11.5	0.06	38.6	141.8	113	0.043	709	631	258	82	38	27	22	18	13	-19	0
14.0	0.06	46.4	170.7	116	0.054	854	763	335	111	50	28	25	20	13	-8	0
16.5	0.06	56.2	206.7	115	0.063	1034	909	317	152	65	38	32	26	21	15	0
19.0	0.06	61.7	226.7	113	0.063	1133	981	257	178	72	40	33	25	22	-12	0
21.5	0.05	61.6	226.5	114	0.064	1133	979	251	182	73	42	34	27	21	-3	0

Note: Italicized data indicates questionable strain gauge readings.

(a) Before testing (b) After testing

Figure A.14.1.1: Photographs of BE14 before and after Test 1.

Load-time history data not available.

Figure A.14.1.2: Load-time history.

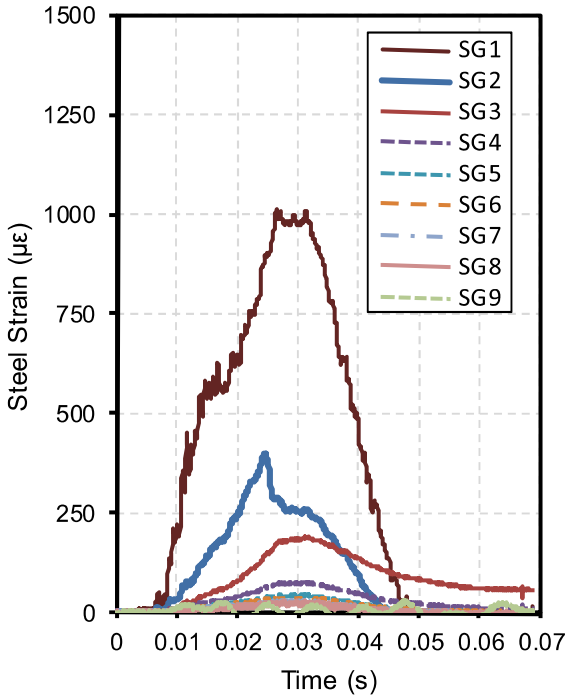

Figure A.14.1.3: Strain-time history.

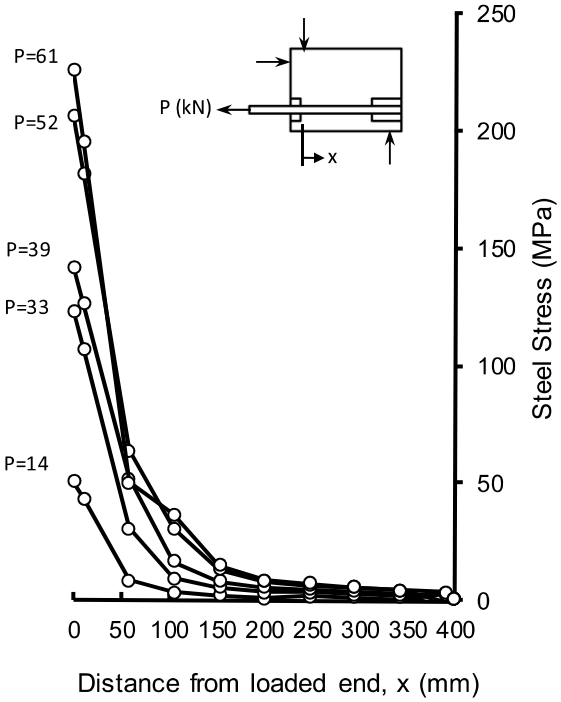

Figure A.14.1.4: Distribution of steel stresses in the bonded region.

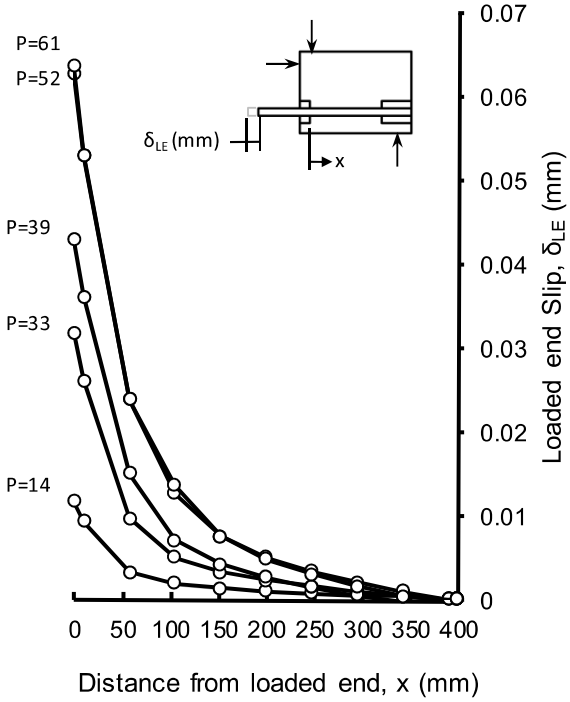

Figure A.14.1.5: Distribution of slip in the bonded region.

A.14.2: Beam-end BE14 – Test 2

BE14 with l_b = 400 mm was subjected to a total of three high strain rate tests. This test, the second of three, was conducted on March 25, 2012. The DPL was used to subject this specimen to a shock wave with a reflected pressure of 295 kPa and reflected impulse of 3570 kPa-ms. The specimen did not fail during this test and reinforcement response was in the strain hardening range. Analysis of the strain gauge data indicated the peak load was at least 159.1 kN, generating a stress in the reinforcement of 585.0 MPa. Time-to-peak load was 10.5 milliseconds and strain rate was 0.28 s^{-1}.

Table A.14.2.1: Experimental data for beam-end BE14 Test 2.

General Test Data						Strain data in the bonded region (×10^{-6})										
Time ms	$\dot{\varepsilon}$ s-1	P_{exp} kN	f_s MPa	l_d mm	δ_{LE} mm	LE	SG1	SG2	SG3	SG4	SG5	SG6	SG7	SG8	SG9	FE
0	0	0	0	0	0	0	0	0	0	0	0	0	0	0	0	0
1.5	1.00	81.4	299.2	140	0.087	1496	1319	479	174	62	35	26	13	21	118	0
3.0	0.47	76.2	280.2	148	0.097	1401	1264	613	235	85	48	37	20	28	112	0
4.5	0.31	75.7	278.4	131	0.109	1392	1303	749	296	109	61	48	27	38	66	0
6.0	0.25	82.9	304.9	144	0.130	1525	1434	887	431	158	78	58	37	40	28	0
7.5	0.28	113.2	416.1	176	0.200	2081	1942	1389	753	318	135	88	58	63	6	0
9.0	0.28	137.1	504.1	183	0.253	2521	2360	1723	988	451	193	113	74	74	18	0
10.5	0.28	159.1	585.0	213	0.695	2930	16032	2085	1282	643	284	143	87	82	18	0
Dynamic loading continued beyond this load but bond failure did not occur.																

Note: Italicized data indicates questionable strain gauge readings.

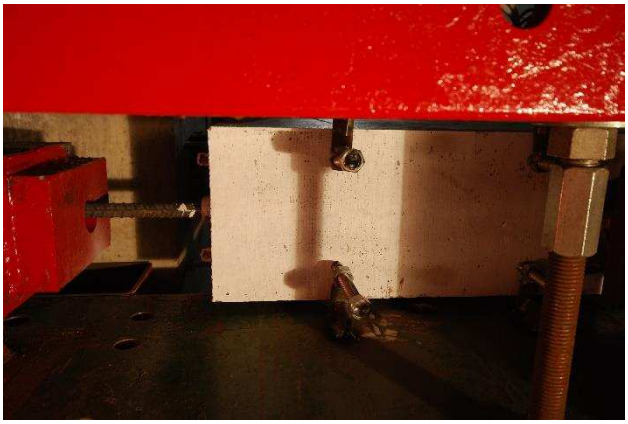

Figure A.14.2.1: Photograph of BE14 after Test 2.

Load-time history data not available.

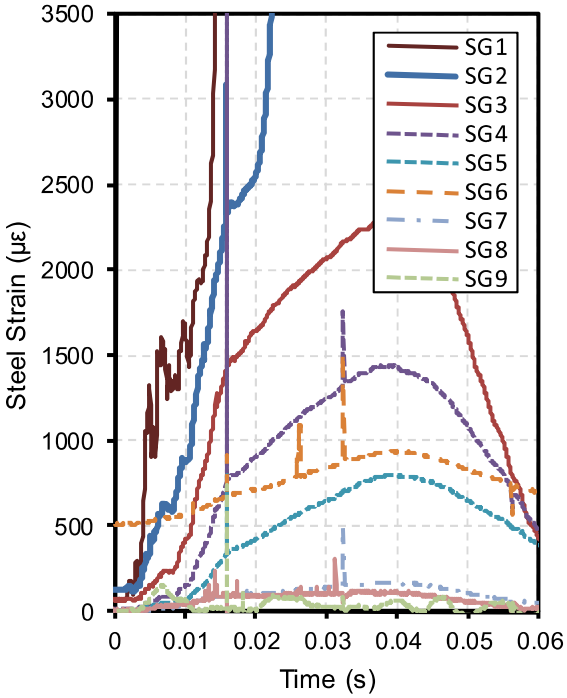

Figure A.14.2.2: Load-time history.

Figure A.14.2.3: Strain-time history.

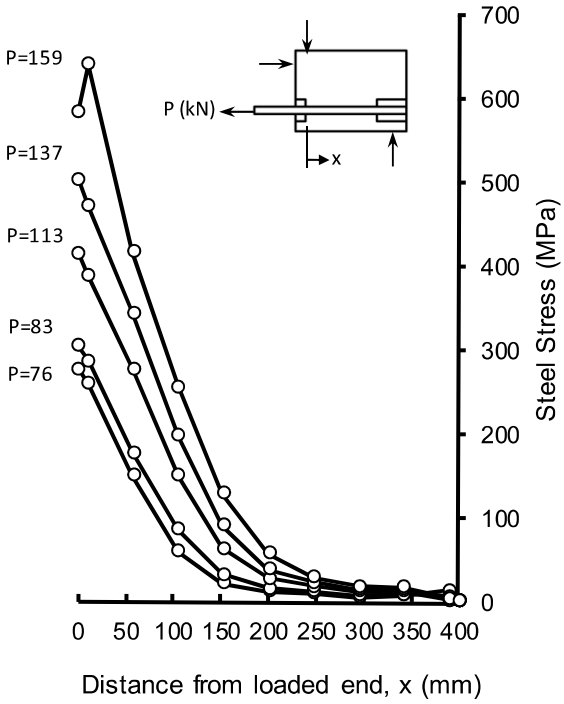

Figure A.14.2.4: Distribution of steel stresses in the bonded region.

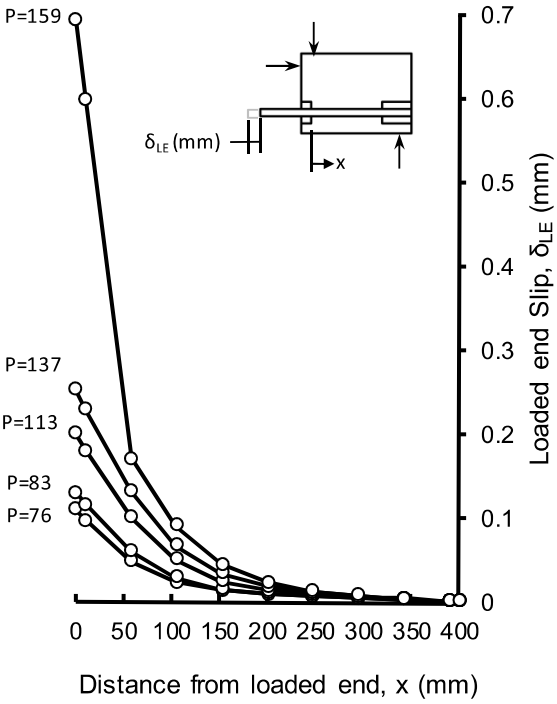

Figure A.14.2.5: Distribution of slip in the bonded region.

A.14.3: Beam-end BE14 – Test 3

BE14 with l_b = 400 mm was subjected to a total of three high strain rate tests. This test, the third of three, was conducted on March 25, 2012. The DPL was used to subject this specimen to the largest shock wave of the entire research program with a reflected pressure of 425 kPa and reflected impulse of 4500 kPa-ms. The specimen failed by rupture of reinforcement 15 mm into the bonded region at the loaded end of the test bar. The crack pattern of the specimen after testing consisted of a narrow crack running parallel to the test bar on the bottom face and another crack spanning the width of the bottom face at the end of the bonded region. The specimen was so heavily damaged that most of the strain gauges were lost during testing. Time-to-rupture was 15 ms with a strain rate of 1.2 s^{-1}. The dynamic rupture stress was estimated to be 738 MPa using a *DIF* applied to ultimate strength of 1.08 (Malvar and Crawford, 1998a). Analysis of the strain gauge data in the bonded region indicated that the entire bonded length of 400 mm was stressed at the time of rupture.

Concerns were raised regarding the safety of operating the DPL at maximum shock tube capacity. The loaded end of the ruptured test bar was propelled 15 meters across the laboratory and the test fixture experienced severe vibrations after the rupture had occurred. As a result, the remaining beam-ends with l_b = 400 mm, BE11, BE12, and BE13, were subjected to the same pressure-impulse which resulted in debonding failure of the l_b = 200 mm specimens. Although this pressure-impulse combination was not sufficient to generate bond failure in the specimens, the bars were stressed past their dynamic yield point and high strain rate bond characteristics were recorded.

(a) After testing

(b) After testing

(c) After testing

Figure A.14.3.1: Photographs of BE14 after Test 3.

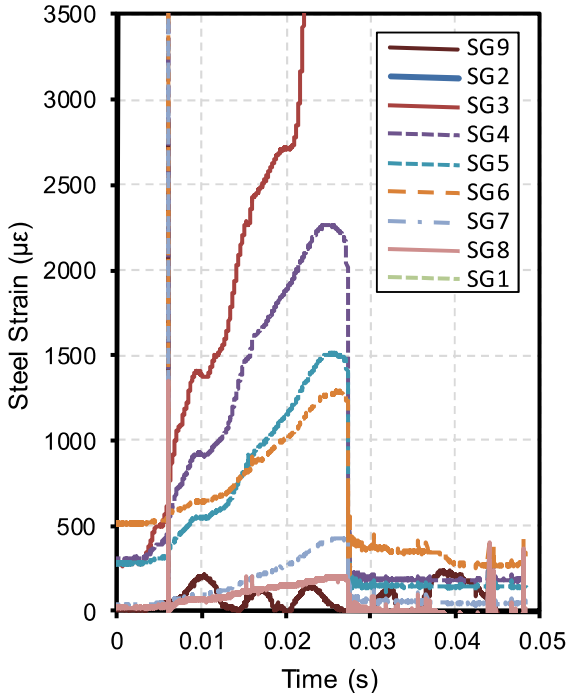

Figure A.14.3.2: Strain-time history.

Appendix B

Lap Splice Beam Test Data

Appendix B contains the complete record results collected during the course of the experimental study on the performance of lap splice beams subjected to high strain rates. The results of a total of twenty-five reinforced concrete lap splice beam tests are provided. Companion Pairs CP1-11 were discussed in Chapter 4. Companion Pair CP0 was intended to serve as a commissioning test and was not covered in Chapter 4, although experimental data was used in the bond database developed in Chapter 5. Details of CP0 are provided in this appendix.

Typical data presented in the appendix includes a written synopsis of each test, the material and cross-sectional properties, and a summary of the relevant experimental results. Resistance curves, steel stress-load history, load-time history and displacement time-history plots are shown. Steel strains recorded by strain gauges placed on the spliced bars are also shown. Note that dynamic steel and concrete strengths are provided for the high strain rate companion tests. These values were calculated following the procedure described in Section 5.2.3. Also provided in this appendix are fully- and partially-bond flexural predictions of resistance and splice stress for each companion beam.

CP1-LSR

Lap splice beam CP1-LSR was subjected to low strain rate testing on September 19, 2013. CP1-LSR was designed with 10M reinforcement, 30 MPa concrete, 25 mm cover, and without transverse reinforcement in the spliced region. The specimen experienced a combined face- and side-splitting tensile failure of the cover concrete with minimal cover loss. Failure occurred at an applied load of 38.4 kN. Based on strain readings, the stress developed in the spliced bars was 431 MPa. Based on a sectional analysis, the stress developed in the spliced bars was 457 MPa. Time-to-failure was 143.6 seconds and strain rate was 1.5×10^{-5} s^{-1}.

Table B.1: Geometry, reinforcing, and material properties for CP1-LSR.

b:	150 mm	Bar:	2-10M	f_c':	32.5 MPa
h:	200 mm	A_b:	100 mm^2	f_y:	431.2 MPa
l_d:	275 mm	d_b:	11.3 mm	ρ:	0.79%
c_b:	26 mm	N:	N/A	c/d:	2.3
c_{so}:	27 mm	A_{tr}:	N/A	$l_d(c_{min}+0.5d_b)$:	8704 mm^2

Table B.2: Summary of experimental test results for CP1-LSR.

Date:	Sept. 19, 2013	δ_f:	14.8 mm	f_s^t:	431 MPa
P_r:	N/A	R_f:	38.4 kN	f_s^{cal}:	457 MPa
I_r:	N/A	t_f:	143.6 s	$\dot{\varepsilon}$:	1.5×10^{-5} s^{-1}

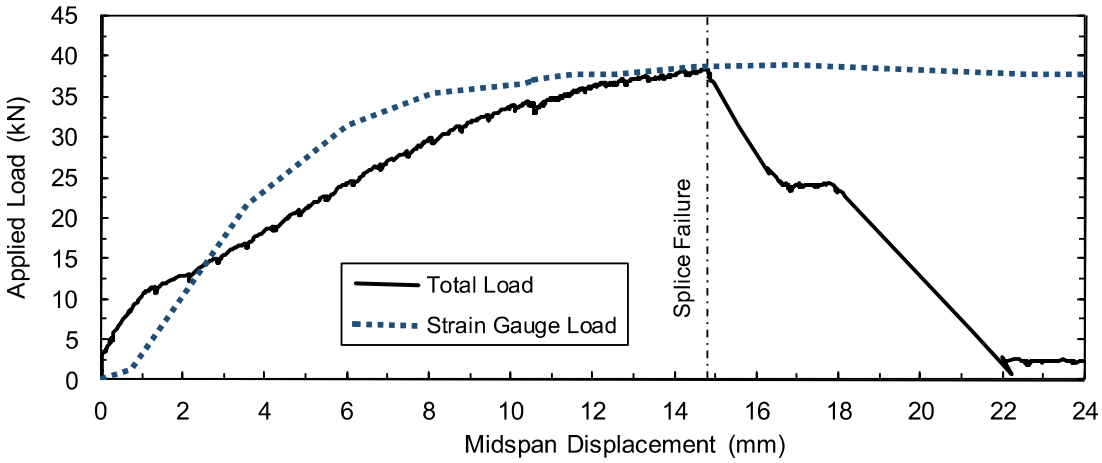

Figure B.1: Load displacement-history plot for CP1-LSR.

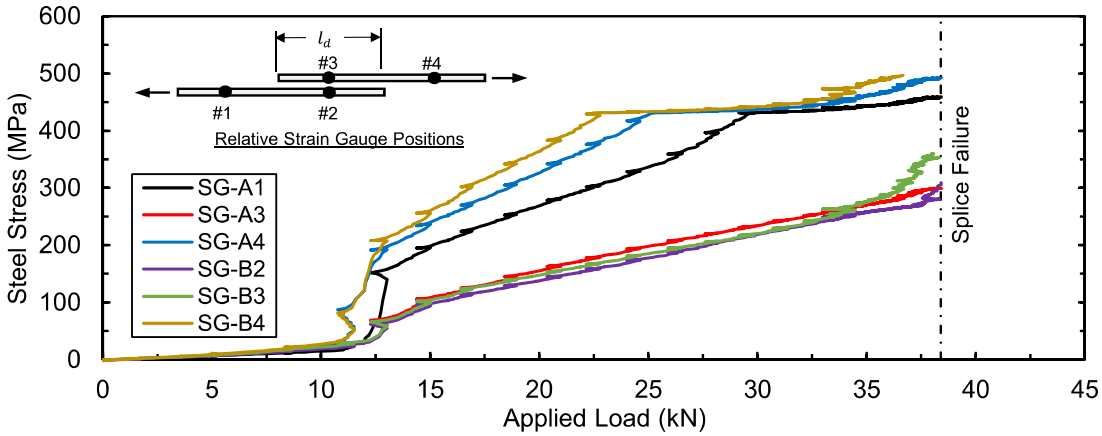

Figure B.2: Steel stress load-history plot for CP1-LSR.

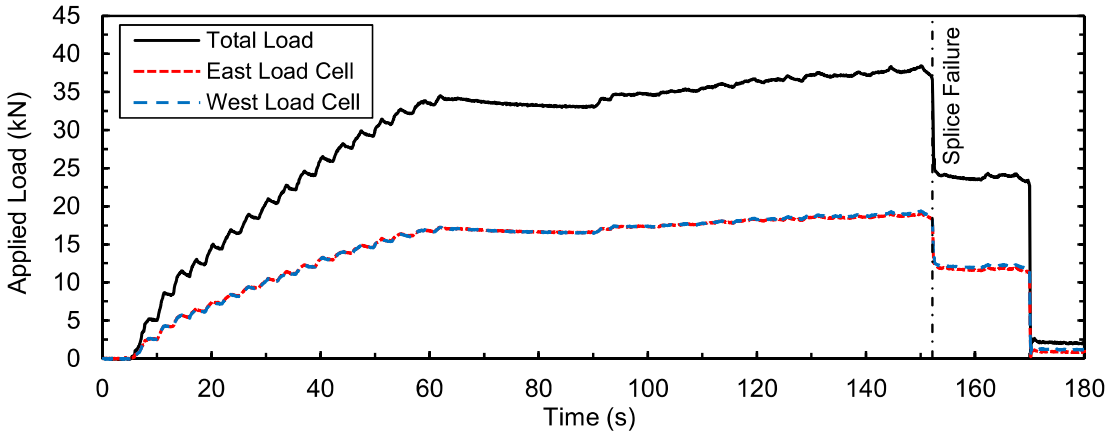

Figure B.3: Load time-history plot for CP1-LSR.

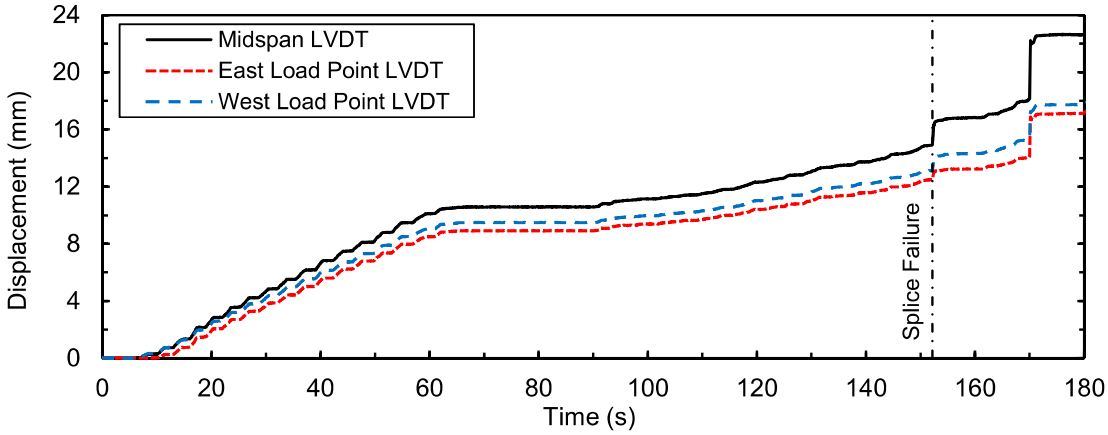

Figure B.4: Displacement time-history plot for CP1-LSR.

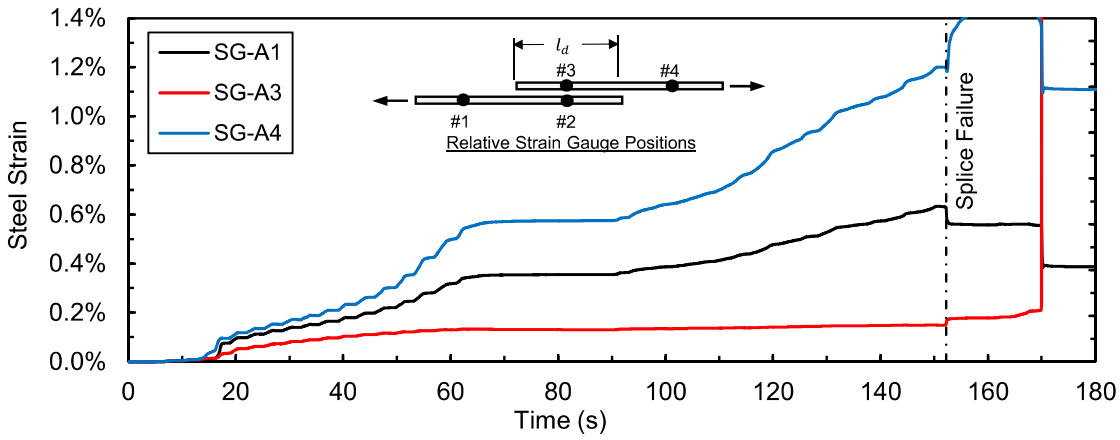

Figure B.5: Test bar "A" strain time-history plot for CP1-LSR.

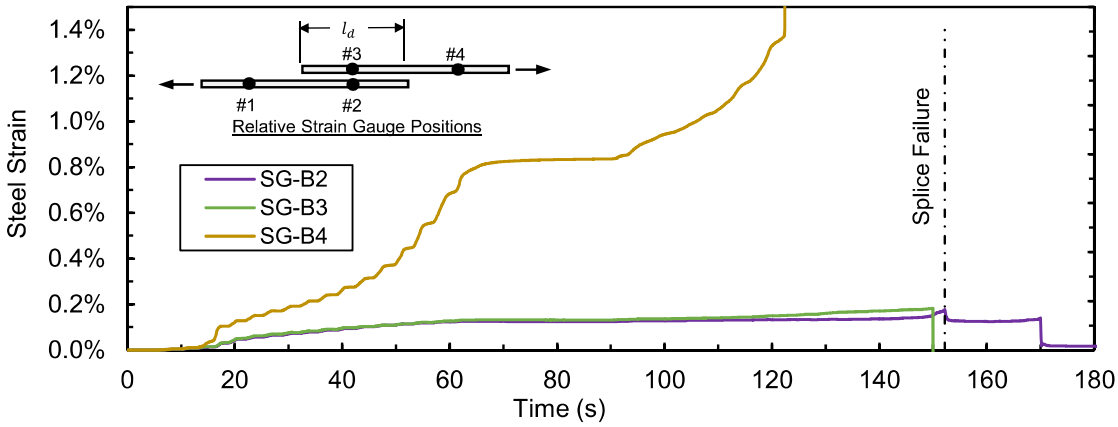

Figure B.6: Test bar "B" strain time-history plot for CP1-LSR.

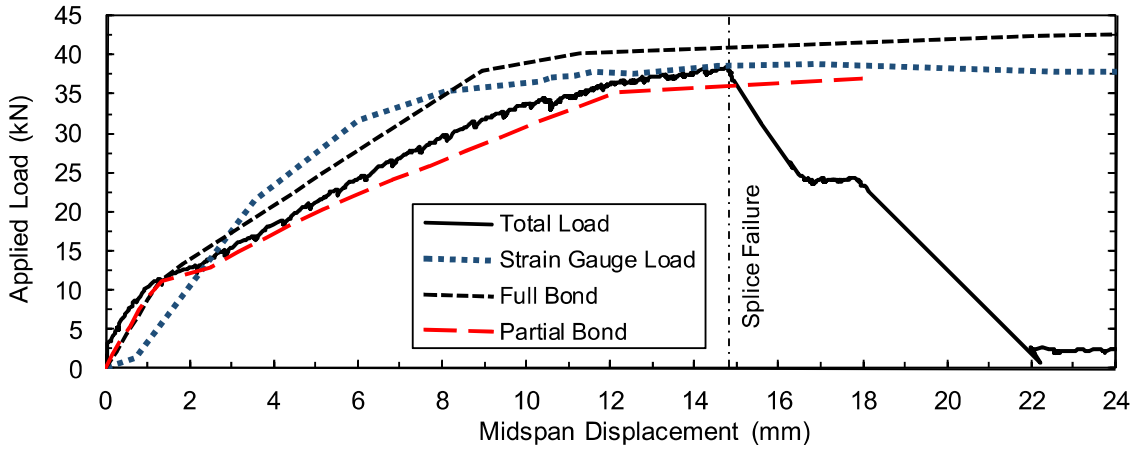

Figure B.7: Comparison of predicted and experimental resistance curves for CP1-LSR.

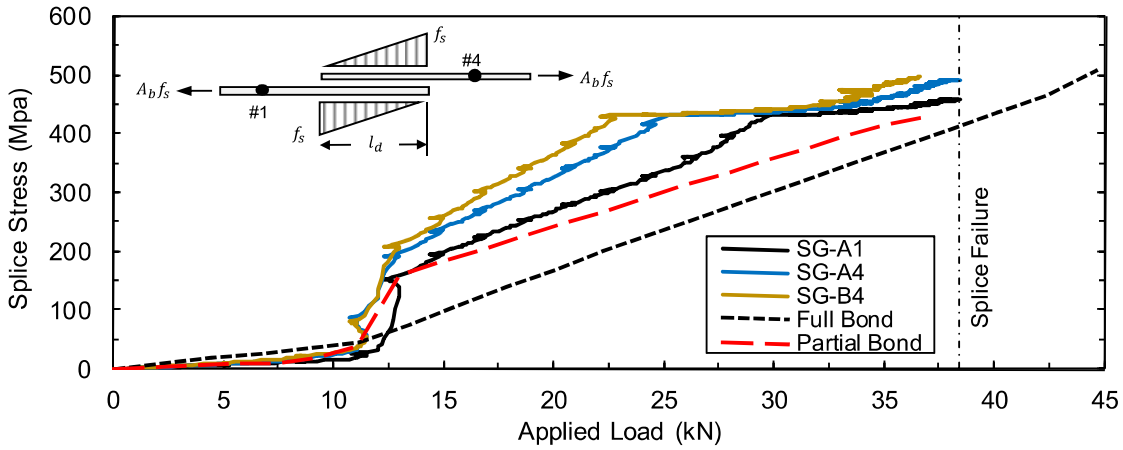

Figure B.8: Comparison of predicted and experimental steel stress developed in spliced reinforcement for CP1-LSR with respect to applied load.

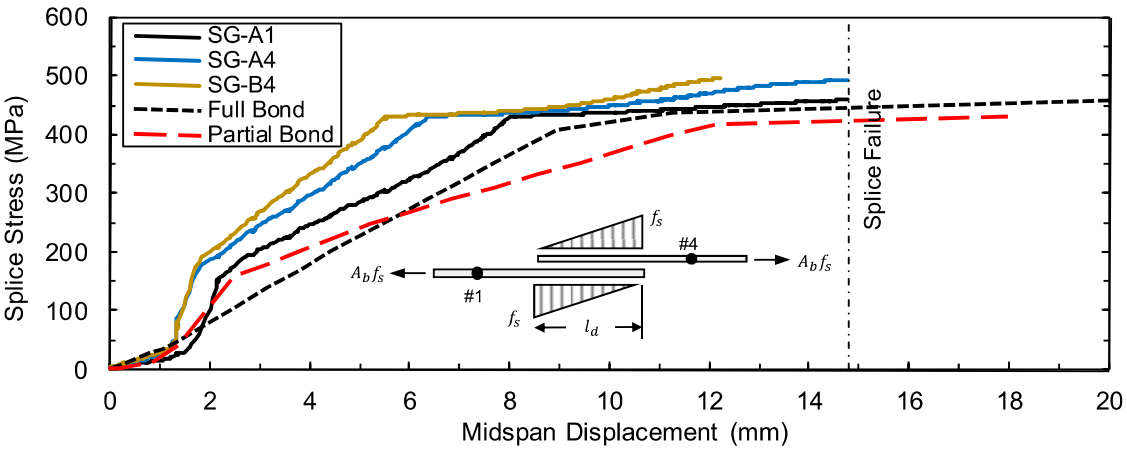

Figure B.9: Comparison of predicted and experimental steel stress developed in spliced reinforcement for CP1-LSR with respect to displacement.

(a) Before low strain rate testing

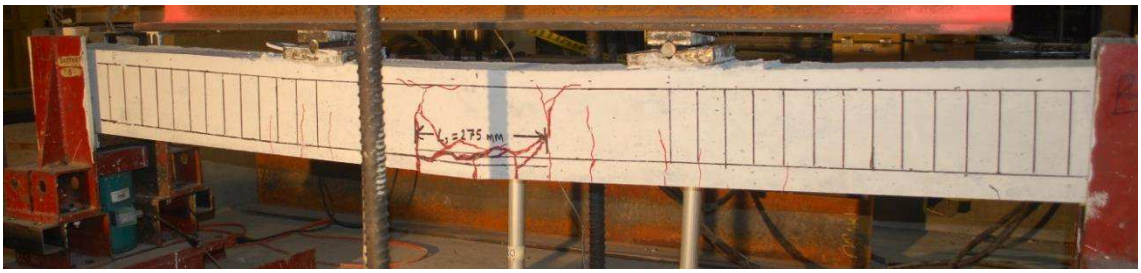

(b) After low strain rate testing

Figure B.10: Photographs of lap splice beam CP1-LSR.

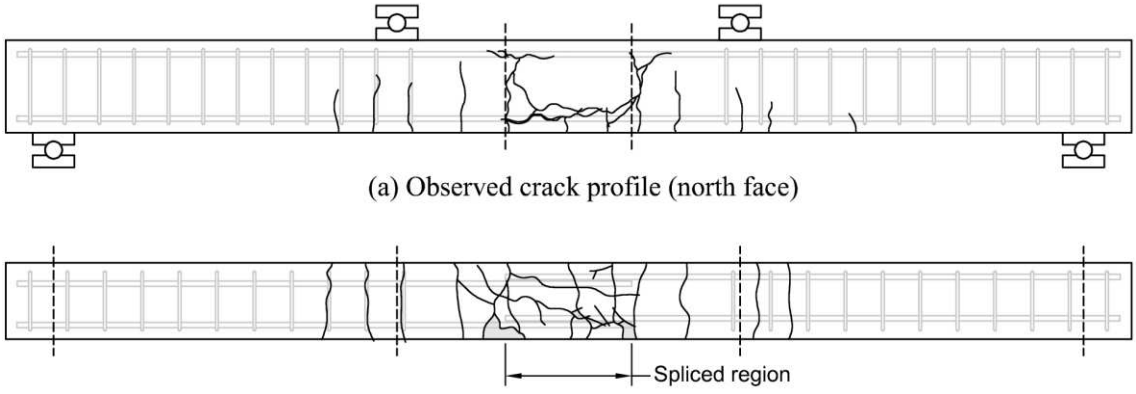

(a) Observed crack profile (north face)

(b) Observed crack profile (bottom face)

Figure B.11: Observed crack profile for lap splice beam CP1-LSR.

CP1-HSR

Lap splice beam Lap splice beam CP1-HSR was subjected to high strain rate testing on October 30, 2013. CP1-HSR was designed with 10M reinforcement, 30 MPa concrete, 25 mm cover, and without transverse reinforcement in the spliced region. The specimen experienced a side-splitting tensile failure of the cover concrete with significant cover loss. The peak dynamic resistance was 47.7 kN. Based on strain readings, the stress developed in the spliced bars was 571 MPa. Based on a sectional analysis, the stress developed in the spliced bars was 575 MPa. Time-to-failure was 15.6 ms and strain rate was 0.18 s^{-1}.

Table B.3: Geometry, reinforcing, and material properties for CP1-HSR.

b:	150 mm	Bar:	2-10M	f'_{dc}:	42.9 MPa
h:	200 mm	A_b:	100 mm^2	f_{dy}:	559.2 MPa
l_d:	276 mm	d_b:	11.3 mm	ρ:	0.79%
c_b:	27 mm	N:	N/A	c/d:	2.3
c_{so}:	25 mm	A_{tr}:	N/A	$l_d(c_{min} + 0.5d_b)$:	8459 mm^2

Table B.4: Summary of experimental test results for CP1-HSR.

Date:	Oct. 30, 2014	δ_f:	50.7 mm	f_s^t:	571 MPa
P_r:	54.8 kPa	R_f:	47.7 kN	f_s^{cal}:	575 MPa
I_r:	432.5 kPa-ms	t_f:	15.6 ms	$\dot{\varepsilon}$:	0.31 s^{-1}

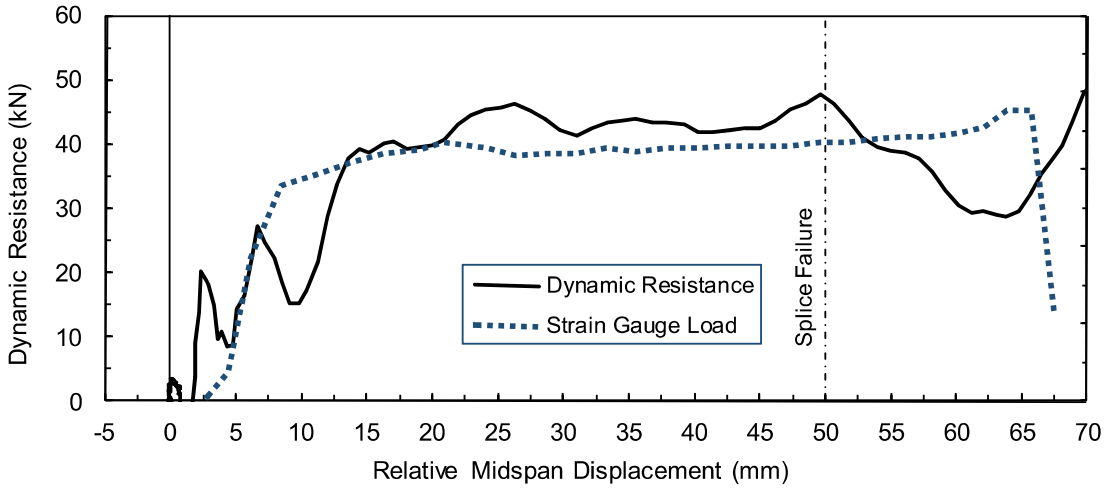

Figure B.12: Load displacement-history plot for CP1-HSR.

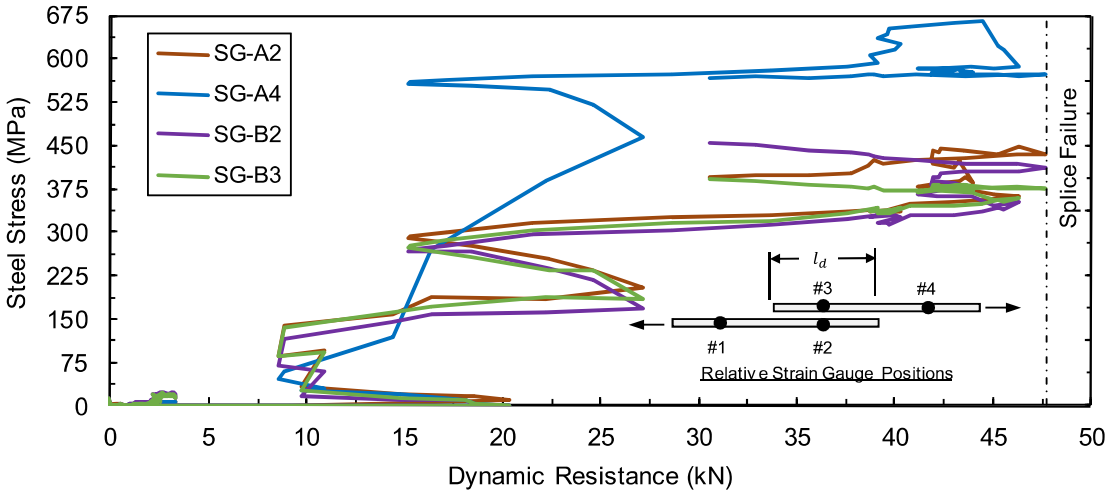

Figure B.13: Steel stress load-history plot for CP1-HSR.

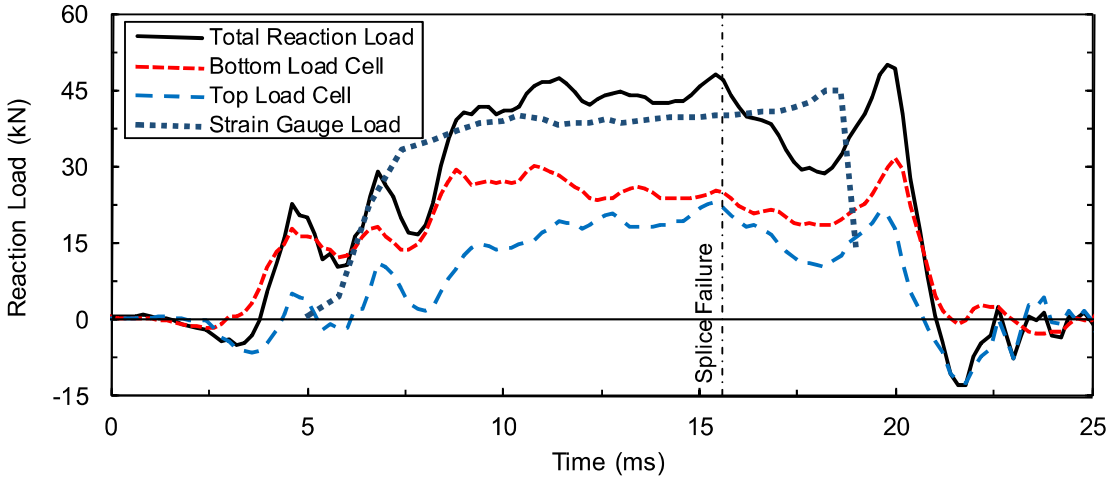

Figure B.14: Load time-history plot for CP1-HSR.

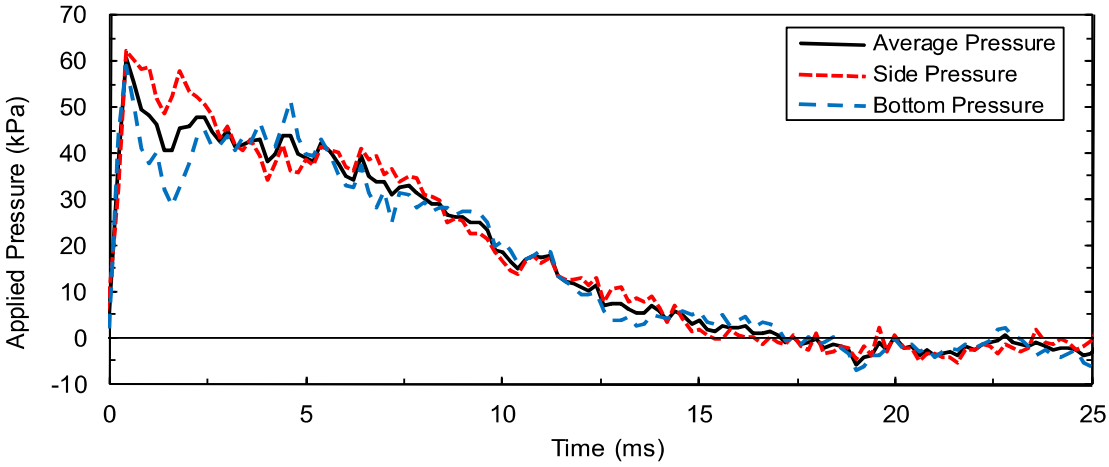

Figure B.15: Pressure time-history plot for CP1-HSR.

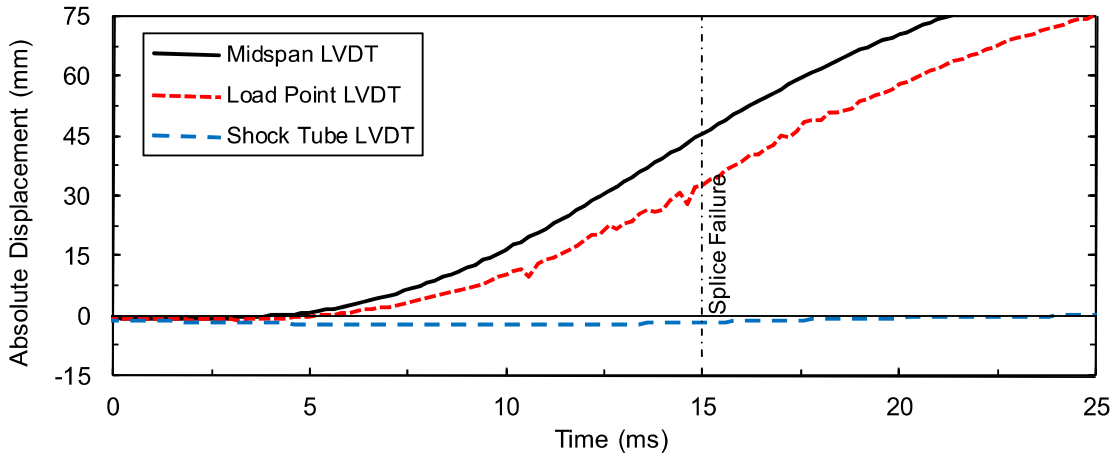

Figure B.16: Displacement time-history plot for CP1-HSR.

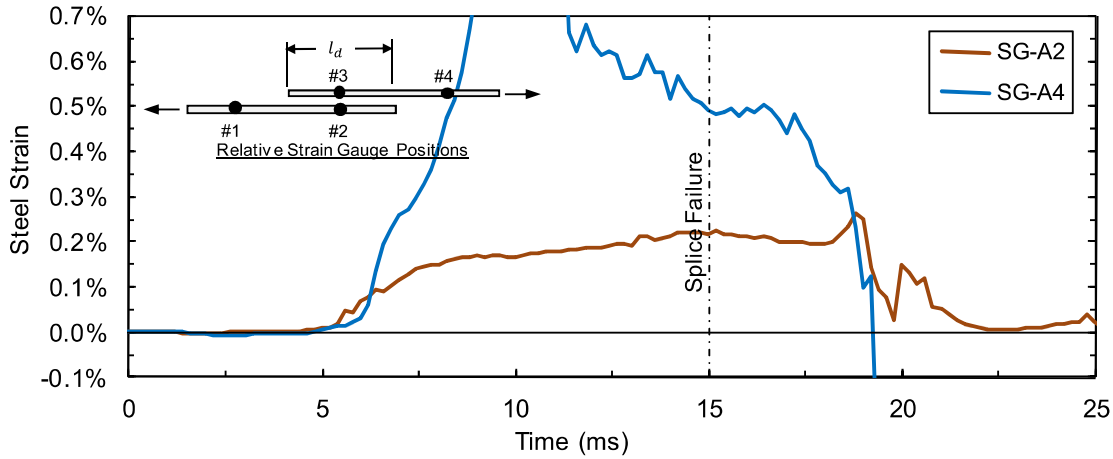

Figure B.17: Test bar "A" strain time-history plot for CP1-HSR.

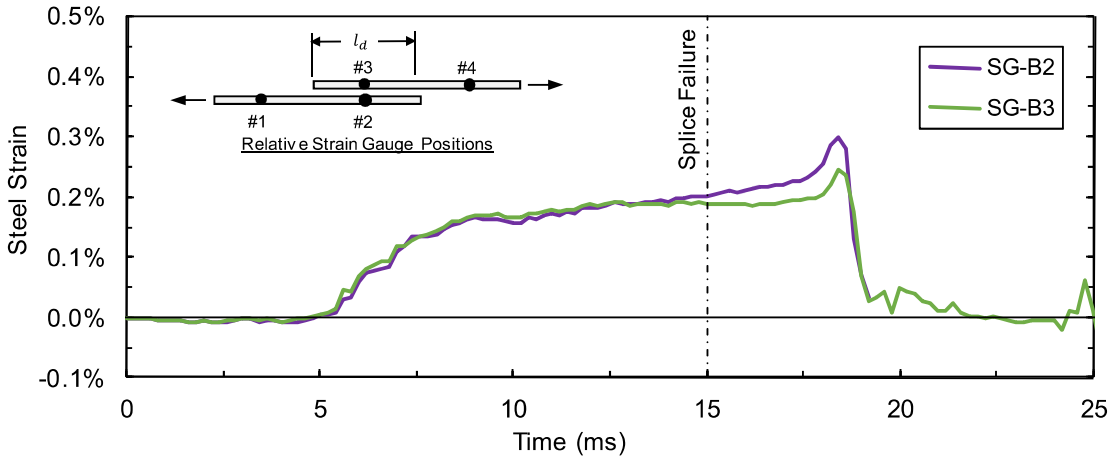

Figure B.18: Test bar "B" strain time-history plot for CP1-HSR.

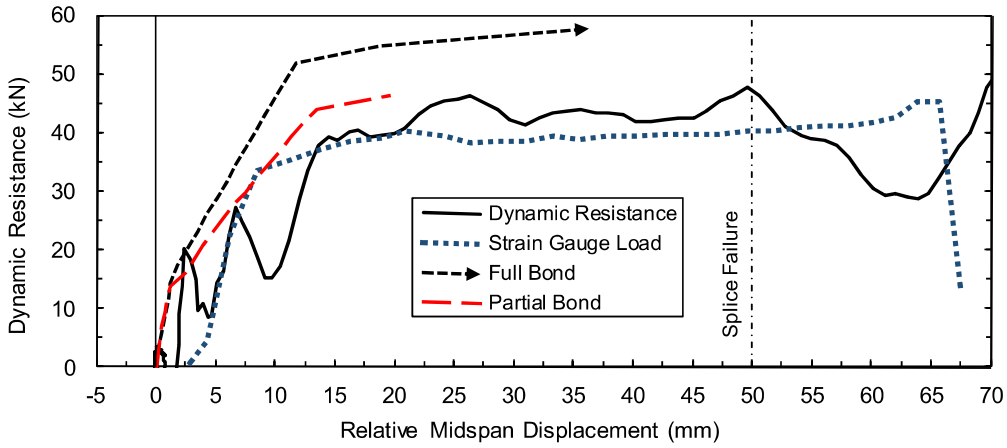

Figure B.19: Comparison of predicted and experimental resistance curves for CP1-HSR.

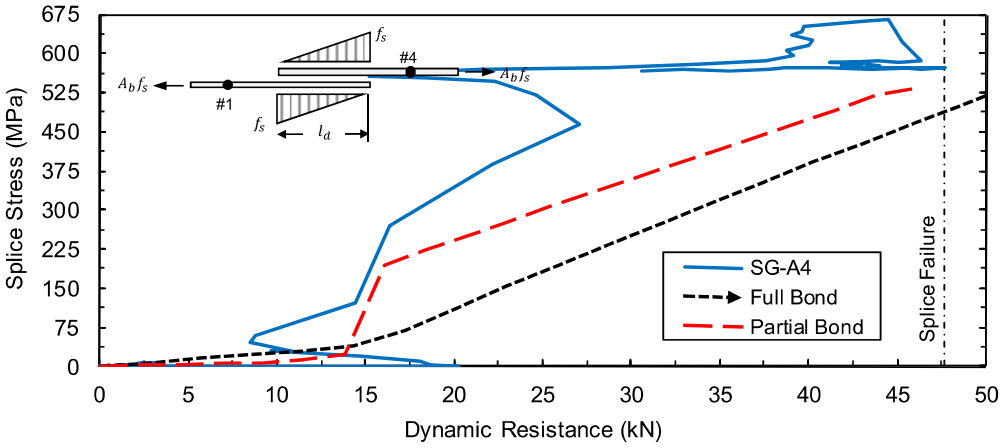

Figure B.20: Comparison of predicted and experimental steel stress developed in spliced reinforcement for CP1-HSR with respect to applied load.

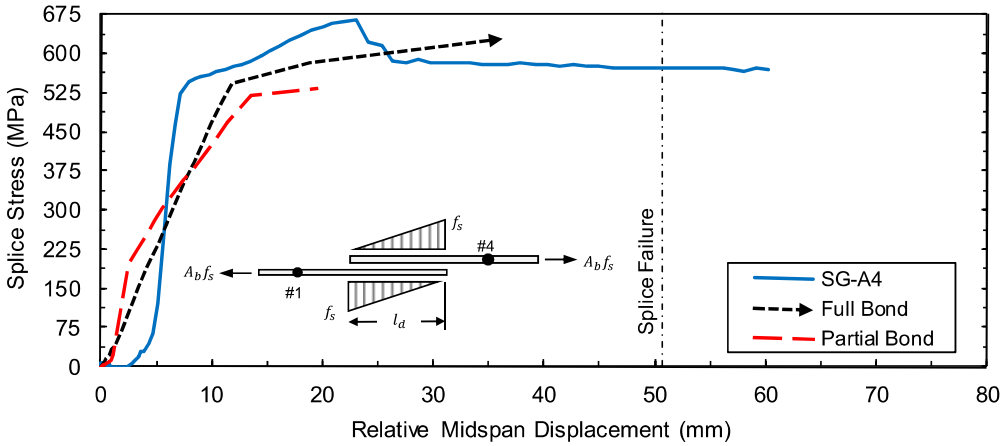

Figure B.21: Comparison of predicted and experimental steel stress developed in spliced reinforcement for CP1-HSR with respect to displacement.

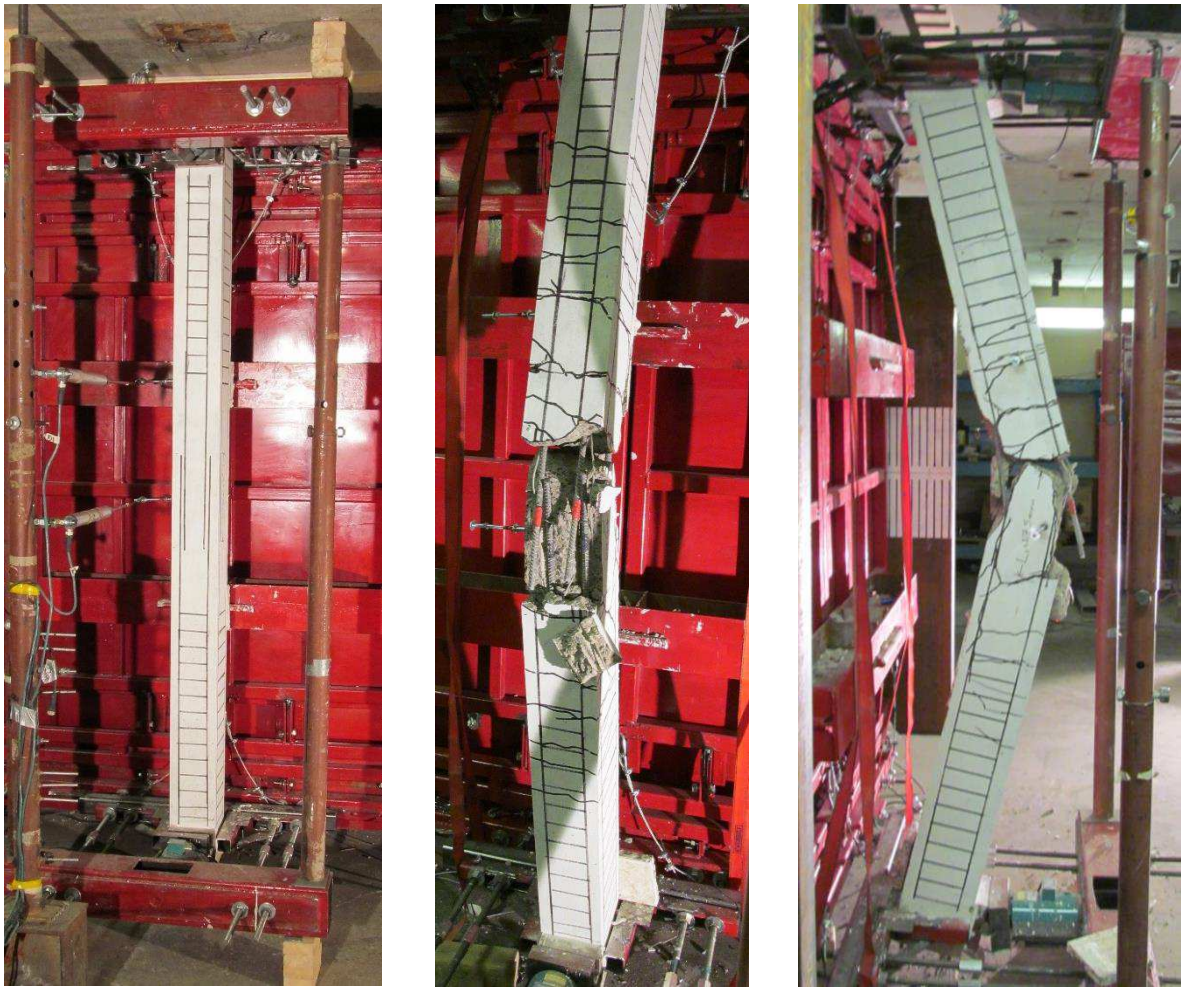

(a) Before high strain rate testing (b) After high strain rate testing (c) After high strain rate testing

Figure B.22: Photographs of lap splice beam CP1-HSR.

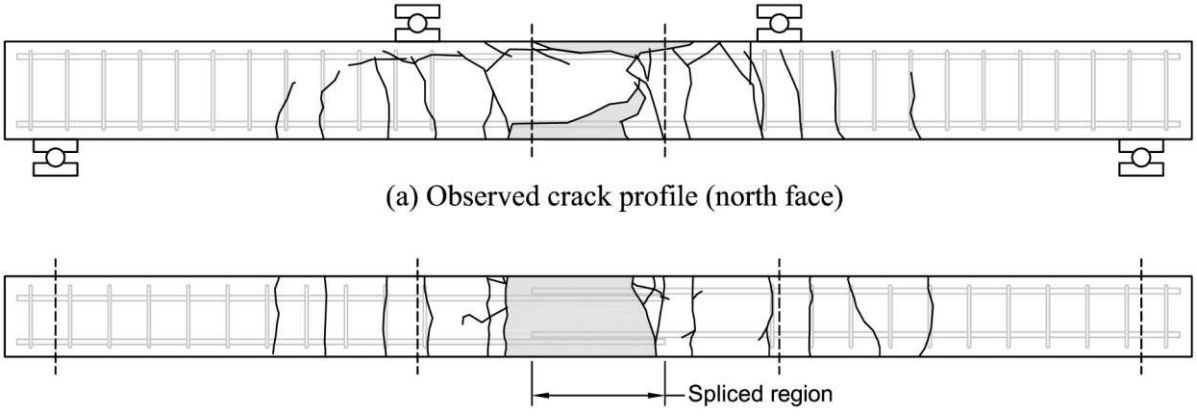

(a) Observed crack profile (north face)

(b) Observed crack profile (bottom face)

Figure B.23: Observed crack profile for lap splice beam CP1-HSR.

CP2-LSR

Lap splice beam CP2-LSR was subjected to low strain rate testing on September 25, 2013. CP2-LSR was designed with 10M reinforcement, 30 MPa concrete, 50 mm cover, and without transverse reinforcement in the spliced region. The specimen experienced a combined face- and side-splitting tensile failure of the cover concrete with minimal cover loss. Failure occurred at an applied load of 45.6 kN. Based on strain readings, the stress developed in the spliced bars was 441 MPa. Based on a sectional analysis, the stress developed in the spliced bars was 468 MPa. Time-to-failure was 123.5 seconds and strain rate was 1.8×10^{-5} s^{-1}.

Table B.5: Geometry, reinforcing, and material properties for CP2-LSR.

b:	240 mm	Bar:	2-10M	f_c':	32.5 MPa
h:	200 mm	A_b:	100 mm^2	f_y:	431.2 MPa
l_d:	168 mm	d_b:	11.3 mm	ρ:	0.58%
c_b:	51 mm	N:	N/A	c/d:	4.4
c_{so}:	49 mm	A_{tr}:	N/A	$l_d(c_{min}+0.5d_b)$:	9181 mm^2

Table B.6: Summary of experimental test results for CP2-LSR.

Date:	Sept. 25,2013	δ_f:	25.8 mm	f_s^t:	441 MPa
P_r:	N/A	R_f:	45.6 kN	f_s^{cal}:	468 MPa
I_r:	N/A	t_f:	123.5 s	$\dot{\varepsilon}$:	1.8×10^{-5} s^{-1}

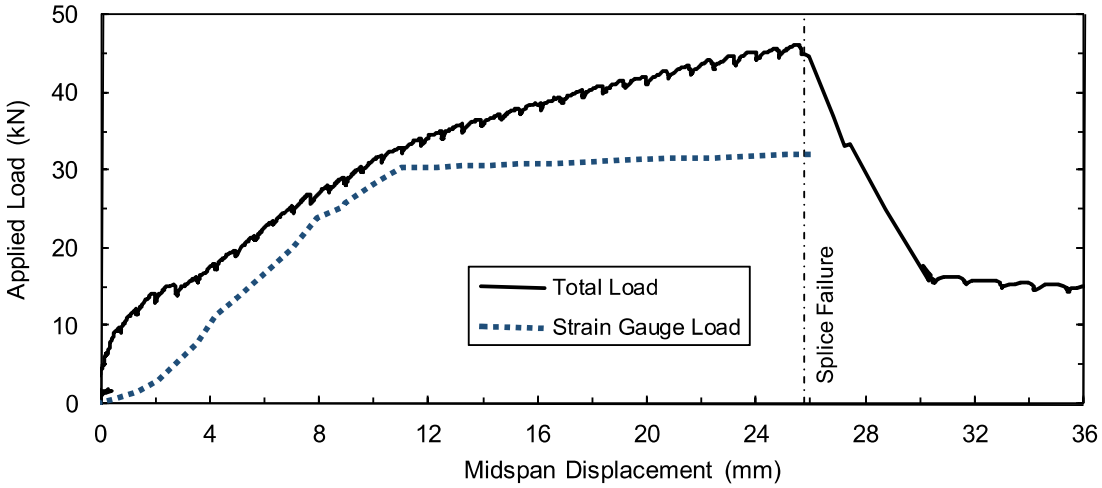

Figure B.24: Load displacement-history plot for CP2-LSR.

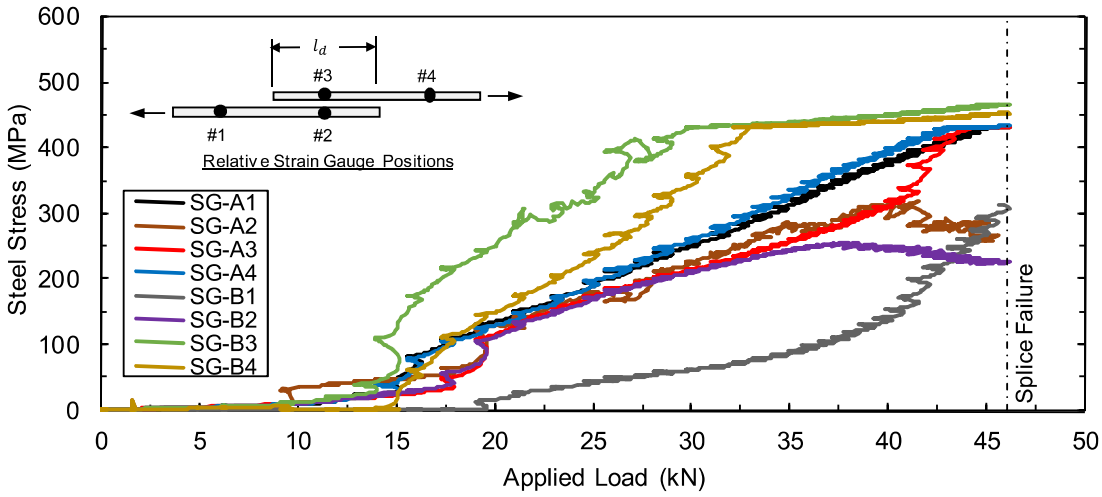

Figure B.25: Steel stress load-history plot for CP2-LSR.

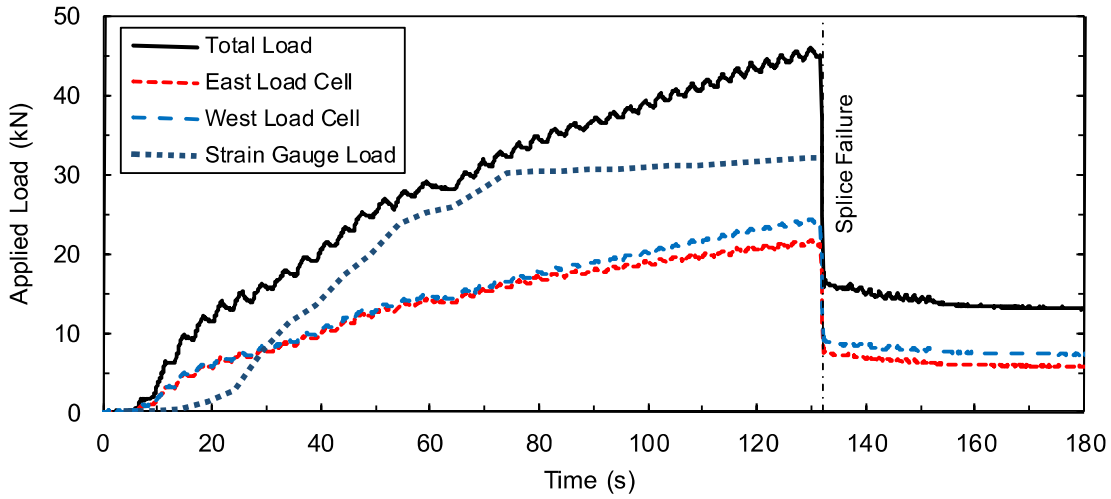

Figure B.26: Load time-history plot for CP2-LSR.

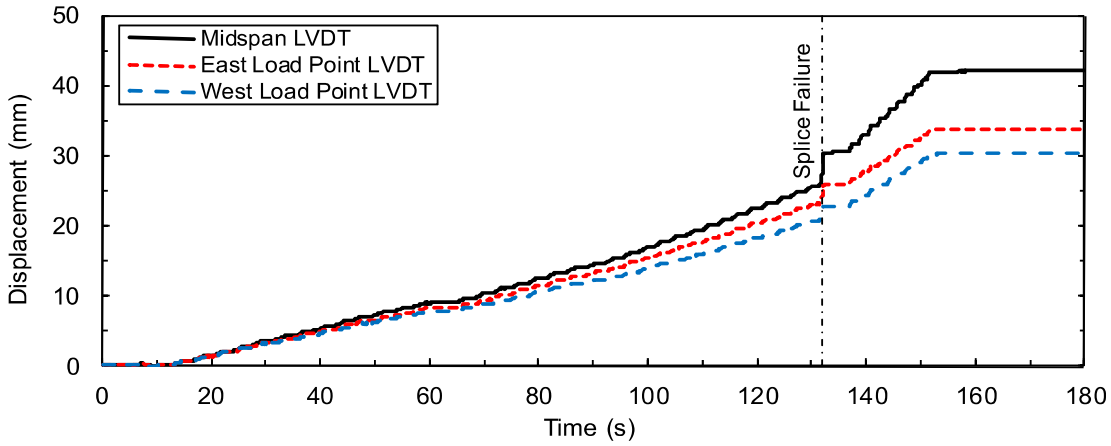

Figure B.27: Displacement time-history plot for CP2-LSR.

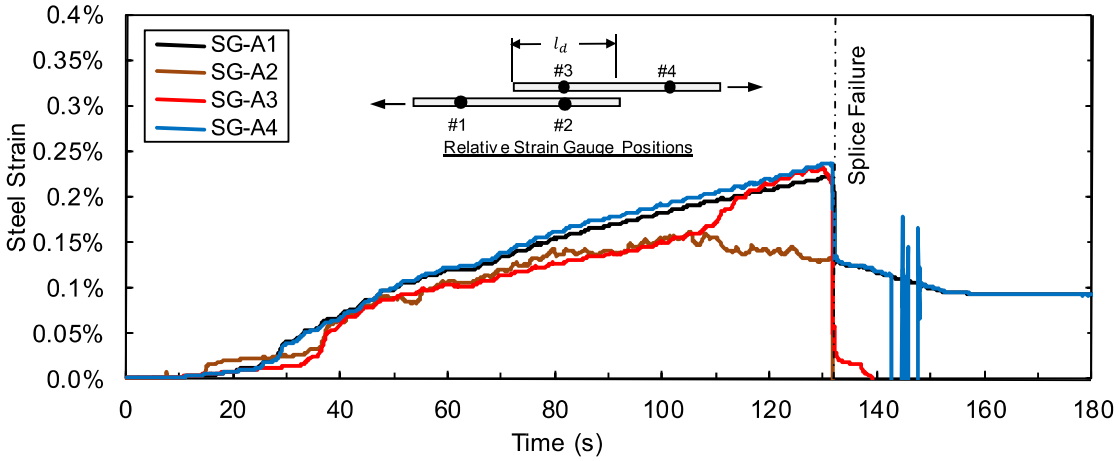

Figure B.28: Test bar "A" strain time-history plot for CP2-LSR.

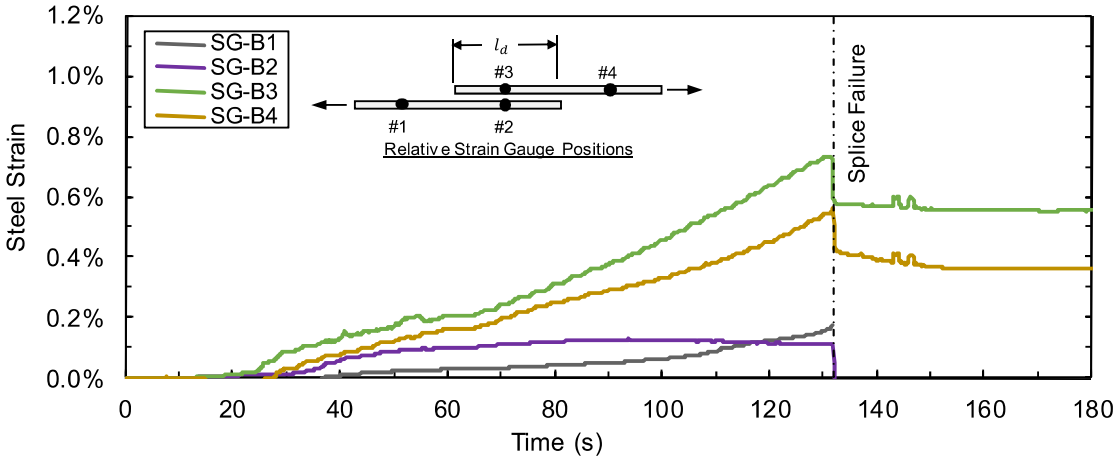

Figure B.29: Test bar "B" strain time-history plot for CP2-LSR.

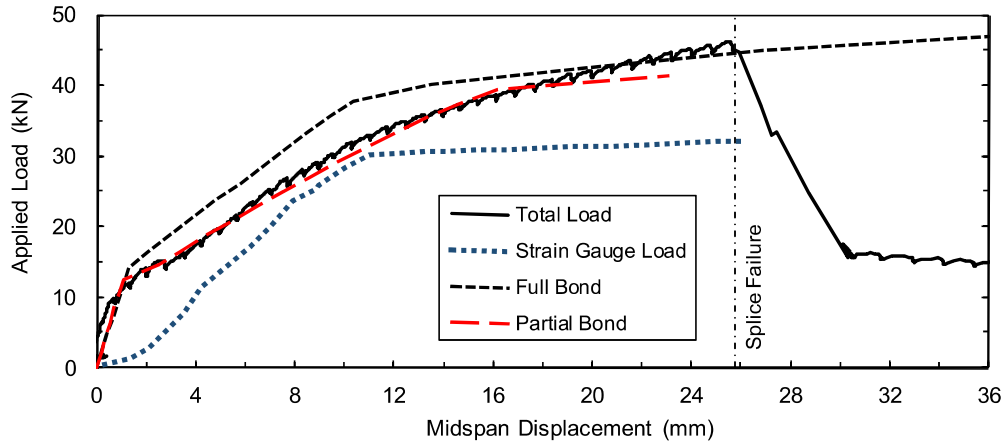

Figure B.30: Comparison of predicted and experimental resistance curves for CP2-LSR.

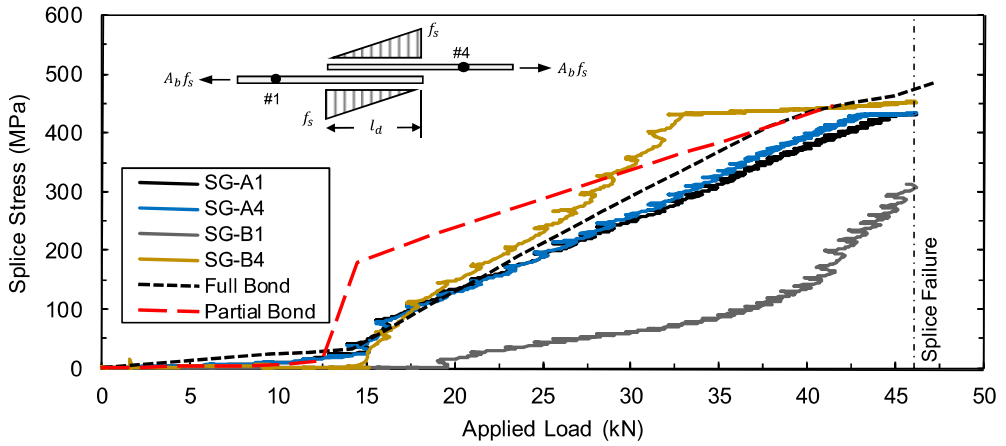

Figure B.31: Comparison of predicted and experimental steel stress developed in spliced reinforcement for CP2-LSR with respect to applied load.

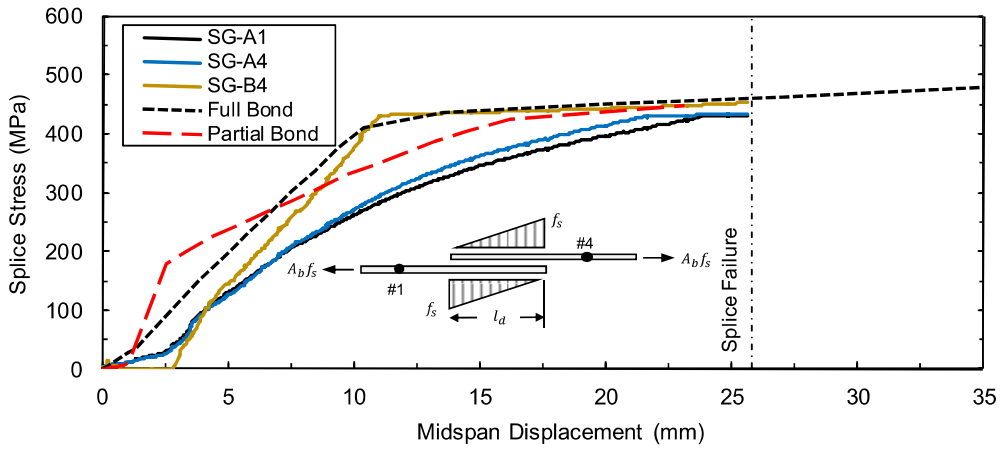

Figure B.32: Comparison of predicted and experimental steel stress developed in spliced reinforcement for CP2-LSR with respect to displacement.

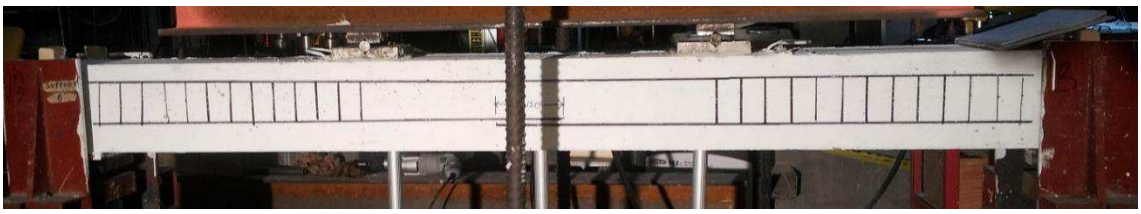

(a) Before low strain rate testing

(b) After low strain rate testing

Figure B.33: Photographs of lap splice beam CP2-LSR.

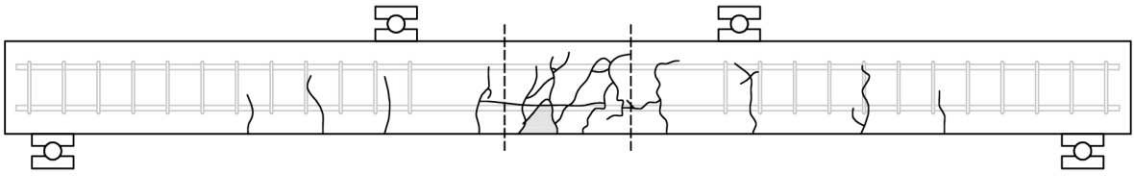

(a) Observed crack profile (north face)

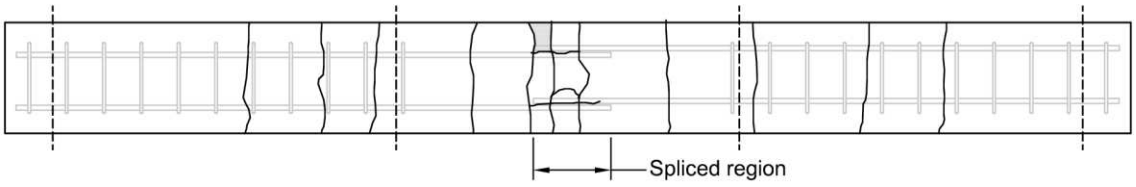

(b) Observed crack profile (bottom face)

Figure B.34: Observed crack profile for lap splice beam CP2-LSR.

CP2-HSR

Lap splice beam CP2-HSR was subjected to high strain rate testing on October 28, 2013. CP2-HSR was designed with 10M reinforcement, 30 MPa concrete, 50 mm cover, and without transverse reinforcement in the spliced region. The specimen experienced a combined side- and face-splitting tensile failure of the cover concrete with minimal cover loss. The peak dynamic resistance was 52.0 kN. Based on strain readings, the stress developed in the spliced bars was 583 MPa. Based on a sectional analysis, the stress developed in the spliced bars was 602 MPa. Time-to-failure was 28.4 ms and strain rate was 0.28 s^{-1}.

Table B.7: Geometry, reinforcing, and material properties for CP2-HSR.

b:	240 mm	Bar:	2-10M	f'_{dc}:	42.7 MPa
h:	200 mm	A_b:	100 mm^2	f_{dy}:	557.4 MPa
l_d:	276 mm	d_b:	11.3 mm	ρ:	0.58%
c_b:	52 mm	N:	N/A	c/d:	4.5
c_{so}:	49 mm	A_{tr}:	N/A	$l_d(c_{min} + 0.5d_b)$:	8744 mm^2

Table B.8: Summary of experimental test results for CP2-HSR.

Date:	Oct. 28, 2014	δ_f:	66.8 mm	f_s^t:	583 MPa
P_r:	52.6 kPa	R_f:	52.0 kN	f_s^{cal}:	602 MPa
I_r:	398.6 kPa-ms	t_f:	28.4 ms	$\dot{\varepsilon}$:	0.28 s^{-1}

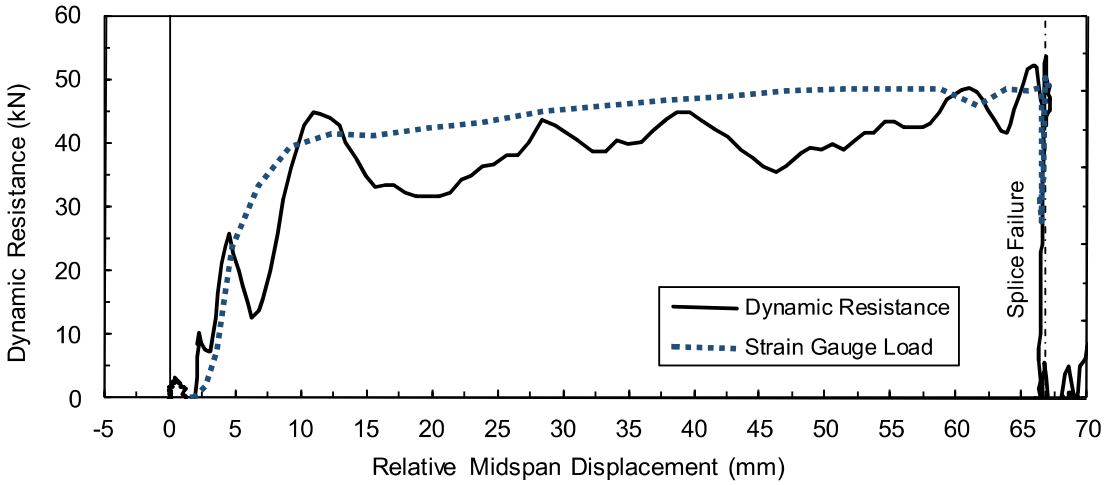

Figure B.35: Load displacement-history plot for CP2-LSR.

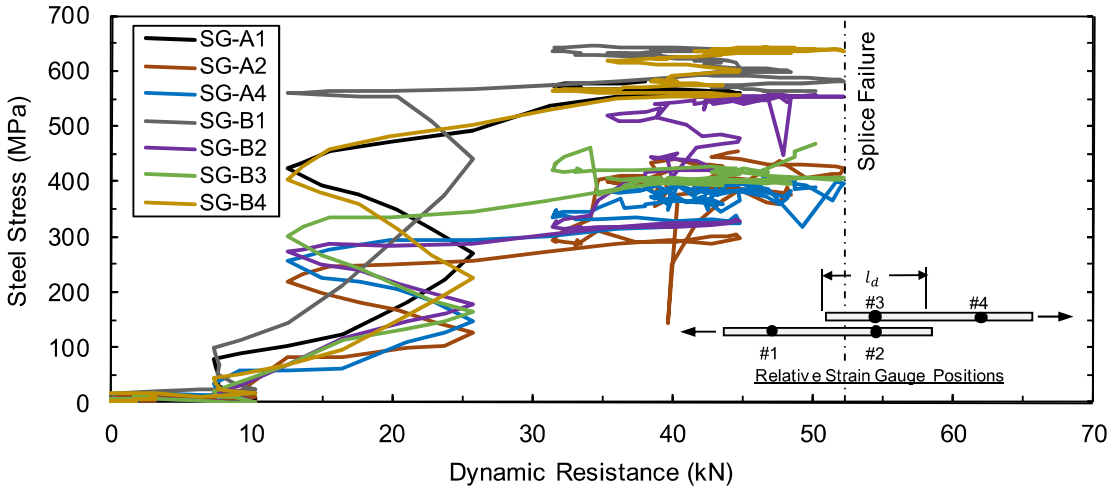

Figure B.36: Steel stress load-history plot for CP2-LSR.

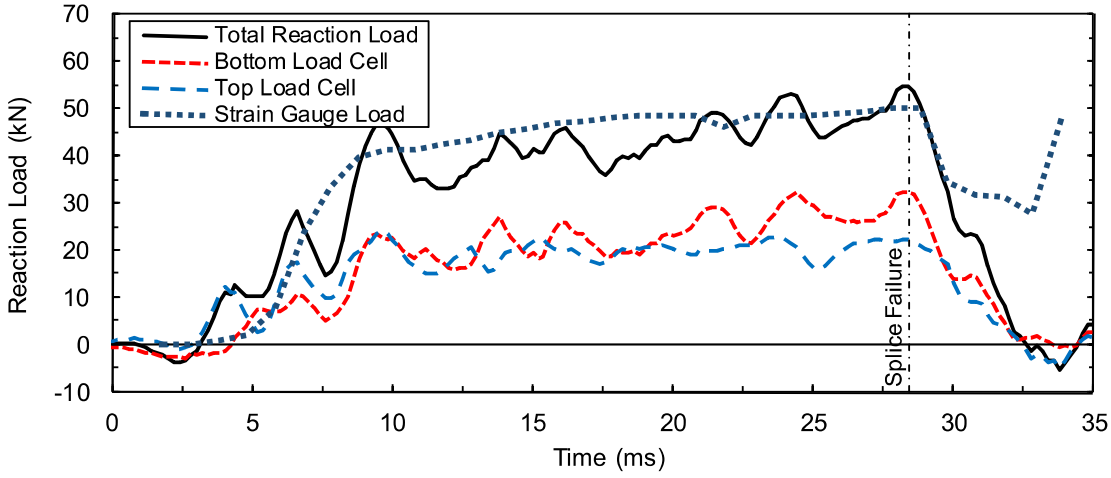

Figure B.37: Load time-history plot for CP2-LSR.

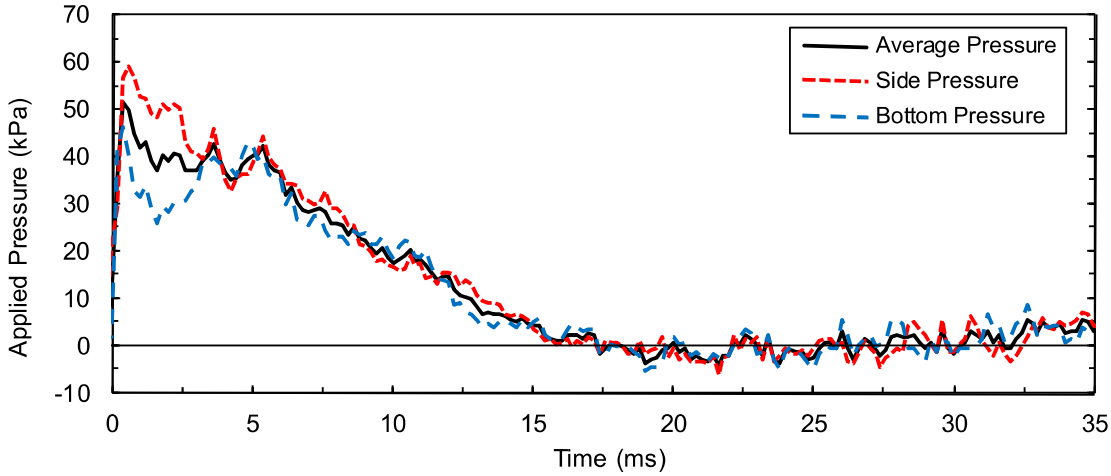

Figure B.38: Pressure time-history plot for CP2-HSR.

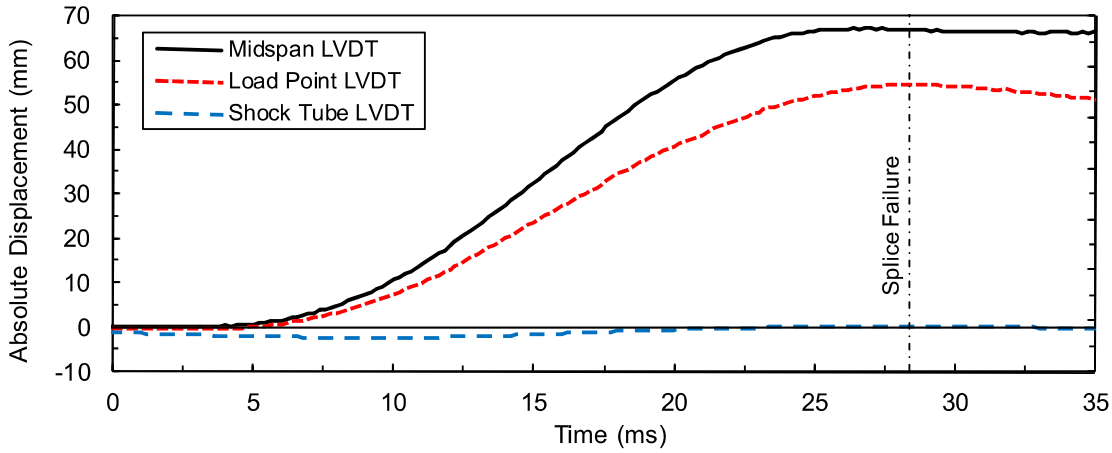

Figure B.39: Displacement time-history plot for CP2-LSR.

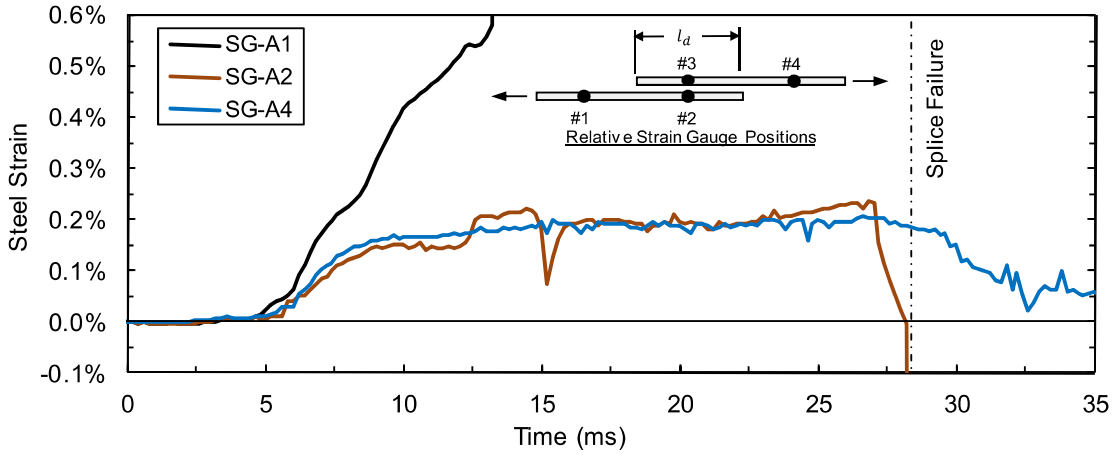

Figure B.40: Test bar "A" strain time-history plot for CP2-LSR.

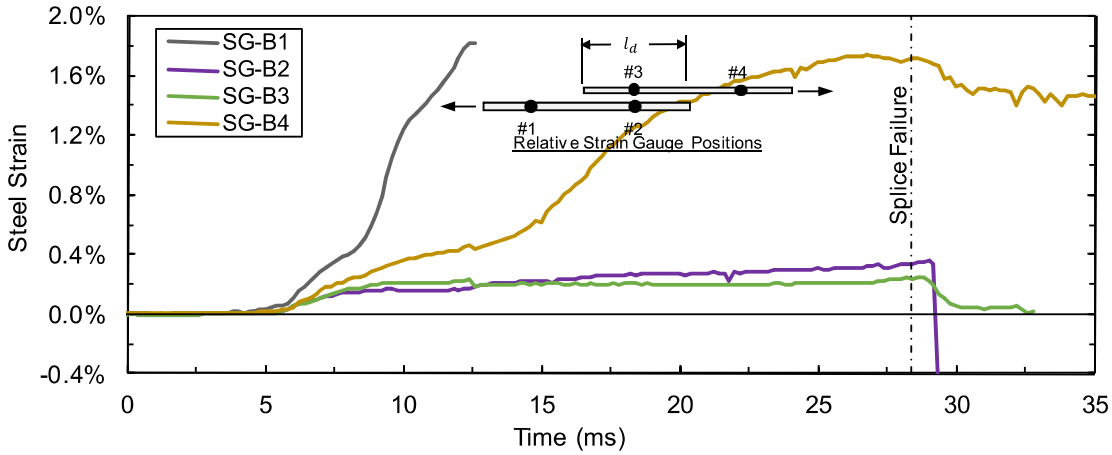

Figure B.41: Test bar "B" strain time-history plot for CP2-LSR.

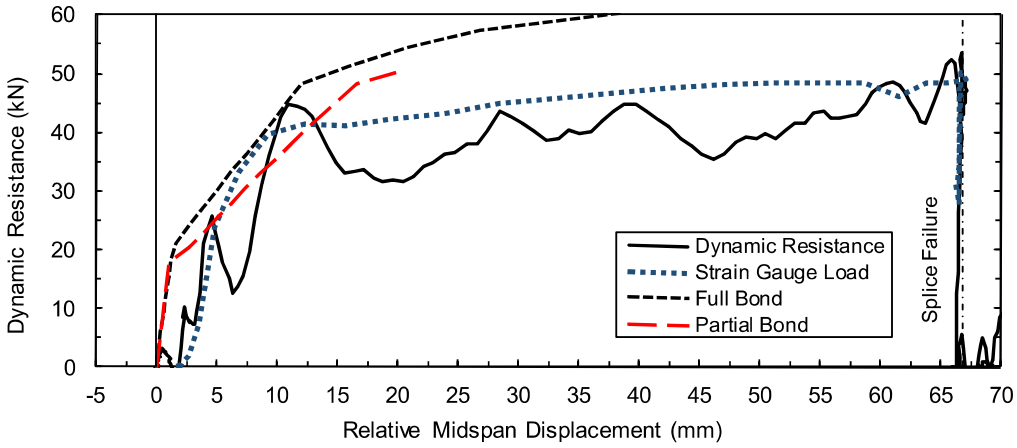

Figure B.42: Comparison of predicted and experimental resistance curves for CP2-HSR.

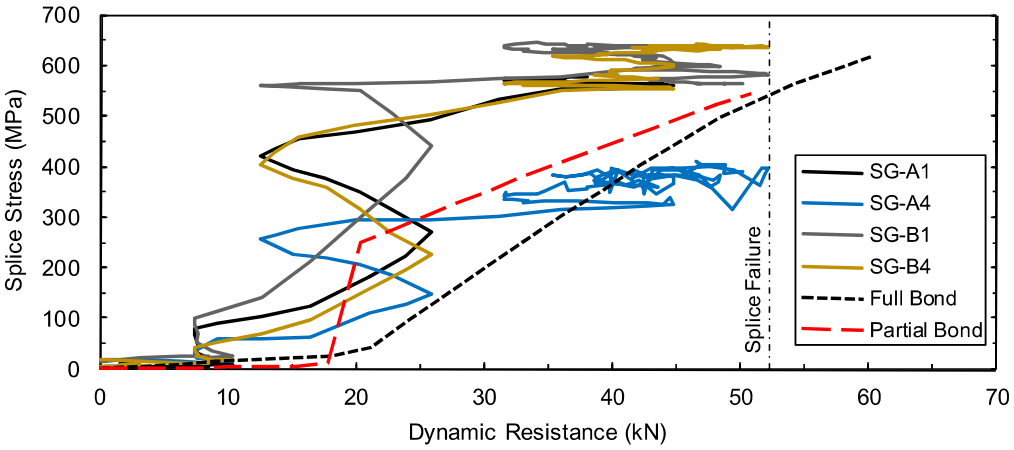

Figure B.43: Comparison of predicted and experimental steel stress developed in spliced reinforcement for CP2-HSR with respect to applied load.

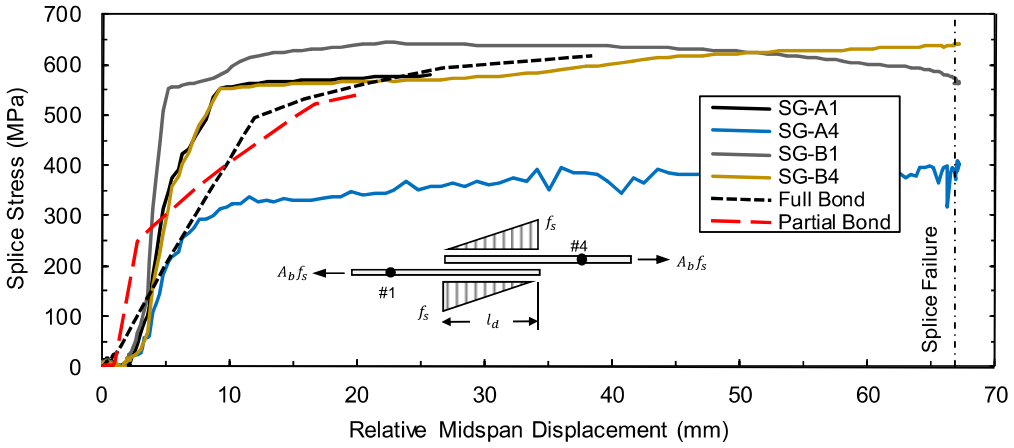

Figure B.44: Comparison of predicted and experimental steel stress developed in spliced reinforcement for CP2-HSR with respect to displacement.

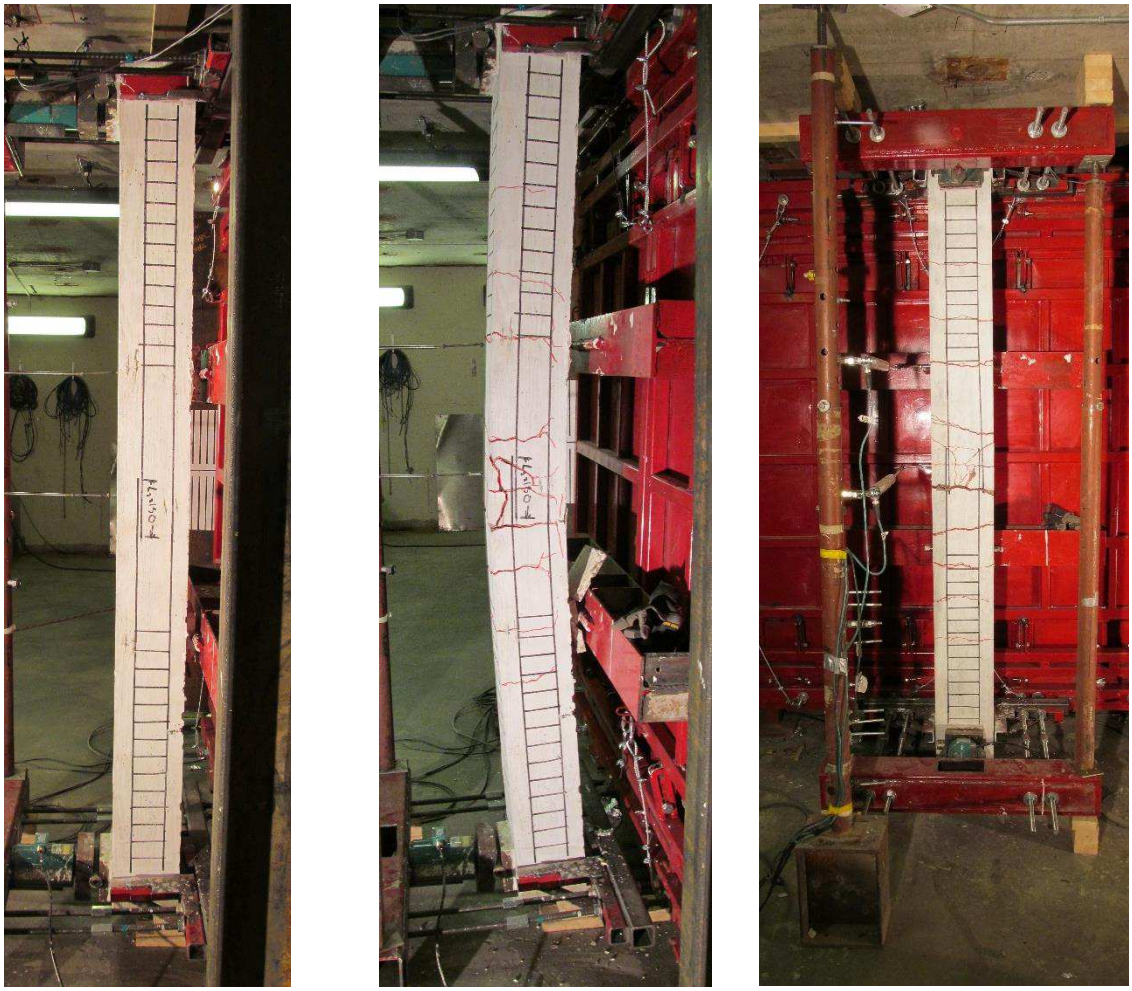

(a) Before high strain rate testing (b) After high strain rate testing (c) After high strain rate testing

Figure B.45: Photographs of lap splice beam CP2-LSR.

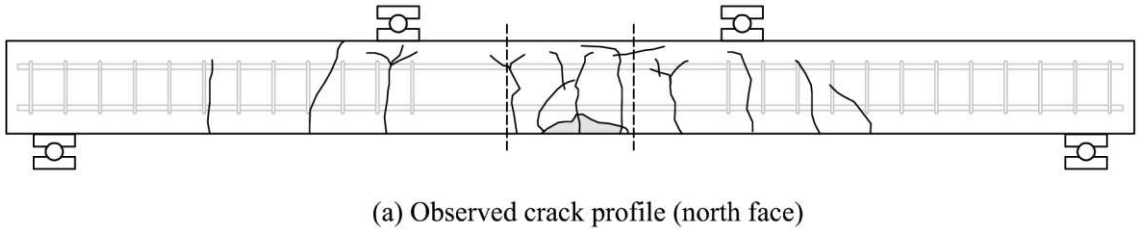

(a) Observed crack profile (north face)

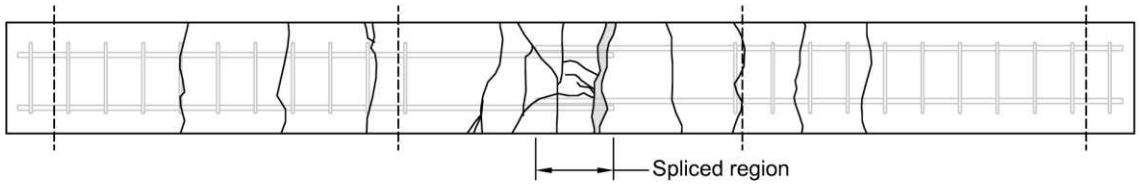

(b) Observed crack profile (bottom face)

Figure B.46: Observed crack profile for lap splice beam CP2-LSR.

CP3-LSR

Lap splice beam CP3-LSR was subjected to low strain rate testing on September 19, 2013. CP3-LSR was designed with 15M reinforcement, 30 MPa concrete, 25 mm cover, and without transverse reinforcement in the spliced region. The specimen experienced a side-splitting tensile failure of the cover concrete with significant cover loss. Failure occurred at an applied load of 122.9 kN. Based on strain readings, the stress developed in the spliced bars was 450 MPa. Based on a sectional analysis, the stress developed in the spliced bars was 462 MPa. Time-to-failure was 320.0 seconds and strain rate was 7.0×10^{-6} s^{-1}.

Table B.9: Geometry, reinforcing, and material properties for CP3-LSR.

b:	165 mm	Bar:	2-15M	f_c':	32.5 MPa
h:	300 mm	A_b:	200 mm^2	f_y:	448.4 MPa
l_d:	493 mm	d_b:	16.0 mm	ρ:	0.91%
c_b:	26 mm	N:	N/A	c/d:	1.6
c_{so}:	24 mm	A_{tr}:	N/A	$l_d(c_{min}+0.5d_b)$:	15776 mm^2

Table B.10: Summary of experimental test results for CP3-LSR.

Date:	Sept. 19, 2013	δ_f:	16.0 mm	f_s^t:	450 MPa
P_r:	N/A	R_f:	122.9 kN	f_s^{cal}:	462 MPa
I_r:	N/A	t_f:	320.0 s	$\dot{\varepsilon}$:	7.0×10^{-6} s^{-1}

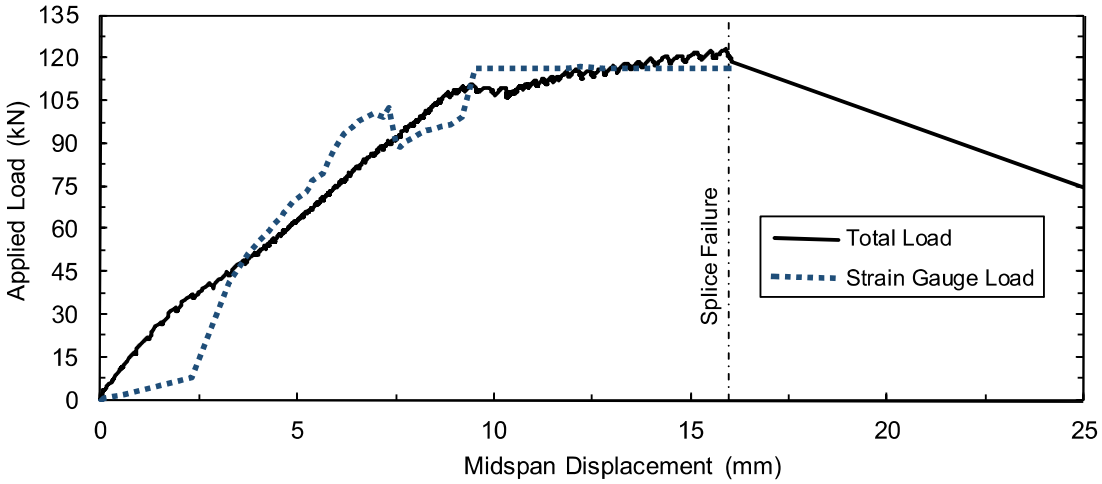

Figure B.47: Load displacement-history plot for CP3-LSR.

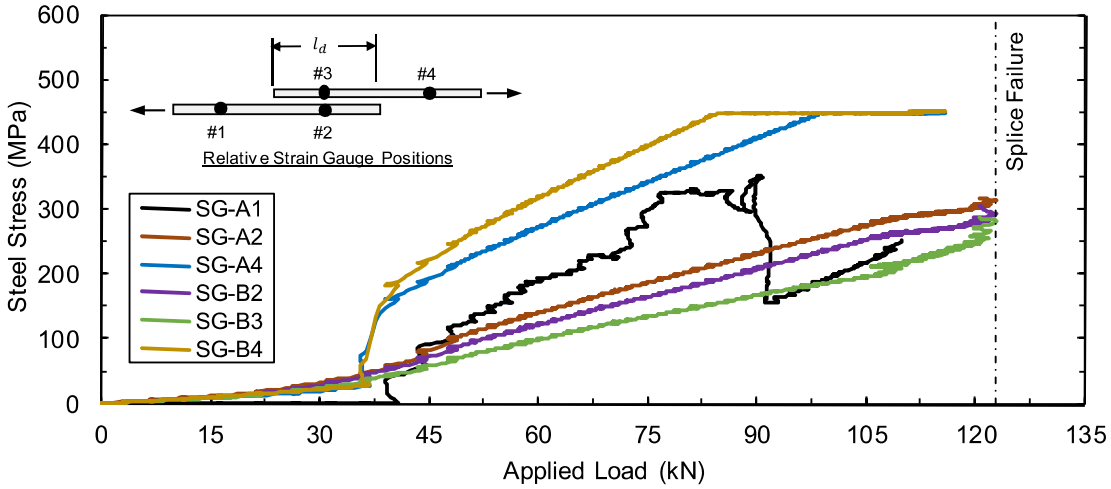

Figure B.48: Steel stress load-history plot for CP3-LSR.

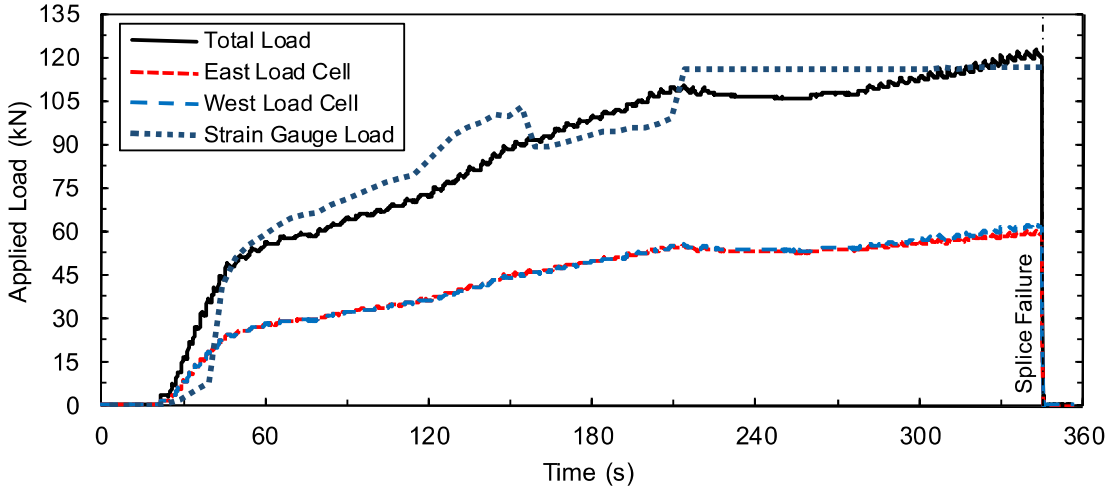

Figure B.49: Load time-history plot for CP3-LSR.

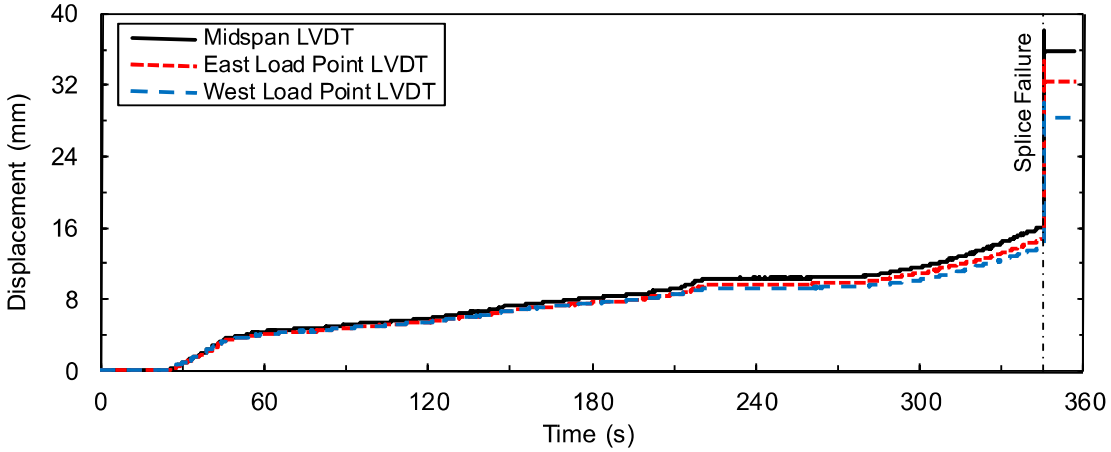

Figure B.50: Displacement time-history plot for CP3-LSR.

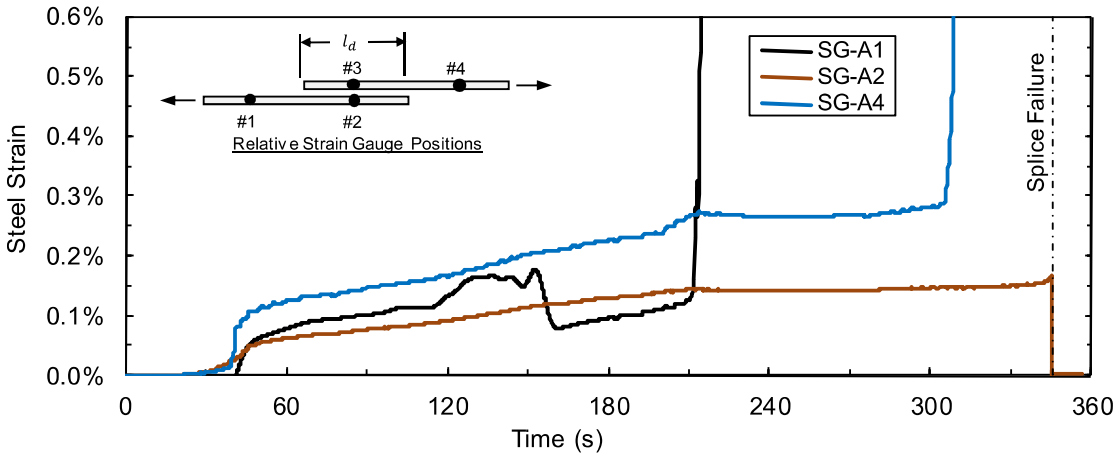

Figure B.51: Test bar "A" strain time-history plot for CP3-LSR.

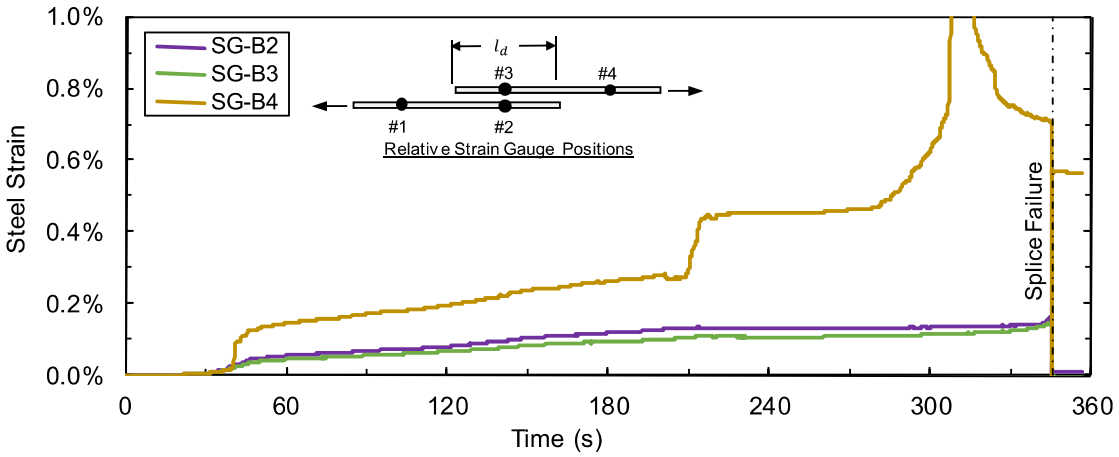

Figure B.52: Test bar "B" strain time-history plot for CP3-LSR.

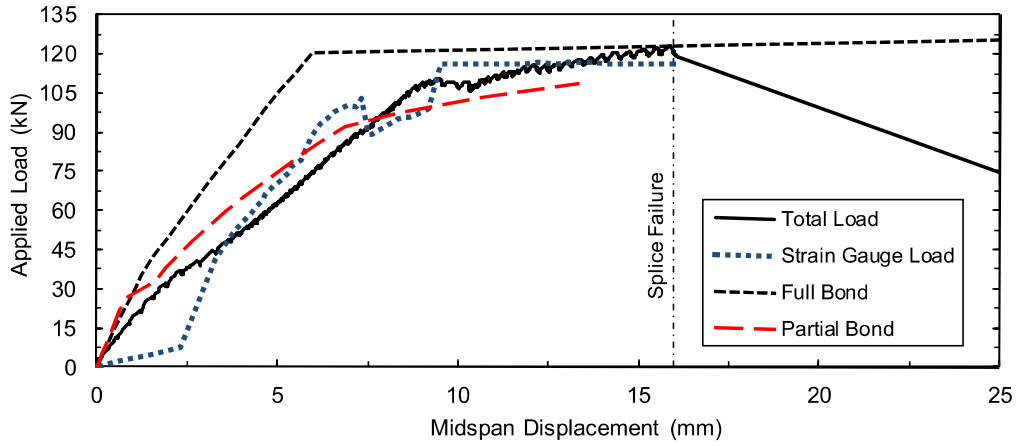

Figure B.53: Comparison of predicted and experimental resistance curves for CP3-LSR.

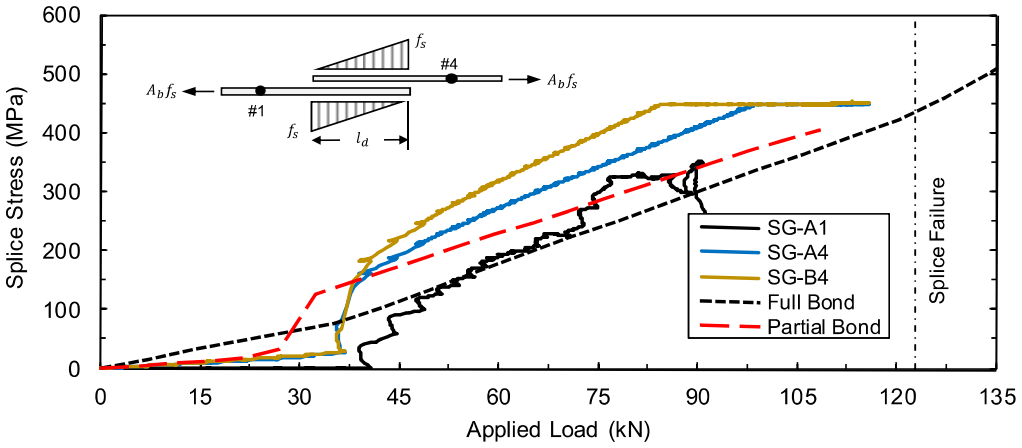

Figure B.54: Comparison of predicted and experimental steel stress developed in spliced reinforcement for CP3-LSR with respect to applied load.

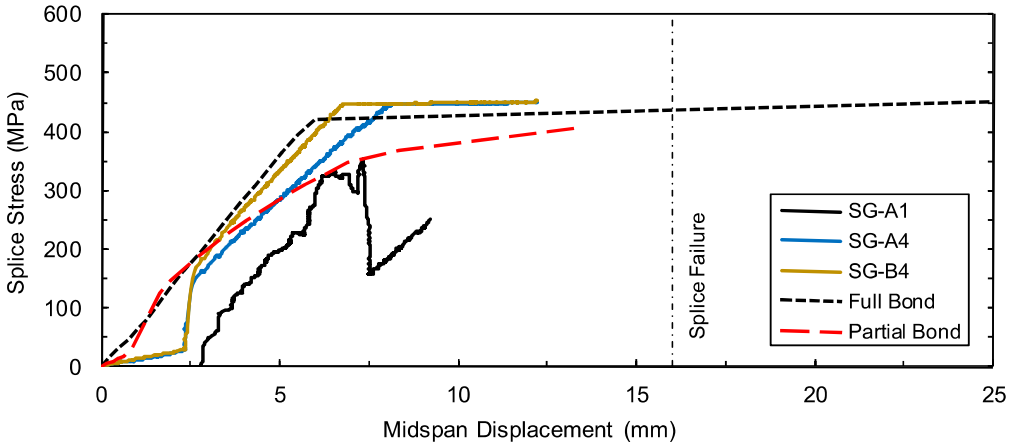

Figure B.55: Comparison of predicted and experimental steel stress developed in spliced reinforcement for CP3-LSR with respect to displacement.

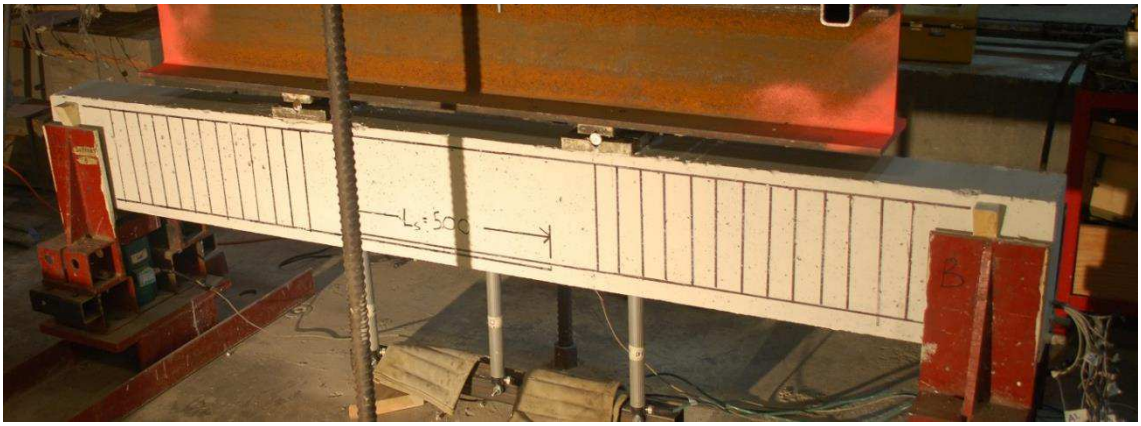

(a) Before low strain rate testing

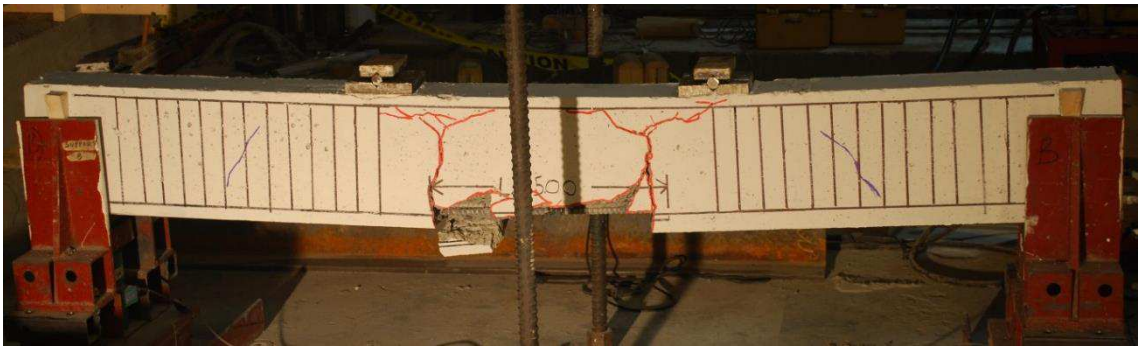

(b) After low strain rate testing

Figure B.56: Photographs of lap splice beam CP3-LSR.

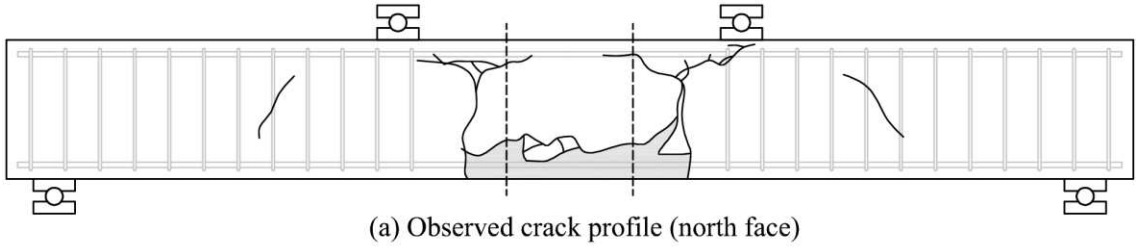

(a) Observed crack profile (north face)

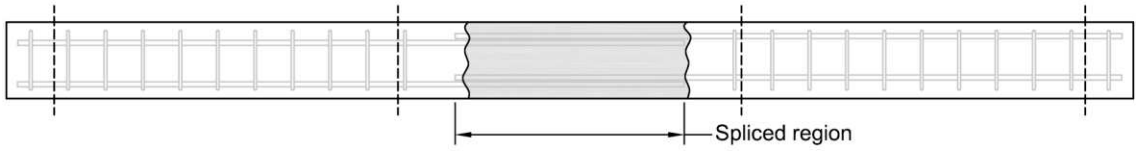

(b) Observed crack profile (bottom face)

Figure B.57: Observed crack profile for lap splice beam CP3-LSR.

CP3-HSR

Lap splice beam CP3-HSR was subjected to high strain rate testing on October 13, 2013. CP3-HSR was designed with 15M reinforcement, 30 MPa concrete, 25 mm cover, and without transverse reinforcement in the spliced region. The specimen showed signs of a combined side- and face-splitting tensile failure of the cover concrete with minimal cover loss. The peak dynamic resistance was 155.0 kN. Based on strain readings, the stress developed in the spliced bars was 566 MPa. Based on a sectional analysis, the stress developed in the spliced bars was 585 MPa. Time-to-failure was 9.0 ms and strain rate was 0.65 s^{-1}.

Table B.11: Geometry, reinforcing, and material properties for CP3-HSR.

b:	150 mm	Bar:	2-15M	f'_{dc}:	43.8 MPa
h:	300 mm	A_b:	200 mm^2	f_{dy}:	587.0 MPa
l_d:	494 mm	d_b:	16.0 mm	ρ:	0.91%
c_b:	26 mm	N:	N/A	c/d:	1.6
c_{so}:	26 mm	A_{tr}:	N/A	$l_d(c_{min} + 0.5d_b)$:	16796 mm^2

Table B.12: Summary of experimental test results for CP3-HSR.

Date:	Oct. 13, 2013	δ_f:	19.0 mm	f_s^t:	566 MPa
P_r:	84.0 kPa	R_f:	155.0 kN	f_s^{cal}:	585 MPa
I_r:	578.5 kPa-ms	t_f:	9.0 ms	$\dot{\varepsilon}$:	0.65 s^{-1}

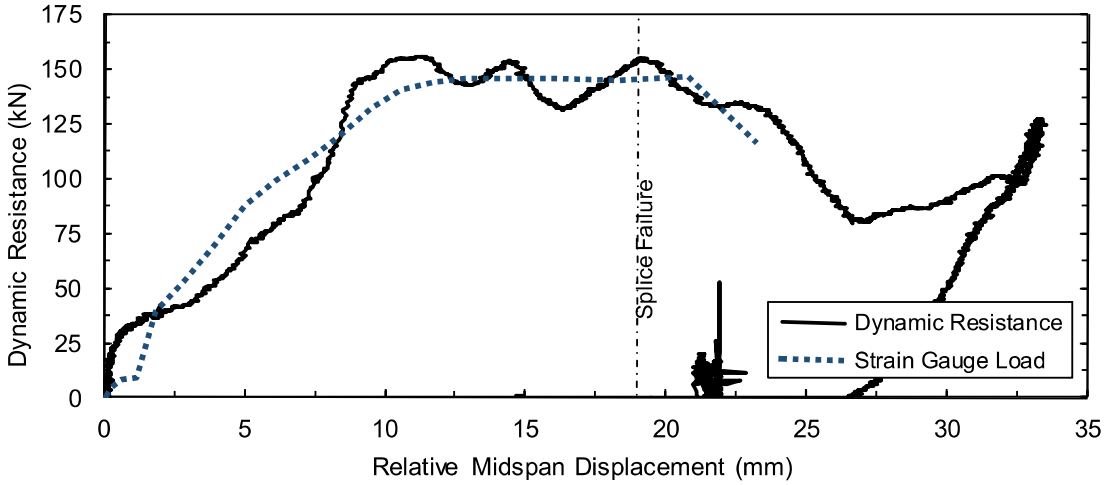

Figure B.58: Load displacement-history plot for CP3-HSR.

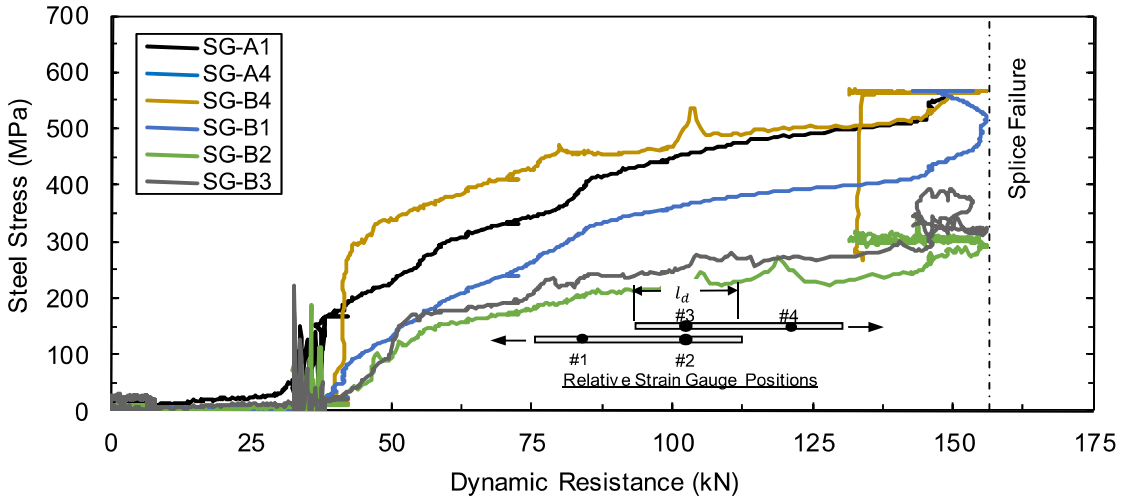

Figure B.59: Steel stress load-history plot for CP3-HSR.

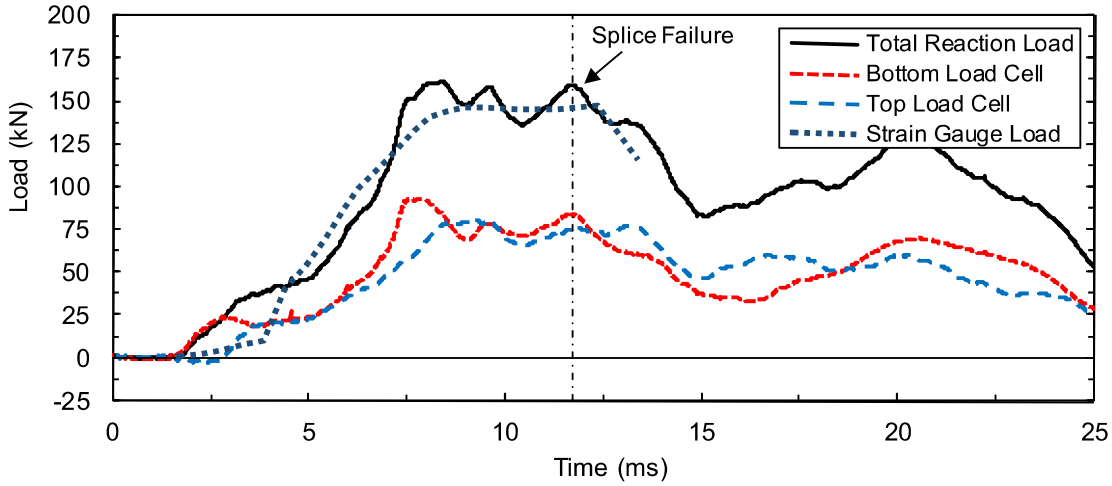

Figure B.60: Load time-history plot for CP3-HSR.

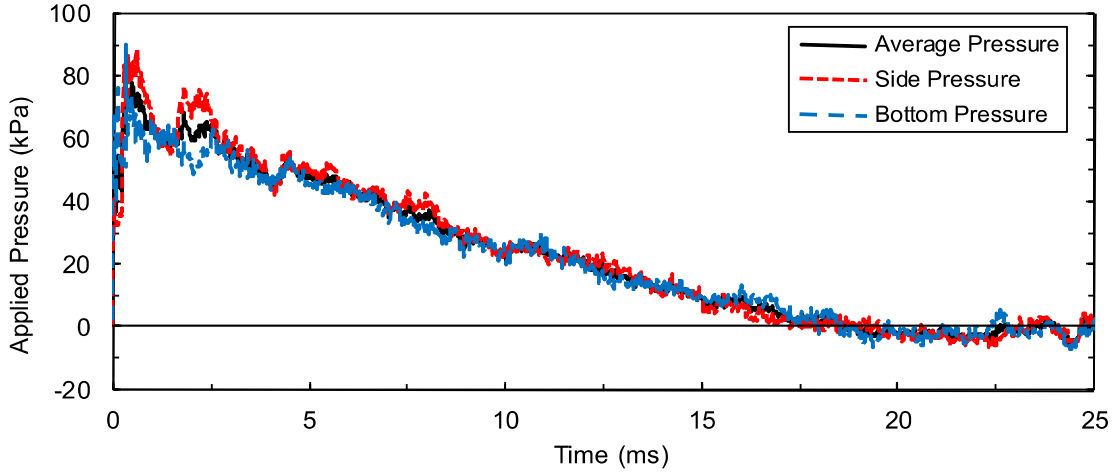

Figure B.61: Pressure time-history plot for CP3-HSR.

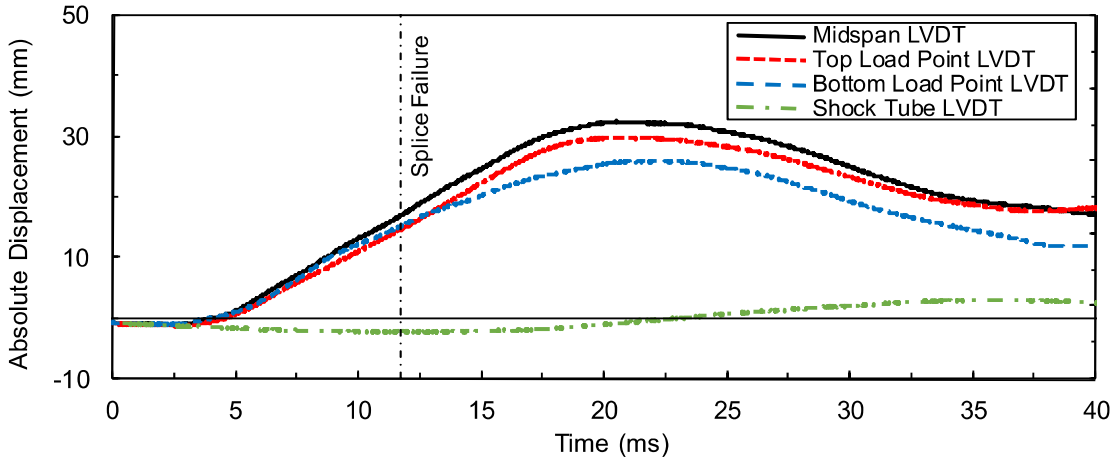

Figure B.62: Displacement time-history plot for CP3-HSR.

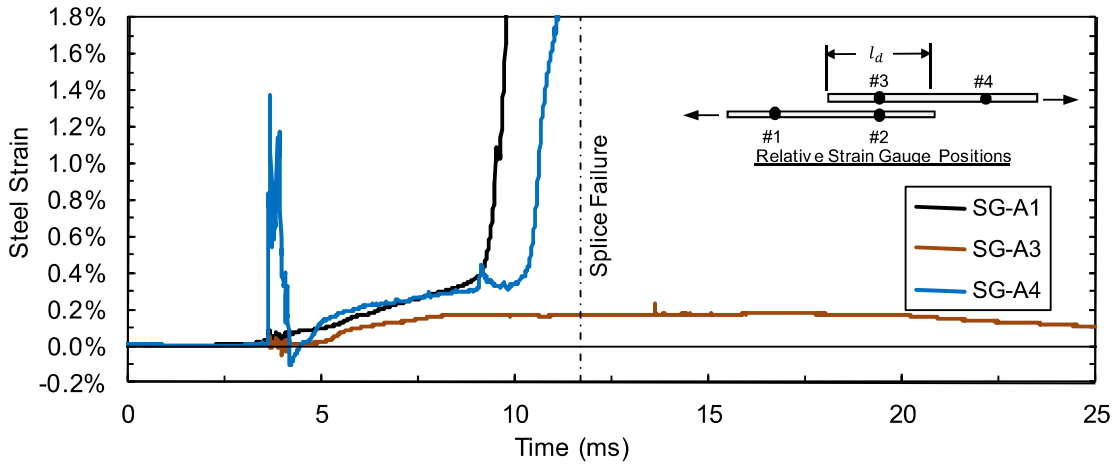

Figure B.63: Test bar "A" strain time-history plot for CP3-HSR.

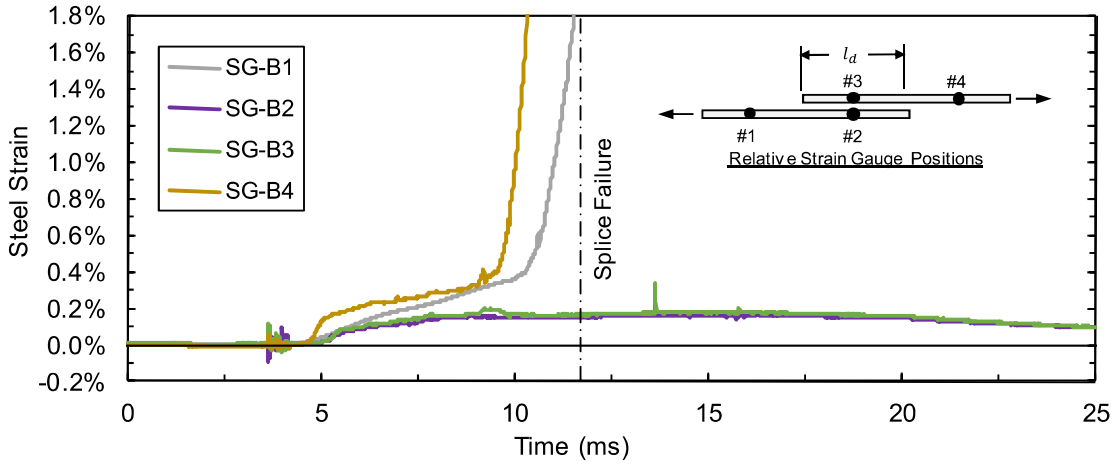

Figure B.64: Test bar "B" strain time-history plot for CP3-HSR.

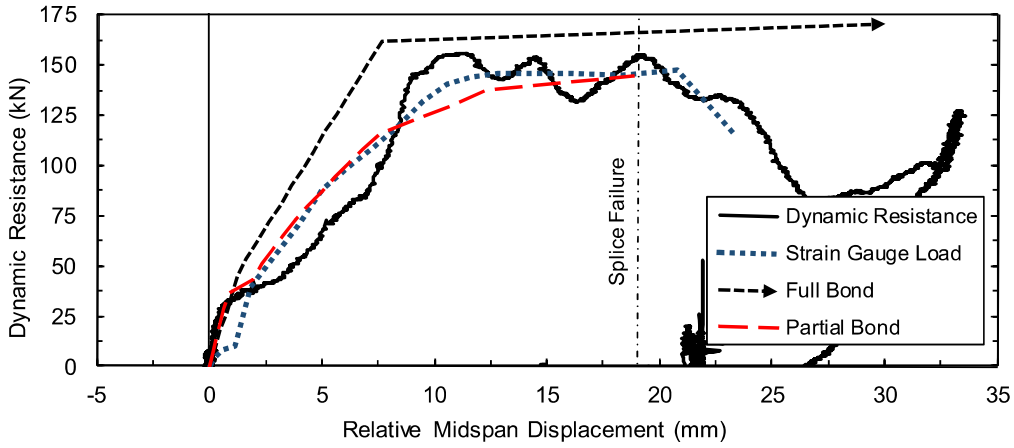

Figure B.65: Comparison of predicted and experimental resistance curves for CP3-HSR.

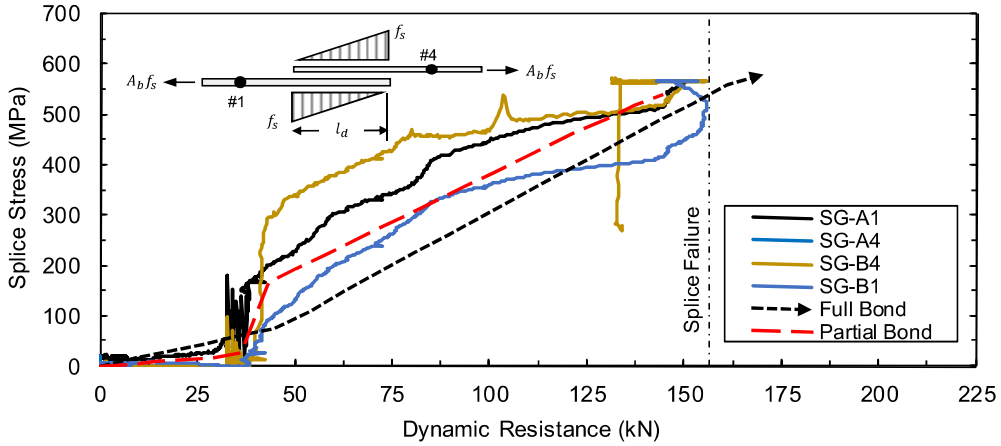

Figure B.66: Comparison of predicted and experimental steel stress developed in spliced reinforcement for CP3-HSR with respect to applied load.

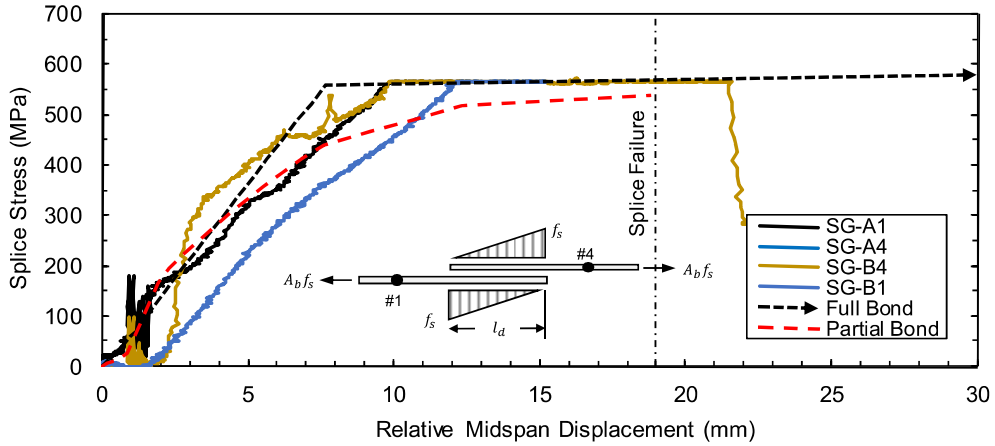

Figure B.67: Comparison of predicted and experimental steel stress developed in spliced reinforcement for CP3-HSR with respect to displacement.

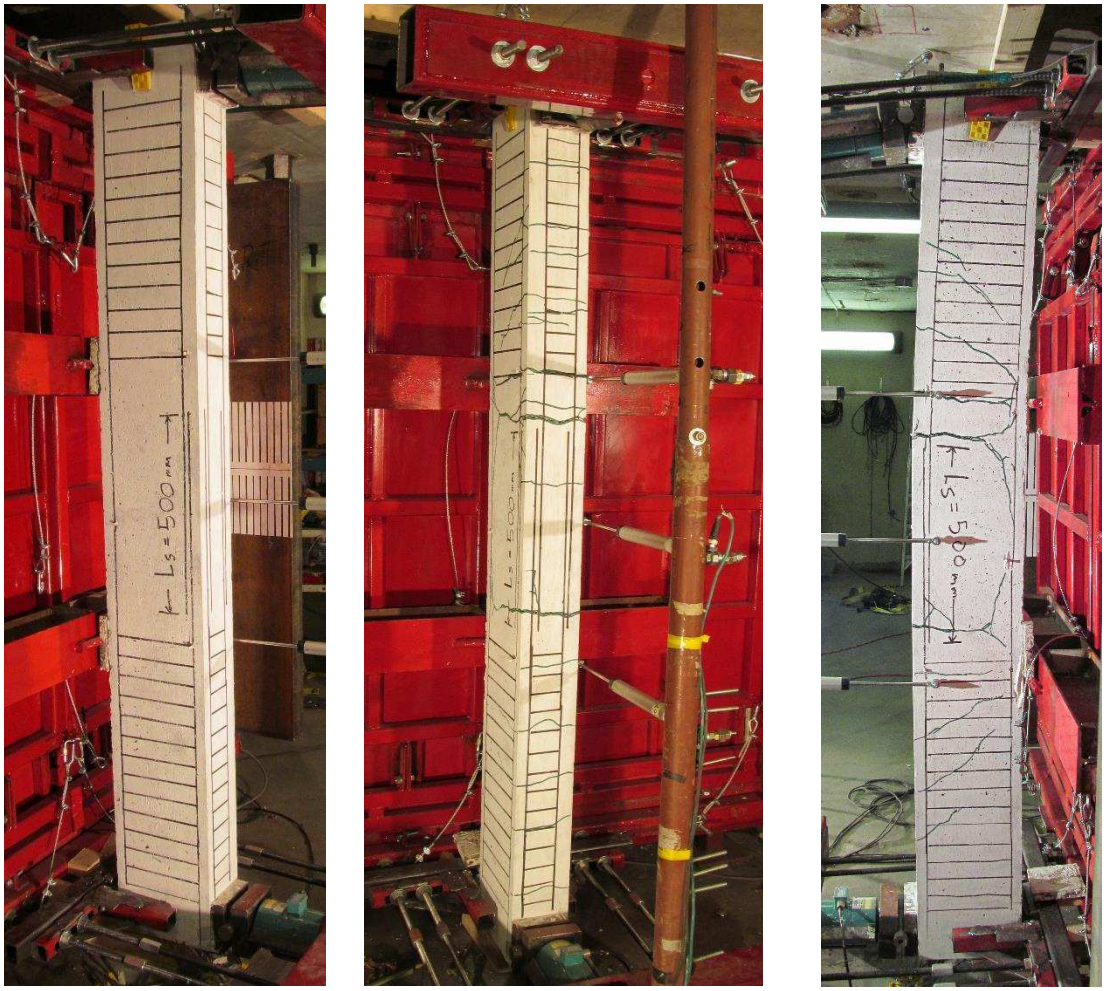

(a) Before high strain rate testing (b) After high strain rate testing (c) After high strain rate testing

Figure B.68: Photographs of lap splice beam CP3-LSR.

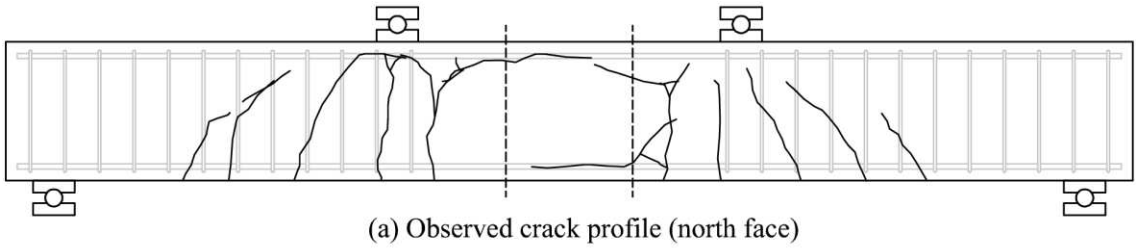

(a) Observed crack profile (north face)

(b) Observed crack profile (bottom face)

Figure B.69: Observed crack profile for lap splice beam CP3-LSR.

CP4-LSR

Lap splice beam CP4-LSR was subjected to low strain rate testing on September 20, 2013. CP4-LSR was designed with 15M reinforcement, 30 MPa concrete, 50 mm cover, and without transverse reinforcement in the spliced region. The specimen experienced a side-splitting tensile failure of the cover concrete with significant cover loss. Failure occurred at an applied load of 114.6 kN. Based on strain readings, the stress developed in the spliced bars was 450 MPa. Based on a sectional analysis, the stress developed in the spliced bars was 458 MPa. Time-to-failure was 412.5 seconds and strain rate was 5.5×10^{-6} s^{-1}.

Table B.13: Geometry, reinforcing, and material properties for CP4-LSR.

b:	265 mm	Bar:	2-15M	f_c':	32.5 MPa
h:	300 mm	A_b:	200 mm^2	f_y:	448.4 MPa
l_d:	272 mm	d_b:	16.0 mm	ρ:	0.63%
c_b:	52 mm	N:	N/A	c/d:	3.3
c_{so}:	52 mm	A_{tr}:	N/A	$l_d(c_{min}+0.5d_b)$:	16320 mm^2

Table B.14: Summary of experimental test results for CP4-LSR.

Date:	Sept. 20, 2013	δ_f:	9.6 mm	f_s^t:	450 MPa
P_r:	N/A	R_f:	114.6 kN	f_s^{cal}:	458 MPa
I_r:	N/A	t_f:	412.5 s	$\dot{\varepsilon}$:	5.5×10^{-6} s^{-1}

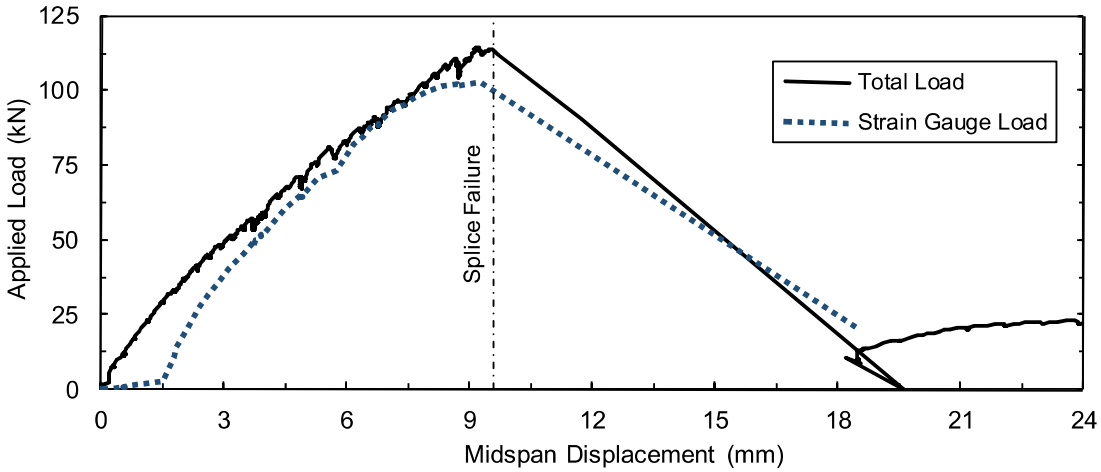

Figure B.70: Load displacement-history plot for CP4-LSR.

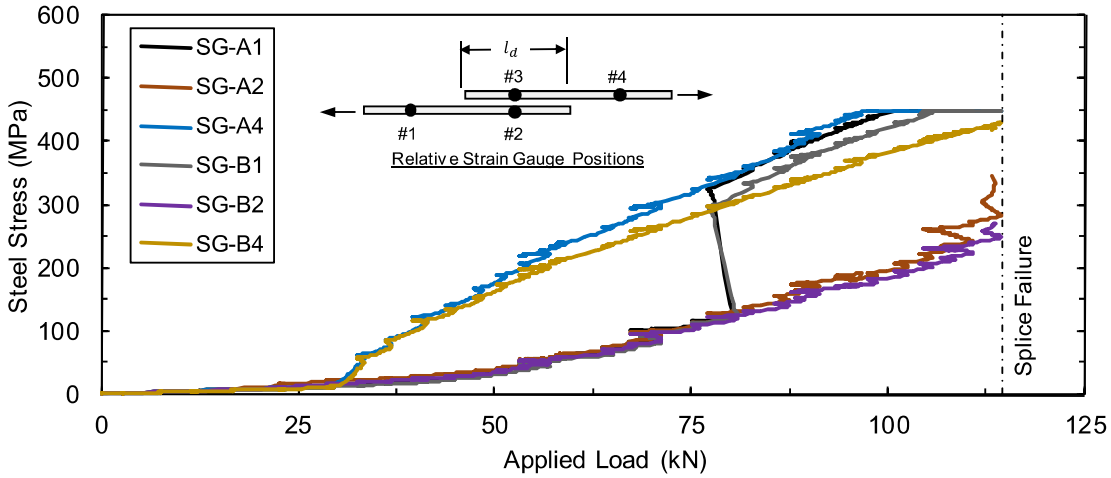

Figure B.71: Steel stress load-history plot for CP4-LSR.

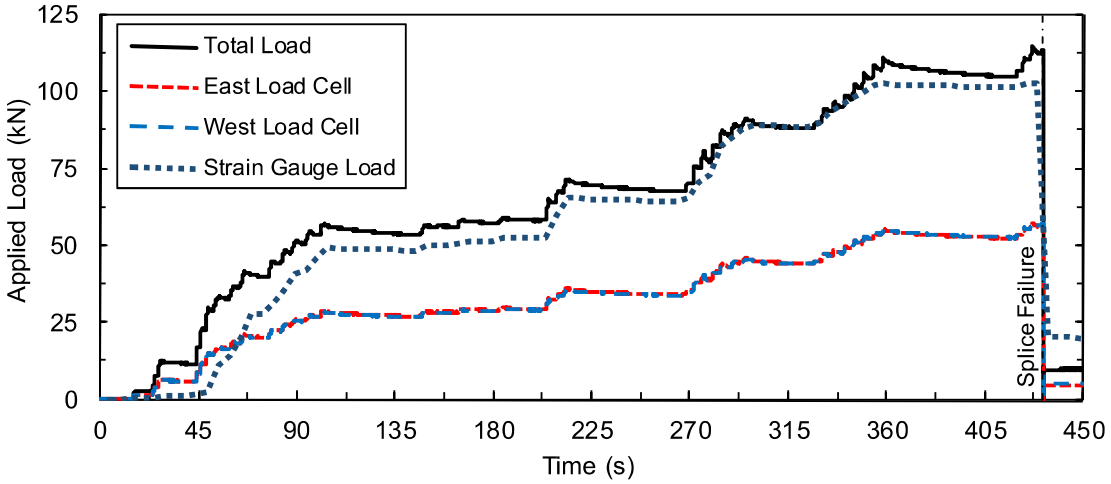

Figure B.72: Load time-history plot for CP4-LSR.

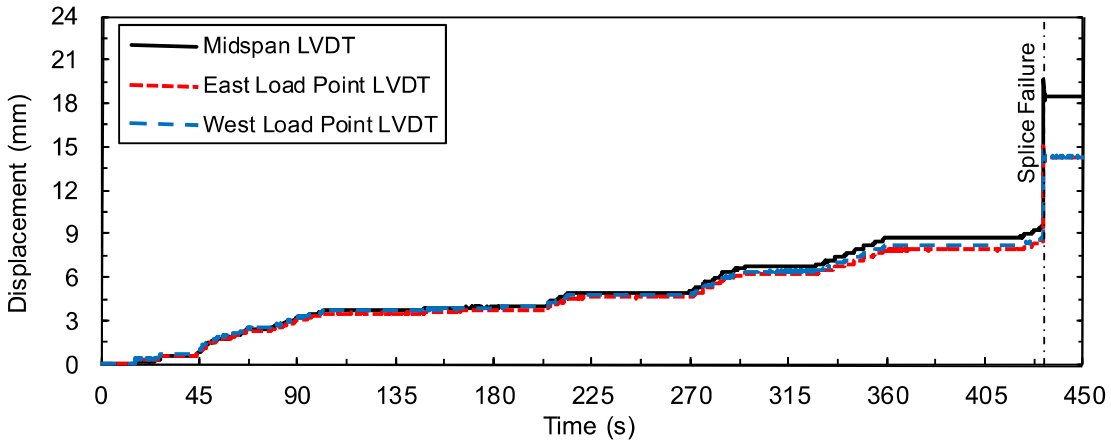

Figure B.73: Displacement time-history plot for CP4-LSR.

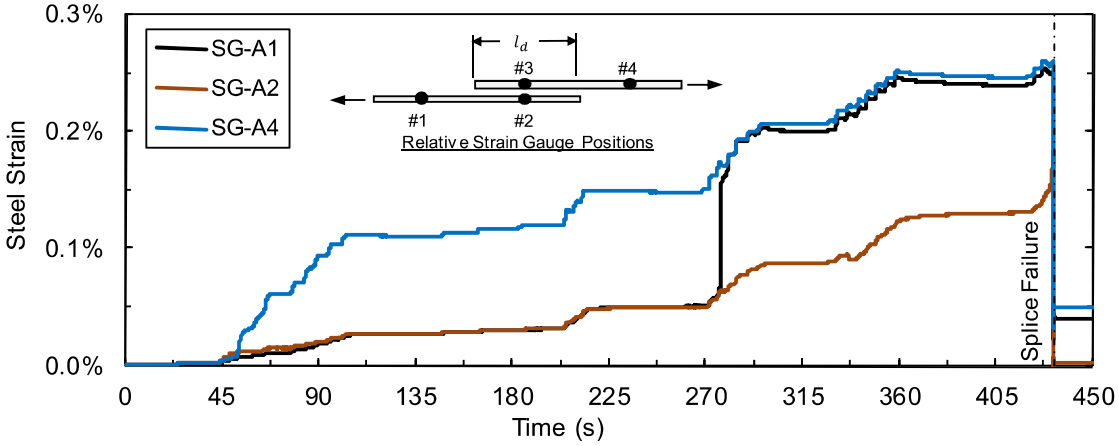

Figure B.74: Test bar "A" strain time-history plot for CP4-LSR.

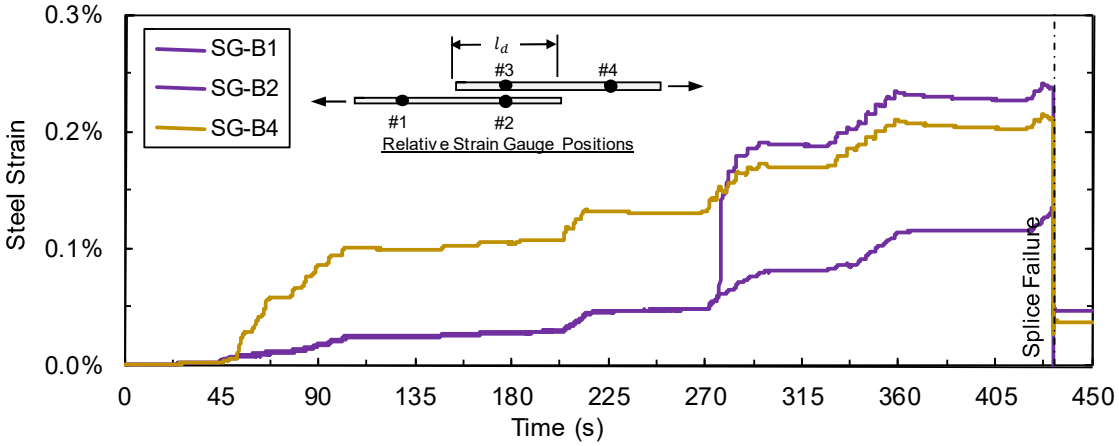

Figure B.75: Test bar "B" strain time-history plot for CP4-LSR.

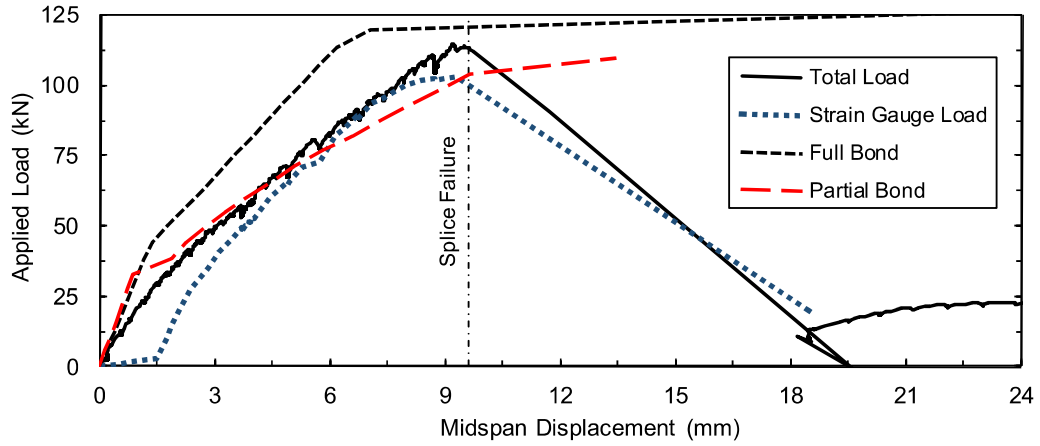

Figure B.76: Comparison of predicted and experimental resistance curves for CP4-LSR.

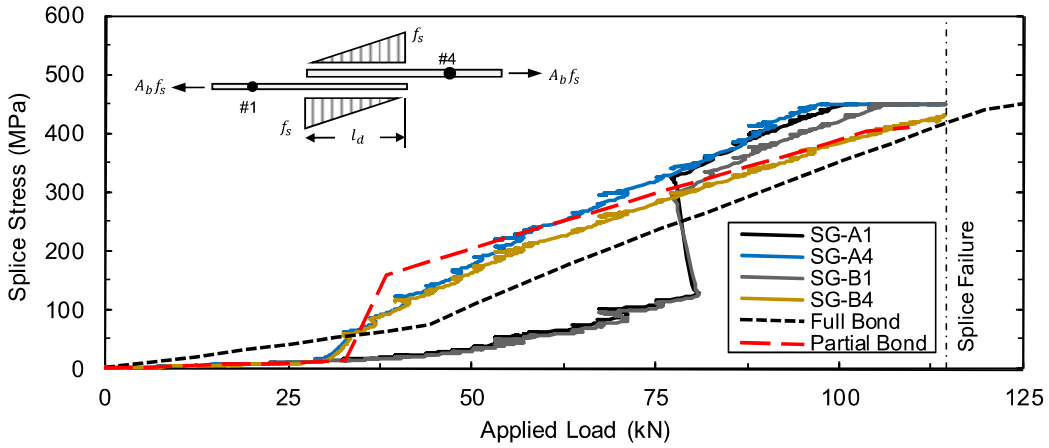

Figure B.77: Comparison of predicted and experimental steel stress developed in spliced reinforcement for CP4-LSR with respect to applied load.

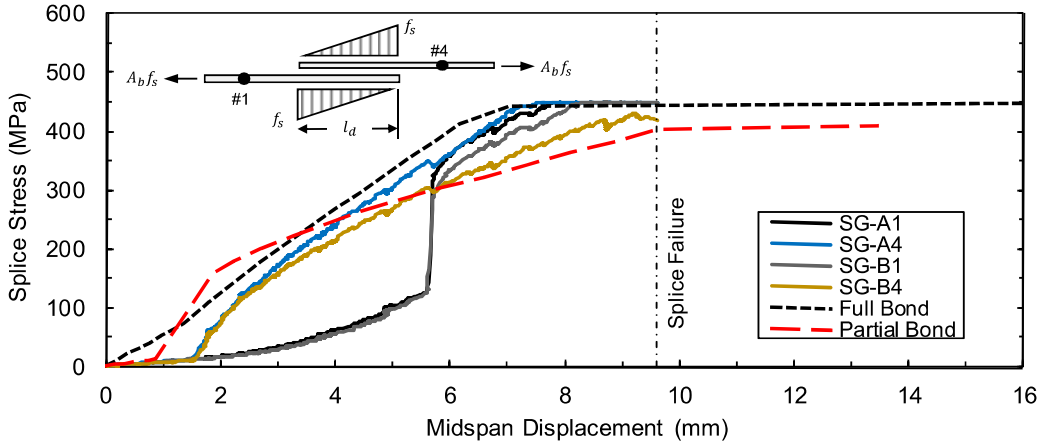

Figure B.78: Comparison of predicted and experimental steel stress developed in spliced reinforcement for CP4-LSR with respect to displacement.

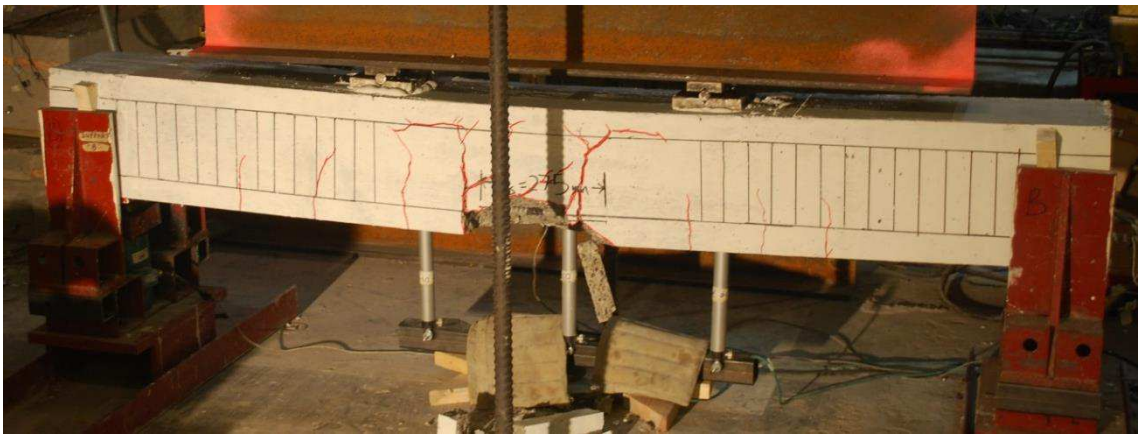

Figure B.79: Photograph of lap splice beam CP4-LSR after testing.

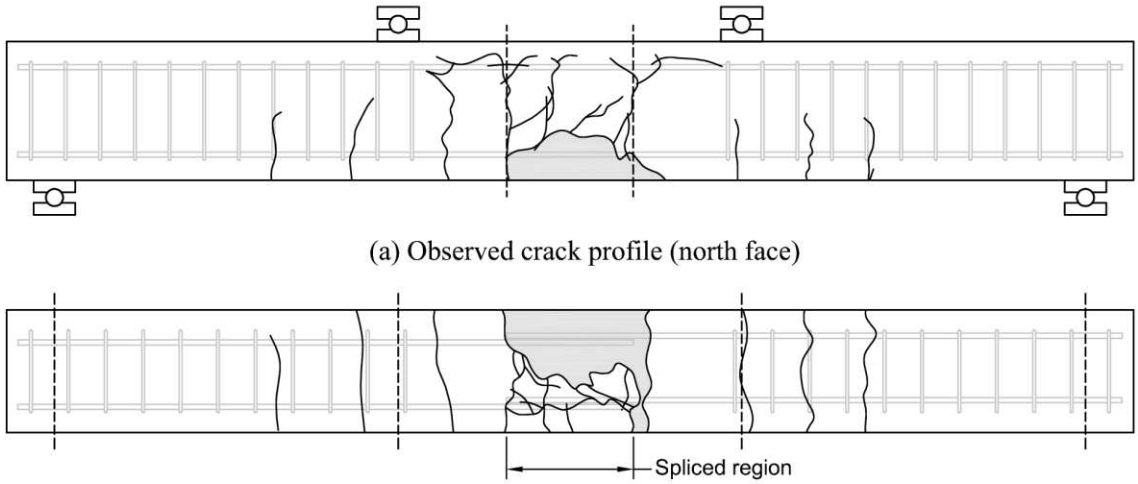

(a) Observed crack profile (north face)

(b) Observed crack profile (bottom face)

Figure B.80: Observed crack profile for lap splice beam CP4-LSR.

CP4-HSR

Lap splice beam CP4-HSR was subjected to high strain rate testing on October 18, 2013. CP4-HSR was designed with 15M reinforcement, 30 MPa concrete, 50 mm cover, and without transverse reinforcement in the spliced region. The specimen experienced a side-splitting tensile failure of the cover concrete with significant cover loss. The peak dynamic resistance was 164.0 kN. Based on strain readings, the stress developed in the spliced bars was 566 MPa. Based on a sectional analysis, the stress developed in the spliced bars was 593 MPa. Time-to-failure was 10.6 ms and strain rate was 1.13 s^{-1}.

Table B.15: Geometry, reinforcing, and material properties for CP4-HSR.

b:	265 mm	Bar:	2-15M	f'_{dc}:	44.6 MPa
h:	300 mm	A_b:	200 mm^2	f_{dy}:	597.0 MPa
l_d:	282 mm	d_b:	16.0 mm	ρ:	0.63%
c_b:	51 mm	N:	N/A	c/d:	3.2
c_{so}:	50 mm	A_{tr}:	N/A	$l_d(c_{min} + 0.5d_b)$:	16356 mm^2

Table B.16: Summary of experimental test results for CP4-HSR.

Date:	Oct. 18, 2013	δ_f:	10.6 mm	f_s^t:	566 MPa
P_r:	91.2 kPa	R_f:	164.0 kN	f_s^{cal}:	570 MPa
I_r:	572.5 kPa-ms	t_f:	15.6 ms	$\dot{\varepsilon}$:	1.13 s^{-1}

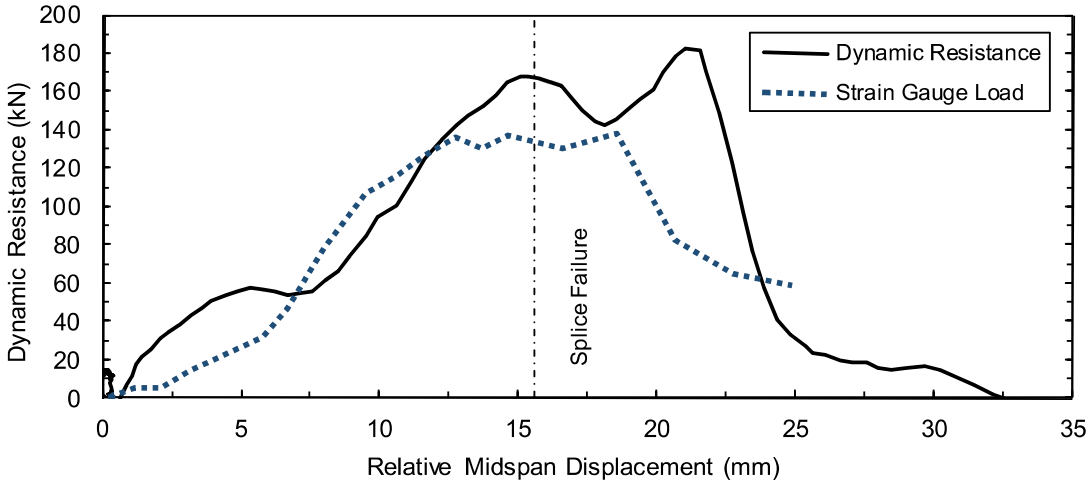

Figure B.81: Load displacement-history plot for CP4-HSR.

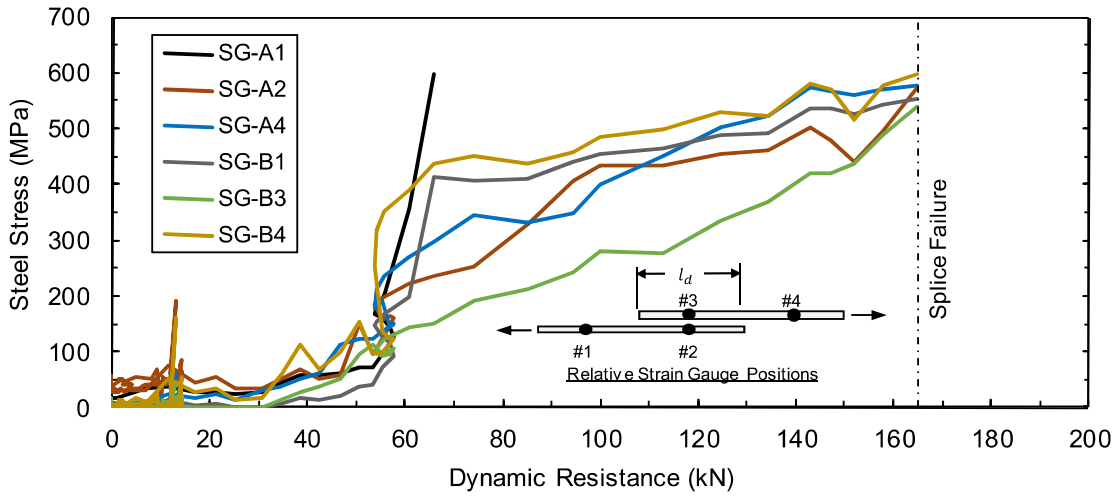

Figure B.82: Steel stress load-history plot for CP4-HSR.

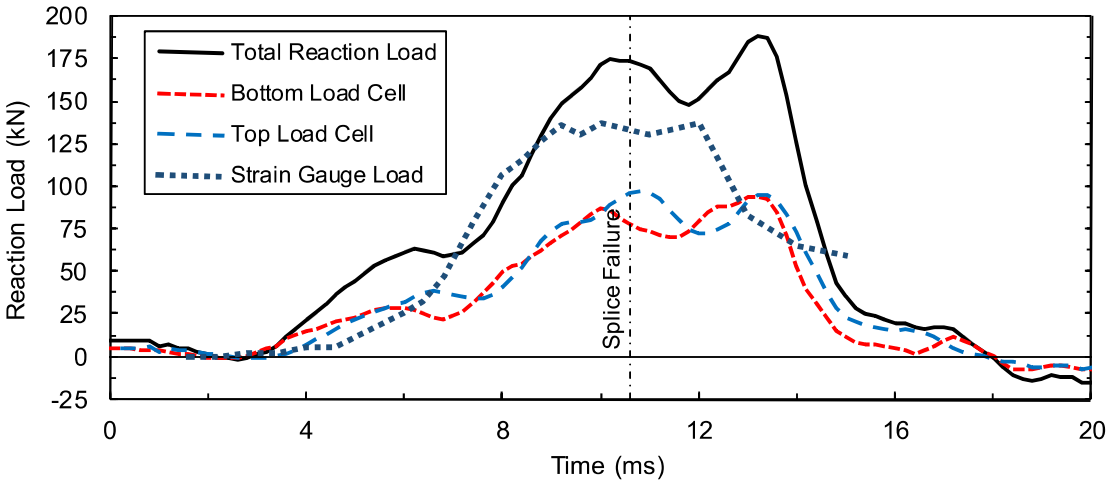

Figure B.83: Load time-history plot for CP4-HSR.

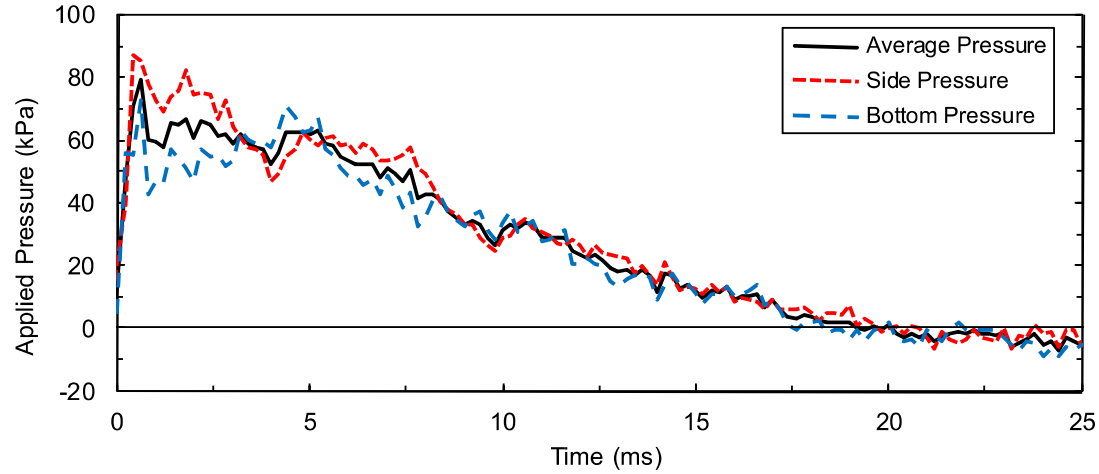

Figure B.84: Pressure time-history plot for CP4-HSR.

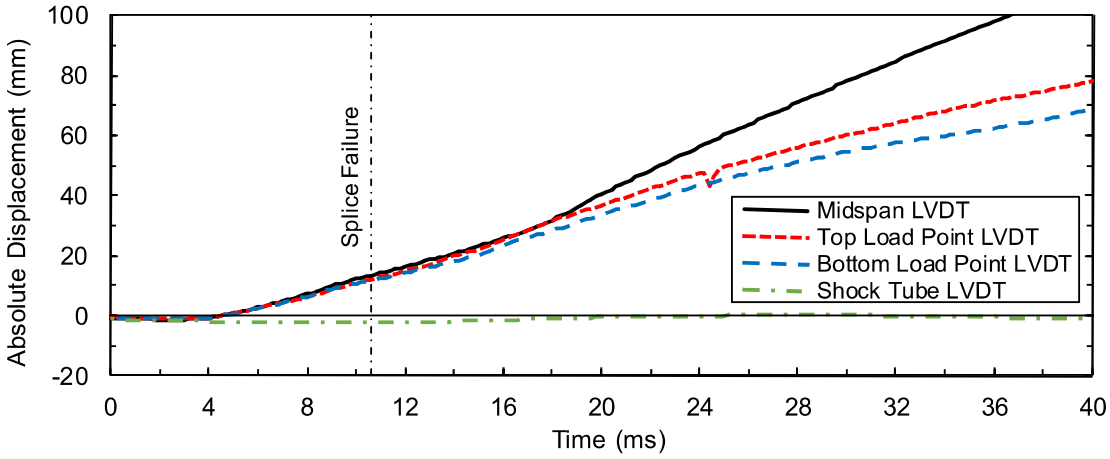

Figure B.85: Displacement time-history plot for CP4-HSR.

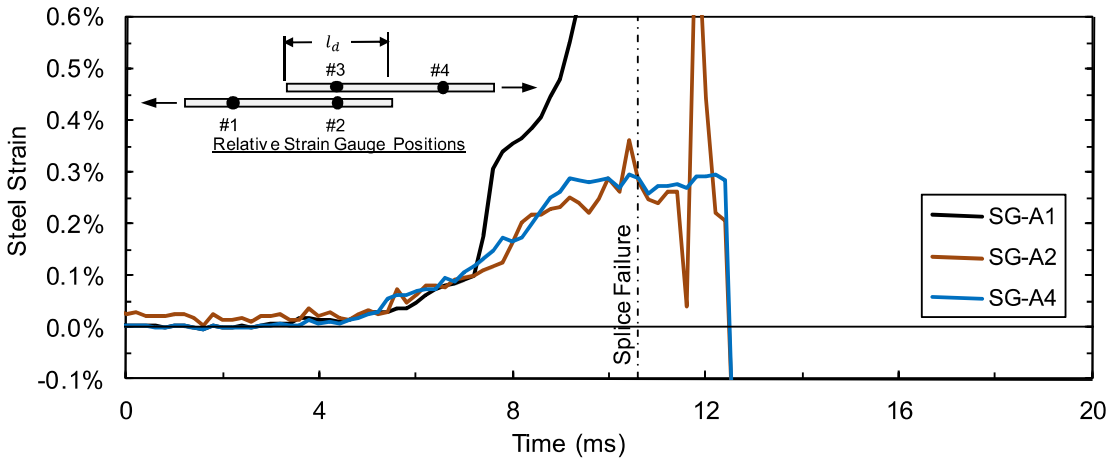

Figure B.86: Test bar "A" strain time-history plot for CP4-HSR.

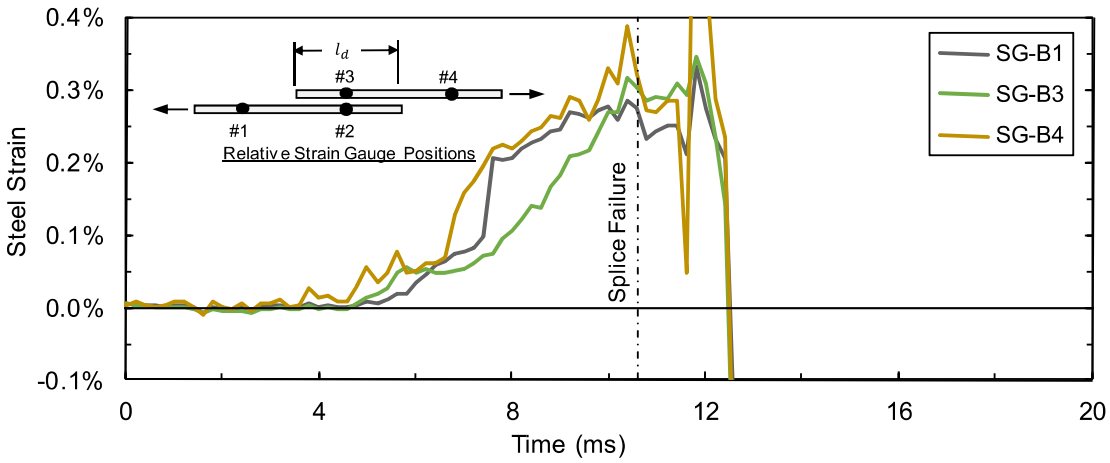

Figure B.87: Test bar "B" strain time-history plot for CP4-HSR.

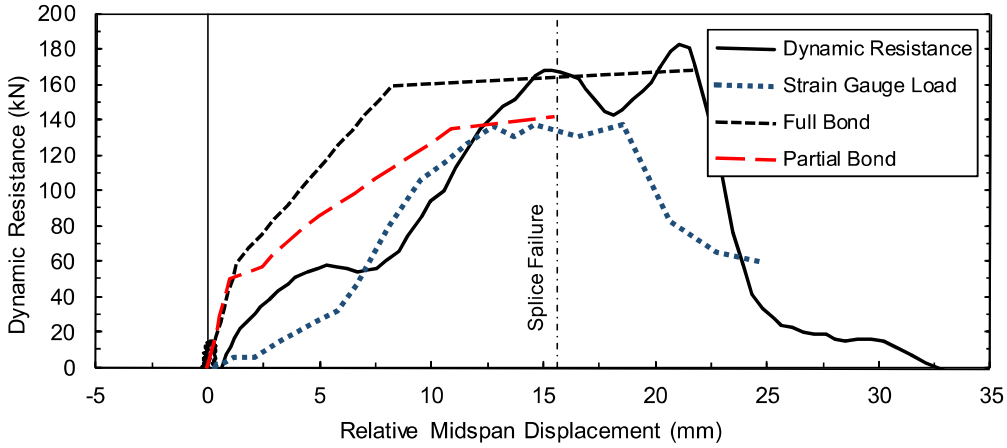

Figure B.88: Comparison of predicted and experimental resistance curves for CP4-HSR.

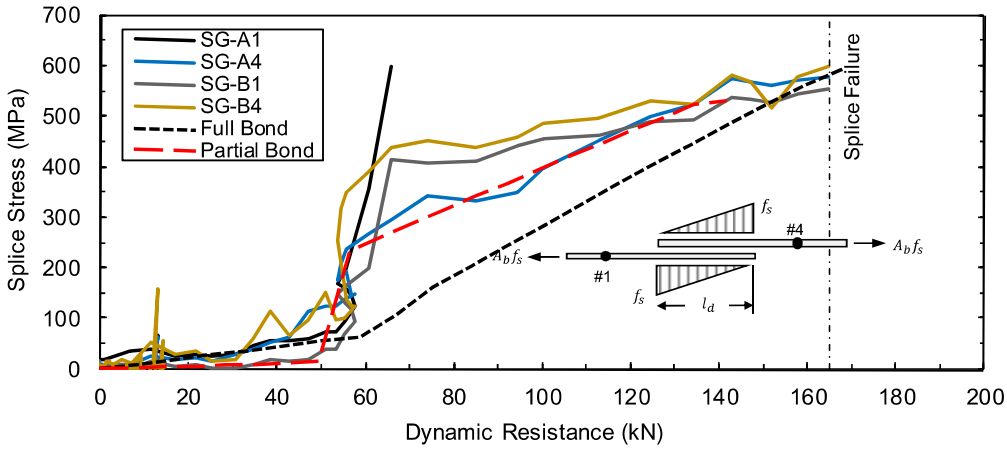

Figure B.89: Comparison of predicted and experimental steel stress developed in spliced reinforcement for CP4-HSR with respect to applied load.

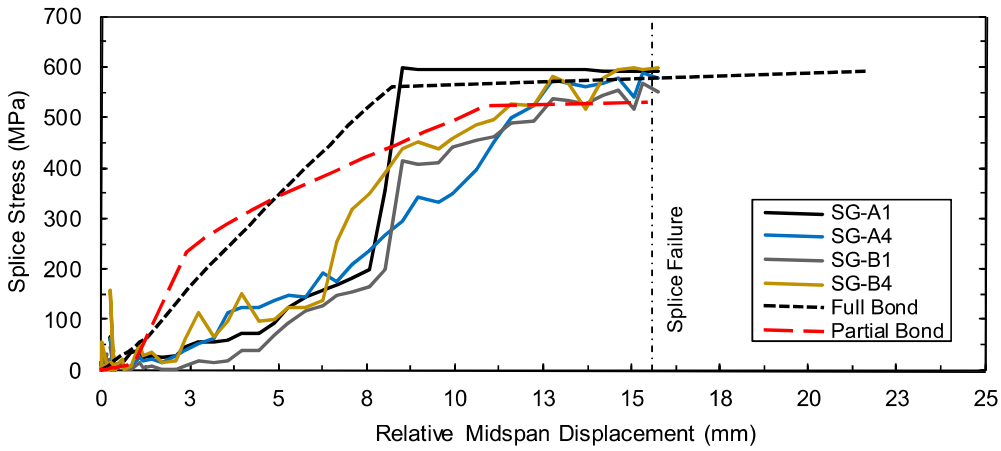

Figure B.90: Comparison of predicted and experimental steel stress developed in spliced reinforcement for CP4-HSR with respect to displacement.

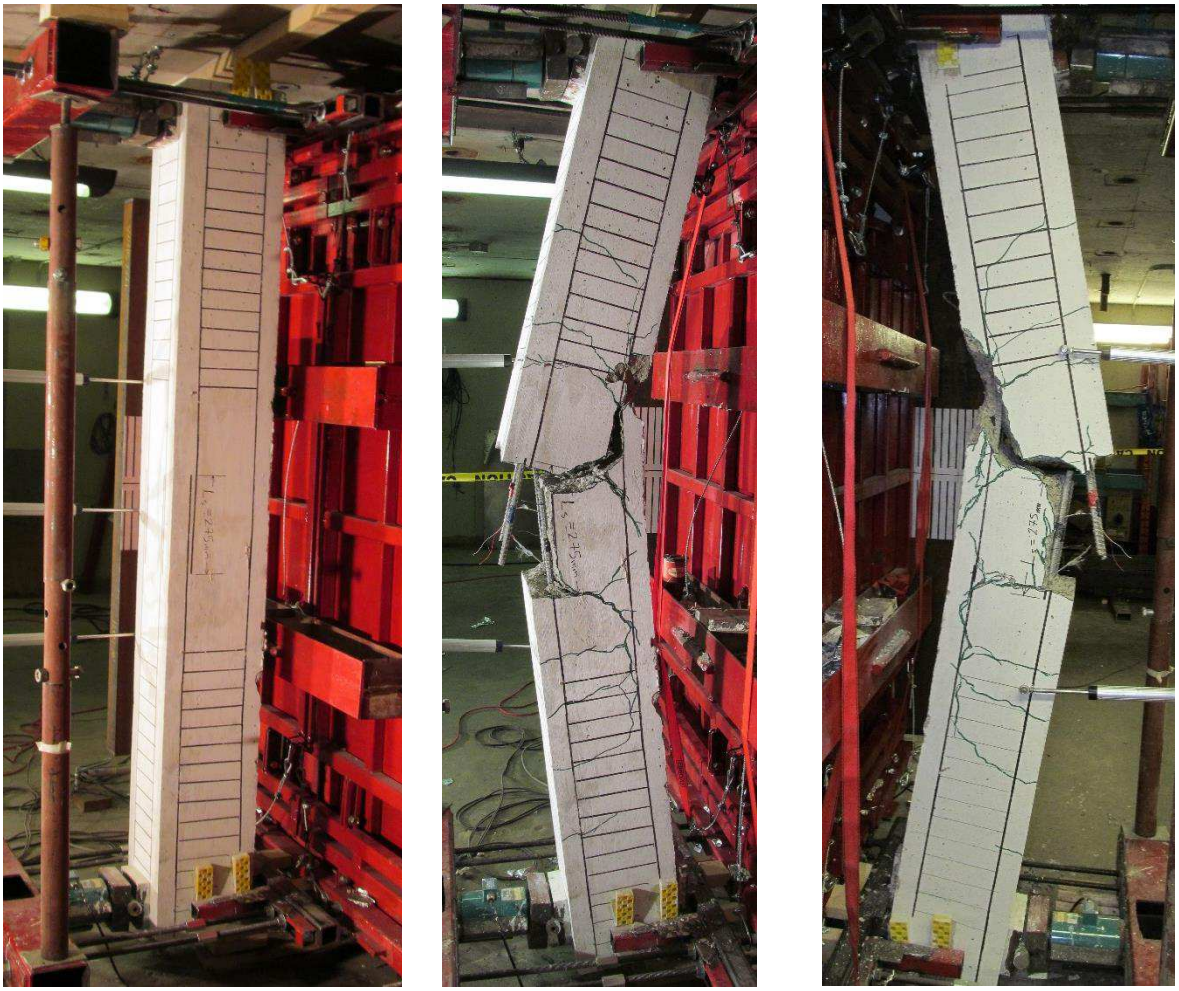

(a) Before high strain rate testing (b) After high strain rate testing (c) After high strain rate testing

Figure B.91: Photographs of lap splice beam CP4-HSR.

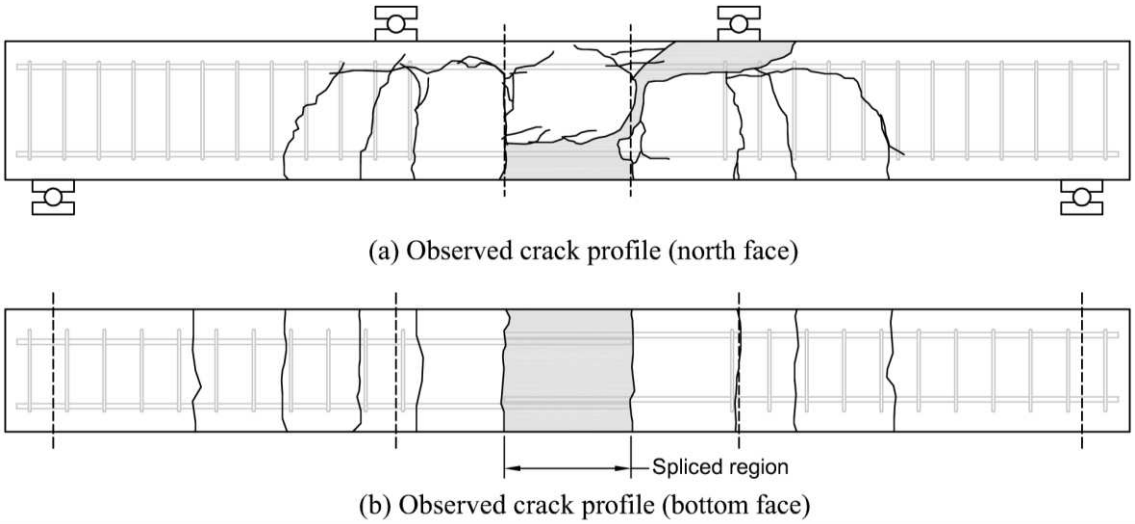

(a) Observed crack profile (north face)

(b) Observed crack profile (bottom face)

Figure B.92: Observed crack profile for lap splice beam CP4-HSR.

CP5-LSR

Lap splice beam CP5-LSR was subjected to low strain rate testing on September 18, 2013. CP5-LSR was designed with 15M reinforcement, 50 MPa concrete, 25 mm cover, and without transverse reinforcement in the spliced region. The specimen experienced a side-splitting tensile failure of the cover concrete with significant cover loss. The onset of lap splice failure occurred at an applied load of 130.6 kN. Based on strain readings, the stress developed in the spliced bars was 448 MPa. Based on a sectional analysis, the stress developed in the spliced bars was 485 MPa. Time-to-failure was 544.0 seconds and strain rate was 4.1×10^{-6} s^{-1}.

Table B.17: Geometry, reinforcing, and material properties for CP5-LSR.

b:	165 mm	Bar:	2-15M	f_c':	48.7 MPa
h:	300 mm	A_b:	200 mm^2	f_y:	448.4 MPa
l_d:	409 mm	d_b:	16.0 mm	ρ:	0.92%
c_b:	28 mm	N:	N/A	c/d:	1.7
c_{so}:	27 mm	A_{tr}:	N/A	$l_d(c_{min}+0.5d_b)$:	14315 mm^2

Table B.18: Summary of experimental test results for CP5-LSR.

Date:	Sept. 18, 2013	δ_f:	10.0 mm	f_s^t:	448 MPa
P_r:	N/A	R_f:	130.6 kN	f_s^{cal}:	485 MPa
I_r:	N/A	t_f:	544.0 s	$\dot{\varepsilon}$:	4.1×10^{-6} s^{-1}

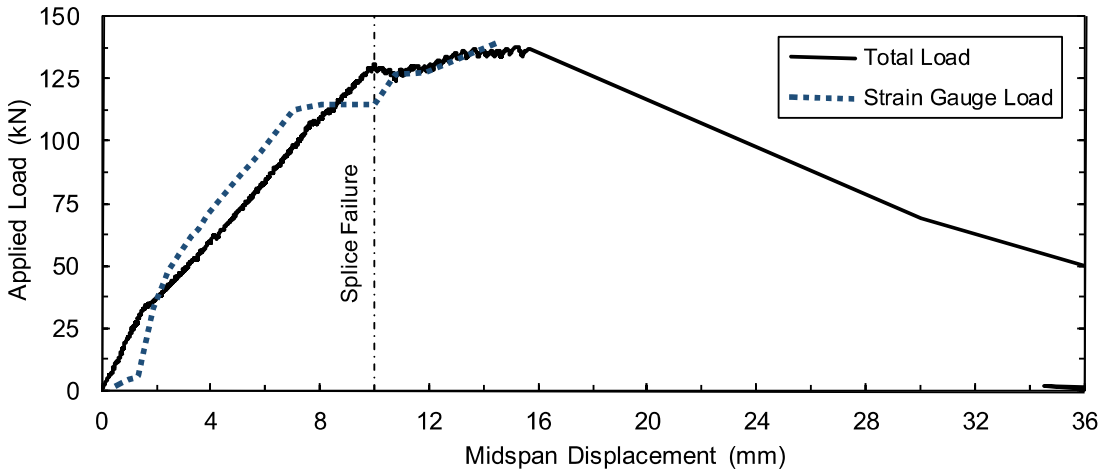

Figure B.93: Load displacement-history plot for CP5-LSR.

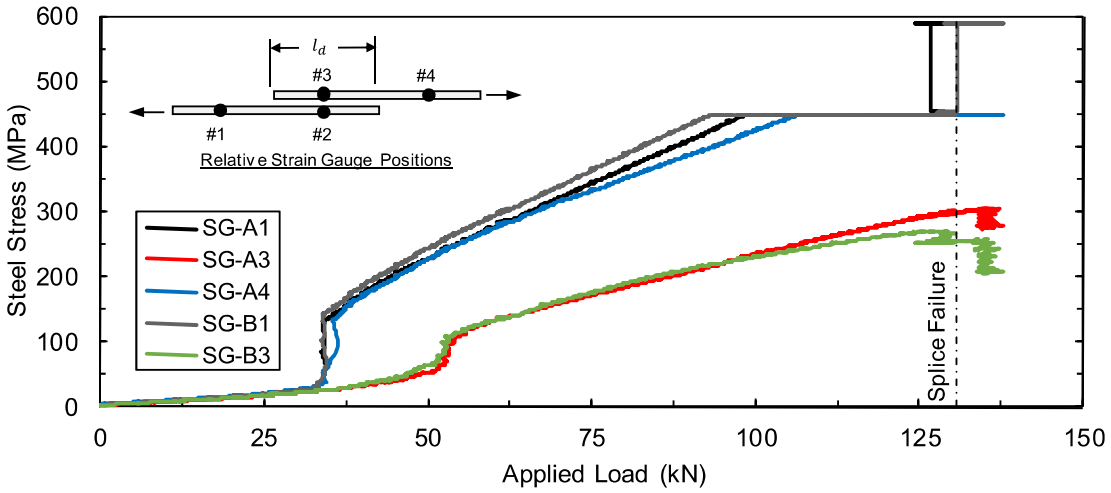

Figure B.94: Steel stress load-history plot for CP5-LSR.

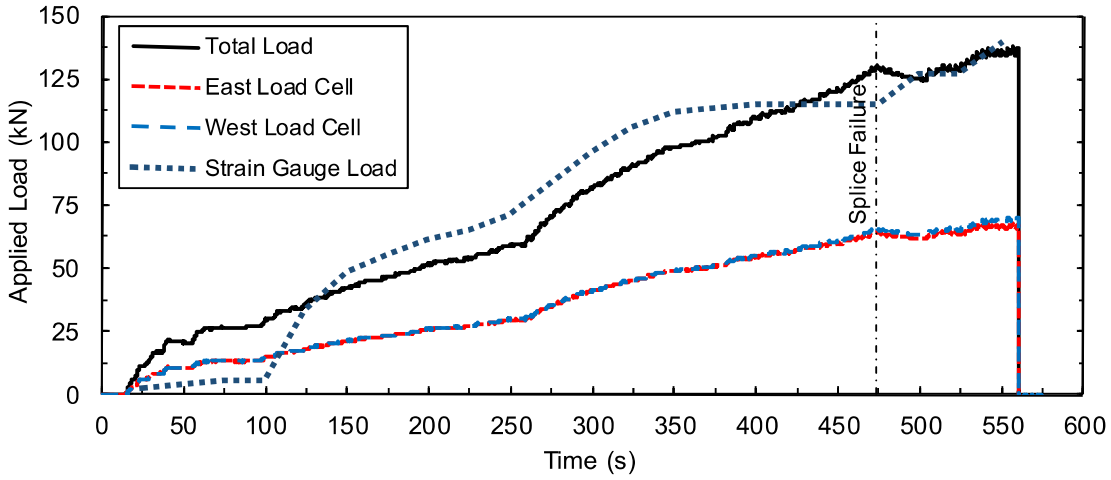

Figure B.95: Load time-history plot for CP5-LSR.

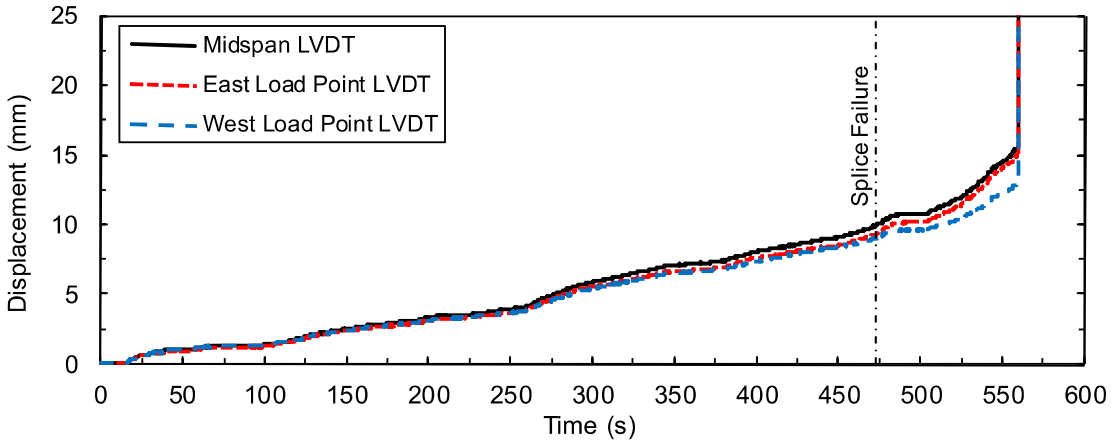

Figure B.96: Displacement time-history plot for CP5-LSR.

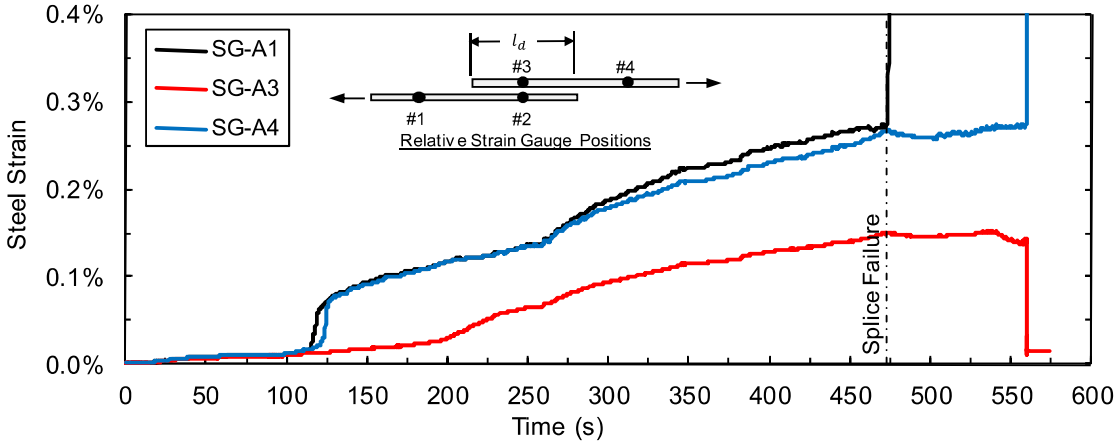

Figure B.97: Test bar "A" strain time-history plot for CP5-LSR.

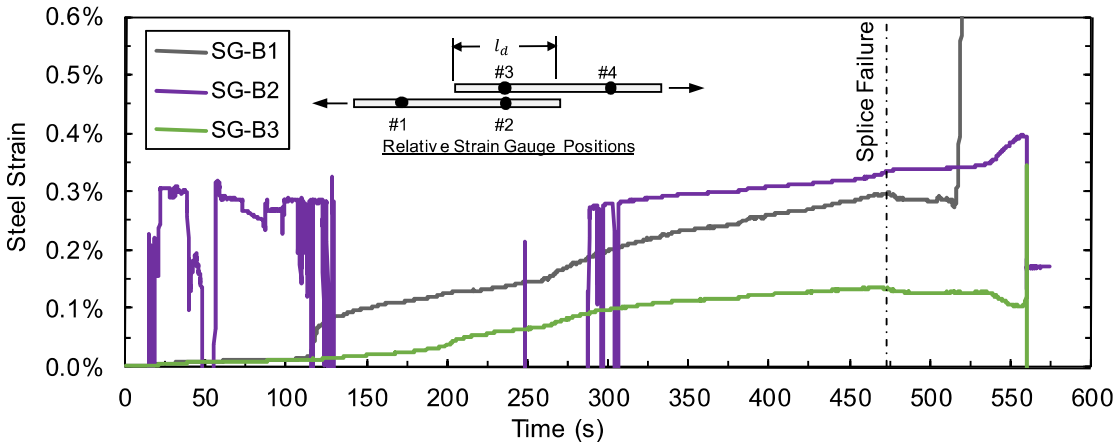

Figure B.98: Test bar "B" strain time-history plot for CP5-LSR.

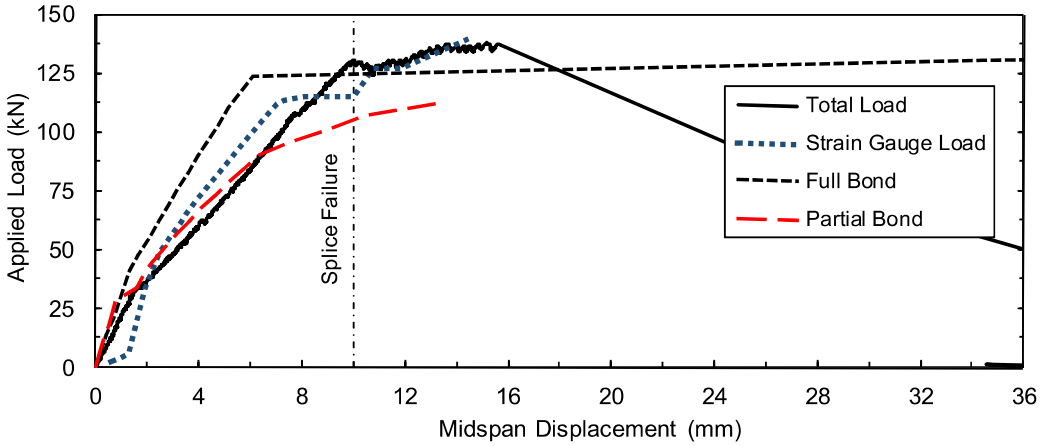

Figure B.99: Comparison of predicted and experimental resistance curves for CP5-LSR.

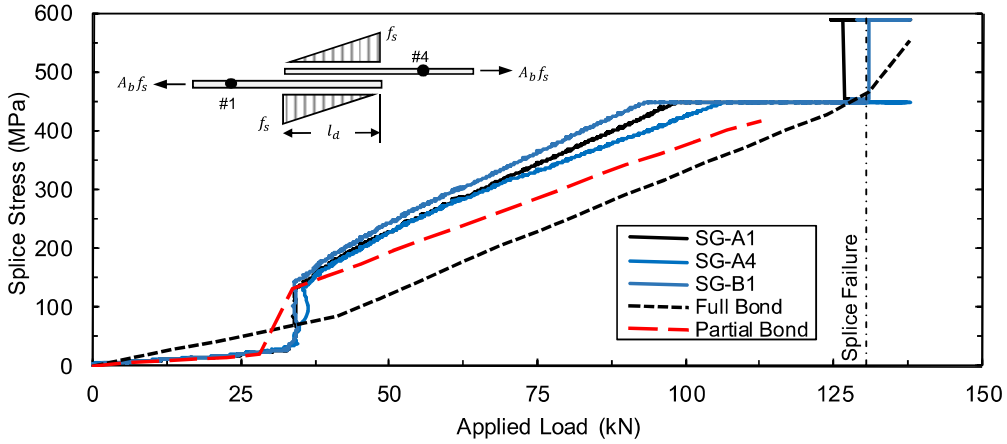

Figure B.100: Comparison of predicted and experimental steel stress developed in spliced reinforcement for CP5-LSR with respect to applied load.

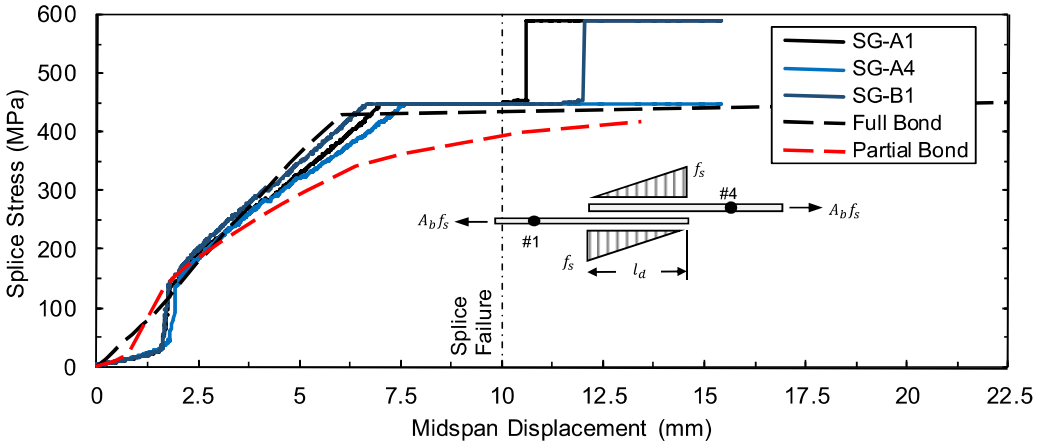

Figure B.101: Comparison of predicted and experimental steel stress developed in spliced reinforcement for CP5-LSR with respect to displacement.

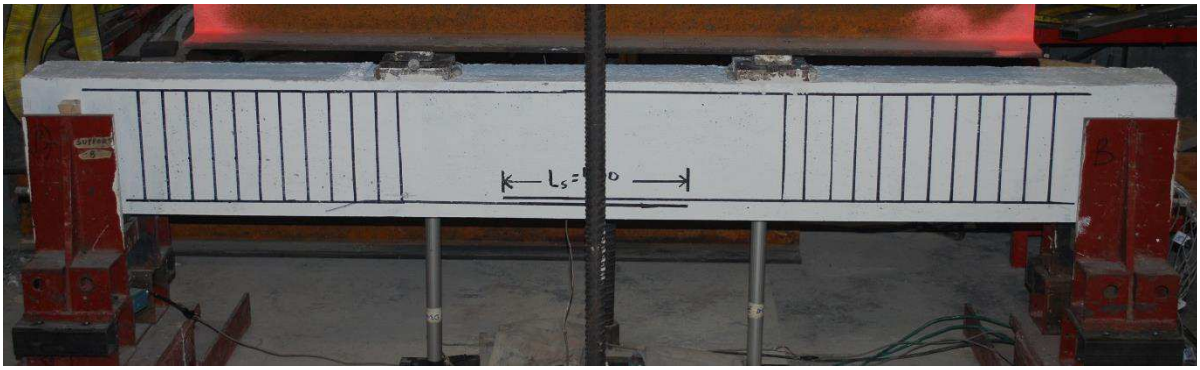

(a) Before low strain rate testing

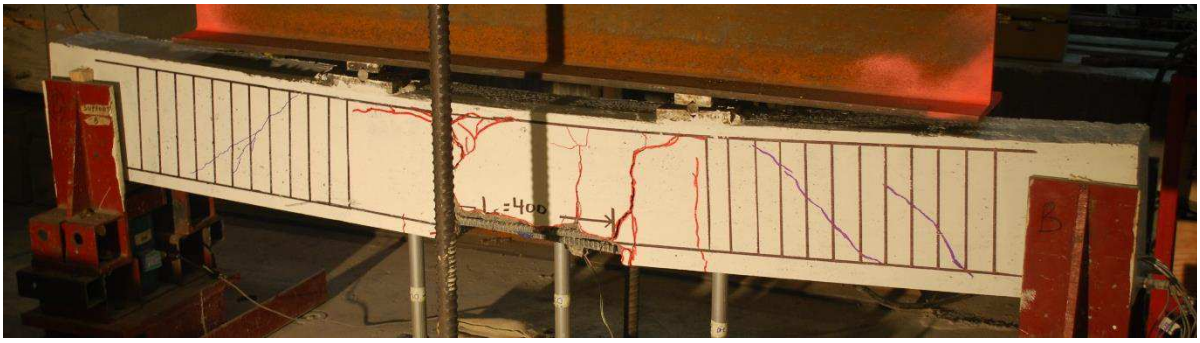

(b) After low strain rate testing

Figure B.102: Photographs of lap splice beam CP5-LSR.

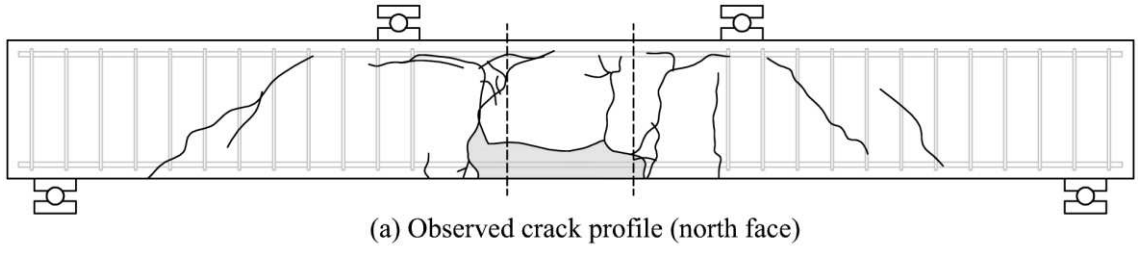

(a) Observed crack profile (north face)

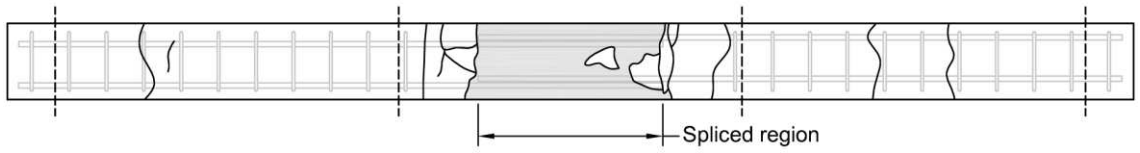

(b) Observed crack profile (bottom face)

Figure B.103: Observed crack profile for lap splice beam CP5-LSR.

CP5-HSR

Lap splice beam CP5-HSR was subjected to high strain rate testing on October 16, 2013. CP5-HSR was designed with 15M reinforcement, 50 MPa concrete, 25 mm cover, and without transverse reinforcement in the spliced region. The specimen experienced a side-splitting tensile failure of the cover concrete with significant cover loss. The peak dynamic resistance was 153.2 kN. Based on strain readings, the stress developed in the spliced bars was 565 MPa. Based on a sectional analysis, the stress developed in the spliced bars was 584 MPa. Time-to-failure was 8.0 ms and strain rate was 0.60 s^{-1}.

Table B.19: Geometry, reinforcing, and material properties for CP5-HSR.

b:	165 mm	Bar:	2-15M	f'_{dc}:	60.0 MPa
h:	300 mm	A_b:	200 mm^2	f_{dy}:	590.3 MPa
l_d:	395 mm	d_b:	16.0 mm	ρ:	0.92%
c_b:	27 mm	N:	N/A	c/d:	1.6
c_{so}:	25 mm	A_{tr}:	N/A	$l_d(c_{min} + 0.5d_b)$:	13035 mm^2

Table B.20: Summary of experimental test results for CP5-HSR.

Date:	Oct. 16, 2013	δ_f:	14.1 mm	f_s^t:	565 MPa
P_r:	82.5 kPa	R_f:	153.2 kN	f_s^{cal}:	584 MPa
I_r:	700.0 kPa-ms	t_f:	8.0 ms	$\dot{\varepsilon}$:	0.60 s^{-1}

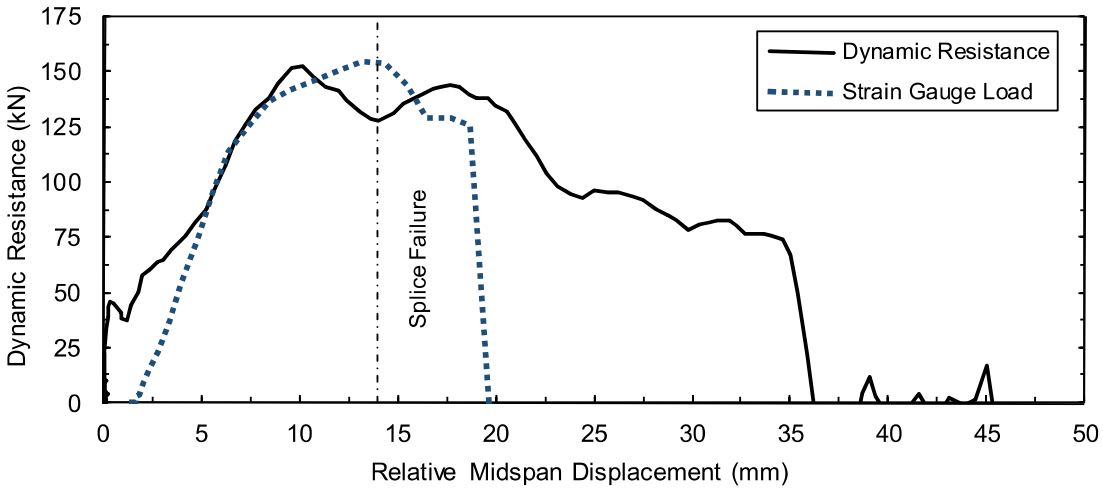

Figure B.104: Load displacement-history plot for CP5-HSR.

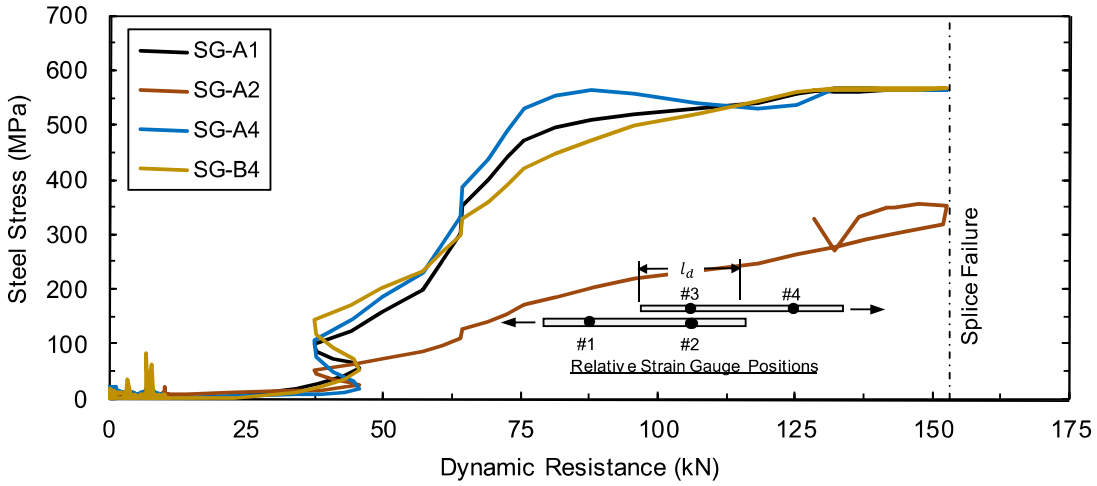

Figure B.105: Steel stress load-history plot for CP5-HSR.

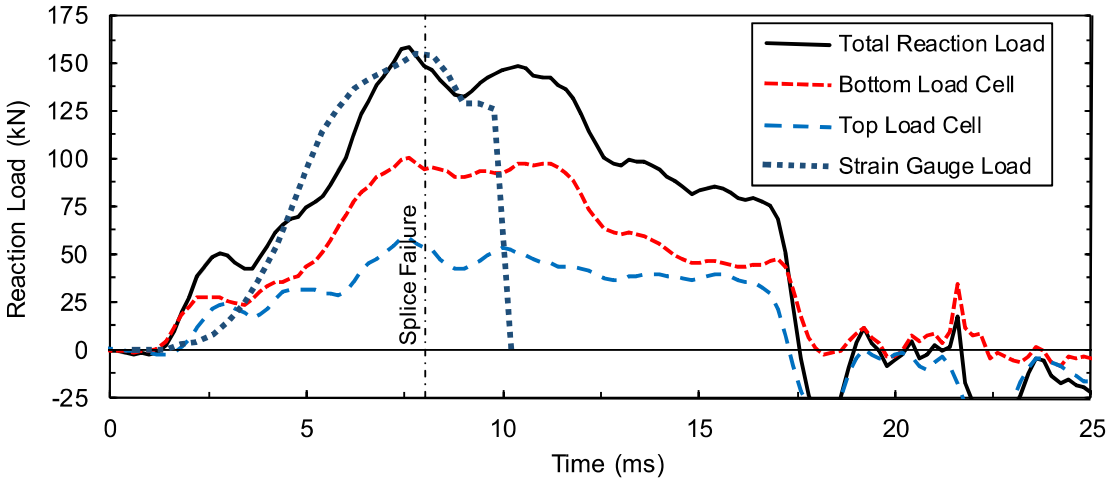

Figure B.106: Load time-history plot for CP5-HSR.

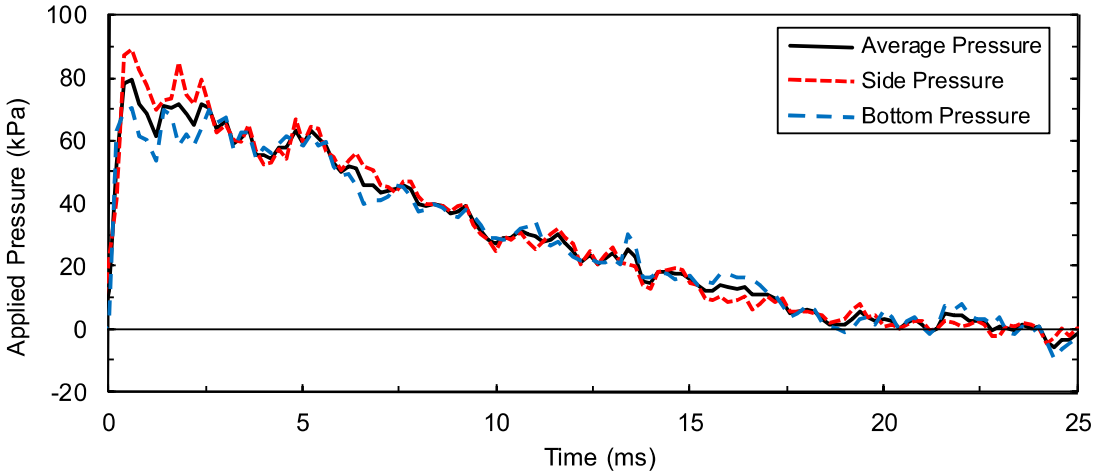

Figure B.107: Pressure time-history plot for CP5-HSR.

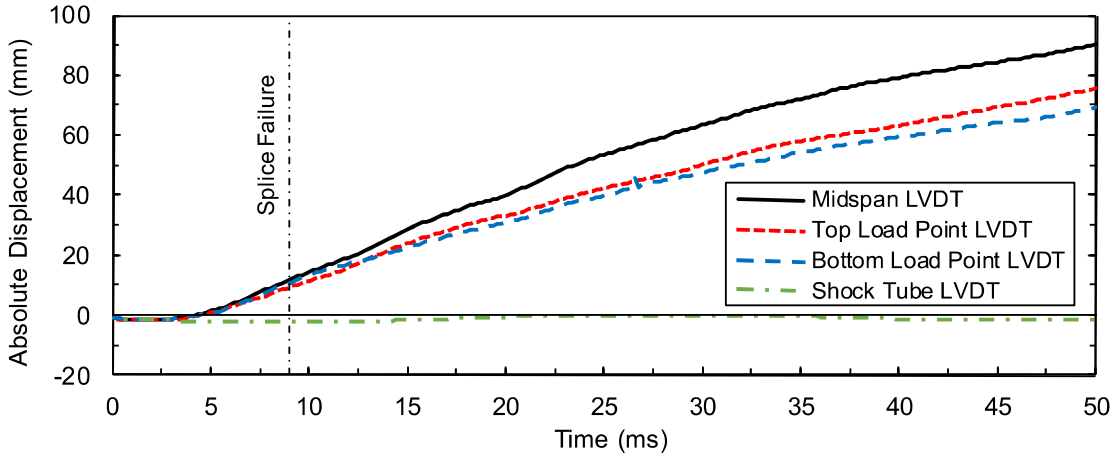

Figure B.108: Displacement time-history plot for CP5-HSR.

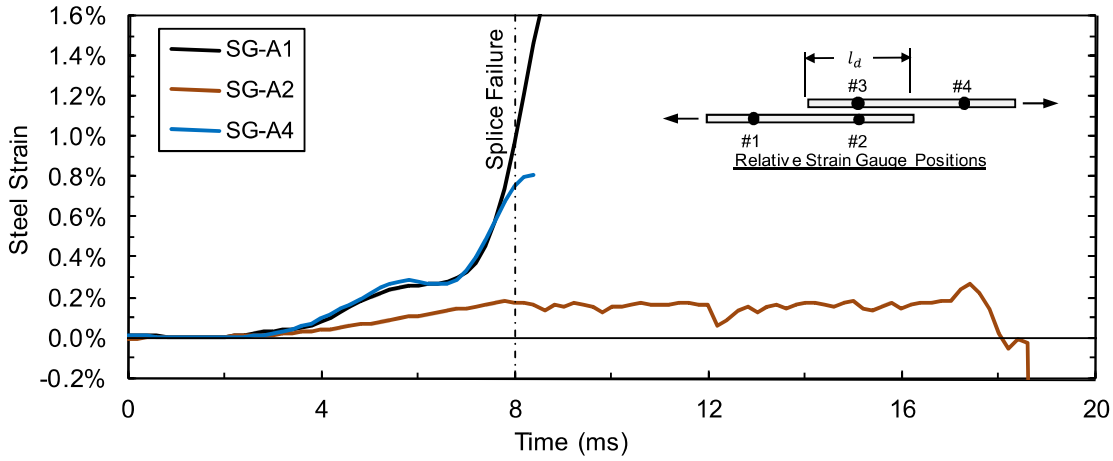

Figure B.109: Test bar "A" strain time-history plot for CP5-HSR.

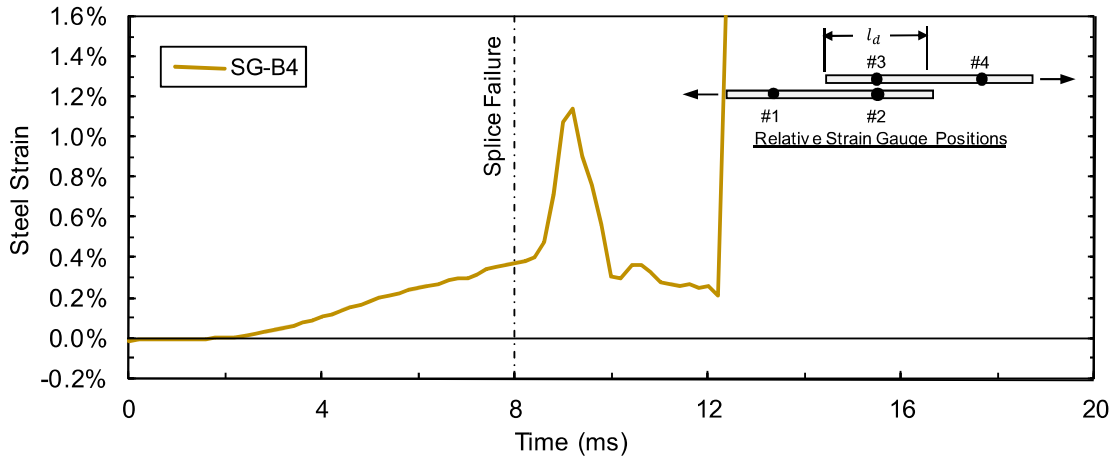

Figure B.110: Test bar "B" strain time-history plot for CP5-HSR.

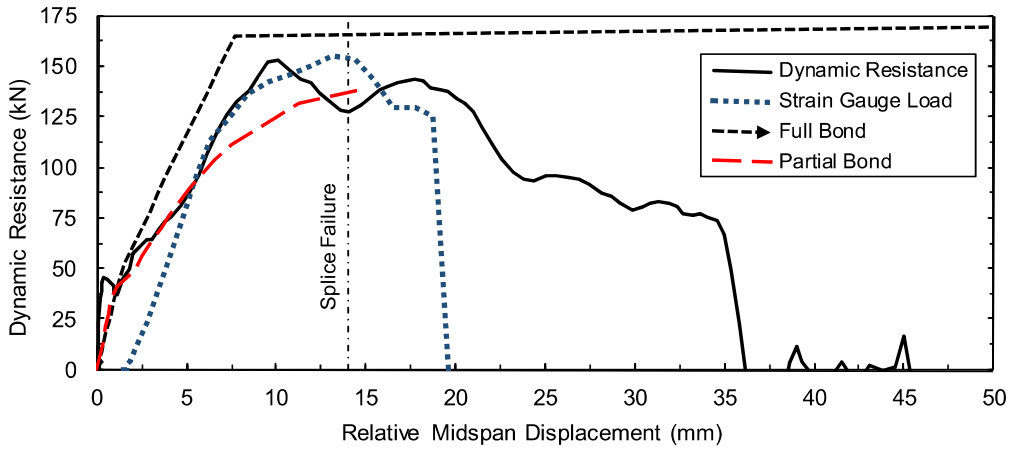

Figure B.111: Comparison of predicted and experimental resistance curves for CP5-HSR.

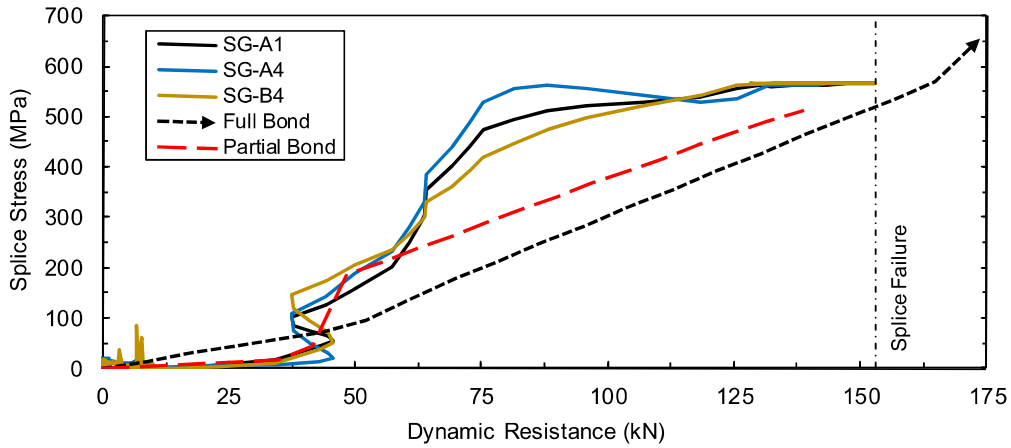

Figure B.112: Comparison of predicted and experimental steel stress developed in spliced reinforcement for CP5-HSR with respect to applied load.

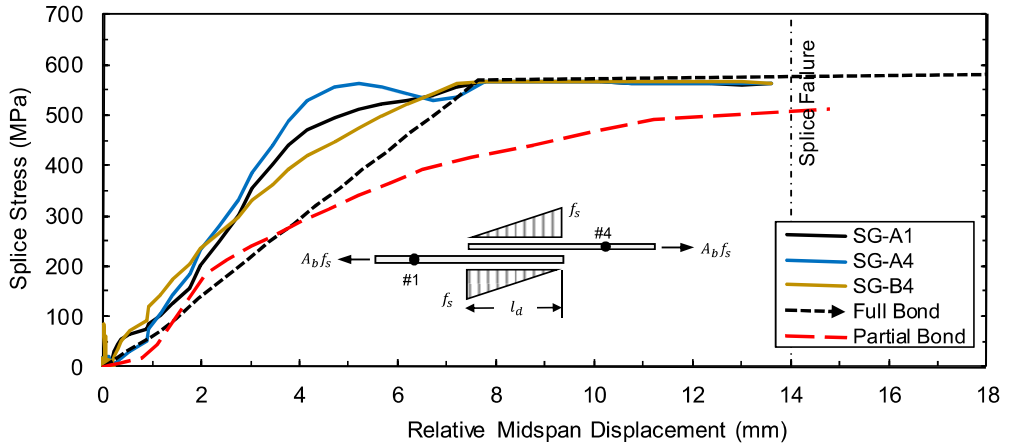

Figure B.113: Comparison of predicted and experimental steel stress developed in spliced reinforcement for CP5-HSR with respect to displacement.

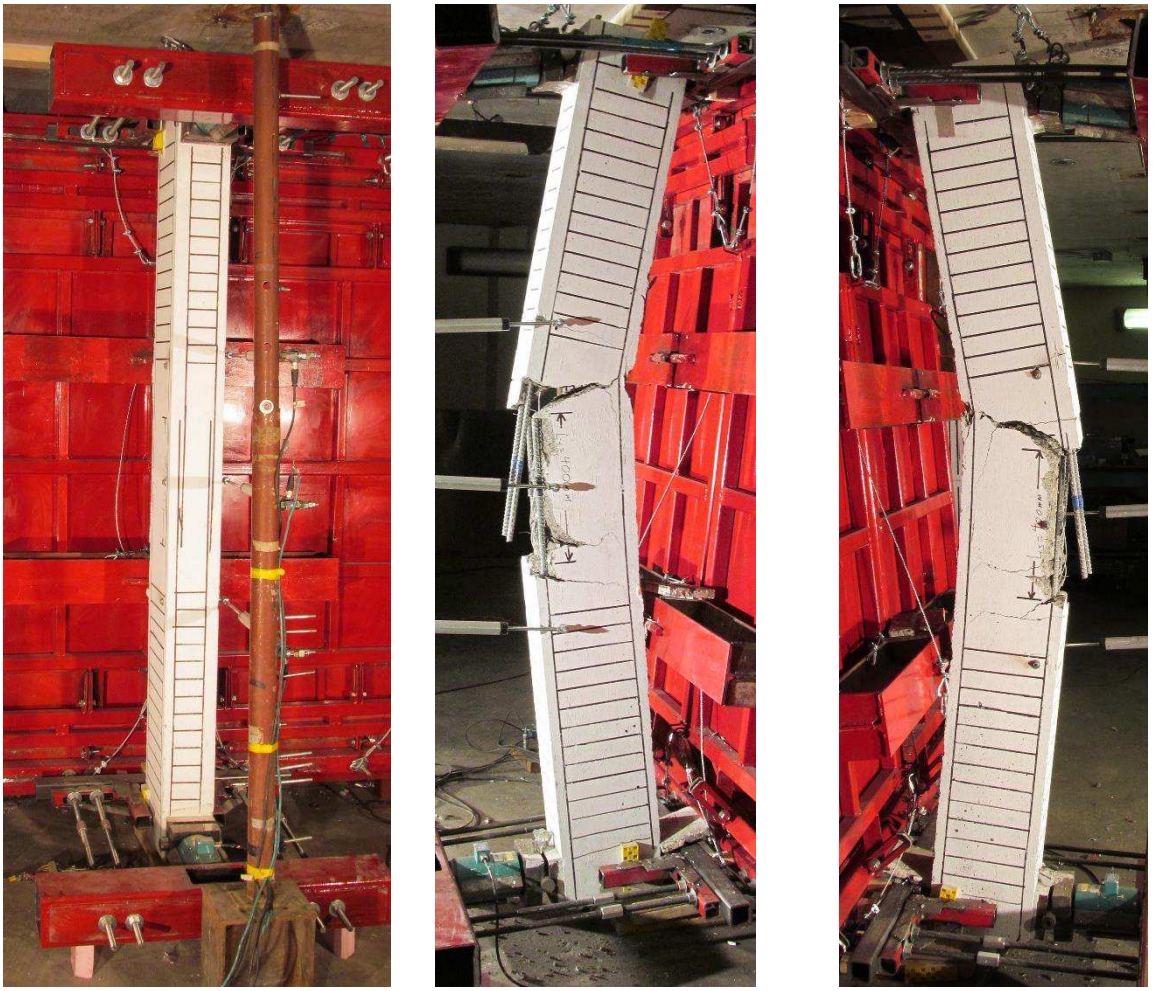

(a) Before high strain rate testing (b) After high strain rate testing (c) After high strain rate testing

Figure B.114: Photographs of lap splice beam CP5-HSR.

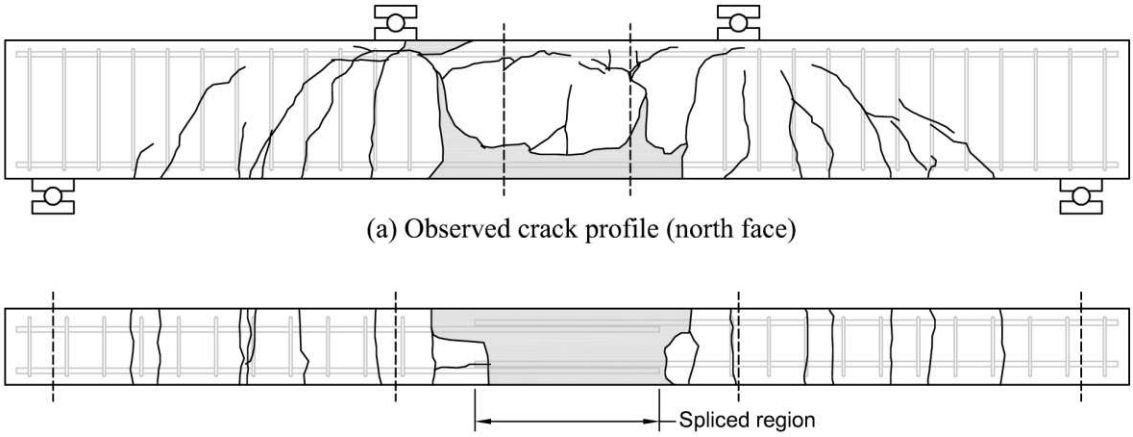

(a) Observed crack profile (north face)

(b) Observed crack profile (bottom face)

Figure B.115: Observed crack profile for lap splice beam CP5-HSR.

CP6-LSR

Lap splice beam CP6-LSR was subjected to low strain rate testing on September 23, 2013. CP6-LSR was designed with 15M reinforcement, 50 MPa concrete, 50 mm cover, and without transverse reinforcement in the spliced region. The specimen experienced a combined side- and face-splitting tensile failure of the cover concrete with significant cover loss. Failure occurred at an applied load of 121.6 kN. Based on strain readings, the stress developed in the spliced bars was 443 MPa. Based on a sectional analysis, the stress developed in the spliced bars was 467 MPa. Time-to-failure was 350.6 seconds and strain rate was 6.3×10^{-6} s^{-1}.

Table B.21: Geometry, reinforcing, and material properties for CP6-LSR.

b:	265 mm	Bar:	2-15M	f_c':	48.7 MPa
h:	300 mm	A_b:	200 mm^2	f_y:	448.4 MPa
l_d:	235 mm	d_b:	16.0 mm	ρ:	0.63%
c_b:	53 mm	N:	N/A	c/d:	3.3
c_{so}:	52 mm	A_{tr}:	N/A	$l_d(c_{min}+0.5d_b)$:	14100 mm^2

Table B.22: Summary of experimental test results for CP6-LSR.

Date:	Sept. 23, 2013	δ_f:	14.1 mm	f_s^t:	443 MPa
P_r:	N/A	R_f:	121.6 kN	f_s^{cal}:	467 MPa
I_r:	N/A	t_f:	350.6 s	$\dot{\varepsilon}$:	6.3×10^{-6} s^{-1}

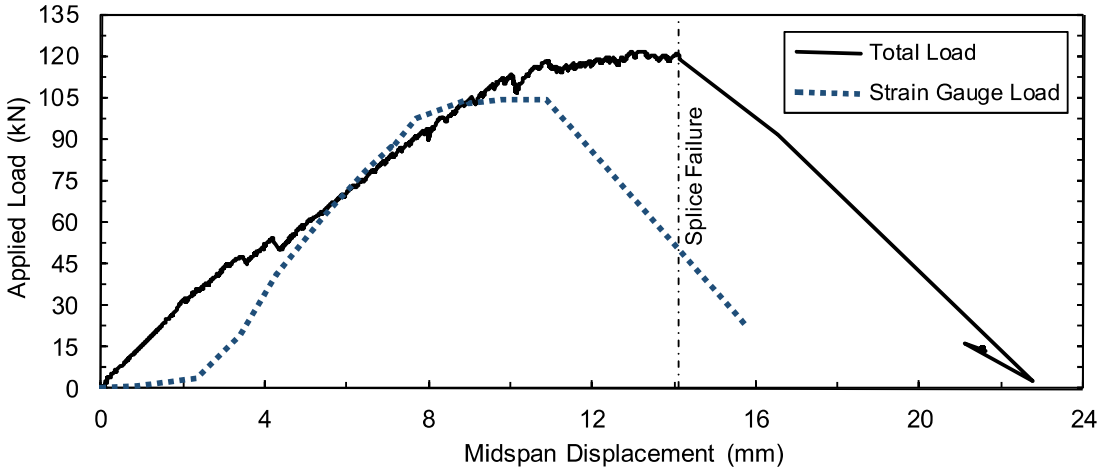

Figure B.116: Load displacement-history plot for CP6-LSR.

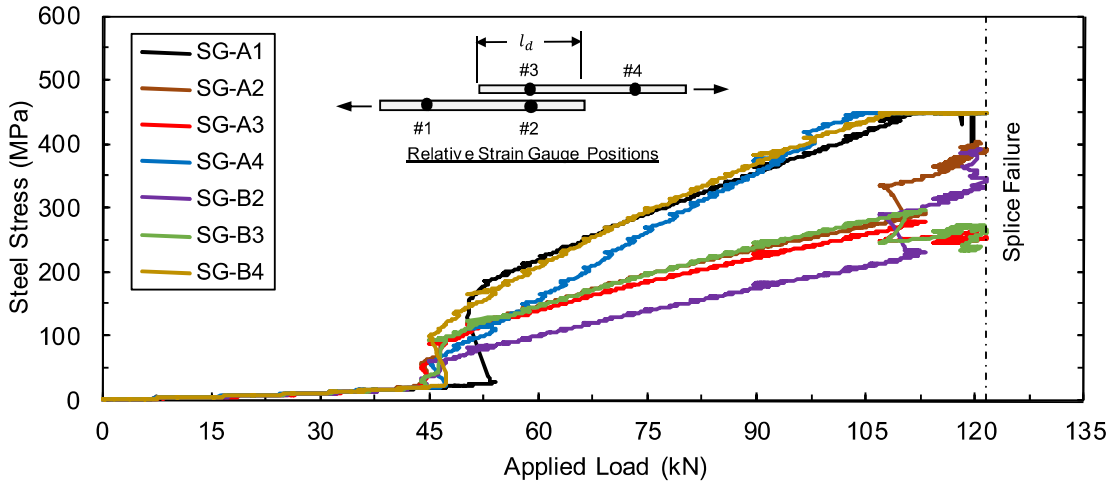

Figure B.117: Steel stress load-history plot for CP6-LSR.

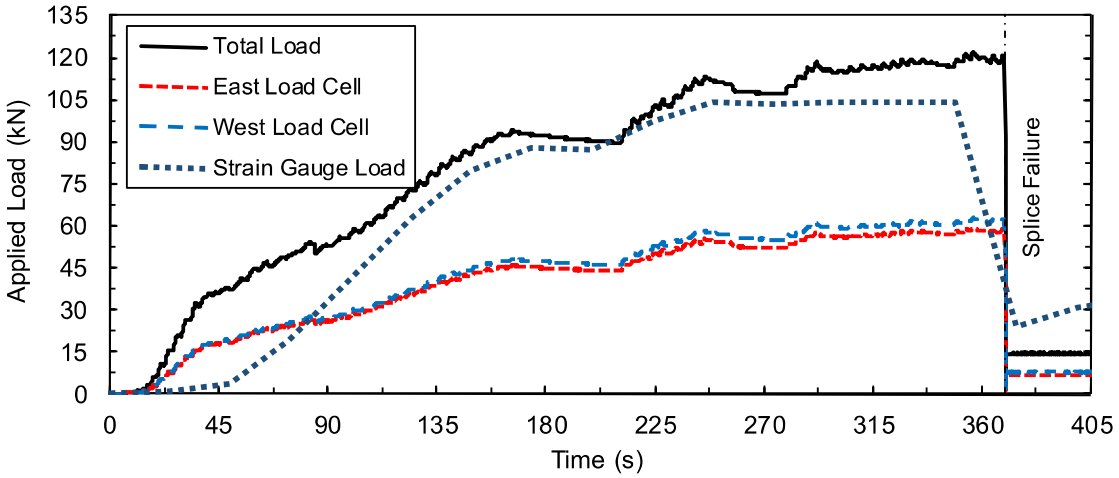

Figure B.118: Load time-history plot for CP6-LSR.

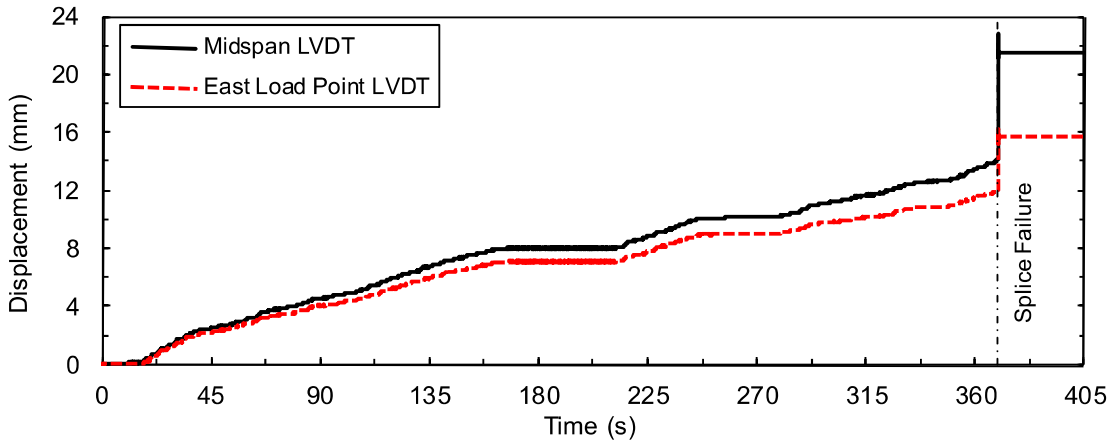

Figure B.119: Displacement time-history plot for CP6-LSR.

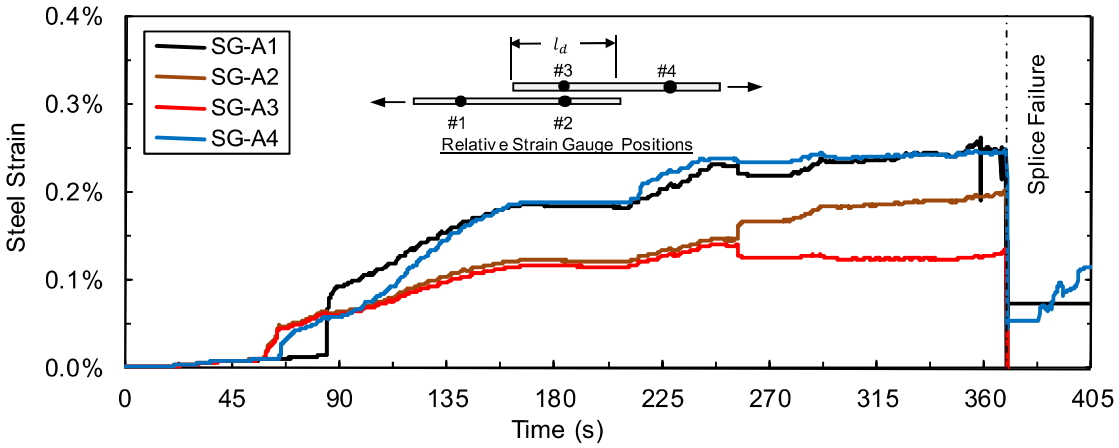

Figure B.120: Test bar "A" strain time-history plot for CP6-LSR.

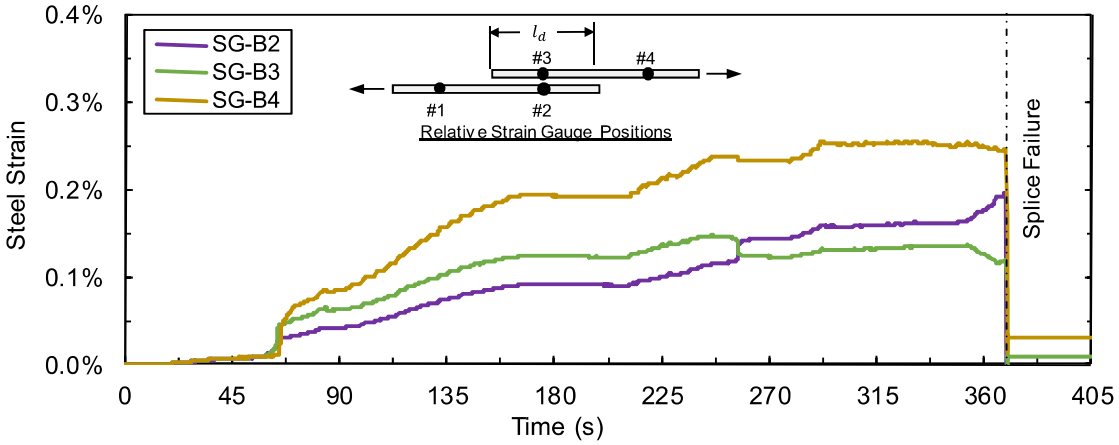

Figure B.121: Test bar "B" strain time-history plot for CP6-LSR.

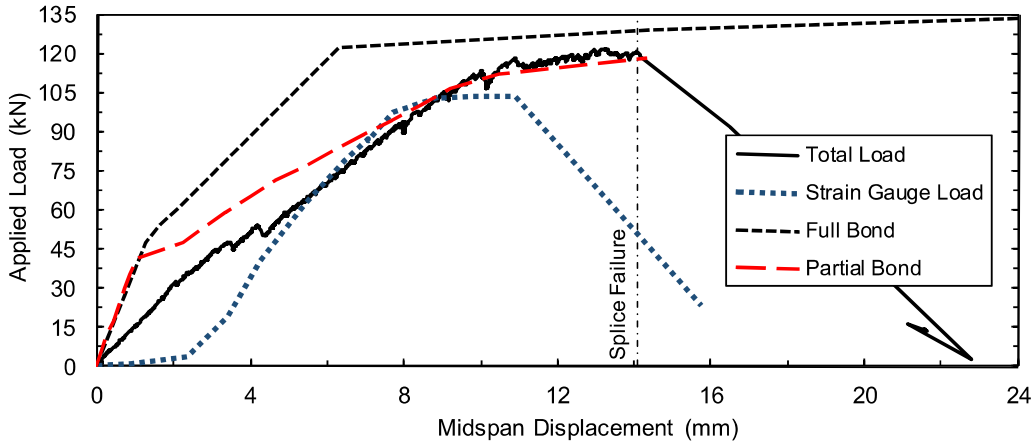

Figure B.122: Comparison of predicted and experimental resistance curves for CP6-LSR.

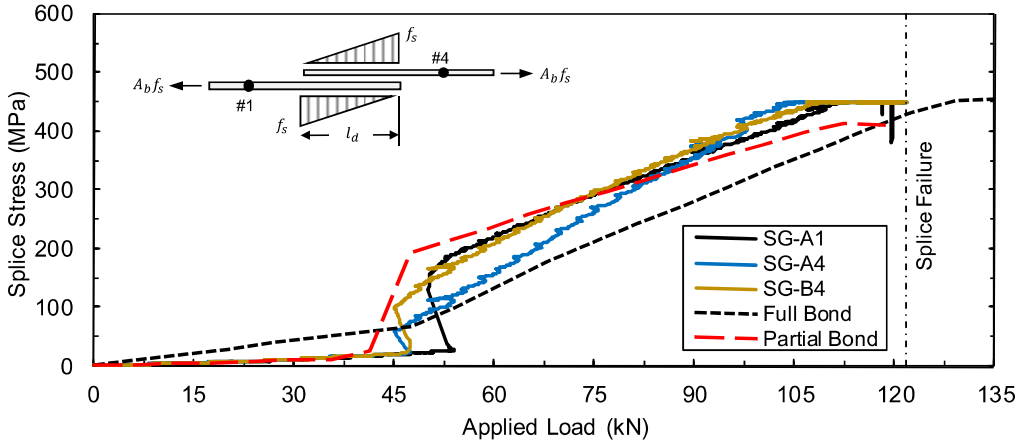

Figure B.123: Comparison of predicted and experimental steel stress developed in spliced reinforcement for CP6-LSR with respect to applied load.

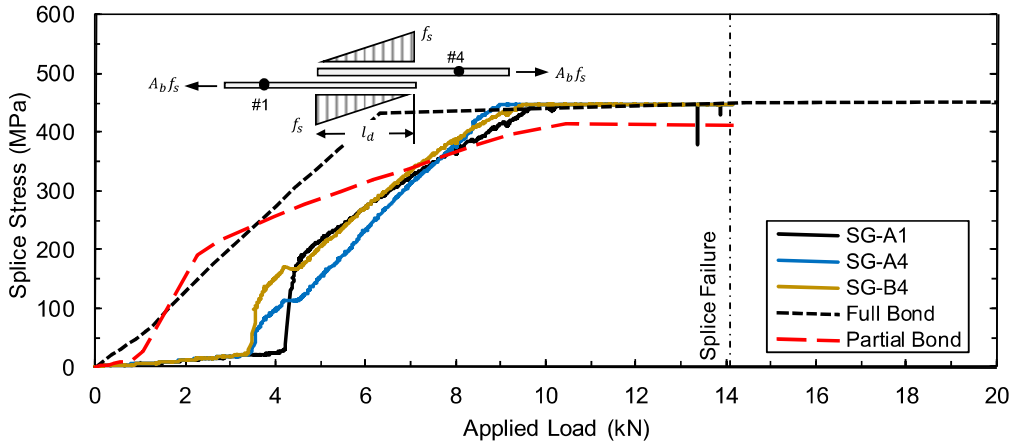

Figure B.124: Comparison of predicted and experimental steel stress developed in spliced reinforcement for CP6-LSR with respect to displacement.

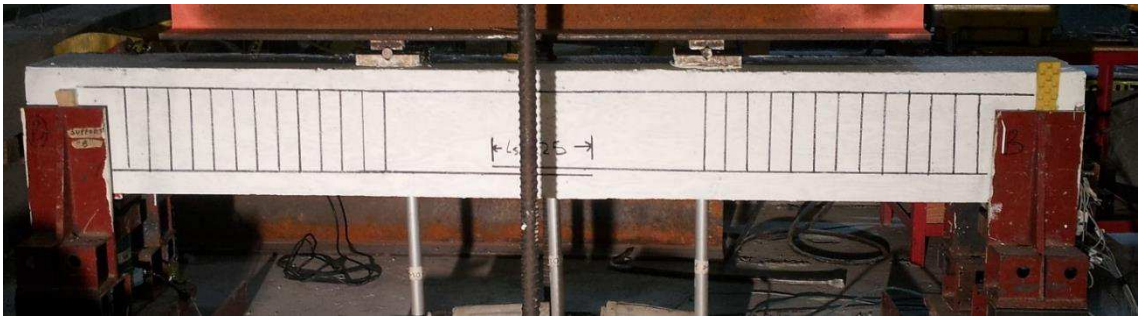

(a) Before low strain rate testing

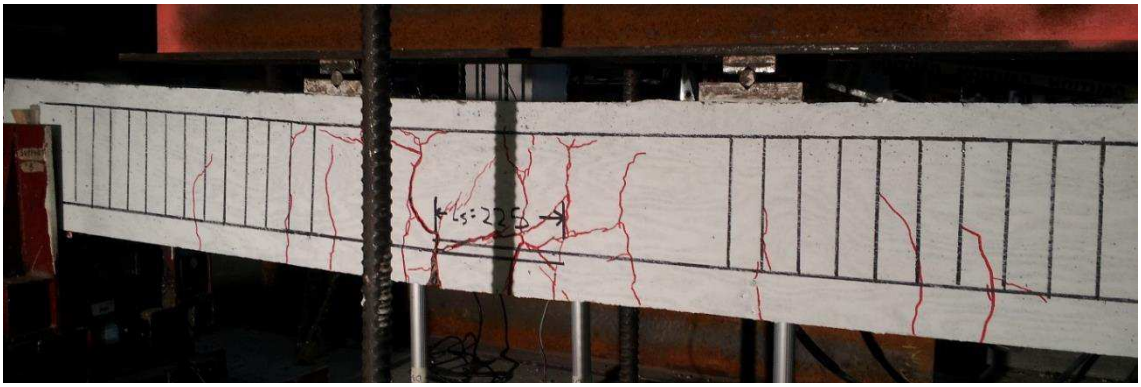

(b) After low strain rate testing

Figure B.125: Photographs of lap splice beam CP6-LSR.

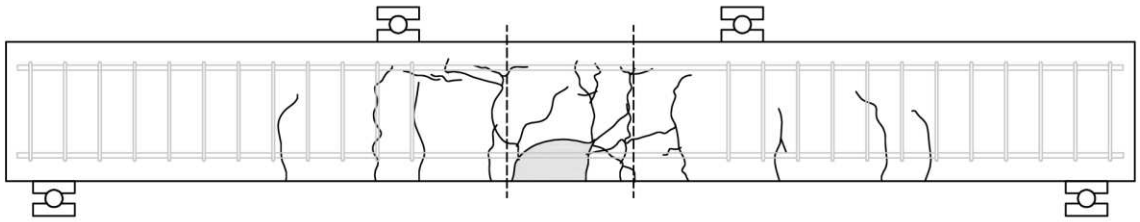

(a) Observed crack profile (north face)

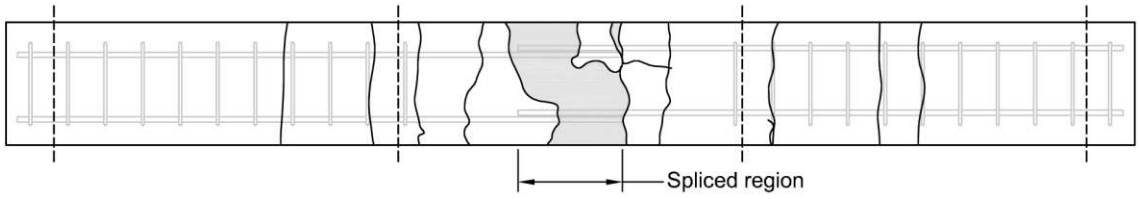

(b) Observed crack profile (bottom face)

Figure B.126: Observed crack profile for lap splice beam CP6-LSR.

CP6-HSR

Lap splice beam CP6-HSR was subjected to high strain rate testing on October 13, 2013. CP6-HSR was designed with 15M reinforcement, 50 MPa concrete, 50 mm cover, and without transverse reinforcement in the spliced region. The specimen experienced a combined side- and face-splitting tensile failure of the cover concrete with minimal cover loss. The peak dynamic resistance was 149.8 kN. Based on strain readings, the stress developed in the spliced bars was 566 MPa. Based on a sectional analysis, the stress developed in the spliced bars was 588 MPa. Time-to-failure was 9.5 ms and strain rate was 0.78 s^{-1}.

Table B.23: Geometry, reinforcing, and material properties for CP6-HSR.

b:	265 mm	Bar:	2-15M	f'_{dc}:	60.3 MPa
h:	300 mm	A_b:	200 mm^2	f_{dy}:	590.3 MPa
l_d:	230 mm	d_b:	16.0 mm	ρ:	0.63%
c_b:	51 mm	N:	N/A	c/d:	3.1
c_{so}:	47 mm	A_{tr}:	N/A	$l_d(c_{min} + 0.5d_b)$:	12650 mm^2

Table B.24: Summary of experimental test results for CP6-HSR.

Date:	Oct. 13, 2013	δ_f:	12.2 mm	f_s^t:	566 MPa
P_r:	92.2 kPa	R_f:	149.8 kN	f_s^{cal}:	588 MPa
I_r:	690.0 kPa-ms	t_f:	9.5 ms	$\dot{\varepsilon}$:	0.78 s^{-1}

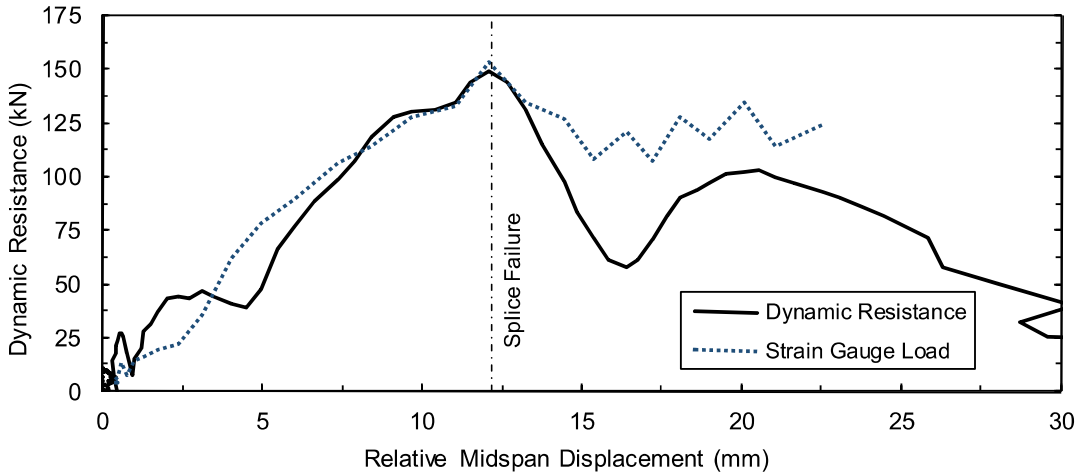

Figure B.127: Load displacement-history plot for CP6-HSR.

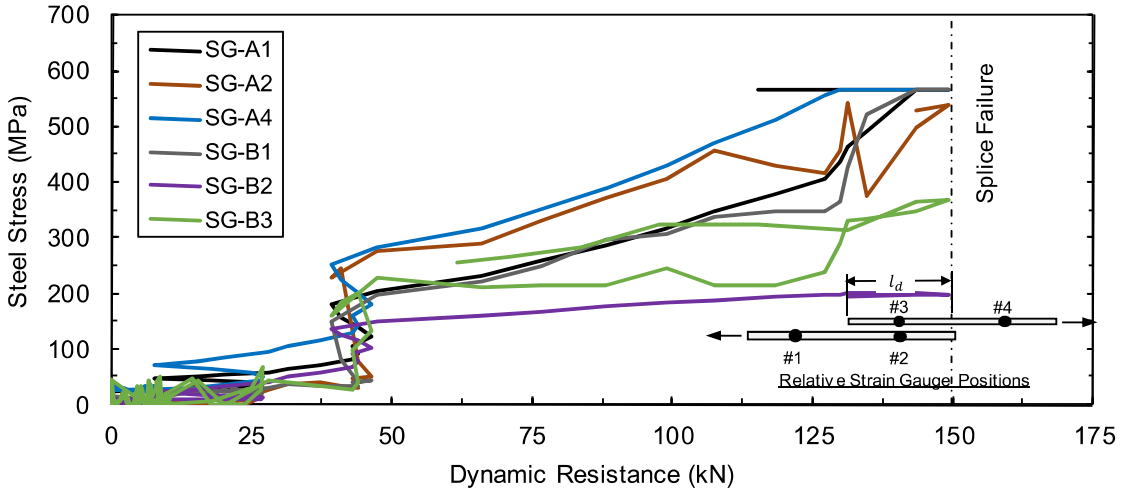

Figure B.128: Steel stress load-history plot for CP6-HSR.

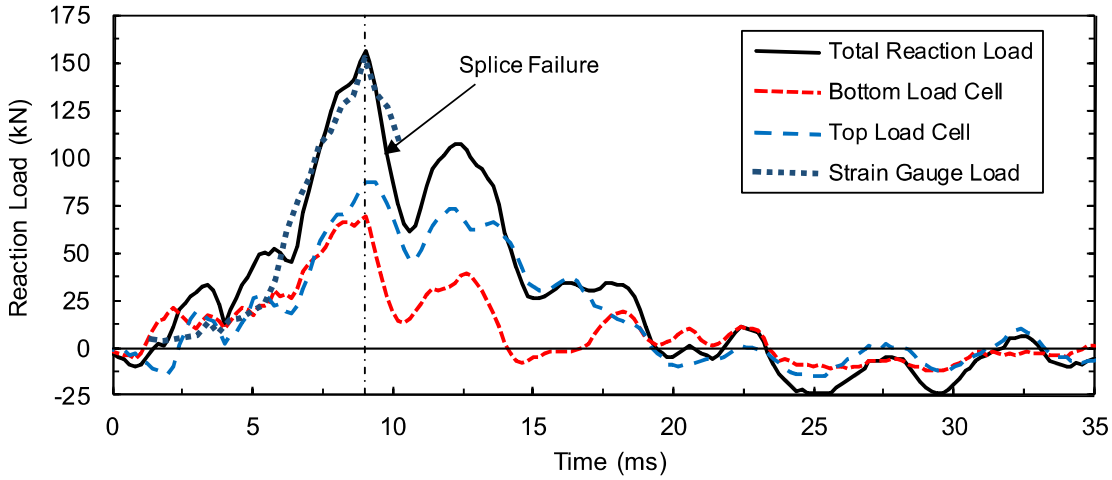

Figure B.129: Load time-history plot for CP6-HSR.

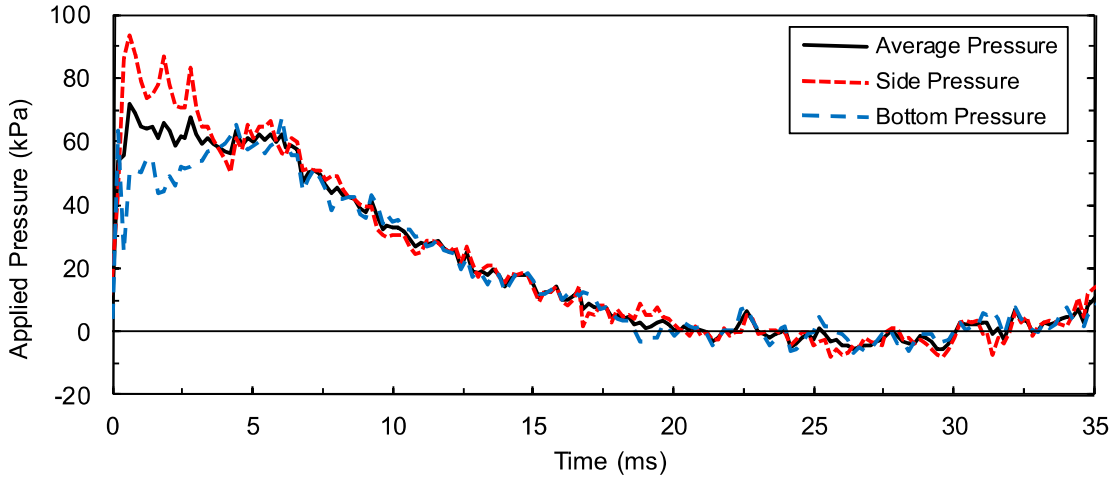

Figure B.130: Pressure time-history plot for CP6-HSR.

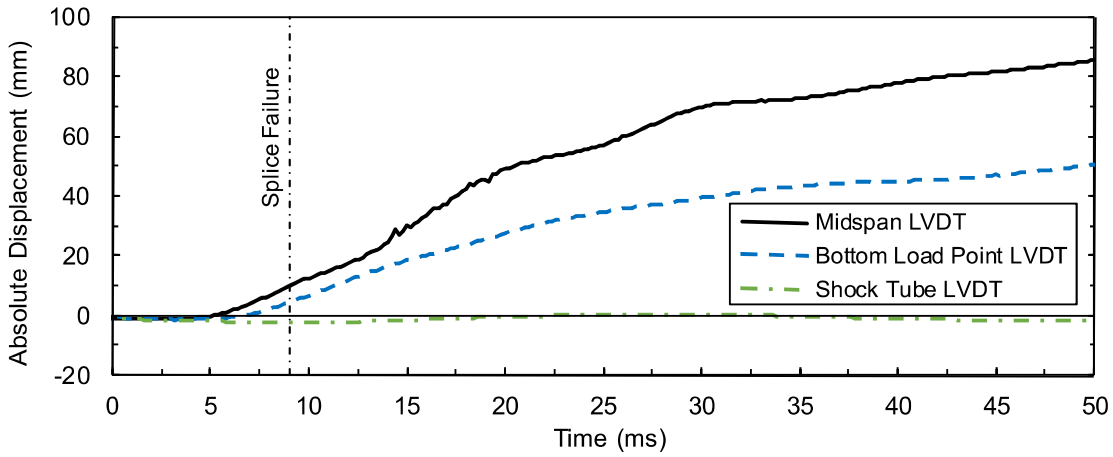

Figure B.131: Displacement time-history plot for CP6-HSR.

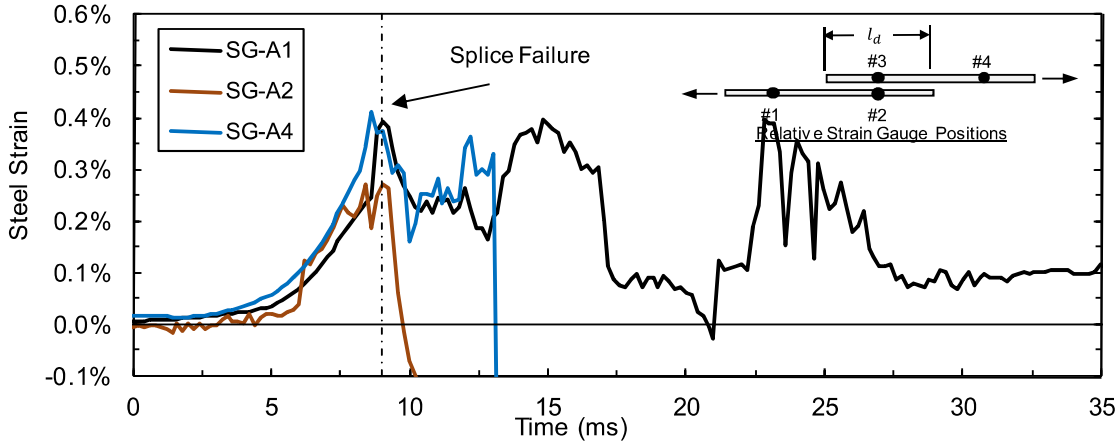

Figure B.132: Test bar "A" strain time-history plot for CP6-HSR.

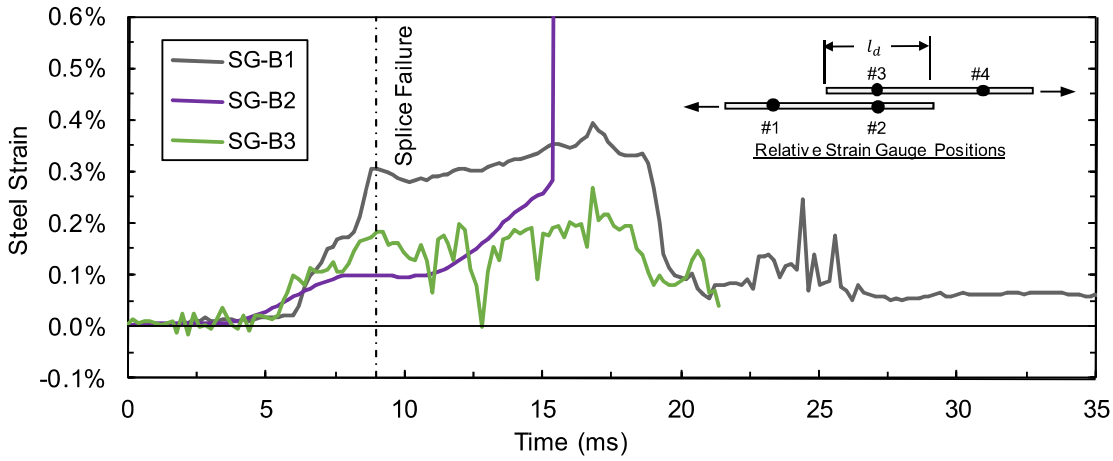

Figure B.133: Test bar "B" strain time-history plot for CP6-HSR.

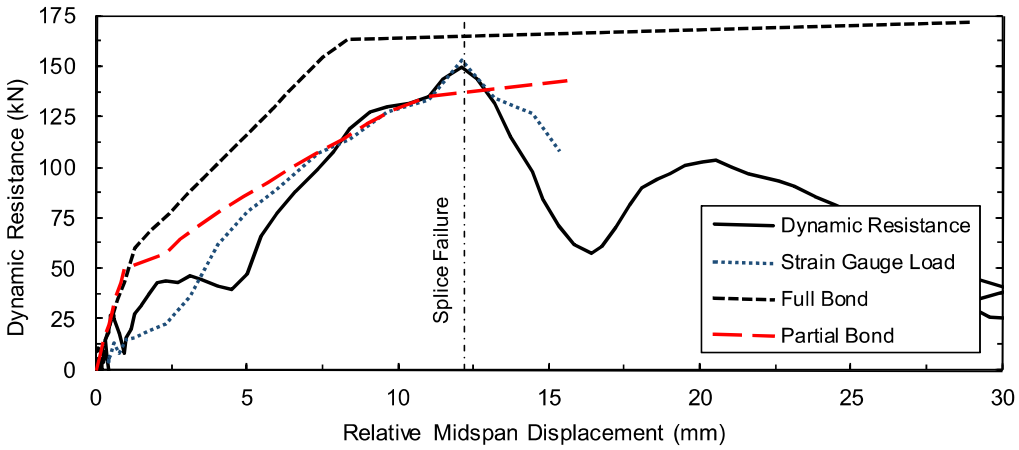

Figure B.134: Comparison of predicted and experimental resistance curves for CP6-HSR.

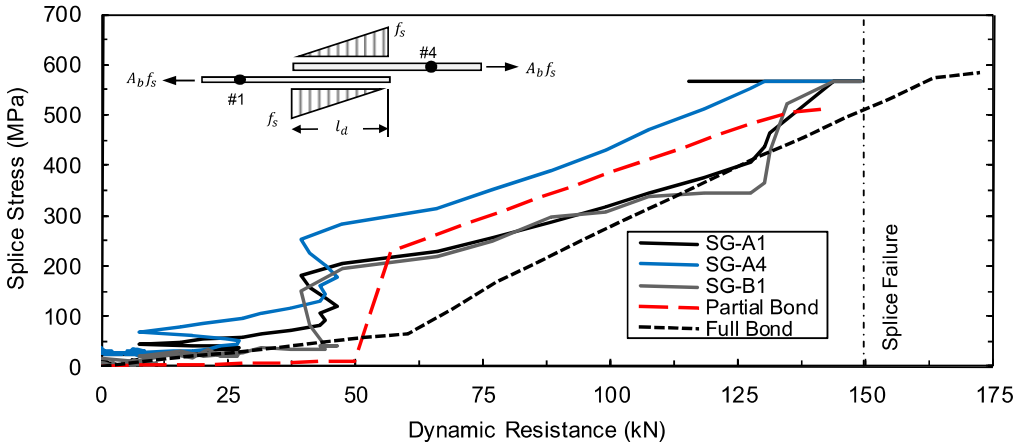

Figure B.135: Comparison of predicted and experimental steel stress developed in spliced reinforcement for CP6-HSR with respect to applied load.

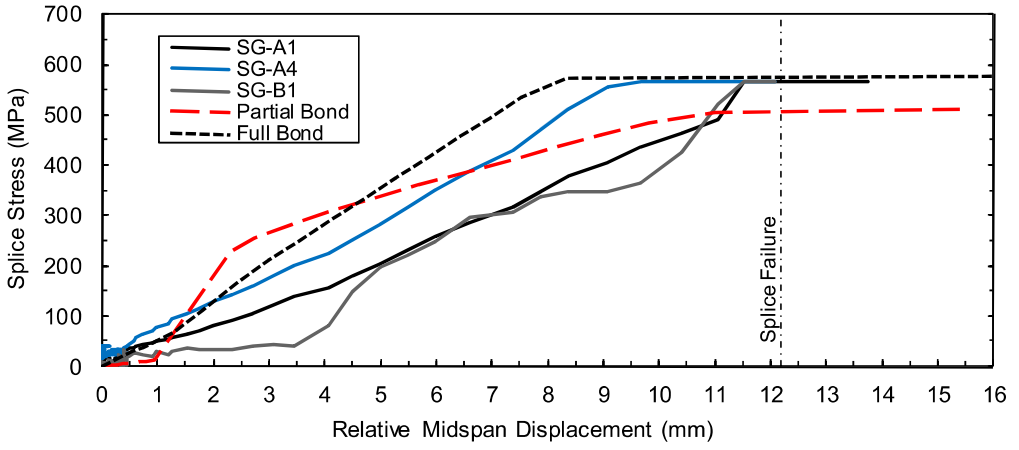

Figure B.136: Comparison of predicted and experimental steel stress developed in spliced reinforcement for CP6-HSR with respect to displacement.

(a) Before high strain rate testing (b) After high strain rate testing (c) After high strain rate testing

Figure B.137: Photographs of lap splice beam CP6-HSR.

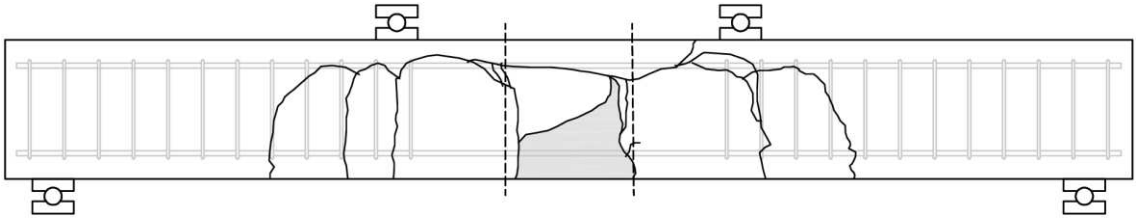

(a) Observed crack profile (north face)

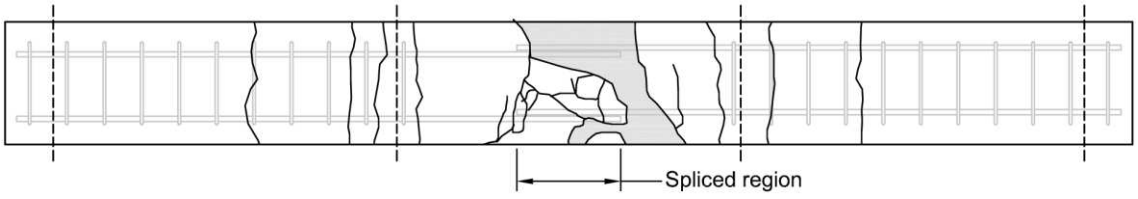

(b) Observed crack profile (bottom face)

Figure B.138: Observed crack profile for lap splice beam CP6-HSR

CP7-LSR

Lap splice beam CP7-LSR was subjected to low strain rate testing on September 25, 2013. CP7-LSR was designed with 20M reinforcement, 30 MPa concrete, 50 mm cover, and without transverse reinforcement in the spliced region. The specimen experienced a face-splitting tensile failure of the cover concrete with minimal cover loss. Failure occurred at an applied load of 182.4 kN. Based on strain readings, the stress developed in the spliced bars was 491 MPa. Based on a sectional analysis, the stress developed in the spliced bars was 491 MPa. Time-to-failure was 322.8 seconds and strain rate was 7.6×10^{-6} s^{-1}.

Table B.25: Geometry, reinforcing, and material properties for CP7-LSR.

b:	280 mm	Bar:	2-20M	f_c':	32.5 MPa
h:	300 mm	A_b:	300 mm^2	f_y:	491.0 MPa
l_d:	415 mm	d_b:	19.5 mm	ρ:	0.91%
c_b:	53 mm	N:	N/A	c/d:	2.7
c_{so}:	54 mm	A_{tr}:	N/A	$l_d(c_{min}+0.5d_b)$:	26041 mm^2

Table B.26: Summary of experimental test results for CP7-LSR.

Date:	Sept. 25, 2013	δ_f:	8.7 mm	f_s^t:	491 MPa
P_r:	N/A	R_f:	182.4 kN	f_s^{cal}:	491 MPa
I_r:	N/A	t_f:	322.8 s	$\dot{\varepsilon}$:	7.6×10^{-6} s^{-1}

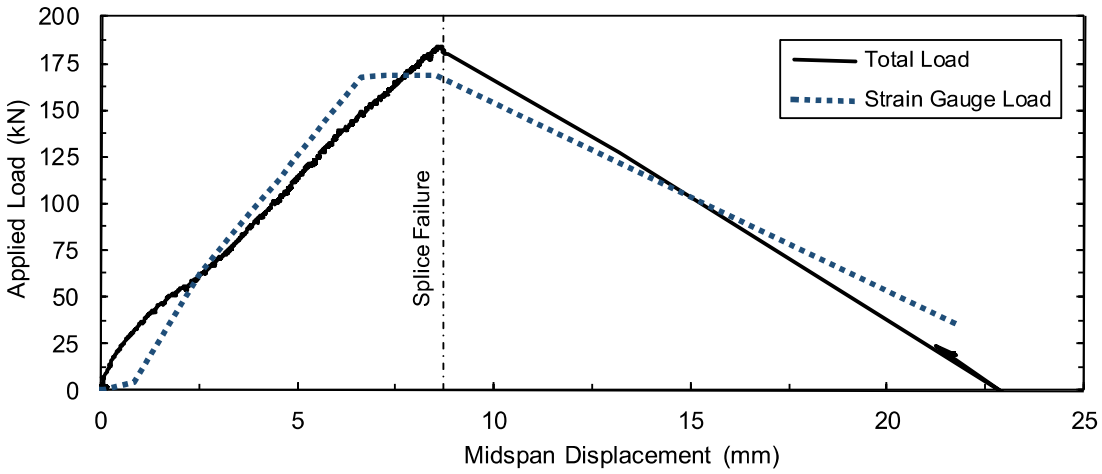

Figure B.139: Load displacement-history plot for CP7-LSR.

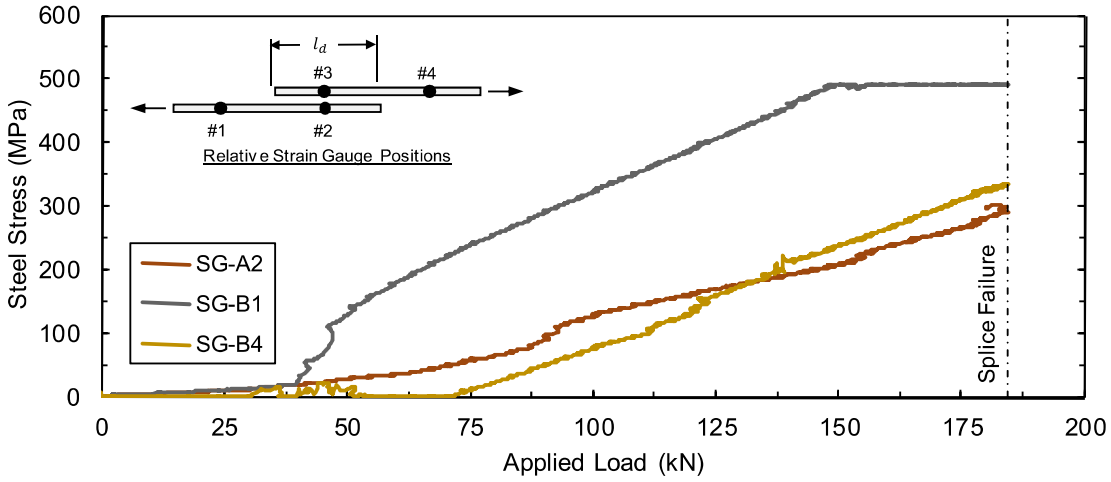

Figure B.140: Steel stress load-history plot for CP7-LSR.

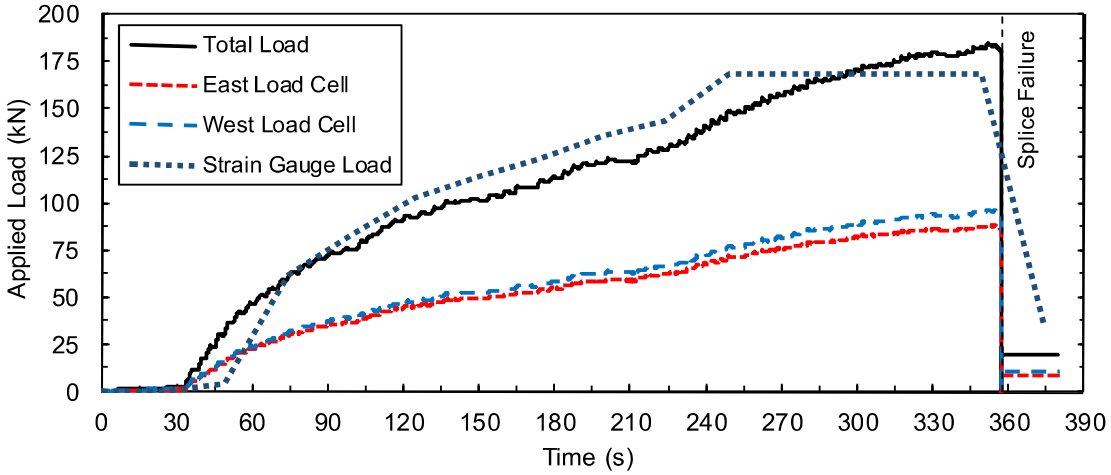

Figure B.141: Load time-history plot for CP7-LSR.

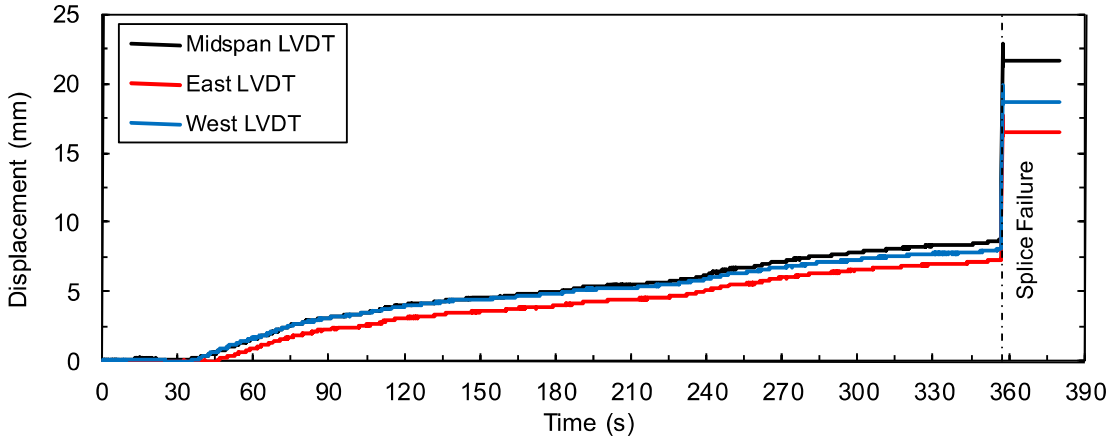

Figure B.142: Displacement time-history plot for CP7-LSR.

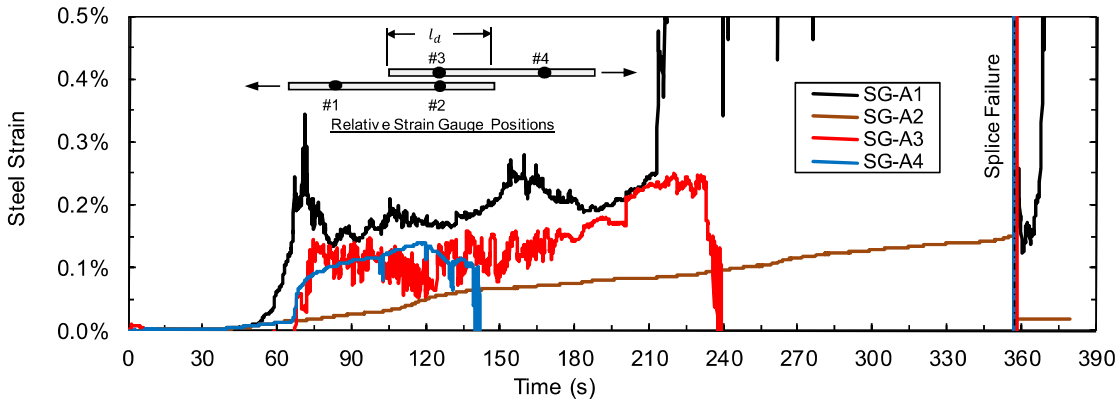

Figure B.143: Test bar "A" strain time-history plot for CP7-LSR.

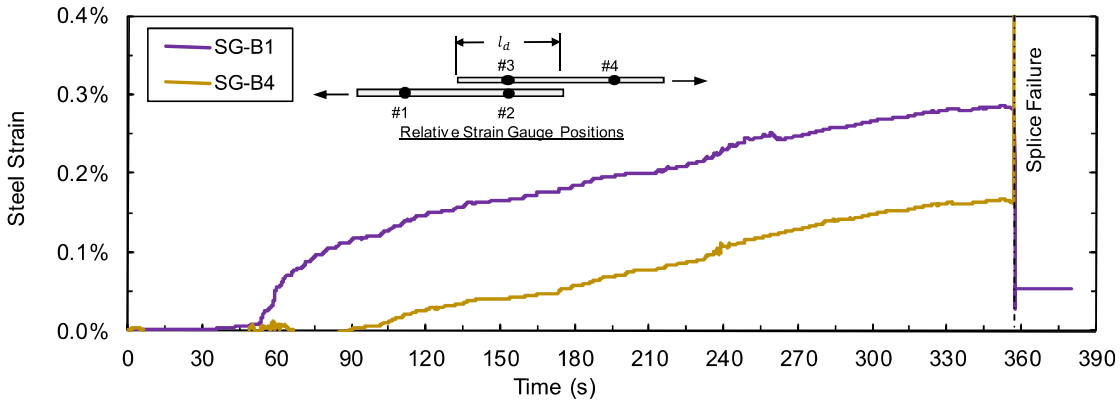

Figure B.144: Test bar "B" strain time-history plot for CP7-LSR.

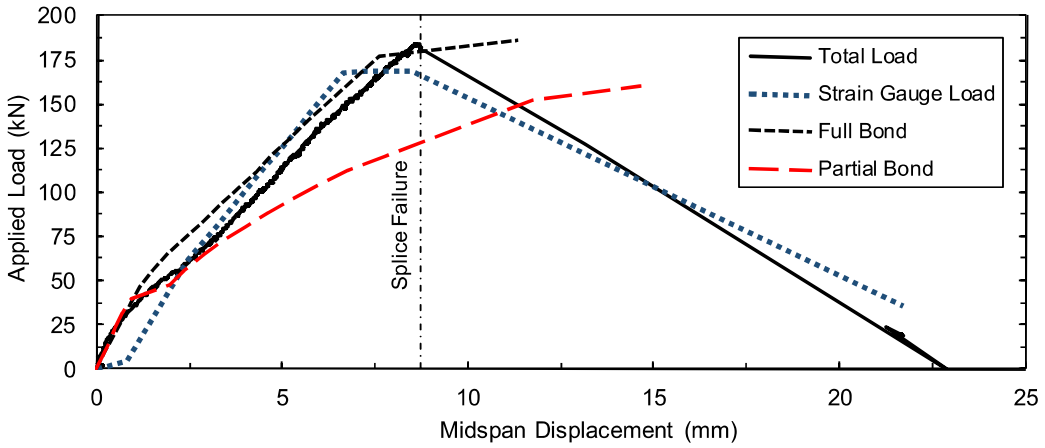

Figure B.145: Comparison of predicted and experimental resistance curves for CP7-LSR.

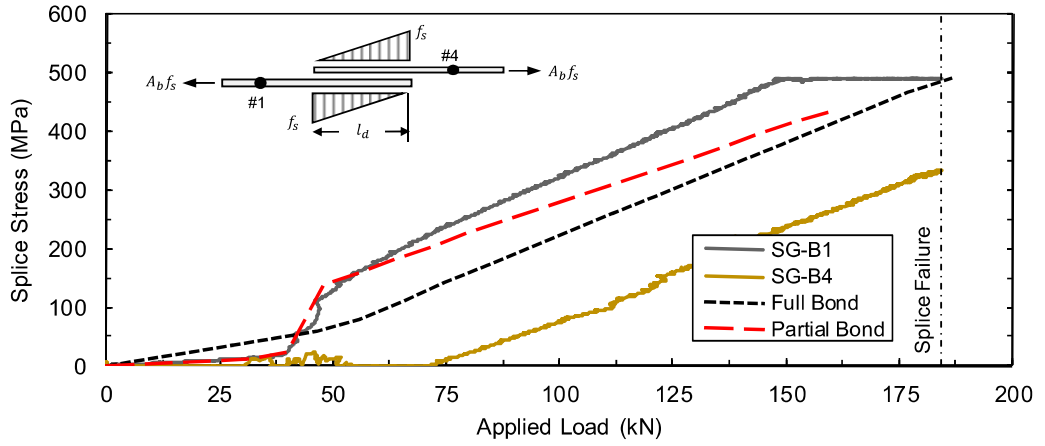

Figure B.146: Comparison of predicted and experimental steel stress developed in spliced reinforcement for CP7-LSR with respect to applied load.

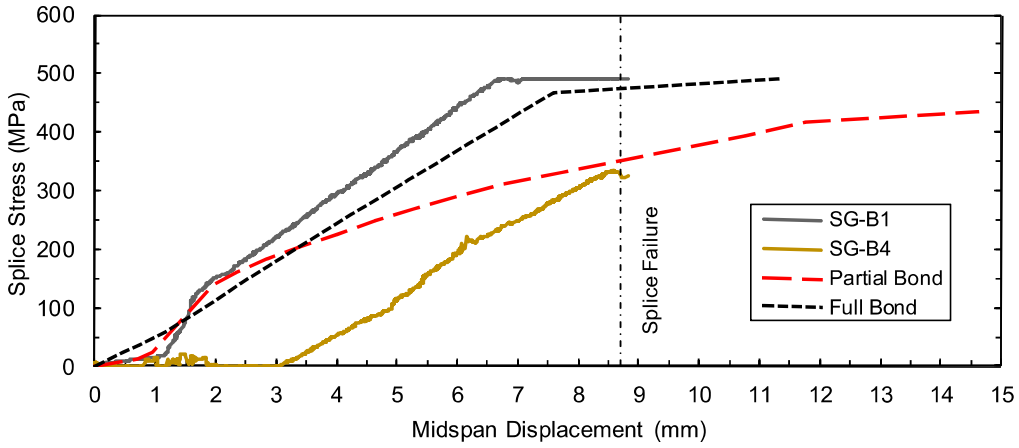

Figure B.147: Comparison of predicted and experimental steel stress developed in spliced reinforcement for CP7-LSR with respect to displacement.

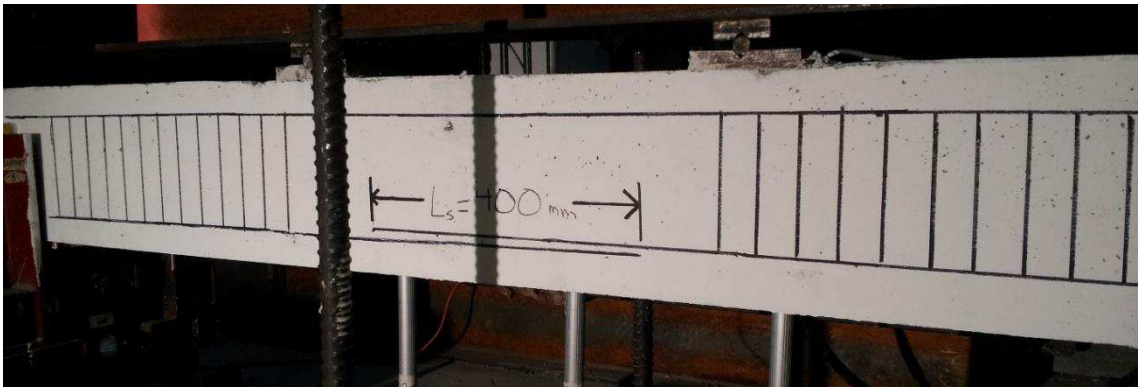

(a) Before low strain rate testing

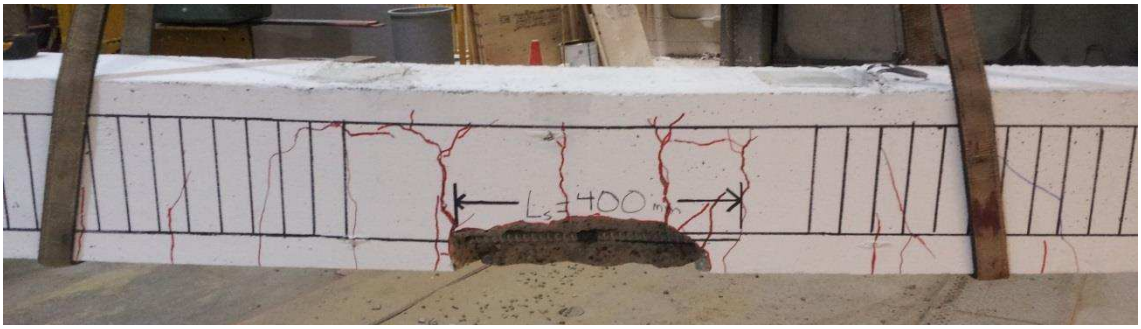

(b) After low strain rate testing

Figure B.148: Photographs of lap splice beam CP7-LSR.

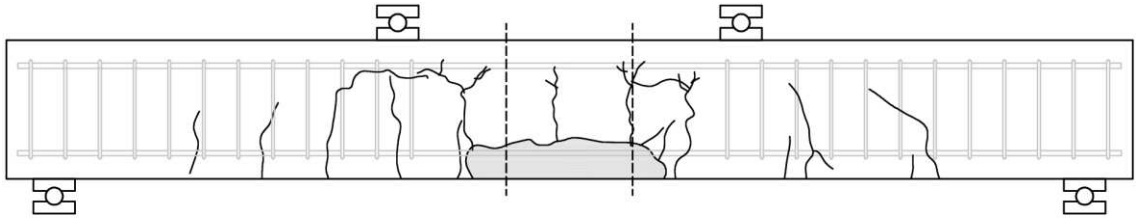

(a) Observed crack profile (north face)

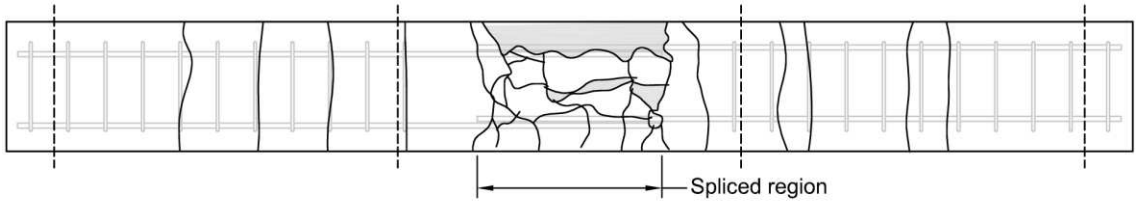

(b) Observed crack profile (bottom face)

Figure B.149: Observed crack profile for lap splice beam CP7-LSR.

CP7-HSR

Lap splice beam CP7-HSR was subjected to high strain rate testing on October 27, 2013. CP7-HSR was designed with 20M reinforcement, 30 MPa concrete, 50 mm cover, and without transverse reinforcement in the spliced region. The specimen experienced a side-splitting tensile failure of the cover concrete with significant cover loss. The peak dynamic resistance was 245.0 kN. Based on strain readings, the stress developed in the spliced bars was 600 MPa. Based on a sectional analysis, the stress developed in the spliced bars was 623 MPa. Time-to-failure was 12.7 ms and strain rate was 0.80 s^{-1}.

Table B.27: Geometry, reinforcing, and material properties for CP7-HSR.

b:	280 mm	Bar:	2-20M	f'_{dc}:	44.1 MPa
h:	300 mm	A_b:	300 mm^2	f_{dy}:	622.3 MPa
l_d:	397 mm	d_b:	19.5 mm	ρ:	0.91%
c_b:	52 mm	N:	N/A	c/d:	2.7
c_{so}:	55 mm	A_{tr}:	N/A	$l_d(c_{min} + 0.5d_b)$:	24515 mm^2

Table B.28: Summary of experimental test results for CP7-HSR.

Date:	Oct. 27, 2013	δ_f:	20.3 mm	f_s^t:	600 MPa
P_r:	100.0 kPa	R_f:	245.0 kN	f_s^{cal}:	623 MPa
I_r:	747.0 kPa-ms	t_f:	12.7 ms	$\dot{\varepsilon}$:	0.80 s^{-1}

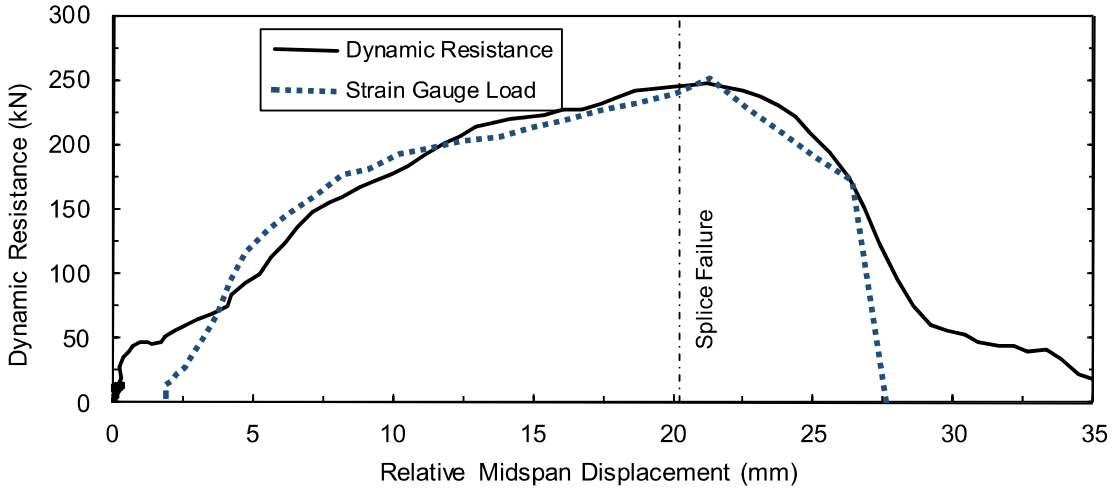

Figure B.150: Load displacement-history plot for CP7-HSR.

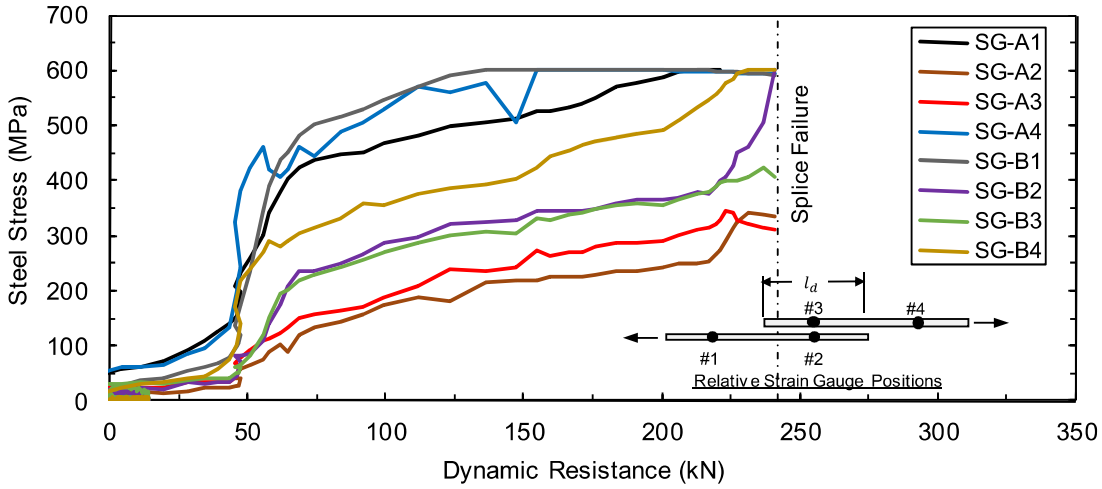

Figure B.151: Steel stress load-history plot for CP7-HSR.

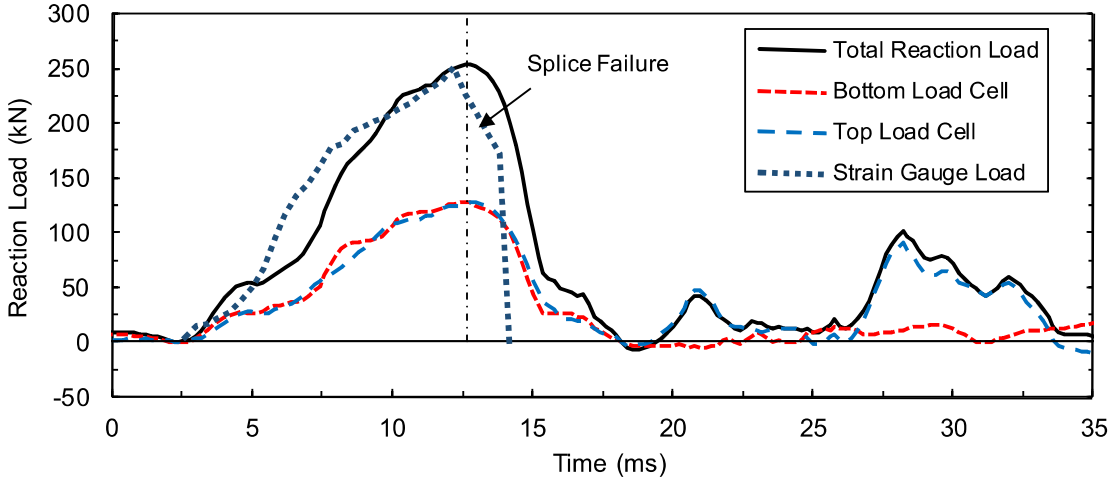

Figure B.152: Load time-history plot for CP7-HSR.

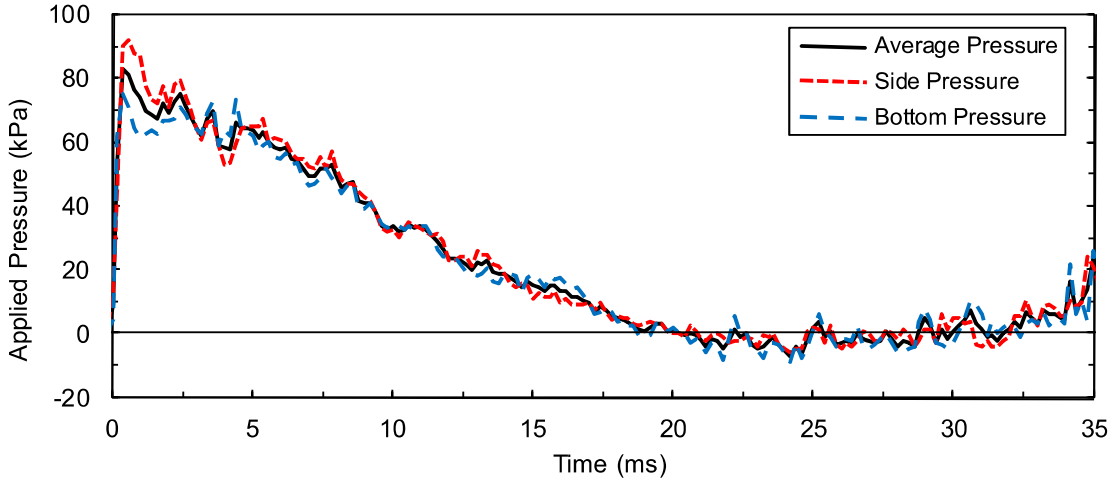

Figure B.153: Pressure time-history plot for CP7-HSR.

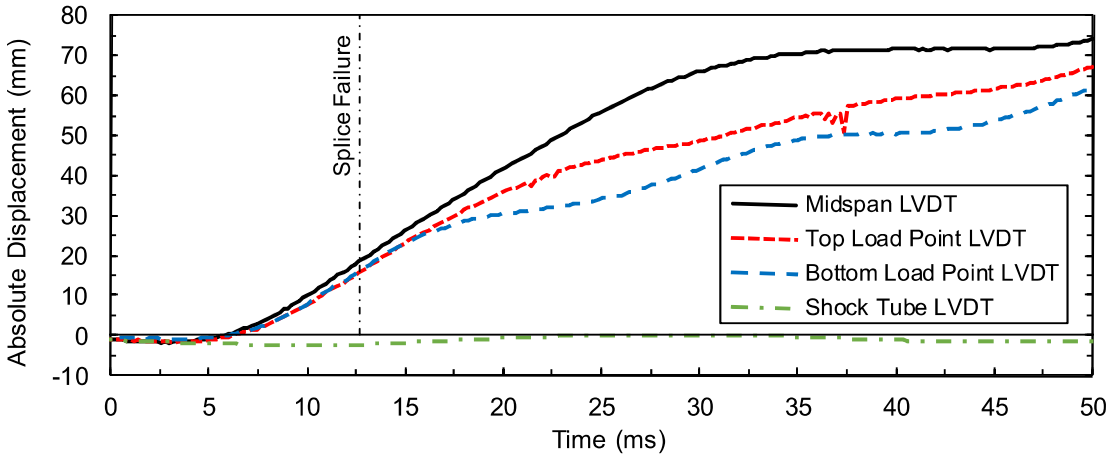

Figure B.154: Displacement time-history plot for CP7-HSR.

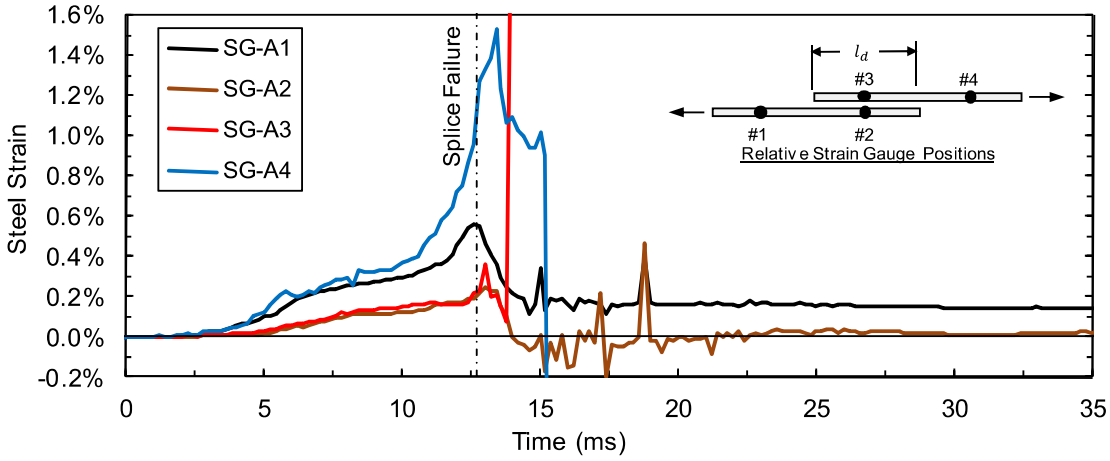

Figure B.155: Test bar "A" strain time-history plot for CP7-HSR.

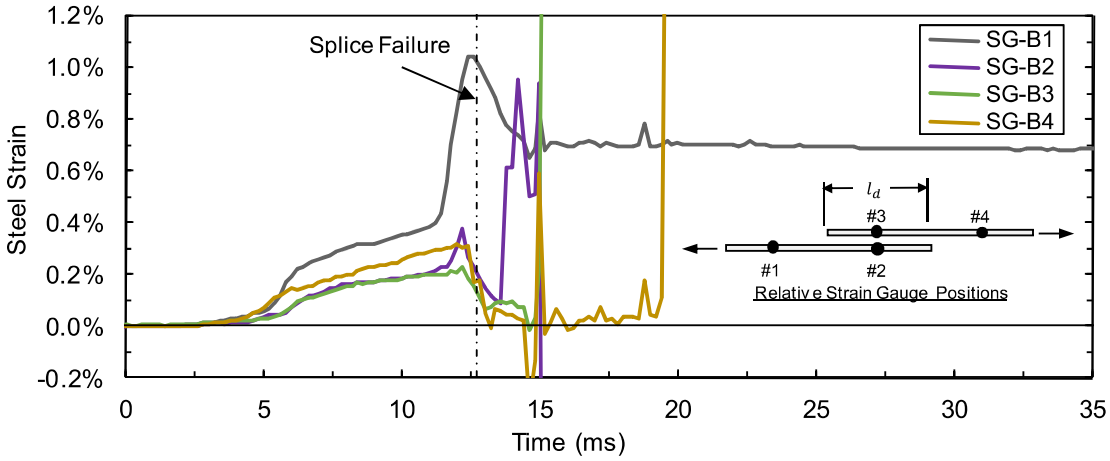

Figure B.156: Test bar "B" strain time-history plot for CP7-HSR.

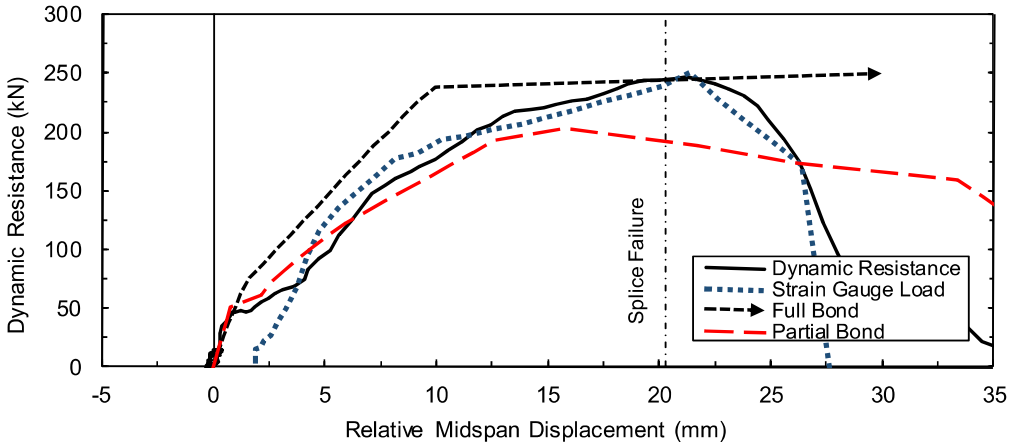

Figure B.157: Comparison of predicted and experimental resistance curves for CP7-HSR.

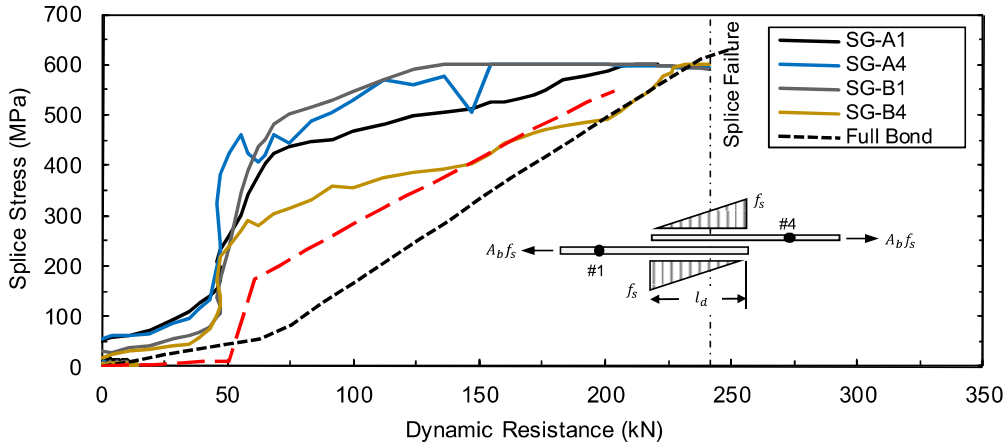

Figure B.158: Comparison of predicted and experimental steel stress developed in spliced reinforcement for CP7-HSR with respect to applied load.

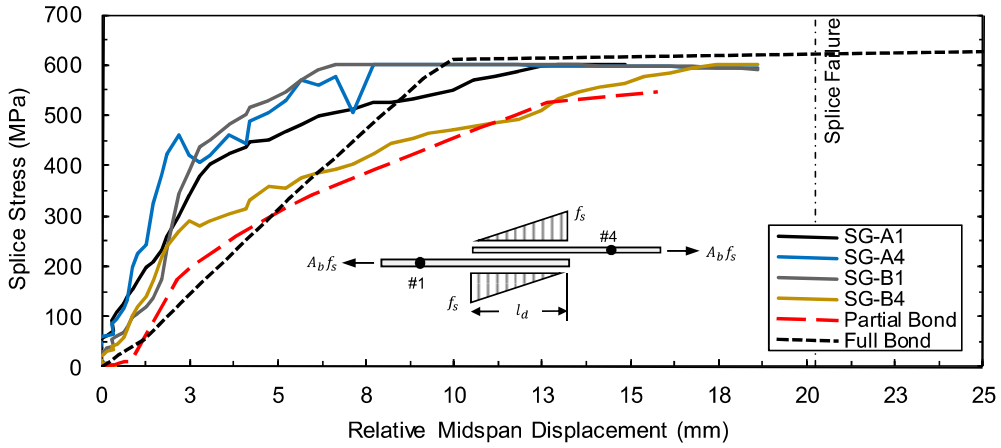

Figure B.159: Comparison of predicted and experimental steel stress developed in spliced reinforcement for CP7-HSR with respect to displacement.

(a) Before high strain rate testing (b) After high strain rate testing (c) After high strain rate testing

Figure B.160: Photographs of lap splice beam CP7-HSR.

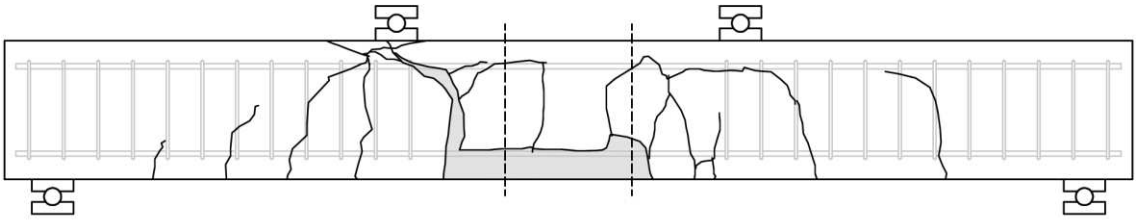

(a) Observed crack profile (north face)

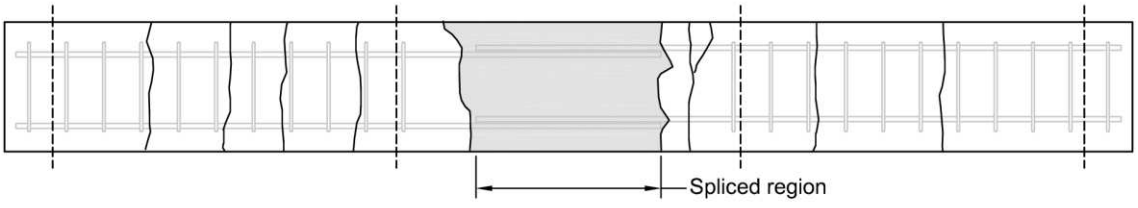

(b) Observed crack profile (bottom face)

Figure B.161: Observed crack profile for lap splice beam CP7-HSR.

CP8-LSR

Lap splice beam CP8-LSR was subjected to low strain rate testing on September 24, 2013. CP8-LSR was designed with 20M reinforcement, 50 MPa concrete, 50 mm cover, and without transverse reinforcement in the spliced region. The specimen experienced a combined side- and face-splitting tensile failure of the cover concrete with negligible cover loss. Failure occurred at an applied load of 185.5 kN. Based on strain readings, the stress developed in the spliced bars was 491 MPa. Based on a sectional analysis, the stress developed in the spliced bars was 491 MPa. Time-to-failure was 570 seconds and strain rate was 4.3×10^{-6} s^{-1}.

Table B.29: Geometry, reinforcing, and material properties for CP8-LSR.

b:	280 mm	Bar:	2-20M	f_c':	48.7 MPa
h:	300 mm	A_b:	300 mm^2	f_y:	491.0 MPa
l_d:	360 mm	d_b:	19.5 mm	ρ:	0.91%
c_b:	53 mm	N:	N/A	c/d:	2.7
c_{so}:	54 mm	A_{tr}:	N/A	$l_d(c_{min}+0.5d_b)$:	22590 mm^2

Table B.30: Summary of experimental test results for CP8-LSR.

Date:	Sept. 24, 2013	δ_f:	10.1 mm	f_s^t:	491 MPa
P_r:	N/A	R_f:	185.5 kN	f_s^{cal}:	491 MPa
I_r:	N/A	t_f:	570 s	$\dot{\varepsilon}$:	4.3×10^{-6} s^{-1}

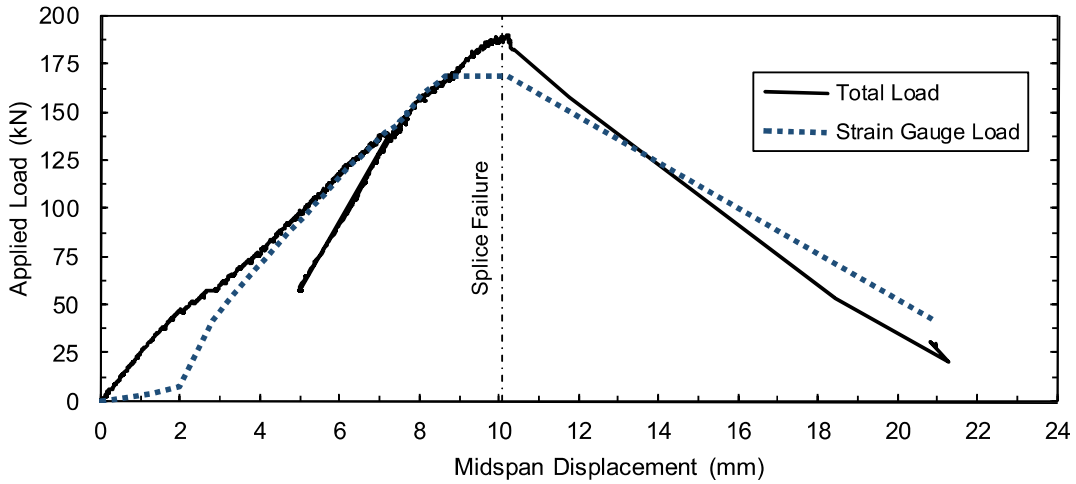

Figure B.162: Load displacement-history plot for CP8-LSR.

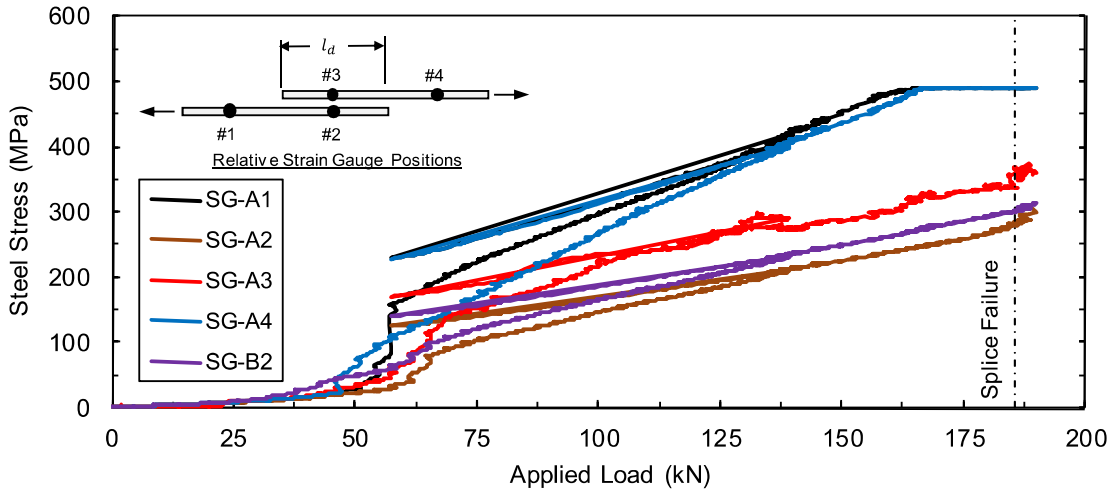

Figure B.163: Steel stress load-history plot for CP8-LSR.

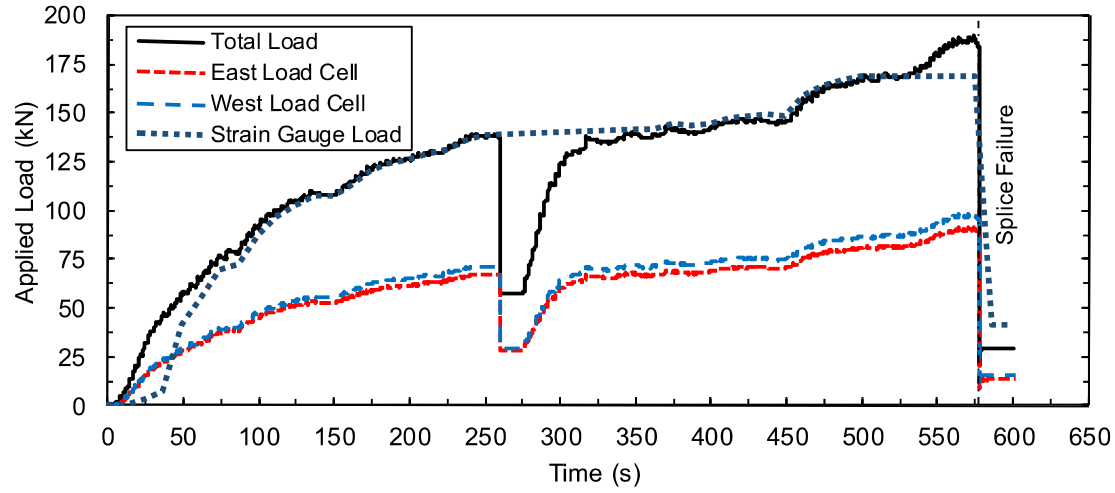

Figure B.164: Load time-history plot for CP8-LSR.

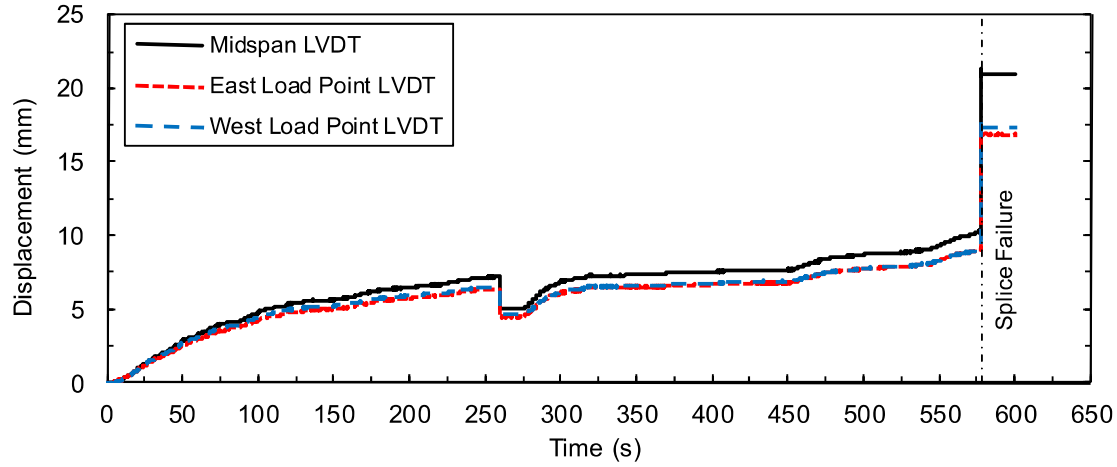

Figure B.165: Displacement time-history plot for CP8-LSR.

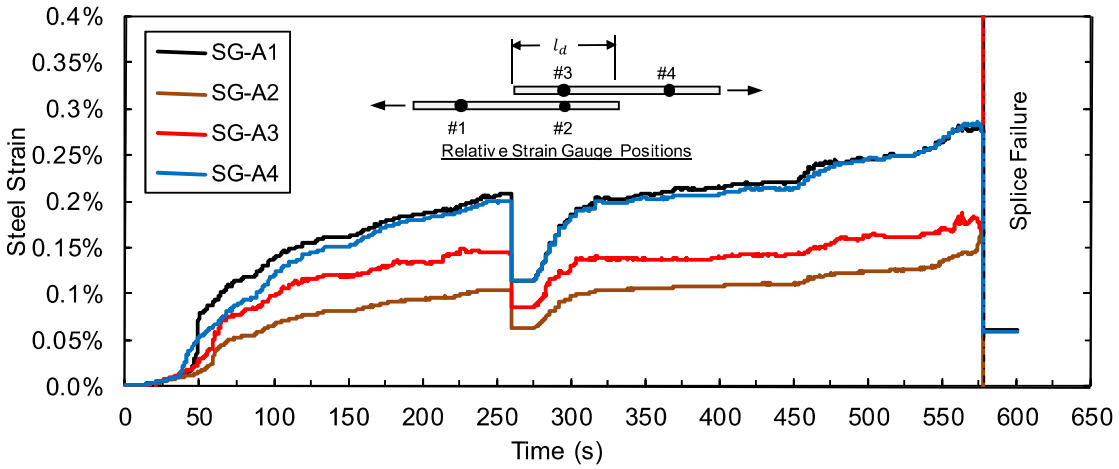

Figure B.166: Test bar "A" strain time-history plot for CP8-LSR.

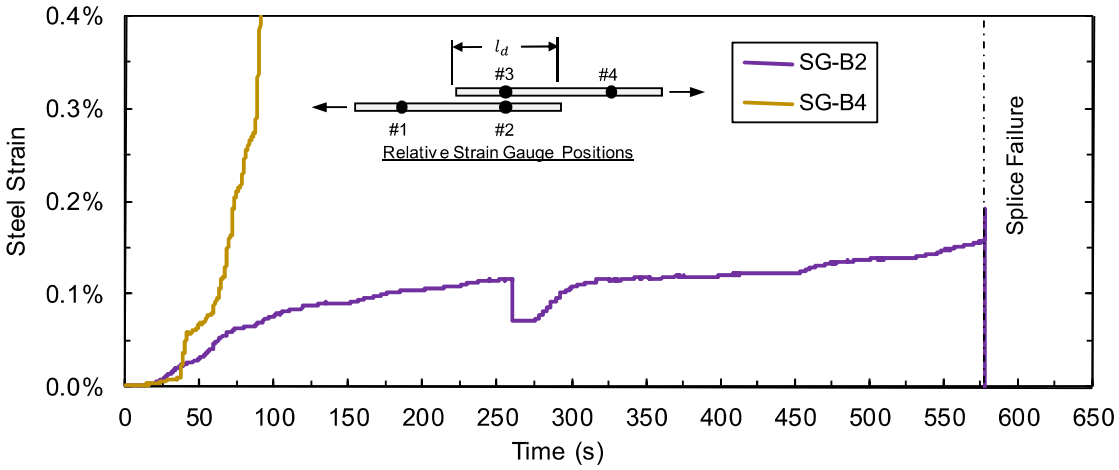

Figure B.167: Test bar "B" strain time-history plot for CP8-LSR.

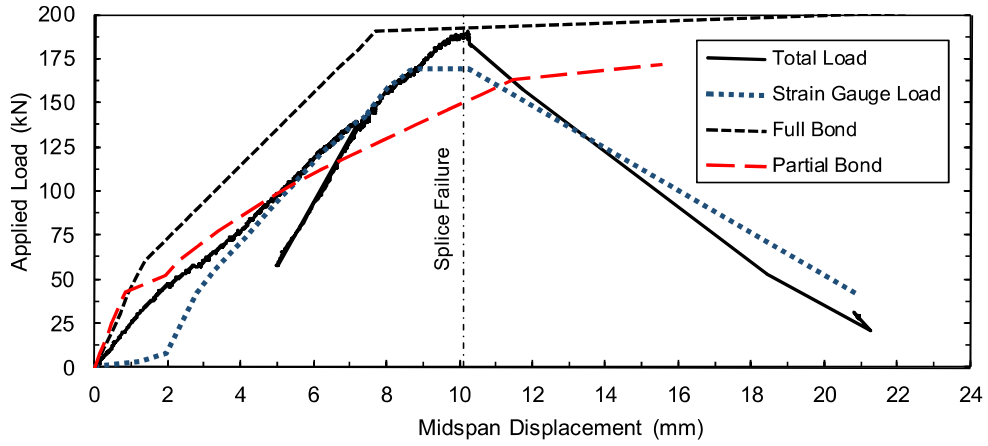

Figure B.168: Comparison of predicted and experimental resistance curves for CP8-LSR.

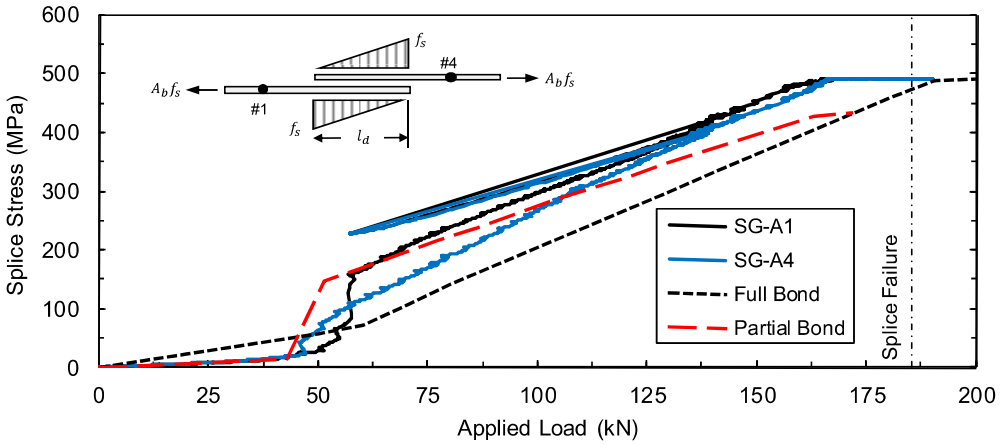

Figure B.169: Comparison of predicted and experimental steel stress developed in spliced reinforcement for CP8-LSR with respect to applied load.

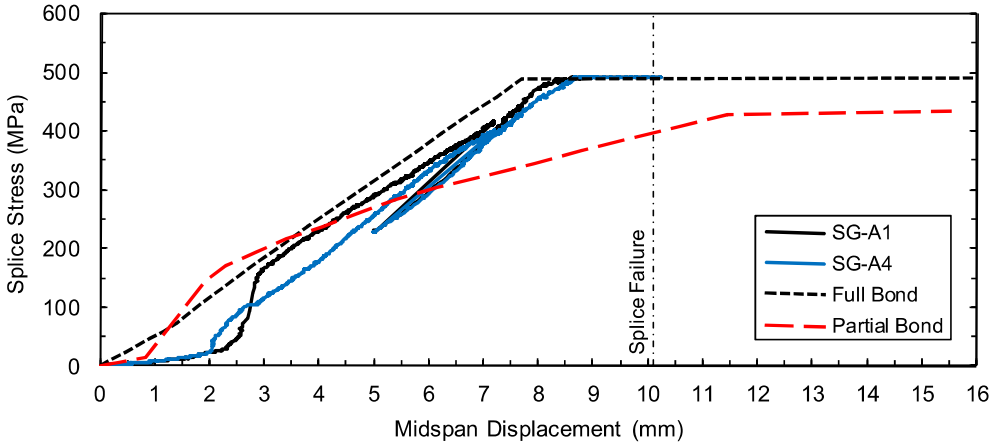

Figure B.170: Comparison of predicted and experimental steel stress developed in spliced reinforcement for CP8-LSR with respect to displacement.

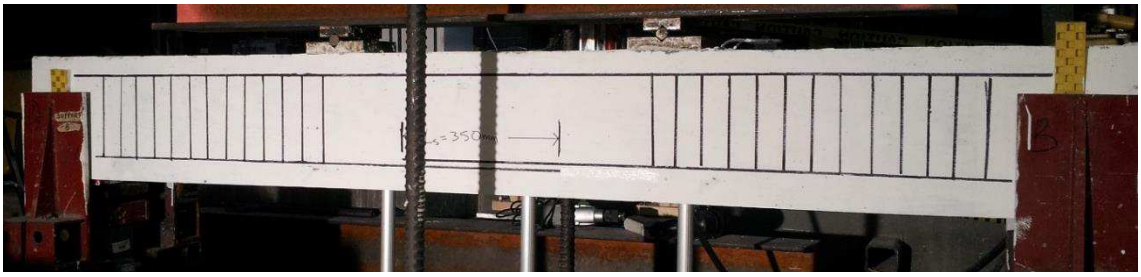

(a) Before low strain rate testing

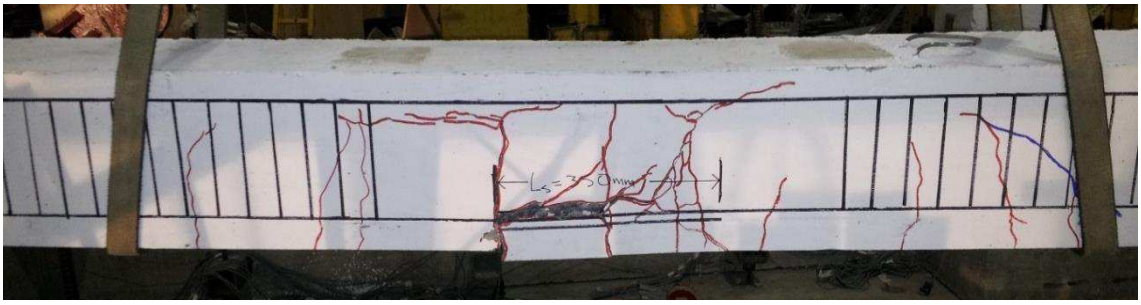

(b) After low strain rate testing

Figure B.171: Photographs of lap splice beam CP1-LSR.

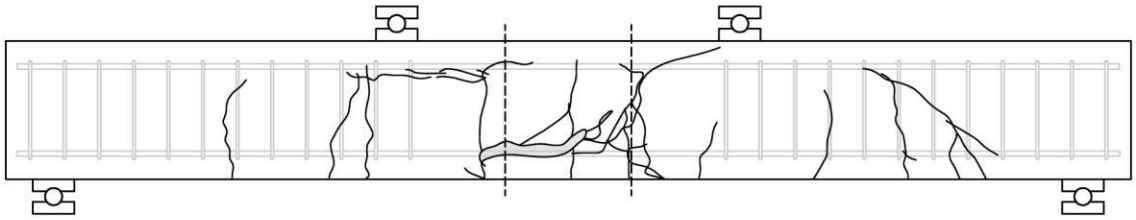

(a) Observed crack profile (north face)

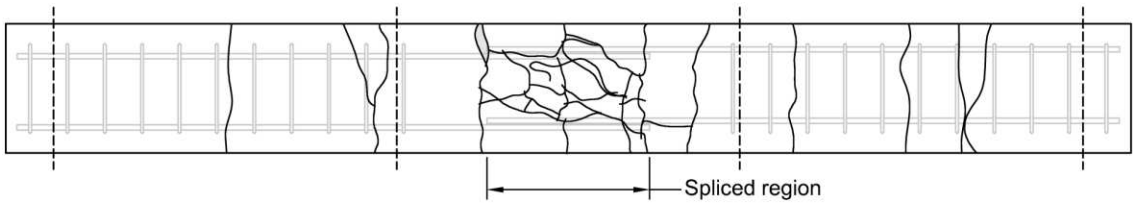

(b) Observed crack profile (bottom face)

Figure B.172: Observed crack profile for lap splice beam CP8-LSR.

CP8-HSR

Lap splice beam CP8-HSR was subjected to high strain rate testing on October 27, 2013. CP8-HSR was designed with 20M reinforcement, 50 MPa concrete, 50 mm cover, and without transverse reinforcement in the spliced region. The specimen experienced the onset of a face-splitting tensile failure of the cover concrete with negligible cover loss. The peak dynamic resistance was 244.0 kN. Based on strain readings, the stress developed in the spliced bars was 595 MPa. Based on a sectional analysis, the stress developed in the spliced bars was 604 MPa. Time-to-failure was 14.0 ms and strain rate was 0.75 s^{-1}.

Table B.31: Geometry, reinforcing, and material properties for CP8-HSR.

b:	200 mm	Bar:	2-20M	f_c':	60.2 MPa
h:	300 mm	A_b:	300 mm^2	f_y:	622.3 MPa
l_d:	361 mm	d_b:	19.5 mm	ρ:	0.91%
c_b:	51 mm	N:	N/A	c/d:	2.7
c_{so}:	53 mm	A_{tr}:	N/A	$l_d(c_{min} + 0.5d_b)$:	21931 mm^2

Table B.32: Summary of experimental test results for CP8-HSR.

Date:	Sept. 23, 2013	δ_f:	20.0 mm	f_s^t:	595 MPa
P_r:	87.0 kPa	R_f:	244.0 kN	f_s^{cal}:	604 MPa
I_r:	671.0 kPa-ms	t_f:	14.0 ms	$\dot{\varepsilon}$:	0.75 s^{-1}

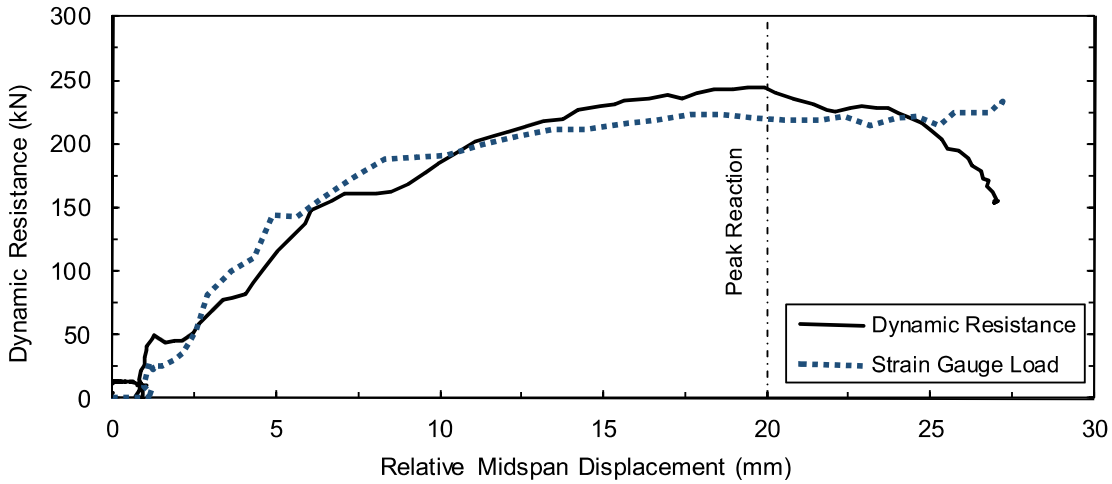

Figure B.173: Load displacement-history plot for CP8-HSR.

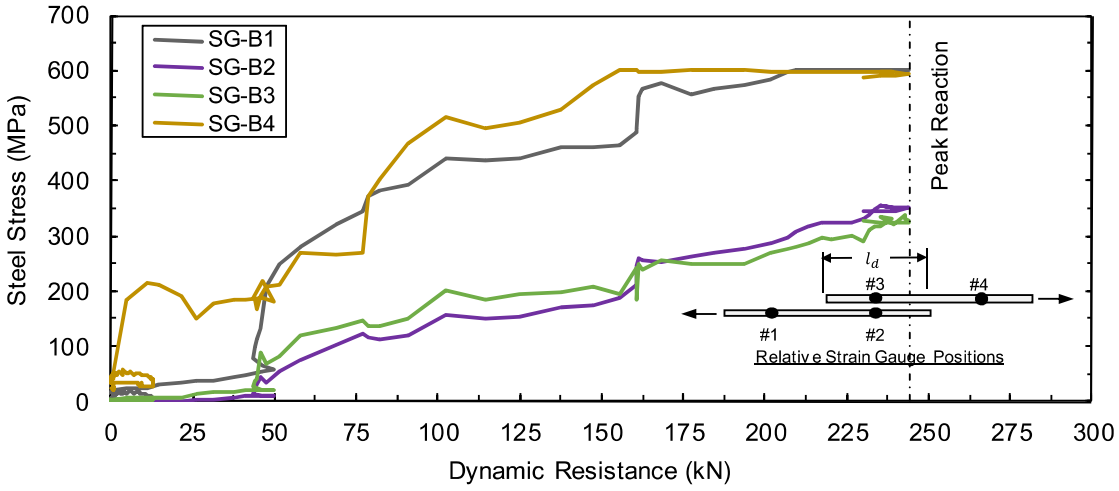

Figure B.174: Steel stress load-history plot for CP8-HSR.

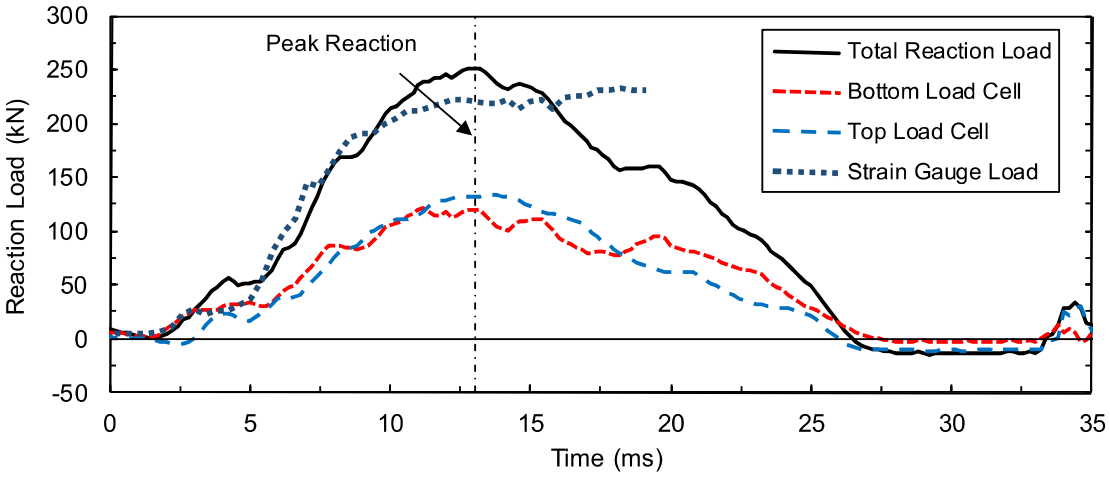

Figure B.175: Load time-history plot for CP8-HSR.

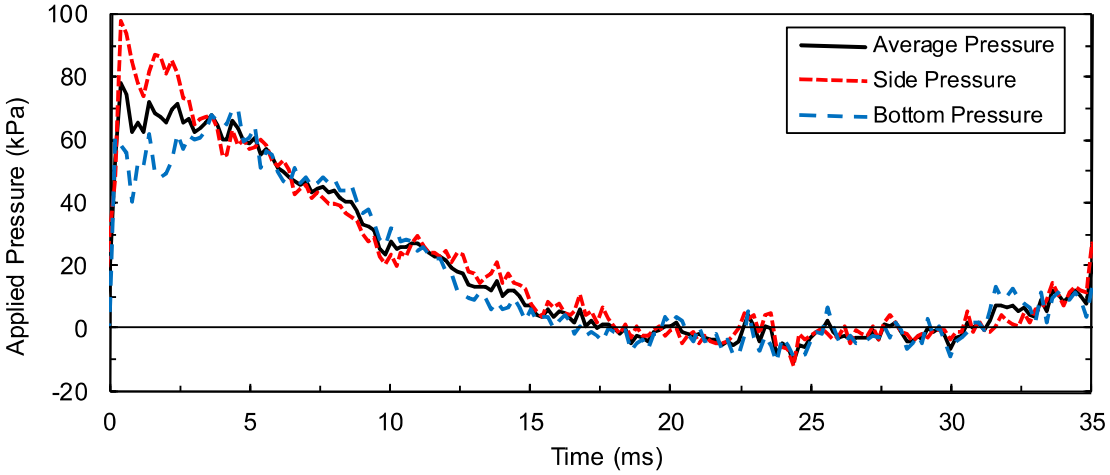

Figure B.176: Pressure time-history plot for CP8-HSR.

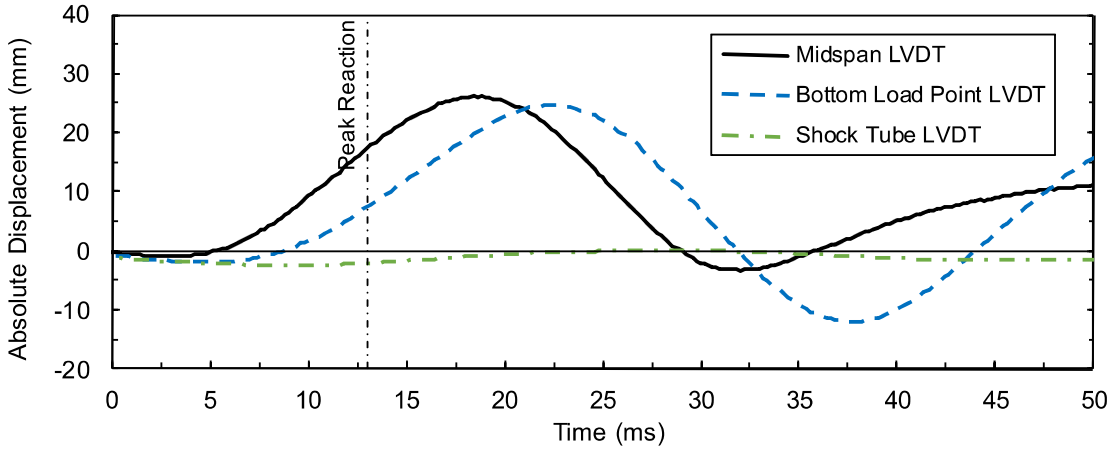

Figure B.177: Displacement time-history plot for CP8-HSR.

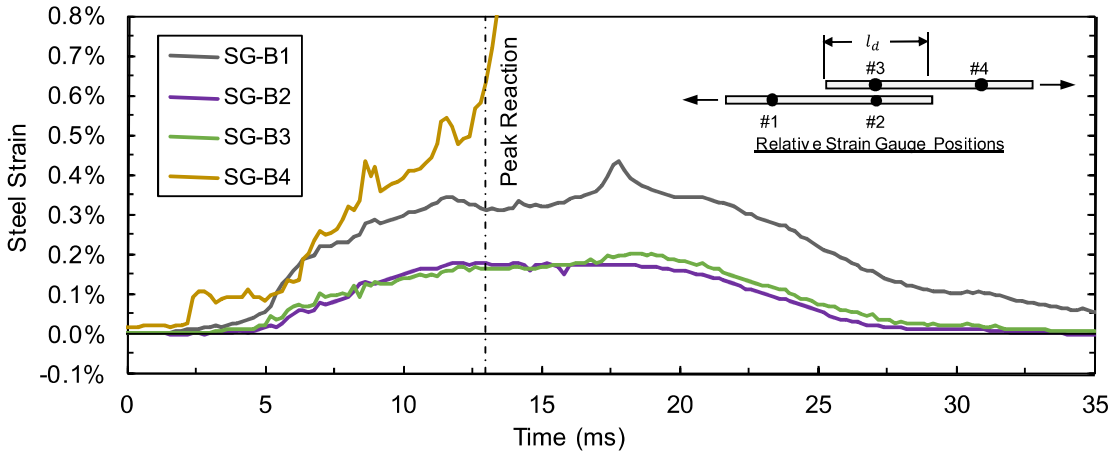

Figure B.178: Test bar "B" strain time-history plot for CP8-HSR.

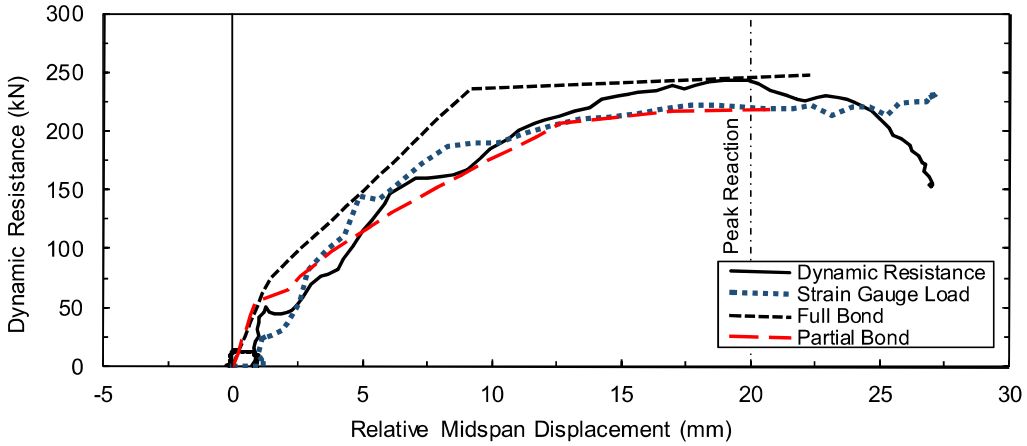

Figure B.179: Comparison of predicted and experimental resistance curves for CP8-HSR.

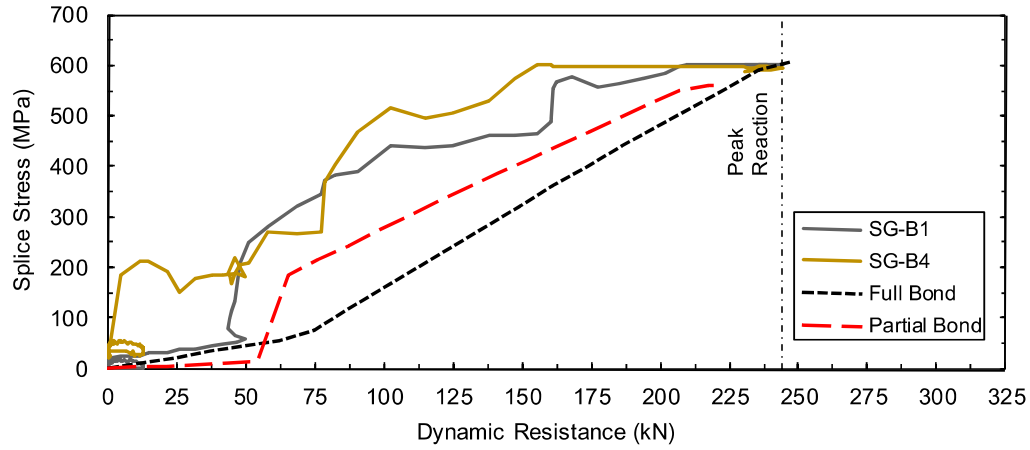

Figure B.180: Comparison of predicted and experimental steel stress developed in spliced reinforcement for CP8-HSR with respect to applied load.

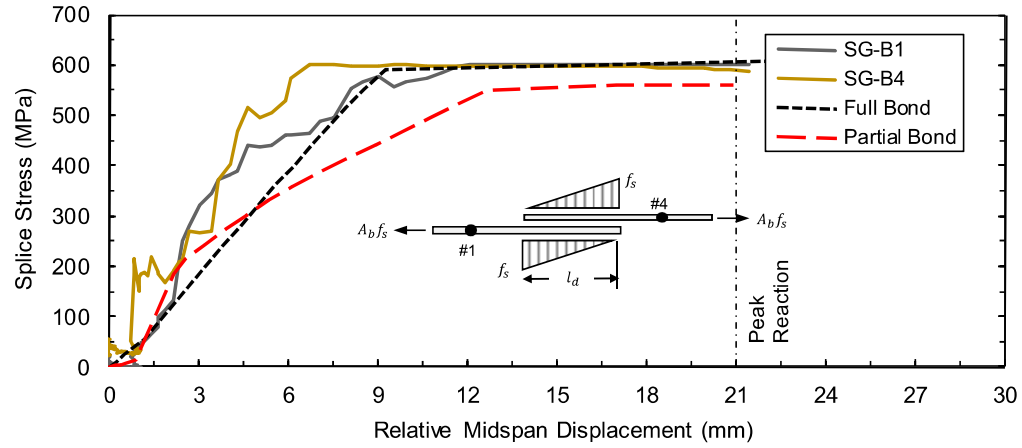

Figure B.181: Comparison of predicted and experimental steel stress developed in spliced reinforcement for CP8-HSR with respect to displacement.

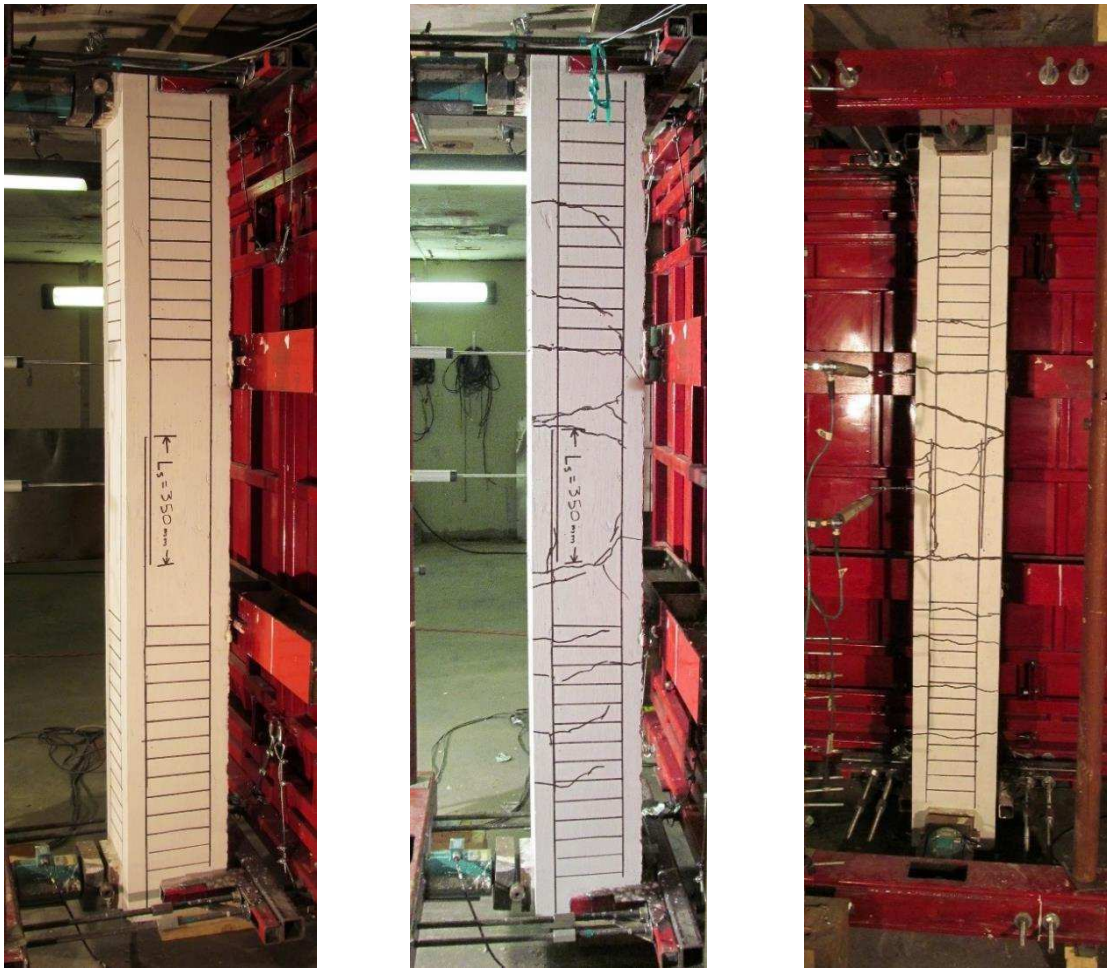

(a) Before high strain rate testing (b) After high strain rate testing (c) After high strain rate testing

Figure B.182: Photographs of lap splice beam CP8-HSR.

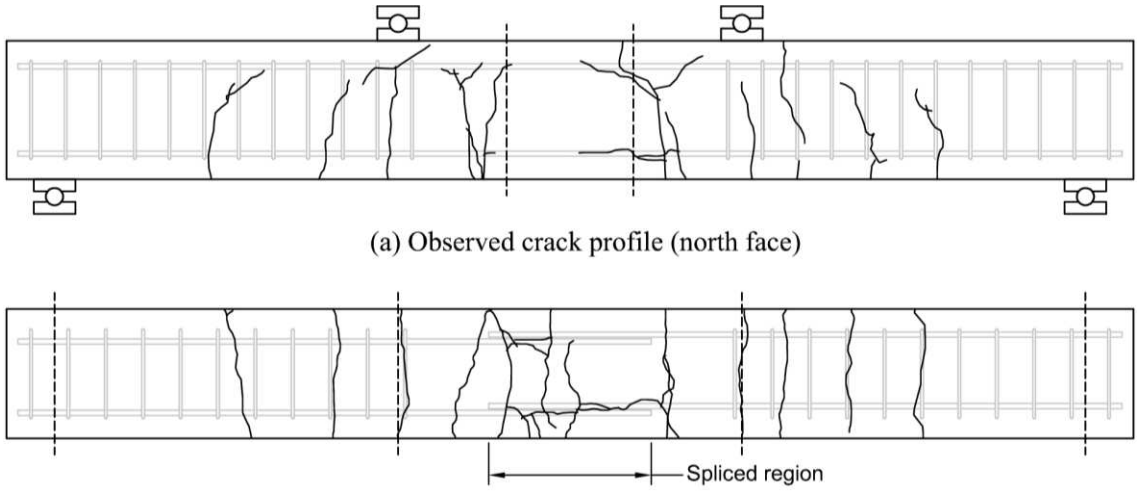

(a) Observed crack profile (north face)

(b) Observed crack profile (bottom face)

Figure B.183: Observed crack profile for lap splice beam CP8-HSR.

CP9-LSR

Lap splice beam CP9-LSR was subjected to low strain rate testing on August 19, 2014. CP9-LSR was designed with 15M reinforcement, 30 MPa concrete, 25 mm cover, and 6-ϕ6.3 mm smooth double leg closed stirrups confining the spliced region. The specimen experienced a combined side- and face-splitting tensile failure of the cover concrete with negligible cover loss. Failure occurred at an applied load of 109.2 kN. Based on strain readings, the stress developed in the spliced bars was 391 MPa. Based on a sectional analysis, the stress developed in the spliced bars was 426 MPa. Time-to-failure was 147.6 seconds and strain rate was 1.3×10^{-5} s^{-1}.

Table B.33: Geometry, reinforcing, and material properties for CP9-LSR.

b:	165 mm	Bar:	2-15M	f_c':	36.9 MPa
h:	300 mm	A_b:	200 mm^2	f_y:	448.4 MPa
l_d:	325 mm	d_b:	16.0 mm	ρ:	0.91%
c_b:	25 mm	N:	6	c/d:	1.7
c_{so}:	28 mm	A_{tr}:	2×31.1 mm^2	$l_d(c_{min}+0.5d_b)$:	10725 mm^2

Table B.34: Summary of experimental test results for CP9-LSR.

Date:	Oct. 19, 2014	δ_f:	9.5 mm	f_s^t:	391 MPa
P_r:	N/A	R_f:	109.2 kN	f_s^{cal}:	426 MPa
I_r:	N/A	t_f:	147.6 s	$\dot{\varepsilon}$:	1.3×10^{-5} s^{-1}

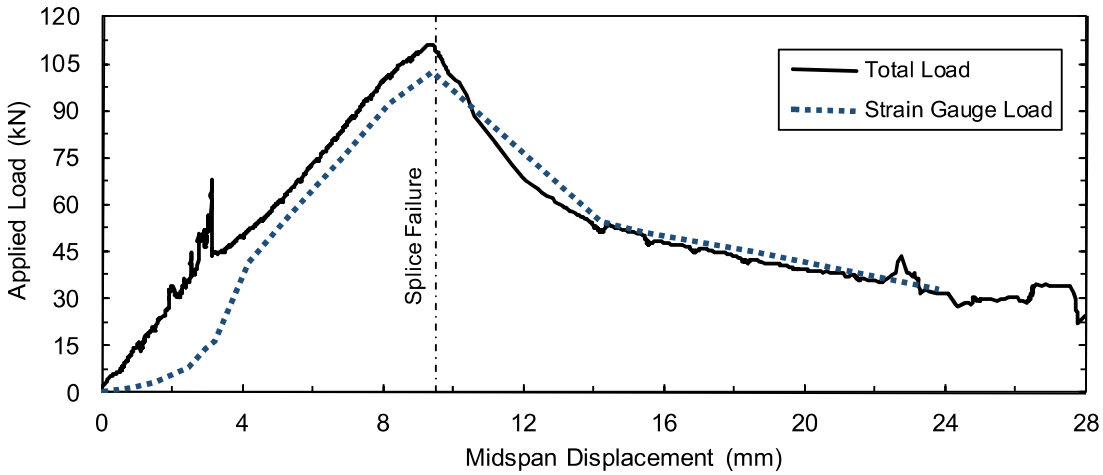

Figure B.184: Load displacement-history plot for CP9-LSR.

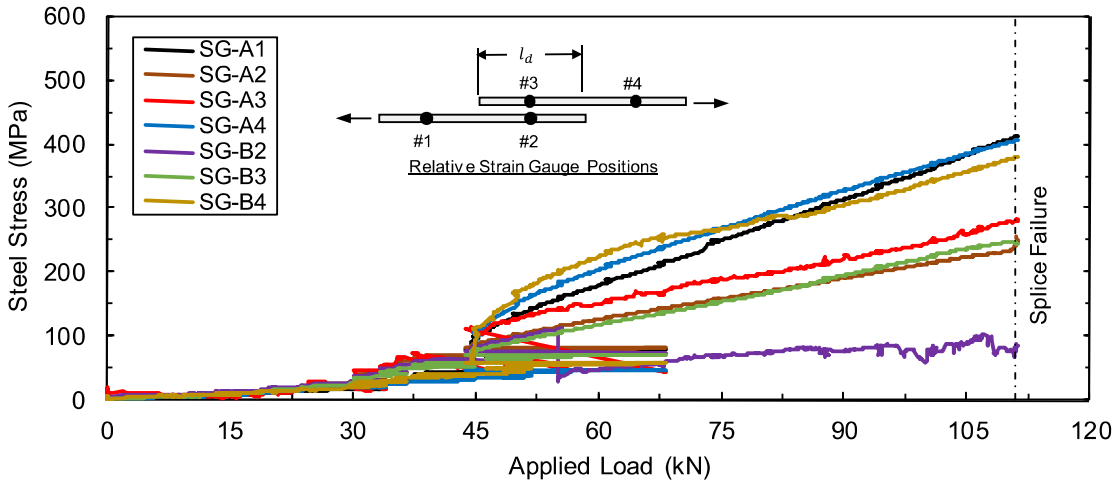

Figure B.185: Steel stress load-history plot for CP9-LSR.

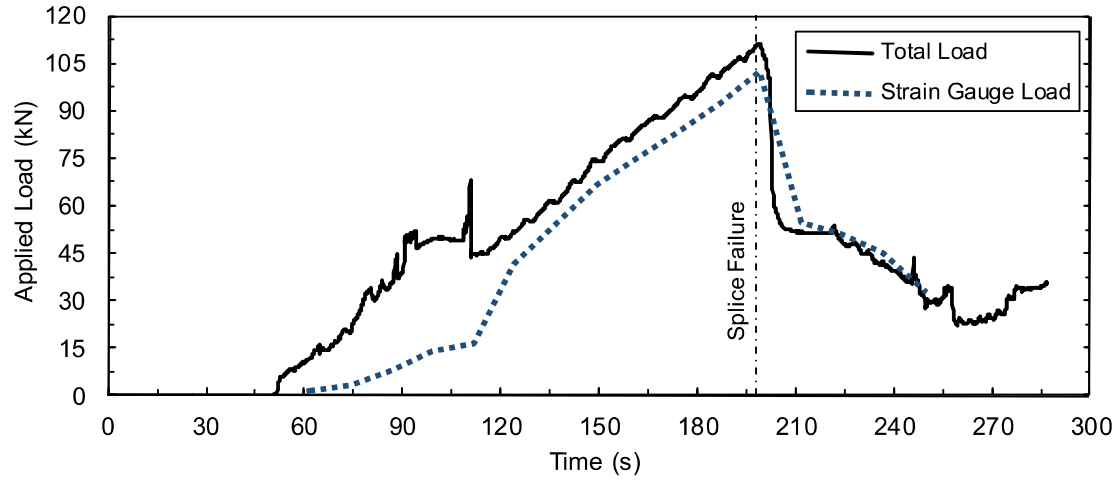

Figure B.186: Load time-history plot for CP9-LSR.

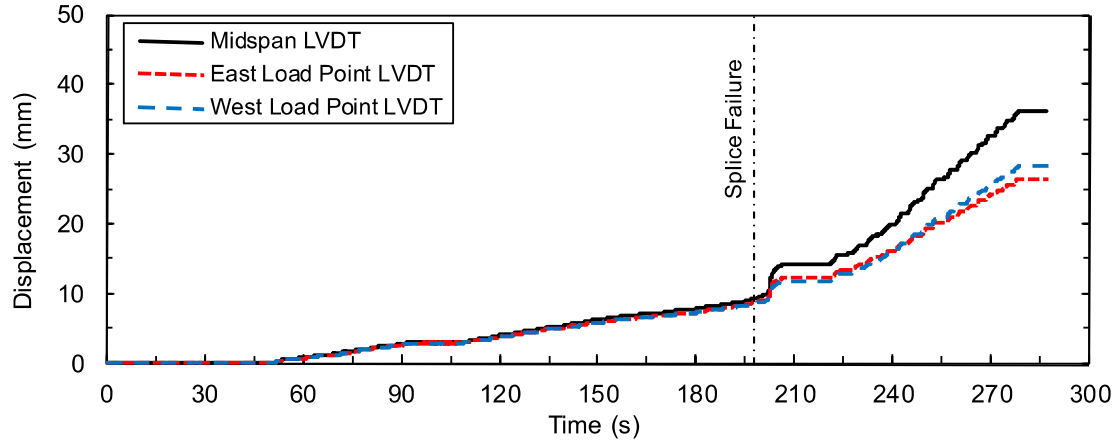

Figure B.187: Displacement time-history plot for CP9-LSR.

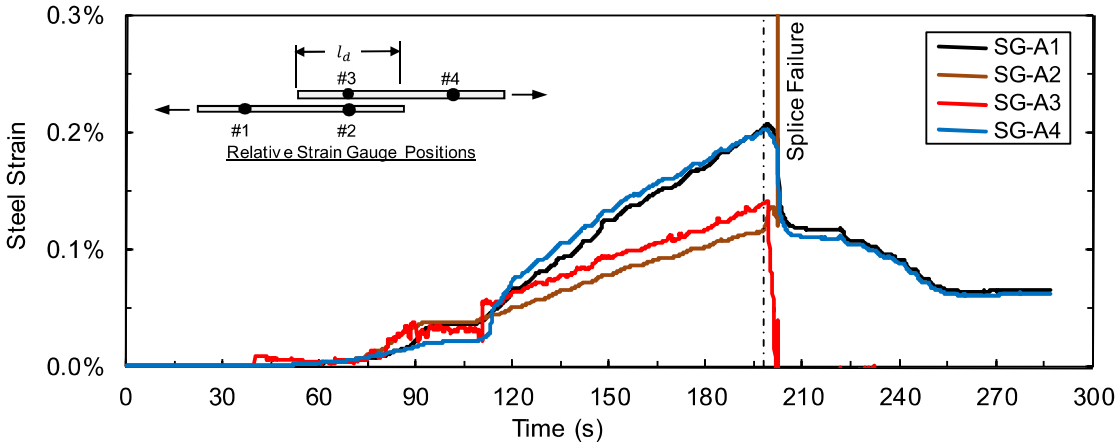

Figure B.188: Test bar "A" strain time-history plot for CP9-LSR.

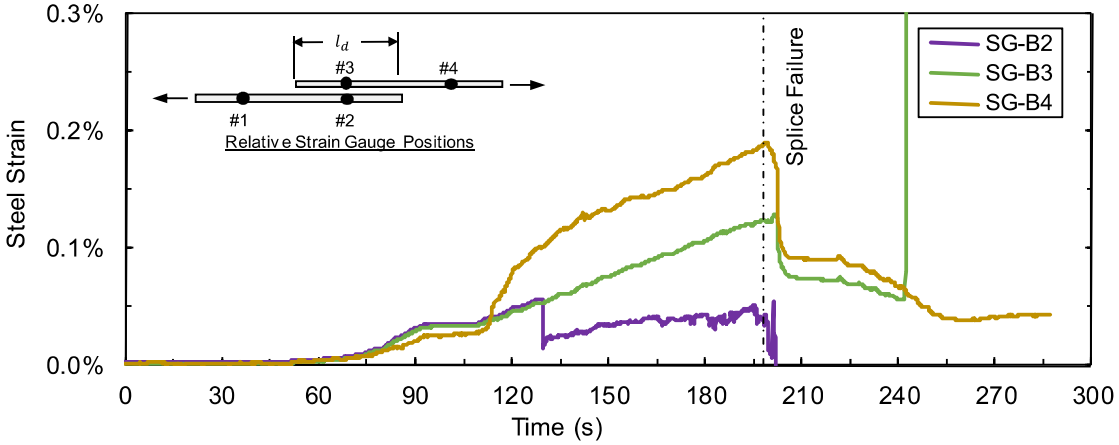

Figure B.189: Test bar "B" strain time-history plot for CP9-LSR.

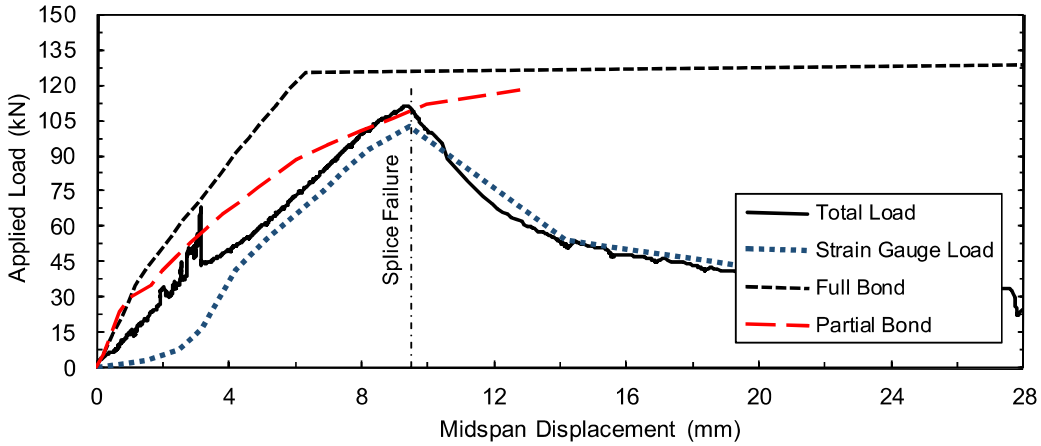

Figure B.190: Comparison of predicted and experimental resistance curves for CP9-LSR.

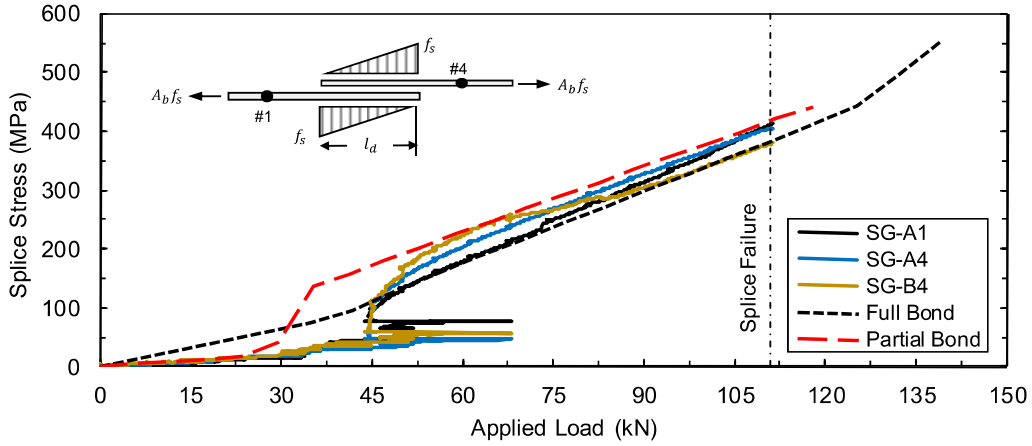

Figure B.191: Comparison of predicted and experimental steel stress developed in spliced reinforcement for CP9-LSR with respect to applied load.

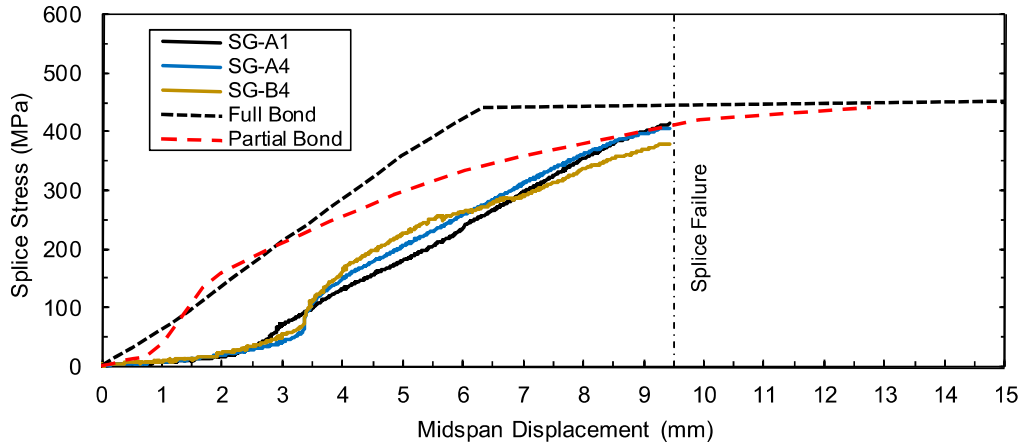

Figure B.192: Comparison of predicted and experimental steel stress developed in spliced reinforcement for CP9-LSR with respect to displacement.

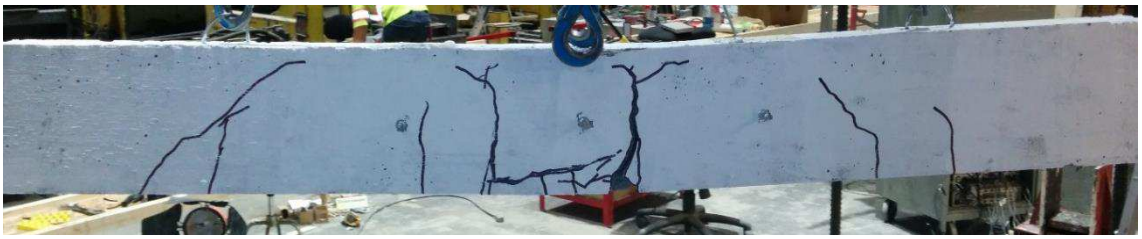

(a) South face after low strain rate testing

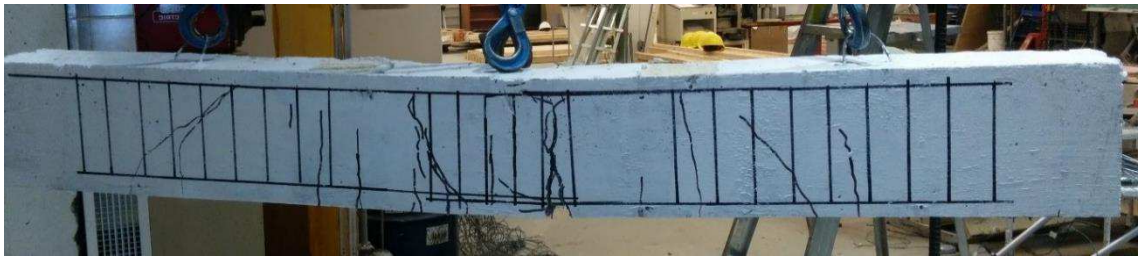

(b) North face after low strain rate testing

Figure B.193: Photographs of lap splice beam CP9-LSR.

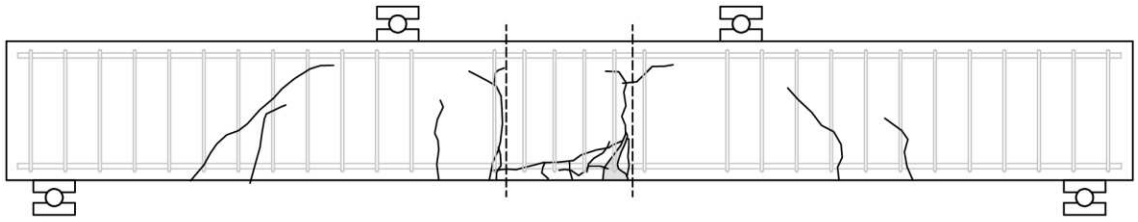

(a) Observed crack profile (north face)

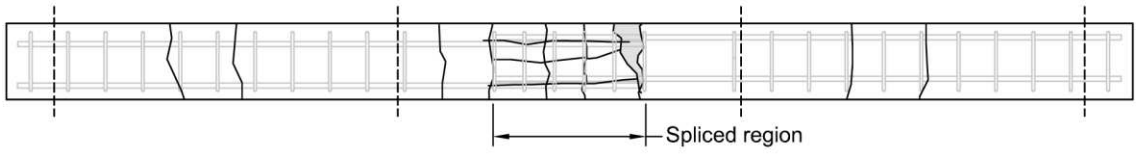

(b) Observed crack profile (bottom face)

Figure B.194: Observed crack profile for lap splice beam CP9-LSR.

CP9-HSR

Lap splice beam CP9-HSR was subjected to high strain rate testing on August 19, 2014. CP9-HSR was designed with 15M reinforcement, 30 MPa concrete, 25 mm cover, and 6-ϕ6.3 mm smooth double leg closed stirrups confining the spliced region. The specimen experienced a side-splitting tensile failure of the cover concrete with significant cover loss. Failure occurred at an applied load of 154.4 kN. Based on strain readings, the stress developed in the spliced bars was 557 MPa. Based on a sectional analysis, the stress developed in the spliced bars was 585 MPa. Time-to-failure was 7.6 ms and strain rate was 0.70 s^{-1}. Note that the bottom load cell yielded noisy readings and the unfiltered records are shown below.

Table B.35: Geometry, reinforcing, and material properties for CP9-HSR.

b:	165 mm	Bar:	2-15M	f'_{dc}:	48.3 MPa
h:	300 mm	A_b:	200 mm^2	f_{dy}:	588.3 MPa
l_d:	325 mm	d_b:	16.0 mm	ρ:	0.91%
c_b:	24 mm	N:	6	c/d:	1.6
c_{so}:	27 mm	A_{tr}:	2×31.1 mm^2	$l_d(c_{min}+0.5d_b)$:	10504 mm^2

Table B.36: Summary of experimental test results for CP9-HSR.

Date:	Aug. 19, 2014	δ_f:	11.1 mm	f_s^t:	557 MPa
P_r:	81.5 kPa	R_f:	154.4 kN	f_s^{cal}:	585 MPa
I_r:	647.0 kPa-ms	t_f:	7.6 ms	$\dot{\varepsilon}$:	0.70 s^{-1}

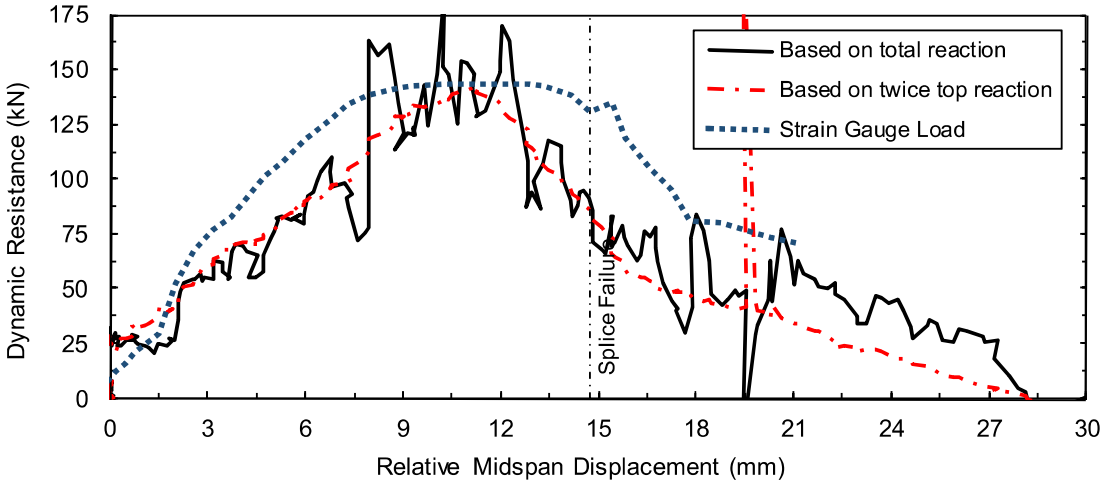

Figure B.195: Load displacement-history plot for CP9-HSR.

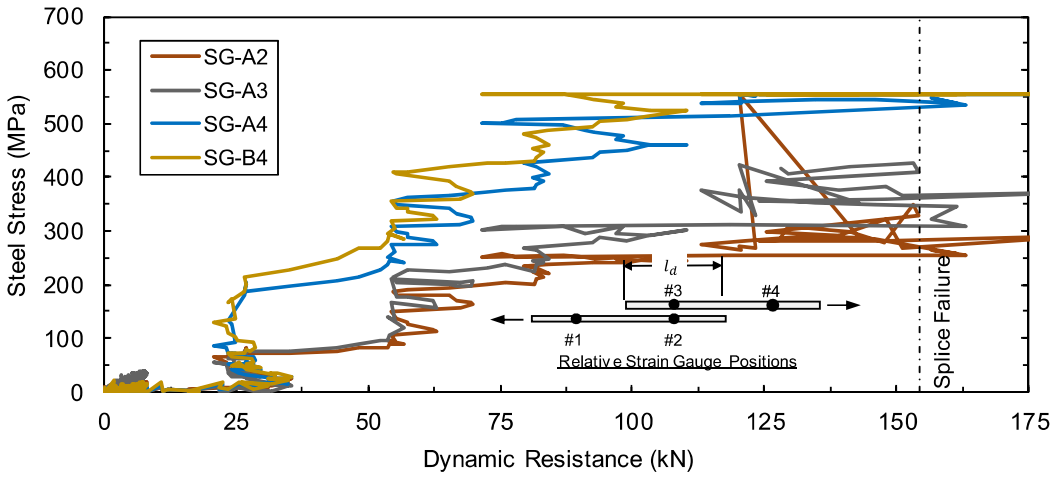

Figure B.196: Steel stress load-history plot for CP9-HSR.

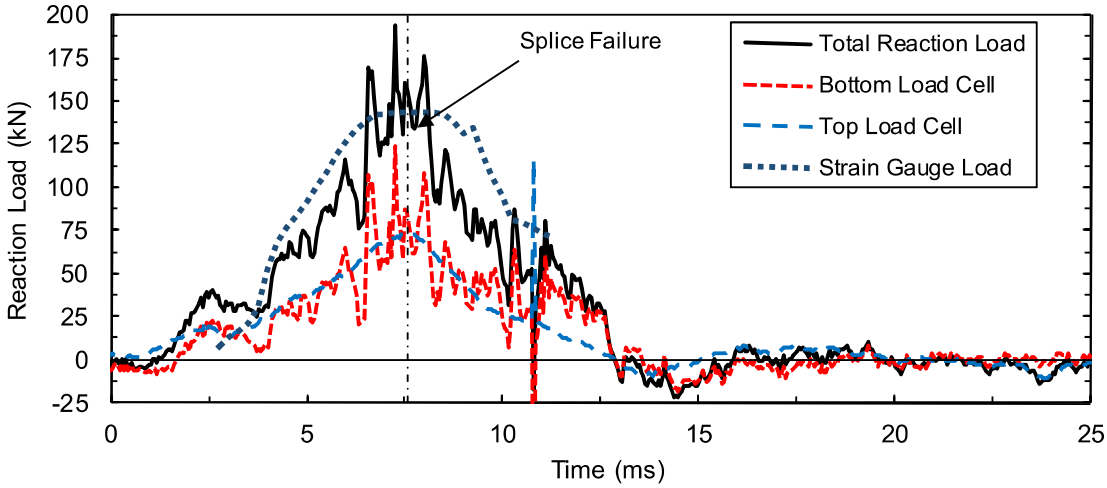

Figure B.197: Load time-history plot for CP9-HSR.

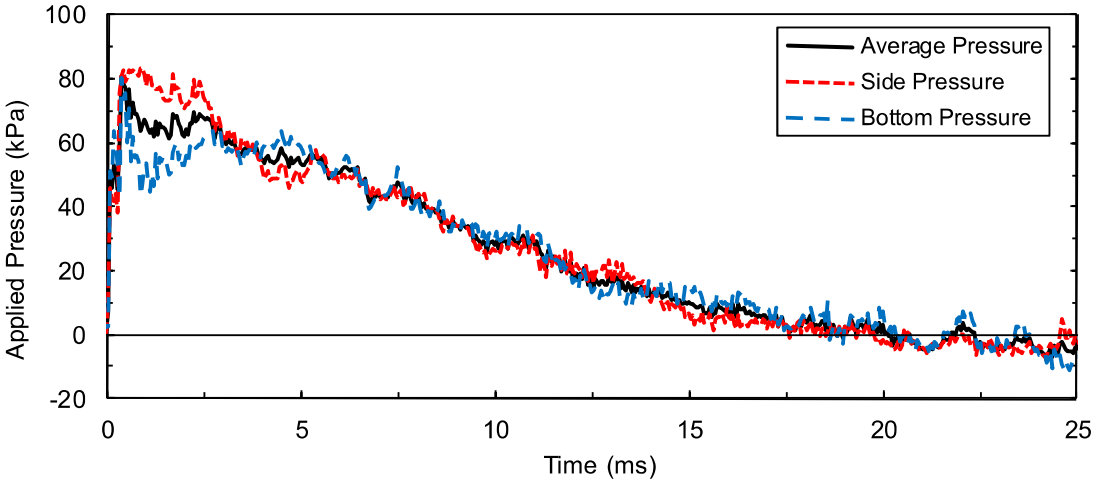

Figure B.198: Pressure time-history plot for CP9-HSR.

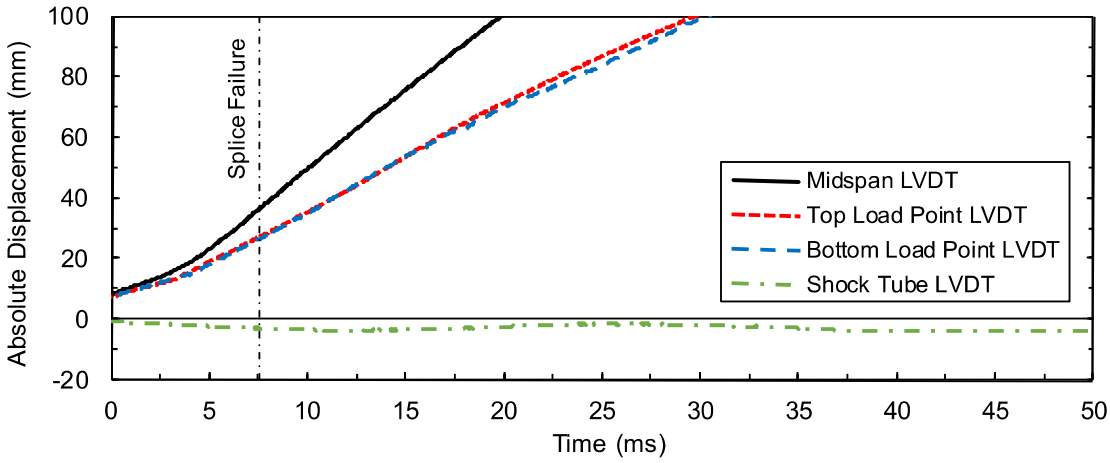

Figure B.199: Displacement time-history plot for CP9-HSR.

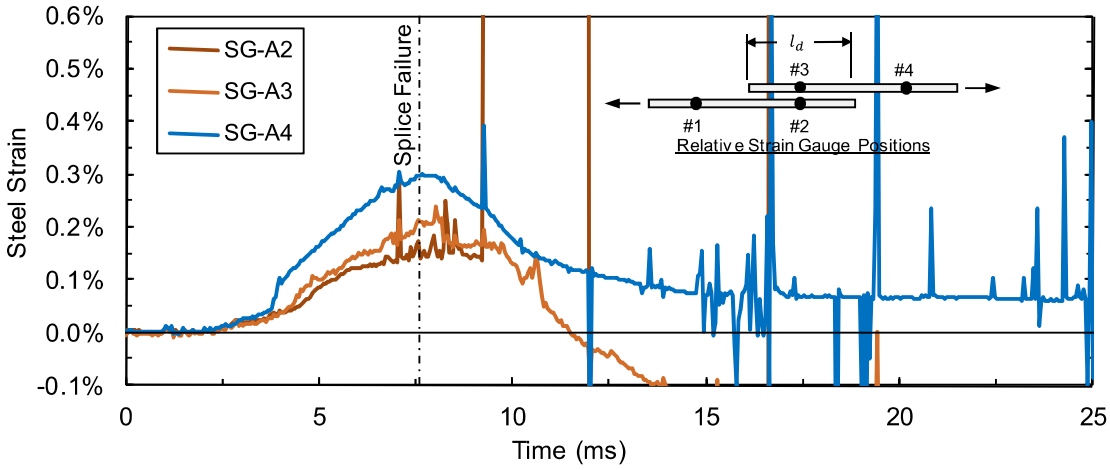

Figure B.200: Test bar "A" strain time-history plot for CP9-HSR.

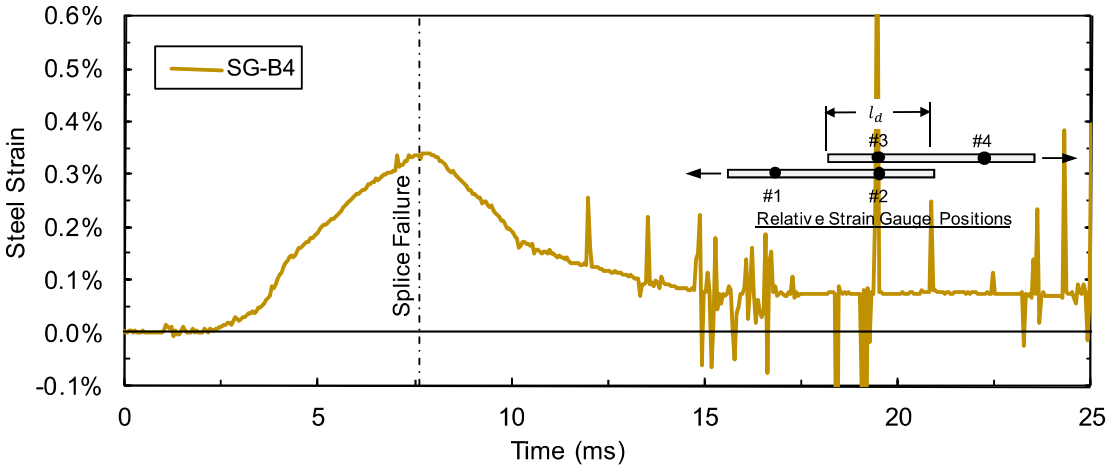

Figure B.201: Test bar "B" strain time-history plot for CP9-HSR.

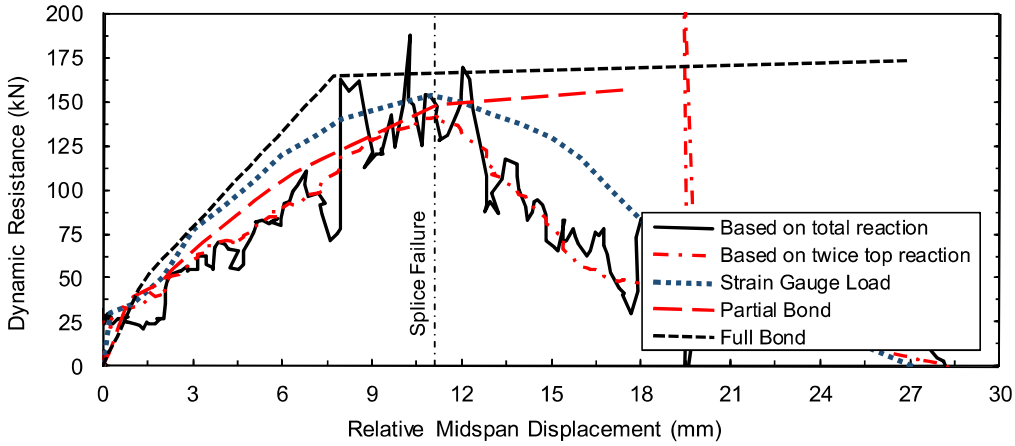

Figure B.202: Comparison of predicted and experimental resistance curves for CP9-HSR.

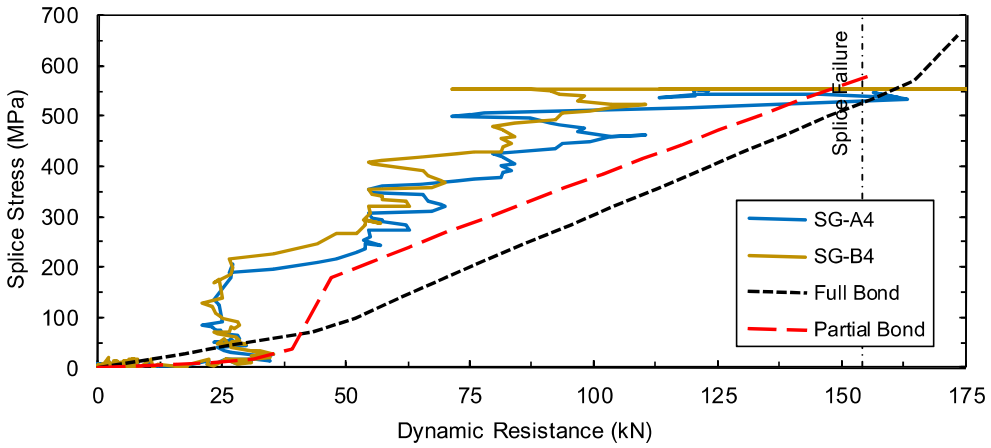

Figure B.203: Comparison of predicted and experimental steel stress developed in spliced reinforcement for CP9-HSR with respect to applied load.

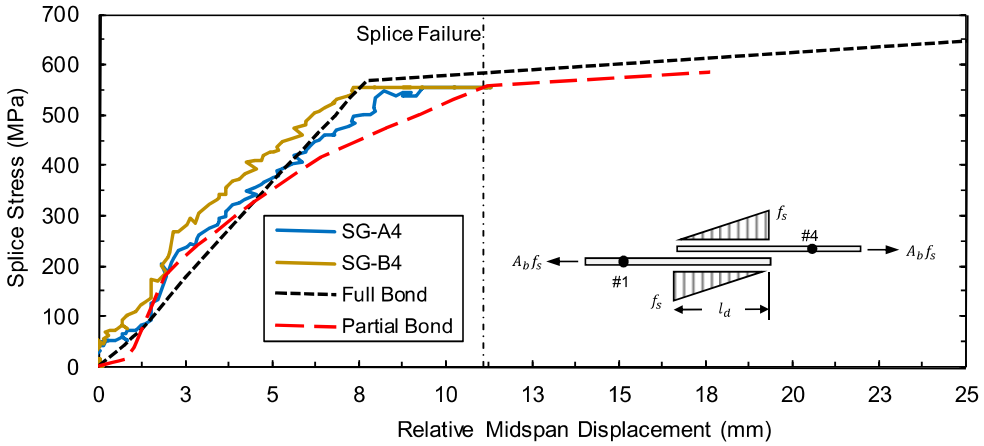

Figure B.204: Comparison of predicted and experimental steel stress developed in spliced reinforcement for CP9-HSR with respect to displacement.

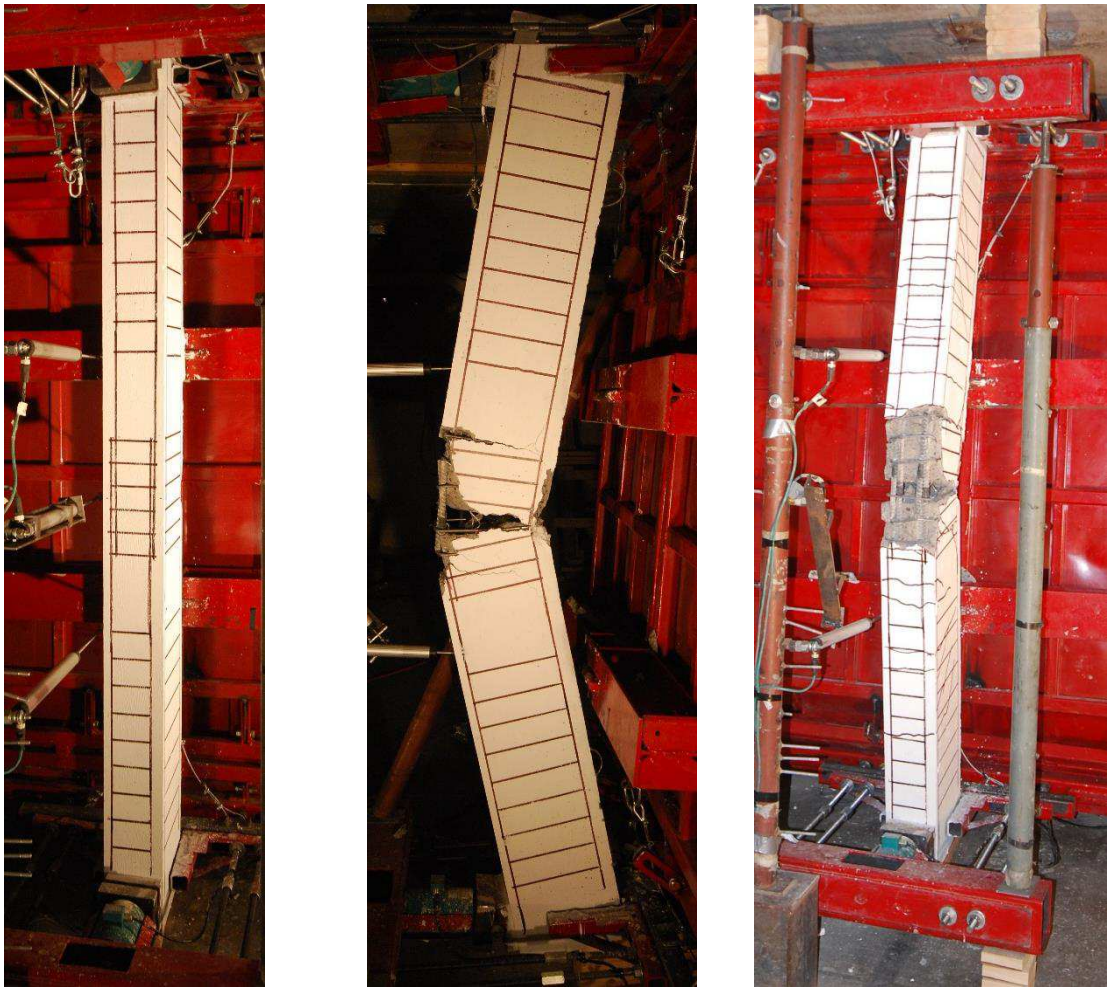

(a) Before high strain rate testing (b) After high strain rate testing (c) After high strain rate testing

Figure B.205: Photographs of lap splice beam CP9-HSR.

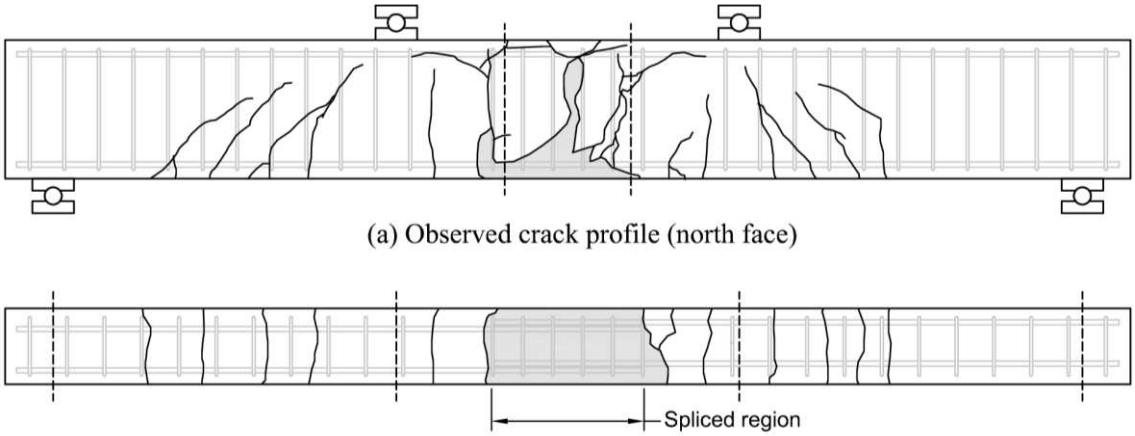

(a) Observed crack profile (north face)

(b) Observed crack profile (bottom face)

Figure B.206: Observed crack profile for lap splice beam CP9-HSR.

CP10-LSR

Lap splice beam CP10-LSR was subjected to low strain rate testing on August 20, 2014. CP10-LSR was designed with 15M reinforcement, 30 MPa concrete, 50 mm cover, and 4-ϕ6.3 mm smooth double leg closed stirrups confining the spliced region. The specimen experienced a predominantly face-splitting tensile failure of the cover concrete with negligible cover loss. Failure occurred at an applied load of 100.1 kN. Based on strain readings, the stress developed in the spliced bars was 428 MPa. Based on a sectional analysis, the stress developed in the spliced bars was 423 MPa. Time-to-failure was 289.5 seconds and strain rate was 7.4×10^{-6} s^{-1}.

Table B.37: Geometry, reinforcing, and material properties for CP10-LSR.

b:	265 mm	Bar:	2-15M	f_c':	36.9 MPa
h:	300 mm	A_b:	200 mm^2	f_y:	448.1 MPa
l_d:	187 mm	d_b:	16.0 mm	ρ:	0.62%
c_b:	48 mm	N:	4	c/d:	3.1
c_{so}:	52 mm	A_{tr}:	2×31.1 mm^2	$l_d(c_{min}+0.5d_b)$:	10472 mm^2

Table B.38: Summary of experimental test results for CP10-LSR.

Date:	Aug. 20, 2014	δ_f:	7.6 mm	f_s^t:	428 MPa
P_r:	N/A	R_f:	100.1 kN	f_s^{cal}:	423 MPa
I_r:	N/A	t_f:	289.5 s	$\dot{\varepsilon}$:	7.4×10^{-6} s^{-1}

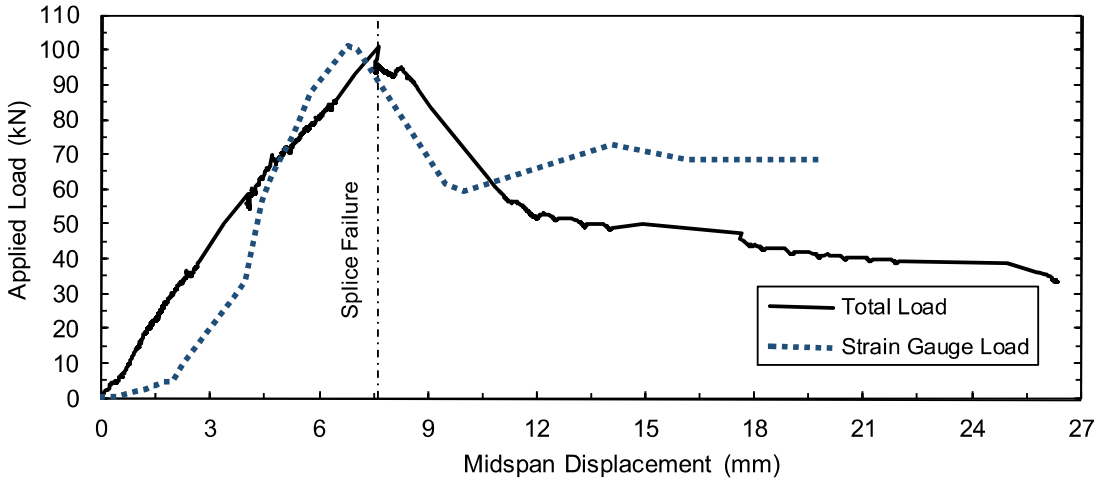

Figure B.207: Load displacement-history plot for CP10-LSR.

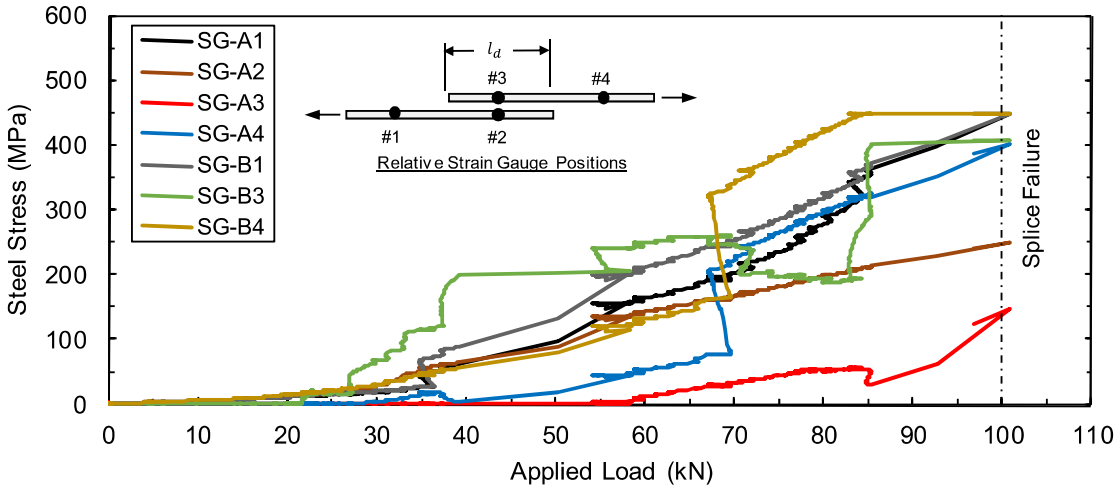

Figure B.208: Steel stress load-history plot for CP10-LSR.

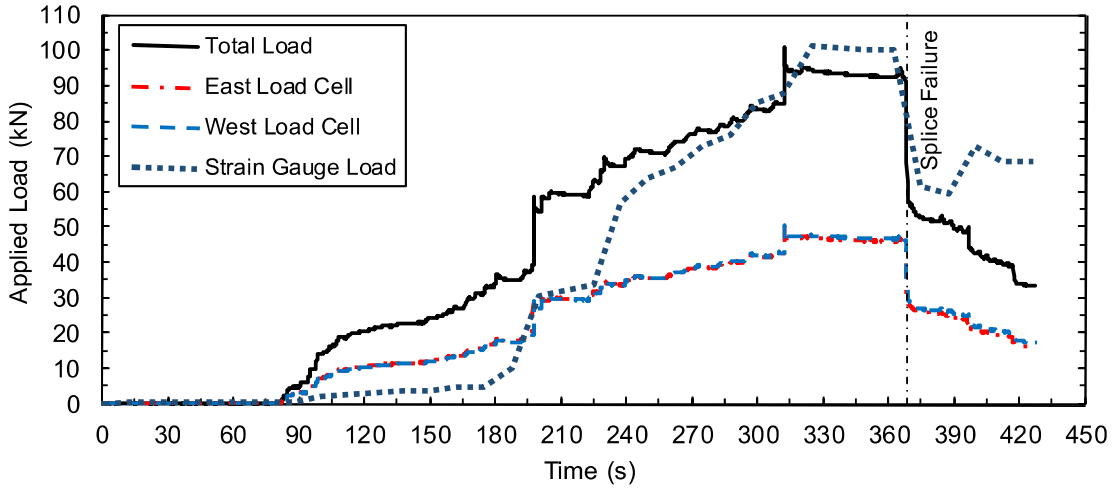

Figure B.209: Load time-history plot for CP10-LSR.

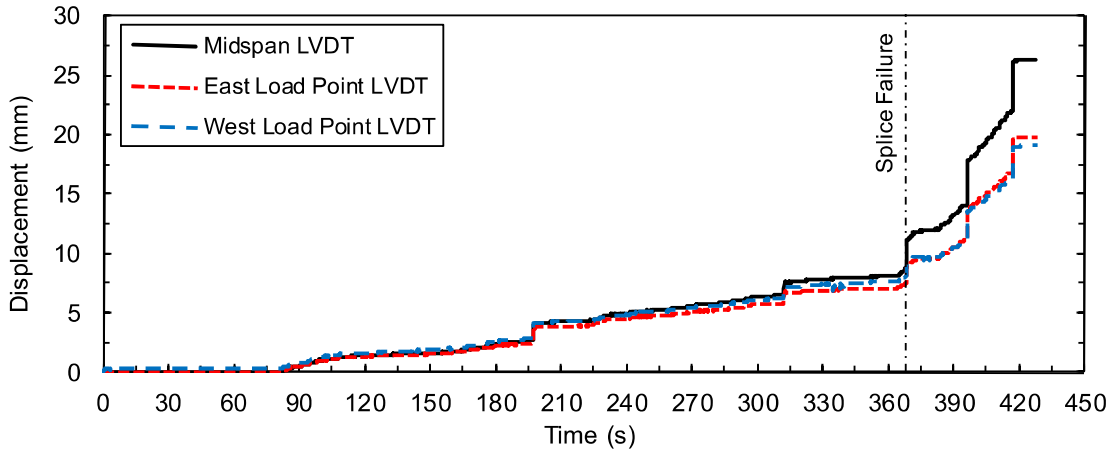

Figure B.210: Displacement time-history plot for CP10-LSR.

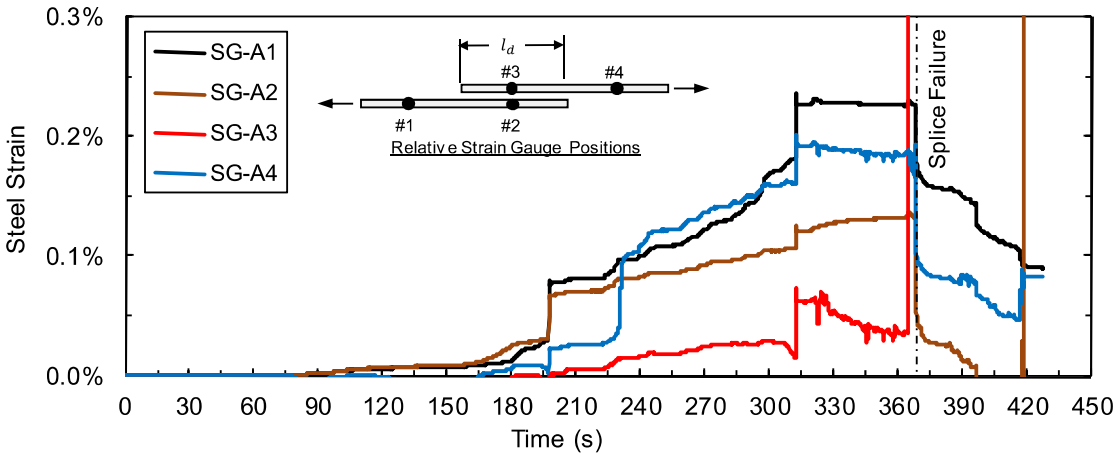

Figure B.211: Test bar "A" strain time-history plot for CP10-LSR.

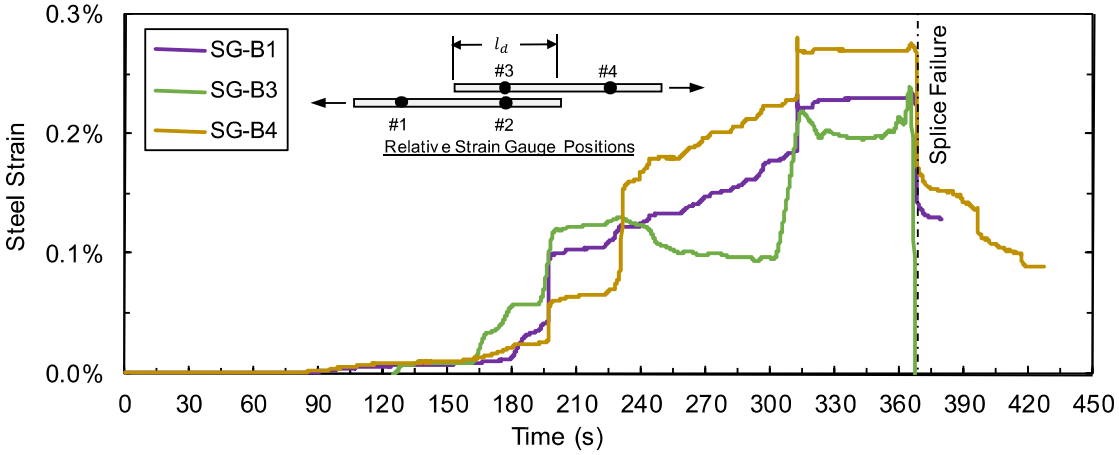

Figure B.212: Test bar "B" strain time-history plot for CP10-LSR.

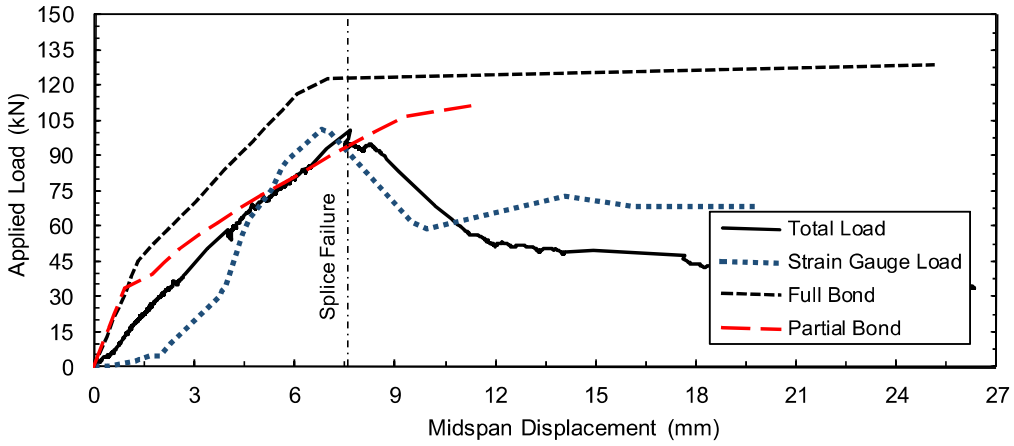

Figure B.213: Comparison of predicted and experimental resistance curves for CP10-LSR.

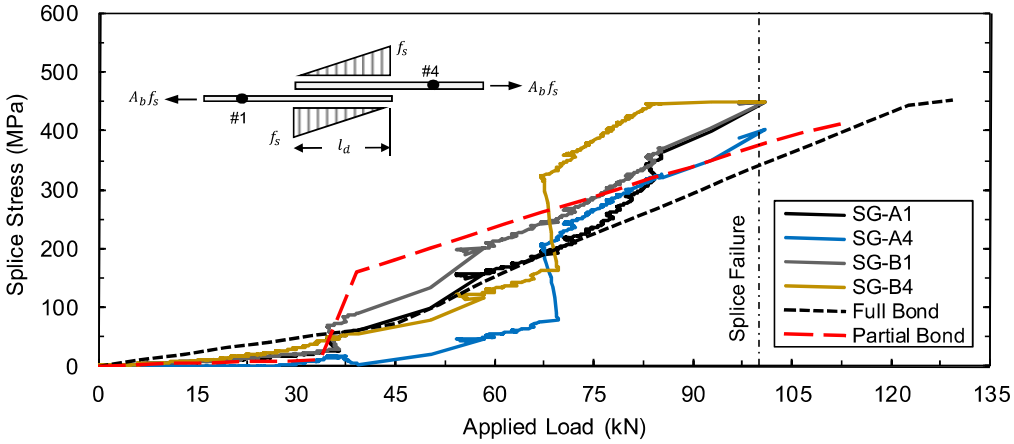

Figure B.214: Comparison of predicted and experimental steel stress developed in spliced reinforcement for CP10-LSR with respect to applied load.

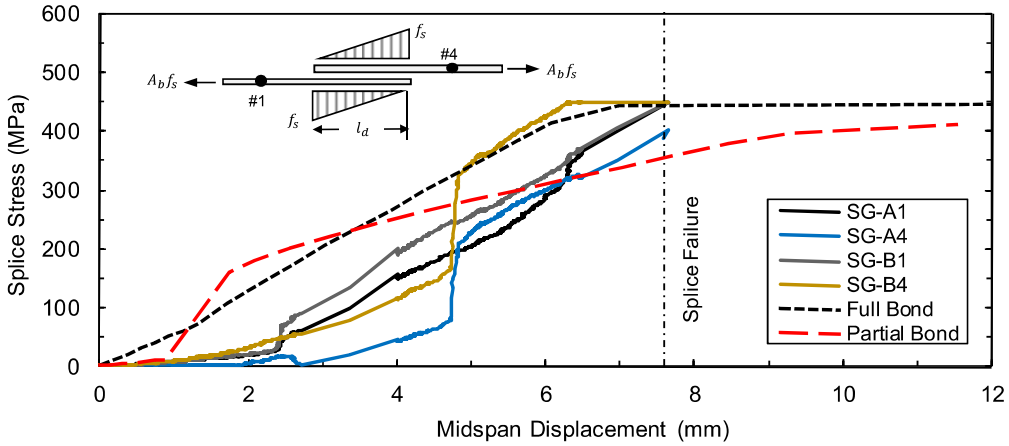

Figure B.215: Comparison of predicted and experimental steel stress developed in spliced reinforcement for CP10-LSR with respect to displacement.

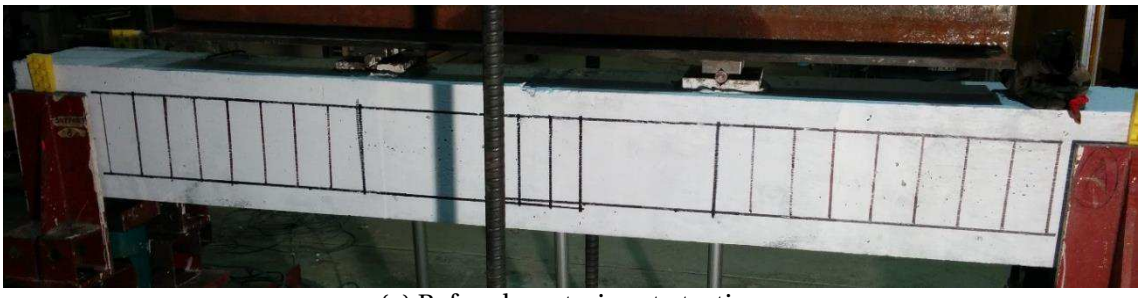

(a) Before low strain rate testing

(b) After low strain rate testing

Figure B.216: Photographs of lap splice beam CP10-LSR.

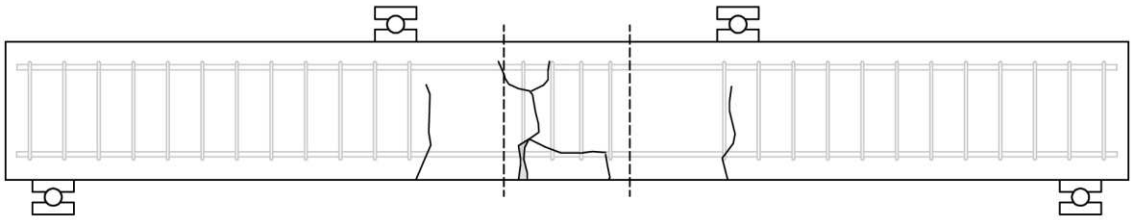

(a) Observed crack profile (north face)

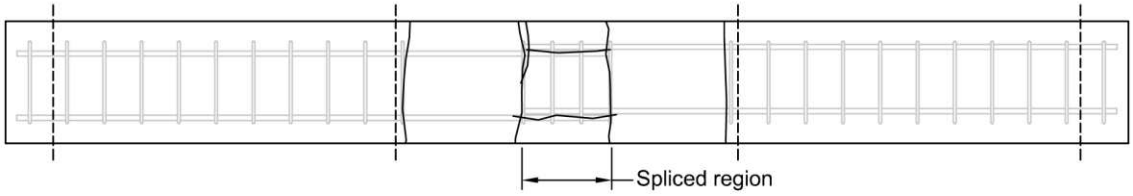

(b) Observed crack profile (bottom face)

Figure B.217: Observed crack profile for lap splice beam CP10-LSR.

CP10-HSR

Lap splice beam CP10-HSR was subjected to high strain rate testing on Aug. 28, 2014. CP10-HSR was designed with 15M reinforcement, 30 MPa concrete, 50 mm cover, and 4-ϕ6.3 mm smooth double leg closed stirrups confining the spliced region. The specimen experienced a side-splitting tensile failure of the cover concrete with significant cover loss. Failure occurred at an applied load of 135.5 kN. Based on strain readings, the stress developed in the spliced bars was 556 MPa. Based on a sectional analysis, the stress developed in the spliced bars was 571 MPa. Time-to-failure was 8.8 ms and strain rate was 0.32 s^{-1}. Note that the bottom load cell yielded poor readings, and that total load was computed based on twice the top reaction.

Table B.39: Geometry, reinforcing, and material properties for CP10-HSR.

b:	265 mm	Bar:	2-15M	f'_{dc}:	47.3 MPa
h:	400 mm	A_b:	200 mm^2	f_{dy}:	573.6 MPa
l_d:	185 mm	d_b:	16.0 mm	ρ:	0.62%
c_b:	49 mm	N:	4	c/d:	3.1
c_{so}:	50 mm	A_{tr}:	2×31.1 mm^2	$l_d(c_{min}+0.5d_b)$:	10567 mm^2

Table B.40: Summary of experimental test results for CP10-HSR.

Date:	Aug. 28, 2014	δ_f:	10.1 mm	f_s^t:	556 MPa
P_r:	82.0 kPa	R_f:	135.5 kN	f_s^{cal}:	571 MPa
I_r:	656.4 kPa-ms	t_f:	8.8 ms	$\dot{\varepsilon}$:	0.32 s^{-1}

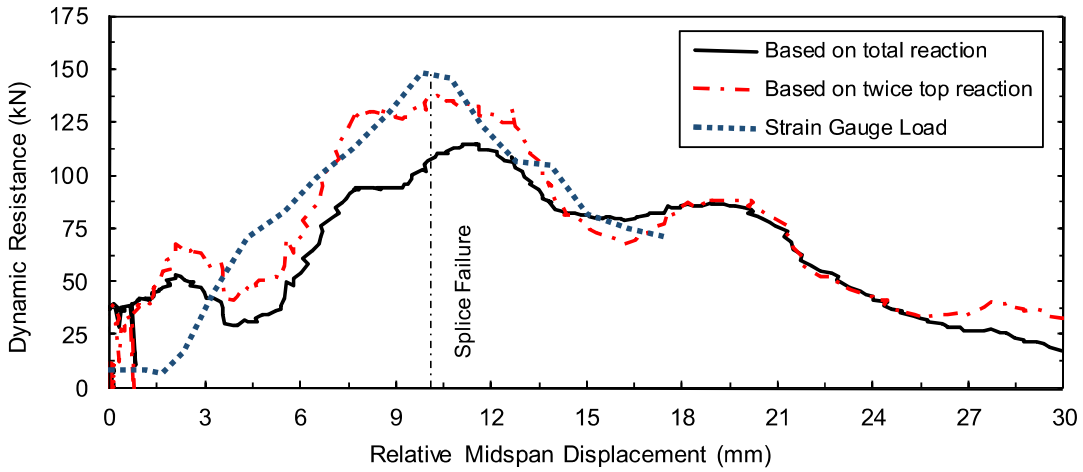

Figure B.218: Load displacement-history plot for CP10-HSR.

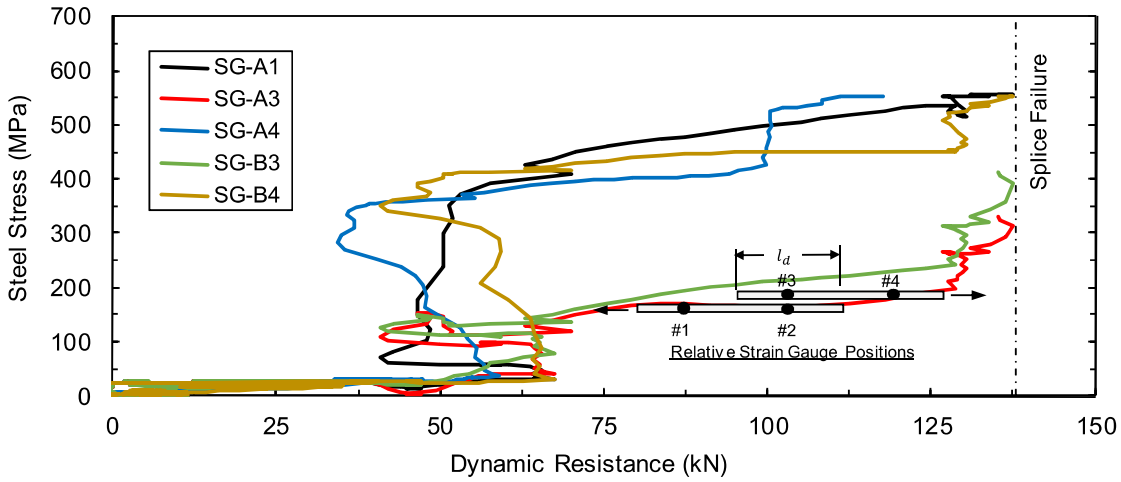

Figure B.219: Steel stress load-history plot for CP10-HSR.

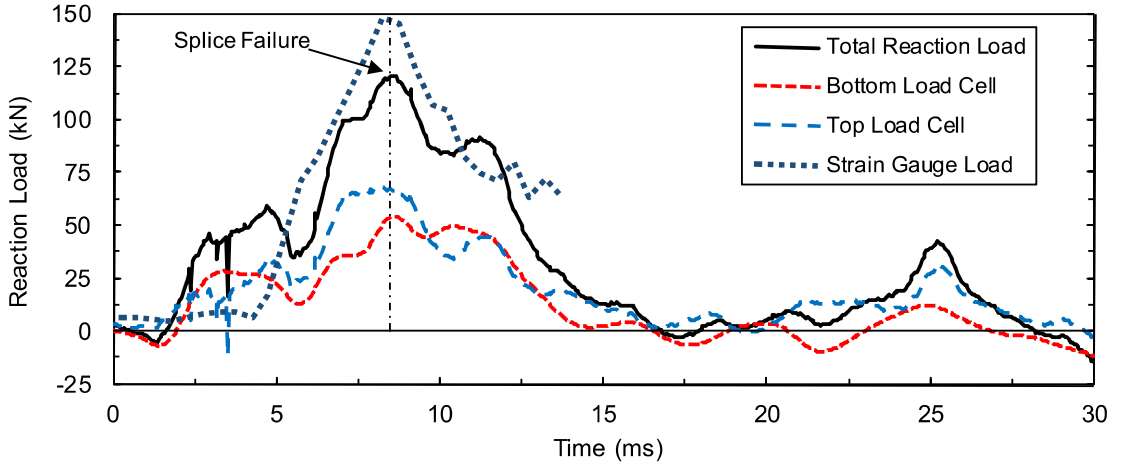

Figure B.220: Load time-history plot for CP10-HSR.

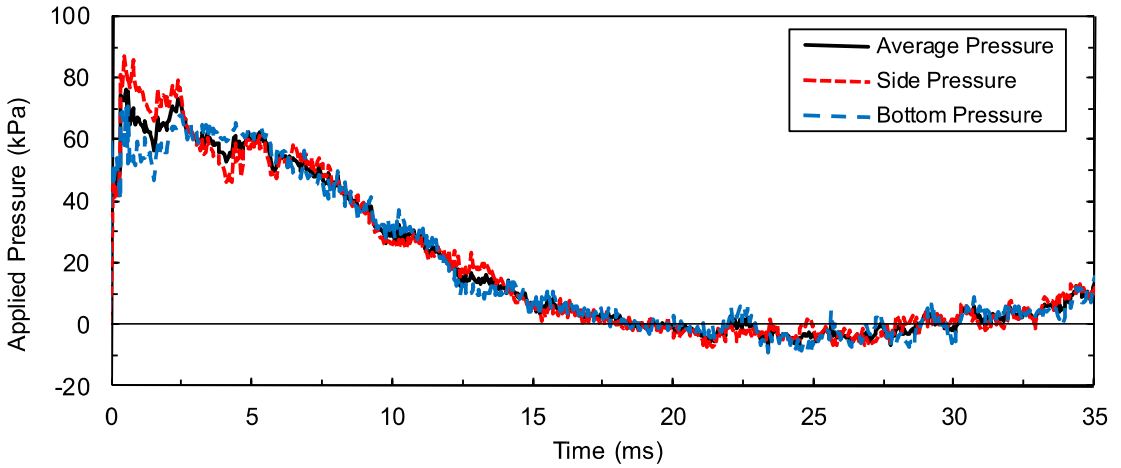

Figure B.221: Pressure time-history plot for CP10-HSR.

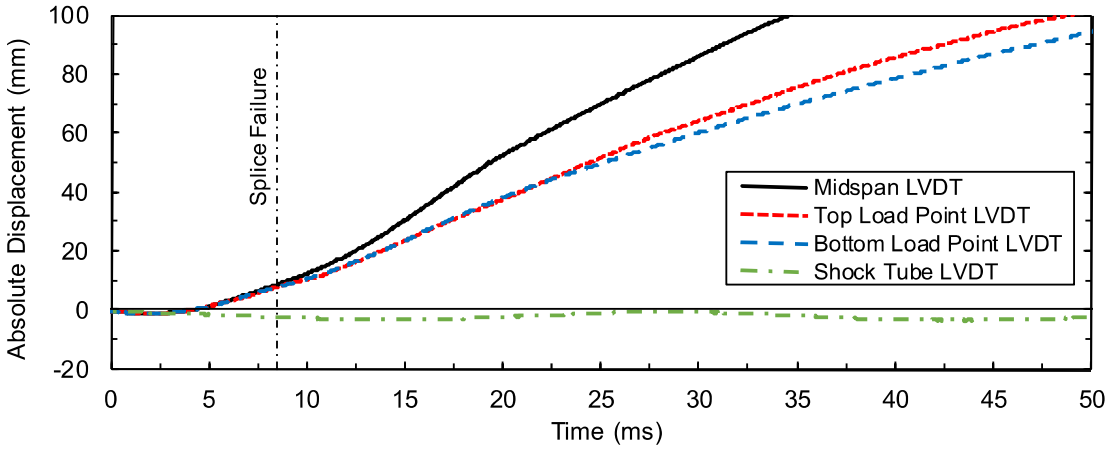

Figure B.222: Displacement time-history plot for CP10-HSR.

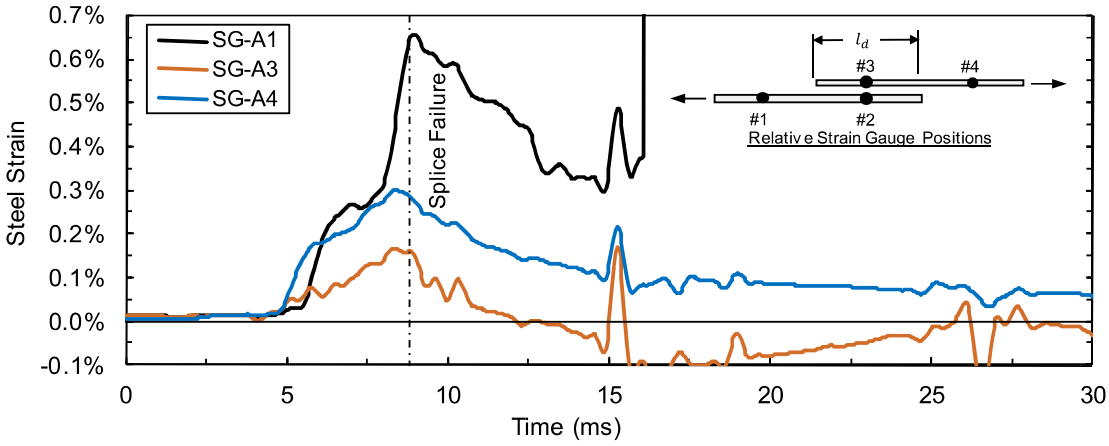

Figure B.223: Test bar "A" strain time-history plot for CP10-HSR.

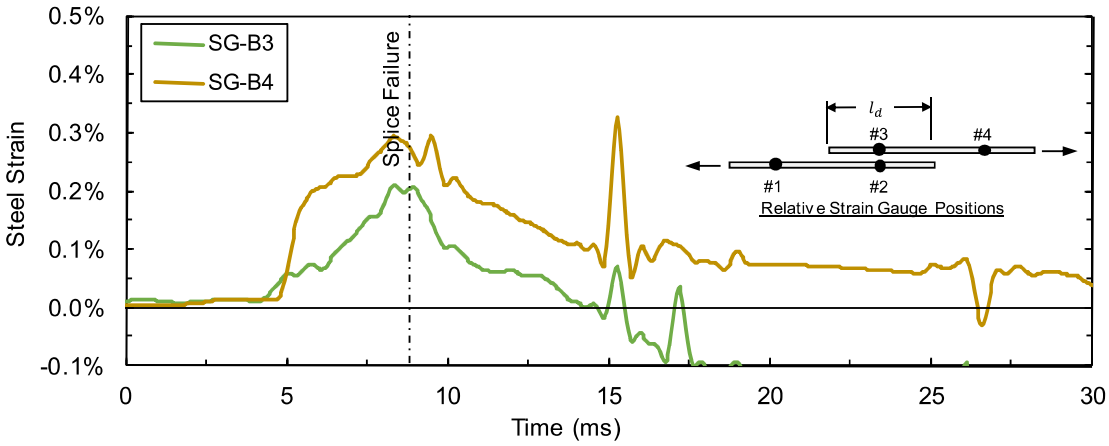

Figure B.224: Test bar "B" strain time-history plot for CP10-HSR.

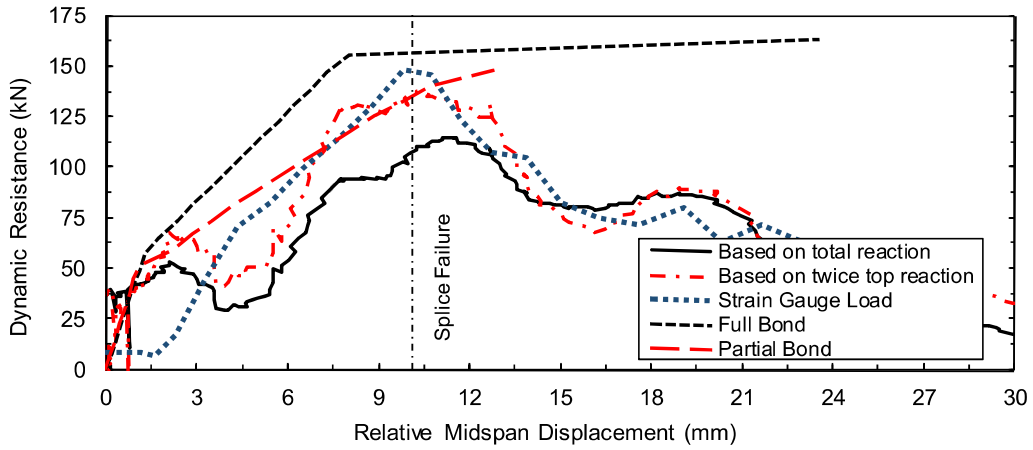

Figure B.225: Comparison of predicted and experimental resistance curves for CP10-HSR.

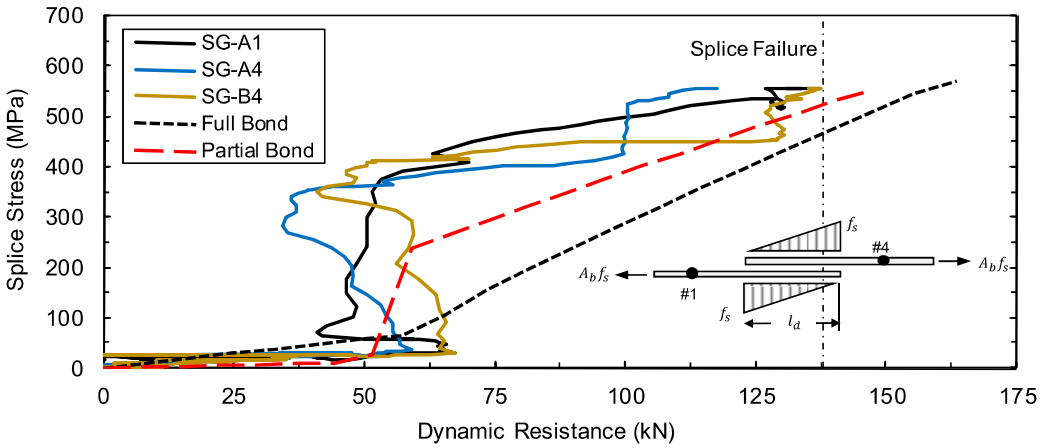

Figure B.226: Comparison of predicted and experimental steel stress developed in spliced reinforcement for CP10-HSR with respect to applied load.

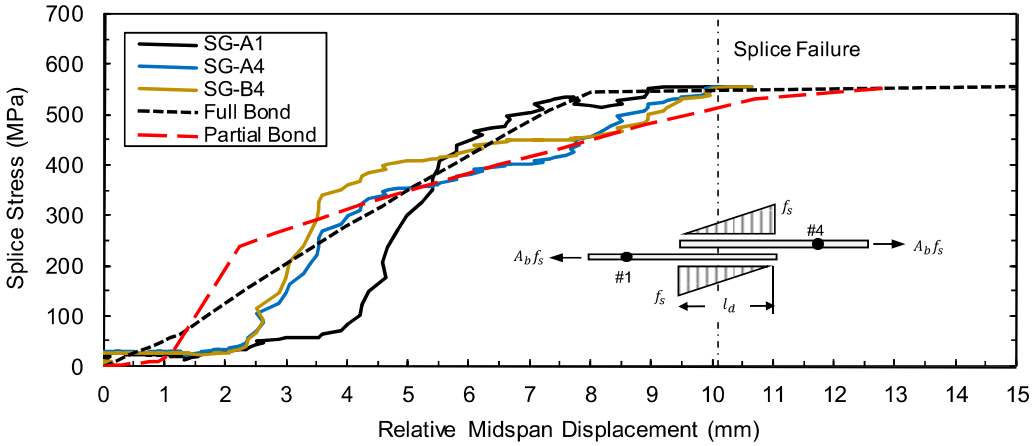

Figure B.227: Comparison of predicted and experimental steel stress developed in spliced reinforcement for CP10-HSR with respect to displacement.

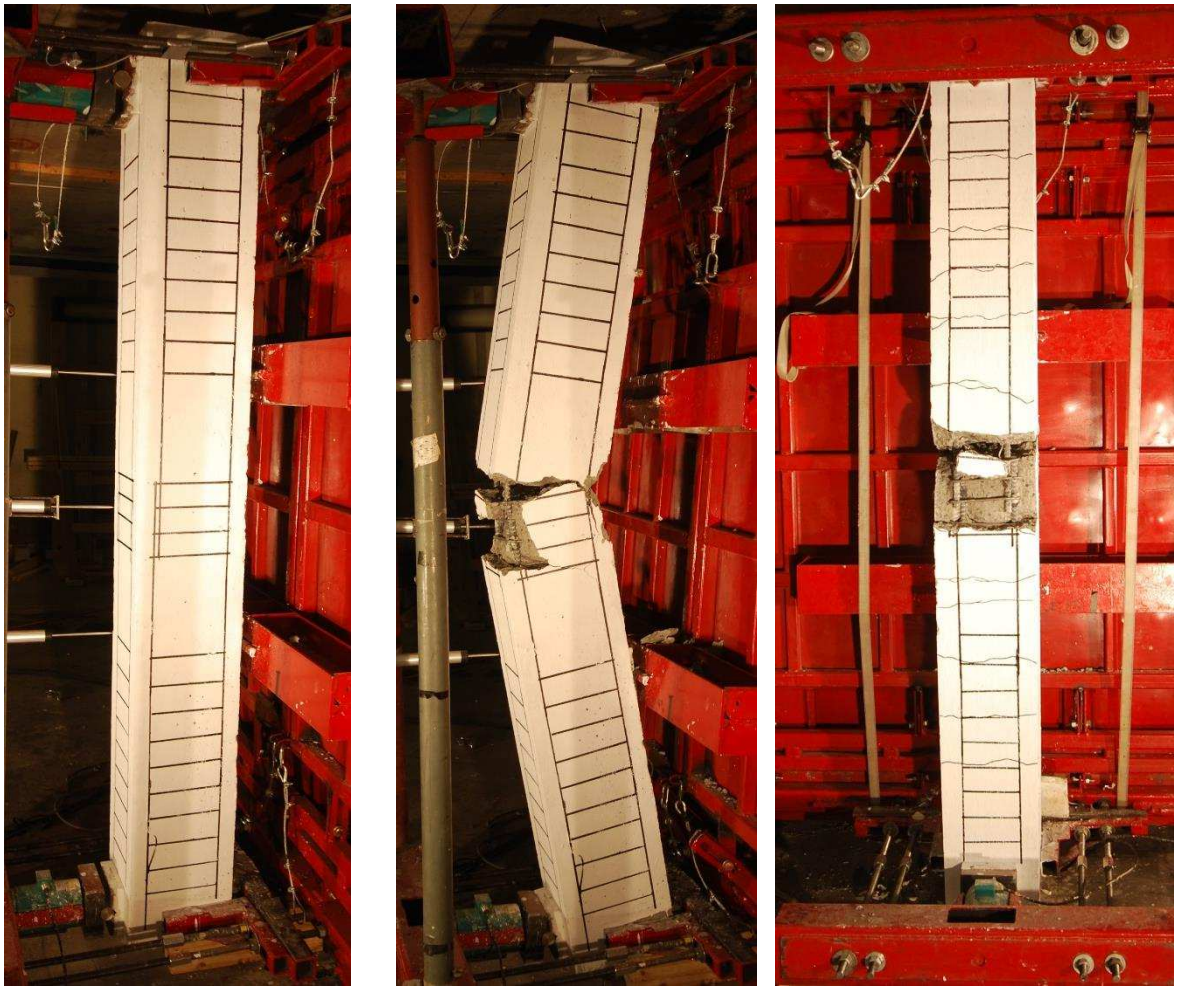

(a) Before high strain rate testing (b) After high strain rate testing (c) After high strain rate testing

Figure B.228: Photographs of lap splice beam CP10-HSR.

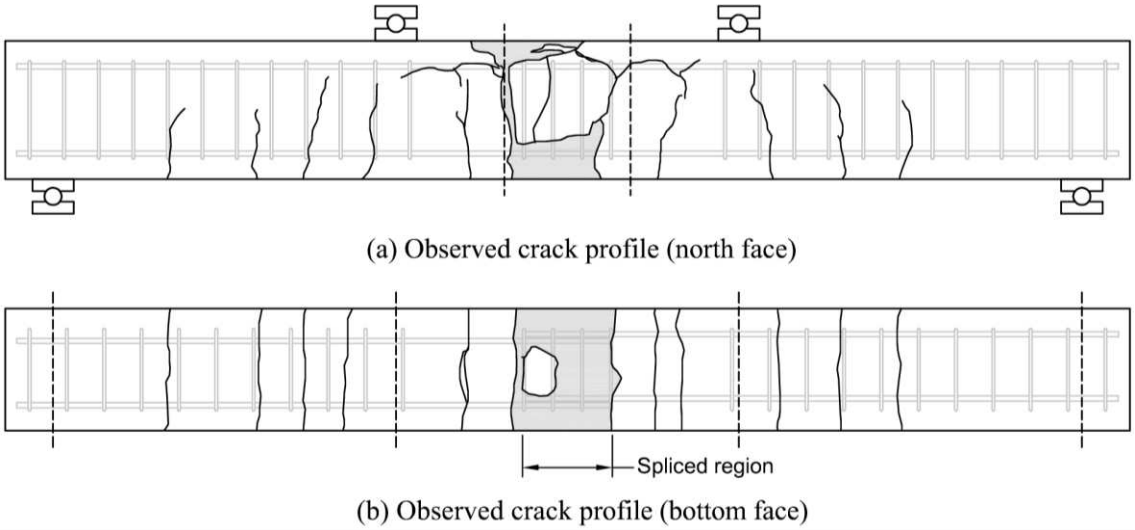

(a) Observed crack profile (north face)

(b) Observed crack profile (bottom face)

Figure B.229: Observed crack profile for lap splice beam CP10-HSR.

CP11-LSR

Lap splice beam CP11-LSR was subjected to low strain rate testing on August 21, 2014. CP11-LSR was designed with 15M reinforcement, 50 MPa concrete, 50 mm cover, and 4-ϕ6.3 mm smooth double leg closed stirrups confining the spliced region. The specimen experienced a predominantly side-splitting tensile failure of the cover concrete with negligible cover loss. Failure occurred at an applied load of 99.4 kN. Based on strain readings, the stress developed in the spliced bars was 417 MPa. Based on a sectional analysis, the stress developed in the spliced bars was 417 MPa. Time-to-failure was 347.7 seconds and strain rate was 6.0×10^{-6} s^{-1}.

Table B.41: Geometry, reinforcing, and material properties for CP11-LSR.

b:	200 mm	Bar:	2-15M	f_c':	45.2 MPa
h:	300 mm	A_b:	200 mm^2	f_y:	448.1 MPa
l_d:	164 mm	d_b:	16.0 mm	ρ:	0.62%
c_b:	49 mm	N:	4	c/d:	3.0
c_{so}:	48 mm	A_{tr}:	2×31.1 mm^2	$l_d(c_{min}+0.5d_b)$:	9184 mm^2

Table B.42: Summary of experimental test results for CP11-LSR.

Date:	Aug. 21, 2014	δ_f:	7.4 mm	f_s^t:	417 MPa
P_r:	N/A	R_f:	99.4 kN	f_s^{cal}:	417 MPa
I_r:	N/A	t_f:	347.7 s	$\dot{\varepsilon}$:	6.0×10^{-6} s^{-1}

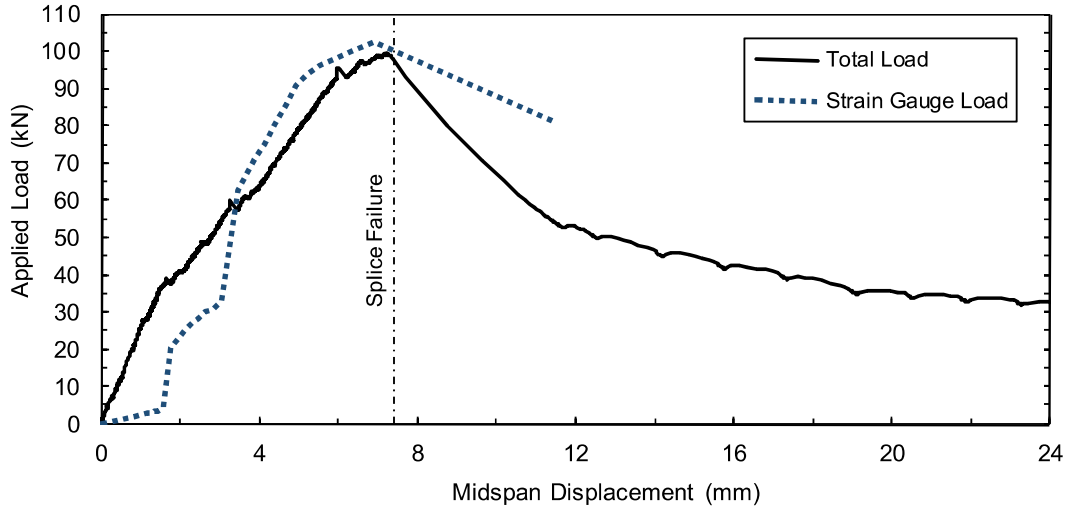

Figure B.230: Load displacement-history plot for CP11-LSR.

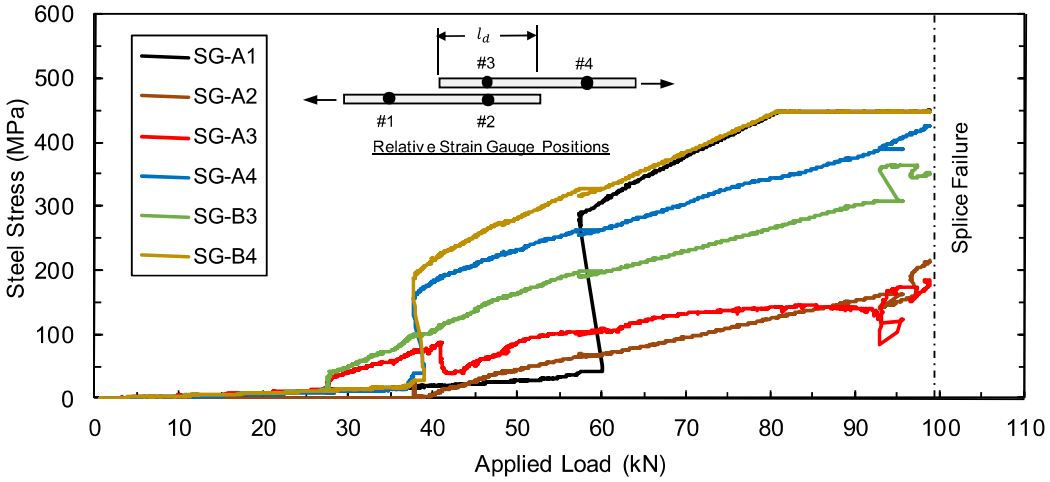

Figure B.231: Steel stress load-history plot for CP11-LSR.

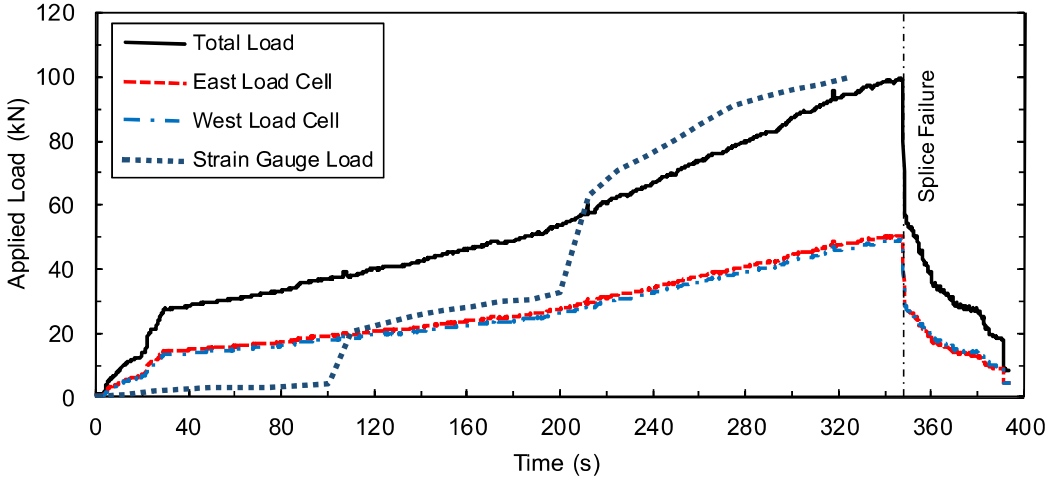

Figure B.232: Load time-history plot for CP11-LSR.

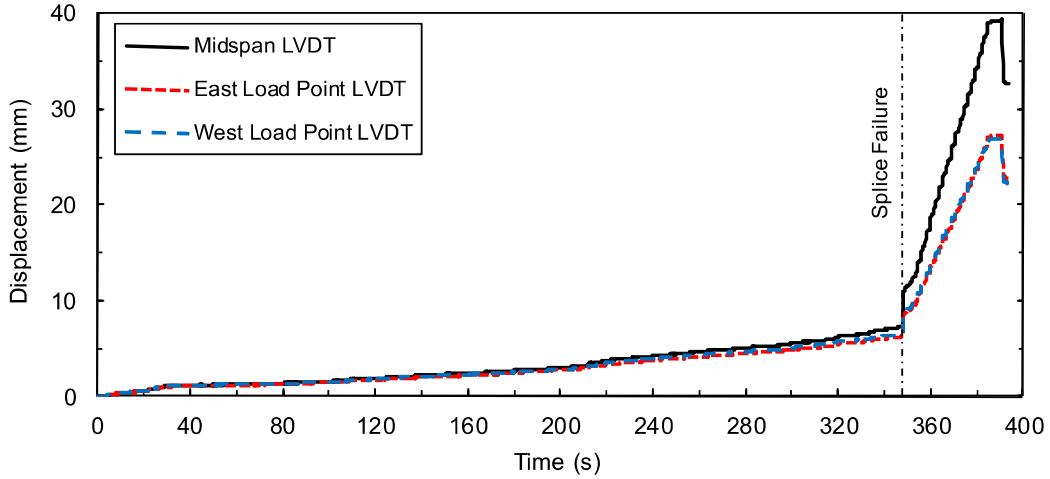

Figure B.233: Displacement time-history plot for CP11-LSR.

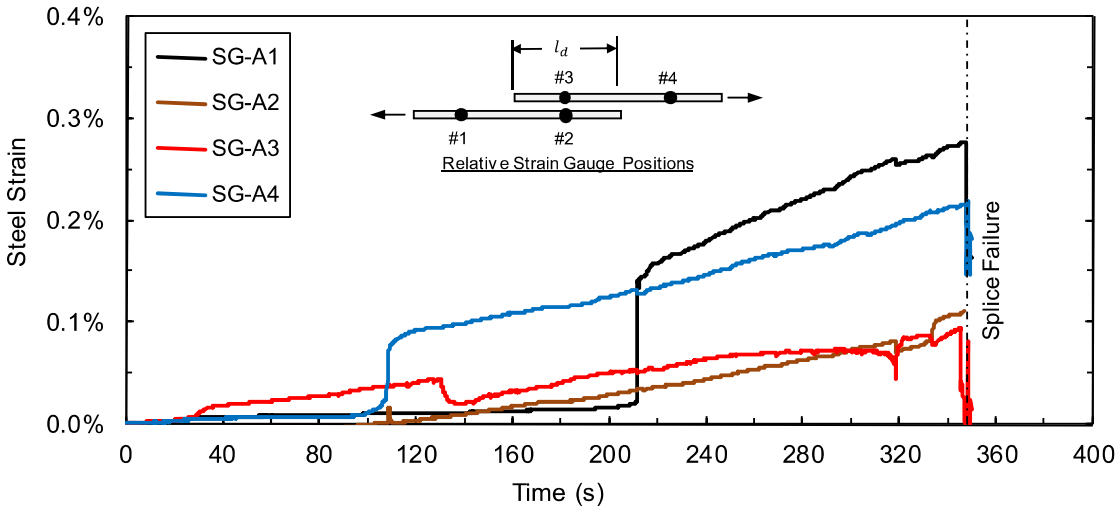

Figure B.234: Test bar "A" strain time-history plot for CP11-LSR.

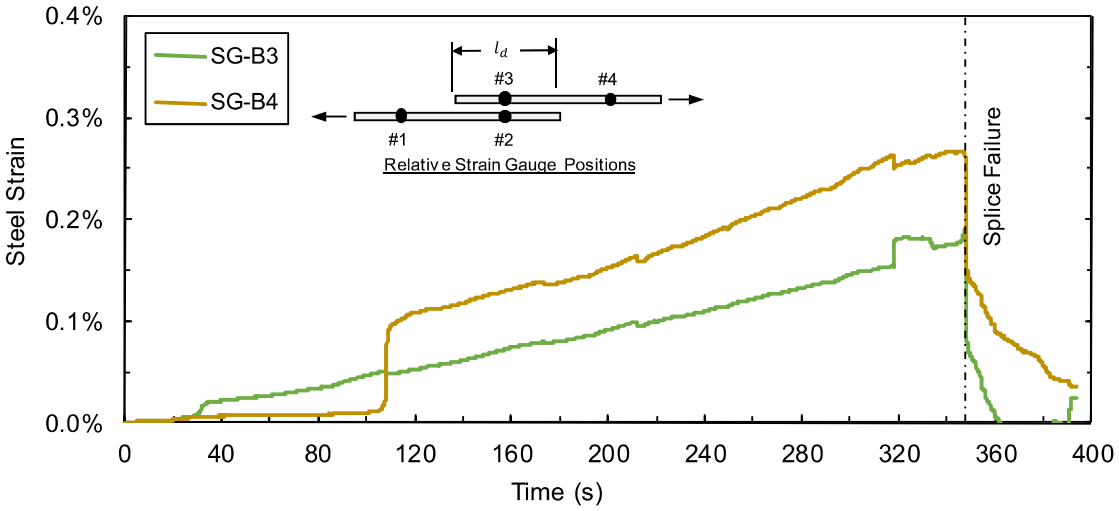

Figure B.235: Test bar "B" strain time-history plot for CP11-LSR.

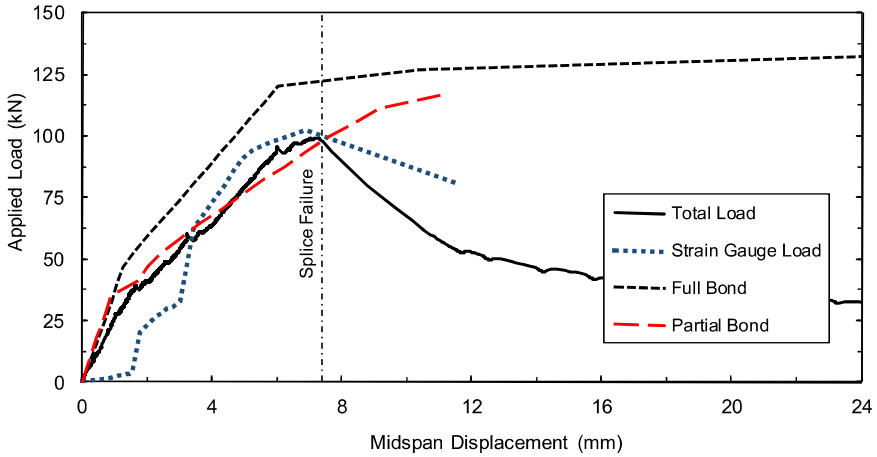

Figure B.236: Comparison of predicted and experimental resistance curves for CP11-LSR.

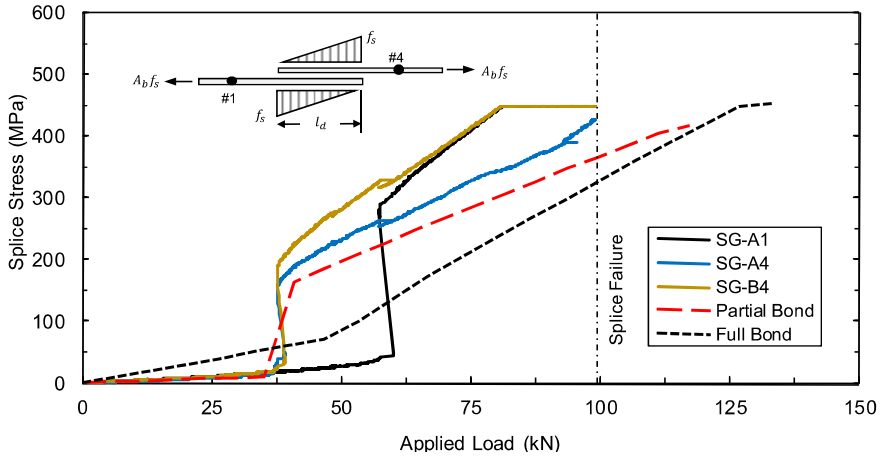

Figure B.237: Comparison of predicted and experimental steel stress developed in spliced reinforcement for CP11-LSR with respect to applied load.

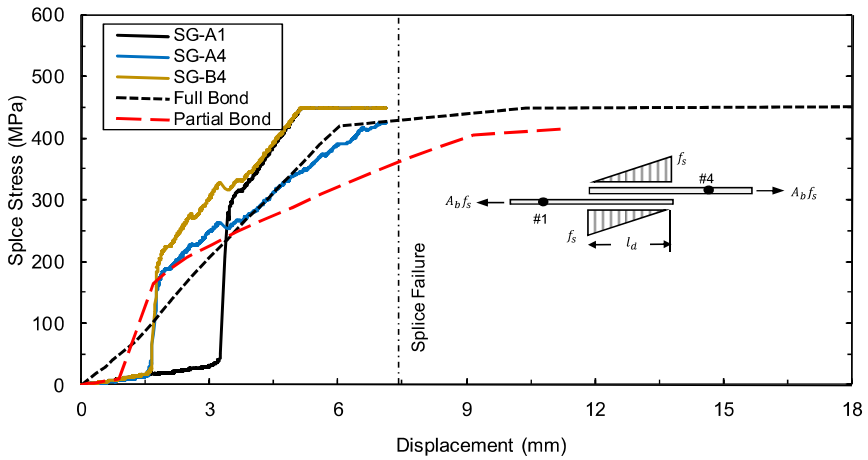

Figure B.238: Comparison of predicted and experimental steel stress developed in spliced reinforcement for CP11-LSR with respect to displacement.

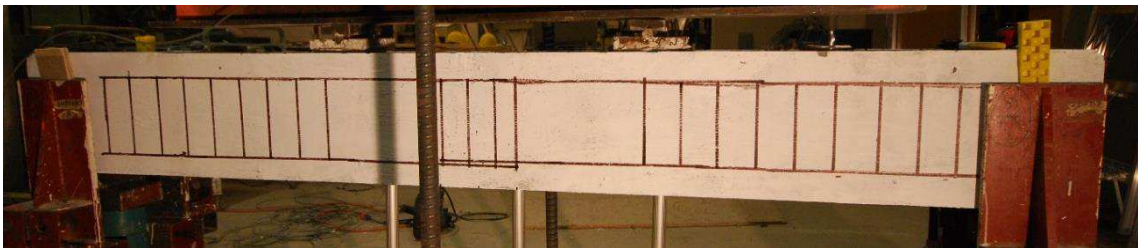

(a) Before low strain rate testing

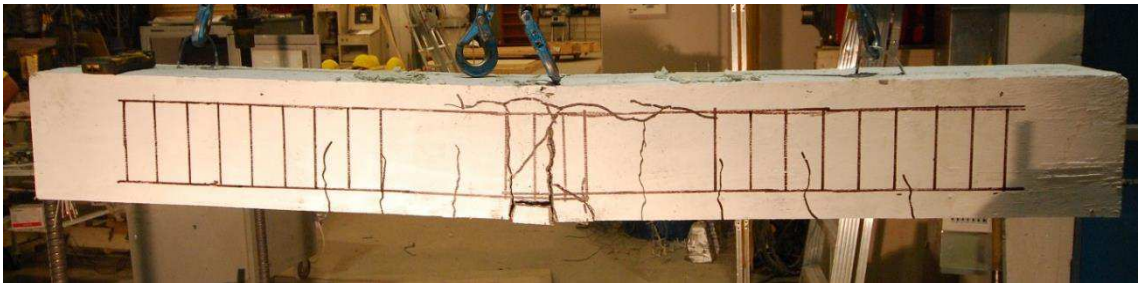

(b) After low strain rate testing

Figure B.239: Photographs of lap splice beam CP11-LSR.

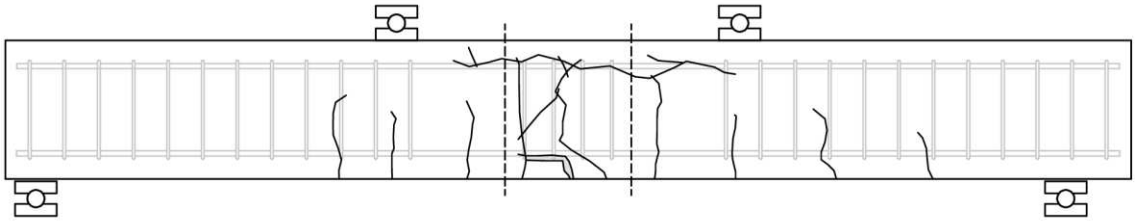

(a) Observed crack profile (north face)

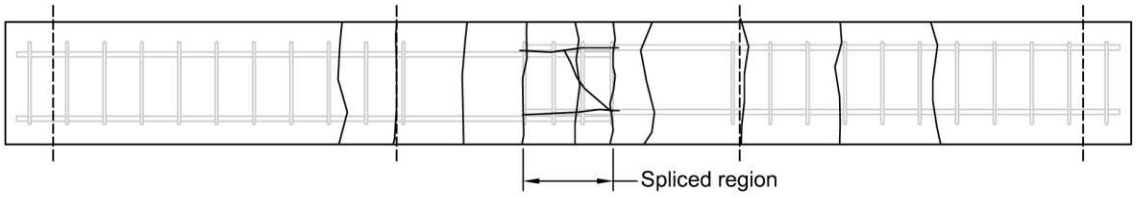

(b) Observed crack profile (bottom face)

Figure B.240: Observed crack profile for lap splice beam CP11-LSR.

CP11-HSR

Lap splice beam CP11-HSR was subjected to high strain rate testing on Aug. 29, 2014. CP11-HSR was designed with 15M reinforcement, 50 MPa concrete, 50 mm cover, and 4-ϕ6.3 mm smooth double leg closed stirrups confining the spliced region. The specimen experienced a side-splitting tensile failure of the cover concrete with significant cover loss. Failure occurred at an applied load of 134.5 kN. Based on strain readings, the stress developed in the spliced bars was 514 MPa. Based on a sectional analysis, the stress developed in the spliced bars was 578 MPa. Time-to-failure was 9.0 ms and strain rate was 0.33 s^{-1}.

Table B.43: Geometry, reinforcing, and material properties for CP11-HSR.

b:	265 mm	Bar:	2-15M	f'_{dc}:	55.7 MPa
h:	300 mm	A_b:	200 mm^2	f_{dy}:	574.9 MPa
l_d:	175 mm	d_b:	16.0 mm	ρ:	0.62%
c_b:	53 mm	N:	4	c/d:	3.1
c_{so}:	48 mm	A_{tr}:	2×31.1 mm^2	$l_d(c_{min} + 0.5d_b)$:	9765 mm^2

Table B.44: Summary of experimental test results for CP11-HSR.

Date:	Aug. 29, 2014	δ_f:	11.0 mm	f_s^t:	514 MPa
P_r:	81.9 kPa	R_f:	134.5 kN	f_s^{cal}:	561 MPa
I_r:	694.0 kPa-ms	t_f:	9.0 ms	$\dot{\varepsilon}$:	0.33 s^{-1}

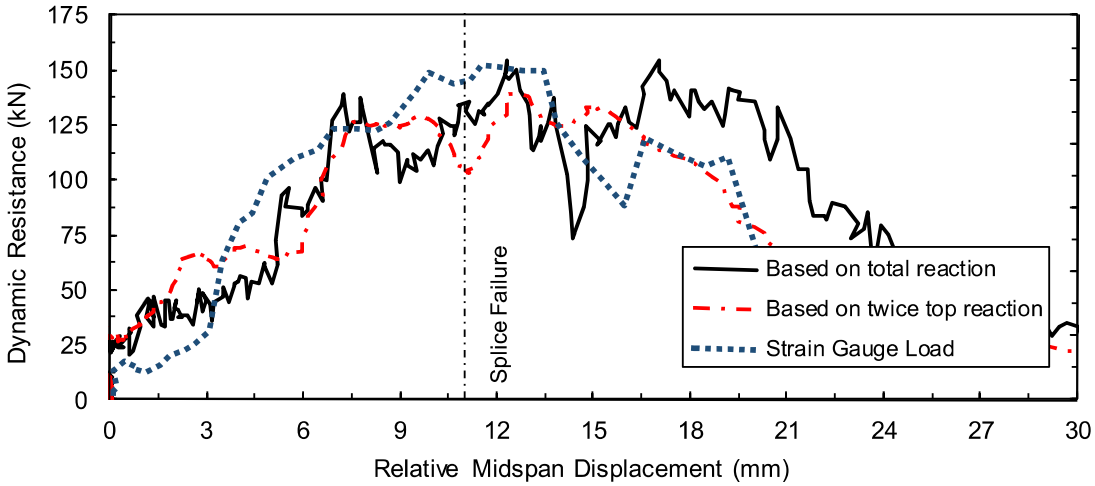

Figure B.241: Load displacement-history plot for CP11-HSR.

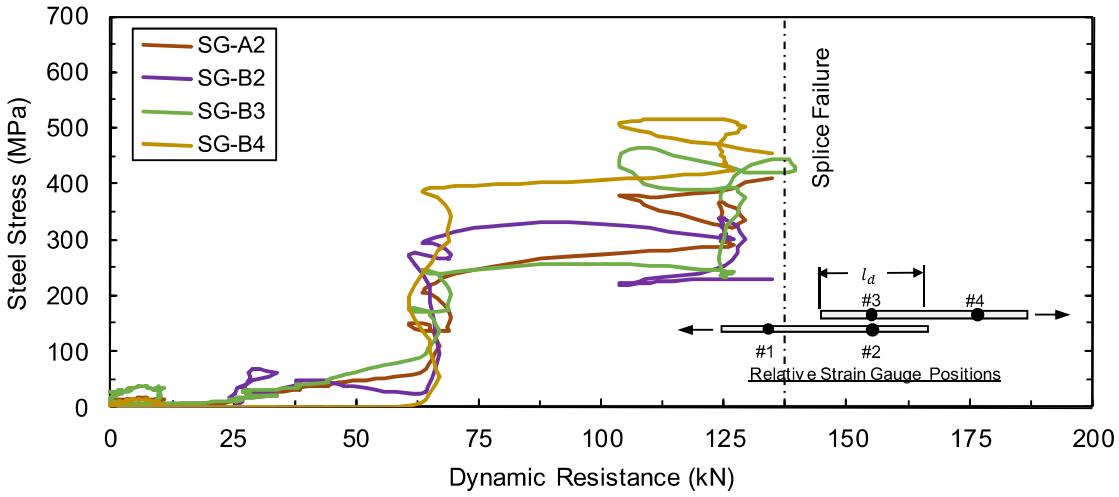

Figure B.242: Steel stress load-history plot for CP11-HSR.

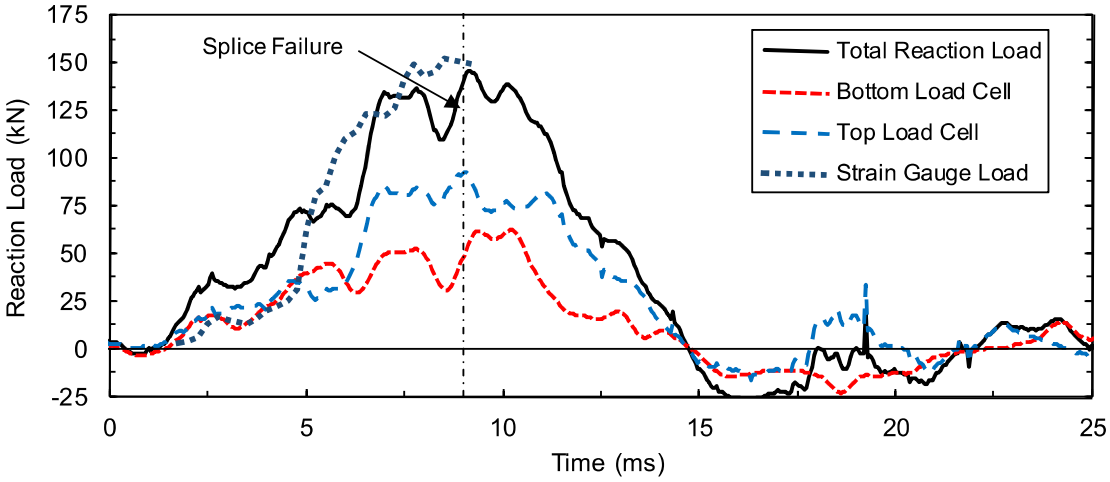

Figure B.243: Load time-history plot for CP11-HSR.

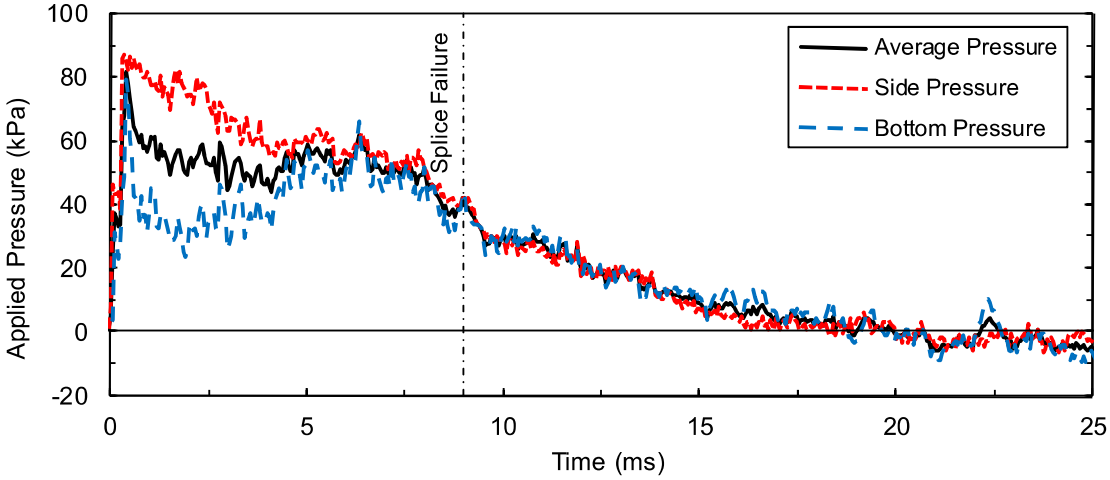

Figure B.244: Pressure time-history plot for CP11-HSR.

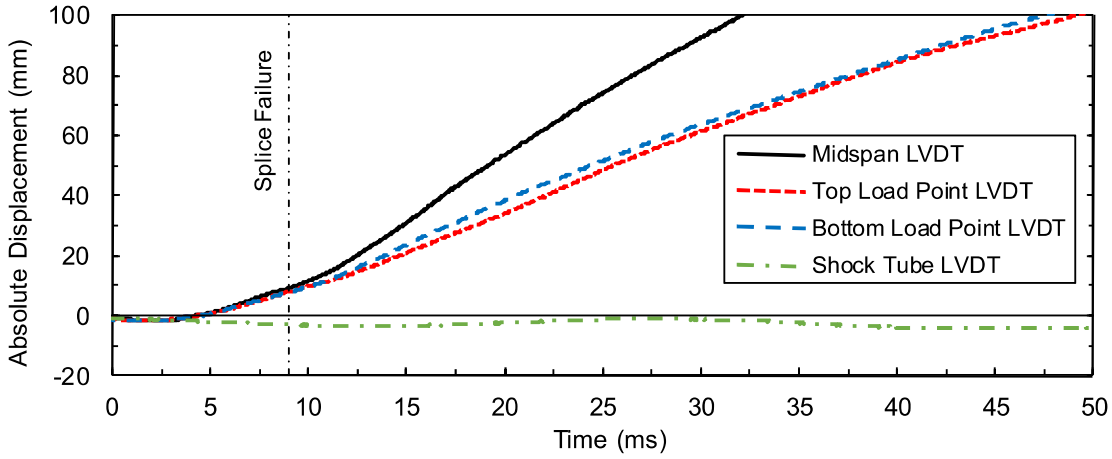

Figure B.245: Displacement time-history plot for CP11-HSR.

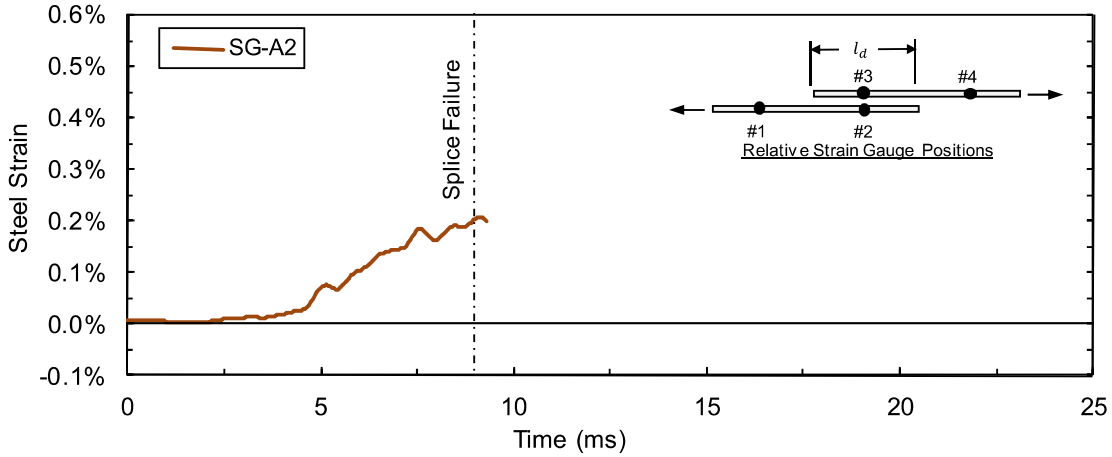

Figure B.246: Test bar "A" strain time-history plot for CP11-HSR.

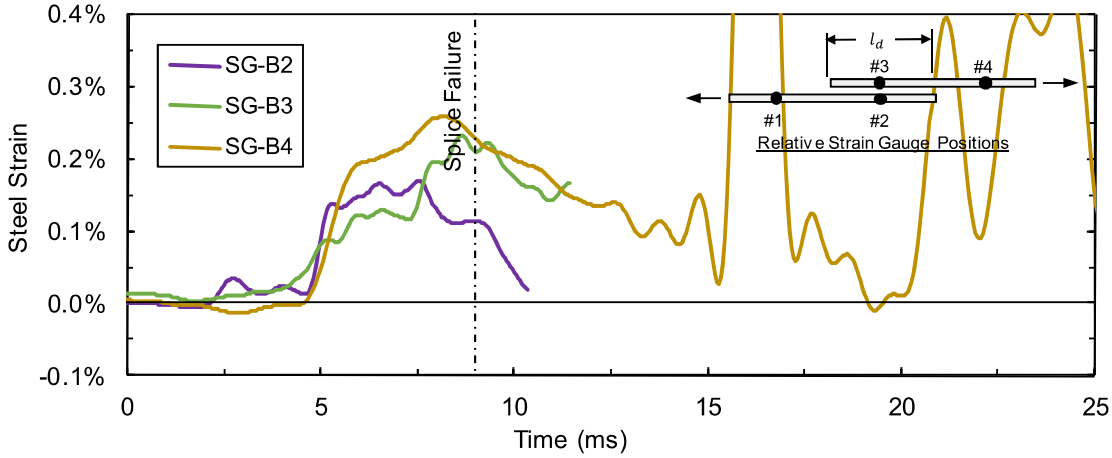

Figure B.247: Test bar "B" strain time-history plot for CP11-HSR.

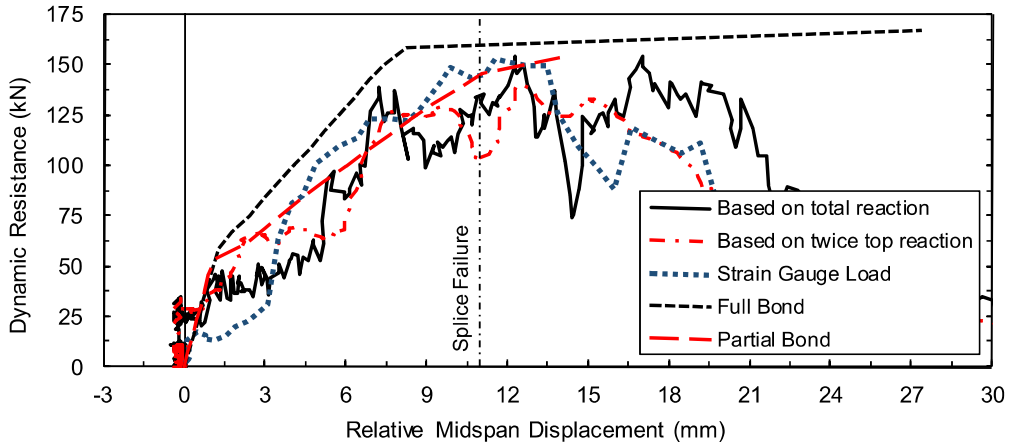

Figure B.248: Comparison of predicted and experimental resistance curves for CP11-HSR.

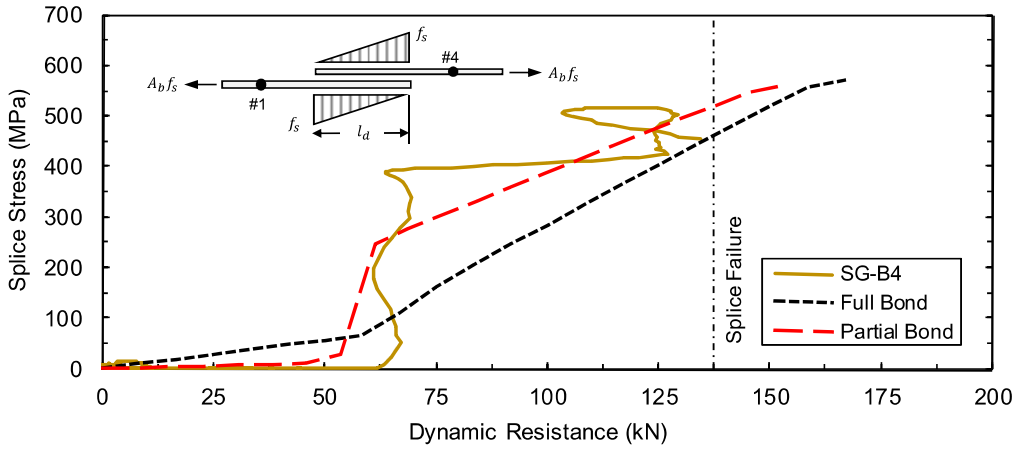

Figure B.249: Comparison of predicted and experimental steel stress developed in spliced reinforcement for CP11-HSR with respect to applied load.

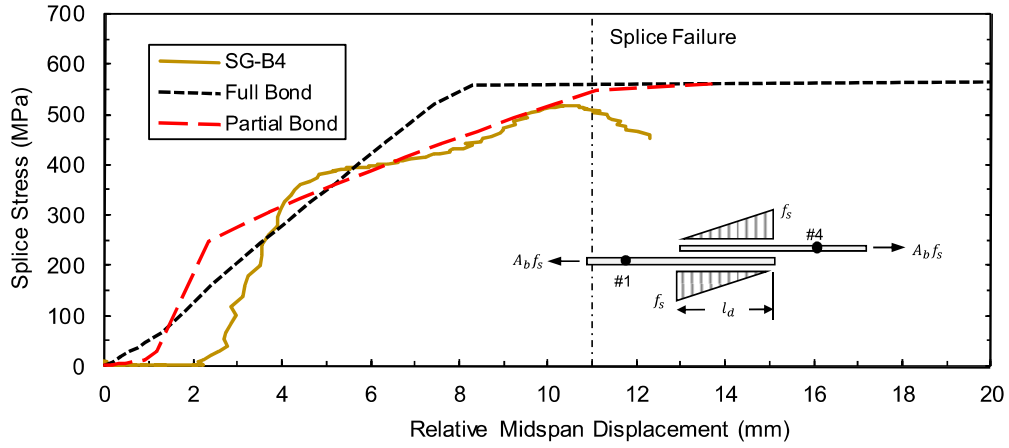

Figure B.250: Comparison of predicted and experimental steel stress developed in spliced reinforcement for CP11-HSR with respect to displacement.

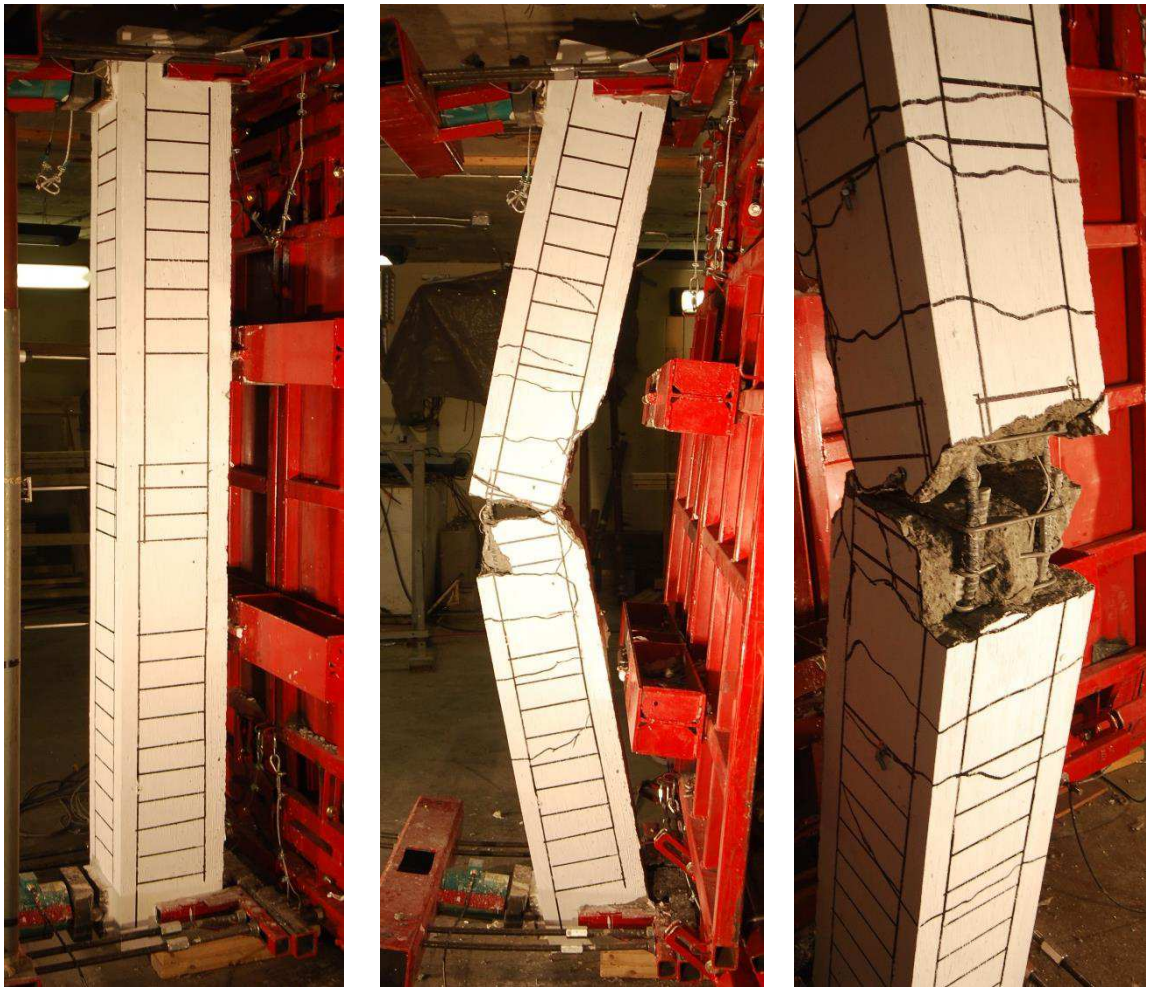

(a) Before high strain rate testing (b) After high strain rate testing (c) After high strain rate testing

Figure B.251: Photographs of lap splice beam CP11-HSR.

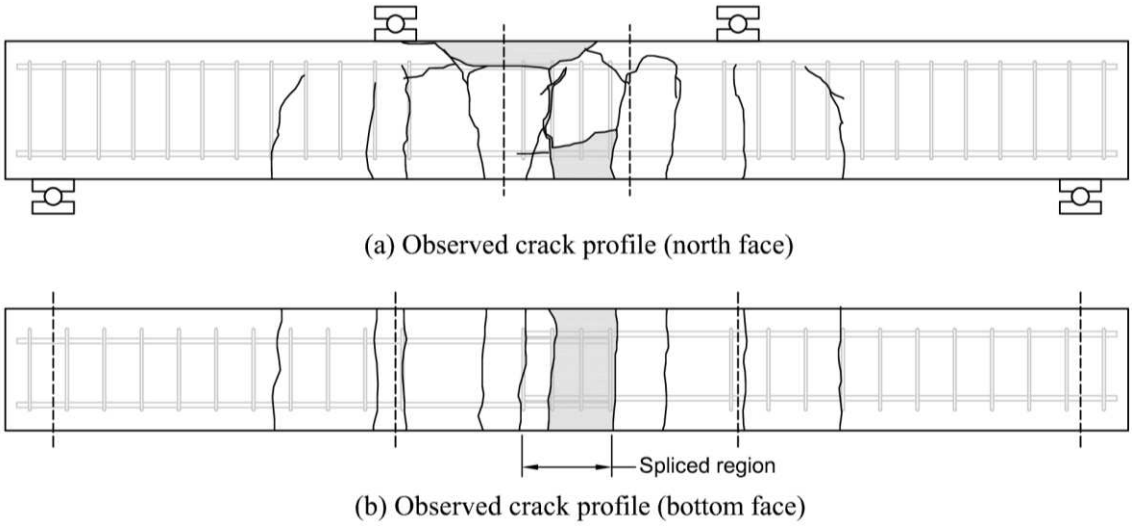

(a) Observed crack profile (north face)

(b) Observed crack profile (bottom face)

Figure B.252: Observed crack profile for lap splice beam CP11-HSR.

CP0-LSR

Lap splice beam CP0-LSR was subjected to low strain rate testing on September 14, 2011. CP0-LSR was designed with 15M reinforcement, 50 MPa concrete, 38 mm bottom cover, 59 mm side cover and without transverse reinforcement in the spliced region. The single splice was centred in the cross-sectional width of the member. The specimen experienced a combined face- and side-splitting tensile failure of the cover concrete with minimal cover loss. Failure occurred at an applied load of 97.6 kN. Based on strain readings, the stress developed in the spliced bars was 470 MPa. Based on a sectional analysis, the stress developed in the spliced bars was 514 MPa. Time-to-failure was 759.0 seconds and strain rate was 3.1×10^{-5} s^{-1}.

Table B.45: Geometry, reinforcing, and material properties for CP0-LSR.

b:	200 mm	Bar:	1-15M	f_c':	45.2 MPa
h:	300 mm	A_b:	200 mm^2	f_y:	470.0 MPa
l_d:	500 mm	d_b:	16.0 mm	ρ:	0.44%
c_b:	38 mm	N:	N/A	c/d:	2.4
c_{so}:	59 mm	A_{tr}:	N/A	$l_d(c_{min}+0.5d_b)$:	23000 mm^2

Table B.46: Summary of experimental test results for CP0-LSR.

Date:	Sept. 14, 2011	δ_f:	36.9 mm	f_s^t:	470 MPa
P_r:	N/A	R_f:	97.6 kN	f_s^{cal}:	517 MPa
I_r:	N/A	t_f:	759.0 s	$\dot{\varepsilon}$:	3.1×10^{-5} s^{-1}

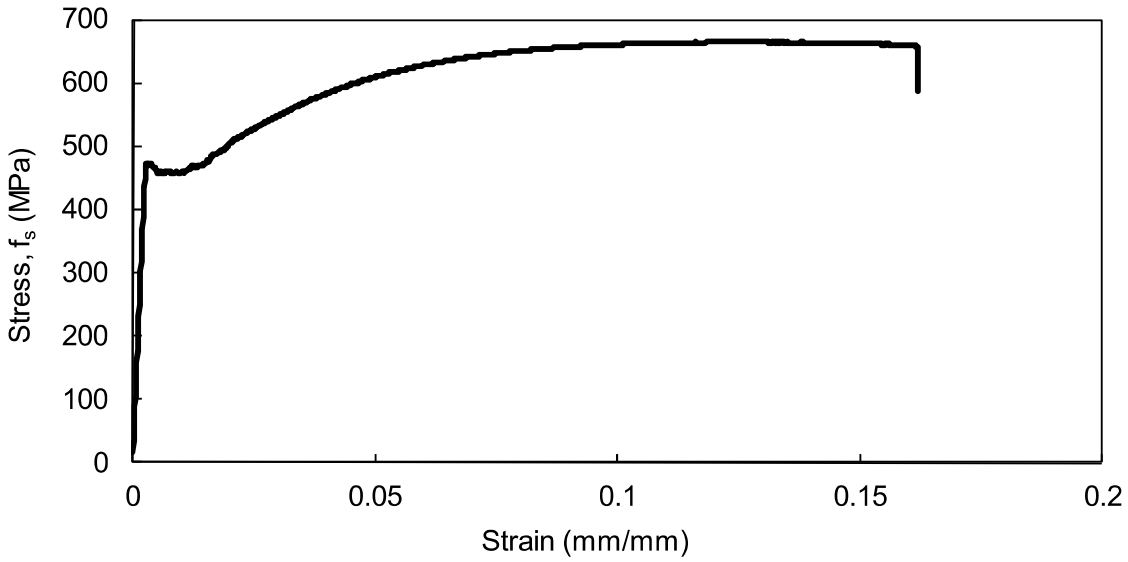

Figure B.253: Static stress-strain curve for 15M rebar used in the CP0 series of tests.

Slightly different strain gauge spacing was adopted for the CPO series of tests. The placement of strain gauges for this series is illustrated in the figure below.

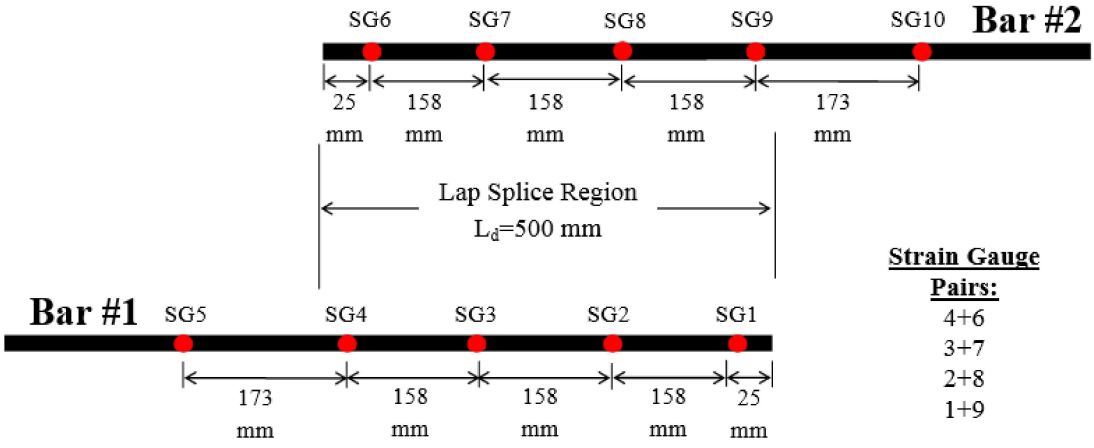

Figure B.254: Strain gauage positioning and nomenclature for CP0 of tests.

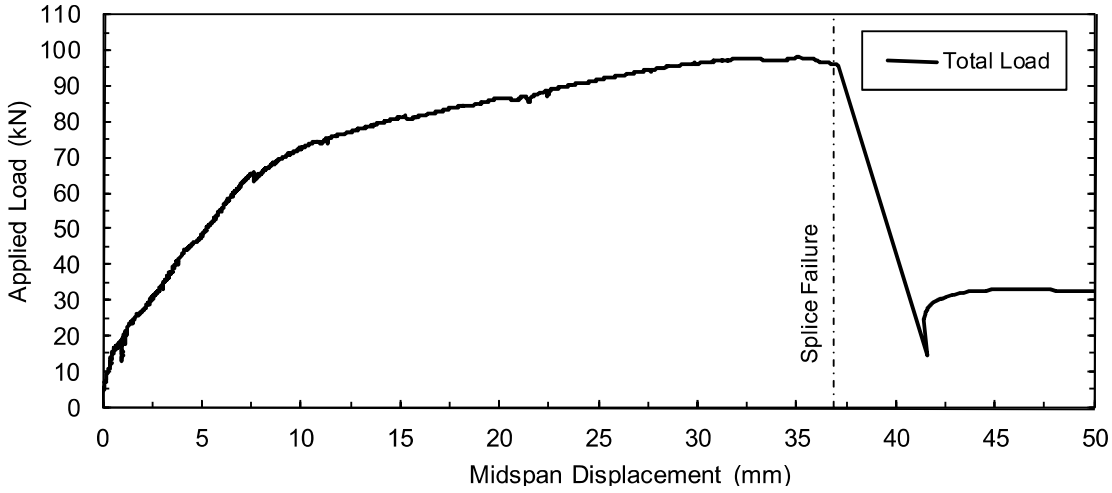

Figure B.255: Load displacement-history plot for CP0-LSR.

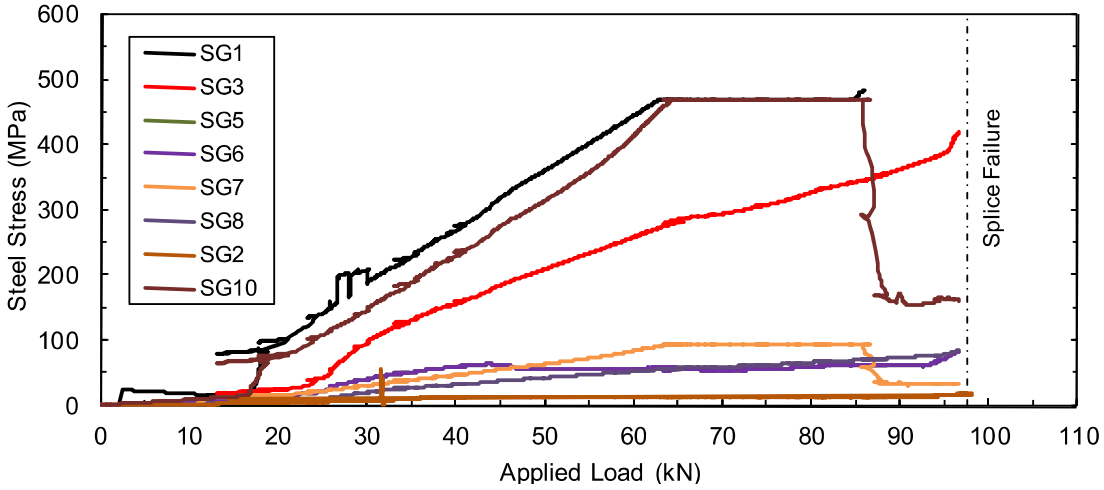

Figure B.256: Steel stress load-history plot for CP0-LSR.

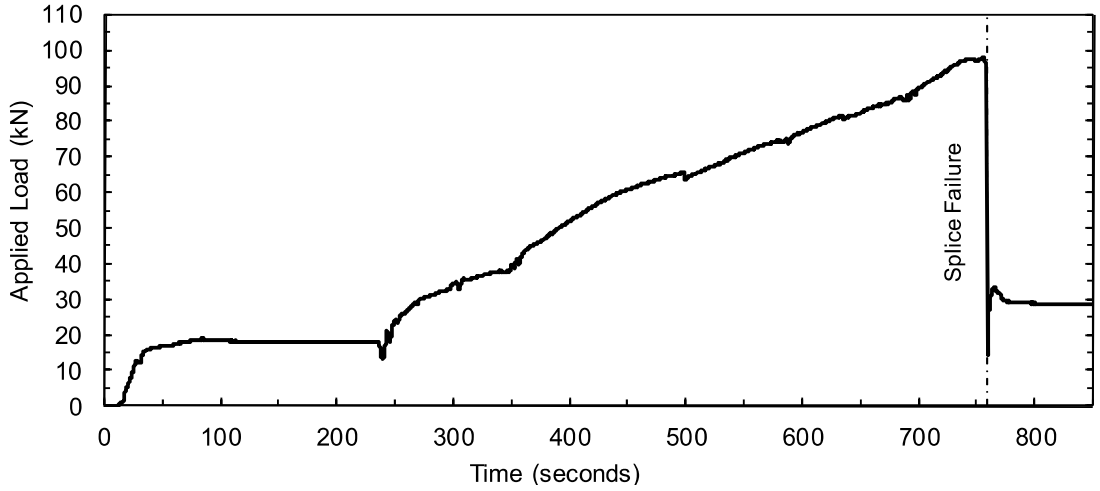

Figure B.257: Load time-history plot for CP0-LSR.

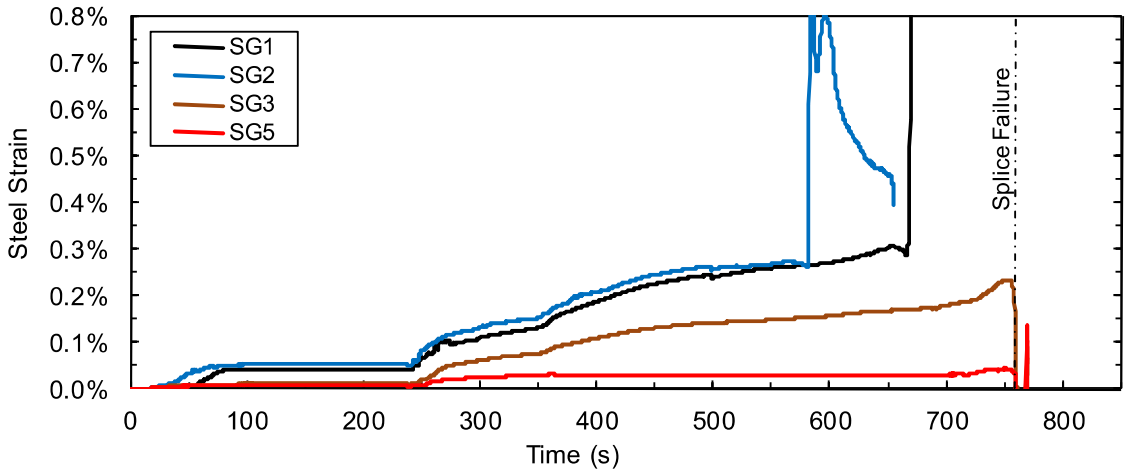

Figure B.258: Test bar "A" strain time-history plot for CP0-LSR.

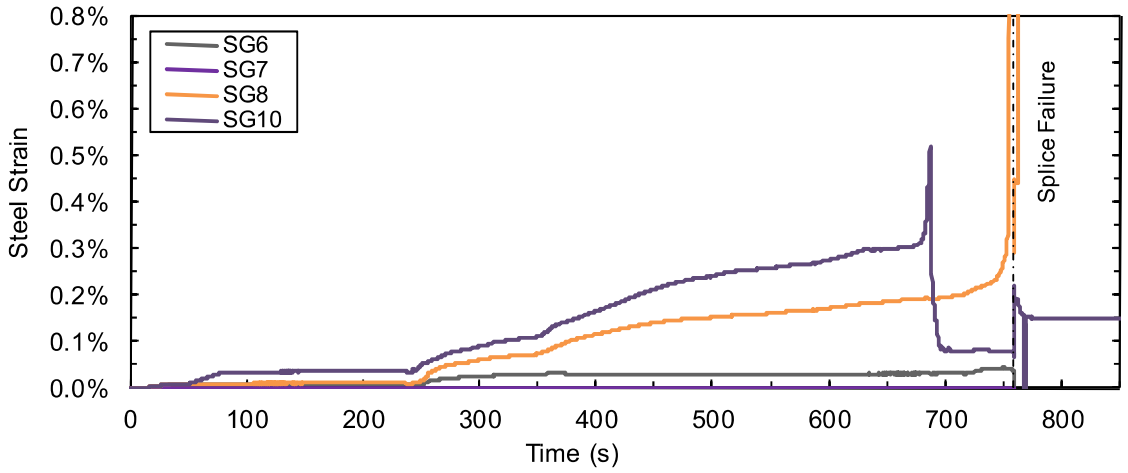

Figure B.259: Test bar "B" strain time-history plot for CP0-LSR.

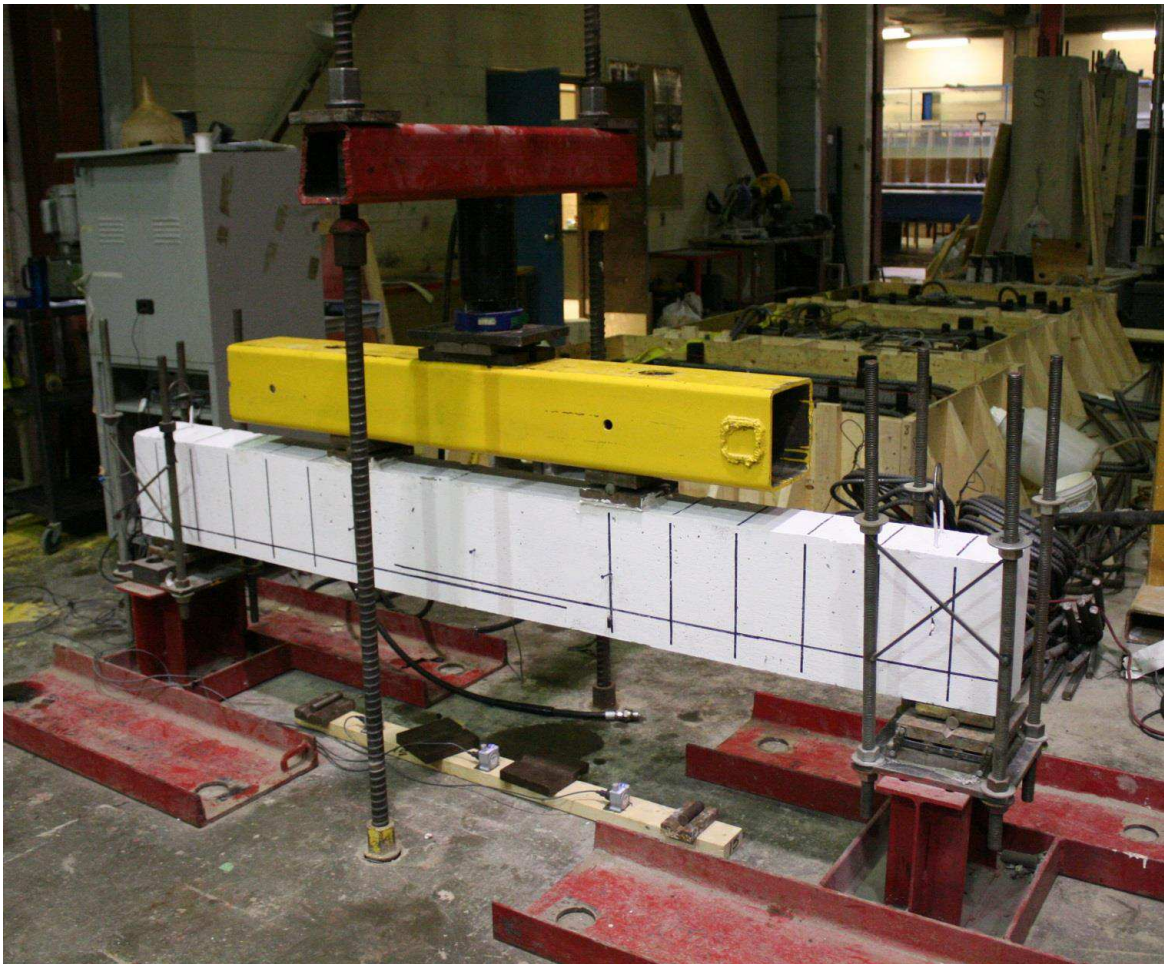

(a) Before testing

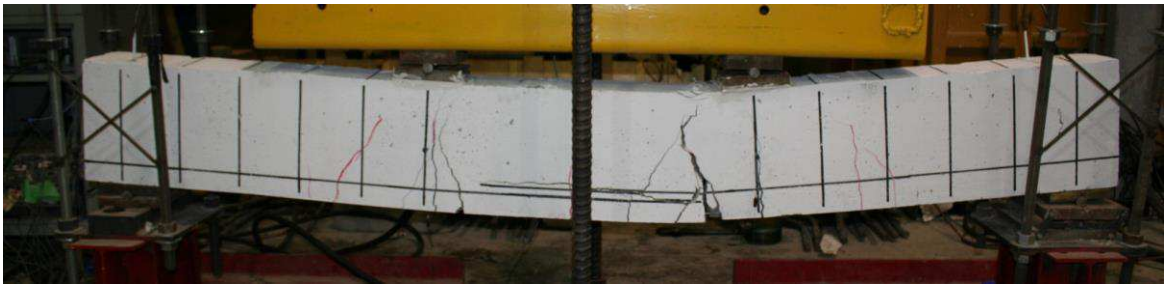

(b) After testing (side face)

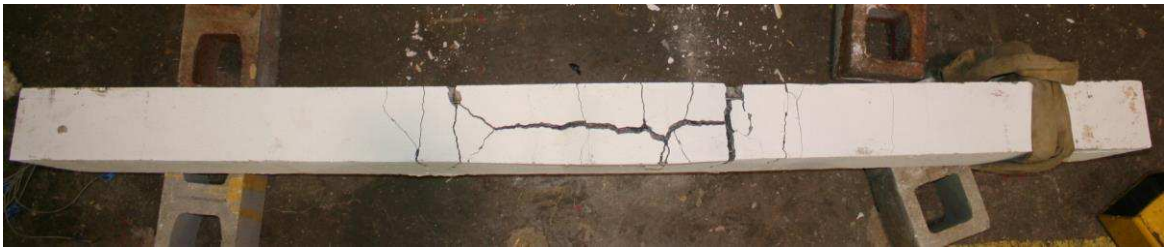

(c) After testing (bottom face)

Figure B.260: Photographs of lap splice beam CP0-LSR.

CP0-HSR1

Lap splice beam CP0-HSR1 was subjected to low strain rate testing on September 7, 2011. CP0-LSR was designed with 15M reinforcement, 50 MPa concrete, 38 mm bottom cover, 59 mm side cover and without transverse reinforcement in the spliced region. The single splice was centred in the cross-sectional width of the member. The specimen experienced a combined face- and side-splitting tensile failure of the cover concrete with minimal cover loss. Load cells were not installed for this test, and load at failure is unknown. However, based on analysis of strain gauge readings, it is estimated that failure occurred when the stress developed in the spliced bars was 631 MPa. Time-to-failure was 18.0 ms and strain rate was 1.1 s^{-1}.

Table B.47: Geometry, reinforcing, and material properties for CP0-HSR1.

b:	200 mm	Bar:	1-15M	f'_{dc}:	57.2 MPa
h:	300 mm	A_b:	200 mm^2	f_{dy}:	613.3 MPa
l_d:	500 mm	d_b:	16.0 mm	ρ:	0.44%
c_b:	38 mm	N:	N/A	c/d:	2.4
c_{so}:	59 mm	A_{tr}:	N/A	$l_d(c_{min} + 0.5d_b)$:	23000 mm^2

Table B.48: Summary of experimental test results for CP0-HSR1.

Date:	Sept. 7, 2011	δ_f:	49.0 mm	f_s^t:	631 MPa
P_r:	87 kPa	R_f:	N/A	f_s^{cal}:	N/A
I_r:	700 kPa-ms	t_f:	18.0 ms	$\dot{\varepsilon}$:	1.1 s^{-1}

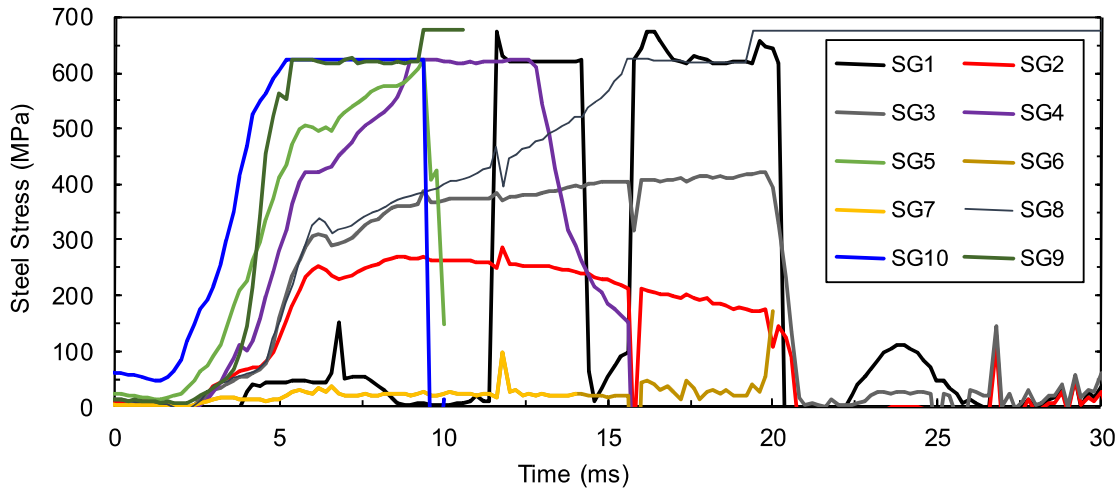

Figure B.261: Steel stress time-history plot for CP0-HSR1.

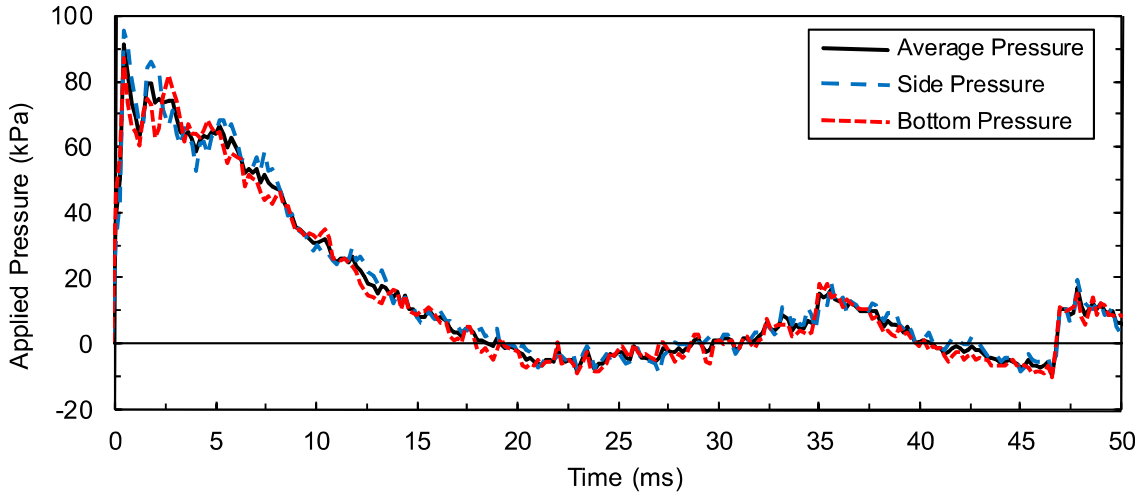

Figure B.262: Pressure time-history plot for CP0-HSR1.

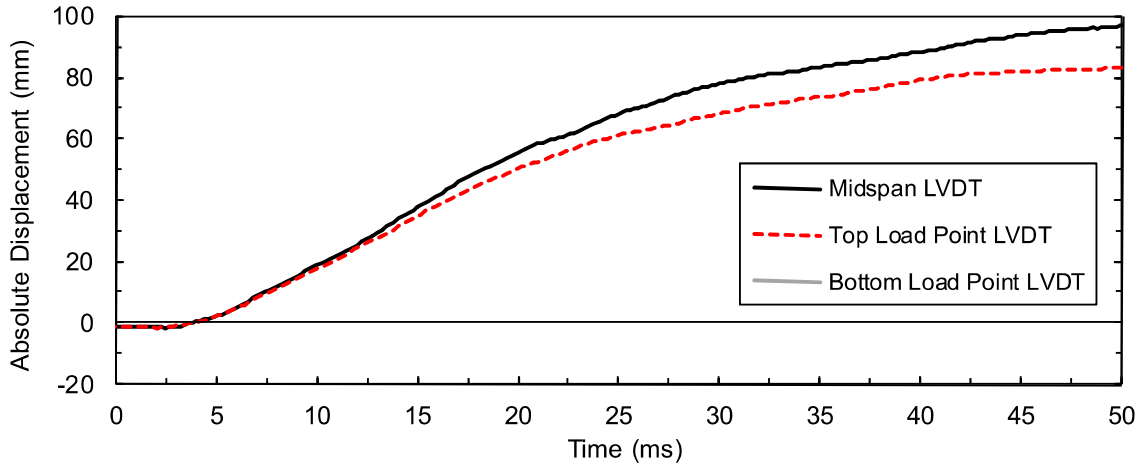

Figure B.263: Displacement time-history plot for CP0-HSR1.

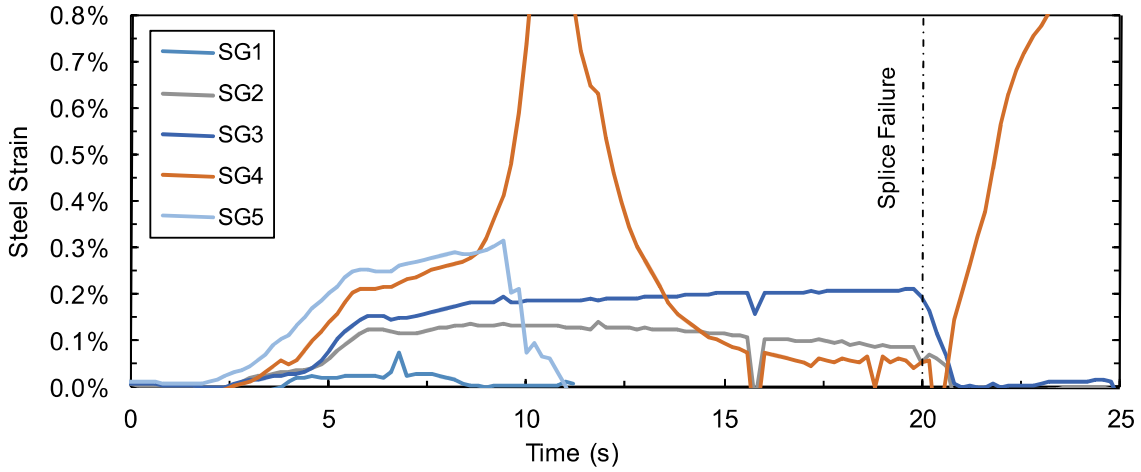

Figure B.264: Test bar "A" strain time-history plot for CP0-HSR1.

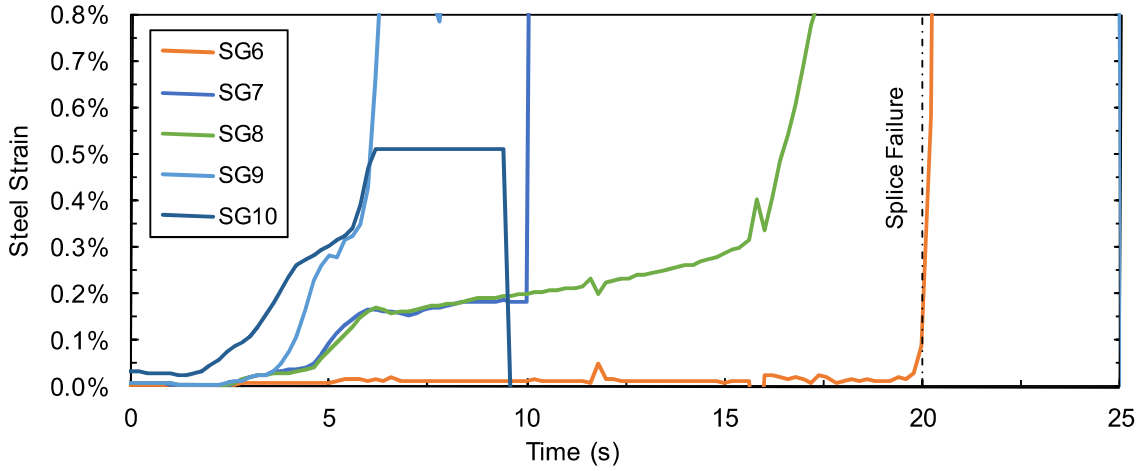

Figure B.265: Test bar "B" strain time-history plot for CP0-HSR1.

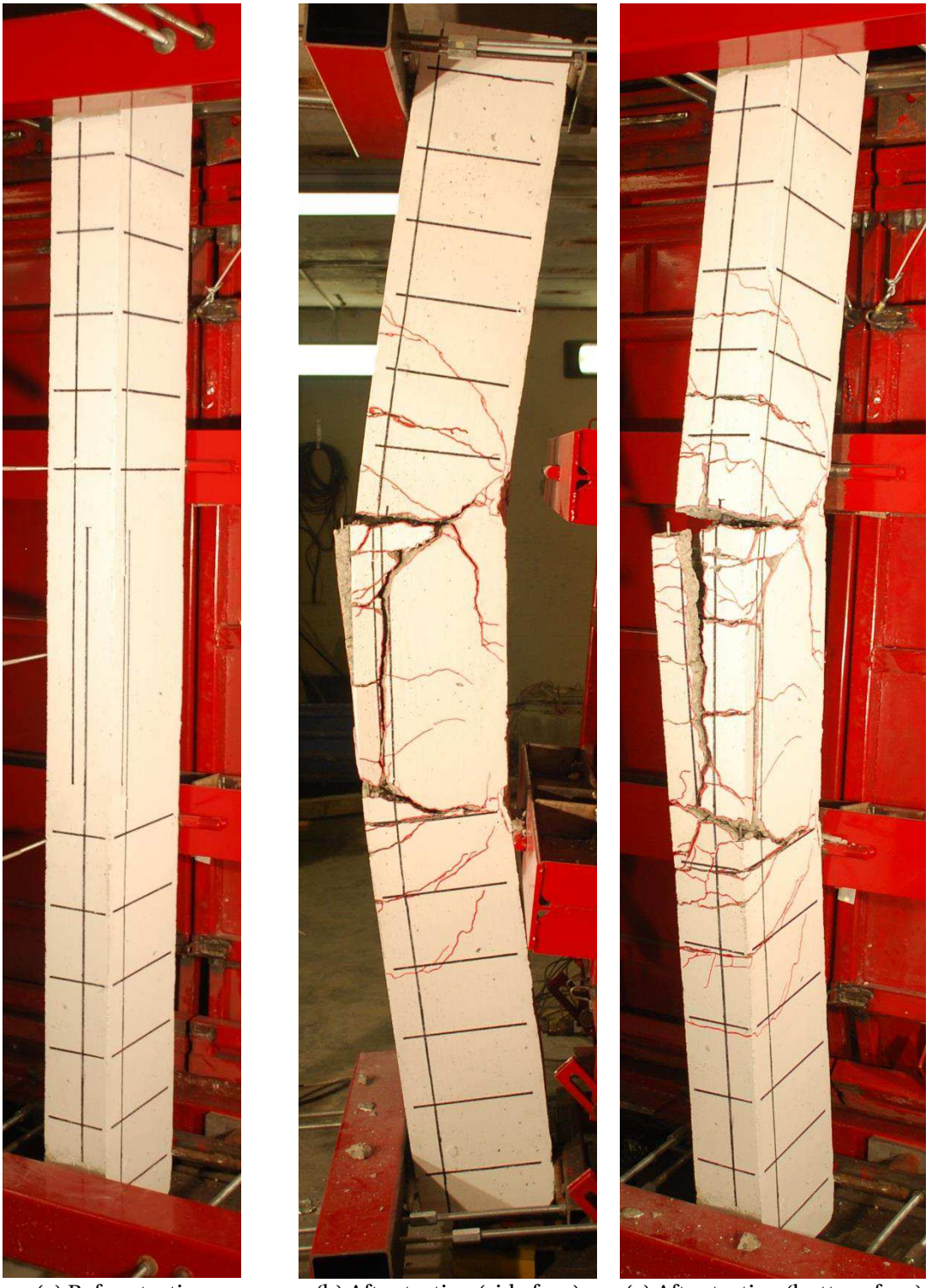

(a) Before testing (b) After testing (side face) (c) After testing (bottom face)

Figure B.266: Photographs of lap splice beam CP0-HSR1.

CP0-HSR2

Lap splice beam CP0-HSR2 was subjected to low strain rate testing on September 7, 2011. CP0-LSR was designed with 15M reinforcement, 50 MPa concrete, 38 mm bottom cover, 59 mm side cover and without transverse reinforcement in the spliced region. The single splice was centred in the cross-sectional width of the member. The specimen experienced a combined face- and side-splitting tensile failure of the cover concrete with minimal cover loss. Load cells were not installed for this test, and load at failure is unknown. However, based on analysis of strain gauge readings, it is estimated that failure occurred when the stress developed in the spliced bars was 624 MPa. Time-to-failure was 19.0 ms and strain rate was 1.1 s^{-1}.

Table B.49: Geometry, reinforcing, and material properties for CP0-HSR2.

b:	200 mm	Bar:	1-15M	f'_{dc}:	57.2 MPa
h:	300 mm	A_b:	200 mm^2	f_{dy}:	613.3 MPa
l_d:	500 mm	d_b:	16.0 mm	ρ:	0.44%
c_b:	38 mm	N:	N/A	c/d:	2.4
c_{so}:	59 mm	A_{tr}:	N/A	$l_d(c_{min} + 0.5d_b)$:	23000 mm^2

Table B.50: Summary of experimental test results for CP0-HSR2.

Date:	Sept. 7, 2011	δ_f:	38.7 mm	f_s^t:	631 MPa
P_r:	87 kPa	R_f:	N/A	f_s^{cal}:	N/A
I_r:	700 kPa-ms	t_f:	19.0 ms	$\dot{\varepsilon}$:	1.1 s^{-1}

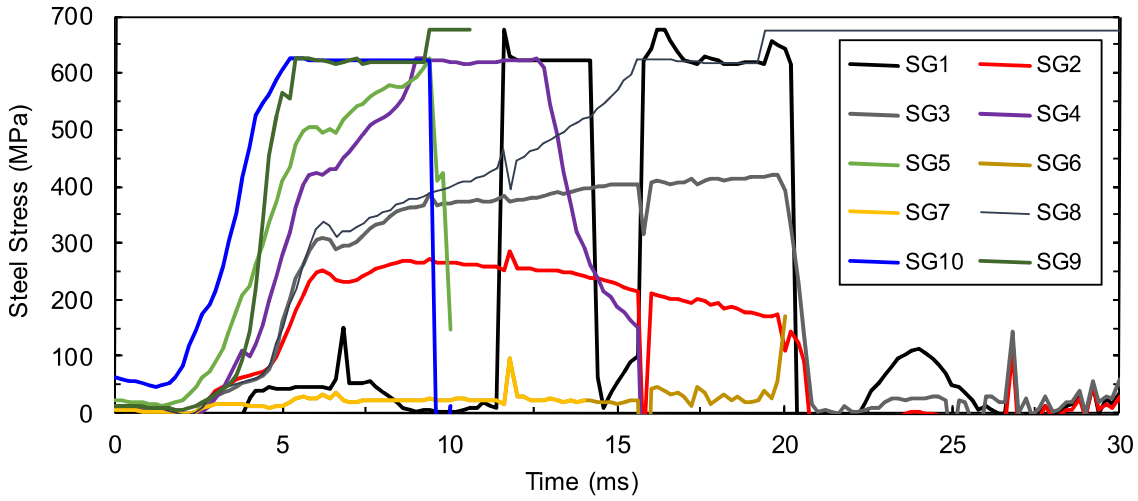

Figure B.267: Steel stress time-history plot for CP0-HSR2.

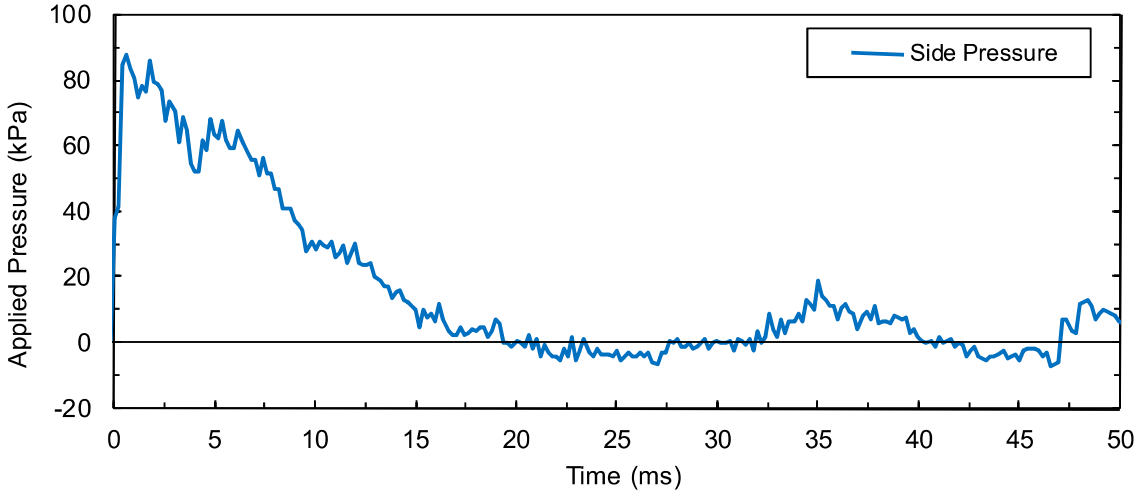

Figure B.268: Pressure time-history plot for CP0-HSR2.

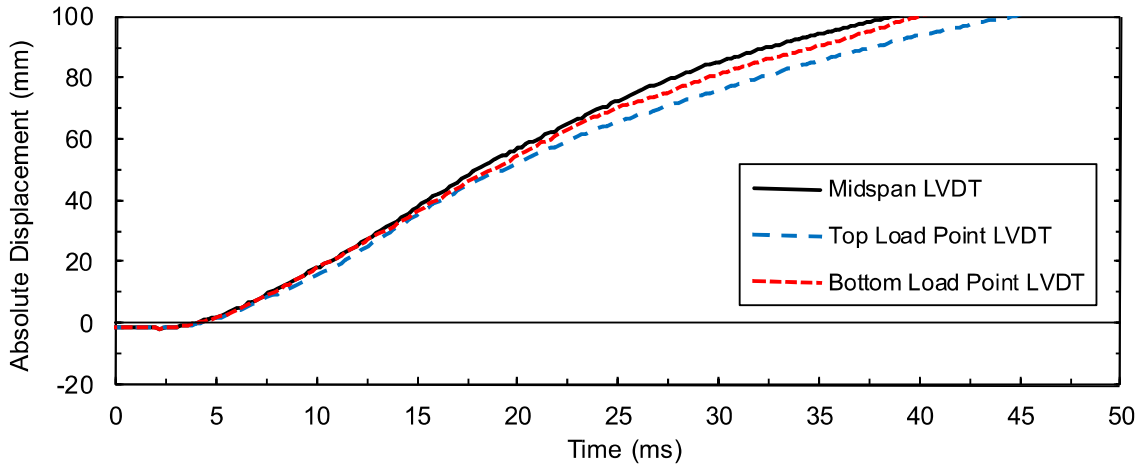

Figure B.269: Displacement time-history plot for CP0-HSR2.

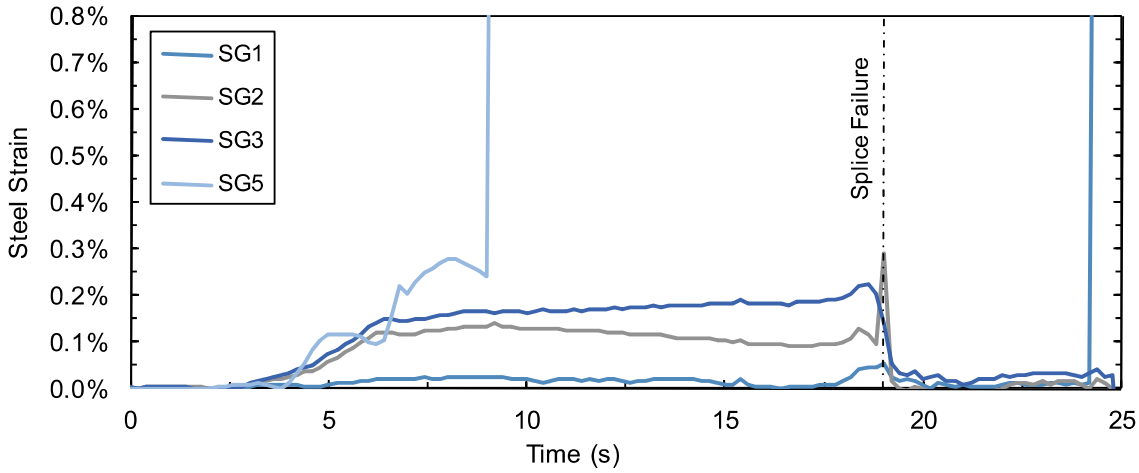

Figure B.270: Test bar "A" strain time-history plot for CP0-HSR2.

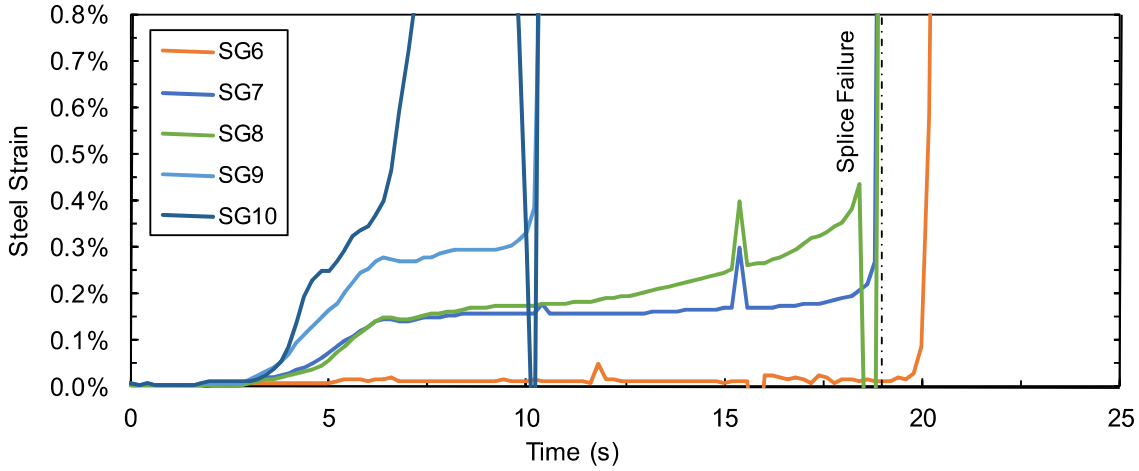

Figure B.271: Test bar "B" strain time-history plot for CP0-HSR2.

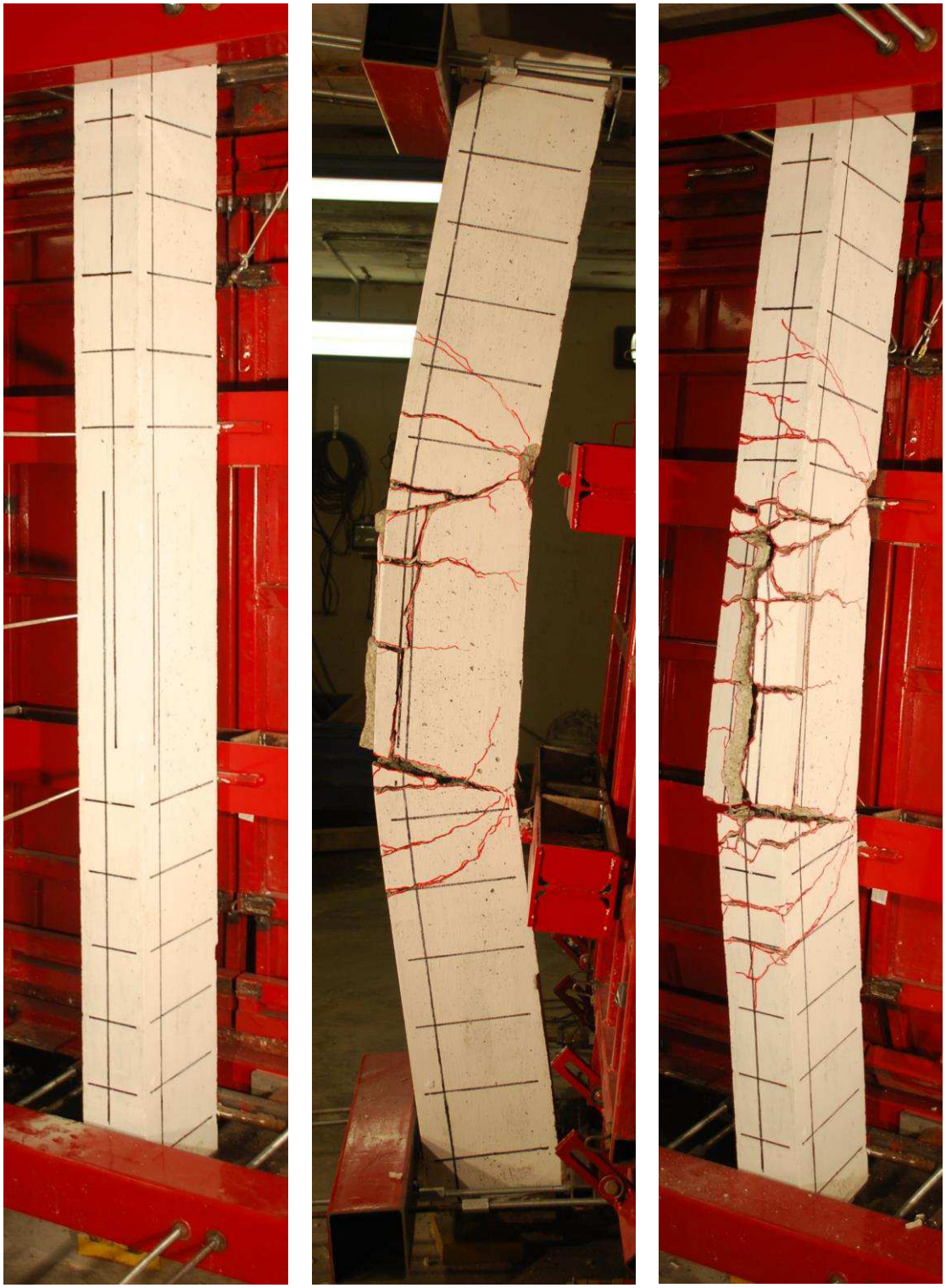

(a) Before testing (b) After testing (side face) (c) After testing (bottom face)

Figure B.272: Photographs of lap splice beam CP0-HSR2.

Appendix C

Dynamic Support Reactions

This appendix presents the derivation of Eqs. (4.1) and (4.2) for the dynamic support reactions of a simply supported beam subjected to equally spaced four-point loading. The equations give consideration to the distributed mass of the beam ($\bar{m}$) and an additional lumped mass (m_c) at the location of each of the load points.

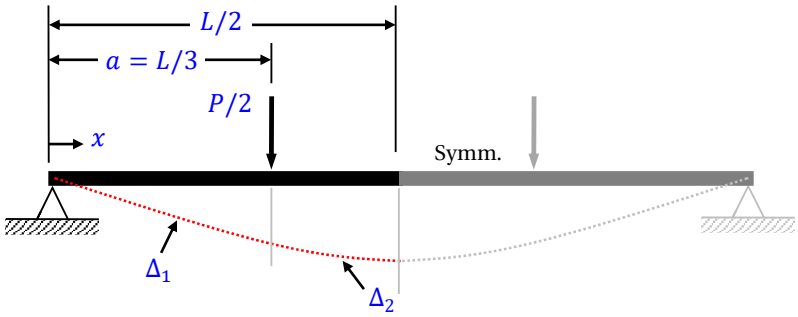

Deflected Shape

$0 \le x \le L/3 \qquad \Delta_1 = \frac{Px}{12EI}(3La - 3a^2 - x^2)$

$L/3 \le x \le L/2 \quad \Delta_2 = \frac{Pa}{12EI}(3Lx - 3x^2 - a^2)$

where $a = L/3$

Maximum deflection at $x = L/2 \quad \Delta_{max} = \frac{23PL^3}{1296EI}$

Mode Shape

$0 \le x \le L/3 \qquad \phi_1 = \frac{\Delta_1}{\Delta_{max}} = \frac{36x}{23L^3}(2L^2 - 3x^2)$

$L/3 \le x \le L/2 \quad \phi_2 = \frac{\Delta_2}{\Delta_{max}} = \frac{36}{23L^2}\left(3Lx - 3x^2 - \frac{L^2}{9}\right)$

Centroid of Distributed Mass

$$\bar{x} = \frac{\int_0^{L/3} x\phi_1 dx \; + \int_{L/3}^{L/2} x\phi_2 dx}{\int_0^{L/3} \phi_1 dx \; + \int_{L/3}^{L/2} \phi_2 dx}$$

$$\int_0^{\frac{L}{3}} x\phi_1 dx \; = \int_0^{\frac{L}{3}} \frac{36}{23L^3}(2L^2x^2 - 3x^4)dx = \frac{4L^2}{115}$$

$$\int_{L/3}^{L/2} x\phi_2 dx = \int_{L/3}^{L/2} \frac{36}{23L^2}\left(3L^2x - 3x^3 - \frac{L^2x}{9}\right)dx = \frac{221L^2}{3312}$$

$$\int_0^{L/3} \phi_1 dx = \int_0^{L/3} \frac{36}{23L^3}(2L^2x - 3x^3)dx = \frac{11L}{69}$$

$$\int_{L/3}^{L/2} \phi_2 dx = \int_{L/3}^{L/2} \frac{36}{23L^2}\left(3Lx - 3x^2 - \frac{L^2}{9}\right)dx = \frac{11L}{69}$$

$$\therefore \bar{x} = \frac{\frac{4L^2}{115} + \frac{221L^2}{3312}}{\frac{11L}{69} + \frac{11L}{69}} = 0.318L$$

Equivalent Lumped Distributed Mass

$$m^* = \left(\int_0^{L/3} \phi_1 dx + \int_{L/3}^{L/2} \phi_2 dx\right)\bar{m} = \frac{22L\bar{m}}{69} = 0.319L\bar{m}$$

Participation Factored for Concentrated Mass

$$\Phi_c = \phi_1\left(x = \frac{L}{3}\right) = \frac{36L}{3 \times 23L^3}\left(2L^2 - \frac{3L^2}{9}\right) = \frac{20}{23} = 0.870$$

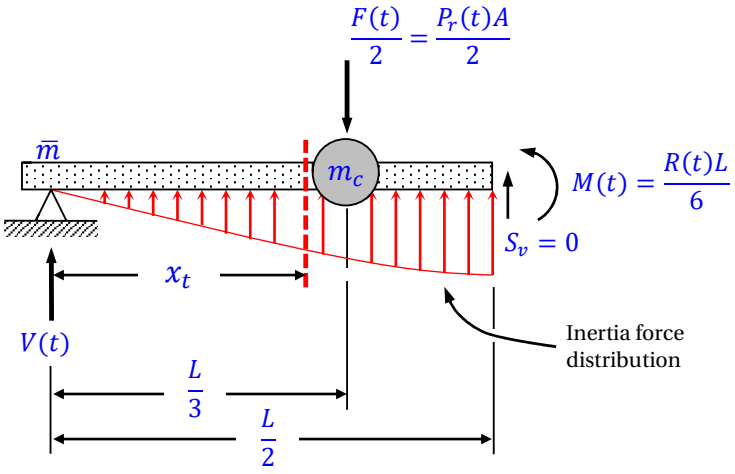

Centroid of Total Inertia Distribution

$$x_t = \frac{\bar{x}m^* + \frac{L}{3}\Phi_c m_c}{m^* + \Phi_c m_c} = \frac{0.101L^2\bar{m} + 0.290Lm_c}{0.318L\bar{m} + 0.870m_c}$$ As shown in Eq. (4.1)

Support Reactions

Referring to the figure above, compute the sum of moments about the centroid of total inertia distribution at $x = x_t$ to establish a relationship for $V(t)$ in terms of the applied force $F(t)$ and internal resistance $R(t)$.

$\circlearrowleft^+ \sum M_{x_t} = 0$

$$V(t)x_t + \frac{F(t)}{2}\left(\frac{L}{3} - x_t\right) - R(t)\frac{L}{6} = 0$$

$$V(t) = R(t)\frac{L}{6x_t} + F(t)\frac{(x_t - L/3)}{2x_t}$$ As shown in Eq. (4.2)

Verification

With $L = 2.232\ m$ ...

$$x_t = \frac{0.503\overline{m} + 0.647m_c}{0.710\overline{m} + 0.870m_c}$$

$$V(t) = \frac{0.372R(t)}{x_t} + \frac{F(t)(x_t - 0.744)}{2x_t}$$

As $m_c \to 0$

$$x_t = \frac{0.503\overline{m} + 0.647 \times 0}{0.710\overline{m} + 0.870 \times 0} = 0.708\ m$$

$$V(t) = \frac{0.372R(t)}{0.708} + \frac{F(t)(0.708 - 0.744)}{2 \times 0.708} = 0.525R(t) - 0.025F(t)$$

The equation for $V(t)$ with $m_c = 0$, above, yields the correct solution for the dynamic support reactions of a simply supported beam subjected to four point bending with distributed mass listed in Table 5.1 of Biggs (1964). As $\overline{m} \to 0$, $V(t) = 0.5R(t)$, meaning that the sum of both of the dynamic support reactions is equal to the internal resistance of the member.

Appendix D

List of Tables

Table 2.1: List of common reinforced concrete bond terminology (ACI, 2003) 21
Table 3.1: Elastic bond-slip parameters obtained through beam-end tests: (a) lb = 200 mm beam-ends, and; (b) lb = 400 mm beam-ends. 44
Table 4.1: Construction details and material properties for lap splice companion pairs. 70
Table 4.2: Low and high strain rate experimental results for lap splice companion pairs. 71
Table 5.1: Database of specimen properties and test results for lap splices without transverse reinforcement. 105
Table 5.2: Database of specimen properties and test results for lap splices with transverse reinforcement. 106
Table 6.1: Construction and reinforcing details of lap splice beams. 131
Table 6.2: Comparison of experimental and predicted low and high strain rate results for the case of partial bond. 132
Table 6.3: Summary statistics for low and high strain rate resistance curve predictions for the case of partial bond. 132

Appendix E

List of Figures

Figure 2.1: Bond force transfer mechanisms (ACI, 2003). 21
Figure 2.2: Free-body diagram of a bonded bar subjected a change in stress. (Wight and MacGregor, 2009) 21
Figure 2.3: Variation in stress in a reinforced concrete beam: (a) reinforced concrete beam; (b) moment diagram; (c) tensile steel stress; (c) variation in tensile stress in reinforcement, and; (d) distribution of bond stress along the reinforcement (Wight and MacGregor, 2009). 22
Figure 2.4: Typical bond splitting cracks (ACI, 2003). 22
Figure 2.5: Influence of high strain rates on concrete properties: (a) compressive strength (Biscoff and Perry, 1991), and; (b) tensile strength of concrete (Malvar and Crawford, 1998b). 23
Figure 2.6: Influence of high strain rates on the yield and ultimate strengths of various steels (Malvar, 1998a). 24
Figure 2.7: Drop weight impactor used by Rezansoff et al. (1975). 25
Figure 2.8: Pull-out specimen studied by Vos and Reinhardt (1982). 25
Figure 2.9: Push-in/pull-out specimen used by Yan (1992). 26
Figure 2.10: Test apparatus and typical pull-out specimens used by Weathersby (2003). 26
Figure 2.11: Typical pull-out specimens studied by Solomos and Berra (2010). 26
Figure 2.12: Beam specimens tested by Toikka (2012) and Toikka et al. (2015) (adaopted from Toikka et al. , 2015). 27
Figure 2.13: Sample bond-slip data presented by Michal et al. (2015). 28
Figure 3.1: Construction and reinforcement details of beam-end specimens. 44

Figure 3.2: Details of the bonded test bar: (a) photograph of formwork construction and PVC bond breakers; (b) schematic of milled slot and strain gauge placement, and; (c) photograph of completed test bar. 45
Figure 3.3: Measured static stress-strain relationship of 20M reinforcement. 45
Figure 3.4: Spacing and nomenclature of strain gauges for beam-end tests. 46
Figure 3.5: Test fixture for (a) static tests, and (b) dynamic tests. 47
Figure 3.6: Idealized schematic of the high strain rate test fixture..... 48
Figure 3.7: Typical specimen failure modes: (a) face splitting failure for static and high strain rate $lb = 200$ mm; (b) face splitting failure for static $lb = 400$ mm; (c) face splitting failure for dynamic $lb = 400$ mm, and; (d) rupture of test bar for high strain rate $lb = 400$ mm..... 48
Figure 3.8: Typical distribution of steel strains in the bonded region. 49
Figure 3.9: Typical distribution of bar slip in the bonded region. 50
Figure 3.10: Static and high strain rate elastic bond-slip relationships for beam-ends: (a) $lb = 200$ mm specimens, and; (b) $lb = 400$ mm specimens. 51
Figure 4.1: Construction and reinforcement details of lap splice beams. 72
Figure 4.2: Static stress-strain relationships of reinforcement. 73
Figure 4.3: Photograph of low strain rate test fixture. 73
Figure 4.4: Illustration of the high strain rate test fixture. 74
Figure 4.5: Photographs of high strain rate test fixture. 75
Figure 4.6: Sample reflected pressure and impulse time-histories. 76
Figure 4.7: Definition of strain rate. 76
Figure 4.8: Typical stages of response observed during low- and high-rate beam tests. 77
Figure 4.9: Free-body-diagram of idealized beam and load transfer device used for derivation of dynamic support reactions. 77
Figure 4.10: Comparison of resistance functions obtained for CP6-HSR. 78
Figure 4.11: Comparison of low and high strain rate member response for lap splices constructed with 10M rebar and not confined by transverse reinforcement. 78
Figure 4.12: Comparison of low and high strain rate member response for lap splices constructed with 15M rebar and not confined by transverse reinforcement. 79
Figure 4.13: Comparison of low and high strain rate member response for lap splices constructed with 20M rebar and not confined by transverse reinforcement. 79
Figure 4.14: Comparison of low and high strain rate member response for lap splices constructed with 15M rebar and confined by transverse reinforcement. 80
Figure 4.15: Comparison of splice damage for beams with 10M reinforcement. 81
Figure 4.16: Comparison of splice damage for beams with 15M reinforcement. 81
Figure 4.17: Comparison of splice damage for beams with 20M reinforcement. 82

Figure 4.18: Definition of bond energy and toughness parameters (adapted from Aoude et al., 2014). 82
Figure 4.19: Effect of high strain rate on bond strength of splices not confined by transverse reinforcement with respect to $cmin/db$ 83
Figure 4.20: Effect of high strain rate on bond strength of splices confined by transverse reinforcement with respect to $cmin/db$ 83
Figure 4.21: Effect of high strain rate on bond strength of splices with and without transverse reinforcement with respect to ls/db. 84
Figure 5.1: Idealized stress-strain relationships. 107
Figure 5.2: Specimen details of the lap splice beams [Chapter 4]. 107
Figure 5.3: Specimens details of the cantilever beam-ends [Chapter 3] 108
Figure 5.4: Specimen details of the lap splice beams tested by Rezansoff et al. (1975) 108
Figure 5.5: Influence of strain rate on the variation of $Tc/fc'1/4$ with respect to $ld(cmin + 0.5db)$. 109
Figure 5.6: Variation of $DIFTc$ with respect to $ld(cmin + 0.5db)$ and rebar size. 109
Figure 5.7: Influence of strain rate on the variation of $Ts/fc'3/4$ for splices confined with transverse reinforcement with respect to $NAtr/n$. 110
Figure 5.8: Variation of $DIFTs$ with respect to $trtdNAtr/n$. 110
Figure 5.9: Low and high strain rate experimental bond strengths compared against those calculated using $DIFTc$ and $DIFTs$ incorporated into the ACI 408R descriptive expression. 111
Figure 5.10: Low and high strain rate experimental bond strengths compared against those calculated using $DIFld$ incorporated into the CSA A23.3 design expression. 111
Figure 5.11: Comparison of low and high strain rate experimental development lengths compared against those calculated using $DIFld$ incorporated into the CSA A23.3 design expression presented in Eq. (5.12). 112
Figure 6.1: Idealized reinforcement lap splice region. 133
Figure 6.2: Idealized bond-slip diagram (adapted from Michal et al, 2015). 133
Figure 6.3: Flowchart for the development of pseudo stress-strain relationships. 134
Figure 6.4: Typical pseudo stress-strain relationship developed for different bond levels. 134
Figure 6.5: Bond-slip relationship proposed by Eligehausen, Popov and Bertéro (1983) 135
Figure 6.6: Stress-strain relationships used in the analytical model. 135
Figure 6.7: Specimen details of the lap splice beams tested Chapter 4. 136
Figure 6.8: Comparison of low and high strain rate experimental resistance curves against those predicted considering full- and partial-bond conditions for splices not confined by transverse reinforcement. 137

Figure 6.9: Comparison of low and high strain rate experimental resistance curves against those predicted considering full- and partial-bond conditions for splices confined by transverse reinforcement..... 140
Figure 6.10: Comparison of experimental and predicted splice stress for companion pair CP4. 141
Figure 6.11: Comparison of experimental and predicted splice stress for companion pair CP6. 142
Figure 6.12: Comparison of experimental and predicted splice stress for companion pair CP8. 143
Figure 6.13: Experimental peak resistance compared against peak resistance predicted using the partially-bonded analysis methodology..... 144